UNIVERSITY OF SOUTHAMPTON

FACULTY OF NATURAL AND ENVIRONMENTAL SCIENCES

Ocean and Earth Science,

National Oceanography Centre, University of Southampton

Global Changes and Variability in Extreme Sea Levels from 1846-2014

by

Robert John Mawdsley

Thesis for the degree of Doctor of Philosophy

March 2016

UNIVERSITY OF SOUTHAMPTON

ABSTRACT

FACULTY OF NATURAL AND ENVIRONMENTAL SCIENCES

Ocean and Earth Sciences

Doctor of Philosophy

GLOBAL CHANGES AND VARIABILITY IN EXTREME SEA LEVELS FROM 1846-2014

by Robert John Mawdsley

Extreme sea levels exert a major control over the coastal zone, and many studies have found that they are changing at locations around the world. This thesis tests the assertion that these changes are predominantly caused by the global rise in mean sea level by investigating the importance of variability, over a range of timescales, in the other main components of sea level. The analysis is undertaken using a quasi-global dataset of 220 tide gauge records that range in length from 28-164 years.

For the first objective, secular (linear) trends in 15 different tidal levels were found to be significant (95% confidence) at between 34% and 63% of the study sites, depending on the tidal level analysed. Significant trends were distributed at sites around the world and at 37 sites the magnitude of the trends was over 1 mm/yr, comparable to the rise in global mean sea level over the 20th century. Spatial patterns were observed on local, regional and global scales. The global rise in mean sea level may be the cause of significantly more positive trends than negative trends occurring in high water levels, but other mechanisms appear more important at many locations.

The second objective assessed changes in the meteorological component of sea level. Significant tide-surge interaction was found at 59% or 81% of the 220 study sites, depending on the method used. At locations that have significant tide-surge interaction skew surge is the better parameter for the representation of the meteorological component. Only 13% of sites had significant secular trends in skew surge. There were significantly fewer negative trends in skew surge than the non-tidal residual, which may be because the influence of phase offsets is removed when using skew surge. Inter-annual variability in skew surge is large, but strong correlations between different regional skew surge and climate indices were not found to be significant in this thesis.

The third objective evaluated how the variability in the tidal and meteorological components of sea level - together with changes in mean sea level - influenced seasonal, inter-annual and secular changes in extreme sea levels. Variability in baseline extreme sea level (i.e. timescales greater than 6 months) was dominated by secular changes in mean sea level and the seasonal and inter-annual variability in mean sea level and skew surge, at most sites. The combined magnitude of the extracted signals reached 2.4 m in the North Sea, but was typically between 0.8 and 1.2 m. Changes in the relative phase of each signal, as well as the magnitude, may alter the magnitude of extreme sea levels. If independent signals in different components and timescales occurred in phase then the baseline extreme sea levels would increase at all sites in this study.

This thesis presents novel findings that show that while secular trends in mean sea level are important to changes in extreme sea levels, significant changes are occurring in all components and over many timescales. Shifts in both the magnitude and phase of signals in all components and over all timescales should be considered in extreme sea level projections. Accurate calculation of extreme sea levels has important implications for applications in the coastal zone, including flood defence, navigation, energy extraction and habitat protection.

Table of Contents

List of Tables

List of Figures

DECLARATION OF AUTHORSHIP

I, ROBERT MAWDSLEY declare that this thesis entitled 'Global Changes and Variability in Extreme Sea Levels from 1846-2014', and the work presented in it are my own and has been generated by me as the result of my own original research. I confirm that:

1. This work was done wholly or mainly while in candidature for a research degree at this University;

2. Where any part of this thesis has previously been submitted for a degree or any other qualification at this University or any other institution, this has been clearly stated;

3. Where I have consulted the published work of others, this is always clearly attributed;

4. Where I have quoted from the work of others, the source is always given. With the exception of such quotations, this thesis is entirely my own work;

5. I have acknowledged all main sources of help;

6. Where the thesis is based on work done by myself jointly with others, I have made clear exactly what was done by others and what I have contributed myself;

7. Parts of this work have been published as:

    a. Parts of Chapters 3 and 4, and the majority of Chapter 5 were published as: Mawdsley, R. J., Haigh, I. D. and Wells, N. C., 2015. Global secular changes in different tidal high water, low water and range levels. Earth's Future, 3: 66–81. doi:10.1002/2014EF000282.
    b. A preliminary paper of the above was published as: Mawdsley, R.J., Haigh, I.D., Wells, N.C., 2014. Global changes in tidal high water, low water and range. In: Green, A.N. and Cooper, J.A.G. (eds.), Proceedings 13th International Coastal Symposium (Durban, South Africa), Journal of Coastal Research, Special Issue No. 70, pp. 343-348, ISSN 0749-0208.
    c. Parts of Chapters 3 and 4, and the majority of Chapter 6 were published as: Mawdsley, R. J. and Haigh, I. D., 2016. Spatial and temporal variability and long-term trends in skew surges globally. Marine Frontiers, 3, doi: 10.3389/fmars.2016.00029

Signed: .....

Date: .....

Acknowledgements

A PhD thesis is a predominantly solitary pursuit, with large expanses of time given over to thought and introspection. This makes the support of colleagues, friends and family all the more vital to stop getting lost in the world of code and wiggly lines. I have been fortunate to have had such people in all aspects of my life during my PhD.

I have been particularly lucky to have had two excellent supervisors. I would like to thank Ivan Haigh for his dedicated supervision, excellent teaching of MATLAB, and kind yet constructive feedback on my writing and presentation skills. All these skills have developed immensely during my PhD, and hopefully this thesis can act as testament to his support. Neil Wells, has imparted his experience and epic knowledge to me throughout the PhD. He along with Carl Amos, have regularly reminded that a PhD should be 'Quantifiable, Repeatable and Predictable', hopefully with your help I have achieved that.

The knowledge and time of a number of other people have been invaluable during my time at NOCS. I would like to thank Mark Pickering for the use of the OTISmpi models runs used to compare against my observed trends. Thanks also go to Francisco Calafat, John Church and Matt Wadey. I would also like to acknowledge the help of Phillip Woodworth, who kindly provided feedback on my two papers.

I am lucky to have a strong and loving family, who have helped during some momentous and tough events during the PhD. Thank you to: Mum (for always being there), Dad (for your encouragement and interest), Hannah (the next Dr. Mawdsley), David (the grown up sibling!), Nana; Buffy and Jack (R.I.P). Thanks also to Sue and Brian for your help throughout the PhD.

The greatest thanks goes to my loving wife, and financial backer, Sophie. We started the PhD as boyfriend and girlfriend and end it as husband and wife, Mummy and Daddy! Thank you for your understanding, patience, support and love throughout the PhD. Doing this while also raising Oscar has required a lot of sacrifices on your part, for which I will be eternally grateful. Thank you as well to Oscar, for although you don't realise it, your smile has helped me forget the bad days instantly.

Definitions and Abbreviations

AMM	Annual Maximum Method
AMO	Atlantic Multi-decadal Oscillation
AO	Arctic Oscillation
AR5	IPCC 5th Assessment Report
BODC	British Oceanographic Data Centre
BOM	Bureau of Meteorology
DTR	Diurnal Tidal Range
EAUS	East Australia
ENSO	El Niño Southern Oscillation
ESL	Extreme Sea Level
GDTR	Greater Diurnal Tidal Range
GESLA	Global Extreme Sea Level Analysis
GIA	Glacial Isostatic Adjustment
GOM	Gulf of Mexico
HW	High Water
IOC	Intergovernmental Oceanographic Commission
IPCC	Intergovernmental Panel on Climate Change
JAP	Japan
JPM	Joint Probability Method
LDTR	Lesser Diurnal Tidal Range
LECZ	Low elevation coastal zone
LGM	Last Glacial Maximum
LW	Low Water
MEDS	Marine Environmental Data Service
MHHW	Mean Higher High Water
MHLW	Mean Higher Low Water
MHW	Mean High Water
MHWN	Mean High Water Neap
MHWNE	Mean High Water Neap-Equatorial
MHWS	Mean High Water Spring
MHWST	Mean High Water Spring-Tropic
MHW88	Mean High Water (88th percentile of Tide)
MLHW	Mean Lower High Water
MLLW	Mean Lower Low Water

MLW	Mean Low Water
MLWNE	Mean Low Water Neap-Equatorial
MLWST	Mean Low Water Spring-Tropic
MSL	Mean Sea Level
MTR	Mean Tidal Range
NAO	North Atlantic Oscillation
NEP	North-east Pacific
NETR	Neap-Equatorial Tidal Range
NMA	Norwegian Mapping Authority
NOAA	National Oceanic and Atmospheric Administration
NP	North Pacific (Oscillation)
NS	North Sea
NTR	Non-tidal residual
NWA-N	North-west Atlantic – North
NWA-S	North-west Atlantic - South
OSU	Oregon State University
PDO	Pacific Decadal Oscillation
POTM	Peaks Over Threshold Method
PSMSL	Permanent Service for Mean Sea Level
QC	Quality Control
RJPM	Revised Joint Probability Method
RLM	R-Largest Method
RMSE	Root Mean Square Error
SCS	South China Sea
SLP	Sea Level Pressure
SLR	Sea Level Rise
SOI	Southern Oscillation Index
SSH	Sea Surface Height
SST	Sea Surface Temperature
STTR	Spring-Tropic Tidal Range
UHSLC	University of Hawaii Sea Level Center
UK	United Kingdom
USA	United States of America
USGS	United States Geological Survey
WAUS	West Australia

Chapter 1: Introduction

1.1 Background

The coastal zone is densely populated and heavily developed because of its strategic importance for transportation, industry, agriculture, fishing and recreation (Pugh and Woodworth, 2014). Development and utilisation of the coastal zone has increased greatly during recent decades and coasts are undergoing tremendous socio-economic and environmental changes (Neumann et al., 2015). The low elevation coastal zone (LECZ; land beneath 10 m from mean sea level (MSL)) comprises only 2% of the total land area of all coastal countries, but currently contains more than 10% of global population (Neumann et al., 2015). Over the past century, the coastal population has grown rapidly and this is expected to continue - by 2060 1.4 billion people will live in this region, equating to approximately 12% of the world's expected 11.3 billion people (Neumann et al., 2015). A large proportion of the coastal population lives in one of 18 megacities (> 10 million population) that are located along the world's coastline (Brown et al., 2013; UN DESA, 2014), several of which are situated in large deltas and are especially susceptible to both coastal and river flooding.

Extreme sea levels (ESL) are a major and regular threat to the LECZ with high ESL causing damaging floods and coastal erosion, and low ESL having implications for navigation and the operation of power plants (Pugh and Woodworth, 2014). Of these impacts, flooding has received the most attention because of the direct impact on human lives, and as such high ESL events have been well documented throughout recent history. A large North Sea coastal flood event in November 1570 drowned an estimated 100,000 to 400,000 people (Lamb, 1991). The Galveston Hurricane of 1900 generated a storm surge of around 5 m, which led to the deaths of between 8,000 and 12,000 people (Emanuel, 2005). In Bangladesh, up to 500,000 people died during Cyclone Bhola in 1970, predominantly because islands in the Ganges Delta were inundated by the resulting storm surge (Frank and Husain, 1971).

The deaths caused by high ESL have typically reduced in recent decades because of the construction of coastal flood defences and/or improvement in flood forecasting and preparedness (e.g. Wadey et al., 2015). However, many events in the 21st century have still resulted in significant loss of life and economic damages. Areas where significant loss of life has recently been cause by ESL include: New Orleans, Louisiana as a result of Hurricane Katrina in 2005; the Irrawaddy Delta of Myanmar in response to Cyclone Nargis in 2008; and the Philippine island of Leyte because of Typhoon Haiyan in 2013 (Pugh & Woodworth, 2014); among many others.

In addition, although the death tolls from ESL have reduced in recent decades, the costs associated with the largest events have increased, especially in developed countries, due to rapid development in coastal regions. For example, damages from Hurricane Katrina in 2005 were estimated to cost $161 billion (World Bank, 2012), making it the costliest natural disaster in US history. The storm surge caused the majority of the damage. This was also the case with Hurricane Ike in 2008 and Hurricane Sandy in 2012, which have respective damage estimates of $42 billion and $70 billion (SwissRe, 2012). The financial impact of ESLs is expected to rise alongside the continued development of the coastal zone. In 2005, the largest 136 coastal cities had an estimated 40 million people and $3,000 billion of assets exposed to independent 1 in 100-year flood events, assuming no flood defences. This exposure is predicted to rise to approximately 150 million people and $35,000 billion of assets by 2070 (Nicholls et al., 2007; Hanson et al., 2011, Stevens et al., 2015).

The impacts of ESL have been mitigated in many regions in recent decades. Mitigation includes the construction of adequate flood defences, as well as, improvements in storm surge modelling and forecasting, community preparedness and emergency response. For example, the 1953 North Sea storm surge killed over 2,500 people, mostly in the Netherlands. In response, extensive coastal defences were built around the North Sea, including the Deltaworks on the Dutch coast and the Thames Barrier in the United Kingdom (UK). This was carried out at the same time as improvements in storm surge modelling and forecasting. Consequently, when a storm surge in December 2013 caused ESLs to exceed the magnitude of the 1953 event at several locations around the North Sea (Wadey et al., 2015) the impact was greatly reduced. There were no flood related deaths in the December 2013 event and the overall damage was estimated at £250 million, compared to a 2014 adjusted value of £1.2 billion for the 1953 flood (Wadey et al., 2015).

Effective mitigation requires an accurate understanding of physical and societal conditions in order to comprehend where and when the risks from ESLs are greatest. This is complicated by the non-stationary nature of ESLs over a range of space and timescales, and means that a thorough understanding of variability of ESLs is needed in order to mitigate against future risks. ESLs are dependent on the variability in, and the combination of, the three main components of sea level: MSL, astronomical tide and non-tidal residual (NTR; Pugh and Woodworth, 2014), with the NTR primarily generated by the meteorological contribution to sea level. Changes in MSL effect ESLs in the following two ways: directly, since a rise (or fall) in MSL will result in a lower (or higher) surge elevation at high-tide being necessary to produce a flooding event; and indirectly, since changes in MSL alter water depth and hence modify the propagation and dissipation of the astronomical tide and meteorological components of sea level. In addition, ESLs can change as a result of variations in the strength and tracks of weather systems, which alter the intensity and/or duration

of storm surges (Seneviratne et al., 2012). Despite concerns of increased coastal flooding, most of the past studies of sea level changes have concentrated on examining only the variations in MSL and by comparison there are far fewer studies of changes in ESLs (e.g. Woodworth and Blackman, 2004).

A number of studies have found evidence for a secular increase in the magnitude of ESL over the last century at many sites around the world, and this increase has been shown to be primarily caused by the direct effect of the secular increase in global MSL (e.g. Woodworth and Blackman; Menéndez and Woodworth, 2010). Secular trends are defined as being persistent over an indefinitely long period, which in this case is the length of the dataset. Therefore, with the rate of increase in MSL predicted to accelerate over the 21st century (Church et al., 2013), the magnitude of ESL may be expected to increase at a similar rate. However, this contradicts the findings of many other studies who have found significant deviations away from a direct linear relationship between the secular trends in ESL and MSL (e.g. Abeysirigunawardena and Walker, 2008; Menéndez and Woodworth, 2010; Mudersbach et al., 2013). Some studies have found significant secular trends in tidal constituents (Ray, 2006; Jay, 2009; Woodworth, 2010) or tidal levels (Flick et al., 2003; Mudersbach et al., 2013; Rasheed and Chua, 2014), while others have inferred changes in the NTR (e.g. Grinsted et al., 2012; Talke et al., 2014; Wahl and Chambers, 2015). Furthermore, each of the main sea level components varies on seasonal and inter-annual timescales, in response to variability in oceanographic, hydrological and meteorological mechanisms (Pugh and Woodworth, 2014). In summary, previous research has found that variations, in both the phase and magnitude of signals in each of the main sea level components, has influenced variability in ESL over time-scales from seasons to centuries. However, the contradiction between the global studies that find that the increase in ESL is primarily a response to the rise in global MSL, and some regional and local scale studies that have observed significant secular changes in the tidal or meteorological components, is an issue that this thesis aims to address.

Therefore, to understand variability in ESLs, a thorough understanding of the variations in all the main components of sea level and their interactions, on a wide-range of time and space scales, is essential. Many projections of ESLs account for the direct effect of the secular increase in MSL, but not for variability or trends in other components or timescales, despite a growing body of evidence suggesting that all components can be important for ESL projections. Understanding of variability in some components and in some locations, is hampered by a lack of research, and therefore this thesis aims to extend and improve upon previous research and to advance the understanding of variability in ESL, on a global scale. This will be undertaken using a global tide

gauge dataset to assess the variability in each of the three main components of sea level separately, on timescales from seasons to centuries, and then in combination.

1.2 Aims and Objectives

The overall aim of this thesis is to quantify the variability and secular trends in each of the three main components of sea level in order to better understand the combined variability and secular trends in ESLs, both spatially on local to global scales and temporally on scales of seasons to centuries. To do this I start by individually assessing the observed changes in the tidal and then non-tidal components of sea level, along with interactions between them, before considering how variability in these two components, and MSL, combine to influence seasonal to century scale changes in ESLs. The analysis is based on a 'quasi-global' tide gauge dataset, with data lengths that vary from 28 to 164 years. To address this aim there are three related objectives, as follows:

- **Objective 1**: To determine the magnitude and spatial distribution of secular changes in tidal levels on a global scale;
- **Objective 2**: To assess the spatial and temporal variability and secular trends in skew surges globally;
- **Objective 3**: To evaluate how the variability in the tidal and non-tidal components of sea level (Objectives 1 and 2), together with changes in MSL, influence the seasonal, inter-annual and secular changes in ESLs.

Note, changes in MSL have been widely documented and therefore there is no individual objective on MSL changes. Instead variations in MSL are considered as part of Objective 3.

For objective 1, different tidal levels are extracted to assess changes in high and low water, and tidal range. Secular trends in each tidal level are calculated and the regional and global coherence of trends is evaluated. The results are compared to the predicted changes in tide from a global tidal model assessment (Pickering, 2014) to investigate the extent to which MSL rise has modified the tide.

For objective 2, skew surge time series are derived using an approach that is effective across all tidal regimes (i.e. semi-diurnal, diurnal and mixed). The strength of tide-surge interaction at each site is evaluated, and the differences between using skew surge and NTR, to assess the meteorological component, are investigated. Secular trends in skew surge and NTR are calculated and then compared. Regional skew surge indices are constructed to assess the coherence in skew surge time series both within regions and between different regions. The correlation between

regional skew surge indexes and climate indices is calculated to investigate the drivers of inter-annual variations in skew surge, at different locations.

Building on objectives 1 and 2, in objective 3 the magnitude and phase of the seasonal, inter-annual and secular variability of each of the three main components of sea level is evaluated individually and then in combination to assess the variability in ESLs across these timescales. The regional variation in the magnitude and phases of the different components is determined. The observed maximum ESL at each site is then compared with a theoretical maximum ESL, which could arise if all independent components combined in phase.

1.3 Structure of Report

The structure of this thesis is as follows: Section 2 presents a literature review, describing the different components of sea level, the current research on observed changes in sea level, methods of representing the components of sea level and ESL and the techniques used to measure sea level and ensure its accuracy. The data used and the specific quality control (QC) procedures applied are outlined in Section 3. This section also describes how sea level records at each site were separated into their component parts. The three objectives are then addressed in Sections 4, 5 and 6, respectively. Section 7 summarises the conclusions and discussions arising from the analysis, and ends with recommendations for further research.

Chapter 2: Background: Literature Review

Sea level (exclusive of wind waves) at any time or location is comprised of a MSL, astronomical tide and a non-tidal component (i.e. NTR), with non-linear interactions between them (Pugh and Woodworth, 2014). ESLs arise as a combination of these components on timescales of seconds to centuries. Section 2.1 describes each of the three main components in turn, and the interactions between them. Current understanding of how these components have changed in the past, or might change in the future, is discussed in Section 2.2. A summary of the impacts of these changes on ESL is presented in Section 2.3. Descriptions of the different methods used to assess sea level components and ESL is given in Section 2.4. Techniques used to measure and ensure accuracy of sea level observations are presented in Section 2.5. A summary, highlighting major current knowledge gaps in the understanding of ESLs is given in Section 2.6.

2.1 Components of Sea Level

Variations in the height of the sea surface are caused by various factors that occur over a wide range of space and time scales (Weisse and Von Storch, 2008). Ignoring the variations in wind waves, the observed sea surface height (SSH), can be regarded as a sum of MSL, tide and a NTR (Pugh and Woodworth, 2014), as defined in Equation 2.1 for a time t:

$$X(t) = \mathrm{MSL}(t) + Tide(t) + NTR(t) \qquad (Eq. 2.1)$$

Each component varies directly in response to many mechanisms and indirectly due to interactions between the components. The remainder of this section will give an overview of each of these three components and describe the mechanisms that cause variations in them.

2.1.1 MSL

The MSL component is the mean level of the sea surface over a defined period, usually a month or year (Araujo, 2006). The simplest method of calculating an annual MSL value is to derive an arithmetic mean (i.e. add all the high frequency measurements of sea level during the defined period and divide by the number of records), but there are more sophisticated methods, such as using low-pass filters (Pugh and Woodworth, 2014).

Sea level measured by tide gauges is relative to a fixed point on land. Therefore, MSL changes at that specific location can be caused by a change in the volume of the water (eustatic) or by

vertical land movement (isostatic) on which the tide gauge is located. Of primary focus for many climate studies is the eustatic rise in MSL resulting either from mass balance from ice sheets to the oceans or thermal expansion of water (Church et al., 2013). Isostatic sea level rise (SLR) may occur because of glacial isostatic adjustment (GIA), in regions that were covered by ice at the last glacial maximum (LGM) (e.g. Norway and Alaska). In these regions, the land is uplifted as the ice load is removed, and here MSL relative to the land is decreasing (Peltier et al., 2001). To compensate for the vertical uplift of land due to GIA the solid earth responds with internal mass movements which creates a surrounding region of the Earth's surface that is correspondingly sinking, known as the 'forebulge' (Peltier et al., 2001). Improved models and precise benchmarking of the tide gauges have recently reduced uncertainty relating to GIA in sea level measurements. On smaller spatial and temporal scales, isostatic SLR can result from land subsidence, caused by increased development of the coastal zone, or the extraction of water or hydrocarbons (e.g. Tokyo or Galveston; Nicholls, 2010).

2.1.2 Tide

Tides are the regular and predictable rise and fall of the sea, directly related in amplitude and phase to a periodic geophysical force (Pugh and Woodworth, 2014). The strength of the primary forces relating to the gravitational attraction and rotation of the Moon and Sun, with respect to Earth, are well defined. However, variations of the orbits, such as the distance away from the Earth or declination, modify the gravitational attraction between the bodies and thus the height of the tide.

The equilibrium tide has three main species of lunar (and solar) tides: long-period tides, with changes over a month or longer that are due to the distance or declination of the orbiting body; diurnal tides controlled by the linear declination and the Earth's rotation; and semi-diurnal tides controlled by the Earth's rotation only (Pugh and Woodworth, 2014). Many factors prevent the equilibrium tide from occurring on Earth, including: the presence of continental boundaries; the depth of the ocean being too shallow for the high water to move at the same speed as the rotating Earth; natural modes of oscillation in the ocean's basins; and the effect of the Earth's rotation on the movement of water (Pugh and Woodworth, 2014). Although observed tides vary from the equilibrium tide their energy exists at the same frequencies and therefore the equilibrium tide acts as a reference for the amplitudes and phases of the observed tide and tidal prediction.

The observed tides can therefore be represented by a series of harmonic constituents that each have a specific amplitude, phase lag and period as described in Equation 2.2 (without nodal corrections, which relate to the variation in each constituent caused by the lunar nodal cycle).

$$X(t) = H_x \cos(\omega_x t - g_x) \qquad Eq. 2.2$$

Where: X is the value of the variable quantity at time *t;* H_x is the amplitude of the oscillation; ω_x is the angular speed that is related to period T_x by: $T_x = 2\pi/\omega_x$ (ω_x is measured in radians per unit time); and g_x is a phase lag relative to some defined time zero (Pugh and Woodworth, 2014).

2.1.3 Meteorological Component of Non-Tidal Residual

The NTR is the component of sea level that remains after subtracting the MSL and tidal components. This mainly contains the meteorologically-induced part of sea level, and is often termed the storm surge. However, other factors are also included in the NTR, and therefore to assess the meteorological component directly, it is necessary to remove, or account for, their effect. Non-meteorological factors are discussed in Section 2.1.4.

Meteorologically forced variation in sea level is caused either by changes in atmospheric pressure or by wind drag on the sea surface. Atmospheric pressure changes sea level through the inverse barometric effect, which is the rise of the sea surface as atmospheric pressure decreases, or vice versa. As the sea surface nears equilibrium in response to atmospheric pressure forcing, the following equation holds:

$$\Delta p_a + \rho g \Delta h = 0 \qquad Eq. 2.3$$

Where: p_a denotes the sea surface atmospheric pressure; ρ is the density of seawater; g is the gravitational acceleration; and h represents the SSH. When average values of $\rho = 1026\ kg/m^3$ and $g = 9.81\ m/s^2$ are taken, then a change of atmospheric pressure of about 1 hPa will case a 1 cm change in SSH.

In the case of storm surges, the pressure affect is usually of secondary importance compared with the direct response of SSH to wind forcing (Weisse and von Storch, 2008). As the wind blows over a body of water it creates a slope on the water surface such that the resulting pressure gradient eventually balances the drag of the wind on the water surface. Equation 2.4 shows that the response of SSH depends on wind speed, fetch and water depth (Weisse and Von Storch, 2008), with elevated SSH resulting from increased wind speed, longer fetch and/or shallower water depth.

$$\frac{\partial h}{\partial x} = \frac{\rho_a}{\rho}\frac{c_d u^2}{Dg} \qquad Eq.2.4$$

Where: h represents the SSH; x is the horizontal distance over which the wind acts on the sea surface (fetch); ρ_a and ρ are the densities of the atmosphere and seawater respectively; D denotes water depth; u is the wind speed; while c_d and g are the drag coefficient and gravitational acceleration, respectively.

As Equation 2.4 suggests, several factors influence the generation of sea level disturbances, including meteorological influences (i.e. wind speed, direction, persistence and spatial distribution, and sea level pressure (SLP)), oceanographic effects (i.e. water density and sea ice cover), and topographic features (i.e. water depth and the width of continental shelf) (Pugh and Woodworth, 2014). The propagation of the sea level disturbance is also influenced by many factors, some of which are the same, including: meteorological influences (i.e. wind persistence and movement of the SLP disturbance), oceanographic affects (i.e. water density and sea ice cover) and topographic features (i.e. water depth, width of continental shelf, and the presence of sand bars and reefs) (Pugh and Woodworth, 2014). The nature of the meteorologically forced signal is dependent on the response of the sea surface to both the generation and propagation mechanism. The responses can be categorised based on three main types, which are namely: (i) storm surges, (ii) seiches and (iii) meteorological tsunamis.

The primary cause of the meteorological component are storm surges, and most of the world's coastline is vulnerable to them. They are generated by two main types of storms. Tropical cyclones transform heat, mainly transferred from a very warm sea surface, into kinetic energy, while extra-tropical storms gain their energy from the horizontal temperature gradient, described in the frontal theory of Bjerknes (von Storch and Woth, 2008). Tropical and extra-tropical storms have difference characteristics, with respect to size and intensity, and their associated storm surges reflect these differences (Gönnert et al., 2001). The storm surges associated with tropical storms typically have a larger amplitude, but a shorter duration (hours to days) and smaller spatial scale (typically smaller than 500 kilometres). Extra-tropical storm surges typically act on larger time (approximately 2 to 5 days) and spatial scales (typically over 1000 kilometres; Weisse and von Storch, 2008), but rarely reach the same magnitude as those generated by tropical storms. Storm surges can also be generated externally. For example, storm surges are often generated to the north of the North Sea and propagate along the east coast of the UK as a long wave (Weisse and von Storch, 2008).

Storm surges generated by tropical cyclones impact the east coast of North America, the Gulf of Mexico, Hawaii, both coasts of Mexico, the Caribbean Sea, the Bay of Bengal, the Arabian Sea, the

South West and East Indian Ocean, the western tropical Pacific, the coastlines around the South China Sea and the coasts of Australia, Japan, Korea (Figure 2.1). Extra-tropical storm surges are common along the east coast of Canada and USA, in Argentina, and all around Europe including the North Sea, the Baltic Sea, the Irish Sea, the Mediterranean Sea, the Adriatic and Aegean seas, and the Black Sea (Gönnert et al. 2001).

Seiches are evident in most inlets and bays, and can be forced by the wind, changes in air pressure, the ocean tide, the internal tide, wave energy impinging on a harbour, earthquakes or landslides (Pugh & Woodworth, 2014). The resonant periods of idealised harbours and inlets can be determined straightforwardly, and all periods are proportional to the reciprocal of the square root of water depth. The longest natural period can be calculated by Merian's formula.

$$\tau = \frac{2L}{\sqrt{gD}} \qquad Eq.2.5$$

Where T is the longest natural period, L is the length, h the average depth of the body of water, and g the acceleration of gravity (Proudman, 1953). In the Adriatic Sea seiches can occur over a range of periods and may produce a SSH displacement of 60-80 cm. Their magnitude coupled with their long decay time, around 10-15 days (Franco et al., 1982), mean that ESLs in Venice, for example, regularly have a contribution from seiches (Lionello et al., 2012).

Meteorological tsunamis (or meteotsunamis) cover a range of phenomena in which meteorological disturbances (e.g. cyclones, frontal squalls, air pressure jumps and thunderstorms) produce long waves in the ocean that propagate until they reach the coastline, where they behave similarly to seismically generated tsunamis. These long waves however are generated over minutes to hours. Many meteotsunamis are generated when a positive sea level change caused by a low-pressure centre is magnified when the cyclone travels in the same direction and at the same speed as long progressive waves in the ocean (approximately$\sqrt{gD}$).

The similarity between meteotsunamis and tsunamis, and to some extent between meteotsunamis and storm surges, has created difficulties in the interpretation of some historical flooding events before seismic and meteorological data were widely available. However, widespread co-incident oceanographic and meteorological monitoring programmes can now detect and attribute these regional scale changes in sea level. Such an event occurred in June 2014 where meteotsunamis in the Balearic Islands, Croatia and the Black Sea over the course of a few days (Šepic et al., 2015), were associated with the same low-pressure system tracking across the Mediterranean Sea. Wave heights during this event reached 3 m in Vela Luka, Croatia (Šepic et al., 2015), but waves of over 5 m have been recorded during previous events (Vučetić et al., 2009). Meteotsunamis have also been recorded in British Columbia (Thompson et al., 2009),

Japan (Hibiya et al., 1982), Korea (Ha et al., 2014) and the English Channel (Tappin et al., 2013; Ozsoy et al., 2016).

Whatever the type of the meteorologically forced sea level, the impacts of a large event are often destructive, particularly when they coincide with large tides. The high frequency variability in this component occurs on timescales from seconds to days, and is the response of the sea surface to many stochastic mechanisms. As such it is the hardest sea level component to predict, and poses the greatest danger for coastal flooding and erosion.

2.1.4 Non-Meteorological Signals in the Non-Tidal Residual

The NTR is influenced by many non-meteorological factors, including: tide-surge interaction (Horsburgh and Wilson, 2007), seismically generated tsunamis, harmonic prediction errors (Pawlowicz et al., 2002), gauge timing errors and tide-river flow interactions (Godin, 1985; Horrevoets et al., 2004). In order to accurately represent the meteorological component, the influence of these factors should be removed from the NTR. Although seismically generated tsunamis generate ESL, they are non-predictable and not linked to climate change and therefore not considered in this study. The methods used to identify and remove seismically generated tsunamis and errors caused by the measurement or analysis are described in Chapter 3.

Non-linear interactions between the three components of sea level lead to variations in one or more of the components. Tide-surge interaction is an important mechanism to consider, and occurs for two main reasons. First, wind stress may be more effective at generating changes in SSH at low tide, because of the reduced water depth compared to high tide (see Equation 2.4). Second, the greater water depth present during a positive storm surge increases the speed of tidal wave propagation, often resulting in the observed high water occurring before predicted high water (Wolf, 1981; Horsburgh and Wilson, 2007; Pugh and Woodworth, 2014). Tide-surge interaction has been studied most in the southern North Sea, where the greatest frequency of positive NTRs are observed to occur on the rising tide (Horsburgh and Wilson, 2007). Tide-surge interactions have also been observed across other continental shelf regions and in shallow water areas, including: the English Channel (Haigh et al., 2010; Idier et al., 2012); Canada (Bernier and Thompson, 2007); Australia (Haigh et al., 2014); the South China Sea (Feng and Tsimplis, 2014); the Bay of Bengal (Antony and Unnikrishnan, 2013); and was observed during Hurricane Sandy off the USA east coast (Valle-Levinson et al., 2013). However, the extent to which tide surge interactions occur has not been assessed for large stretches of the world's coastline.

2.2 Variations in Sea Level

Sea levels vary on temporal scales of seconds to millennia and understanding how the variations interact with each other is imperative for determining sea levels in the future. This section describes the current research and understanding of the variations on different time scales for the three main components of sea level and ESL. Each section starts by looking at the secular (centennial scale) variation before moving to inter-annual and seasonal variations, which are the timescales focused on in this study.

2.2.1 MSL

A central tenet of climate change research is that global warming has led to an eustatic rise in MSL over the last century. The Intergovernmental Panel on Climate Change (IPCC) 5th Assessment Report (AR5) (Church et al., 2013) states that there is 90-100% probability that during the period 1901 to 2010 the mean rate of global MSL rise was 1.7 ± 0.2 mm/yr, and that between 1993 and 2010 this rate was higher at 3.2 ± 0.4 mm/yr. These results from sea level recorders with the support since 1993 of satellite altimetry data, show that there is a 66-100% probability that an acceleration in the rate of MSL rise has occurred, with estimates that range from 0.000 ± 0.002 mm/yr^2 to 0.013 ± 0.006 mm/yr^2 (Hartmann et al., 2013). The observed acceleration (Woodworth et al., 2011; Haigh et al., 2014) is expected to continue, with estimates of MSL rise of between 0.26 and 0.97 m by 2100 (Rhein et al., 2013). The primary mechanisms causing global MSL rise between 1993 and 2010, were ocean thermal expansion (accounting for about 35%), glacier mass loss (accounting for a further 25%, not including that from Greenland and Antarctica; Church et al., 2013). The ocean thermal expansion, mass transfer from ice sheets and glaciers and the estimated change in land water storage (which is relatively small) account for approximately 65% of the observed global MSL rise for 1901–1990, and 90% for 1971–2010 and 1993–2010 (Church et al., 2013).

Although secular variation in MSL is predominantly caused by these three mechanisms, many more factors affect MSL on short time scales. Another important question is whether, given that tide gauges only provide a partial coverage of the ocean, water may have been redistributed around the ocean. For example, Miller and Douglas (2007) argued that the apparent 20th century acceleration seen at the eastern boundary of the North Atlantic Ocean could have been an artefact of the spin-down of the sub-tropical gyre. The question of redistribution is also relevant to the quasi-global altimetry dataset. In the regions such as the western Pacific and South China Sea (SCS) increases of over 10 mm/yr have been observed over the last 20 years (Meysiggnac and Cazenave, 2013). Merrifield (2011) found this increased rate of sea level rise to coincide with an

increase in the speed of the trade winds. Other studies have suggested the large rate of SLR in the western Pacific is related to the response of the ocean to the El Nino Southern Oscillation (ENSO; Church and White, 2011). The ENSO has a periodic cycle of between 3 and 7 years, caused by variations in equatorial wind patterns. The responses to regional climatology include steric effects caused by the increased seawater temperature in the region (Peng et al., 2013), as well as changes in regional wind patterns. Decreases of MSL in the SCS accompanied by increases of 10-20 cm along the eastern Pacific coast have been observed, persisting for many months during El Niño events (Rong et al., 2007; Cayan et al., 2008). These aspects stress the importance of considering 'trends' and 'accelerations' in sea level alongside those of large scale patterns of ocean variability."

MSL values are also effected by variations in atmospheric pressure: either directly, through the inverse barometric affect (Pugh & Woodworth, 2014); or indirectly, through the influence of atmospheric pressure on annual variations in heating, oceanic currents and regional winds. Monsoon winds can generate large seasonal variations, while steric affects can be seen in MSL around the world (Peng et al., 2013; Amiruddhin et al., 2015). These seasonal variations are typically greatest in the northern hemisphere, where maximum values are observed in September after a summer of heating and seawater expansion (Pugh & Woodworth, 2014). However, regions near river outflows (e.g. Bay of Bengal, Gulf of Bohai or the St. Lawrence River) can have seasonal cycles of up to 1 m (Tsimplis and Woodworth, 1994).

Other processes such as eddies can cause variability in MSL over a few days. The observed properties of eddies vary considerably, but in the ocean the word is used to describe features with length scales of order 10-100 km, and with timescales of 10-30 days (Gill, 1982). Their amplitude in terms of vertical displacement of isopycnals can be over 100 m, but associated variation in SSH is typically 5-25 cm (Chelton et al., 2007). They occur predominantly offshore, since they are associated with large currents predominantly, and their impact is short-lived since they generally propagate westward at a few centimetres per second (Gill, 1982).

2.2.2 Tide

Changes in tides are known to have occurred over thousands of years, in response to large (up to 130 m) variations in MSL associated with glacial and inter-glacial cycles (Egbert et al., 2004; Green, 2010), and over much longer time-scales with the evolution of ocean basins and continents (Sündermann and Brosche, 1978; Müller et al. 2011). However, for many applications, tides have generally been considered to have undergone little change over the last century. It is often presumed in the projection of ESLs, that they will not change over the next century, because the

astronomical forces that generate them are virtually constant (Cartwright and Tayler, 1971; Cartwright and Edden, 1973; Cartwright, 1985).

However, several studies have detected measureable changes in tides during the 20th century and early part of the 21st century at a number of locations (Woodworth, 2010). For example, significant trends in the mean tidal range (MTR), calculated from mean high water (MHW) and mean low water (MLW), have been observed over the timespan of direct sea level measurements. These trends have been observed: at sites around the United Kingdom (UK; Woodworth et al., 1991; Haigh et al., 2010); in the German Bight (Töppe & Führböter., 1994; Hollebrandse, 2005; Mudersbach et al., 2013); around the coastline of Japan (Rasheed & Chua, 2014); and at many sites around the United States of America (USA; Flick et al., 2003). The amplitudes of particular major tidal constituents have also been shown to change over these timescales, including: at individual sites (e.g. Cartwright (1971) for St. Helena in the South Atlantic; Cartwright (1972) for Brest in France; Araújo and Pugh, (2008) for Newlyn in the UK); in regional studies (e.g. Amin (1993) for Australia; Ray (2006, 2009), and Jay (2009) for the USA; Araújo (2006) for the West European Coast; Torres & Tsimplis (2011) for the Caribbean Sea; Mudersbach et al. (2013) for the German Bight; Zaron & Jay (2014) for open ocean sites in the Pacific Ocean); and in two comprehensive studies that assessed quasi-global sea level datasets (Woodworth, 2010; Müller et al., 2011). In many of these studies, the magnitude of observed changes in both tidal levels and tidal constituents was comparable to increases in MSL at certain sites. For example, during the latter half of the twentieth century, Anchorage in Alaska and Wilmington in North Carolina, were found to have trends in diurnal tidal range (DTR) of over 5 mm/yr (Flick et al., 2003), while trends in MTR in the German Bight exceeded 3 mm/yr (Töppe & Führböter, 1994; Mudersbach et al., 2013). Therefore, changes in the tide are large enough, at certain locations, that they should be accounted for in coastal engineering, management and planning applications, where sea level is an important factor (Woodworth et al., 1991; Müller et al., 2011).

With the astronomical forcing remaining near constant over the timespan of tide gauge observations, these measureable changes in tidal levels and tidal constituents are likely caused by changes in terrestrial factors, such as water depth and coastal geomorphology, which generate differences in the timing and magnitude of the observed tide (Pugh & Woodworth, 2014). Possible terrestrial mechanisms have been summarised in previous papers (e.g. Woodworth, 2010; Müller, 2012) and include: interactions between the tide and the continuum of the non-tidal variations (Munk & Cartwright, 1966); changes in water depth due to variations in global MSL and/or isostatic changes in the solid earth, which lead to modifications in tidal wavelengths (e.g. Flather et al., 2001; Müller et al., 2011; Pickering et al., 2012); morphological changes in coastal waters, harbours or estuaries (e.g. Bowen, 1972; Araújo et al., 2008); changes in the internal tide,

expressed as small changes in its surface expression (e.g. Ray and Mitchum, 1997; Mitchum and Chiswell, 2000; Colosi and Munk, 2006); and seasonal variations caused by changes in sea ice cover (St. Laurent et al., 2008), mean currents (Cummins et al., 2000) and water column stratification (Kang et al., 2002; Müller, 2012) (Note: the latter could have a large influence over longer time-scales as global warming causes widespread changes in the global oceans).

The well-documented rise in global MSL over the past 150 years (Church et al., 2013) has been explored as a potential mechanism causing the observed regional changes in the tide. For example, Woodworth et al. (1991) found a positive correlation between the trends in MTR and MSL around the UK. Müller et al. (2011) illustrated, using a global tidal model, that a 1 m increase in MSL could lead to a 1-2 % change in the amplitude of major constituents, while modelling studies of the North Sea suggest that the change in tidal wave speed, in response to MSL change, can lead to spatially variable and non-linear responses (Pickering et al., 2012; Ward et al., 2012; Pelling et al., 2013; Pickering, 2014). These responses, that include standing wave resonance from the reflection of the incident tidal wave, frictional effects, coastline geometry, and inertial effects (van Rijn, 2011), mean that although some regional patterns are observed, at other sites, local effects appear to dominate (Woodworth et al., 2010).

All these mechanisms can also lead to changes in the tide on seasonal to decadal timescales, while variations in astronomical forcing also becomes important over these periods. All lunar constituents are affected by the 18.61-year nodal cycle, which is the response of the tide to the amplitude of the lunar declination (Pugh and Woodworth, 2014). Increases in the range of the lunar declination increases the amplitude of the diurnal lunar tides, but there is a corresponding decrease in the amplitude of the semi-diurnal tides. The 8.85-year cycle of lunar perigee is determined by the Moon's elliptical orbit around the Earth, with its phase described by the positions of least and greatest distance known as perigee and apogee, respectively (Pugh & Woodworth, 2014). The main influence of the lunar perigean cycle is to increase the amplitude of semi-diurnal constituents over a 4.4-year cycle. The lunar nodal modulation dominates over the lunar perigean modulation in regions where the tide is mixed or diurnal in form, but this is reversed in semi-diurnal tidal regimes (Haigh et al., 2011).

2.2.3 Meteorological Component

The factors influencing the generation and propagation of storm surges are documented in Section 2.1.3, and show that changes to a number of parameters can cause variations. Research has shown that these characteristics are non-stationary, with variations occurring on scales from

seconds to centuries, and influenced by both internal natural variability and anthropogenic climate change.

The meteorological component of sea level is the response of the sea surface to storms. A growing body of literature suggests that climate change could alter the frequency, intensity and tracks of storms and therefore the associated changes in the meteorological component (Church et al., 2013). An increase in sea surface temperatures (SST) would raise the ambient potential intensity (as defined by Bister and Emmanuel, 1998) through which tropical cyclones move, and should shift the distribution of intensities upwards (Seneviratne et al., 2012). Observations demonstrate a strong positive correlation between SST and potential intensity (Emanuel, 2000), but recent research suggests that local potential intensity is controlled by the difference between local SST and spatially averaged SST in the tropics (Vecchi and Soden, 2007). This suggests that increasing SST due to global warming by itself does not yet have a fully understood physical link to increasingly strong tropical cyclones (Seneviratne et al., 2012). Furthermore, a number of processes could counteract the increase in potential intensity, including increases in vertical wind shear (Vecchi and Soden, 2007) or an increase in the saturation deficit of the middle troposphere (Emanuel et al., 2008). As such, confidence remains low for centennial changes in tropical cyclone activity, even after accounting for past changes in observing capabilities (Hartmann et al., 2013). However, in the North Atlantic the frequency and intensity of the strongest cyclones has increased since the 1970s (Kossin et al., 2007). In addition, a net increase in frequency and intensity of extra-tropical storms, coupled with a poleward shift in storm tracks has been observed since the 1950s in both the North Atlantic and North Pacific (Hartmann et al., 2013).

The relatively short observational data set of meteorological conditions makes detecting secular changes difficult, because of large inter-annual variability (Hartmann et al., 2013). Therefore, sea level records have often been used as a proxy for storminess (e.g. Zhang et al., 2000; Araújo and Pugh, 2008; Menéndez and Woodworth, 2010; Haigh et al., 2010), since some hourly sea level records extend back over 100 years. These studies have generally investigated changes in the NTR, or ESLs (which includes all components of sea level).

The most comprehensive of these studies, by Woodworth and Blackman (2004) and Menéndez and Woodworth (2010), found that at most sites there was no significant trend in NTR over the 20th century. At these sites, an increase in ESL was observed at a similar rate to the increase seen in MSL. This was also observed by studies of the Mediterranean (Marcos et al., 2009), the English Channel (Araújo and Pugh, 2008; Haigh et al., 2010), the Caribbean (Torres and Tsimplis, 2013), the U.S. East Coast (Zhang et al., 2000; Thompson et al., 2013), and the South China Sea (Feng and Tsimplis, 2014). This suggests that changes in the meteorological component, and therefore the

meteorological conditions that drive them, were not significant over the 20th century and early part of the 21st century, at most locations.

However, Menéndez and Woodworth (2010) did observe significant (at 95% confidence) secular trends in NTR at some sites. These included increases in the Caribbean and the Gulf of Mexico; and decreases around most of Australia and parts of the east coast of the USA north of Cape Hatteras. Grinsted et al. (2012) also observed decreases in storm surge activity along the north-east US coast, but Talke et al. (2014) found evidence for an increase in annual maximum storm tide (which includes the tidal component) at New York. Significant differences between the trends in ESL and MSL have been observed for several other regions, including: the Mediterranean, at Camargue (Ullmann et al., 2007), Venice (Lionello et al., 2005) and Trieste (Raicich, 2003); the German Bight (Mudersbach et al., 2013); and sites along the western coastline of North America (Bromirski et al., 2003; Cayan et al., 2008; Abeysirigunawardena and Walker, 2008).

Although sea level records have provided an extended dataset to assess whether changes in storminess have occurred, they are still not long enough to remove all the effects of the seasonal and inter-annual variations. As with MSL, storm surge generation varies in response to regional climatology. ENSO has one of the most widespread influences on climate variability, stretching across the Pacific and into the Atlantic. For example, the number of hurricanes in the Atlantic is known to reduce during strong El Niño events (Bell and Chelliah, 2006). However, Menéndez and Woodworth (2010) found a small positive correlation between the Niño 3 index and the magnitude of the NTR at sites between Cape Hatteras and Cape Cod. In the Caribbean, Torres and Tsimplis (2013) found that 2 out of the 5 sites they studied were anti-correlated with ENSO, but Menéndez and Woodworth (2010) found no significant relationship. Woodworth and Menéndez (2015) found that in most regions ESLs largely followed the pattern of MSL response to ENSO. By contrast, the tropical west Pacific and the coast of Australia showed a negative correlation (Feng et al., 2014). Positive correlation was observed between ENSO, the number of storms that make landfall (Feng and Tsimplis, 2014) and the magnitude of the NTR (Menéndez and Woodworth, 2010) in China, although Feng and Tsimplis (2014) found that neither ENSO nor the Pacific Decadal Oscillation (PDO) was an indicator of a change in magnitude of ESL. Elsewhere in the Pacific, increases in ESL at sites in British Columbia were attributed to a strong positive trend in the PDO (Abeysirigunawardena and Walker, 2008).

In the North Atlantic, the North Atlantic Oscillation (NAO) is the most dominant regional climate signal. Marcos et al. (2009) found that the median and higher percentiles of sea level (i.e. inclusive of MSL) were both strongly correlated with NAO. However, the correlation between NAO and the NTR was weaker. Haigh et al. (2010) showed that there was a weak negative correlation to the

winter NAO throughout the English Channel and a stronger significant positive correlation at the boundary with the southern North Sea. This latter finding is supported by Menéndez and Woodworth (2010) who found a positive correlation with the Arctic Oscillation (AO) and NAO, for most sites around the UK (but not the English Channel) and Scandinavia. In the western Atlantic, Talke et al. (2014) and Ezer and Atkinson (2014) both observed anti-correlation between NAO and their different measures of storm surge activity.

2.3 Extreme Sea Levels

Section 2.2 has documented the changes observed in each of the three main components of sea level, on seasonal, inter-annual and secular timescales. However, although the analysis of individual components and timescales is useful to determine important mechanisms, for most practical purposes it is necessary to assess the total combined sea levels.

ESLs are a combination of signals of different timescales in each of the three main components of sea level (Pugh and Woodworth, 2014), and this combination depends on both the magnitude and phase of each signal. Therefore, while high ESLs are often caused by individual large storm surges, their magnitude, and therefore their impact on the coastal zone, can be modulated by variations in the magnitude of the low-frequency signals on seasonal to secular timescales. Consequently, even if the observed frequency or intensity of individual storm surges does not increase as predicted (Seneviratne et al., 2012), then the magnitude of ESLs may still increase because of variations in the low-frequency signal of sea level.

ESLs occur more frequently at any peak in the low-frequency signal. On seasonal timescales increases in ESL frequency are observed during spring tides (Pugh and Woodworth, 2014), in response to steric changes in MSL (e.g. Amiruddhin et al., 2015) or because of the dominance of particular storm seasons (e.g. Zhang et al., 2000). Changes in the magnitude of the seasonal cycle on inter-annual (e.g. Feng et al., 2015) or secular (Wahl et al., 2014) timescales may also change ESLs. On inter-annual scales, increases in the frequency of ESL have been observed during peaks in the nodal cycle of the tide (e.g. Haigh et al., 2011) or because of increases in the MSL or meteorological component in response to variations in regional climate (e.g. Marcos et al., 2015). On secular timescales, the magnitude of ESL at most locations has increased during the 20th century as a direct response to the global rise in MSL (e.g. Menéndez and Woodworth, 2010). However, at many other sites the secular trend in ESL has been found to be different than the trend in MSL. This difference may be related to the inter-annual variability in regional climate (e.g. Abeysirigunawardena and Walker, 2008), increases in the amplitude of tide (e.g. in the German

Bight; Mudersbach et al. 2013), or changes in storm surges characteristics (e.g. in north-east USA; Grinsted et al., 2012).

ESLs may also alter in response to variations in the phase of a signal. The relative phases of seasonal or inter-annual signals in each component are not constant (e.g. Feng et al., 2015), and an increase in ESL would occur if a phase shift increased the constructiveness between different signals. This has been assessed for the Swan River in western Australia (Eliot, 2012), where coastal flooding events are largely restricted to the period from May to July due to the relative phase of seasonal cycles in MSL and the tide. However, on inter-annual timescales peaks in the MSL and meteorological component have not occurred simultaneously since 1960.

The magnitude of sea level is a combination of signals of different timescales and components. Observed changes in the magnitude of some signals are large, but even a small increase in the constructiveness of different signals, caused by a phase shift, may increase the magnitude of an ESL enough to cause a flooding event.

2.4 Methods of Characterising Sea Level Components

This section summarises the different methods available for characterising or assessing sea level components. Characterisation of MSL is limited to the different ways of calculating of MSL, which was discussed in Section 2.1.1. Therefore, this section focuses on the many methods that are used to assess the level of the tidal and meteorological components, and of ESL.

2.4.1 Tide

Much of the variability in the tide, especially in the open ocean, can be represented by a small number of tidal constituents, as represented by Equation 2.2. These constituents reflect the response of ocean to individual variations in astronomical forcing, i.e. the M_2 constituent is the Principal Lunar Constituent.

Examining changes in tidal constituents is useful to understand the processes responsible for the observed changes in tides. However, it is difficult to quantify in terms useful to practitioners (i.e. coastal engineers, port authorities, planners, etc.), exactly how these observed changes in individual tidal constituents combine to alter the observed tide at a specific site. For practical purposes therefore, tidal levels are often used. Generally, these levels are calculated from a particular phase of the tide, either high or low tide, although these can depend on locally adopted definitions (Pugh and Woodworth, 2014).

To use these levels as a reference or to assess secular changes, they are typically averaged over a period of 18.61 years, so that the effects of the lunar nodal cycle are averaged out (Woodworth, 2010). Previous studies that have assessed changes in tidal levels (e.g. Töppe & Führböter, 1994; Woodworth et al., 1991; Flick et al., 2003; Mudersbach et al., 2013; Rasheed & Chua, 2014) have exclusively analysed MTR or DTR, and associated tidal high water (HW) and low water (LW) levels. However, there are many more tidal levels that can be used. These may describe the difference between the mean higher high water (MHHW) and mean low high water (MLHW) of the semi-diurnal tide, or changes between the mean spring (tide) high water (MHWS) or the mean neap (tide) high water (MNHW).

2.4.2 Meteorological Component

Many studies that assess the meteorological component use the NTR, and assume that the non-meteorological factors that can affect the NTR are not significant. However, as documented in Section 2.1.4, there are many regions where significant tide-surge interaction has been observed (e.g. Horsburgh and Wilson, 2007), and therefore tide and surge should not be regarded as independent at all locations.

Recently, several studies have used the parameter 'skew surge', rather than the NTR, to assess the meteorological component of sea level in north-west Europe (Batstone et al., 2013; Dangendorf et al., 2014), and in the USA (Wahl and Chambers, 2015). A skew surge is the difference between the maximum observed sea level and the maximum predicted tidal level regardless of their timing during the tidal cycle. There is one skew surge value per tidal cycle. A skew surge is thus an integrated and unambiguous measure of the storm surge that represents the true meteorological component of sea level (Haigh et al., 2015). For the UK, Batstone et al. (2013) suggested that variations in skew surge heights are independent of the tidal level, and therefore by using them, one does not have to consider the complications of non-linear tide-surge interactions.

Different aspects of either the NTR or skew surge can be assessed and these can lead to different conclusions. These threshold include: annual maximum (e.g. Talke et al. 2014), monthly maximum (e.g. Menéndez and Woodworth, 2010), storm duration, storm count and storm intensity (e.g. Zhang et al., 2000; Haigh et al., 2010) or high percentiles (e.g. Menéndez and Woodworth, 2010).

2.4.3 Extreme Sea Levels

Many of the measures of the NTR or skew surge (listed above) can also be used for ESLs. The aim of any method is to extract a subset of the largest (or smallest) events which can be used to

represent the extremes. Two types of method can be used to estimate ESL: (i) direct, in which the extremes of observed sea level are analysed; and (ii) indirect, where the tide and meteorological components of sea level are modelled separately and ESL is inferred.

There are three main direct methods: the annual maximum method (AMM), peaks over threshold method (POTM) and the r-largest method (RLM). The AMM has been widely used to assess ESL (e.g. Menéndez and Woodworth, 2010; Talke et al., 2014), but there are problems with its application to sea level, and it is highly inefficient in its use of data. The complex combination of deterministic (tide) and stochastic (oceanographic and meteorological) processes, mean that necessary assumptions of independence and identical distribution between the time-series do not always hold true (Tawn and Vassie, 1991). The other two methods exploit more of the data but, like the AMM, they do not distinguish between different components of sea level. Direct methods have been used regularly to assess ESL or NTR (as shown in Section 2.2), since they do not require knowledge of tide–surge interaction, which can be a significant feature of the data, as, discussed in Section 2.1.4.

Direct methods, such as the AMM or the extraction of percentiles, can generate a regular time-series that can also be used for the analysis of trends or inter-annual variability in sea level. Caution should be exercised when using the maximum monthly or annual values, since the maximum is representative of only one value and may be skewed by a single large event. The spatial extent of storm surges (especially those generated by tropical storms) means that the highest sea level generated by the storm may not always occur at the tide gauge. As such the use of high percentiles of sea level has been preferred in many studies of (e.g. Menéndez and Woodworth, 2010). For example, the 99.9^{th} percentile of sea level, which in an hourly time-series relates to the 8^{th} highest value per year, has often been used as a proxy for ESL. While it is still influenced by the largest events the skewing effect of single events is reduced.

Indirect methods started with the development of the joint probabilities method (JPM), by Pugh and Vassie (1978), and importantly analyses the tide and non-tidal components separately. The revised joint probability method (RJPM) developed by Tawn and Vassie (1989) improved the estimation of ESL. Principally the changes were made to improve estimation of ESL at sites: where the storm surge was responsible for a large proportion of the sea level and where less than 10 years of data were available (IOC, 2006). In both the JPM and RJPM, each of the components is analysed separately before a convolution of the two creates the probability distribution (Coles and Tawn, 2005). This convolution can be adapted so that the meteorological component becomes a function of tidal level, and therefore reflects the level of tide-surge interaction (IOC, 2006). Although these indirect methods are not used in this thesis, because we do not conduct

any extreme value analysis, they are a regularly used method in ESL studies, especially those that investigate variability on all temporal scales. The skew surge JPM method has recently been developed by Batstone et al. (2013) and used to assess ESLs around the UK. The use of skew surge removes the need for the assessment of tide-surge interaction in the convolution of the tidal and meteorological components.

2.5 Sea Level Observations

There are two main methods of measuring sea level: sea level recorders and satellite altimetry. The benefits of satellite altimetry include the measurement of large swaths of the ocean with every satellite pass and a near-global coverage. However, the orbit of the satellite means that the sea level at a specific location is only measured every few days. Variations of the tidal and meteorological components of sea level require at least hourly observations and therefore the remainder of this section only discusses measurements using sea level recorders.

2.5.1 Types of Sea Level Recorder

Direct measurements of water level have been made for millennia, with river levels in the Nile linked to temples so that priests could warn of imminent floods (Pugh, 1987). The tide poles used by the ancient Egyptians were still the standard instrument used in the 18th century as regular sea level measurements began to be made and used as a tool for aiding navigation to and from ports. The majority of sea level records are at the coast, and most of these are still at major ports, but a few sea level recorders have been installed in the open ocean, such as the pressure recorders deployed in the Southern Ocean (e.g. Hibbert et al., 2010).

The first self-recording gauge, designed by Palmer, began operating at Sheerness in the Thames Estuary (Palmer, 1831). This gauge used a float in a stilling well connected to a system of wire pulleys and gearing to move a pen over a paper chart. Modern float gauges record the data digitally, but still require a vertical structure so that the recording system can be mounted above the stilling well. A narrow connecting hole damps out the rapid elevation changes caused by wind waves, but allows the sea level in the well to adjust to longer period variations. Various issues can arise due to marine growth, icing in the winter and frictional effects on the float, and as such regular checks are essential. A number of solutions have been developed to counter these problems but data anomalies are caused by these issues. Errors can also result from water density differences between the inside and outside of the well, while the presence of strong currents flowing past the water inlet can lead to drawdown (i.e. the Bernoulli effect) in the well levels

(Pugh and Woodworth, 2014). Despite these limitations float gauges have been the standard method of measuring and recording sea levels over the last 150 years and they have only recently begun to be phased out (Pugh, 1987).

Acoustic reflection gauges are often used as replacements to float gauges and these can be used in existing stilling wells, or as separate installations. These send a pulse of sound from a sensor and record the time (t) taken for the signal to return. The distance is calculated by:

$$depth = \frac{tC_a}{2} \qquad (Eq. 3.1)$$

Where C_a is the speed of sound in air. Corrections must be made for variations of C_a with air temperature, pressure and humidity. These adjustments can be made by recording the travel time of a sound pulse over a known standard distance, but these can still be affected by temperature gradients within the stilling well (Pugh and Woodworth, 2014).

The same principle of timing a reflected signal is used in radar reflection gauges. The radar gauge is positioned several metres above the surface of the sea and does not require extensive fixings to fixed coastal infrastructure. Therefore, they are increasingly popular due to their relatively low cost and ease of installation and maintenance. The vertical system measures the range, either by recording the time taken for the signal to return to the sensor, or the phase shift between two waves from a frequency-modulated continuous-wave system. Unlike acoustic measurements, radar range gauges are not affected by either temperature or temperature gradients. Analysis of these measurements has been limited so far, and there are concerns about wave bias in the sea level measurements, false measurements due to debris passing under the beam and damage to the instrument during large events. However, radar gauges are now the first choice for many sea level agencies (Pugh and Woodworth, 2014).

All the above methods require a vertical system, but at sites where this is not possible, a pressure measuring system can be used. A pneumatic bubbler system has been used extensively in these locations and works by releasing compressed air, at a metered rate, along a thin tube to a pressure point fixed underwater. The pressure point is normally a vertical cylinder with a closed top and open bottom. A small 'bleed hole' is drilled about half way down the cylinder. Air from the tube enters the cylinder, becomes compressed, and pushes down the water inside the chamber. When the water is pushed down to the level of the bleed hole the air bubbles are released through the hole and travel back to the surface. As the surface of the sea varies, the pressure exerted on the pressure point changes. The variation in pressure is transmitted up the tube to a recording instrument. The sea level is calculated according to the law:

$$h = \frac{p - p_a}{\rho g} \qquad Eq. 3.2$$

Where: h is the height of the sea level above the bleed hole; p is the measured pressure; p_a is atmospheric pressure; ρ is the seawater density; and g is the gravitational acceleration (Pugh and Woodworth, 2014). Errors again can be created by inaccurate density values, particularly in estuaries where it will vary significantly over the tidal cycle.

Tide gauge measurements are deemed acceptable if they have an accuracy of less than 1 cm, according to the Inter-governmental Oceanographic Commission (IOC; 2006). Many modern day instruments are accurate to approximately 3 mm, but all instruments used in this study meet the minimum requirements of the IOC. Statistical errors for some aspects of this study, such as the extraction of high and low waters will be small even if the accuracy of each measurement was poor (e.g. to many centimetres) .The large number of measurements obtained during a full year would ensure that statistical errors would only be of millimetric magnitude (Woodworth et al., 1991). In addition, systematic errors only become important to trend studies if values with errors from different sources in different years are employed in the same time series analysis (Woodworth et al., 1991).

2.5.2 Benchmarking

Over long periods, neither the land nor sea levels are constant and therefore, to understand sea levels, it is necessary to decouple the sea level and land signals (IOC, 2006). The location or the type of instrument may vary over time, and therefore to maintain accurate sea-level measurements across these changes, a clearly defined and stable zero level or datum is required (Pugh and Woodworth, 2014). This stability has not always been achieved and therefore discontinuities in the sea level measurements occur.

2.5.3 Quality Control

The quality control of sea level measurements needs to take place at all stages of analysis, since some small errors may resemble natural phenomena. However, errors should be considered with care and only rejected if there is independent evidence of a malfunction (Pugh and Woodworth, 2014). If not, there is a danger of removing real but unexpected events, which is a particular problem when using the data to assess ESLs.

One method of detecting errors in the sea level measurements is to plot the NTR against time. Common errors in sea level recorders have a well-defined pattern in the NTR, as Figure 2.2 shows for a month of synthetic errors. Some key errors include:

- Datum shifts: These appear as jumps in the NTR and unless there is an accurate benchmarking survey to reference the different datums to each other, then the two datasets are incompatible and not suitable for change analysis, as described in Section 2.5.2. These jumps might relate to changes in the location of the gauge (either vertically or horizontally) or a rapid land movement caused by an earthquake.
- Phase shifts: Abrupt but often small shifts in the phase of the tide can be generated by the repositioning of a sea level recorder or a slip of the pen recording the data (in older records). Gradual phase shifts can be caused by drifts in the instrument caused by marine growth in the stilling well or electronic drift in recording equipment. The effects of phase offsets include the smearing of tidal energy, which has been detected in South Pacific tide gauges and shown to give false negative trends in the amplitudes of key constituents (Zaron & Jay, 2014).
- Outliers. Abrupt changes in the NTR that appear as spikes, and may be erroneous records or natural events, such as tsunamis (either geological or meteorological), seiches or storm surges. Therefore, great care should be exercised when removing any data. Independent verification of naturally generated outliers is often possible, especially in more recent data, where there is improved documentation of notable atmospheric or geological events.

Further checks can be made by the comparison of time-series or trends in any of the components between neighbouring sites.

2.6 Summary and Knowledge Gaps

Assessing secular changes in ESL is complex because each of the three main components that combine to generate ESL, vary on seasonal, inter-annual and secular time-scales. Variations on all these timescales and the relative magnitude of each component, control the occurrence of ESLs. A key contradiction exists in the published literature. The secular change in ESLs is similar to the increase in global MSL at most locations, but there are a number of sites where significant changes in the tide and/or the meteorological component have also been observed. Therefore, this study assesses the magnitude and distribution of changes in each of the sea level components, and investigates how they combine to generate ESL.

For the tidal component, most studies have investigated the changes in individual tidal constituents, rather than in tidal levels, which have a direct relevance to a wide range of practical applications. Examining changes in tidal constituents is useful to understand the processes responsible for the observed changes in tides. However, it is difficult to quantify in terms useful to practitioners exactly how changes in individual tidal constituents combine to alter the observed tide at a specific site. Past studies that have assessed changes in tidal levels have been limited to small data dense regions, and exclusively analysed MTR or DTR, and the associated tidal high water (HW) and low water (LW) levels. Many more tidal levels are available and regularly used for a variety of applications. Before now, it has not been clear whether changes in different tidal levels are consistent, or whether changes in tidal levels match those observed in the main tidal constituents. Therefore, the first objective of this thesis is to determine the magnitude and spatial distribution of secular changes in the tidal levels on a global scale, addressing these particular issues.

Although much research has been conducted to determine the temporal variability of storm surge activity on inter-annual and secular time-scales, the majority of past studies have focused on assessing changes in the NTR. Skew surge can better quantify the meteorological component of sea level, by removing the effect of phase offsets and tide-surge interactions. However, until now (to my knowledge) they have only been used to assess changes in the meteorological component around north-west Europe and the USA. Little research has been conducted into tide-surge interaction in many regions, and therefore it would be prudent to identify further regions where this may have an important impact on the magnitude of ESL. Furthermore, few studies have examined the spatial coherence in storm surge variability along stretches of coastlines and between regions. This is despite the that fact that regional climatic variability can account for much of the inter-annual variability in the meteorological component of sea level. Therefore, the second objective is to assess the spatial and temporal variability and secular trends in skew surge globally, again addressing these issues.

Most studies of ESLs have assessed the changes in the total combined sea level, and not the individual components that better reflect the mechanisms that generate the variations. Secular changes in MSL are well documented and the growing understanding that secular changes in the tidal and meteorological components are spatially widespread, and large at some sites, means that all components should also be accounted for in ESL projections. Furthermore, variability in all sea level components, and therefore in ESL, also occurs on seasonal and inter-annual timescales. Studies on these timescales have typically investigated the variability in individual components, but the largest ESLs are generated by the simultaneous occurrence of peaks in different sea level components. Understanding how variability in each component, and on each timescale, could

combine is essential to better comprehend potential changes in the future. Therefore, the third objective is to examine how the magnitude and phase of signals in different components and time scales, combine to generate ESLs, once again addressing these particular issues.

Table 2.1: Summary of Previous Studies into Changes in Tides

Authors	Year	Location	Methods	Key Findings	Limitations
Cartwright	1971	St. Helena	Observations. Changes in constituents	Changes in major constituents are oceanic in nature.	Constituents only
Cartwright	1972	Brest	Observations. Changes in constituents	Changes in major constituents since 1700s, probably oceanic in nature.	Constituents only
Woodworth et al.	1991	UK	Observations. Linear trends in tidal levels (MTR)	Sig. trends in tidal levels at some sites. Positive correlation with trend in MSL.	Only MTR; Data end in 1990.
Amin	1993	Australia	Observations. Linear trends in constituents	Changes in magnitude and phase of major constituents.	Constituents only
Toppe & Fuhrboter	1994	North Sea	Observations. Linear trends in tidal levels (MTR)	Increase in MTR in the German Bight caused primarily by decrease in MLW.	Only MTR.
Flick et al.	2003	U.S.A	Observations. Linear trends in tidal levels (MTR and DTR)	Large increases in tidal levels along all US coastlines.	Only MTR & DTR.
Hollebrandse	2005	North Sea	Observations and modelling of tidal levels (MTR)	Closure of inland seas on Dutch coast have a local affect (upto 200 km) on the magnitude of MTR. Other local affects are related to water extraction and port development.	
Ray	2006	U.S.A	Observations. Linear trends in constituents	Increae in M2 constituent related to resonant period of Bay of Fundy approaching M2 period.	Constituents only
Araujo	2006	West European Coast	Observations. Linear trends in constituents	Secular (and short term) changes in constituents.	Constituents only
Araujo and Pugh	2008	Newlyn	Modelled response of constituents to SLR and channel develop scenarios	Changes in the bathymetry of the inlet channel are the most significant contribution to the tidal changes.	
Jay	2009	U.S.A	Observations. Linear trends in constituents	Changes in both M2 and K1 constituents mean mechanism of increase in magnitude throughout NW Pacific is not frequency based.	Constituents only
Ray	2009	U.S.A	Observations. Linear trends in constituents	Consistent increase in S2 constituent along US East Coast	Constituents only
Woodworth	2010	Global	Observations. Linear trends in constituents	Trends in major constituents at sites around the world	Constituents only
Muller et al.	2011	Global	Observations and modelling. Linear trends in constituents	Widespread changes in the magnitude of major constituents, with no clear correlation to MSL trends.	Constituents only
Torres & Tsimplis	2011	Carribean	Observations. Linear trends in constituents	Sig. trends in S2 consituents	Constituents only
Pickering et al.	2012	North Sea	Modelled response of constituents to SLR scenarios; no-flood	Spatially variable and non-linear changes caused by shift in amphidromic points, typically only large changes with >2m SLR.	Constituents only
Pelling et al.	2012	North Sea	Modelled response of constituents to SLR scenarios	Increase in M2 magnitude in Bay of Fundy in response to SLR.	Constituents only
Pelling et al.	2013	North Sea	Modelled response of constituents to SLR scenarios	Reponse to SLR scenarios has a large impact from the decision to allow flooding or no flooding along the coastline.	Constituents only
Mudersbach et al.	2013	North Sea	Observations. Linear trends in tidal levels (MTR)	Changes in observed HW are different to MSL trends, possibly because of changes in tidal constituents in the S. North Sea. Different trends are evident between 1918-1952 and 1953 to 2008.	
Rasheed & Chua	2014	Japan	Observations. Linear trends in tidal levels (MTR and DTR)	Changes in tidal levels and constituents at many sites around Japan, but with trend direction that contradicts Woodworth (2010)	Only MTR & DTR; No mention of data QC.
Zaron & Jay	2014	Pacific Islands	Observations. Linear trends in constituents	Smearing of data from phase offsets may lead to the false detection of positive trends in individual constituents.	Constituents only

Table 2.2: Summary of Previous Research into Changes in NTR and ESL

Authors	Year	Location	Methods	Key Findings	Limitations
Zhang et al.	2000	U.S. East Coast	10 sites, looking at different measures of the storm: duration, intensity and frequency. They then broke these up into ET and TS.	No significant trends in NTR; Large inter-decadal fluctuations in all measures; EOF analysis shows relative importance of modes relating to ET and TS events to sites along the coast.	
Raicich etal.	2003	Adriatic	Observations from Trieste	ESL increase larger than MSL increase	
Bromirski et al.	2003	San Francisco	Separate NTR using a window of 4096-hr (approx. 170-days) on a demeaned and detrended signal. Splits years into high NTR and low NTR, so can then plot against SLP anomalies across the Pacific.	There is a broad region of highly significant negative anomalies across midlatitudes of the central and eastern North Pacific with high NTR years.	Assumes that the energy in the NTR does not change significantly at tidal frequencies, which may not be the case where strongly tide-surge interactions occur.
Woodworth & Blackman	2004	Global	Calculate percentiles and correlate against regional indices.	Regions of correlation between ESL and regional climate indices	Simple analysis using just percentiles and basic correlation with indices.
Bernier & Thompson	2006	NW Atlantic	Modelling using 40 years of hindcast data compared to observations.	Small reduction caused by changes in atmospheric conditions	
Ullmann et al.	2007	Camargue	Annual maximum used as ESL proxy.	ESL increase larger than MSL increase. Increased frequency of surge generating winds from SE and changes in hydrodynamics along the Camargue coastline.	AM used.
Cayan et al.	2008	California	Calculates a 99.9th percentile of sea level from entire dataset, then counts the number of exceendences for a set of years.	Increase in the exceedence of the 99.99th percentile of sea level of 20 and 30 times respectively at San Fran. And La Jolla. Positive sea level anomalies occurred for months during El Nino events.	
Abeysirigunawardena & Walker	2008	British Columbia	Annual Maximum of ESL	Rate of increase in ESL approx. double that of MS L with the extra due to positive phase of PDO.	AM used.
Marcos et al.	2009	Southern Europe	Analysis of ESL and surge. 10-largest values, but ensuring that the events are seperated by more than 72 hrs	The NAO is correlated with the median as well as with the higher-order percentiles of SL, correlation with NTR is much weaker. Trends in ESL similar to those in MSL. This could be due to shift in storm tracks on changes in strength.	
Menendez & Woodworth	2010	Global	Monthly maximum of ESL & surge. Uses a magnitude (MM) and frequency approach. Comparison with climate indices.	Majority of change in ESL is caused by increase in MSL. Many different contributions to changes in ESL (e.g. nodal/perigean cycles, interannual regional climatology, seasonal cycles and long-term trends).	Indices are a very simplistic method of understanding changes in regional climate.
Haigh et al.	2010	English Channel	Uses high percentiles of surge values and Winter NAO index	Trends in ESL similar to those in MSL. Weak negative correlation to the winter NAO through out the Channel and a stronger significant positive correlation at the boundary with the southern North Sea.	
Sweet & Zervas	2011	U.S. East Coast	Sea level anomalies (>0.05m) and daily storm surges (>0.3m) are extracted for each cool season (October to April).	Increase in extra-tropical storms are correlated to El Nino phase of ENSO.	
Zhang & Church	2012	Pacific	Sea level variability derived from altimeter date seperated into interannual, decadal and long-term trend.	SLR in western tropical Pacific partially due to basin-scale decadal climate variability.	

Grinsted et al.	2012	U.S. East Coast	Surge index created from squared day-to-day difference in local sea level, which minimizes long-term trends in MSL, or from changes in coastal morphology.	Signifcant trend in large surge events roughly equating to storm size since 1923; More cyclones in warm years; Katrina sized events 2x as likely in warm years than cold years.	Difficult to compare to other studies due to unique index. No comparison to usual methods using NTR etc.
Merrifield et al.	2013	Global	Calculates open ocean annual max values using satellite and model data and a scaling of 2.5 times SD, calculated from TG sites.	The time-averaged annual maximum water level correlates significantly with, and scales as 2.5 times, the water level standard deviation.	
Mudersbach et al.	2013	S. North Sea	Trend analysis of percentiles (80,85,90,95,99,99.9th) for observed sea level and median reduced sea level.	Changes in observed HW are different to MSL trends, possible because of changes in tidal cons in the S. North Sea. However, the median reduced SL trends are only signifcant at 66% level. Different trends are evident between 1918-1952 and 1953 to 2008.	Significance of trends in median reduced SL is stated at lower confidence level than many studies (66%; 1 SD).
Sweet & Park	2014	U.S.	Use thresholds relative to MHHW to determine 'nuisance' flood levels. Correlated against ENSO using multiple regression analysis.	Nuisance coastal flooding is increasing along U.S. coastlines. Event rates accelerate as water level distributions exceed elevation thresholds. Tipping points for coastal inundation are surpassed in the coming decades.	
Ezer & Atkinson	2014	U.S. East Coast	Uses number of hours for the sea level is certain level above MHHW.	The increase in minor flooding can be predicted from SLR and tidal range. Frequency of extreme storm surge flooding events is less and affected by the NAO.	Uses a fixed MHHW throughout at all sites, but only mentions changes in tides for Wilmington.
Feng & Tsimplis	2014	China	Assessment of ESL and surge. Indices include PDO and ENSO	Neither of PDO and ENSO is found to be an indicator of changes in the size of extremes. ENSO appears to regulate the number of tropical cyclones that reach the Chinese coasts.	
Haigh et al.	2014	Australia	Extending records out to many thousands of years by building statistical models of tropical cyclone behaviour to generate synthetic event sets artificially.	Systematic understimation of tropical cyclone-induced surge in recorded dataset, due to dearth of data (but temporally and spatially).	
Torres & Tsimplis	2014	Carribean	Assessed ESL and surge at 5 tide gauges.	No evidence of increase in storm activity, but ESL increase caused by MSL. Negative correlation of ESL with ENSO at 2/5 . Stable estimates obtained from 30 yrs where few TC surges, but 40 yrs needed where TC surges are common.	
Talke et al.	2014	New York	Uses Annual Max. Storm Tide (AMST), but the graph (Figure 2) average these over 36 years.	Half of long-term variance is anti-correlated with NAO.	AMST will have issues regarding skewed trends from one storm event, although this is I think reduced by using 36-yr average.

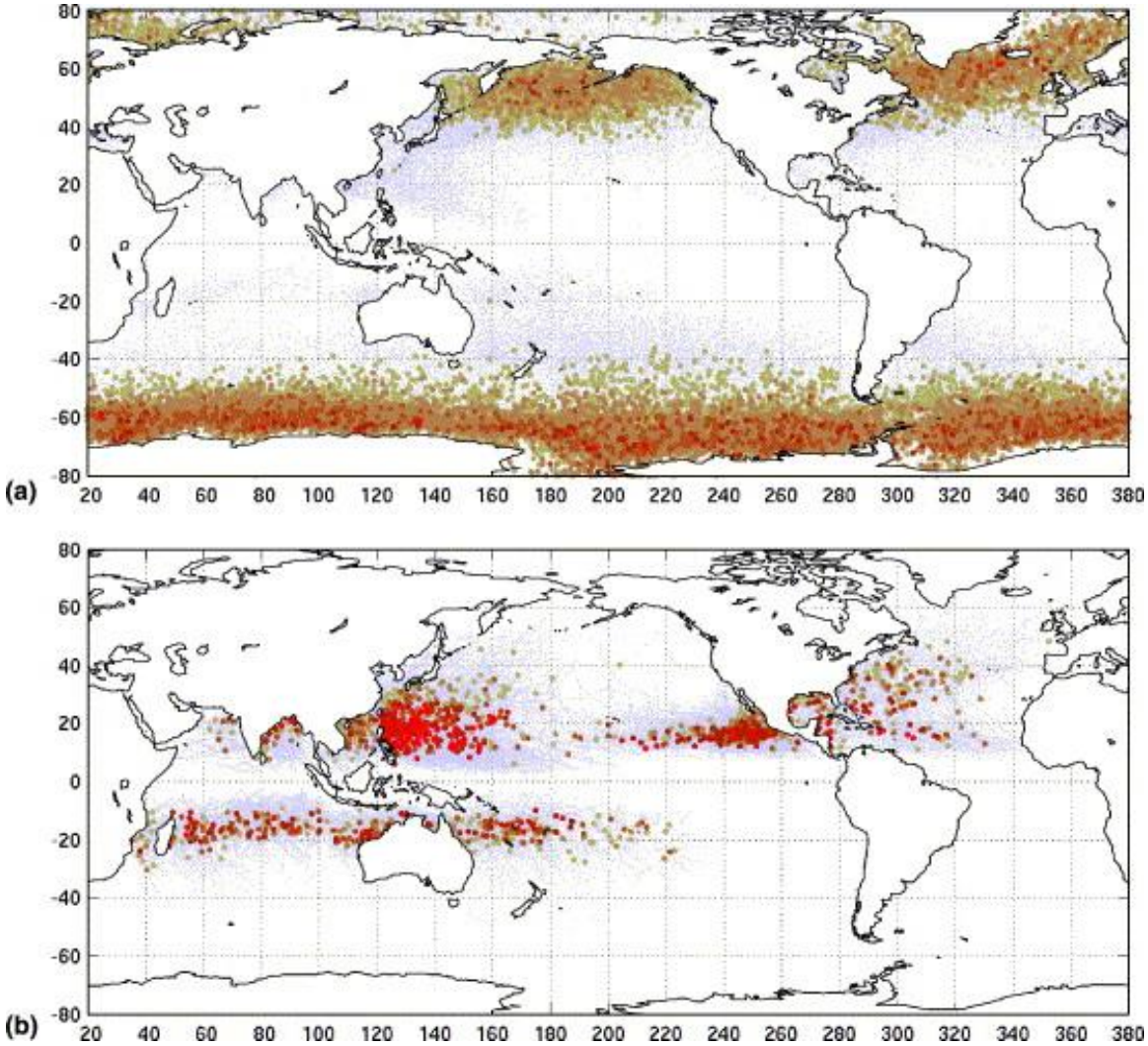

Figure 2.1: The location of storm tracks (light dots) and the points of maximum intensity for each storm system (dark circles), for: (a) extratropical storms (storm tracks from the GISS/NASA extratropical storm atlas); and (b) tropical storms (hurricane track data from NHC/NOAA and JTWC/US Navy). (Source: Alves, 2006).

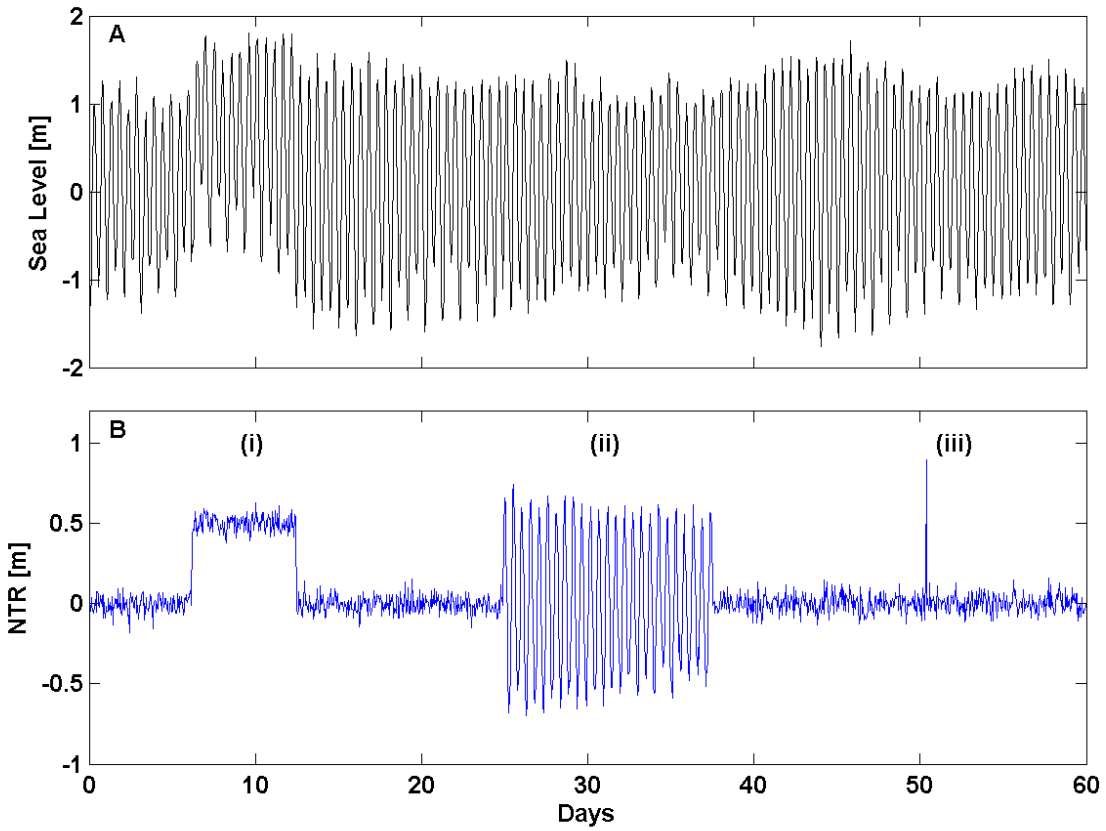

Figure 2.2: Example time series showing (A) total sea level, and (B) the NTR. Common errors in tide gauge measurements are observed in the NTR as a result of: (i) a 0.5 m datum offset, (ii) phase offset of 1 hour, and (iii) an isolated error of 0.9 m. Detection of errors (ii) and (iii) is difficult in the sea level time-series.

Chapter 3: Data

Three main data sources were used in this study, namely: (i) tide gauge data; (ii) predictions from a global tidal model; and (iii) climate indices. These are each described in the following sections.

3.1 GESLA Dataset

The GESLA dataset is the source of all sea level observations used in this thesis. This dataset of high frequency sea level records (< 1 hour) was originally collated by staff from the Permanent Service for Mean Sea Level (PSMSL) at the National Oceanography Centre, Liverpool in the UK and the Antarctic Climate & Ecosystems Cooperative Research Centre in Australia. The GESLA dataset has primarily been used to assess changes in ESLs (e.g. Woodworth & Blackman, 2004; Menéndez & Woodworth, 2011; Hunter, 2012; Hunter et al., 2013) but, it has also been used to assess changes in the main tidal constituents (Woodworth, 2010). It is probably the best source of information available for such global wide studies (Woodworth, 2010).

The original GESLA dataset comprised records from 452 unique locations with the data ending in 2008 at the latest. I extended all data sets, where possible, through to the end of 2013, and added three new datasets, at Knysna and Mossel Bay in South Africa, and Luderitz in Namibia. Records were extended using research quality data downloaded from the following web sites: University of Hawaii Sea Level Center (UHSLC) for global sites; British Oceanographic Data Centre (BODC) for the UK; National Oceanic and Atmospheric Administration (NOAA) for the USA; Marine Environmental Data Service (MEDS) for Canada; Bureau of Meteorology (BOM) for Australia; and Norwegian Mapping Authority (NMA) for Norway. All data used in this study was hourly.

3.1.1 Quality Control Procedures

Since the QC procedures of the different institutes varied, further data checks consisting of identifying and removing errors, as classified in Section 3.1.3, at all sites. The extra QC procedures are detailed for each site in Appendix A, and include the following specific visual checks:

1. Visual check for large values in the NTR time series.

a. If the NTR values followed a regularly sinusoidal pattern, which was not a consistent feature throughout the time series, then the values were classed as a phase offset, and flagged as invalid.
b. If the NTR values were a spike of an individual value, then they were classed as spikes and flagged as invalid.
c. If the NTR values showed a consistent shift away from zero, then the period of change was compared with documentation, and removed if it was thought to be a datum shift.

2. Visual checks of the magnitude and phase of tidal constituents. Where jumps in either were observed, then the harmonic analysis was checked to see if all necessary tidal constituents could be resolved on a year of data.

The extra quality control removed obvious timing errors and reduced the 'smearing' of tidal energy across a wider range of frequencies. This 'smearing' can reduce the energy attributed to tidal constituents during harmonic analysis (Zaron & Jay, 2014).

A considerable amount of knowledge regarding the processes affecting sea levels on temporal scales of hours to weeks is required since many signals that are not meteorological forced, such as tsunamis, can appear similar to those that are meteorological forced, such as meteotsunamis. Tsunami signals that had a clear earthquake source, as documented by the United States Geological Survey (USGS), were removed. The occurrence of these non-meteorological related events are unpredictable and can skew results, particularly when assessing the meteorological component of sea level. Small tsunami signals are difficult to separate from the NTR, and therefore some events remain in the data. The tsunamis removed in this dataset are catalogued and linked to recorded earthquakes by the USGS, in Appendix B.

3.1.2 Data Requirement

The data requirements for ESL analysis are strict. Events ranging from hours (e.g. tropical storm surges, tidal high water), to decades (e.g. the lunar nodal cycle) must be captured and accurately resolved. The following requirements were imposed on the GESLA sites after QC:

- Data must be of research quality. Data downloaded from UHSLC or BODC websites have been through QC procedures. Further checks, as detailed in Section 3.1.1, were conducted to remove some remaining erroneous data caused by timing errors and outliers.
- Data must be hourly to capture variability in the tidal and meteorological components, and to ensure consistency between sites. Data sampled at higher frequencies than 1 hour are resampled on to give hourly records at all sites.

- Each year of data must contain at least 75% of potential hourly values. Seasonal cycles influence all three components and a high percentage of data is required for these cycles to be accurately resolved each year.
- The dataset must span at least 28 years and contain 15 years (Woodworth et al., 1991) that conform to the above requirements in that period. This allows representation of decadal variations in tide, such as the lunar nodal cycle.
- Data must extend past the year 2000, so that as far as possible the data from all sites is directly temporally comparable.

After these criteria were applied, 220 sites in the GESLA dataset were deemed eligible for analysis (Figure 3.1) and these have been used throughout this thesis. Details of each of the 220 sites are documented in Appendix C. For some sections of this thesis, these requirements are overly conservative. For example, the seasonal cycle can be calculated from a 5 year window (e.g. Marcos and Tsimplis, 2007). However, the limitations are imposed so that the same sites can be used in all analysis sections.

The GESLA dataset has a geographical bias, since the distribution of sea level records, especially those that meet the criteria, are primarily located in North America, Europe, Australia and Japan, as shown in Figure 3.1. The nature of tide gauges also creates a geographical bias towards coastal sites and away from the open ocean. However, many different coastal morphology types are represented in the data from estuarine (e.g. Wilmington, USA) to Pacific Islands (e.g. Pago Pago, American Samoa). Equally, the temporal distribution of the data is inconsistent across regions for similar reasons – the difficulty in maintaining a tide gauge for many years. Longer datasets that provide more detailed information regarding the consistency of trends across the 20th century are again concentrated around North America, Europe and Australia. Of the 14 sites over 100 years long, all but one are in North America. Research conducted by Woodworth (2010) has shown the trends observed at sites over the last 30 years are generally the same as those observed over longer timescales, but there are exceptions to this rule.

3.1.3 Extraction of sea level components

The sea level records were separated into their three main component parts: MSL, tide and NTR. Typically, researchers have calculated annual MSL values and removed this from sea level records, but a 30-day running mean is used in this thesis. Both methods extract the signals caused by global average sea level change and land movement related to glacial isostatic adjustment (GIA) or localised land subsidence. However, the running mean also extracts the variability on timescales less than a year. The majority of intra-annual variability has oceanographic (e.g. steric

properties or ocean currents) or meteorological (e.g. Monsoon winds or pressure changes), not gravitational, origins. A disadvantage to the 30-day running mean is that it will include some energy from other components. Tidal constituents such as the annual (Sa) and semi-annual (Ssa) are included in the running mean, and some high-frequency energy will be removed from the non-tidal residual through aliasing. These effects are however, expected to be negligible.

The remaining record, without MSL, was divided into calendar years, with each year then run through the harmonic analysis software T_Tide (Pawlowicz et al., 2002), to separate the tide and NTR. The Rayleigh criterion states that 67 constituents can be extracted from 1 year of sea level data (Foreman, 1977). However, noise in the sea level data and the small magnitude of some tidal constituents means that not all 67 constituents are deemed significant from the harmonic analysis. Only the amplitude and phase of constituents with a signal to noise ratio greater than 2 were used to generate the tidal signals for each year. Analysing the records in this way meant that the nodal cycle was not removed at this stage but it is accounted for later in the analysis. The NTR was calculated by subtracting the predicted tide and the 30-day running average MSL from the measured sea level time-series. Note, other methods exist for extracting the NTR, such as that used by Bromirski et al. (2003).

3.2 Tidal Model

Outputs from the OTISmpi tidal model from Pickering (2014) were compared to the GESLA dataset. OTISmpi solves the non-linear shallow water equations using a finite differences time stepping method. Details of the model and its validation can be found in Egbert et al. (2004) and references therein. The results are from the newer fully global North Pole in Greenland version of $1/8^{th}$ degree OTISmpi (Egbert et al., 2004), where the lack of an open boundary condition or data assimilation allows the model to evolve to a future tidal equilibrium (due to the SLR perturbation). Specific choices regarding the model setup are detailed in Pickering (2014).

3.3 Regional Climatology

Previous research (e.g. Menendez and Woodworth, 2010; Marcos et al., 2015) has indicated that the NTR in some regions is correlated with regional climate indices. In this thesis, the spatial variability in the meteorological component is compared with these climatic indices. Climate indices generally use one parameter to characterise changes in regional climate and are widely

used because of the ease of application. Typical parameters are SST and SLP, and changes in either can indicate macro-scale changes in regional climate. I used 8 climate indices, namely: the Atlantic Multi-decadal Oscillation (AMO); AO; NAO; Niño 3; Niño 4; North Pacific (NP); PDO; Southern Oscillation Index (SOI). The NAO index was downloaded from the Climate Research Unit of the University of East Anglia (http://www.cru.uea.ac.uk/cru). The other indices were obtained from the NOAA (http://www.cpc.ncep.noaa.gov).

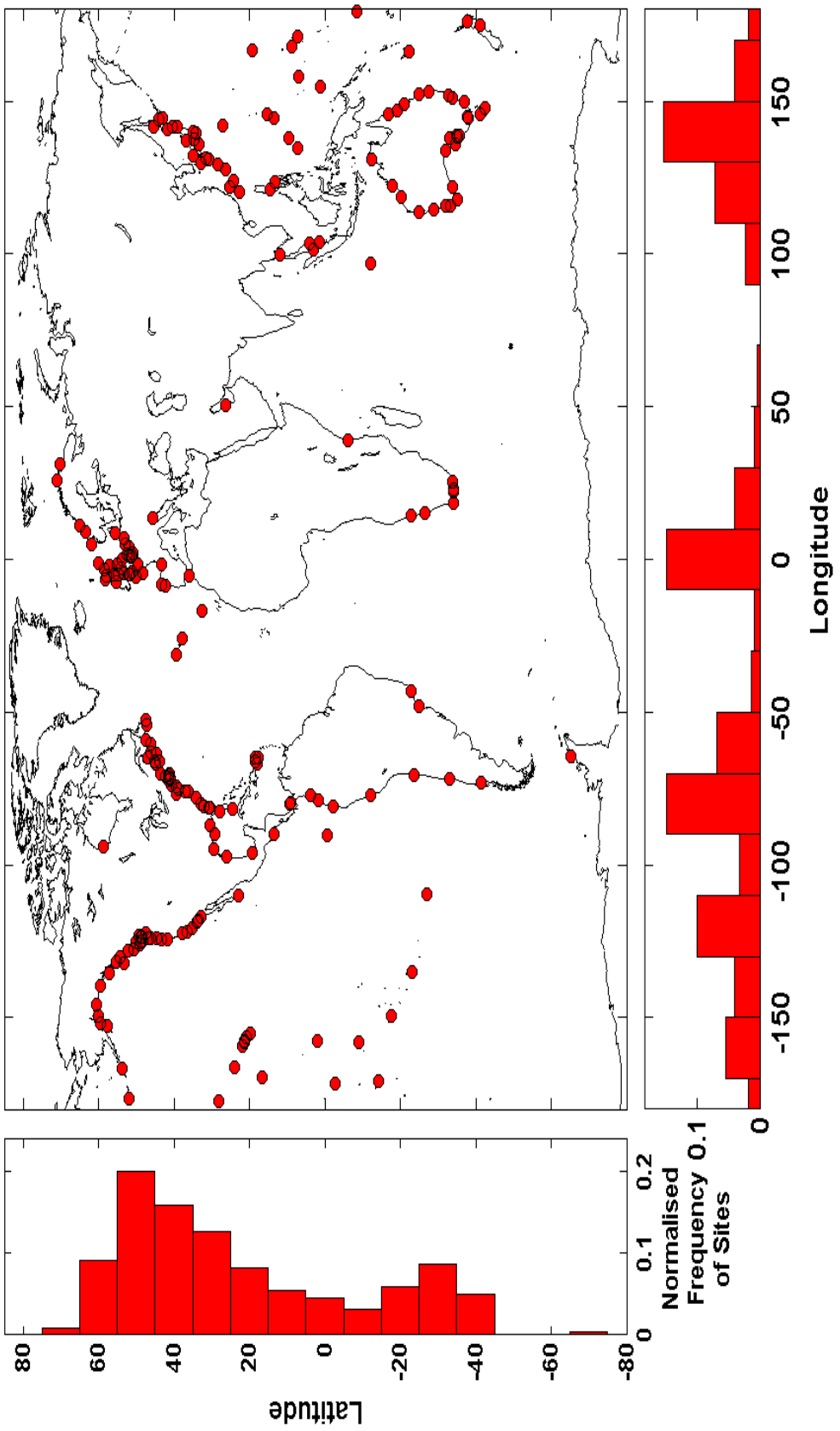

Figure 3.1: Location map of the 220 selected sites used in the analysis. Normalised frequency histograms are plotted along the x-axis for longitude and y-axis for latitude..

Chapter 4: Secular changes in tidal levels

The remainder of this thesis concentrates on the three objectives outlined in Chapter 1. The first of these was to determine the magnitude and spatial distribution of secular changes in tidal levels. The majority of this chapter is adapted from the following publication:

> *Mawdsley, R. J., Haigh, I. D. and Wells, N. C. (2015), Global secular changes in different tidal high water, low water and range levels. Earth's Future, 3: 66–81. doi:10.1002/2014EF000282*

4.1 Introduction

Tides are a major control on the coastal zone. For example, coastal communities are vulnerable to extreme high sea levels and coastal flooding (Nicholls et al., 2007), in which tides play an important role along the majority of the world's coastlines (Haigh et al., 2011; Pugh and Woodworth, 2014). Navigation to and from ports is constrained by the height and timing of high and low water (Gill & Schultz, 2001). Tidal range influences the spatial extent of species in coastal ecosystems (Stumpf & Haines, 1998), while tidal currents control sediment transport (Allen et al., 1980) and the tidal energy potential (Mackay, 2009). Furthermore, tidal levels relative to chart datum are used as the legal basis for many national and international boundaries (Pugh & Woodworth, 2014). Therefore, any changes to tides have wide ranging and important practical and scientific implications.

Studies that have assessed changes in tides have been summarised in Section 2.2.2, but as outlined in Section 2.6 there are several key knowledge gaps. The aim of this chapter is to address several of these gaps by determining the magnitude and spatial distribution of secular changes in tidal levels on a global scale.

There are two specific objectives. The first objective is to compare the magnitude of trends in a range of different tidal levels and assess the spatial distribution of changes. The second objective is to establish if MSL is the main mechanism forcing observed changes in the tide, by comparing the observed changes with predicted changes from the OTISmpi tidal model (Pickering, 2014).

4.2 Methodology

Data from both tide gauge records and the OTISmpi model were used and the methodology for extracting the various tidal levels is described below.

4.2.1 Tide Gauge Analysis

The extraction of the tidal component from the sea level records was described in Chapter 3, but further analysis was required to analyse changes in various tidal levels. Previous studies have found changes in some tidal levels, specifically MTR and DTR, but many others exist. This study investigates the changes in 15 different tidal levels (5 HW levels, 5 LW levels and 5 tidal ranges), which are detailed in Table 4.1.

Tidal levels are all reported relative to MSL and were calculated from different subsets of the extracted daily or twice daily predicted tidal HWs and LWs. Every tidal HW and LW was extracted by locating the turning points of the tide time-series. Time-series of MTR were calculated by subtracting the annual mean of all LWs from the annual mean of all HWs. Time series of greater DTR (GDTR) were computed by subtracting the annual mean of each daily lower LW, from the annual mean of each daily higher HW; while time series of the lesser DTR (LDTR) were calculated using the lower HW and the higher LW for each day. Periods of larger or smaller tides were defined to determine whether changes are occurring in the spring-neap (which dominates in semi-diurnal regions) or equivalent tropic-equatorial cycle[1] (which dominates in diurnal regions). These both have an approximate 14-day period relating to the phase and declination of the Moon, respectively (Zetler & Flick, 1985). As illustrated in Figure 4.1, these periods were defined using the highest HW of successive 14-day periods. The time between each pair of consecutive highest HW was split into quarters, with the spring-tropic period defined as the quarter before (Q4) and the quarter after (Q1) a highest HW; and the neap-equatorial period was defined as quarter 2 (Q2) and quarter 3(Q3). This definition ensured that the two periods contained mutually exclusive HWs and LWs. Spring-tropic tidal range (STTR) was calculated from the mean of all HWs minus the mean of all LWs in the spring-tropic period, with the same true for neap-equatorial tidal range (NETR) and the neap-equatorial period.

Typically tidal levels are calculated over an 18.6-year periods to capture all combination of tides over a lunar nodal cycle (NOAA, 2010). However, this assumes stationarity in the tidal levels,

[1] The term tropic-equatorial cycle is not used much in science but both the International Hydrographic Office (IHO) and National Oceanographic and Atmospheric Association (NOAA) use it to refer to the 14-day cycle in the diurnal tide (Pugh, personal communication) and as such I use it here. It also enforces the fact that the mechanisms that drive changes in semi-diurnal and diurnal tides are different.

which this study tests by calculating an annual value for each tidal level to allow a linear regression model with a nodal term to be fitted. . Equation 4.1 gives the example for MTR.

$$MTR(t) = a + bt + c\cos(\omega t - d); \qquad \text{Eq. 4.1}$$

Where: t is time in years; b is the linear trend in MTR, $\omega = 2\pi/18.61$ radians per year; and a, c and d are constants. The nodal term $c * \cos(\omega t - d)$ is included to ensure that trends are not biased by the lunar nodal cycle (Woodworth, 2011). Figures 4.2a, b and c show the fits of the above regression model to tidal levels calculated for Brest in France, with the nodal variation included. Time-series with the nodal cycle removed are shown in Figures 4.2d, e and f. Throughout the chapter confidence intervals are quoted at the 95% confidence level (i.e. approximately two standard errors) and were estimated using a Lag-1 autocorrelation function to allow for any serial autocorrelation in the residuals (Box et al., 1994). From here on when I use the term significant trends, this means the trends are statistically (at 95% confidence) different from zero.

To assess whether the difference between the number of sites with positive or negative was statistically significant, a chi-squared (χ^2) test was used. The χ^2 test calculates the probability that the observed dataset is different to an expected dataset. In this case, if the two are different then it demonstrates that the difference between the number of positive and negative trends is significant.

4.2.2 Comparison with Tidal Model

The observational dataset provides good coverage of many coastlines, but it does under-represent certain regions as discussed in Section 3.1.2. Therefore, to compliment the observations and aid discussion on the spatial patterns of change and the potential mechanisms behind them I used outputs from a global tidal model.

This study used the Oregon State University (OSU) OTISmpi model, the details of which are described in Section 3.2. For the analysis, MHW calculated from the observations and the model were compared. In the model, MHW was based on 4 major constituents (M_2, S_2, K_1 and O_1) since the addition of further constituents did not improve results enough to justify the increase computational expense (Pickering, 2014). Pickering (2014) conducted extensive analysis to find a spatially consistent description of MHW, which proved difficult because of movement between regions of diurnal or semi-diurnal tides. To rectify the issue he identified an optimal percentile, the 88.8th, of the ranked SSH time series to represent MHW globally. For comparison, the MHW

from observational results has been calculated in the same way. This differs from traditional definition of MHW and therefore in this thesis it will be referred to as MHW88.

Two runs were initially analysed: a uniform 0.5 m SLR (SLR_p5); and a global average 0.5 m SLR, with GIA adjustments (SLR_p5_GIA). Both used fixed present day coastlines and the calculated change relates to the difference in magnitude of the MHW88 in the control and the SLR scenario run. Both 0.5 m SLR scenarios were run by Mark Pickering during his PhD, but results from them were not published anywhere or included in his PhD thesis. The outputs from the model are therefore entirely the work of Mark Pickering, but the comparisons presented here between the model runs and the observed tidal levels are novel results of this study. Both showed similar results and therefore the more realistic SLR scenario was used. This was considered to be SLR_p5_GIA.

For analysis, three different groups of model grid-points were assessed: all grid-points, coastal grid-points, and grid-points nearest each of the 220 selected sites. The first and third subsets are self-explanatory, but the coastal grid-points were determined by creating a 3x3 grid around a point. If one of the points in that grid was classed as land, the central point was classed as coastal. If no points classed as land were present then the data was from the open ocean and was not selected.

Any direct comparison of the model and tide gauge observations is complicated since their outputs are in different formats, and their magnitudes are not directly comparable. The model output is an absolute difference in MHW88 between the two runs, while the change in the tide gauge observations is a trend in mm/yr. We can roughly compare the two outputs if assumptions are made regarding the rate of MSL rise. Therefore, the 50 cm increase in global MSL applied in the model would take 166 years at the current rate of increase (~3 mm/yr), and therefore a 10 mm increase in MHW88 over this time period equates to a rate of ~0.06 mm/yr. Changes on this scale in the tide gauges would not be detectable over the natural variability in the tide gauge observations.

4.3 Results

4.3.1 Secular Trends in Sea level Observations

Results from the analysis show that significant (95% confidence) secular changes have occurred in all tidal levels, and at sites on every continent and around every ocean basin, over the time-span

of the observations. Global maps showing where trends in MHHW, MLLW and GDTR are significantly positive (red dots), significantly negative (blue dots), or not significant (black dots), are shown in Figures 4.3a, b and c respectively. Similar plots showing trends in the other tidal levels are included in Appendix D. From Figure 4.3 it is clear that although changes are observed around the world, there is no discernible global pattern. However, several regions do exhibit spatial coherence, as is evident in the magnitude of the trends in GDTR for North America, Europe and Australasia (see zoomed in plots of these data-dense regions in Figure 4.4).

On the north-west American coast, nearly all sites have significant positive trends in GDTR and MHHW and significant negative trends in MLLW. This is also observed in the German Bight (Figure 4.4b), Australia and south-east Asia (Figure 4.4c) and South Africa; although these last two regions have lower data coverage and therefore may not capture all the changes occurring in the tide. Regions exhibiting spatially coherent decreases in GDTR and MHHW, and increases in MLLW are typically smaller and the coherence within these areas is weaker. They include areas on the north-east American coast (Figure 4.4a), which alternate with small regions where trends have the opposite sign, and Japan (Figure 4.4c). Even within regions of mostly coherent signals, there are local variations. For example, negative trends in MHHW at Tofino, Canada and Willapa Bay, USA, contrast with the positive trends observed at other sites along the north-west American coast. In other regions, the sign of the trend is the same as neighbouring sites but the magnitude is very different. Wilmington, North Carolina in the USA, has a trend in GDTR of 5.2 mm/yr (Figure 4.5i), while surrounding sites have trends of less than 1 mm/yr.

The largest positive trend observed in any tidal level was the 6.1 ± 1.2 mm/yr increase in STTR at Calais, France (Figure 4.5d). The largest negative trend was 3.5 ± 1.6 mm/yr in STTR at Churchill in Canada (Figure 4.5e). The magnitude of trends in HW levels varied from 3.1 ± 0.5 mm/yr in MHWST at Calais (Figure 4.5d), to -2.0 ± 0.9 mm/yr in MHWST at Churchill (Figure 4.5e), while the magnitude of trends in LW levels lay between 1.6 ± 0.8 mm/yr in MLWST at Delfzijl in the Netherlands (Figure 4.5f) and -3.5 ± 1.0 mm/yr in MLWST at Wilmington, in USA (Figure 4.5i). Large trends of over 5 mm/yr were observed in different tidal regimes, ranging from mixed-diurnal micro-tidal, such as Manila in the Philippines (Figure 4.5g), to semi-diurnal macro-tidal, such as Calais (Figure 4.5d).

Determining realistic percentage change is difficult, since the magnitude of some tidal levels, such as MLHW, can have values close to zero. Therefore, in these cases, small changes in magnitude equate to large changes in percentage terms. However, the maximum trends by magnitude reported above, equate to changes of 1.0 % per year in both STTR and MHWST at Calais (Figure 4.5d), 2.1 % per year in GDTR at Manila (Figure 4.5g) and 4.4 % per year in STR at

Wilmington. Global maps of the percentage change in MHHW, MLLW and GDTR are presented in Figures 4.6a, b and c and show the regionally coherent patterns described above as, well as the sites with localised trends. Similar maps for all other tidal levels listed in Table 4.1 are included in Appendix D, and show comparable patterns of spatial coherence, although with slightly different numbers of positive and negative significant trends.

The percentage of sites with significant trends varies depending on the selected tidal level, from 34% for MHWNE to 63% for MLLW, as shown in Figure 4.7. The stacked bar chart shows the frequency and percentage of sites where trends of each tidal level are significant positive (red), significant negative (blue) and non-significant (black). This figure also shows that for tidal range and HW levels there are more positive trends than negative trends, while for LW levels the opposite is true. For all tidal levels a χ^2 test was used to determine whether the difference between the number of positive and negative trends was statistically significant (note I only did this for the positive and negative trends that were themselves significant at the 95% confidence level). The rejected null hypothesis was that there would be an equal number of significant positive and negative trends for each tidal level. This null hypothesis assumed that the distribution of sites was not geographically biased towards regions with or without coherent spatial signals. For all tidal range and HW levels, there were significantly more positive than negative trends; while for all LW levels there were significantly more negative trends.

Although the largest changes occurred in the spring-tropic tidal levels, changes occurred in all tidal levels. At many sites, there are significant differences in the trends observed between each of the five different tidal levels used for tidal range, HW and LW. Differences between trends in tidal levels are presented for selected sites in Figure 4.8, and for all sites in Appendix D. Each plot shows the magnitude of trends in the five tidal ranges, listed on the x-axis, as large green dots, with the limits of the 95% confidence level shown as small green dots. The contribution to the tidal range trend of the associated HW level is represented by the red bar, while the trend in the associated LW level is shown by the blue bar (see Table 4.1 for associated tidal levels). A positive trend in HW level and a negative trend in the LW level, both have a positive contribution on the trend in tidal range, and vice versa for a decrease in HW levels and increase in LW level. For example, at Brest in France the negative trend in MHHW of -0.11 mm/yr (Figure 4.2d) and the positive trend in MLLW of 0.10 mm/yr (Figure 4.2e) both give a negative contribution towards the magnitude of the trend in GDTR of -0.21 mm/yr (Figure 4.2f).

At 38 of the 220 sites, significant (95% confidence) differences exist between at least one pair of tidal ranges. At six sites, the trends in tidal ranges have different signs. These sites are: Vernadsky in Antarctica (Figure 4.8g) and Kaohsiung in Taiwan, where trends in GDTR and LDTR have

opposite signs; Bunbury in Australia (Figure 4.8i), where it is GDTR and MTR; Stornoway (Figure 4.8c) in the UK, where STTR and NETR have opposite signs; and Port Pirie in Australia where the difference in trend signs occurs between MTR and NETR. Most significant differences occur between the STTR and NETR, such as at San Francisco (Figure 4.8f) in the USA, Wyndham (Figure 4.8j) in Australia, Lowestoft in the UK, Pohnpei in Micronesia and Port Elizabeth (Figure 4.8h) in South Africa, among others. Significant differences also occur between GDTR and LDTR. Along with those listed above, these occur at Hamada and Toyama in Japan, Keelung in Malaysia and Seward (Figure 4.8a) in Alaska, USA. Differences between HW levels and LW tidal also occur. However, the sites where differences are observed are not all the same, meaning that in total 56 sites have significant differences in trends of the same set of tidal levels (i.e. tidal range, HW or LW). Sites with differences between at least two HW levels include Aburatsu in Japan, Flores in the Azores and Walvis Bay in Namibia. Sites with differences between at least two LW levels include Campbell River in Canada, St. Petersburg in the USA and Williamstown in Australia.

In summary, changes in tidal levels are globally distributed and the magnitude of trends is large at some locations. Magnitudes in STTR reaches 6.1 mm/yr at Calais, which is greater than the MSL rise observed at this site. Although the largest changes in magnitude are in the spring-tropic tidal levels (i.e. STTR, MHWST and MLWST), there were large changes in all tidal levels analysed. Results also show importantly, that at 38 sites significant differences in trends between at least one pair of tidal ranges (i.e. between STTR and NETR) exist, and a further 18 sites have differences between a pair of either HW or LW levels. Despite differences between trends in tidal levels, the spatial patterns are similar between all tidal levels, although with the direction of the trend reversed for LW levels. Regionally coherent increases in HW levels and decreases in LW levels are observed on the western North American coast, around Australia and in the German Bight, while decreases in HW levels and increases in LW levels are observed for small areas on the eastern North American coast and around the Japanese coast. Although no clear global pattern is visible, there are significantly more positive than negative trends in tidal range and HW levels, and vice versa for LW levels.

4.3.2 Assessment of MSL as the Causal Mechanism

The greater number of positive than negative trends in tidal range and HW levels, and vice versa for LW levels, suggests that a global mechanism has an influence on changes in the tide. An initial assessment of the effect of the MSL rise on changes in tidal levels is presented in Figure 4.9, where scatter plots show the trends in MSL and MTR for each site. For global sites, or a subset of UK sites only no significant correlation is observed, and this pattern is repeated for all tidal levels.

The tide gauge dataset is geographically biased, as described in Section 3.1.2, and this may have generated this difference between the number of trends with a particular sign. Therefore, the trends in tidal levels calculated from sea level observations were compared with predictions from a global tidal model.

The magnitude of the changes in MHW88 between the model run with 0.5 m of SLR and the control run are shown in Figure 4.10. Grid points where the difference exceeds 2 mm (Figure 4.10a) or 10 mm (Figure 4.10b) are coloured red for increases and blue for decreases. All changes in MHW88 are concentrated around the coast but there are regions in the south Atlantic and the South China Sea, where increases over 2 mm occur in the open ocean. However, all changes in MHW88 greater than 10 mm are confined to coastal regions, as shown in Figure 4.10b.

The number of positive and negative changes (greater than 10 mm) in the model are calculated for two subsets: coastal grid-points and grid-point nearest to the observations, as shown in Figure 4.11. For the coastal subset 10.1% of the grid-points were positive but only 7.5% were negative. For the grid-point nearest to the observations subset, 9.5% were positive and only 7.3% were negative. Despite the similar ratios of positive to negative, only the coastal subset gives a significant χ^2 test statistic (at the 95% level) for the difference between the number of positive and negative changes. This is because of the greater number of grid-points in the coastal subset. However, the number of positive to negative changes (greater than 10 mm) in the grid-point nearest to the observation subset is significant at the 90% level.

The comparison between the trends in observations and the change in the model shows a weak positive correlation (0.28). However, this correlation does not show clearly in the two regional maps shown in Figure 4.12, which present the model results overlaid with the sign of the trend in MHW88 calculated from the observations, separated into significant positive trends (red), significant negative trends (blue) and non-significant trends (grey). There are areas where the sign of the changes in the model and the trend of the observations are the same, such as the Gulf of Mexico (Figure 4.12a), but in most instances the comparison is poor. Visual comparison is difficult on a global scale, but a global map is presented in Figure 4.13 for interest.

4.4 Discussion

To my knowledge, this is the most comprehensive assessment of changes in tidal levels to date. Using sea level data from 220 sites round the world, significant changes have been found in the time-series of 15 commonly used tidal levels at sites around the world. While this chapter

analyses changes in tides at some new sites, the spatial patterns observed are broadly consistent with changes observed in previous studies using either tidal levels or major tidal constituents.

The largest spatially coherent trend observed was along the western North American coast, which is consistent with the increased amplitude of the M_2 and K_1 constituents found by Jay (2009) at sites north of 18 °N. Along the east coast of North America, the decrease of up to 10 % in the amplitude of the S_2 constituent observed by Ray (2009), is also observed in this study (see Appendix Figure D5.1) but this pattern is not replicated in the tidal level changes in this study. Instead, there is an alternating pattern of smaller regions of increases and decreases (Figure 4.4a). This pattern is also observed in the response of tidal constituents and MTR to scenarios of sea level rise in a global ocean modelling study undertaken by Pickering (2014). Results in this region correspond most closely to his 2 m sea level rise scenario (generated from 1 m of meltwater from each of Greenland and western Antarctica). However, in this scenario, patterns in other regions compare poorly with the findings of this paper. Extra runs of the model, where a 0.5 m SLR has been applied to the global tidal model have been used in this study, and show a weak positive correlation. However, the 1/8th degree model doesn't resolve the tide along complex coastlines (Green, personal communication) and therefore it is not evident whether the difference results from the resolution and complexity of the model or if mechanisms other than SLR are the primary driver for changes in tidal levels.

Around Australia, the coherent positive trends observed in tidal range and HW levels are consistent with the increased amplitude of the M_2 and S_2 constituents at most sites, as shown by Woodworth (2010). The generally positive trends in tidal range and HW levels continues through the sparse dataset in south-east Asia, but there is a consistent decrease in tidal range and HW levels around Japan. Woodworth (2011) found similar patterns in the magnitude of M_2 and K_1 constituents around Japan, but Rasheed and Chua (2014) found increases in MTR, DTR, MHW and MHHW over the same region. On smaller spatial scales, a coherent increase was observed in both MTR (De Ronde, 1983; Töppe & Führboter, 1994) and the amplitude of major constituents in the German Bight (Woodworth, 2010). These results are consistent with these findings and those that show that consistent spatial trends do not extend, across the North Sea, to the UK (Woodworth et al., 1991; Haigh et al., 2010).

Although no spatial coherence has been observed around the UK, trends in MTR have previously been shown to have a positive correlation with trends in MSL (Woodworth et al., 1991). In other studies, changes in MSL have been suggested as a cause of secular changes in the tide, because the propagation of the tidal wave is controlled by water depth. Many studies using hydrodynamic models have investigated the response of the tide to changes in MSL. Several of these studies

focused on the north-west European shelf, and the North Sea in particular, where spatially variable and non-linear responses were observed (Flather et al., 2003; Pickering et al., 2012; Ward et al., 2012; Pelling et al., 2013; Pickering, 2014). These changes manifest as small shifts in the position of amphidromic points (Pickering et al., 2012; Ward et al., 2012), but the direction and distance of the shift is dependent on the coastal boundary conditions imposed (Pelling et al., 2013). Where vertical walls were applied at the present day coastline, changes were caused by the alteration of the propagating tidal wave. However, when the coast was allowed to flood the response was controlled by the increased dissipation of the newly flooded cells (Pelling et al., 2013). The consistent increase in the magnitude of tidal range and HW levels observed at Dutch and Danish sites in this study, agrees with findings of the modelling studies (Pickering et al., 2012; Pelling et al., 2013), suggesting that the model's findings and the proposed mechanisms (e.g. shift in amphidromic points) are valid.

Modelling studies generally suggest that the magnitude of MSL rise at which changes in tides are likely to become important is large (> 2 m) (e.g. Flather et al., 2003; Pickering et al., 2012). This chapter, along with previous studies of historic changes, suggests that significant variations in tides are occurring already, but there is contrasting evidence as to whether this is caused by MSL change. Woodworth et al. (1991) found a positive correlation between trends in MSL and MTR at UK site, but this study finds no significant correlation for any tidal level, even for UK sites, as shown in Figure 4.9. Conversely, there are more positive than negative trends in tidal range and HW levels, and vice versa for LW levels. This finding suggests that one or more mechanisms are affecting tides on a global scale. Since the gravitational forces driving the tides are virtually constant over the observed timescales, the most likely cause of global change in tides is global MSL rise. The model comparisons conducted in this study, show that although changes in MSL do change tidal levels across the world (mostly along the coast), the correlation between the model results and observations is only weakly positive (Figure 4.13). These contradictory findings suggests that MSL is an important mechanism at many sites but that other mechanisms may dominate on a regional or local scale, as explored below.

There are a number of mechanisms associated with the rise in sea level, which can cause changes in the tides. The movement of amphidromic points is one such mechanism, and has been suggested for the changes in North Sea (Pelling et al., 2013), and the coherent increase in the amplitude of the M_2 and K_1 constituents along the western North American coast (Jay, 2009). This study also finds increases in these two constituents (see Figure D5.1) along with a coherent increase in MHW along the western North American coast in the observations, but not in the model simulation (Figure 4.12). This suggests that mechanisms other than SLR are responsible for these changes. However, possible causes of the shifts which include changes in the internal tide

due to changes in stratification (Jay, 2009), and changes in the mean vorticity of the upper ocean in response to large-scale changes in wind-driven circulation (Kolker and Hameed, 2007) are speculative and require further research. The scale of the spatial coherence suggests large scale ocean processes are the cause, but because increases are observed in both diurnal and semi-diurnal constituents, frequency dependent mechanisms such as resonance were ruled out along the western North American coast (Jay, 2009).

However, frequency dependent mechanisms are important in other regions. The amplitude of the tide increases where the natural resonance of the basin is close to the frequency of a major constituent. Standing wave resonance is responsible for most large tidal ranges, including the largest in the world in the Bay of Fundy which is close to resonance with the dominant M_2 tidal constituent (Pelling & Green, 2013). The primary resonant period of the Bay of Fundy and the whole of the Gulf of Maine is believed to be between 12.5 and 13.3 hours (Greenberg et al., 2012). With MSL rise, this period is expected to decrease and move closer to the M_2 period of 12.42 hours. This study finds that significant positive trends in MTR in the Gulf of Maine (Figure 4.4a) are primarily caused by an increase in the amplitude of the M_2 tidal constituent. The system is non-linear though, with a double peak in resonance observed in the Gulf of Maine (Arbic et al., 2007; Müller, 2008), meaning that future MSL change will have complex effects on the tide. Nonetheless, SLR and the subsequent shift in resonance is believed to be an important factor in the increases observed in the amplitude of the M_2 constituent (Ray, 2006; Woodworth, 2010; Müller et al., 2012), and tidal range and HW levels at a number of sites in this study, such as in the Gulf of Maine.

The mechanisms of frequency dependence and energy dissipation, that have been shown to be important on regional scales, can also affect local scales. Bathymetric changes in coastal waters, harbours or estuaries are a suspected major cause of changes in the tide. These changes include: natural changes such as vertical land movements, and accretion and erosion in river deltas (Araújo et al., 2008); changes in river discharge (Jay et al., 2011; Ray, 2016); or anthropogenic causes such as dredging of a navigation channel or creation of a sea wall. Changes in instrumentation can also lead to discontinuities but these effects should be removed during quality control. The examples of Tofino, Canada and Willapa Bay, USA, where negative trends in MTR contrast with the positive trends in MTR observed at other sites along the north-west American coast, show local effects are important. However, this is highlighted most clearly by the annual values of GDTR at Delfzijl (Figure 4.5f), and its neighbouring site Den Helder, in the Netherlands, which show a discontinuity around 1978. Realignment of the Dutch coast as part of the Deltaworks programme, where the largest engineering schemes finished around 1978 (Bijker, 2002) may have influenced the tides in this region. Verification of the cause of the changes of the tides along the German and Dutch

coast is not possible with the GESLA dataset since no high-resolution sea level data are available before the start of the Deltaworks. A modelling study by Kang et al. (2013) of the Yellow Sea showed that the tidal regime there changed in response to large-scale land reclamation on the Korean coast.

The trend in MHHW at Delfzijl is 2.0 mm/yr, which is a similar magnitude to the 2.9 mm/yr trend observed in MSL at this location. The increase in global MSL over the 20th century is estimated to be 1.7 mm/yr and this has accelerated over the latter part of the 20th century to over 3 mm/yr (Church et al., 2013). Its impact on extreme high sea levels is a major concern, and since trends in HW levels are in addition to the effect of MSL change, large underestimation of extreme high sea levels will occur where changes in tide are not accounted for. For example, current calculations of ESLs around the UK do not account for changes in the tide (McMillan et al., 2011), despite the fact that significant changes have been reported since the early 1990s at several sites (Woodworth et al., 1991).

A first step in improving the estimation of ESLs would be to include changes in tide. However, because this study has shown that trends vary between tidal levels, accounting for the complexity of the changes in tides is difficult. ESLs occur more regularly at peaks in various tidal cycles, including spring-neap and lunar-nodal cycles (Cartwright, 1974; Amin, 1979; Zetler & Flick, 1985; Haigh et al., 2011). This is because the base level upon which a storm surge event adds is greater during spring-tropic tides and around the peak of the lunar-nodal cycle. Changes in the magnitude of spring-tropic tidal levels, such as MHWST, will therefore lead to larger changes in magnitude of ESLs, than changes in neap-equatorial tidal levels. Most differences between trends in tidal levels are between the spring-tropic and neap-equatorial tidal levels as the high or low waters they include are mutually exclusive. These findings show that the tide is changing in far more complex ways than would be revealed if just changes in time-series of MTR or DTR were assessed. It is also clear that calculating the trend of a particular tidal level should be done directly and not inferred from other levels without prior investigation.

Although changes in tidal levels were analysed at 220 tide gauge sites around the world, the results are still limited by the availability of data in several regions. Datasets in some under-represented areas such as India and China are difficult to access while in Africa, records are rare and typically short. Considerable recent effort has been made to create a network of tide gauges around the coast of Africa (Woodworth et al., 2007), which will help ensure a more representative global dataset for future studies. The nature of tide gauges also creates a geographical bias towards coastal sites and away from the open ocean. However, many different coastal morphology types are represented in the data from estuarine (e.g. Wilmington, USA) to Pacific

Islands (e.g. Pago Pago, American Samoa). These data sparse regions could skew the results, since a key assumption is that the geographical distribution of sites was not biased towards regions with trends of a particular sign.

Using results from a tidal model provides a global assessment and the results show that there are significantly more positive trends than negative trends at grid-points along the coast (Figure 4.11). This suggests that the observational dataset is not biased towards regions with trends of a particular sign. However, caution should be exercised since the resolution of the model does not capture the full complexity of the tide at the coast. Data quality issues are also a particular problem with tidal data analysis, because small changes in the location of the tide gauge or in the surrounding coastal morphology can lead to clear shifts in the magnitude or phase of tidal constituents or levels. Determination of what constitute real change can be difficult, with both natural and anthropogenic mechanisms often acting on the tide. As discussed above, discontinuities in the trends in tidal levels, such as Delfzijl (Figure 4.5f), mean the linear trend applied to all sites is not always the most suitable model (Visser et al., 2015). However, the changes in tidal levels at these sites are real, even if their cause is most likely anthropogenic, and they are included in the analysis.

4.5 Conclusions

A quasi-global sea level dataset at 220 tide gauge sites was used to analyse changes in 15 different tidal levels: five HW levels; five LW levels; and five tidal ranges (calculated from the difference of the respective tidal high and low water levels). The results show that statistically significant trends are evident in all tidal levels at many sites around the world. For each of the 15 tidal levels assessed, between 34 % and 63% of the selected sites had trends that were significantly (95 % confidence) different from zero. A coherent global pattern of change is not evident, but regionally consistent patterns are observed in the north-east Pacific, the German Bight, and around the coast of Australia and Japan. There are significantly more positive trends in tidal range and HW levels, and more negative trends in LW levels. This suggests a global mechanism has an impact on trends but no correlation is found between the trend in MSL and the trend of any tidal levels, despite previous studies observing a correlation, and hydrodynamic models showing that MSL rise can cause changes in the tide. Comparisons against a global tidal model support the theory that SLR is an important mechanism, but that other mechanisms are also acting to change tidal levels, especially in the north-east Pacific.

The magnitudes of the trends are similar to rates observed in MSL at some locations. Thirty-seven sites had a trend greater than 1 mm/yr in MTR, and while for MHW this number was only eight,

the magnitudes of these changes means that they are similar to trends in MSL. At 56 sites, I find significant differences occurred between the magnitudes of different tidal levels within the same set (i.e. tidal range, HW or LW). In six cases, the sign of the trend is different. The largest differences between tidal level trends were between spring-tropic and neap-equatorial tidal levels, and this has implications for ESL analysis. High ESLs are more likely to occur during spring-tropic periods and increases in HW during this period would result in larger increases in ESLs.

The number and global distribution of sites with significant changes, and the large magnitude of these changes at certain sites, strongly suggests that trends in the tide should be considered when predicting ESLs in the future for applications including coastal defences, navigation, coastal management and tidal power extraction. The inclusion of changes in tides for prediction of future sea levels is complicated by the finding that there are differences in trends, both in terms of magnitude and some cases sign, between different tidal levels. Inadequate understanding of the mechanisms causing the observed changes further complicates prediction, and therefore excludes them from current predictions of extreme sea levels. Further work is necessary to separate out the impact of mechanisms occurring on global, regional and local scales.

Table 4.1: Summary of selected tidal levels and the description of their calculation.

Tidal Range Level	**HW/LW Levels**	**Description**
Great Diurnal Tidal Range (GDTR)	Mean Higher High Water (MHHW) Mean Lower Low Water (MLLW)	Annual average of highest high water minus the lowest low water of each day.
Mean Tidal Range (MTR)	Mean High Water (MHW) Mean Low Water (MLW)	Annual average of all high waters minus the average of all low waters.
Lesser Diurnal Tidal Range (LDTR)	Mean Lower High Water (MLHW) Mean Higher Low Water (MHLW)	Annual average of lowest high water minus the highest low water of each day.
Spring-Tropic Tidal Range (STTR)	Mean High Water Spring-Tropic (MHWST) Mean Low Water Spring-Tropic (MLWST)	Annual average of all high waters minus all low waters during spring-Tropic periods.
Neap-Equatorial Tidal Range (NETR)	Mean High Water Neap-Equatorial (MHWNE) Mean Low Water neap-Equatorial (MLWNE)	Annual average of all high waters minus all low waters during neap-equatorial periods.

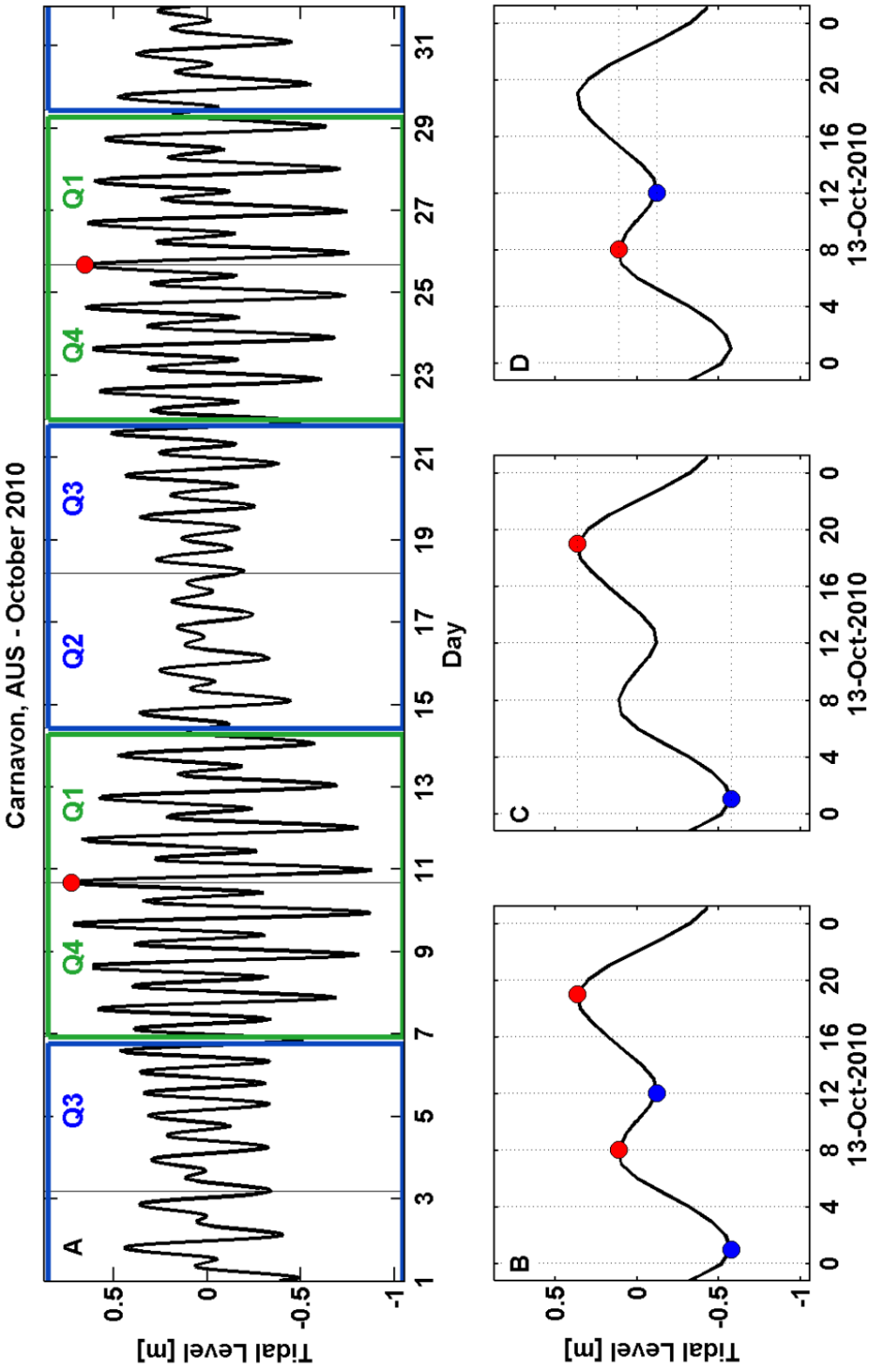

Figure 4.1: Example, from Carnavon, Australia, of the HW and LW subsets used for calculation of the different tidal levels. (A) periods of spring-tropic (green box) and neap-equatorial (blue box) periods based upon the timing of the highest high water of a 14-day period; (B) daily HW and LW used for MTR calculation; (C) daily highest HW and lowest LW used for GDTR calculation; (D) daily lowest HW and highest LW used for LDTR calculation.

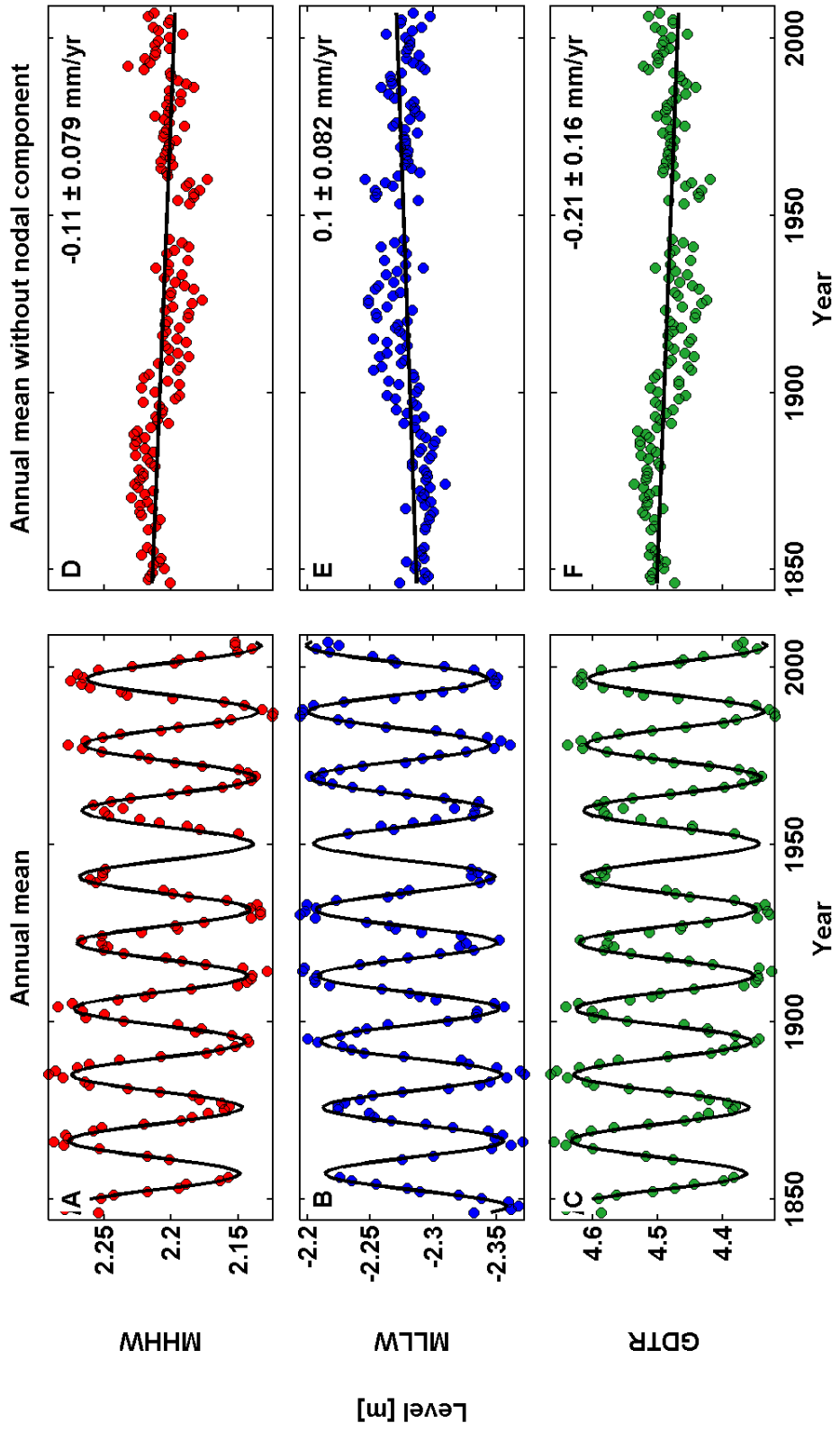

Figure 4.2: (A-C) Time series of annual values of MHHW, MLLW and GDTR relative to MSL at Brest in France, (D-F) and the same time series with the variation caused by the lunar nodal cycle removed. The fitted model with or without the lunar nodal component is plotted as black line.

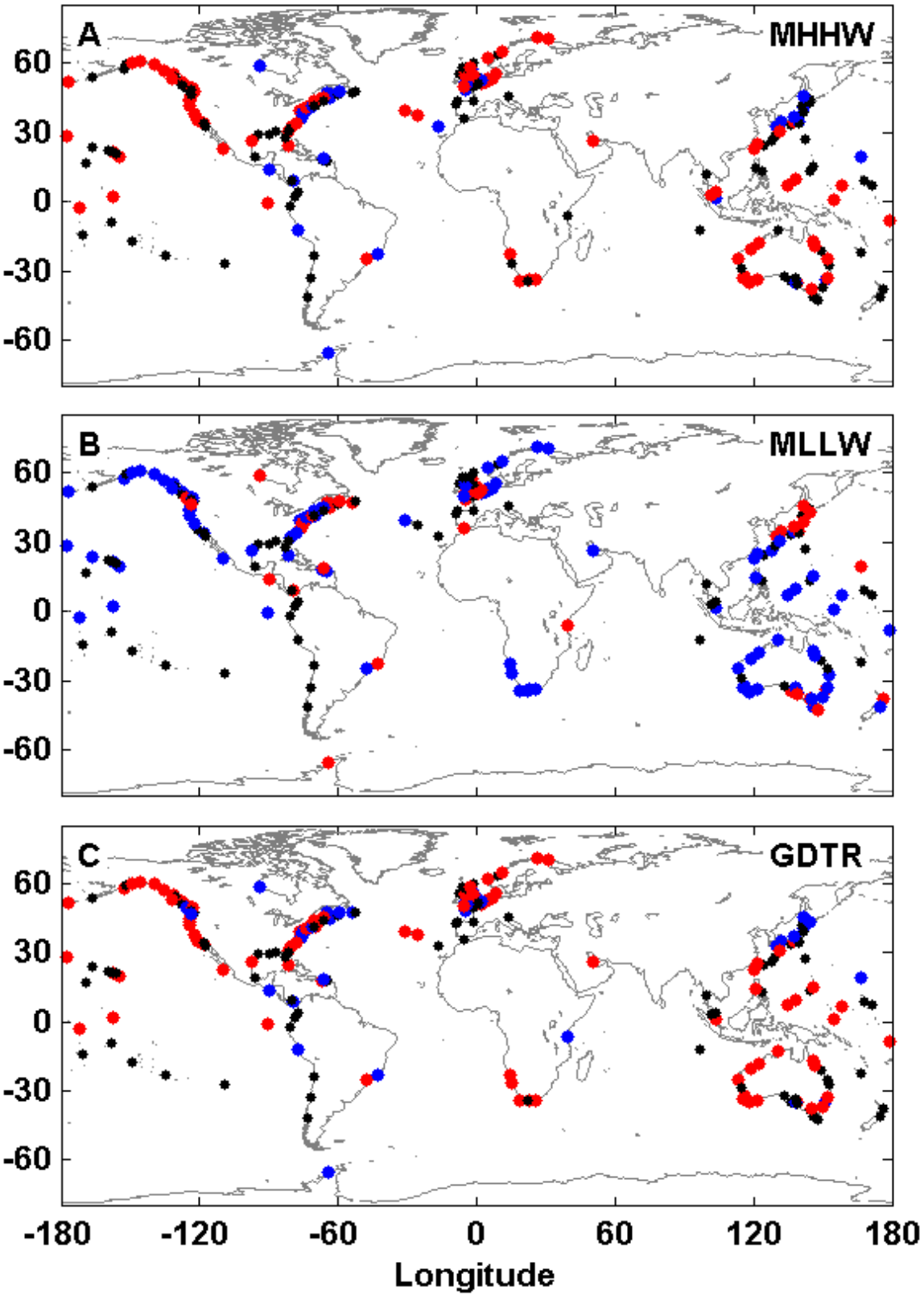

Figure 4.3: Global map showing where trends in MHHW (A), MLLW (B) and GDTR (C) are: significant positive (red), significant negative (blue) or not significant (black). Significance means trend is significantly different to zero.

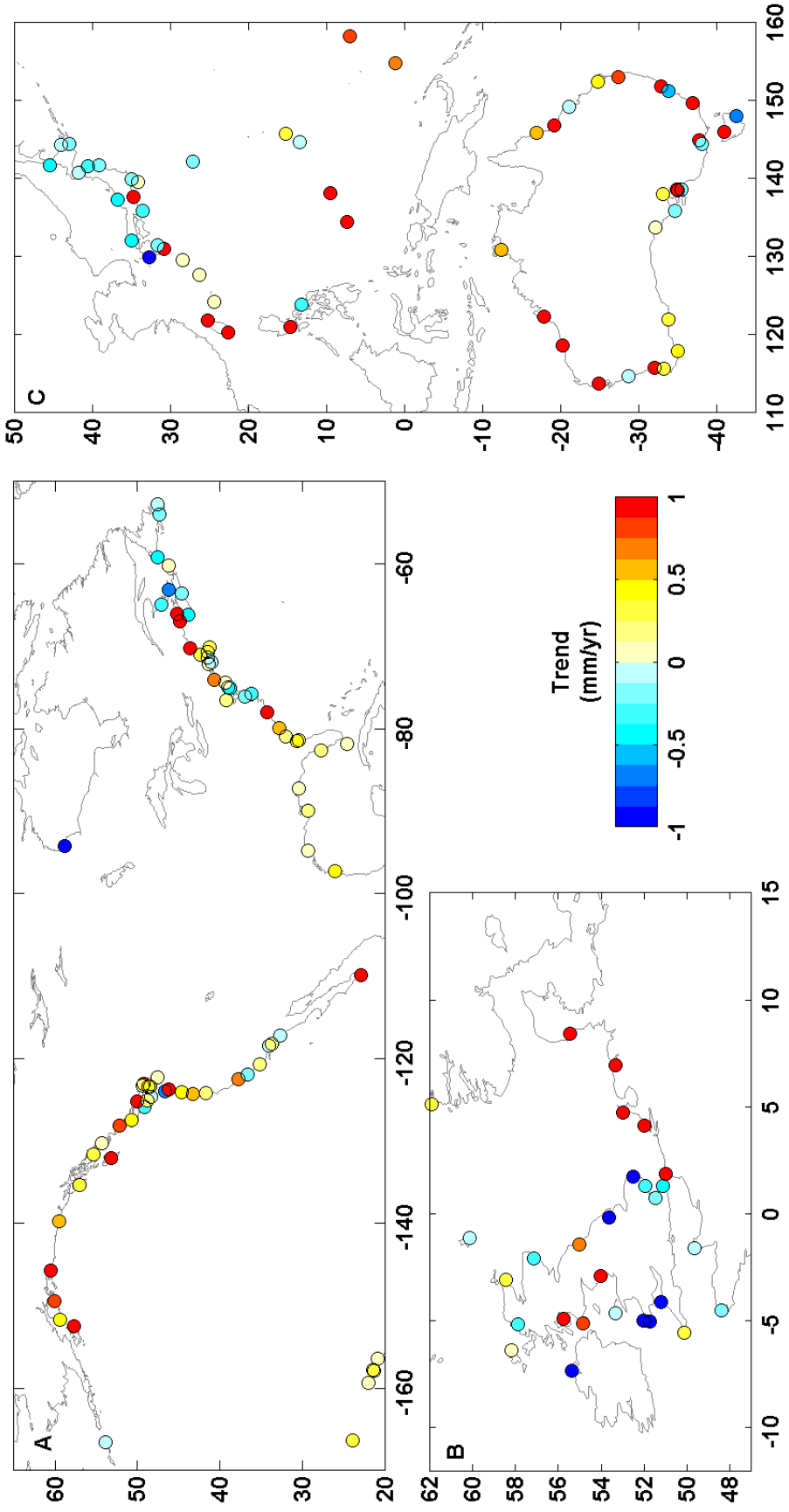

Figure 4.4: Regional maps of North America (A), north-west Europe (B) and Japan and Australasia (C) showing magnitude of changes in GDTR.

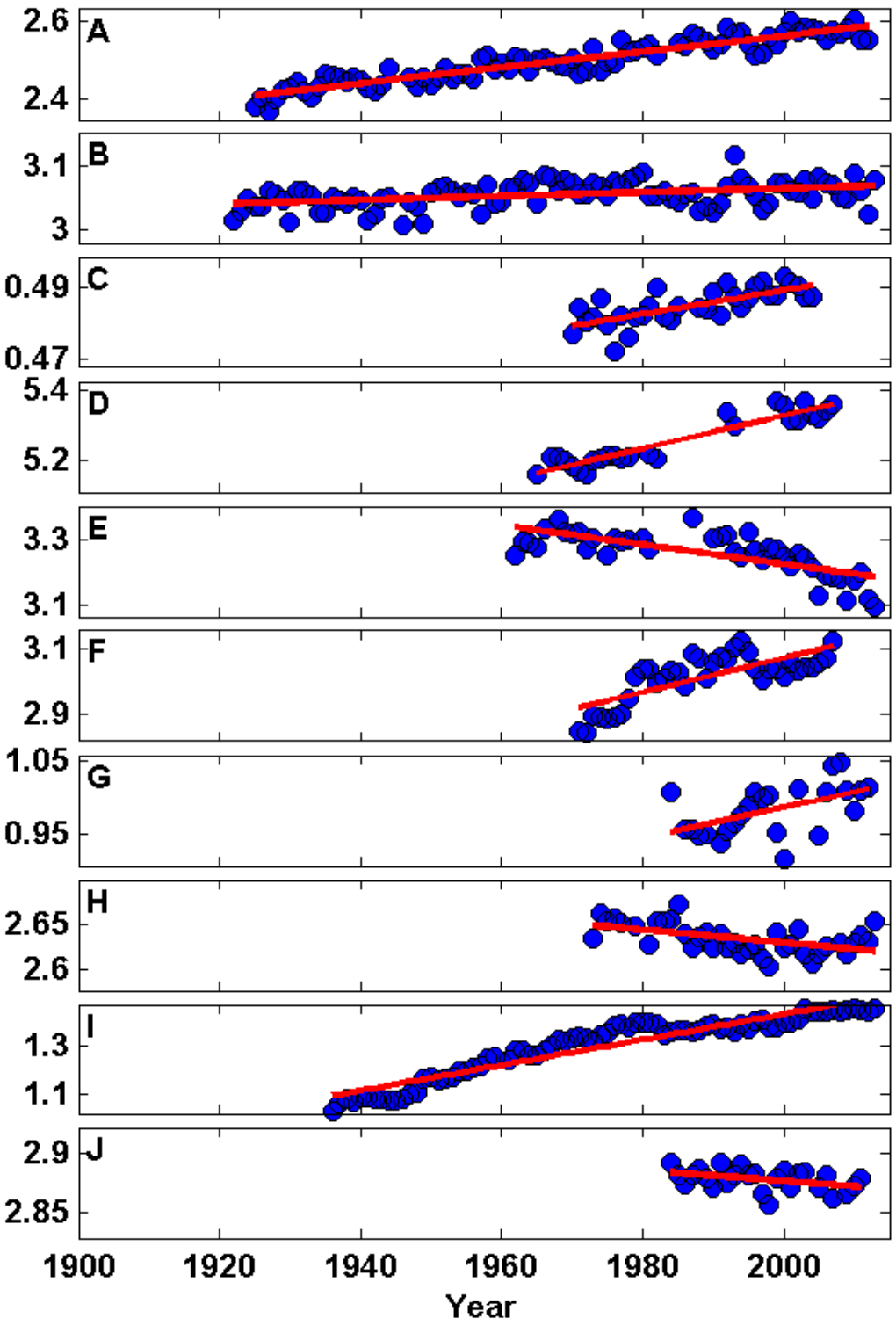

Figure 4.5: Time series of annual GDTR values (in metres) without nodal component for 10 selected sites: (A) Astoria, USA, (B) Boston, USA, (C) Bunbury, Australia, (D) Calais, France, (E) Churchill, Canada, (F) Delfzijl, Netherlands, (G) Manila, Philippines, (H) Willapa Bay, USA, (I) Wilmington, USA, (J) Zanzibar, Tanzania.

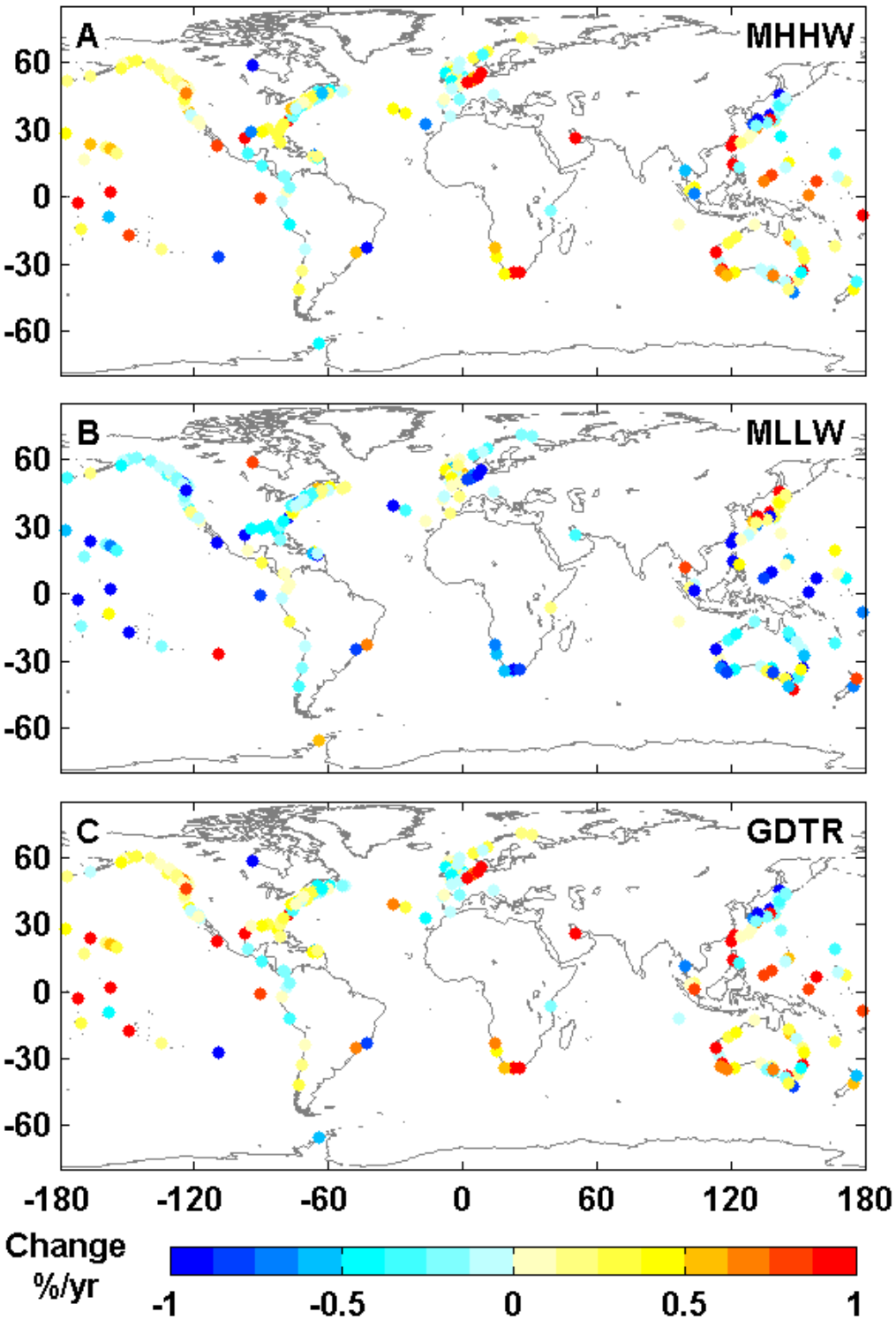

Figure 4.6: Global map showing percentage changes in %/year for MHHW (a), MLLW (b) and GDTR (c) for all locations.

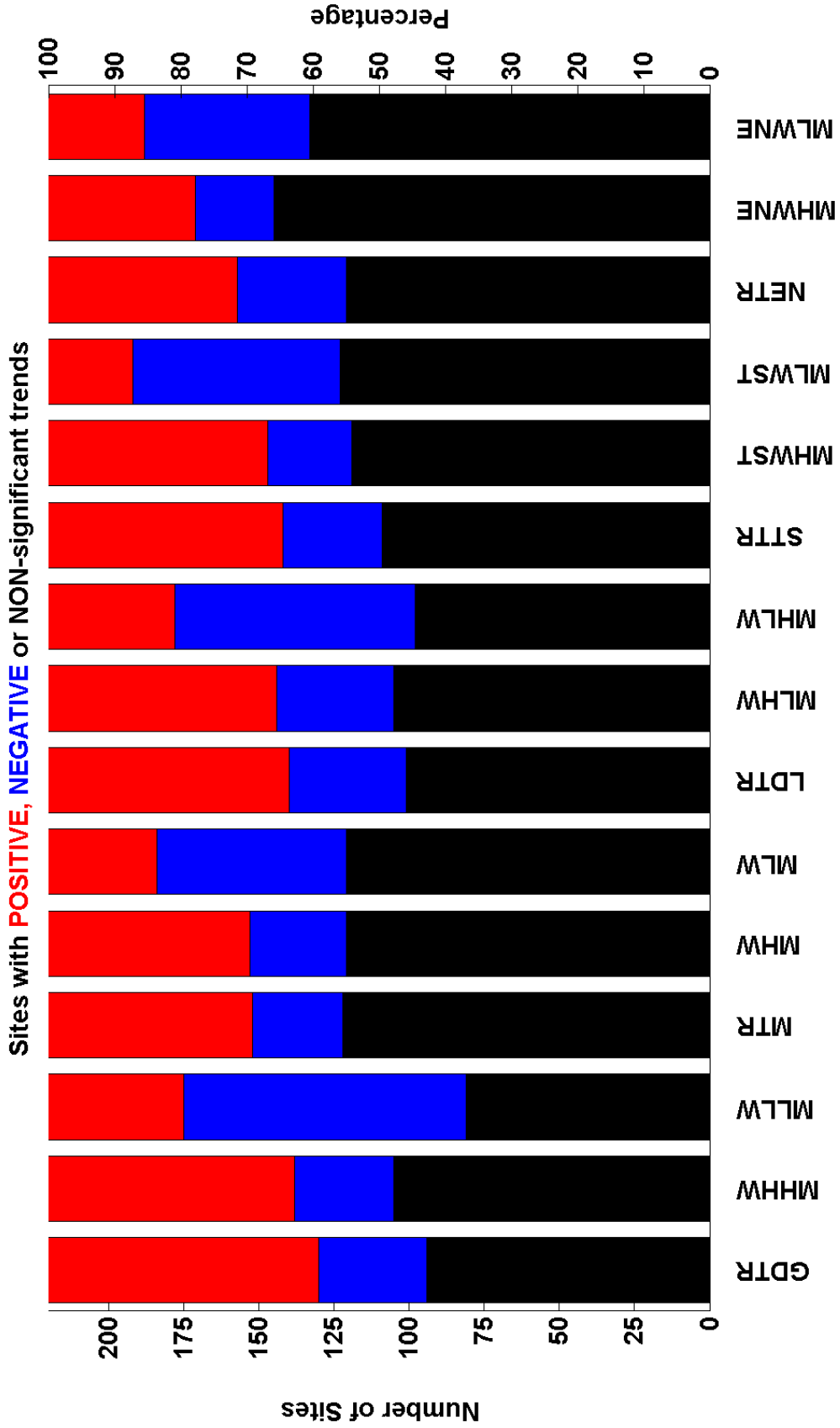

Figure 4.7: Stacked histograms showing the frequency and percentage of sites with significant positive trends (red), significant negative trends (blue) and non-significant trends (black). Significance means trend is significantly different to zero.

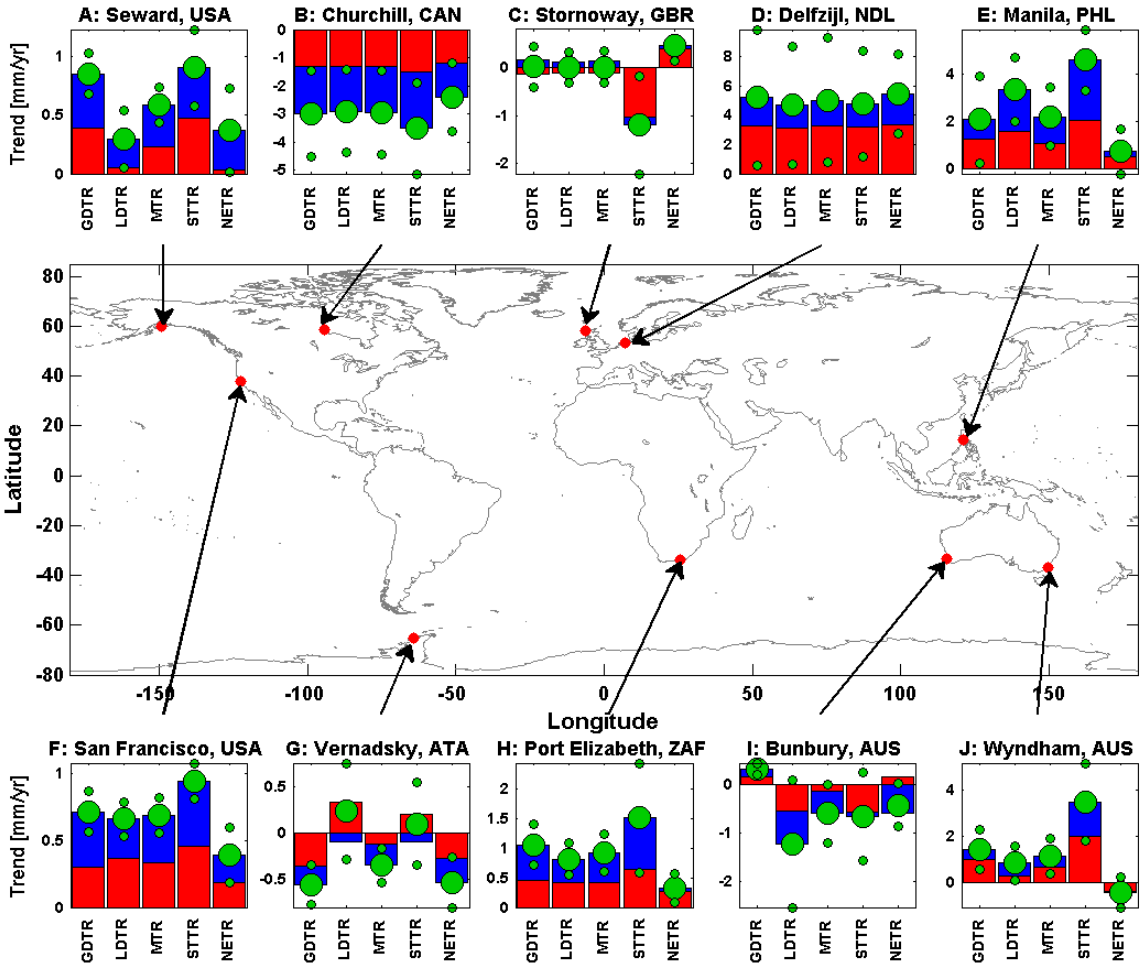

Figure 4.8: Map showing position of selected sites (red dots). Plots surrounding the map show the magnitude of linear trends in tidal levels at 10 sites referenced in the text. The trend in tidal ranges (large green dots) is plotted with 95% confidence limits (small green dots) for five tidal ranges (see Table 1). Stacked bar charts show the contribution towards the tidal range trend of changes in the respective HW subsets (red) and LW subsets (blue). For example, at Delfzijl the contribution toward STTR from HW is positive (i.e. trend in MHWST is positive) and the contribution from LW is also positive (i.e. negative trend in MLWST).

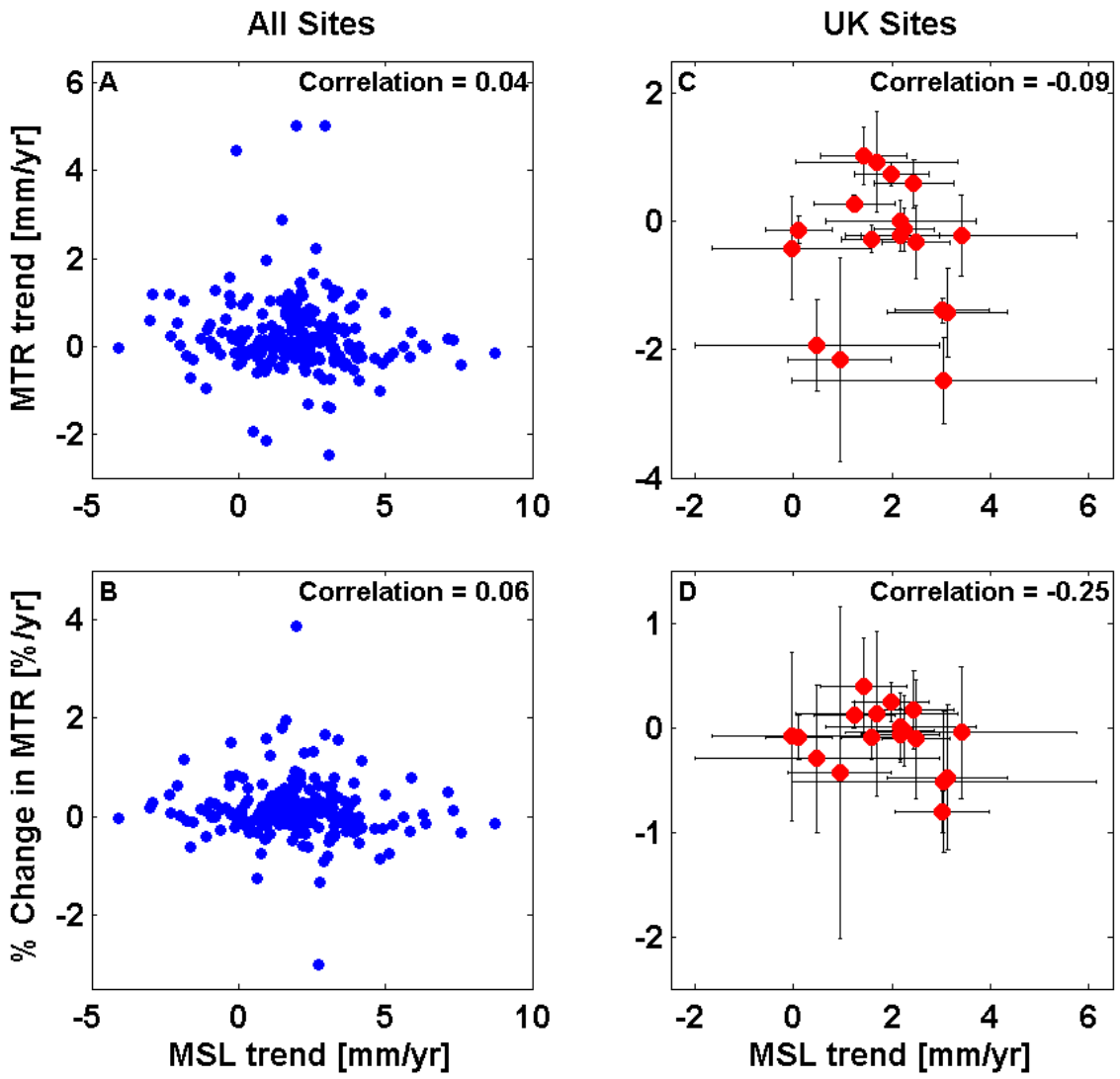

Figure 4.9: Scatter plots showing correlation coefficients for MTR trend (a,c) and percent change in MTR (b,d) against MSL trend for global sites (a,b) and UK sites (c,d).

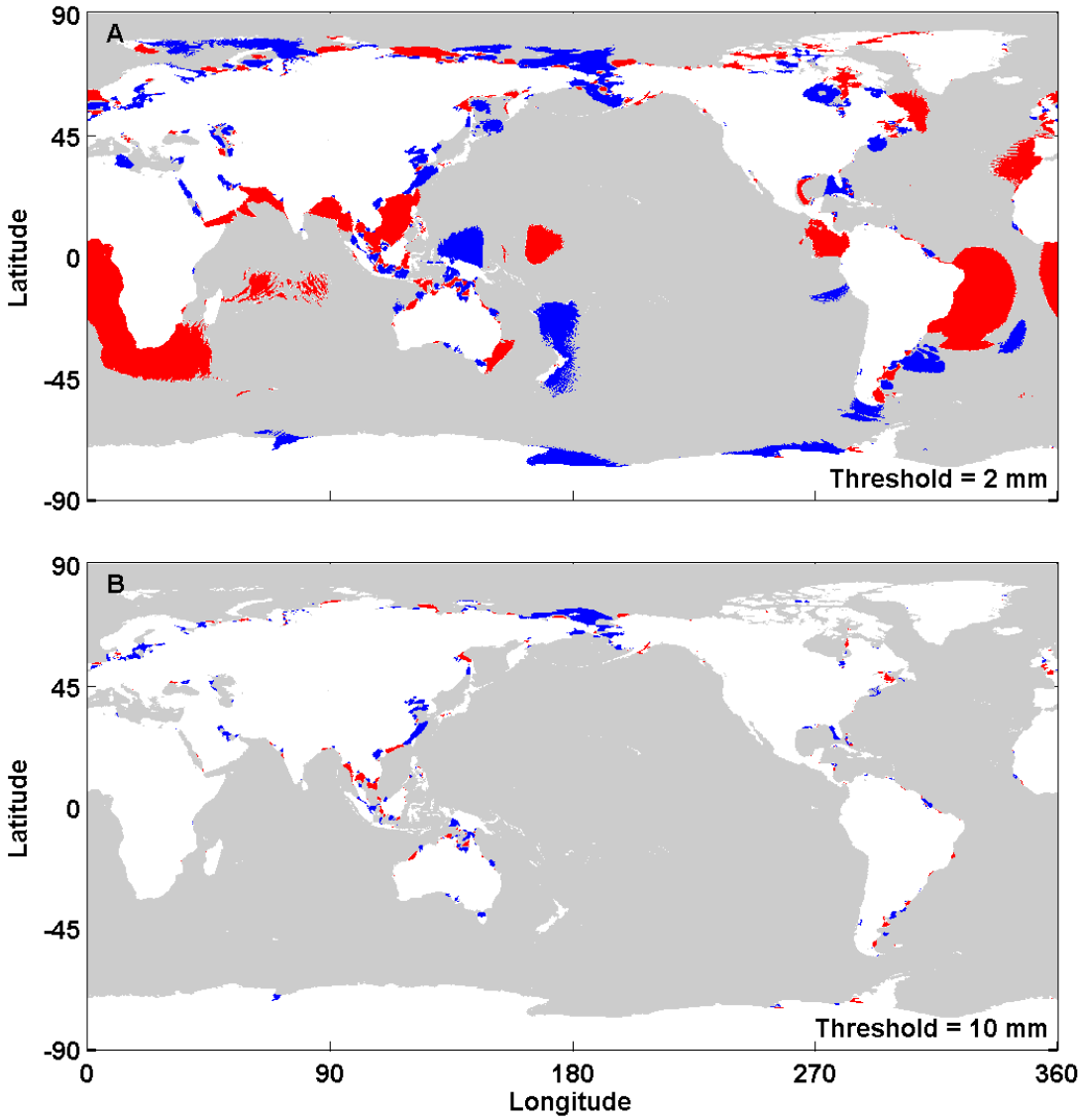

Figure 4.10: Global map showing the direction of change of magnitude of MHW88. The 2 maps show where changes are greater than (top) 2 mm, (bottom) 10 mm. Colours show where trends are positive (red), negative (blue) or not-significant (grey).

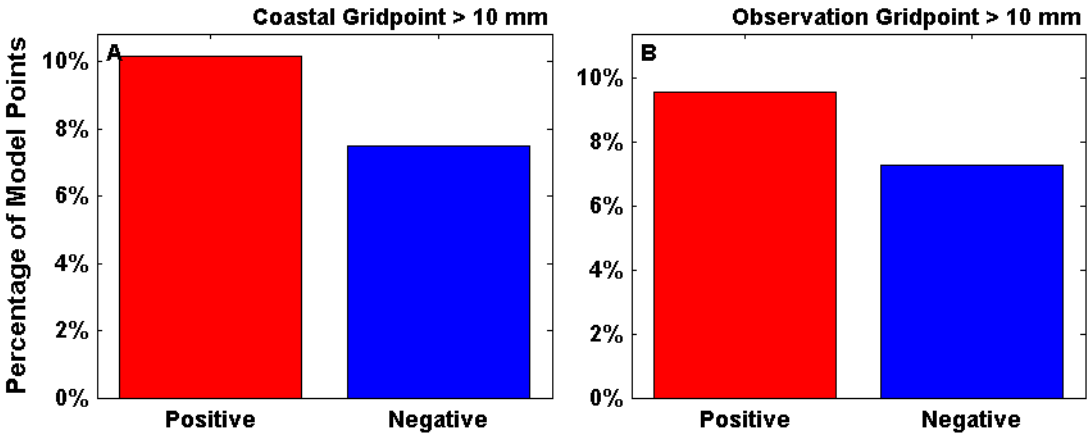

Figure 4.11: Bar charts showing the number of positive and negative changes in MHW88 greater than 10 mm for (A) all coastal grid-points, and (B) the nearest grid-point to the observations.

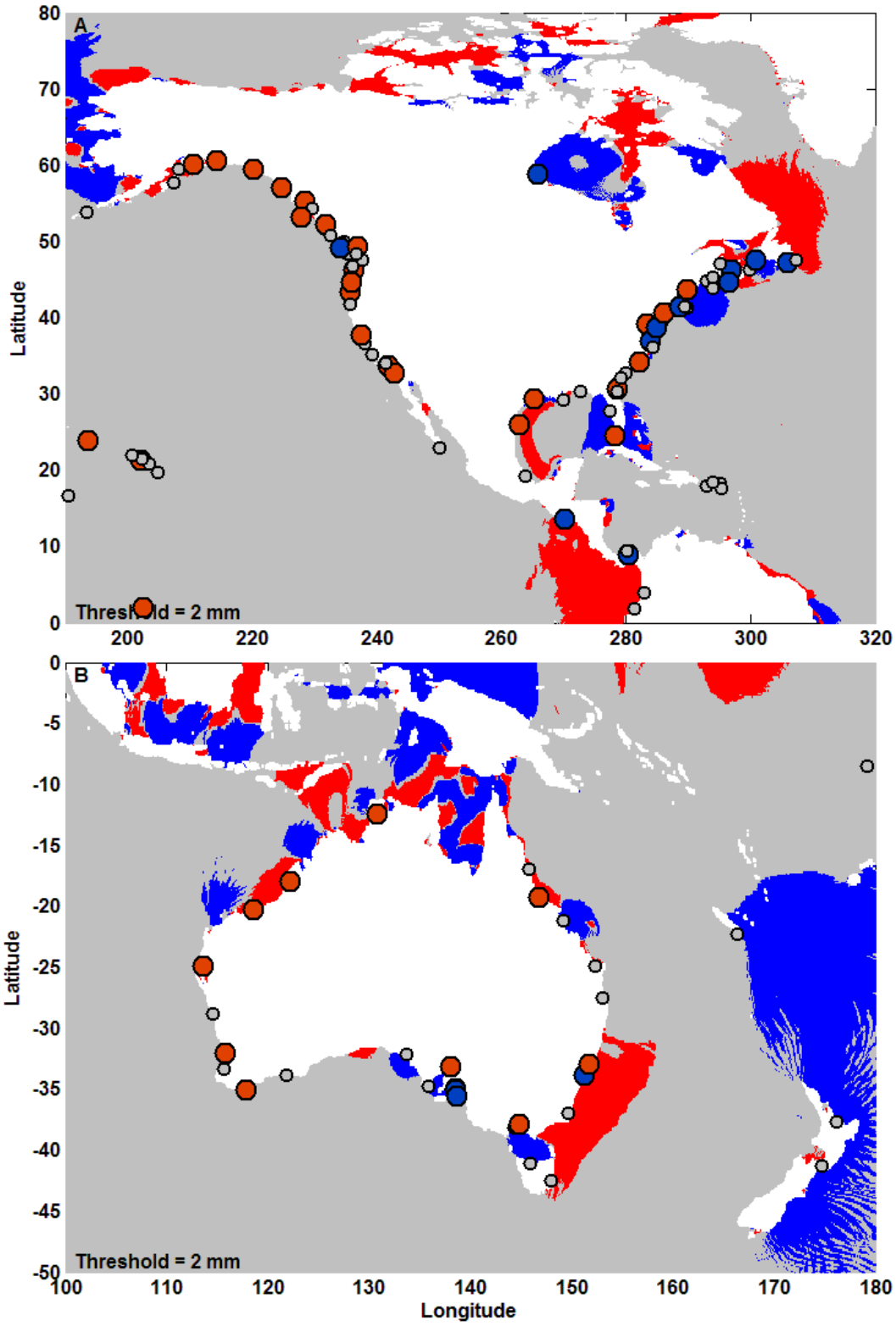

Figure 4.12: Regional maps of (A) North America and (B) Australia, showing the direction of change of magnitude of MHW88, for both the model (shaded regions) and 220 selected sea level records (dots). Colours show where trends are positive (red), negative (blue) or not-significant (grey). Significance for the model is classed as > 10 mm change between control and SLR scenario run, while for observed sea level it relates to the 95% confidence level.

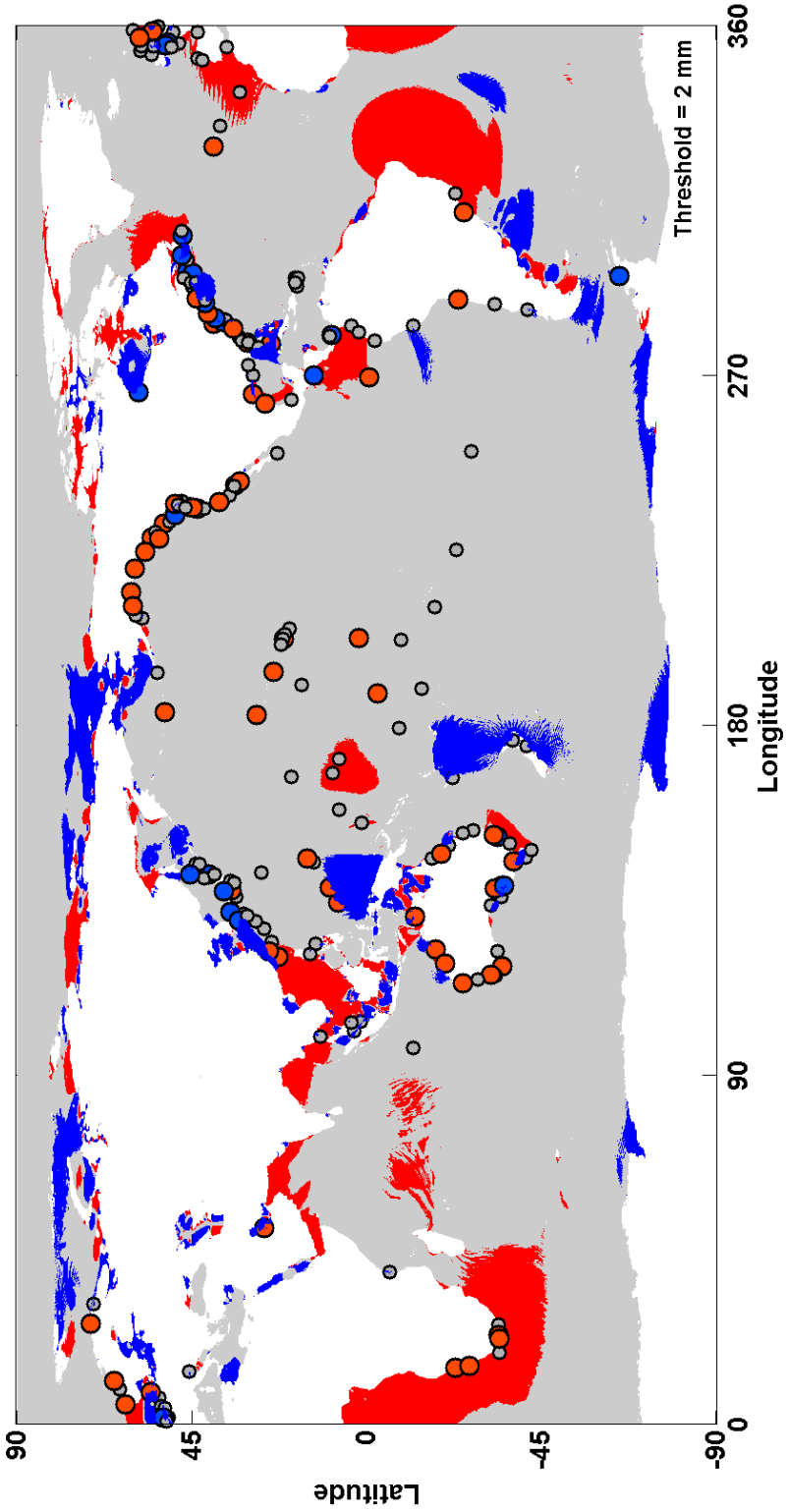

Figure 4.13: Global map showing the direction of change of magnitude of MHW88, for both the model (shaded regions) and 220 selected sea level records (dots). Colours show where trends are positive (red), negative (blue) or not-significant (grey). Significance for the model is classed as > 2 mm change between control and SLR scenario run, while for observed sea level it relates to the 95% confidence level.

Chapter 5: Spatial and Temporal Variability in Skew Surge

This chapter investigates the meteorological component of sea level and assesses the spatial and temporal variability and secular trends in skew surges globally. It is adapted from the following publication:

> *Mawdsley, R. J. and Haigh, I. D. (2016), Spatial and temporal variability and long-term trends in skew surges globally. Frontiers in Marine Science, 3, doi: 10.3389/fmars.2016.00029.*

5.1 Introduction

Storm surges and the resulting extreme high sea levels are among the most dangerous events influencing the coastal zone, and have been responsible for many devastating natural disasters, both in terms of loss of life (e.g. Typhoon Haiyan in November 2013) and economic losses (e.g. Hurricane Sandy in October 2012) (Pugh and Woodworth, 2014). The widespread social, economic and environmental impacts associated with such events have driven research to better understand their generating mechanisms and propagation into shallow coastal areas. However, the large number of stochastic processes that influence the meteorological component of sea level over a range of time and space scales, mean that they remain difficult to predict over periods longer than a few days. Understanding the risks associated with storm surges and how these might change in the future is therefore essential to aid coastal zone management and sustainable developmental planning in coastal regions (Wong et al., 2014).

The previous studies that have assessed changes in the meteorological component of sea level have been described and compared in Section 2.2.3. Although the meteorological component can be generated by seiches and meteotsunamis, these events are poorly resolved in hourly data, and as such the findings in the chapter will relate primarily to storm surges. The aim of this chapter is to assess the spatial and temporal variations in storm surges over the 20th century and early part of the 21st century at a quasi-global scale, addressing the issues highlighted in Section 2.6.

There are four specific objectives in this chapter. The first objective is to determine the extent of tide-surge interaction, at each of the 220 study sites, and to examine the scale of the differences between skew surge and NTR values. The second objective is to compare how the use of skew

surge or NTR, effects the assessment of trends in the meteorological component. The third objective is to assess the extent to which there is spatial coherence in skew surge variability, both locally (i.e. between adjacent tide gauge sites) and regionally (i.e. across ocean basins). The fourth and final objective is to compare inter-annual variation in skew surge to regional climate.

5.2 Methodology

This chapter uses the tidal and NTR time-series, whose extraction is described in Section 3.1.3, and the time-series of tidal HW and LW, whose identification is described in Section 4.2.1. For every predicted HW at each site, a skew surge value was calculated. Batstone et al. (2013) used a method that identified the maximum predicted and observed water levels between successive LWs. However, this approach was inappropriate in mixed tidal regimes. The global nature of this study required a method that works across all tidal regimes. Therefore, skew surge was calculated by finding the largest local maxima in the observed sea level, within a ±3 hour window of the time of each predicted HW (Figure 5.1). Most observed HW occurred within this window, but if no observed HW were found then the window size was extended to ±6 hours. In a mixed tidal regime, the coupling of each observed HW to each predicted HW is more complicated. Therefore, Two criteria were introduced to ensure that the observed HW is primarily caused by the predicted HW to which it is coupled. Firstly, if the predicted HW occurs between a double low tide no observed HW was assigned to it. Secondly, if a second predicted HW is closer in time to an observed HW than its coupled predicted HW, the coupling was removed between that predicted and observed HW. These caveats mean that some predicted HW did not have an associated observed HW, but this method captured a mean of 95% of observed HWs at all sites. Two sites (Bunbury and Hoek van Holland) had an observed HW assignment less than 80%, because many observed HWs occurred around double low tides and were removed.

The study then examined the differences between the skew surge and NTR time series, at each of the 220 study sites, by using four methods to determine the extent of tide-surge interaction. Initially the maximum values of skew surge and NTR from the entire time series were compared, where concurrent values in both time series occur for an event at each site. For example, the maximum NTR at Galveston, USA was generated by Hurricane Ike in September 2008, however, the tide gauge stopped recording just before the predicted HW and no corresponding skew surge value for this particular tidal cycle could be calculated. Also compared were the maximum skew surge value and the maximum NTR at HW (if tide-surge interaction was negligible the two values should be similar). The χ^2 test was first used to assess tide-surge interaction by Dixon and Tawn (1994) but was modified by Haigh et al. (2011) to quantify the level of tide-surge interaction at each site, by comparing the number of peaks in NTR against the level or phase of the tide. The χ^2

test calculates the probability that the observed dataset is different to an expected dataset. In this case, if the two are different then it demonstrates that tide-surge interaction is significant. Dixon and Tawn's (1994) approach, from here on called the tidal-level method, involved splitting the astronomical tidal range into five equi-probable bands. If the tide and NTR were independent processes, the number of NTR peaks per tidal band would be equal, but if interaction is significant the number of NTR peaks per tidal band would differ. As Haigh et al. (2010) pointed out, this method does not distinguish that interaction tends to be different on the ebb and flood phases of the tide (Horsburgh and Wilson, 2007). Haigh et al. (2011) therefore modified the method to compare the relative timing of the peak NTR to the predicted HW, and this method is from here on called the tidal-phase method. The tide was divided into 13 hourly bands between 6.5-hours before and after high water. With no tide–surge interaction the expected number of occurrences in each of the 13 bands would be the same. See Haigh et al. (2010) for the mathematical details. The same 13 hourly bands were used to assess tide-surge interaction in the tidal-phase method, but 6 equi-probable bands are used for the tidal-level method. The results from both methods are based on the largest 200 NTR events, where an event is defined by a 72-hour window centred on the peak NTR, to ensure that each NTR peak is independent event. Statistical significance for the χ^2 test is given for a p-value <0.05.

Next, the secular trends in the skew surge time-series were assessed at each site, and compared these to trends calculated from the NTR time-series. This study used the percentiles method (e.g. Menéndez and Woodworth, 2010; Haigh et al., 2010), which ranks the parameter values for each year. The 50^{th} percentile of the NTR time-series (the median) approximates to zero, while the 99.9^{th} percentile is about the level of the 8^{th} highest hourly sea level value. For skew surges, the tidal regime at each site affects the annual number of HWs. In semi-diurnal regimes there are approximately 705 skew surge values a year, whereas for a diurnal regime an average of 352 skew values would occur. Therefore, the 99^{th} percentile represents a value between the 4^{th} and 7^{th} highest values in the skew surge time series. Trends were calculated for these percentiles, using linear regression, while standard errors were estimated using a Lag-1 autocorrelation function to allow for any serial autocorrelation in the time-series (Box et al., 1994). For the rest of this chapter, the term 'significant trend' signifies that a trend is statistically (at 95% confidence level) different from zero.

High percentiles represent the largest events at each site, but the large year to year variability present in the higher percentile time-series can obscure the inter-annual signals and secular trends. To assess the extent to which there is spatial coherence in skew surge variability, correlation coefficients were calculated between the skew surge percentile time-series for each pair of sites. Groups of sites with strong correlation between them, were identified and

designated as coherent regions. Regional skew surge indices were created by calculating the mean of the de-trended and normalised time-series of the 99th percentile of skew surge, for each site in that area. The regional skew surge indices were only derived for the period from 1970-2010, when there was sufficient overlap of data among sites in each region, but increase the temporal comparison by using individual long time-series from each region. The regional skew surge indices were filtered using a locally regressed least squares (Loess) approach (Cleveland and Devlin, 1988), which through testing gave the lowest standard error. This non-parametric method combines a multiple regression model with a nearest-neighbour model. Each point of the Loess curve was fitted using local regression, using a 2nd degree polynomial to the points within a 10-year window centred on that point. These filtered time-series are used to assess the temporal variations in the regional skew surge indices and the correlation of those indices between each other and against the regional climate indices, listed in Section 3.3. The significance of the correlations are calculated using a Lag-1 autocorrelation function (Box et al., 1994).

5.3 Results

5.3.1 Tide-surge interactions

The first objective was to identify any tide-surge interaction, at each of the 220 study sites, and this was done using the 4 methods detailed in Section 5.2. The difference between the maximum skew surge value and the maximum NTR over the whole time series, is shown for each site in Figure 5.2a. Small differences indicated sites where tide-surge interaction was negligible. Results showed that the difference is largest in regions surrounded by shallow bathymetry, such as the German Bight, Northern Australia, the Gulf of Panama and parts of the east coast of North America. However, there are other sites with large differences, including: sites in northern Australia (Port Hedland, Broome, Wyndham, Townsville and Bundaberg); Easter and Wake Islands in the Pacific Ocean; Funchal on Madeira, Portugal; and Yakutat in Alaska. At 120, 80 and 20 sites, the difference is larger than 10 cm, 20 cm and 50 cm, respectively. The difference between the maximum skew surge and the maximum NTR observed at the time of predicted HW showed that 137 sites have a value of zero, as shown in Figure 5.2b. However, sites in the North Sea, the US east coast, north-west Australia and a few other individual locations have non-zero values which suggests that in these regions the tide-surge interaction shifts the peak in NTR away from predicted HW.

Figures 5.2c-d present the magnitude of the χ^2 test statistic as a coloured dot (where $p < 0.05$) and a black dot where the statistic is not significant at this level. The results for the tidal-level method are shown in Figure 5.2c, and show that tide-surge interaction is statistically significant (95% confidence) at 130 of the 220 sites (59%). These sites included those identified in Figures 5.2a-b, but also included sites on the Malay Peninsula and along the coast of Washington and Oregon, USA. The results for the tidal-phase method, are shown in Figure 5.2d, and show that tide-surge interaction is statistically significant at 175 of the 220 sites (81%). As mentioned earlier, Haigh et al. (2010) modified Dixon and Tawn's (1994) original χ^2 test statistic as it did not distinguish that interaction tends to be different on the ebb and flood phases of the tide. Interestingly, these results show the tidal-phase method identifies a greater number of sites at which tide-surge interaction is statistically significant.

At several sites the differences between the maximum skew surge and NTR values are large, but the χ^2 statistic values are small. This is often caused by the impact of one large storm. For example, at Wake Island, Pacific, it is Typhoon Ioke in 2006 (skew surge = 0.97 m, NTR = 1.45 m), at Broome, Australia it is Cyclone Rosito in 2000 (skew surge = 0.82 m, NTR = 2.24 m) and for Townsville, Australia it is Cyclone Yasi in 2011 (skew surge = 0.93 m, NTR = 2.10 m). At Easter Island, Chile the event in June 2006 is a high frequency signal, similar to seiching, but further research is needed to determine its cause (skew surge = 0.51 m, NTR = 1.18 m).

The difference between skew surges and NTRs at a site can vary considerably between individual events as a result of the timing of the peak in the NTR relative to the predicted HW. This is illustrated in Figure 5.3 for 8 selected sites. The scatter sub-plots show the magnitude of the 200 largest NTR events plotted against the magnitude of the associated skew surge. The histogram sub-plots show the time of the peak in NTR for the 200 events relative to time of predicted HW. The colours on each plot display the maximum NTR (green), the top 10 NTRs (red), the top 25 NTRs (blue) and the remainder of the top 200 NTRs (black). At Atlantic City, USA (Figure 5.3a), Galveston, USA (Figure 5.3d) and Naze in Japan (Figure 5.3f), the largest skew surge and largest NTR occurred during the same event. However, at the other selected sites, the timing of the peak NTR relative to the HW means that the largest skew surge and largest NTR are not coincident. For example, at Immingham, UK, the maximum NTR occurred 6 hours before predicted HW and because the MTR (as defined in Section 4.2.1) is 4.8 m, the magnitude of the skew surge was only the 56th largest from the top 200 NTR events (Figure 5.3e). The timing relative to predicted HW is less important where MTR is small. At Galveston, USA (MTR = 0.24 m) for example, the largest NTR (with the values caused by Hurricane Ike removed) occurred during Hurricane Carla in 1961. The peak NTR occurred at the same time as predicted HW, and 7 of the 10 largest events occur within 3 hours of predicted HW (Figure 5.3d).

As mentioned earlier, tide-surge interaction has been most studied in the southern North Sea, where the largest positive NTRs tend to occur on the rising tide. This pattern can be clearly observed in the results for Immingham shown in Figure 5.3e. However, the shape of these distributions vary around the world. For example, at Fremantle in Australia (Figure 5.3c) most peaks in NTR occur near the time of predicted HW, while for Charleston (Figure 5.3b) and Seattle (Figure 5.3h) in USA, the majority of peaks in NTR occur on the ebb tide.

5.3.2 Skew Surge and NTR Comparison

The second objective was to determine if using skew surge to assess changes in the meteorological component, gave different results compared to using the NTR. The finding that, tide-surge interaction is evident at a large proportion of the study sites, suggests that trends in skew surge and NTR may differ.

The trends calculated for the 95th, 99th and 99.9th percentiles of the NTR time-series are plotted in Figure 5.4, against the trends in skew surge time-series for the same three percentiles. Given the differences in sampling of the two parameters, as summarized in Section 5.2, comparisons of trends in different percentiles gives an understanding of how to relate the percentiles of the two parameters to each other. If the trends were the same between skew surge and NTR, all points would lie along the 1:1 ratio line shown on each panel. Trend differences between the skew surge and the NTR are generally small, with trends in the same percentiles of the two parameters showing the closest comparison (i.e. the closest 1:1 match occurs between the 99th percentile of both parameters). The colour of each dot in Figure 5.4 represents the height of MTR at that site. Sites with the largest difference between trends in skew surge and NTR typically have a large MTR. These sites include Broome, Australia, Ilfracombe, UK and Hoek van Holland, Netherlands, and these sites also have a large tide-surge interaction (as shown in Figures 5.2c-d). At three further sites, Calais (France), Darwin (Australia) and Eastport (USA), the trend in skew surge is significantly larger than the trend in NTR (i.e. the 95% confidence intervals of the two trends do not overlap). The trends at Calais and Eastport change from significant negative trends (at the 95% level) to positive trends that are significant at the 66% level. The root mean squared error (RMSE) between skew surge and NTR trends are listed for each panel in Figure 5.4, and are largest for the 99.9th percentile, since trends in this percentile can be affected by individual large events.

The time-series of the 99th (blue) and 99.9th (red) percentiles of skew surges are presented in Figure 5.5 for selected sites, along with the linear trends in these time-series and the corresponding 95% confidence intervals. The variability around the 99.9th percentile, which captures only the annual maximum of skew surge, is large relative to the magnitude of the linear

trend and therefore very few significant trends are detected. Therefore the 99th percentile of skew surge is used throughout the rest of the paper. Previous global studies, including Menéndez and Woodworth (2010), used the 99th percentile of NTR, so this choice allows direct comparison with the results of that study.

Linear trends calculated for the 99th percentile of skew surge and NTR are shown for each site in Figure 5.6a and 5.6b respectively. Significant trends are shown as coloured dots, with the colour representing the magnitude of the trend. Overall there are few significant trends in the skew surge time-series, with significant negative trends at 18 sites and significant positive trends at 11 sites. For the NTR there are significant negative trends at 33 sites and significant positive trends at only 5 sites. There are 15 sites with negative trends in both parameters, and 4 sites with positive trends in both.

Trends were calculated at sites with enough years for the last 20, 40, 60 and 80 years, and compared to the trend of the entire time series. These results are presented in Appendix E and show that the number of positive and negative trends are roughly similar, and low in relation to the number of sites. Despite the low numbers of sites with significant trends there are some regions with consistent trends between neighbouring stations, such as coherent decreases around north Australia and the Atlantic coast of southern Europe.

5.3.3 Spatial variability of skew surge

The third objective was to assess the extent to which there is spatial coherence in skew surge variability, both locally (i.e. between neighbouring sites) and regionally (i.e. across ocean basins). For each site in turn, correlation coefficients were calculated between the unfiltered 99th percentile time series at that site and each of the other 219 sites. The results are shown in Figure 5.7. There are distinct regions where strong positive correlations occur among neighbouring sites. These include the north-east Pacific, north-west Atlantic and sites in northern Europe. Interestingly, sites on the west coast of the US are weakly anti-correlated (at the 66% level) with several sites in northern Europe.

The strong correlation between groups of sites implies that regional skew surge indices could be created that represented the average skew surge conditions for a particular region; similar to what other studies have done for MSL (e.g. Shennan and Woodworth, 1992; Woodworth et al., 1999, 2009; Haigh et al., 2009; Wahl et al., 2013; Thompson and Mitchum, 2014; Dangendorf et al., 2014). Eight regions were identified where a large density of sites meant that strong positive correlations existed between them. These regions, and the sites of which they are comprised, are detailed in Table 5.1 and include the: north-east Pacific (NEP), Gulf of Mexico (GOM), north-west

Atlantic South (NWA-S), north-west Atlantic North (NWA-N), North Sea (NS), west Australia (WAUS), east Australia (EAUS) and Japan (JAP).

An example of the creation of a regional index is shown in Figure 5.8 for the north-east Pacific. The de-trended, normalised time-series from each of the 11 selected sites in the region are plotted in Figure 5.8a, with an arbitrary offset. These time series are overlaid in Figure 5.8b. The thicker red line shows the regional time-series that has been created by averaging time-series from the 11 sites. The locations of the sites used to calculate the regional time-series are shown in Figure 5.8c, as red dots.

There is considerable inter-annual variability in the regional indices. To better investigate this variability a Loess filter was fitted to each of the 8 regional skew surge indices. The filtered time series are shown in Figure 5.9a, and show that concurrent peaks are observed in multiple regional skew surge indices, most notably in 1992-93 in the north-west Atlantic (North and South indices) and the North Sea. Peaks in skew surge in the southern North Atlantic throughout the 1990s appear to lag peaks in the Gulf of Mexico by approximately one year. Storm seasons for these regions are summer and winter respectively and the lag may be a result of this or a delay in the response to changes in regional scale climatology.

Correlations among the 8 regional skew surge indices are shown in Figure 5.10b. Between many regions, there is a strong correlation ($r > 0.5$), but at the 95% level these are not significant, due largely to the reduction in the number of effective observations when autocorrelation is accounted for. Strong correlations exist between: the two north-west Atlantic indices ($r = 0.65$, $p = 0.02$), the Gulf of Mexico and both two north-west Atlantic indices (South: $r = 0.37$, $p = 0.33$; North: $r = 0.31$, $p = 0.4$), the North Sea and north-west Atlantic – South ($r=0.65$, $p = 0.12$). Only this last correlation is significant at the 80% level.

The regional skew surge indices were only calculated for the period 1970-2010, because there were fewer sites with valid data outside of this period and this increased the variability in the indices. To allow longer temporal comparisons between regions, individual sites were selected from each region that were both long and highly correlated with the regional index. The 8 sites with long records, across the 8 regions, are shown in Figure 5.9b. Note, these time series have also be subjected to the same Loess filter, applied to the regional time series. The simultaneous peak in the 1990s, mentioned above, is also present in the individual sites. However, a peak in the signal in the filtered time series at Charleston and Atlantic City, USA in the 1960s is not clear at Immingham, UK. The reverse is true in the late 1980s, where an increase at Immingham is not present at Charleston or Atlantic City.

5.3.4 Comparison of skew surge to climate indices

The fourth objective is to compare inter-annual variations in skew surge with fluctuations in regional climate. Correlation coefficients were calculated between the 8 regional skew surge indices and each of the 8 regional climate indices. The results are shown in Figure 5.11.

There are no statistically significant correlations at the 95% level, again largely because of the large degree of autocorrelation in the filtered time-series. Strong positive correlations ($r > 0.5$) occur between: the North Sea and NAO ($r = 0.60$, $p = 0.28$), the Gulf of Mexico and Niño 4 ($r = 0.52$, $p = 0.19$) and western Australian and SOI ($r = 0.59$, $p = 0.31$). Strong negative correlations ($r < -0.5$) occur between the north-east Pacific and AO ($r = -0.57$, $p = 0.28$) and NAO ($r = -0.50$, $p = 0.40$), the Gulf of Mexico and AO ($r = -0.53$, $p = 0.32$), western Australia and NP ($r = -0.56$, $p = 0.28$), and eastern Australia and Niño 4 ($r = -0.52$, $p = 0.19$). The correlations detailed above that involve Niño 4 are the only correlations significant at the 80% level.

The peak observed in the north-east Pacific index in 1997-98 (Figure 5.9a), corresponds to one of the strongest El Niño events in the time-series. The peak observed in both the Seattle record and the north-east Pacific index in 1982-83 corresponds to another strong El Niño event, however, the El Niño event of 1972 is not evident in the skew surge time series. Also, the typically positive Niño 3 values observed through the early 1990s coincide with a trough in the north-east Pacific index. The presence of a peak in north-east Pacific index during only the strongest El Niño events suggest a complex relationship between skew surge and the magnitude of variability in regional climate.

5.4 Discussion

One of the key goals of this chapter was to determine if different results are obtained when using skew surge to assess changes in the meteorological component of sea level, compared to the more traditional NTR. While the NTR primarily reflects the meteorological contribution, it may also contain harmonic prediction errors or timing errors, and non-linear interactions, which can bias the analysis. It is for this reason that this chapter assessed the alternative use of skew surges. The advantage of using skew surge is that it is an integrated and unambiguous measure of the storm surge (Haigh et al., 2015). Changes in skew surges have only previously been assessed (to my knowledge) at sites around the north-west Europe (Batstone et al., 2013; Dangendorf et al., 2014) and the USA (Wahl and Chambers, 2015). Both of these regions generally display semi-diurnal tidal behaviour, but the new method works well in all tidal regimes.

Significant tide-surge interaction occurred at 130 of the 220 sites analysed (59%) based on the tidal-level method, and 175 sites (81%) based on tidal-phase approach. These sites include those previously reported, as well as regions not previously identified in the literature, such as the Gulf of Panama and the Malay Peninsula. It was also found that tide-surge interaction is not limited to locations with large adjacent areas of shallow bathymetry. Smaller but still statistically significant interactions occur along the Pacific coast of North America, on a number of Pacific Islands and around the Iberian Peninsula. The topography of these sites is highly variable. Some sites are in shallow water such as Willapa Bay, USA, which is in a large bay, and Astoria, USA, which is influenced by the Columbia River. Other sites are on volcanic islands rising steeply from the ocean floor, such as Papette, French Polynesia and Pohnpei, the Federated States of Micronesia. For both these island sites there is an increased frequency of peaks in NTR around the time of predicted HW, a pattern that is also observed at Galveston, USA (Figure 5.3d).

In some regions the timing of the peak NTR relative to tidal-phase, and therefore the level of tide-surge interaction has a local signal. For example, around the UK, peak NTR usually occurs away from predicted HW (Horsburgh and Wilson, 2007; Haigh et al., 2010; Olbert et al., 2013), and in the North Sea, Horsburgh and Wilson (2007) showed that the external surge component will always peak away from predicted HW. However, at Larne and Bangor in Northern Ireland, peak NTR most frequently occurred at predicted HW (Olbert et al., 2013). These sites have similar tidal conditions and are geographically close but highlight that small changes in bathymetry and tidal range can influence the pattern of tide-surge interaction.

Individual storm characteristics vary from the average pattern, and where these deviations occur in the largest storm surges the difference in skew surge magnitude can be important. At Wake Island in the Pacific, Typhoon Ioke generated a NTR of 1.5 m but a skew surge of only 1.0 m, because the peak NTR for this event occurred 5 hours before predicted HW (see Appendix E, Figure E3.10, Site 434). However, no significant tide-surge interaction is observed at this site and the peak NTR for an event like Typhoon Ioke could have occurred at the same time as predicted HW. Conversely, at Brest, France, where significant tide-surge interaction usually means that peaks in NTR occurred away from predicted HW, the maximum NTR (caused by the so-called Great Storm in October 1987) occurred at the same time as predicted HW. Therefore, although the skew surge is a more reliable indicator of the average meteorological influence on sea level, individual storm surges may have different characteristics. Parameterisation of any physical process aims to use one value to represent a complex system, and this must be considered when skew surge is used in ESL calculations. This is especially true in regions with small tidal ranges or those affected by tropical cyclones. The rapid peak in storm surge associated with tropical

cyclones reduces the influence of storm surge on tidal propagation, and may lead to a more uniform distribution of the peak NTR timing relative to predicted HW.

Although tide-surge interaction is evident at most of the study sites, large differences between trends in skew surge and NTR values only occurred at a few sites. The largest differences occurred at sites along the north-coast of Australia or the French coast of the English Channel, and this resulted in the reversal of trends at Calais and Darwin. Both locations have macro-tidal regimes with significant tide-surge interaction. The general similarity in trends means the results of this study can be compared to previous studies which used NTR. Menéndez and Woodworth (2010) found more negative trends in NTR than positive trends globally. I also find more negative trends in NTR, but no statistically significant difference between the number of positive and negative trends in skew surge. The findings are consistent with those of Wahl and Chambers (2015) for the US, who found a greater number of sites had significant trends in NTR compared to skew surge. The number of sites with significant trends in skew surge and NTR may be generated from chance, but a formal assessment has not been made here, because of the spatially non-homogenous dataset. Methods such as that of Livezey and Chen (1983) could be adapted to assess whether the number of trends is statistically significant. Even so, there are a greater number of negative trends in NTR than skew surge and this may be caused by timing errors or changes in the tide-surge interaction. Timing errors are particular evident in early records that have been digitised from paper charts and are often associated with issues with the older mechanical tide gauges (Pugh and Woodworth, 2014). Therefore, timing errors are more prevalent in the early part of the tide gauge records, and if they are included in the analysis they may introduce a negative bias into the NTR time-series. By definition, time-series of skew surges are not influenced by such timing errors. Another possible reason for the difference in trends is that the magnitude of the tide-surge interaction is changing through time, because of changes in the phase or magnitude of the tide (see Section 4). Previous studies in the North Sea (Horsburgh and Wilson, 2007) and English Channel (Haigh et al., 2010) however, found no significant changes in tide-surge interaction over time. This was not investigated in this study.

Little spatial coherence was observed in the magnitude and sign of the trends among sites, mainly because the trends were insignificant at most sites. However, in northern Australia a number of sites display significant negative trends in skew surge (Figure 5.6) and in NTR, which is consistent with Menéndez and Woodworth (2010), while these findings also support their research showing positive trends at sites in the Gulf of Mexico and along the Atlantic coast of Florida. However, most other findings vary from those of Menéndez and Woodworth (2010). A decrease occurred at sites in southern Europe, and an increase at a number of sites in southern Australia. No coherent trend along the north-east coast of America is observed in this study, which agrees with Zhang et

al. (2000) but contradicts the increase found in this region by both Menéndez and Woodworth (2010) and Grinsted et al. (2012). Differences between this study and those of Menéndez and Woodworth (2010) may be the result of further QC, or the inclusion of new data. New data along the north-east coast of America included large storms surges in 2010 and 2012, generated by Hurricanes Irene and Sandy, respectively. Appendix E, Figures E3.1 to E3.4 show that trends over the last 20-80 years change depending on the period studied, and therefore extra data can vary results. In other studies of ESL, changes may also be caused by the inclusion of tide, such as the increases in New York (Talke et al., 2014), western Northern America (Bromirski et al., 2003; Cayan et al., 2008; Abeysirigunawardena and Walker, 2008) and the German Bight (Mudersbach et al., 2013). In Chapter 4 significant increases in tidal HW were found in all these regions, and this may have contributed towards the increase in ESL found in other studies, and the lack of trends in skew surge identified by this thesis, in these areas. With the growing literature regarding changes in tide (e.g. Jay, 2009; Woodworth, 2010; Pickering et al., 2012; Pelling et al., 2013), and considering the results of Chapter 4, it is essential that studies of the meteorological component use parameters that relate solely to meteorological forcing and not other drivers of change, such as the tide or tide-surge interaction.

The number of statistically significant trends is low, in part, because of the large inter-annual variability in the high percentiles of skew surge. The creation of filtered regional skew surge indices removed the high frequency variability and helped to reveal underlying inter-annual variability and the spatial coherence between regions. However, despite strong correlations between some regions around the North American coastline and across the Atlantic to the North Sea, none of the correlations are significant at the 95% level. Just prior to completing this study a similar investigation by Marcos et al. (2015) showed, using the GESLA dataset, that the intensity and frequency of ESL unrelated to MSL display a regional coherence on decadal time-scales. Their finding points towards large-scale climate drivers of decadal changes in storminess (Marcos et al., 2015). The strong correlations between neighbouring sites show that these large scale climatic drivers are important, but their significance is difficult to assess in short datasets that have a high degree of temporal auto-correlation.

Comparisons of regional storm surge time-series and climate indices have been undertaken in numerous past studies. Menéndez and Woodworth (2010) found the Niño 3 index had a positive correlation with the magnitude of NTR in the eastern Pacific and a negative correlation in the western equatorial Pacific. The magnitude of an El Niño appears to influence the north-east Pacific index, with peaks in the index associated with the largest El Niño events in 1982-83 and 1997-98, but a trough in the index during small but positive values of the Niño 3 index in the early 1990s. Also in the Pacific the PDO was previously shown to correlate positively with sites in the

north-east Pacific (Abeysirigunawardena and Walker, 2008), however this study does not find any significant correlation. The findings of this study relating to the North Sea index support previous studies (e.g. Haigh et al., 2010) that find a positive correlation with the NAO, although the correlation is not significant. Studies by Ezer and Atkinson (2014) and Talke et al. (2014) found anti-correlation between the NAO and sites on the US east coast, but this study finds very weak (and non-significant) positive correlations. The method of using filtered regional skew surge indices, means that although strong correlations ($r > 0.5$) are observed between some regional skew surge indices and climate indices, they are not deemed significant at the 95% level. The effect of autocorrelation in the calculation reduces the degrees of freedom (effective observations) from 40 to less than 8 for all correlation calculations, and therefore increases the size of the confidence intervals. The significance of correlations may improve with increased data length or reduced filter size, however, filters are a widely used and during the development of the methodology the 10 year Loess filter was found to give the lowest RMSE. In this study skew surge time-series have been correlated against climate indices, but it would be more appropriate to use wind and pressure datasets, as these are the parameters that directly cause storm surges. Future work, could repeat this work using meteorological re-analysis datasets, like Bromirski et al. (2003), Calafat et al. (2013) and Wahl and Chambers (2016) did to assess storm surge variability in their regional studies.

One of the main limitations of this study (and other studies) remains the relatively small number of sites and the limited number of storm captured by the length of the time-series available. Although the GESLA dataset is probably the most comprehensive collection of hourly sea level data, there are still many under-represented regions in the database. The 8 regional indices all cover data dense regions since this is where the strongest correlations are, but even here the small number of datasets longer than 40 years limited the length of the regional skew surge indices. The application of the filter, which is necessary to extract relationships between the datasets, meant that the confidence intervals increased and the significance of the correlations decreased. There is a need for either more sites or better access to data in under-represented areas, especially areas that are prone to large storm surges, such as the Caribbean, the Bay of Bengal and countries around the South China Sea. Conversely, the already global nature of the study does not allow for a detailed understanding of the findings presented here. Further work conducted on a local to regional scale, should be undertaken to assess the mechanisms that are driving the tide-surge interaction, and control its specific signature. Such assessment could consider differences in the tide-surge interaction for tropical and extra-tropical storms, the influence of slope angle or shelf width, or the effect of changes in bathymetry.

5.5 Conclusion

This chapter has used time series of skew surge to assess changes in the meteorological component of sea level on a quasi-global scale for the first time. Past studies that have assessed changes in meteorological component have tended to focus on the NTR, which could be biased by contributions from non-meteorological factors. This study also assessed the spatial and temporal variability in the skew surge, using regional indices.

First, the extent of tide-surge interaction was determined, at each of the 220 study sites, as this controls the scale of the differences between skew surge and NTR values. Using χ^2 test statistics statistically significant (95% confidence) levels of tide-surge interaction were found at 130 of the 220 sites (59%) based on tidal-level and 175 sites (81%) based on tidal-phase. The tide-surge interaction is strongest in regions of shallow bathymetry such as the North Sea, north Australia and the Malay Peninsula. However, non-standard distributions were also observed at sites on open ocean islands, although at these sites the peak in NTR often tended towards the time of predicted HW rather than away from it, as experienced in shallow water areas (e.g. North Sea).

Second, it was assessed whether different results were obtained when using skew surges to estimate changes in the meteorological component, compared to the more traditional NTR. At most sites the trends in skew surge were similar to those of NTR. Where the differences in trends were large, the sites tended to have a large tidal range, such as those in northern Australia and northern France. However, at most sites the trends in skew surges were not statistically significant and approximately equal numbers of positive and negative trends were observed. Despite this, there were more negative trends in the NTR. This suggests that using skew surge improves the calculation of trends, because phase offsets caused by timing errors are not present in time series of skew surges.

Third, the extent to which there is spatial coherence in skew surge variability was examined, both locally (i.e. among adjacent tide gauge sites) and regionally (i.e. across ocean basins). Eight regions were identified where strong positive correlations among neighbouring sites allowed the creation of a regional skew surge index. A number of strong correlations ($r > 0.5$) between regions were found, including: positive correlation between the two regions on North American Atlantic coast, positive correlation between the north-west Atlantic – south and the North Sea; and negative correlation between the North Sea and north-east Pacific. However, these trends were not significant at the 95% level, since the high degree of autocorrelation in the filtered dataset increased the size of the confidence intervals.

Finally, inter-annual variations in skew surge were compared with fluctuations in regional climate. Again strong correlations were observed, but they were not significant at the 95% level. Correlations significant at the 80% level included those between the Gulf of Mexico and eastern Australia and the Niño 4 index.

Table 5.1: Details of sites included in each of the regional skew surge indices.

Regional Index Name (and abbreviation)	**Sites Included in Index**
North East Pacific (NEP)	**Canada**: Bella Bella, Port Hardy, Tofino, Campbell River, Point Atkinson, Vancouver, Bamfield, Victoria, Patricia Bay. **USA**: Seattle, Neah Bay.
Gulf of Mexico (GOM)	**USA**: Port Isabel, Galveston, Grand Isle, Pensacola, St. Petersburg, Key West.
North-west Atlantic – South (NWA-S)	**USA**: Fernandina Beach, Mayport, Fort Pulaski, Charleston, Wilmington.
North-west Atlantic – North (NWA-N)	**USA**: Duck Pier, Chesapeake Bay, Baltimore, Lewes, Cape May, Atlantic City, New York (Battery), New London, Montauk, Newport, Boston, Woods Hole, Portland, Nantucket, Eastport.
North Sea (NS)	**Denmark**: Esbjerg. **Netherlands**: Delfzijl, Den Helder. **France**: Calais **UK**: Dover, Sheerness, Lowestoft, Immingham, North Shields, Aberdeen, Wick.
Western Australia (WAUS)	**Australia**: Darwin, Broome, Port Hedland, Carnarvon, Geraldton, Fremantle, Bunbury, Albany, Esperance
Eastern Australia (EAUS)	**Australia:** Wyndham, Thevenard, Port Lincoln, Port Pirie, Port Adelaide, Port Lonsdale, Victor Harbour, Geelong, Williamstown, Burnie, Spring Bay, Fort Denison, Newcastle, Brisbane, Bundaberg, Mackay, Townsville, Cairns.
Japan (JAP)	**Japan:** Nishinoomote, Aburatsu, Kushimoto, Maisaka, Miyakejima, Mera, Ofunato, Hachinohe, Hakodate

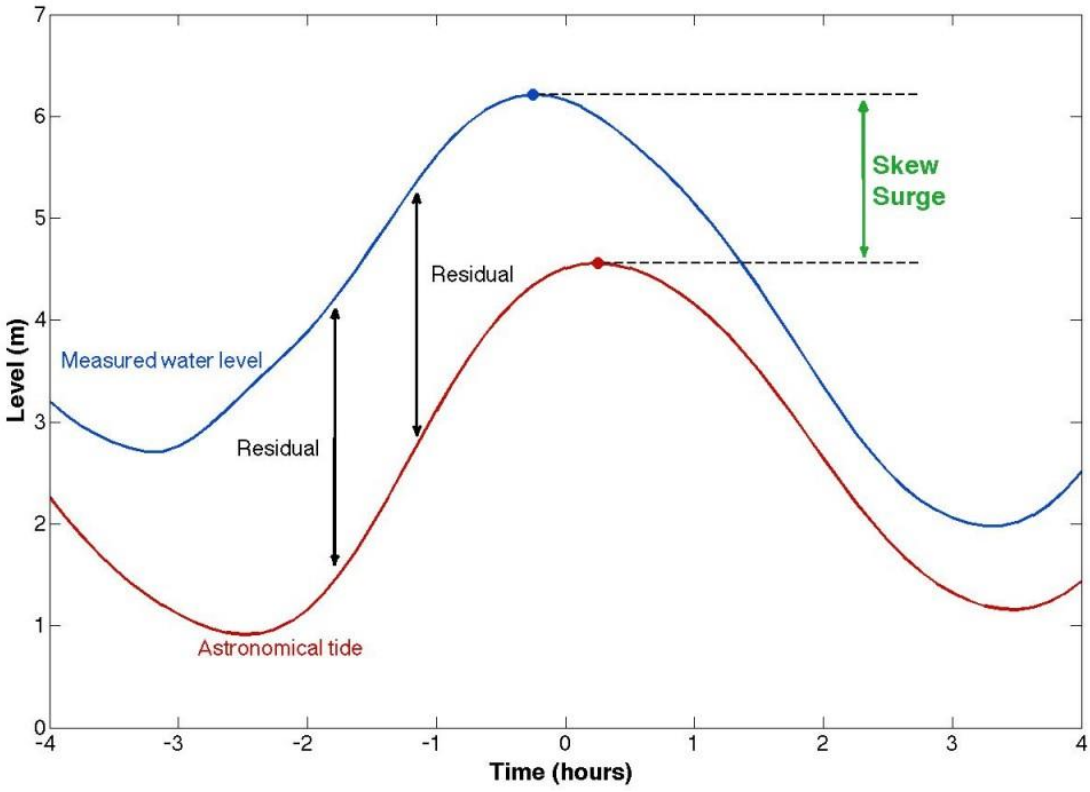

Figure 5.1: Schematic example of a storm surge event and the different calculation methods for the NTR and skew surge.

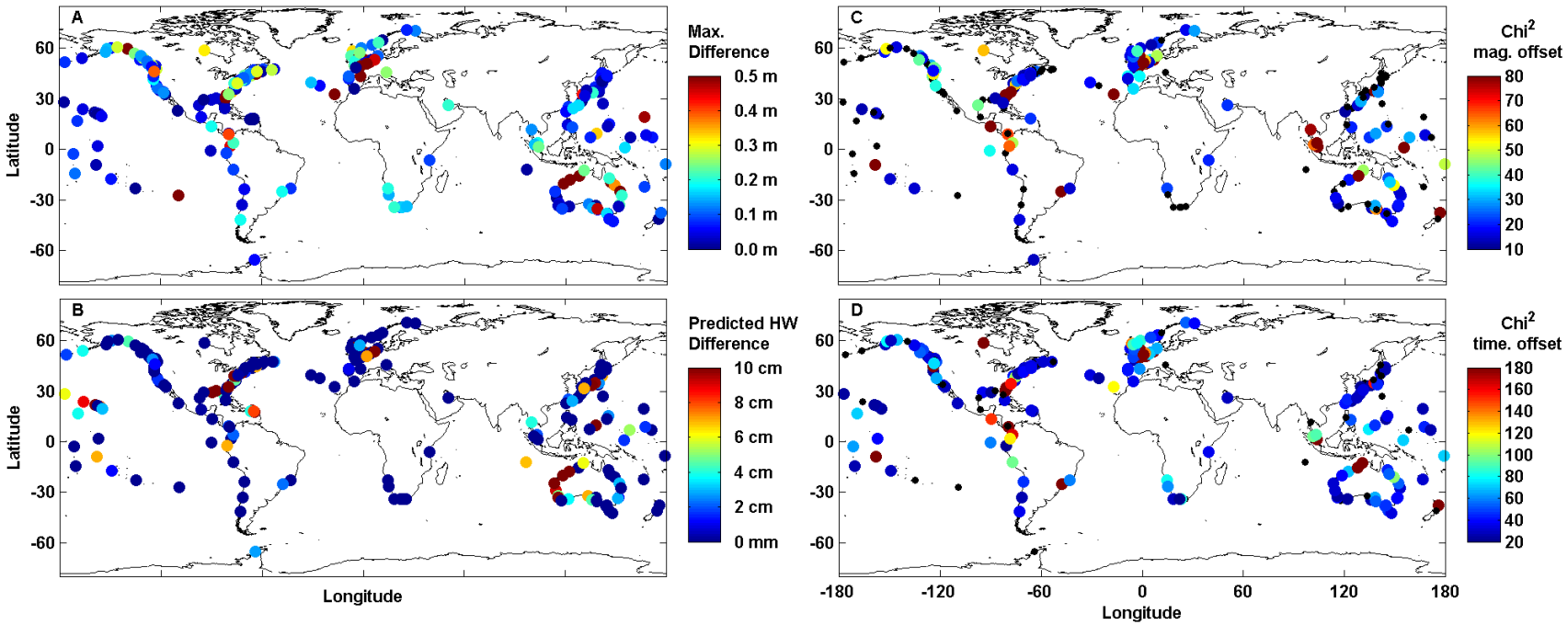

Figure 5.2: Global maps of the 220 selected sites showing: a) difference between the maximum NTR and the maximum skew surge value. b) difference between the maximum skew surge value and the maximum NTR occurring at the same time as predicted HW c) χ^2 values showing magnitude of tide at time of peak NTR for the 200 largest NTR. d) χ^2 values showing time of peak NTR relative to predicted HW for the 200 largest NTR event. Black dots (c-d) show non-significant values in the chi-squared test (based on p-values larger than 0.05).

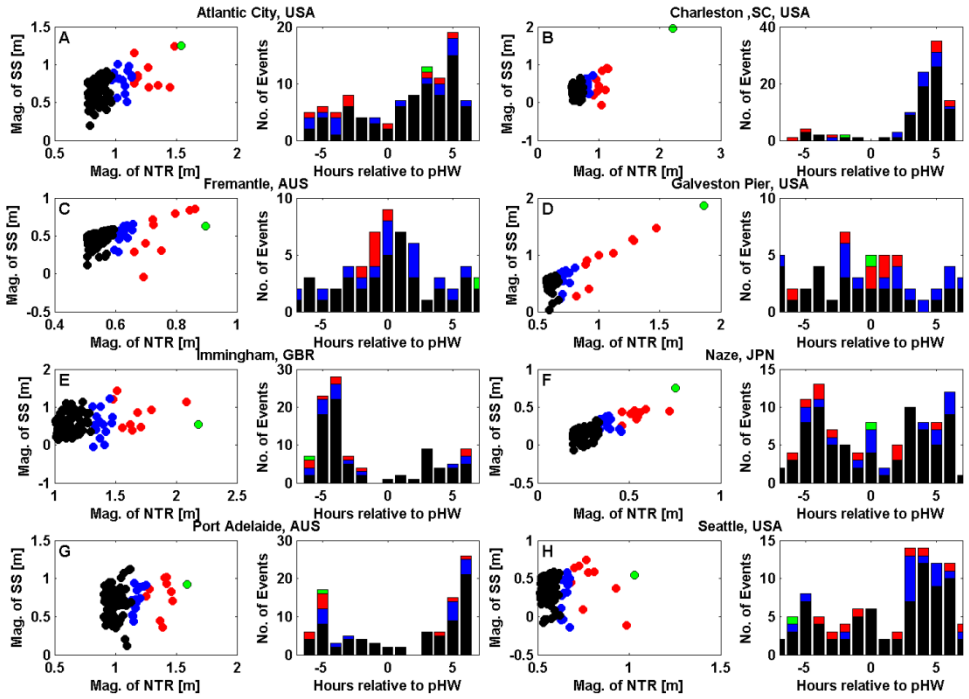

Figure 5.3: For 8 selected sites: a) Atlantic City, USA; b) Charleston, USA; c) Fremantle, Australia; d) Galveston, USA; e) Immingham, UK; f) Naze, Japan; g) Port Adelaide, Australia; h) Seattle, USA. Left, scatter plot of 200 largest NTRs and the associated skew surge value, right histogram of the time of the peak NTR relative to predicted high water. Both plots are coloured according to magnitude with green showing the maximum NTR, red the top 10 NTRs and blue the top 25 NTRs, black are the remainder of the top 200 NTRs.

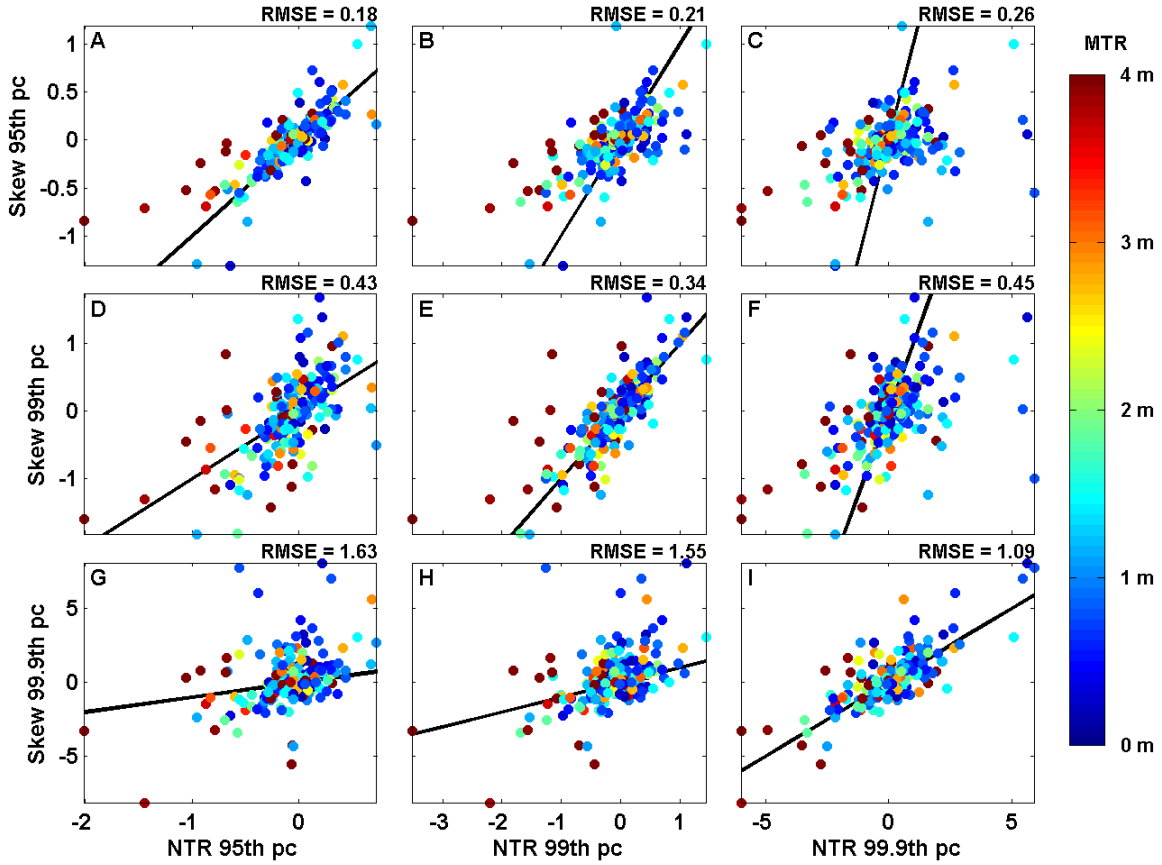

Figure 5.4: Comparison of trends for different percentiles of NTR (on the x-axis) and skew surge (on the y-axis). Each point is shaded according to the average MTR at each site. The black line shows 1:1 ratio. The RMSE value for each plot is the value for the best fit.

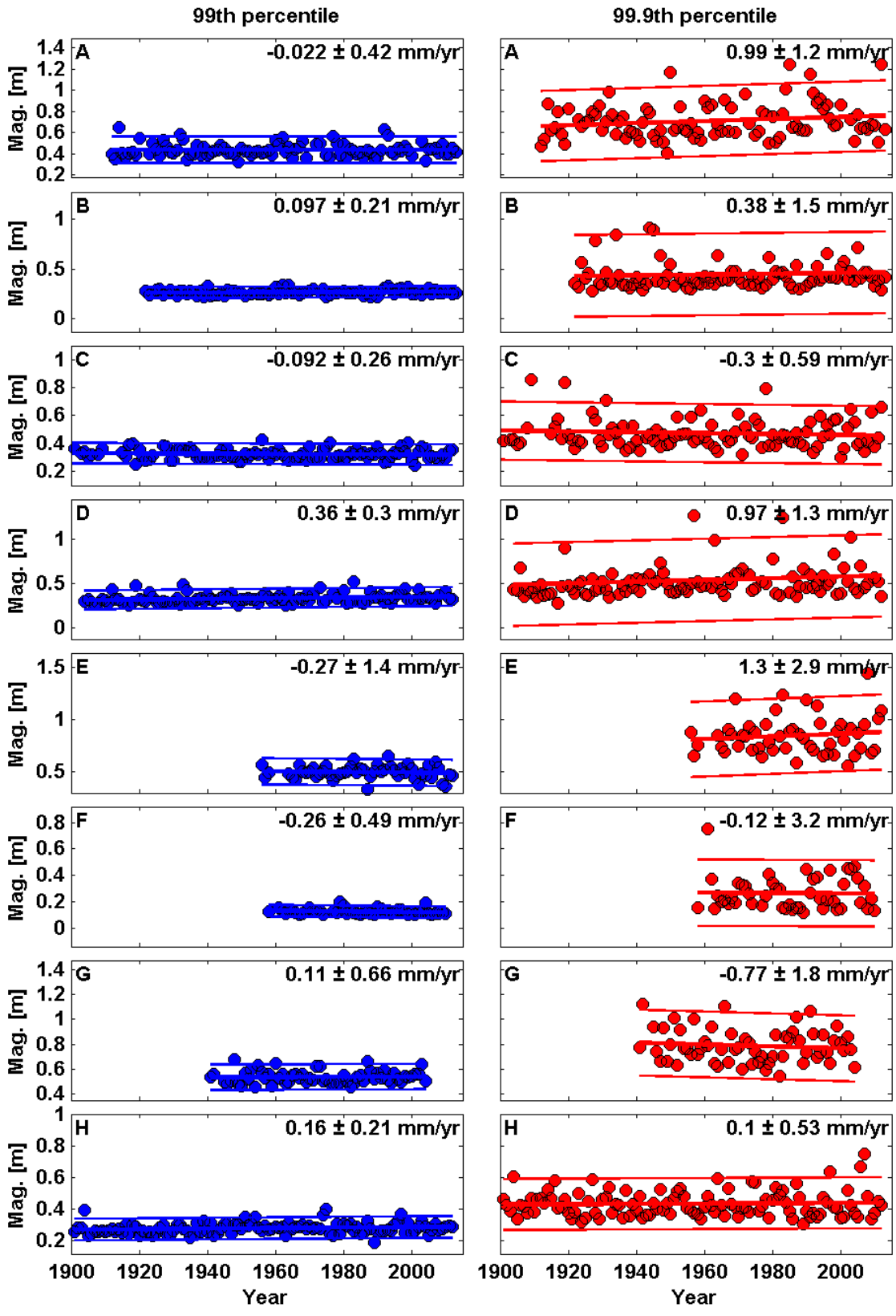

Figure 5.5: Time series plots of annual values of the 99th (blue) and 99.9th (red) percentiles for skew surge at 8 selected sites: a) Atlantic City, USA; b) Charleston, USA; c) Fremantle, Australia; d) Galveston, USA; e) Immingham, UK; f) Naze, Japan; g) Port Adelaide, Australia; h) Seattle, USA.

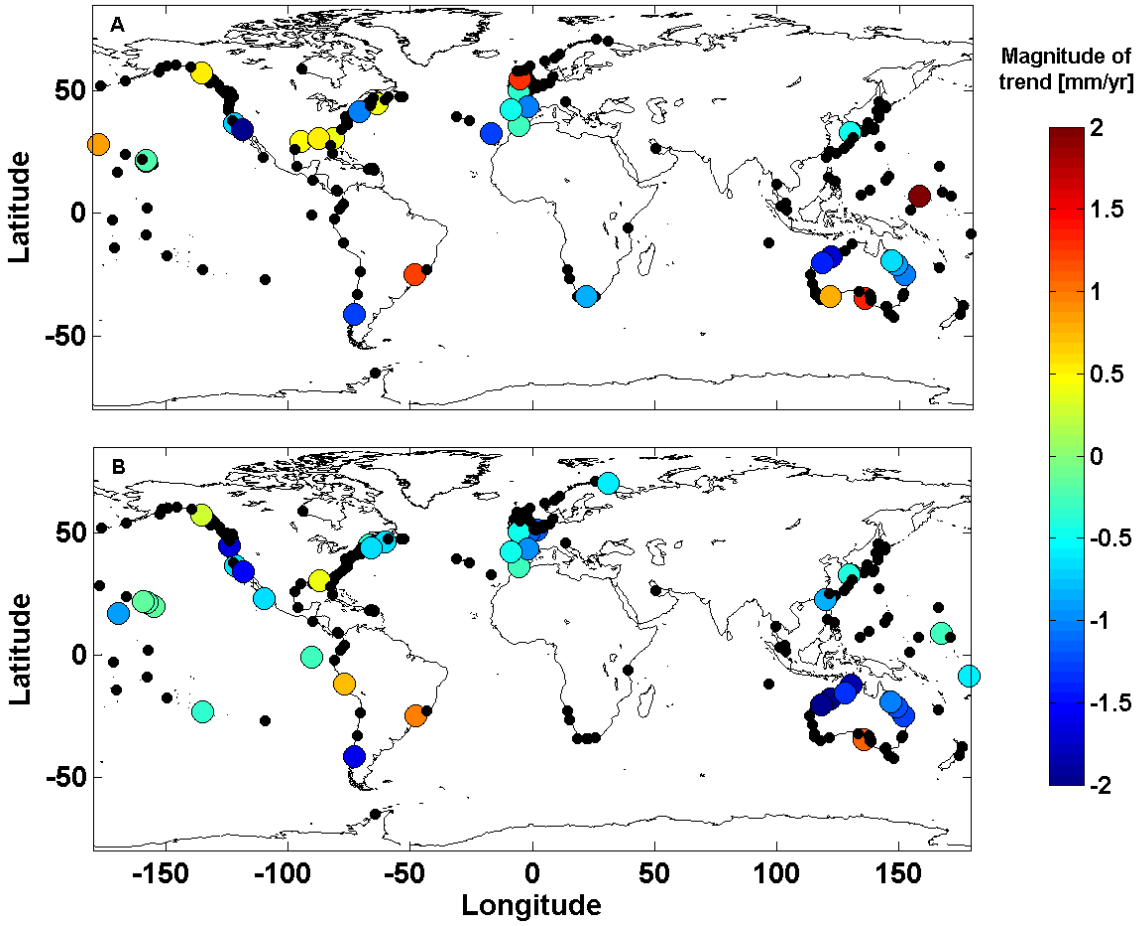

Figure 5.6: Shows the magnitude of the trend in in the 99th percentile of (a) skew surge and (b) NTR, for the 220 sites analysed. Coloured dots show that the trend is significant at the 95% level.

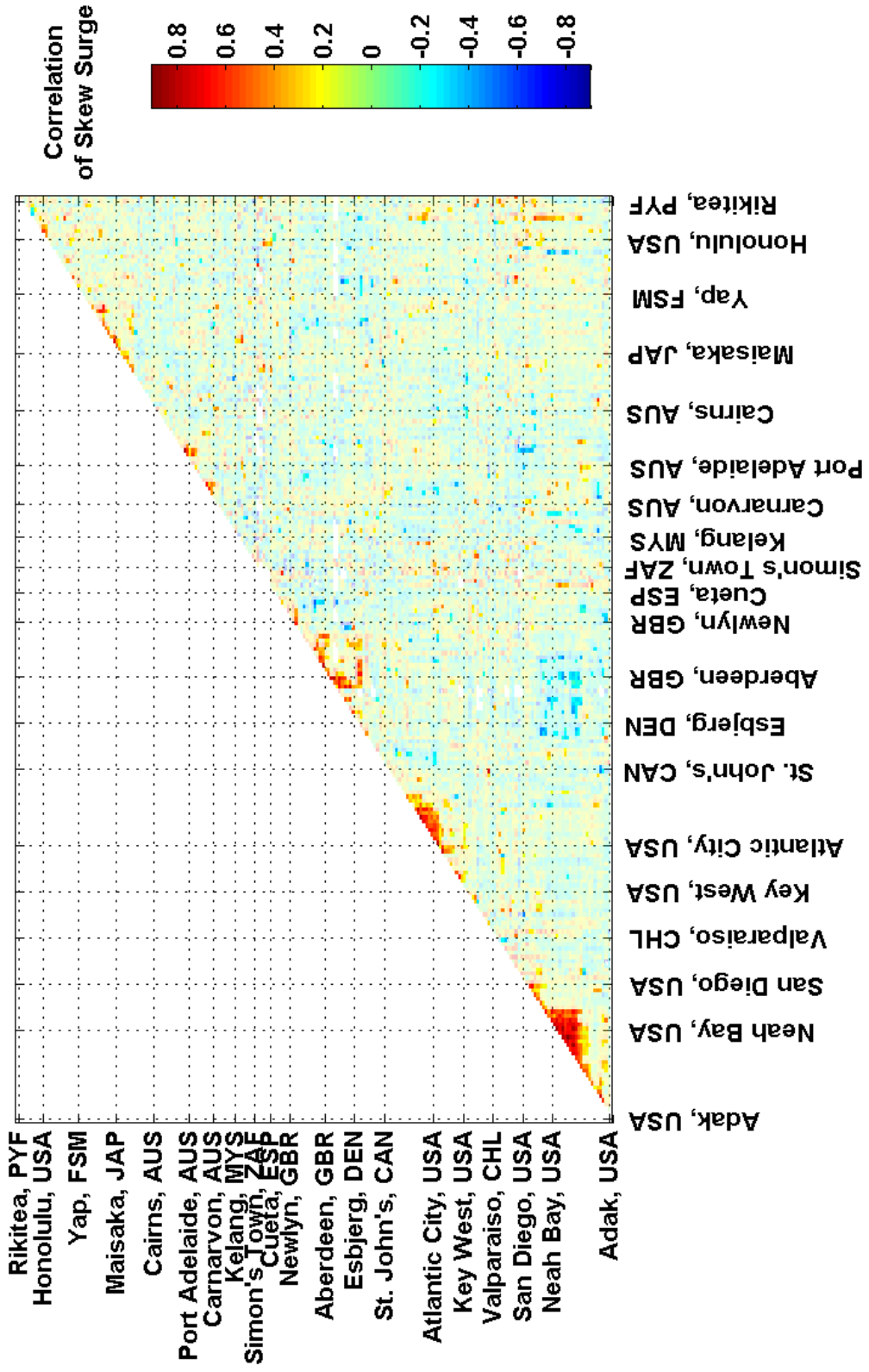

Figure 5.7: Correlation between each site. Each site is plotted along an imaginary coastline running from Alaska down the west and up the east coast of the America, across to the Atlantic to Norway, down through Europe around Africa, around the Indian Ocean, up the western Pacific Ocean and then across the Pacific Islands to the east. Sites with correlations at the 66% level are shown as bold colour.

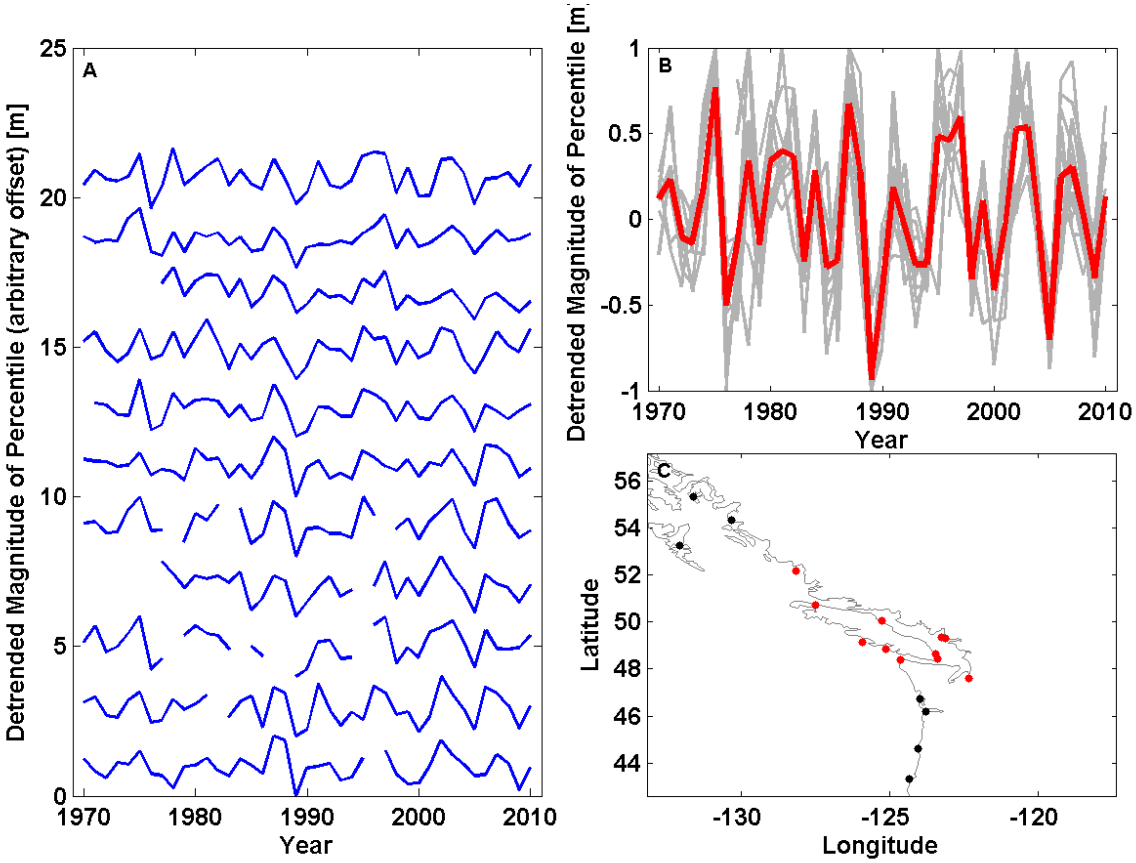

Figure 5.8: Creation of regional skew surge index for the north-east Pacific. A) The de-trended time series of the 99th percentile for each site from north to south (see Table 5.1 for site ID), B) All the time-series with the mean of all sites plotted in red, and C) the sites included in this region highlighted in red.

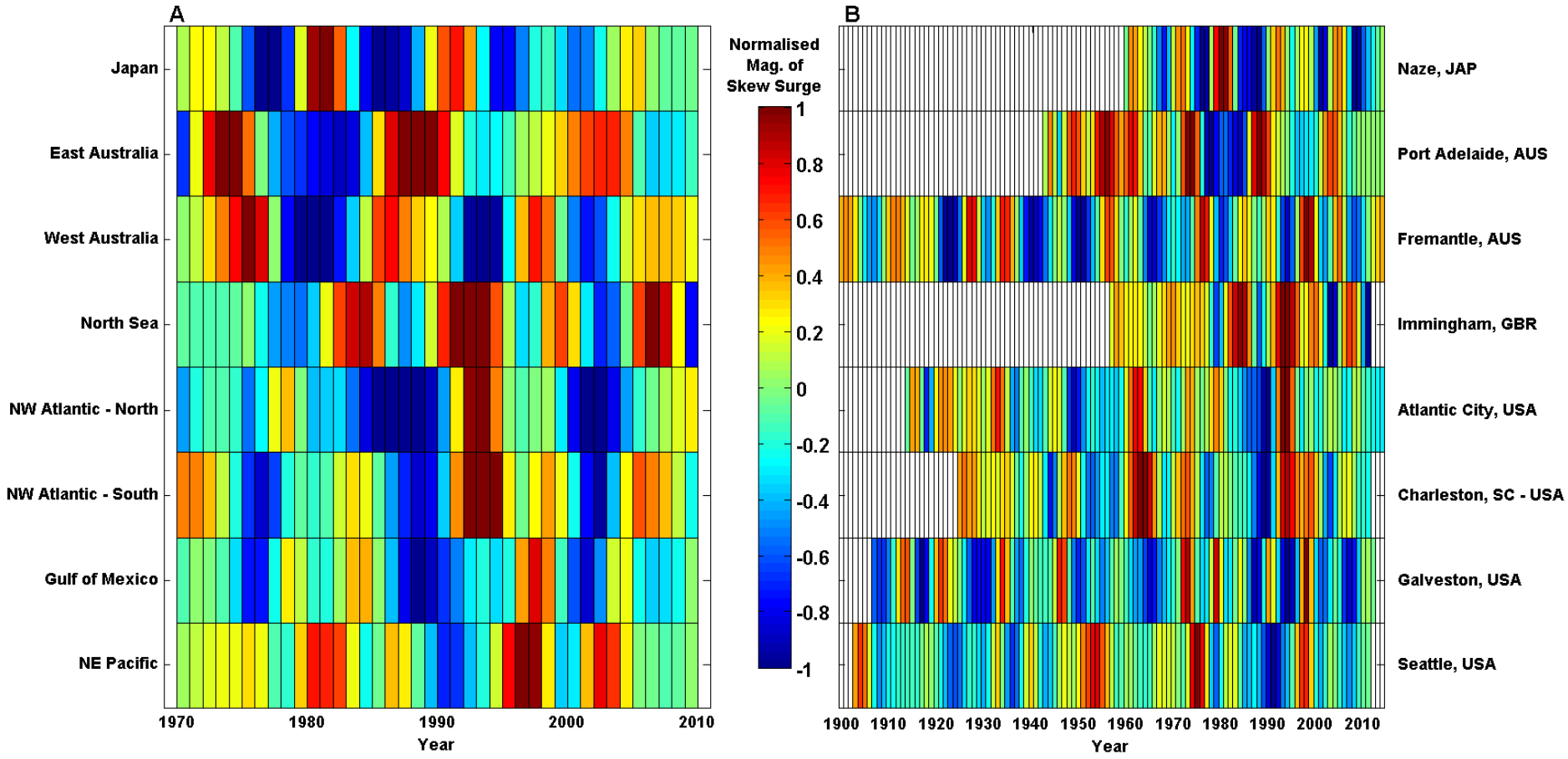

Figure 5.9: Temporal variability of 8 selected regions as shown by the de-trended normalised and then filtered magnitude of skew surge for : A) regional skew surge indices; B) selected long site from each region, which has a strong correlation with the regional skew surge index.

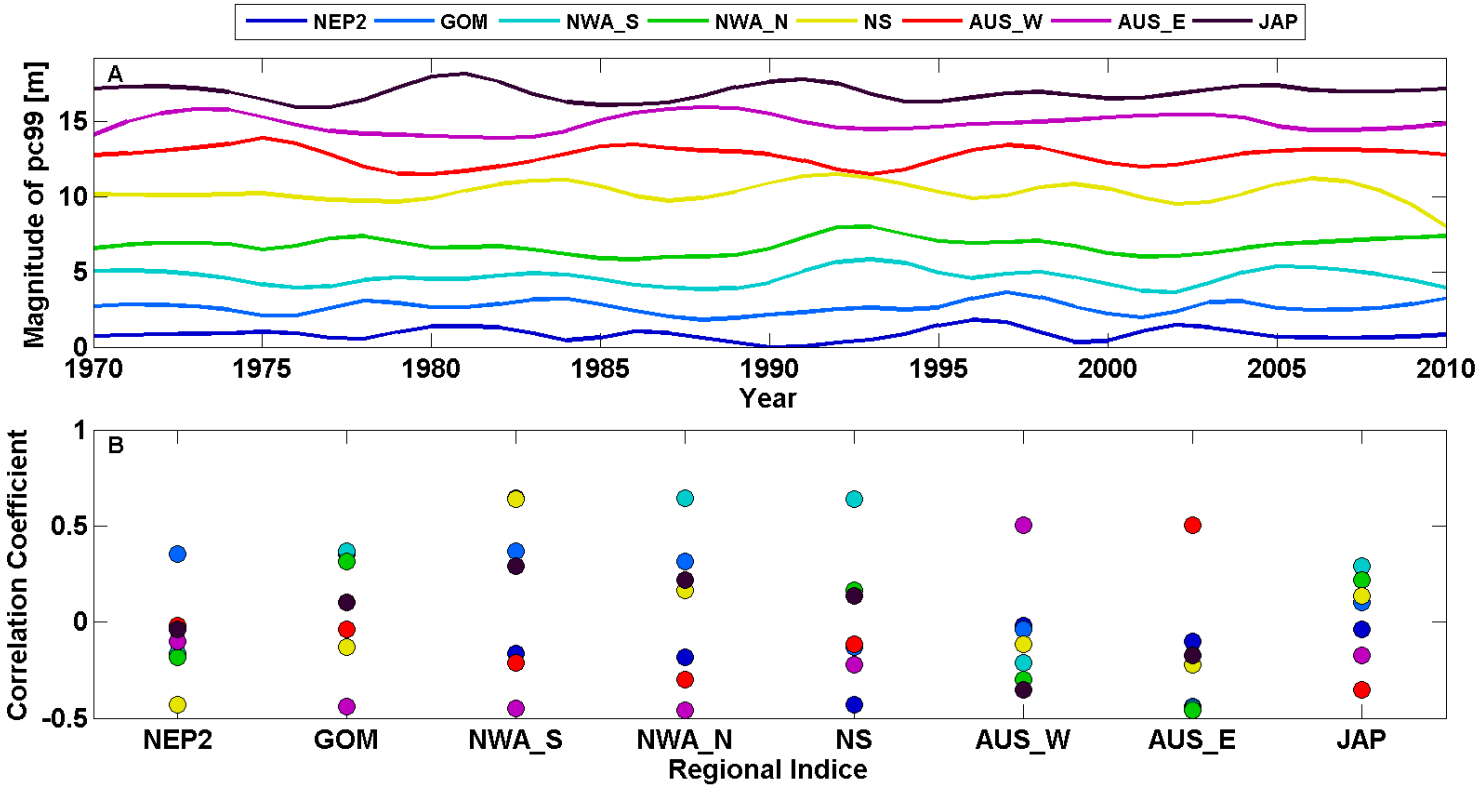

Figure 5.10: a) Stacked time series of filtered regional skew surge indices, with arbitrary offset applied, b) Correlation of each filtered regional skew surge index against the others.

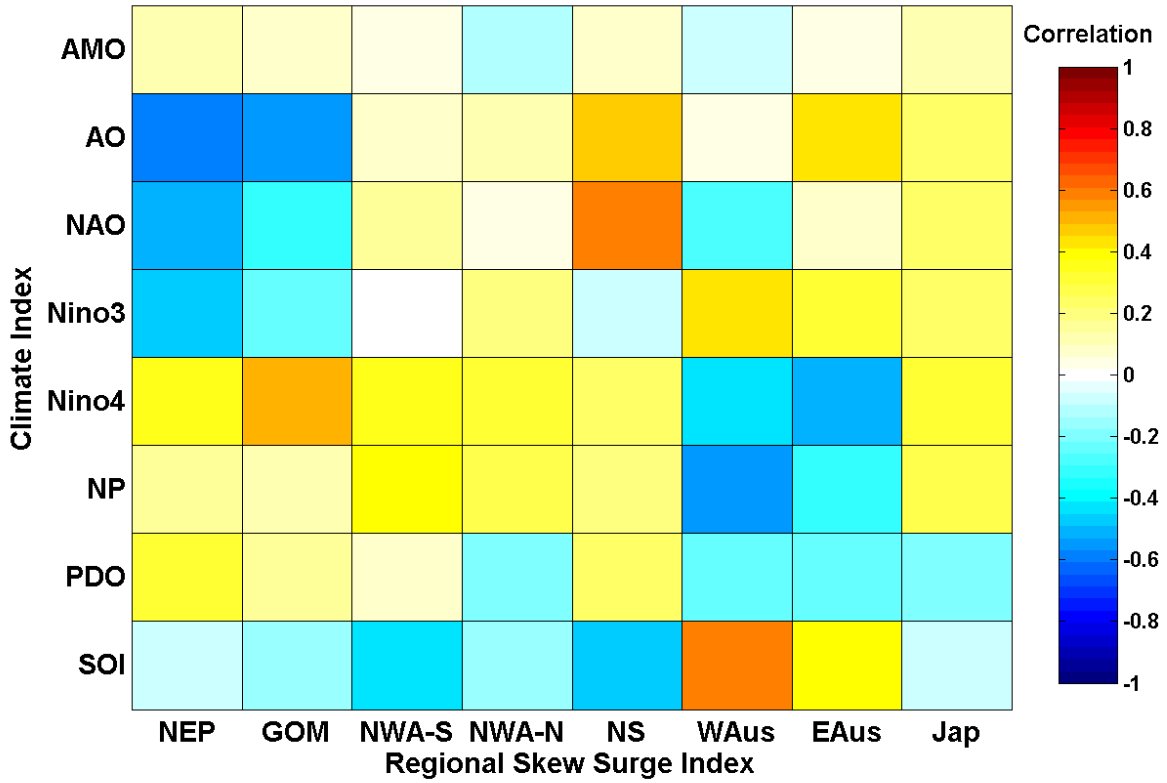

Figure 5.11: Correlation of regional indices of skew surge against key climatic indices.

Chapter 6: Component analysis of extreme sea level

This chapter brings together the findings of the previous two chapters to assess how the magnitude and phase of each sea level component combines to influence ESL. A version of this chapter will shortly be submitted for publication.

6.1 Introduction

High ESL and resulting coastal flooding, are a severe threat to both human life and the billions of dollars' worth of assets along the coastline. The coastal zone is the most densely populated region in the world, containing more than 10% of the global population in 2000 in less than 2% of the world's total land area (Neumann et al., 2015). With the rapid growth of population in coastal regions, shorelines are becoming increasingly developed. This is leading to an increase in the economic impact of ESL despite many improvements in storm surge forecasting and flood protection in recent decades. ESL have a regular and devastating impact on the coastal zone as demonstrated during Cyclone Haiyan in 2013, where over 5,000 people lost their lives (Pugh and Woodworth, 2014), or during Hurricane Katrina, in 2005, where much of the $160 billion of damage was caused by the storm surge (World Bank, 2012). Coastal defences are designed to withstand a storm event with a particular return period (e.g. 1 in 200 years in the United Kingdom), but because the mechanisms that generate ESL are non-stationary, these thresholds need to be reassessed regularly. To estimate them accurately requires a thorough understanding of the variability of ESL on time-scales of hours to centuries.

The previous studies that have assessed changes in ESL, and the individual sea level components that effect ESL, have been described and compared in Section 2. The aim of this chapter is to evaluate how the variability in the tidal and non-tidal components of sea level (Objectives 1 and 2 described in Chapters 4 and 5), together with changes in MSL, influence the seasonal, inter-annual and longer-term changes in ESLs, addressing the issues highlighted in Section 2.6. Note, variability on time scales shorter than six months are not considered here. The intention is to consider the 'baseline' variability (longer than several months) upon which the high frequency variability of individual storm surge events could be considered. The first objective of this chapter is to separate the three main components of sea level (i.e. MSL, tide and meteorological) into seasonal, inter-annual and secular signals, and assess the maximum range and relative importance of each signal. The second objective is to determine the magnitude of the combined variability of all the extracted signals and examine how this varies around the world. The third objective is to assess

the phasing of the seasonal and inter-annual signals to determine if, and when, different signals have acted constructively (i.e. in phase) in the historical records available. Considering findings from these first three objectives, the fourth objective is to estimate a theoretical maximum ESL taking into account the dependence between the signals. The final objective is to estimate the secular trends in ESLs at each site, and to determine at which sites the secular trend in the tidal or meteorological component, is greater than the secular trend in MSL.

6.2 Methodology

For all 220 study sites (shown in Figure 3.2), monthly time-series were derived for each of the three main components of sea level. Parameters were chosen that represented the higher percentiles of each component so that changes that will influence high ESL are captured. The monthly maximum of the 30-day running mean was used so that variations in sea level caused by changes in currents or the passage of eddies are included. For the astronomical tidal component, a monthly mean of MHHW is used to account for peaks in the tide due to the semi-diurnal, diurnal, spring/neap or tropic equatorial cycles. The meteorological component was represented by the monthly maximum skew surge. This parameter has been shown, in Chapter 5, to represent the meteorologically forced variations in sea level better than the NTR (Batstone et al. 2013). At each of the sites, each of the three primary component time-series were then separated into a secondary time-series representing: (i) seasonal; (ii) inter-annual; and (iii) secular, signals.

A seasonal cycle was extracted from each of the three primary components using annual and semi-annual cosine waves and a least squares approach (e.g. Amiruddhin et al., 2015, Feng et al., 2015). This method gives a regular seasonal cycle with a fixed amplitude and phase, hence variability in the magnitude or phase is not captured (Marcos and Tsimplis, 2007; Feng et al., 2015). However, the variability in the seasonal cycle, which may be caused by regional climate, is included in the inter-annual cycle. As described in Section 3, some energy from the seasonal cycle in skew surge may be captured by the MSL seasonal cycle, although the effect of this is expected to be small.

To extract the inter-annual signal for the tide, two fixed phase and amplitude cosine waves were fitted to the records, with periods of 18.61 years and 4.425 years to represent the nodal and perigean cycles (Haigh et al., 2011). Unlike the tidal component, the inter-annual variability in the MSL and skew surge time-series is irregular, because they are predominantly controlled by stochastic macro-scale climate variability (Menéndez and Woodworth, 2010). To extract the inter-annual signals for the MSL and skew surge time-series, a locally regressed least squares (Loess)

filter was used (Cleveland and Devlin, 1988), which through testing gave the lowest standard error. This non-parametric method combined a multiple regression model with a nearest-neighbour model. Each point of the loess curve was fitted to the points using local regression, using a 2nd degree polynomial to the points within a 36-month window centred on that point. Testing showed that the 36-month window was suitable since it was not influenced by the seasonal cycle. However, it smoothed the data to allow the inter-annual signal to be better observed, and captured a larger degree of variability compared with using larger window lengths.

The magnitude of the inter-annual signals in MSL and skew surge, were largely influenced by subjective choices in the creation of the filter. As such, the length of the averaging window had a large influence on the magnitude, as well as the method used to fill gaps in the data. Gaps in the data were filled to make the time-series continuous, a requirement necessary to apply the filter. The gaps were filled with zeros, which reduced the amplitude of the signal near the gaps, but was deemed preferable to the unrealistically high values introduced if an interpolation routine was used to fill the gaps. The selected method meant that where records contained many gaps, the filtered time series tended towards a flat-line. At seven sites (Calais, France, Fernandina Beach, USA, Harwich, UK, Mossel Bay, South Africa, Tumaco, Colombia, Veracruz, Mexico and Walvis Bay, Namibia) the inter-annual variability was zero because of this, and these were removed from further analysis. One further site, Miyakejima in Japan, was removed from the analysis because land subsidence caused by a volcanic eruption in 2000 created an erroneously large inter-annual and secular signals in MSL.

For the seasonal and inter-annual signals, the magnitude is represented by the maximum to minimum range of values from each time-series. The magnitudes of secular trends were calculated for each of the three component time-series using linear regression, and are quoted with 95% confidence intervals (i.e. approximately two standard errors). Standard errors were estimated using a Lag-1 autocorrelation function to allow for any serial autocorrelation in the time-series (Box et al., 1994). In this chapter, the term ‘significant trend’, signifies that the trend was statistically (at 95% confidence) different from zero, unless otherwise specified. Changes due to secular trends in each component are calculated over 100-years so that they give an estimate of the centennial scale variability. This method assumes that a linear trend is appropriate for representing the secular rate of change.

In total 10 signals were extracted for each site; three seasonal signals (one for each of the main sea level components); four inter-annual components (two for tide), and three secular linear trend estimates (one for each of the main sea level components). Figure 6.1a shows a combined time-series for Seattle, USA, calculated by adding the 10 extract signals (black) shown in Figure 6.1b against the monthly maximum sea level. This demonstrates how much of the total

variability in sea level is represented by the extracted signals. For Seattle the comparison is good, but at other sites, particularly those affected by tropical storms the captured variability is lower. Examples of this are presented for five further sites in Appendix F. Each of the 10 extracted time-series are plotted in Figure 6.1b, with from bottom to top: the three secular (linear), the four inter-annual, and the three seasonal signals. The magnitude listed next to each signal is the range (from maximum to minimum value in the time-series of each signal) calculated over the whole length of data at that site. Figure 6.1c shows the seasonal cycles for one year for MSL, tide and skew surge, and the combined cycle (the sum of the three seasonal cycles). Figure 6.1d shows the inter-annual signals over the length of the data at that site for MSL, nodal tide, perigean tide and skew surge, and the combined signal (the sum of the four inter-annual signals). The maximum values of each seasonal and inter-annual time-series are shown as coloured dots.

Finally, the magnitudes of the 10 extracted signals were used to calculate the largest 'theoretical' ESL that could occur, at each of the sites, if the peaks in independent signals occurred simultaneously in a given year. The inter-annual nodal and perigean cycles in the tide ($MHHW_n$ and $MHHW_p$) are not dependent on any of the other signals, but the other signals are often interdependent because the same oceanographic or atmospheric forcing drives them. Therefore, dependence was assumed between the three seasonal cycles (MSL_s , $MHHW_s$ and SS_s), the three secular trends (MSL_l, $MHHW_l$ and SS_l) and the inter-annual signals of MSL and skew surge (MSL_{ia} and SS_{ia}). Dependence between seasonal cycles was accounted for by adding the three seasonal cycles over a year and calculating the maximum from that combined seasonal cycle. This insures the relative phases of the three seasonal signals are taken into account. This was repeated for other dependencies as detailed in Equation 6.1:

$$Theoretical\ Max. = \max(MSL_s + MHHW_s + SS_s) + \max(MSL_{ia} + SS_{ia}) + \max(MHHW_n) + \max(MHHW_p) + \max(MSL_l + MHHW_l + SS_l) \qquad \text{Eq. 6.1}$$

6.3 Results

6.3.1 Global variation in the magnitude of sea level components

The first objective is to assess the magnitude (i.e. range) of each of the 10 signals and examine the spatial variability. The maximum range in the three seasonal signals is shown in Figure 6.2. Seasonal cycles in MSL are greatest in the SCS and East China Sea, with large values also around

the North Sea, along the Pacific coast of Alaska and Canada, the Atlantic coast of Florida and northern Australia (Figure 6.2a). However, some regions with large seasonal MSL cycle are not represented in the study. The seasonal signal in the tide is typically small at most sites, but large cycles do occur at sites with larger tidal ranges, such as north-west Australia and around Vancouver Island, Canada (Figure 6.2b). The seasonal cycle in skew surge is largest in the southern North Sea, but with a large signal also observed along the US east coast north of Chesapeake Bay (Figure 6.2c).

The maximum range in the four inter-annual signals is shown in Figure 6.3. Inter-annual variability in MSL is largest on both sides of the equatorial Pacific, but is also large in the Great Australian Bight and around Vancouver Island, Canada (Figure 6.3a). The largest magnitude of the nodal cycle in the tide is seen in Malaysia and at sites in the southern United Kingdom (Figure 6.3b). The perigean cycle is two orders of magnitude smaller than the nodal and has its largest magnitude in north-east Australia, and at Malin Head, Ireland (Figure 6.3c). The inter-annual signal in skew surge is largest in the southern North Sea, the Great Australian Bight and the US east coast between Cape Hatteras and New York (Figure 6.3d).

The linear trends in each of the three components are shown in Figure 6.4, scaled up to 100 years for comparison. Secular changes in MSL are greatest in the Gulf of Mexico and Philippines (although these findings may be confined to the specific tide gauge locations), with typically large values along the east coast of North America and in the western Pacific (Figure 6.4a). The largest secular changes in the tide are observed in the southern North Sea and at other select sites (Figure 6.4b). The nature of variations in the tide means that changes are observed at local as well as regional scales. Secular changes in skew surge are generally small (Figure 6.4c). Where large changes are observed (as discussed in Chapter 5) they are often generated by individual large storms, such as Hurricane Katrina for Grand Isle, USA, however, a consistent positive trend in skew surge is observed in the North Sea (Figure 6.4c).

The spatial distribution of magnitudes for each extracted cycle across the 212 study sites, are presented as boxplots in Figure 6.5. Each red line on Figure 6.5 marks the median magnitude of each of the 10 signals. The ends of the box represent the 25^{th} and 75^{th} percentiles, the feathers show the range from the 2.5^{th} to the 97.5^{th} percentiles and the red crosses show the outliers beyond that range. The largest median value of any signal, across the study sites, is 0.19 m in secular MSL (scaled up to a 100-year period). The median variability of seasonal MSL, inter-annual MSL and seasonal skew surge are of the same order of magnitude (0.15 m, 0.18 m and 0.11 m respectively). The largest variability of any signal at any site is 1.57 m, which occurs in the secular MSL, at Manilla in the Philippines. The maximum values show that, in addition to the cycles mentioned above, signals in the seasonal tide, nodal tide, secular tide, inter-annual skew surge

and secular skew surge, all exceed 0.2 m at some sites (Figure 6.5). However, median values of the variability in perigean tide, nodal tide, secular tide and secular skew surge, across the 212 study sites, are all less than 0.04 m.

6.3.2 Magnitude of the combined variability in ESL

Having assessed the magnitude of the 10 signals individually across the study sites, the second objective was to determine how the combined magnitude of the 10 extracted signals varied around the world. The combined variability was calculated as the sum of the absolute magnitude of all 10 signals. Therefore, negative secular trends are plotted as having a positive contribution to the combined range of the variability. The calculation of the magnitude for each signal was described in Section 6.2. Stacked bar charts of the combined variability of each signal are presented in Figure 6.6, for five data dense region, namely: (a) the Pacific coast of USA and Canada; (b) the Gulf of Mexico and Atlantic coast of USA and Canada; (c) Europe; (d) Australia; and (e) Japan.

The magnitude of combined variability is typically between 0.8 and 1.5 m, along the Pacific coast from Alaska to northern California (Figure 6.6a). However, three sites in Alaska (Kodiak Island, Seldovia and Yakutat) have variability in the secular MSL signal of approximately 1 m, due to the negative trend generated by GIA. Large contributions throughout this region also come from the seasonal and inter-annual signals in MSL, while on the eastern coast of Vancouver Island the seasonal cycle of the tide is large. South of San Francisco the combined variability decreases to below 1 m, because the magnitude of the seasonal and inter-annual signals of both MSL and skew surge decrease (Figure 6.6a).

Through the Gulf of Mexico and along the Atlantic coast of the USA and Canada the combined variability ranges from 0.7 to 1.5 m (Figure 6.6b). Secular increases in MSL are large along the Texas and Louisiana coasts, but there is also a large contribution from the seasonal and inter-annual variability in MSL throughout the Gulf of Mexico and along the US east coast to Wilmington. In Wilmington, there is also a large contribution from the secular tidal signal. North of Wilmington there is a gradual shift of dominance from MSL to skew surge variability, so that north of New York the seasonal and inter-annual contribution is larger in skew surge than MSL. (Figure 6.6b). The nodal and secular tidal signals in the Bay of Fundy both have a magnitude of approximately 0.1 m and are therefore an important contributor to the total variability at Eastport, USA and Saint John, Canada.

The largest combined variability of any site is 2.4 m at Delfzijl, Netherlands (Figure 6.6c). The seasonal and inter-annual signals of skew surge dominate in the whole of the North Sea. The

combined variability of the west coast of the UK ranges from 1.2 to 1.7 m, and has contributions from the seasonal and nodal tide of up to 0.2 m in the Irish Sea and Bristol Channel. At sites in the Bristol Channel, seasonal and inter-annual variability is approximately equal in range for the three components, because of these large signals in the tide. The combined variability for Norway, the English Channel and the Iberian Peninsula ranges from 0.7 to 1.1 m, but reduces to 0.5 m for Cueta, on the African side of the Straits of Gibraltar.

There are considerable differences in the combined variability around the coast of Australia (Figure 6.6d), with two areas exhibiting large combined variability. In the north the combined variability ranges from 1.2 to 1.7 m, with large contributions from seasonal, inter-annual and secular variability in MSL, and from the seasonal tidal signal, which is 0.4 m in Broome. The large combined variability in the Great Australian Bight, with a typical range of 1.2 to 1.3 m, has a large contribution from the seasonal and inter-annual signals in both MSL and skew surge. The combined variability from Geelong to Cairns is typically smaller, between 0.5 and 0.9 m, but a large secular MSL signal increases the combined variability at Brisbane. Very small seasonal and inter-annual skew surge signals are observed along this coastline, despite the regular occurrence of tropical cyclones from Brisbane to Cairns.

At sites around Japan, the combined variability is small, ranging from 0.5 to 1.3 m. The variance between sites is primarily controlled by variations in the secular MSL signal, while the seasonal cycle of MSL dominates variability on other timescales at all sites (Figure 6.6e). The seasonal MSL cycle is largest at sites around southern Japan (south of 36°N), on both the Pacific and Sea of Japan coasts. The skew surge and tidal signals are consistently small across all sites. Note, the order of the sites in Figure 6.6e runs along the Pacific coast of Japan to northern island of Hokkaido, before moving through sites in the Sea of Japan.

6.3.3 Relative phases of seasonal and inter-annual signals of sea level components

The third objective is to assess the phasing of the seasonal and inter-annual signals and determine where and when they acted constructively (i.e. in phase). The method of estimating the seasonal cycle means that the phases of the three seasonal cycles are fixed relative to each other, with the peak occurring at the same time every year. The phases of the seasonal cycles of MSL, tide and skew surge are compared in Figure 6.7. The location of each site is represented by a circle, which is divided into three segments to show the percentage of the combined seasonal cycle that is attributed to MSL (the segment starting from 00:00 going anti-clockwise), skew surge (the segment starting from 00:00 and going clockwise), and tide (the segment in between). The colour

of each segment represents the month in which the peak of each seasonal cycle occurs. For example, a circle with three equal segments all coloured blue, would indicate that each component has a seasonal cycle with the same magnitude that peaks in September.

Results in Figure 6.7 show a clear differentiation between the northern and southern hemispheres, mostly attributed to the timing of the peaks in MSL. Along the Pacific coast of Alaska and Canada, the peaks in MSL and skew surge occur between November and January. The peaks in MSL and skew surge along the Atlantic coast of North America north of Chesapeake Bay (Figure 6.8a) and around Europe (Figure 6.8b) also occur at this time. Around Japan the peak in MSL occurs in August and September (Figure 6.8c), while the peak in skew surge occurs between August and November, at most sites. In the southern hemisphere, the peaks in MSL generally occur between March and June, but the timing of the peak in skew surge is more variable. Around northern Australia, the peak occurs in January to February, while for the rest of the coast the peak occurs from June to August (Figure 6.8d). At most other sites in the southern hemisphere, the peak occurs from June to August as well. Concurrent peaks in seasonal cycles therefore occur in the north-west Pacific, around Japan and at some sites along the Canadian Atlantic coast, in the North Sea and along the south Australian coast (Figure 6.7a).

A similar analysis for the inter-annual signals is shown in Figure 6.9a-d, for the same four regions. Here, however, the colour relates to the year in which the peak in the inter-annual signal occurs. Peaks in the tidal inter-annual signal are repeated and the colour relates to the first occurrence. At the majority of sites MSL dominates the inter-annual signal, including at nearly all sites along the North American coast, sites around Australia (except in the Great Australia Bight), around Japan, sites in the Pacific and around southern Africa. North-west Europe is the only region where the inter-annual signals of the skew surge (southern North Sea) and tide (Bristol Channel) are larger than MSL.

The longer the time series the lower the probability of concurrent peaks in the inter-annual cycles. In some regions, the peak in the inter-annual MSL signal occurred simultaneously at a number of neighbouring sites. At sites along the Pacific coast of North America, the peaks in the inter-annual MSL signal occurred either in 1982 or 1997, and coincide with large El Niño events (Figure 6.9a). In the western Pacific, from Taiwan to the Kyushu Island, Japan, the peak at many sites occurred in 1998, which coincides with a large La Nina event (Figure 6.9d). Around Australia, the timing of peaks is more variable, but in the north-west a number of sites peaked in 2011, while in the south most sites had a peak between 1995 and 1999 (Figure 6.9c). Around the UK, there is a split between the North and South, with peaks in Scotland occurring in 1989, while the peaks around most of England and Wales occurred in 2005-2006 (Figure 6.9b).

Comparing the timing of peaks in inter-annual signals requires that all sites plotted have data for the periods plotted. Figures 6.9a-d plot data for the common period from 1980 to 2013, but at some sites longer periods can be compared. Therefore, Figure 6.10a and 6.10b show this analysis for sites in North America for the periods 1920-2013 and 1950-2013, respectively. At sites along the Pacific coast of Canada and America, the peaks in MSL still occurred in either 1982 or 1997, even for data back to 1920. Unfortunately, due to sparsity of long data sets outside of North America it is not possible to describe regional patterns over these longer periods in other parts of the world. However, at the few sites in north-west Europe and Australia that do extend back to 1950, there is not the same consistency in the peak year, suggesting that the period 1980-2013 was not exceptional at these locations.

6.3.4 Theoretical maximum variability in ESL

The fourth objective was to estimate a theoretical maximum ESL, taking into account the dependence between signals. If assumptions about independence are correct in Equation 6.1 then the observed maximum ESL should not be larger than the theoretical maximum ESL at all sites, and Figure 6.11 shows this to be the case. Most sites have a ratio of observed to theoretical maximum ESL between 1:1 (equal) and 1:2 (observed maximum is half the theoretical maximum). Only at the following sites was the theoretical maximum ESL more than double the observed maximum ESL: St. Petersburg, Port Isabel and Fort Pulaski, in Florida and Georgia, USA; Simon's Town in South Africa, Luderitz in Namibia, Legaspi in Philippines; Rikitea in French Polynesia; Funchal in Madeira; Hachinohe, Hakodate and Hamada in Japan; and Ilfracombe and Milford Haven in The UK.

Figure 6.11a-g shows how the magnitude of individual signals in the 7 largest signals (the seasonal, inter-annual and secular signal in MSL, the seasonal and nodal cycles in tide and the seasonal and inter-annual signals in skew surge), affect the ratio of observed to theoretical maximum ESL. The seasonal cycle in MSL increases the difference between the theoretical and observed maxima (Figure 6.11b), while large seasonal and inter-annual signals increase the magnitude of both maxima (Figure 6.11f and 6.11g). There were three main reasons for the large difference found between the maximum observed and theoretical ESLs. The peak in the inter-annual MSL and/or skew surge occurred during a trough in tidal nodal cycle or early in a dataset when the secular MSL signal peaks in the present day. Alternatively, the peak in the observed value coincided with a trough in the seasonal cycle.

6.3.5 Magnitude of change in ESL

The final objective is to calculate the magnitude of the secular change in ESL at each site. The linear trends in the 99th percentile of sea level (which is widely used as a proxy for high ESL) are shown in Figure 6.12a for each of the 220 sites. ESLs are increasing at most sites, in agreement with previous studies (e.g. Menéndez and Woodworth, 2010). The magnitude of the trend varies between -12.9 ± 1.3 mm/yr in Churchill, Canada and 16.4 ± 8.7 mm/yr in Manilla, Philippines. However, the majority of trends across the sites are close to the mean and median values of 2.0 and 2.1 mm/yr respectively, which closely corresponds with the 1.7 mm/yr global MSL rise observed over the 20th century (Church et al., 2013). The secular trends presented in Figure 6.12a match closely the regional signal of global MSL rise presented in Figure 6.4a, but at some locations the magnitude of the trend is different. For example at Manilla and Churchill, the change also has a contribution from land subsidence and GIA, respectively.

Significant trends exist in the tidal and meteorological components at some sites, as shown in Chapters 4 and 5, respectively. However, as Figure 6.12b shows that the component with the largest secular trend is predominantly MSL. The largest significant trend of any component occurs in: MSL for 61% of sites, MHHW for 10% of sites, the 99th percentile of skew surge for 5% of sites, while at the remaining 54 sites no component has a significant trend. At all sites where MHHW or skew surge has the largest significant trend, the trend in MSL is not significant. However, of these sites the trend in MHHW is larger than that of MSL at: Astoria (USA); Calais (France); Christmas Island (Kiribati); Heimsjoe (Norway); Heysham and Immingham (UK); Newcastle (Australia); and Queen Charlotte City and Vancouver (Canada). The sites where the trend in the 99th percentile of skew surge is large than that of MSL, include: Easter Island (Chile); Mackay (Australia); and Santa Monica (USA).

6.4 Discussion

ESLs are by definition rare events and therefore their prediction in a non-stationary environment is difficult on timescales of years to decades. This chapter looked at variability in the main components of sea level on time scales greater than six months, and assessed the baseline conditions of ESL, upon which high frequency variability, associated with individual events, adds.

This study supports previous findings that secular trends in high ESL, have increased at most sites around the world during the 20th century (Woodworth and Blackman, 2004; Menéndez and Woodworth, 2010). On secular time scales, the rise in global MSL is driving changes in ESL (e.g.

Menéndez and Woodworth, 2010), and at most sites secular trends in tidal levels or skew surge are smaller in comparison (Figure 6.4). However, the largest trends in tidal levels, as shown in Chapter 4 are of the same order of magnitude, and should therefore be considered in ESL projections. For example, secular changes in tidal levels are not included in the assessment of ESL around the UK coast at present (McMillan et al., 2011).

Most variability of baseline ESL (on time scales longer than 6 months) occurs in the MSL signals on seasonal, inter-annual and secular timescales. However, the median values of seasonal and inter-annual signals in skew surge are of the same order of magnitude, and the maximum values in all the signals except the perigean tide, exceed 0.2 m across the study sites.

The magnitude of the variability on seasonal and inter-annual scales means that assessing the phase and magnitude of these is clearly important. A number of studies have analysed seasonal cycles in sea level components. This study presents a combined seasonal cycle (annual plus semi-annual signals), and therefore comparisons against the peak in the annual MSL cycle, used in some previous studies, may show differences of 1-2 months, such as in northern Japan (Tsimplis and Woodworth, 1994; Feng et al., 2015). However, the timing of peaks in seasonal MSL cycle in this study generally compare well to previous research, both globally at most sites (Tsimplis and Woodworth, 1994), and regionally for Australia (Haigh et al., 2014) and the South China Sea (Feng et al., 2015). Seasonal cycles in MSL, range in magnitude from 0.03 m to 0.45 m, in this study. These magnitudes agree well with previous studies (e.g. Merrifield et al., 2013; Feng et al., 2015). Vinogradov and Ponte (2010) showed, using satellite altimetry data, that the seasonal cycle in MSL measured by tide gauges are comparable to, but larger than, those in the nearby shallow ocean (< 200m depth). However, along the coasts of China and Russia, the annual amplitude in altimetry data was found to be underestimated by 25% compared to tide gauges (Feng et al., 2015).

The seasonal tide has both astronomical (Pugh and Woodworth, 2014) and terrestrial (e.g. Muller, 2012) forcing mechanisms. Peaks in the astronomical forcing are caused by variations in the declination of the Moon and Sun, and occur in March and September for semi-diurnal regimes and in June and December for diurnal regimes (Pugh and Woodworth, 2014). Seasonality in oceanographic, meteorological and hydrologic factors are the terrestrial mechanisms that generate seasonality in the tide. These can include stratification of the water column (Kang et al., 2002; Muller, 2012), sea-ice cover (St. Laurent et al., 2008), ocean currents (Cummins et al., 2000) or large-scale wind patterns (Kolker and Hameed, 2007). The largest seasonal signals in this study are in regions of large tidal range, such as north-west Australia and Vancouver Island. These large seasonal cycles have been identified by previous studies (e.g. Muller et al., 2014). Around Vancouver Island the changes have been linked to changes in stratification due to freshwater

influx (Foreman et al., 1995) or changes in wind-driven currents (Cummins et al., 2000). Muller et al. (2014) observed large changes in coastal and polar regions, with relative changes in the amplitude of the M_2 constituent of 5-10%. However, the GESLA dataset has very few sites in the Arctic and therefore this study does not capture these changes. The relative magnitude of astronomical and terrestrial forcing influences the phase of the seasonal tidal cycle.

The skew surge signal is exclusively influenced by storm surges, and therefore the phase of the seasonal cycle is controlled by the main storm season in that region. In the mid- to high-latitudes peaks generally occur in winter months (i.e. November to February for the northern hemisphere), while for the tropics peaks are controlled by the timing of tropical cyclones. In some regions definitive cyclone seasons exists, such as June to November in the North Atlantic, while in the western Pacific tropical cyclones can occur at any time of year. Comparisons with the global study of Menéndez and Woodworth (2010) are good, although peaks on the Australian west coast occur 1-2 month earlier in this study. Interestingly the peak in seasonal skew surge for all locations around North America occurs between December and February, which supports Menéndez and Woodworth (2010). The switch of the dominant storm system, from hurricanes to extra-tropical storms, observed by Zhang et al. (2000) is therefore, not seen in the phase of the seasonal skew surge.

The magnitude of inter-annual signals in MSL and skew surge is influenced by the filter used to extract the signal. Any comparison with other studies is limited by the assumptions made during the creation of the filter. An assessment of the absolute magnitude of the inter-annual signal is therefore not appropriate, but regions of higher variability can be assessed. Sites with large inter-annual variability in skew surge occur on the edge of extra-tropical storm tracks, such as the east coast of North America above New York, the North Sea and the Great Australian Bight. Merrifield et al. (2013) identify these regions as the transition between high and low variability in the high frequency (< 1 month) component. The large variability is likely caused by small shifts in the predominant storm track position that occur on inter-annual scales. These may be linked to variations in the NAO (e.g. Sickmoeller et al., 2000; Weisse et al., 2005; Feser et al., 2015) or the Northern and Southern Annular Modes (e.g. Yin, 2005). The largest variability in the inter-annual MSL signal occurs on both sides of the equatorial Pacific, along the Pacific coast of North America and in northern Australia. Zhang and Church (2012) identified ENSO as the main forcing mechanism for these areas, while PDO influenced variability along the Pacific coast of North America.

Inter-annual cycles of the tide are different since they are sinusoidal, and controlled by astronomical forcing. The last peak in the nodal cycle (in this dataset) occurred in 1997. The

largest magnitude occurs in Malaysia and Philippines, which supports the findings of Haigh et al. (2011), who found a large modulation of the signal in the SCS. Large nodal cycle variations are also observed in areas of large tidal range such as in the UK (Bristol Channel and Morecambe Bay) and Canada (Bay of Fundy), but these changes are small relative to tidal range. Timing of the peaks correspond to the ratio of diurnal to semi-diurnal tides, since peaks in the nodal cycle increase the amplitude of the lunar diurnal tide, but decrease the lunar semi-diurnal tide (Pugh and Woodworth, 2014).

The relative phases of seasonal or inter-annual signals are important, since a shift in the phase could increase or decrease the combined magnitude. Only in a few regions did peaks in all three seasonal cycles occur simultaneously in the same month. The constructive cycles that occur at sites around Vancouver Island and most of Japan, and odd sites in Australia, Malaysia and the Pacific Islands, mean that only increases in the magnitude of the seasonal cycles would increase the combined seasonal cycle. Where the cycles do not act constructively, or have not in the past, small shifts in the phase of any signals could increase the magnitude of ESL. A theoretical maximum ESL is calculated by assuming maximum constructiveness between independent signals. At all sites, the observed maximum ESL is smaller than the theoretical maximum ESL, and at some sites, the latter is double the magnitude of the former. At many of these sites, the reason for the large difference is that peaks in the inter-annual signal of MSL and skew surge were out of phase with the nodal cycle. Other reasons include the peaks in the inter-annual signals occurring early in a dataset with a large positive secular trend and the peak in inter-annual signal occurring during a trough in the seasonal cycle (Figure 6.9).

Changes in ESL can therefore either arise by changes in the magnitude of different signals or in shifts of the relative phases due to changes in the forcing mechanisms or the statistical probability of constructive signals. Many mechanisms may change the baseline ESL and they vary in magnitude and likelihood. For example, secular trends in global MSL are 'virtually certain' to continue increasing through the 21st century (Church et al., 2013), and the observed acceleration (Woodworth et al., 2011; Haigh et al., 2014) may also continue (Church et al., 2013). The secular trend in ESL is similar to that of MSL at most sites (e.g. Menéndez and Woodworth, 2010). Based on this, the magnitude of ESL can be expected to continue increasing, at most sites, and at a rate determined by the regional signal of MSL rise (Meyssignac and Casenave, 2012). However, as shown in Chapter 4, secular trends in tidal levels have a similar magnitude to trends in MSL at some locations, while increases in storm surge magnitude and frequency have been predicted (Seneviratne et al., 2012). At present, few changes in storm surges have not been observed in previous research (e.g. Menéndez and Woodworth, 2010) or in this thesis (Chapter 5), but an possible consequence of climate change is the increase in the frequency of the most intense

cyclones (Bister and Emanuel, 1998). However, apart from the Atlantic (Kossin et al., 2007) significant evidence of this change has not been observed, due in large part to the lack of reliable meteorological data before 1970 (Seneviratne et al., 2012).

For both seasonal and inter-annual signals, changes in either the phase or magnitude may result in changes in ESL. Signals in MSL and skew surge on seasonal and inter-annual timescales are strongly dependent because their forcing mechanisms are similar. However, some decoupling of these signals may occur, such as the timing of peaks in the seasonal cycles of sites along the US east coast and Japan. This will be because of the different response of the components to changes in air pressure, winds or local heating density affects, or where river runoff is large (Pugh and Woodworth, 2014). Changes in the magnitude of inter-annual signal in MSL and skew surge, and the regional climates that drive them, are a matter of much debate. Some evidence suggests that the characteristics of ENSO or NAO are changing (Seneviratne et al., 2012), but the lack of sites with long records make resolving the inter-annual variability difficult. Peaks in the inter-annual MSL cycles occurred in 1982 or 1997 for most sites around the Pacific, and are associated with large El Niño events. These two ENSO events were the largest of the 20th century based on the Multivariate ENSO index (Wolter and Timlin, 1998).

The seasonal cycle in each component is more regular, and therefore the annual and semi-annual cycles can be well represented by cosine waves (e.g. Amiruddhin et al., 2015; Feng et al., 2015). However, magnitude and timing of the meteorological, oceanographic and hydrological processes that control the seasonal signals vary. As such the phase and magnitude of the seasonal MSL cycle have been observed to vary in response to these processes (Plag and Tsimplis, 1999; Marcos and Tsimplis, 2007; Hunicke and Zorita, 2008; Vinogradov et al., 2008; Torres and Tsimplis, 2013; Dangendorf et al., 2013; Wahl et al., 2014; Feng et al., 2015). The forcing mechanisms, described above, also change on secular time-scales, with positive trends in the amplitude of the seasonal MSL cycle observed around southern Europe (Marcos and Tsimplis, 2007) and along the US east coast (Wahl et al., 2014). An improvement of the analysis would be to account for the variability in the seasonal cycle, however, given the focus and global nature of this study this was not possible here. Some of the variability not captured by the seasonal cycle will be included in the inter-annual signal in this study.

There are a number of regions where large seasonal cycles exist but are not presented in this study, due to the geographical bias in the GESLA dataset. Therefore, the large seasonal MSL signals in the Bay of Bengal, St. Lawrence bay, the Gulf of Carpenteria and the Bohai sea (e.g. Tsimplis and Woodworth, 1994), are not presented. Determination of the phase and magnitude of the seasonal cycle could be calculated from many more sites, since the seasonal cycle can be

calculated using a 5-year window (e.g. Marcos and Tsimplis, 2007). Limitations from other sections of the thesis limit the number of sites used to 220.

6.5 Conclusions

The aim of this chapter was to understand how the three main components of sea level vary over different timescales and how the combined variability in these individual components influences ESL. Using 220 sites from the GESLA dataset, seasonal, inter-annual and secular signals were extracted from each of the three main sea level components. From these time-series, assessments were made of the magnitude of each signal, the combined variability in ESL resulting from these signals, the phase coherence between different components and calculated a theoretical maximum ESL.

The first objective was to estimate the magnitude of signals in MSL, tide and skew surge, on seasonal, inter-annual and secular timescales. Seasonal cycles in all three components and inter-annual signals of MSL and skew surge have the largest variability. The variability caused by the secular trend in MSL and the nodal cycle of the tide are smaller, but on the same order of magnitude. The number of signals with similar magnitudes shows that the assessment of variability in ESL requires understanding of the mechanisms affecting all three components on a range of timescales.

The second objective was to estimate the combined variability in the baseline ESL, by adding together the magnitude of the 10 extracted signals. In regions including the southern North Sea, northern Australia and Vancouver Island, a number of different signals have large magnitudes. Therefore, the combined variability in these regions exceeds 1.3 m, and reaches up to 2.4 m in the southern North Sea. This suggests that the variability, on periods longer than 6 months, can combine to generate particular periods that are more favourable for a high ESL to occur.

The third objective was to assess the relative phase of the seasonal and inter-annual signals in the three main components, and determine where and when these signals have acted constructively. (i.e. occurred in phase). Concurrent peaks were found in the seasonal cycle around Vancouver Island and at most Japanese sites, which cause the seasonal cycle in ESL to increase in magnitude. Elsewhere, peaks in the seasonal and inter-annual signals of the three components do not occur simultaneously and therefore a shift in phase, caused by changes in the forcing mechanisms or from the probability of independent signals acting constructively, would increase the baseline ESL.

The relative phasing of the seasonal and inter-annual signals mean that not all signals are independent of each other. Therefore, the fourth objective was to account for the dependence

between signals in estimating a theoretical maximum ESL. At all sites presented, the observed maximum ESL is smaller than a theoretical maximum ESL, calculated by assuming constructiveness between all independent signals. At some sites, the theoretical maximum is double the observed maximum, and these large differences are usually caused by the signals of the nodal cycle and inter-annual MSL acting destructively or peaks in the inter-annual signal occurring early in a data set that has a large positive secular trend in MSL.

Finally, the secular change in ESL at each site, supports findings from previous research showing an increase in ESL at most sites, but with a magnitude at most sites that is similar to the rise in global MSL. The largest increases observed are in the western equatorial Pacific and northern Australia (a response to the variability in ENSO), and the Gulf of Mexico and the Philippines (a response to land subsidence). However, the magnitude of variability in all components and on timescales from seasonal to secular, means that projections of ESL will not be accurate unless they are all accounted for.

This chapter does not give absolute values of ESL, but rather calculates a baseline ESL, upon which a high-frequency signal, associated with individual storms, would add. It shows that large variations occur in many different signals that effect ESL and these can combine to generate periods when the baseline ESL is high. Secular changes in ESL are caused by secular increase in MSL at most sites, but variability in other components and timescales is also important. By assessing the relative phasing of seasonal and inter-annual signals for the first time on a global scale. There are many sites where peaks in the three main components of sea level do not occur concurrently. Therefore, if the phase of all independent signals shifted so that they all acted constructively the magnitude of the baseline ESL could double. Changes in the phase of each signal, as well as the magnitude, should therefore be considered in projections of ESL.

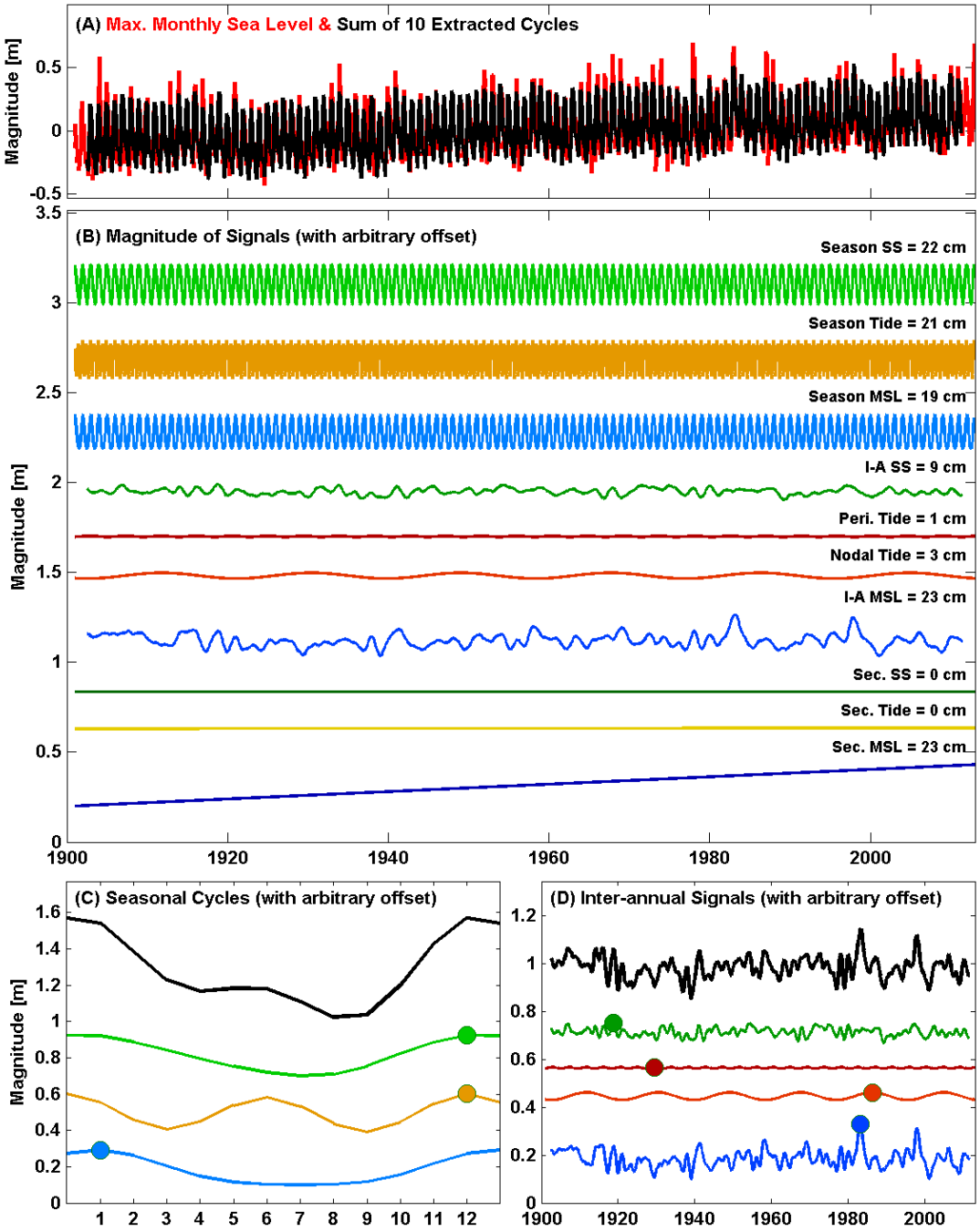

Figure 6.1**:** Example of the extracted signals for Seattle, USA: (A) shows the time-series of the monthly maximum sea level (red) compared to the combined time-series from the 10 extracted signals (black); (B) shows all 10 extracted signals, with their magnitude calculated from the maximum to minimum range over the entire time-series; (C) the three seasonal cycles, along with a combined seasonal signal (black line); (D) the four inter-annual signals, along with a combined inter-annual signal (black line). Maximum values of each seasonal and inter-annual time-series are shown as a coloured dot.

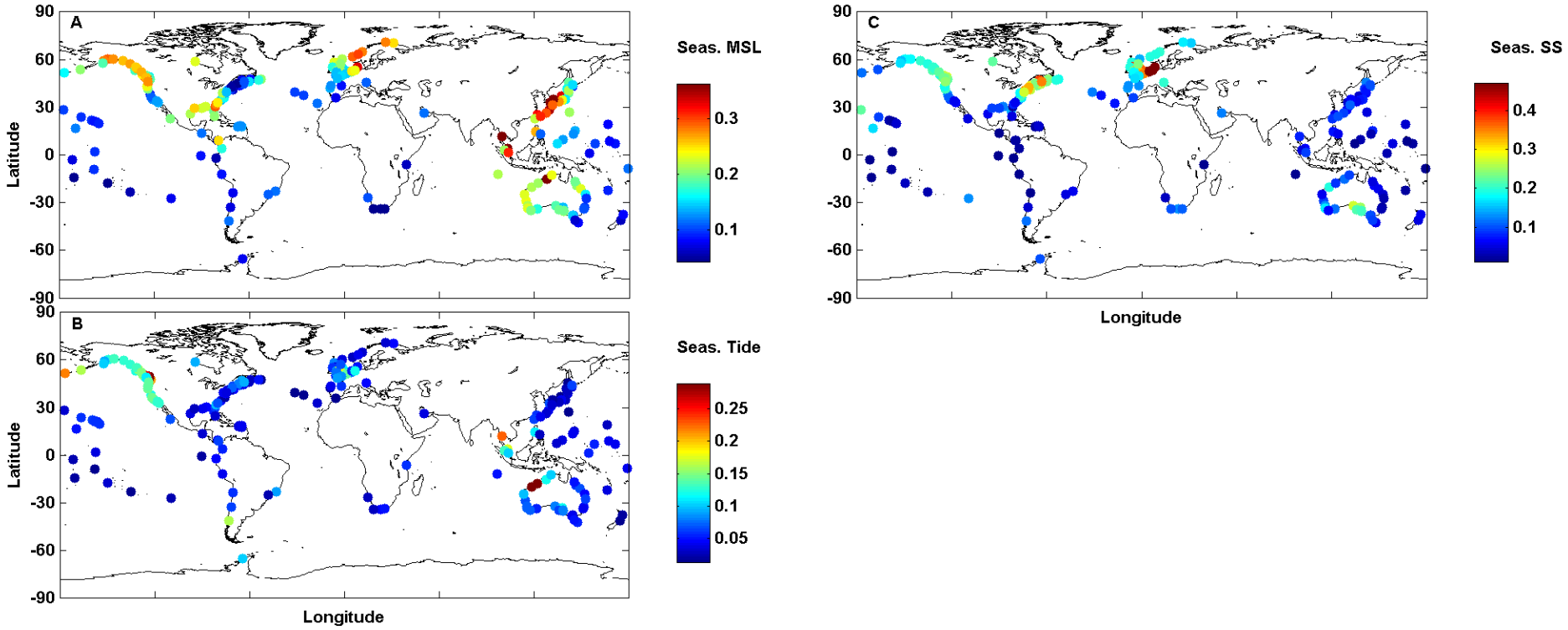

Figure 6.2: Map of the magnitude (in metres) of the three seasonal cycles of (A) MSL, (B) tide, and (C) skew surge. The colour of the dot represents the magnitude of the variability. Note, there is a different scale for each plot.

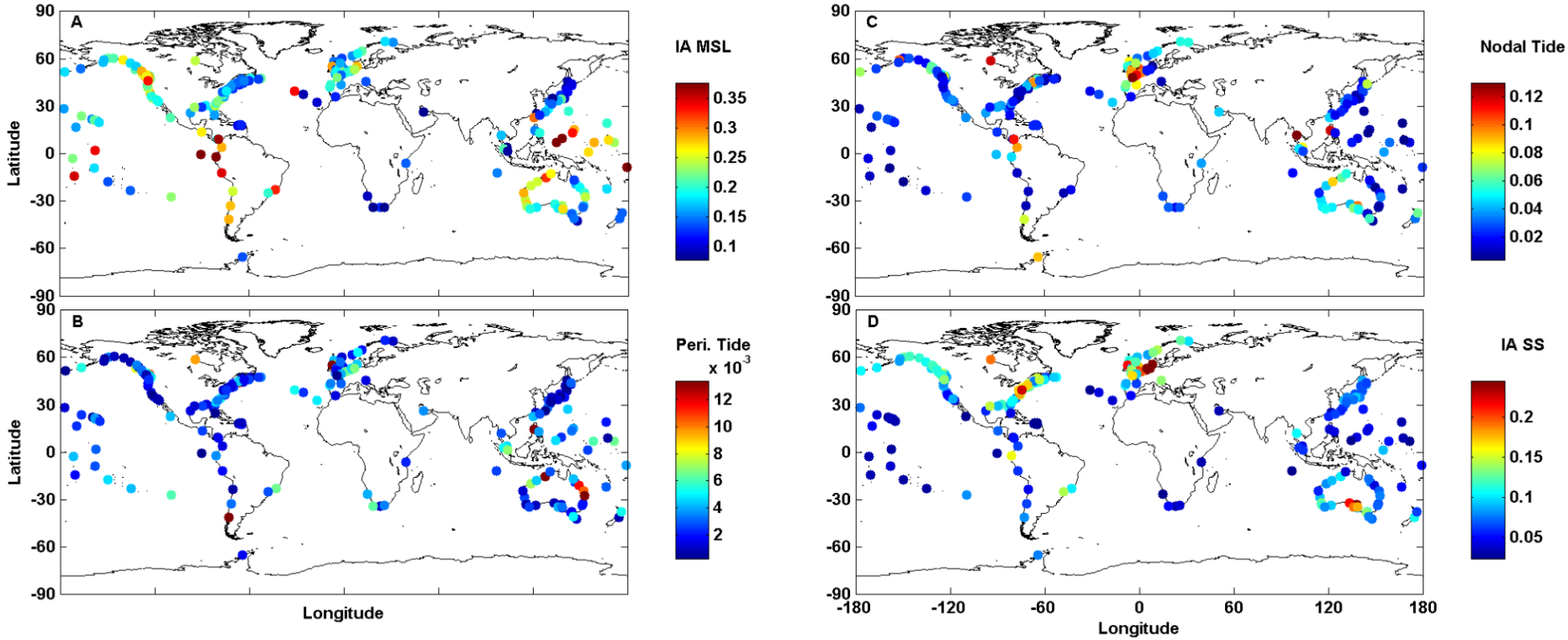

Figure 6.3**:** Map of the magnitude (in metres) of the four extracted inter-annual signals of: (A) MSL, (B) perigean tide, (C) nodal tide, and (D) skew surge. The colour of the dot represents the magnitude of the variability. Note, there is a different scale for each plot.

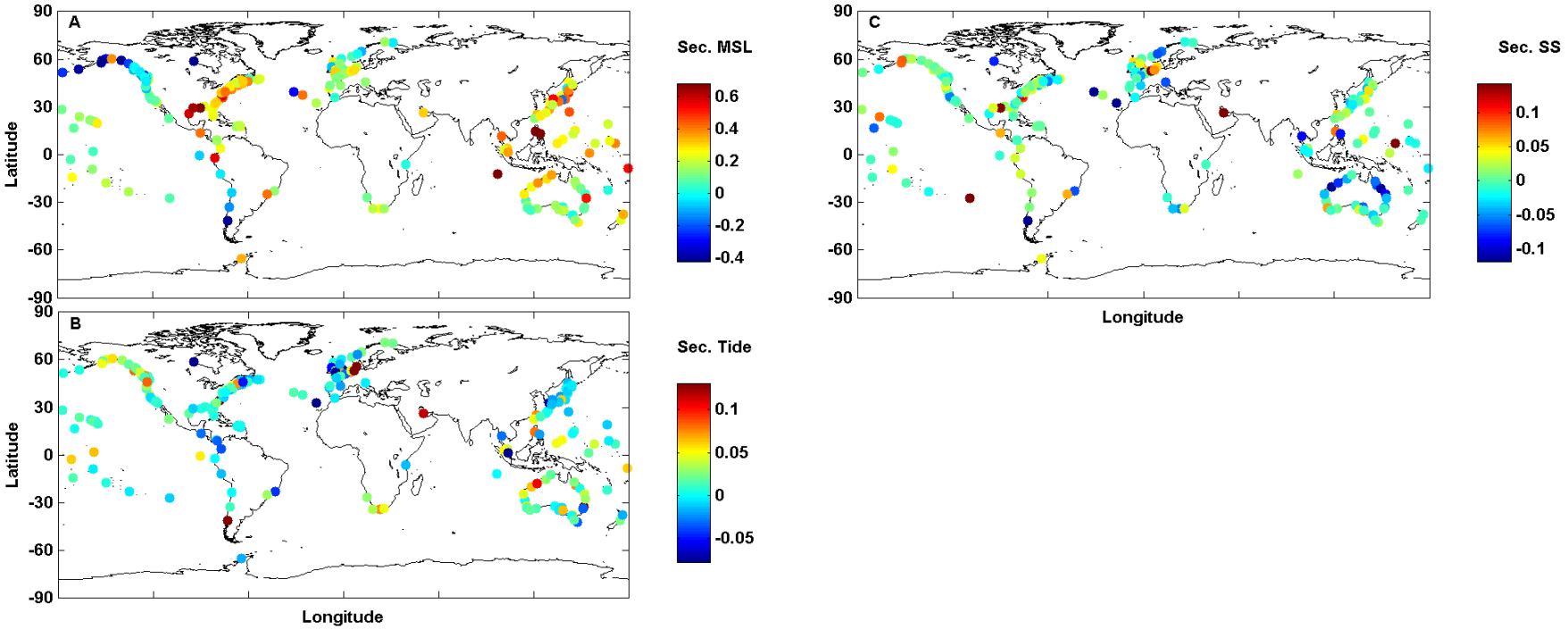

Figure 6.4**:** Map of the magnitude (in metres) of the change in sea level (over 100 years) due to the secular trend in: (A) MSL, (B) tide, and (C) skew surge. The colour of the dot represents the magnitude of the variability. Note, there is a different scale for each plot.

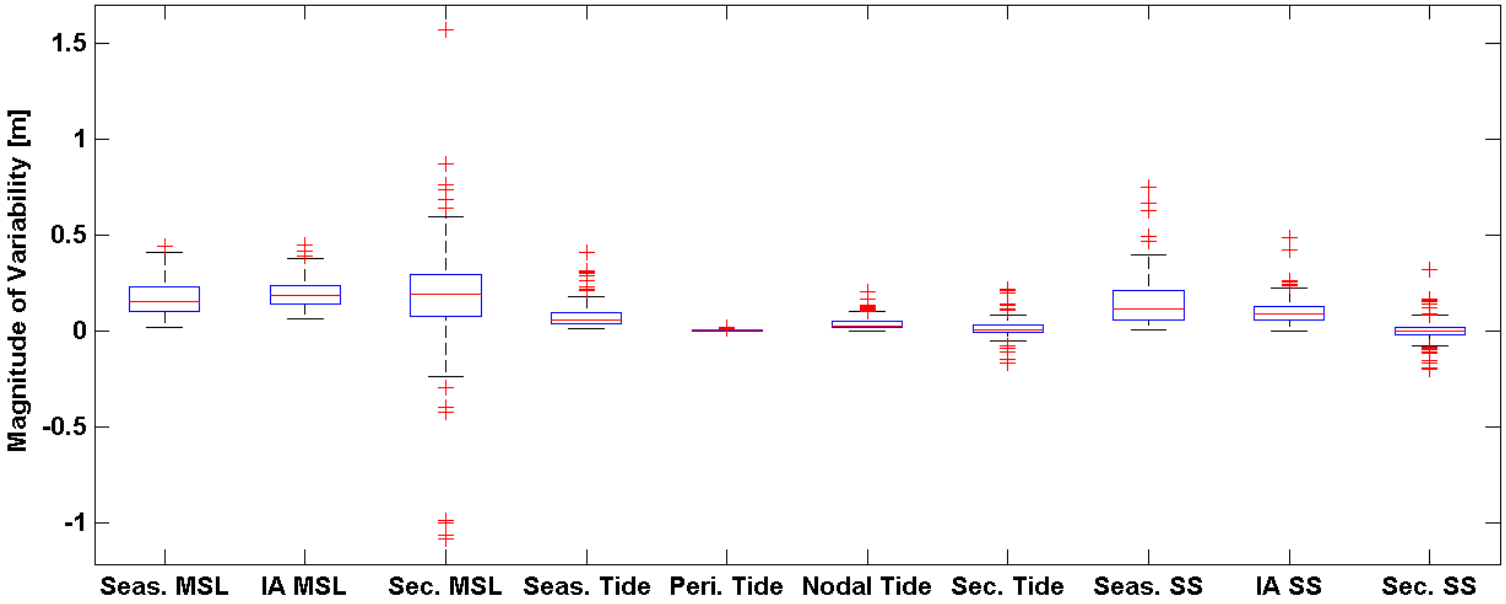

Figure 6.5**:** Box plots showing the distributions of the magnitude of each extracted cycle. The box represent values between the 25th and 75th percentile, the red line plots the median value (50th percentile). The feathers of the box extend to the 2.5th percentile and 97.5th percentile, with the red crosses show the value that are outside of this last range. Secular signals shows that change that would occur over 100-years based on the linear trend calculated over the length of data at each site, while the seasonal and inter-annual signals are calculated from the maximum to minimum range of values from each time-series.

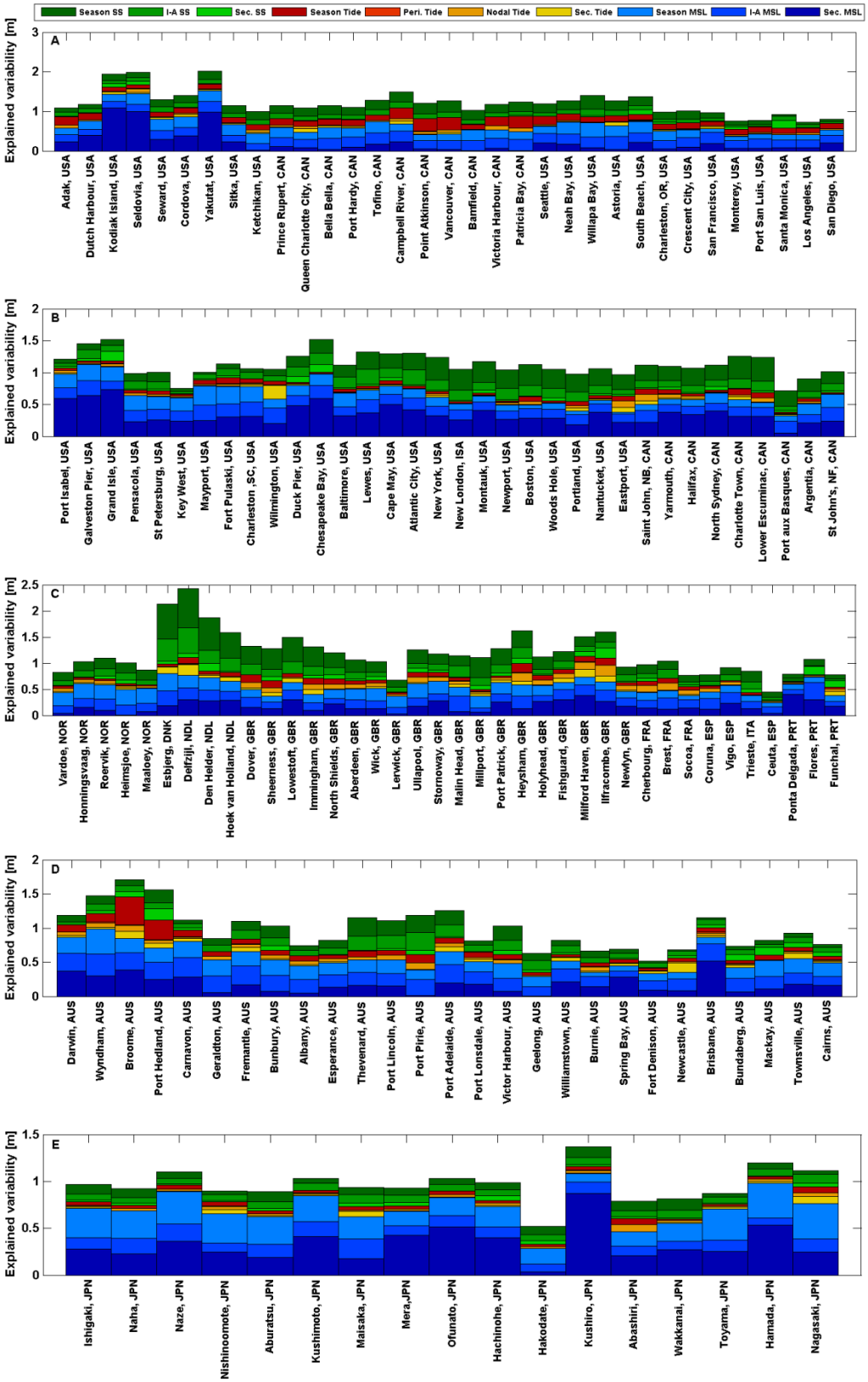

Figure 6.6**:** Stacked bar chart of combined variability for sites along sections of coastline in: a) western North America, b) eastern North America, c) Europe, d) Australia, e) Japan.

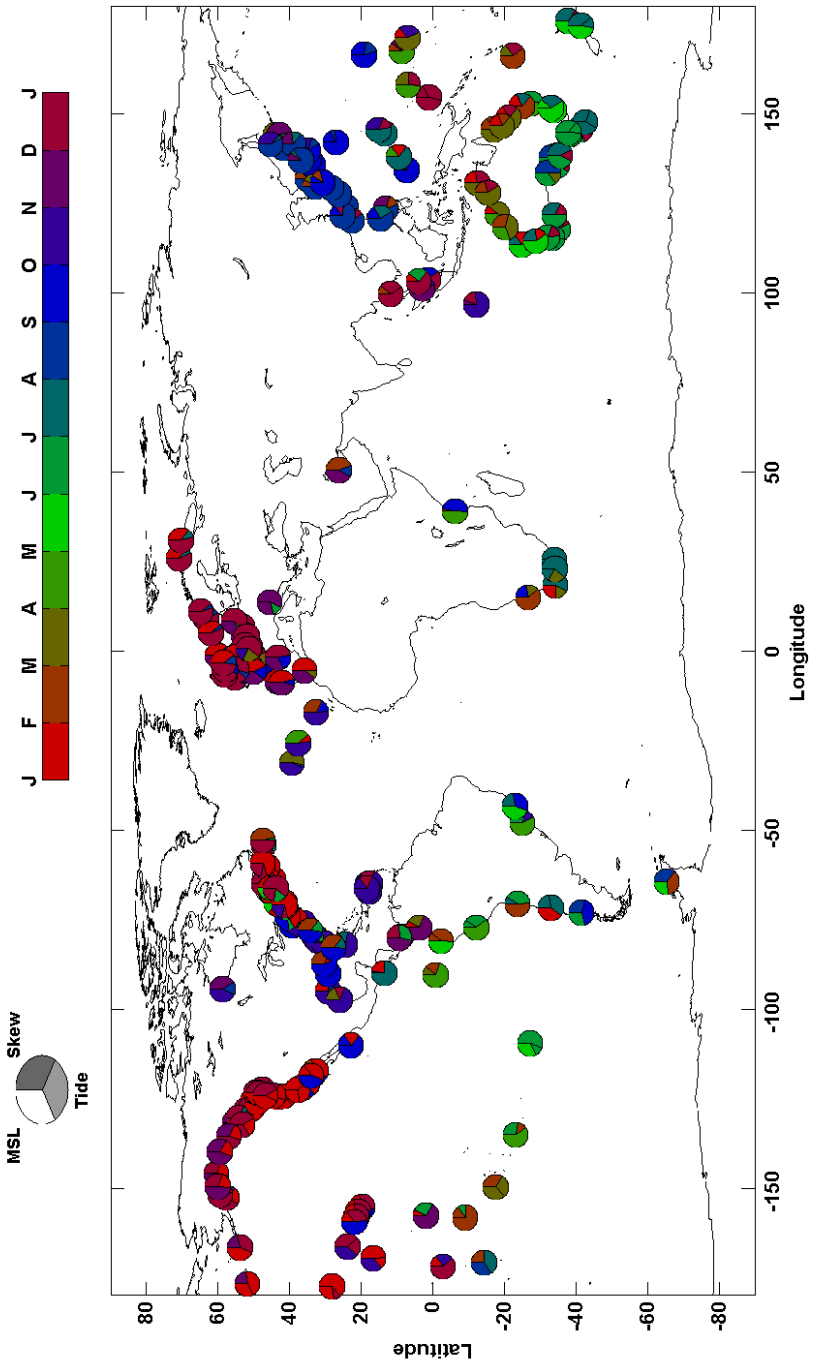

Figure 6.7**:** Global map showing the relative magnitude and timing of peaks in the seasonal cycles of MSL, tide and skew surge for each of the 212 study sites. Each circle is divided into three segments for the seasonal cycles of MSL, tide, SS, with the segments plotted in this order anti-clockwise from 00:00 hrs. The size of the each segment shows the percentage of seasonal variability given by each component, and the colour corresponds to the month in which the peak in each seasonal cycle occurred.

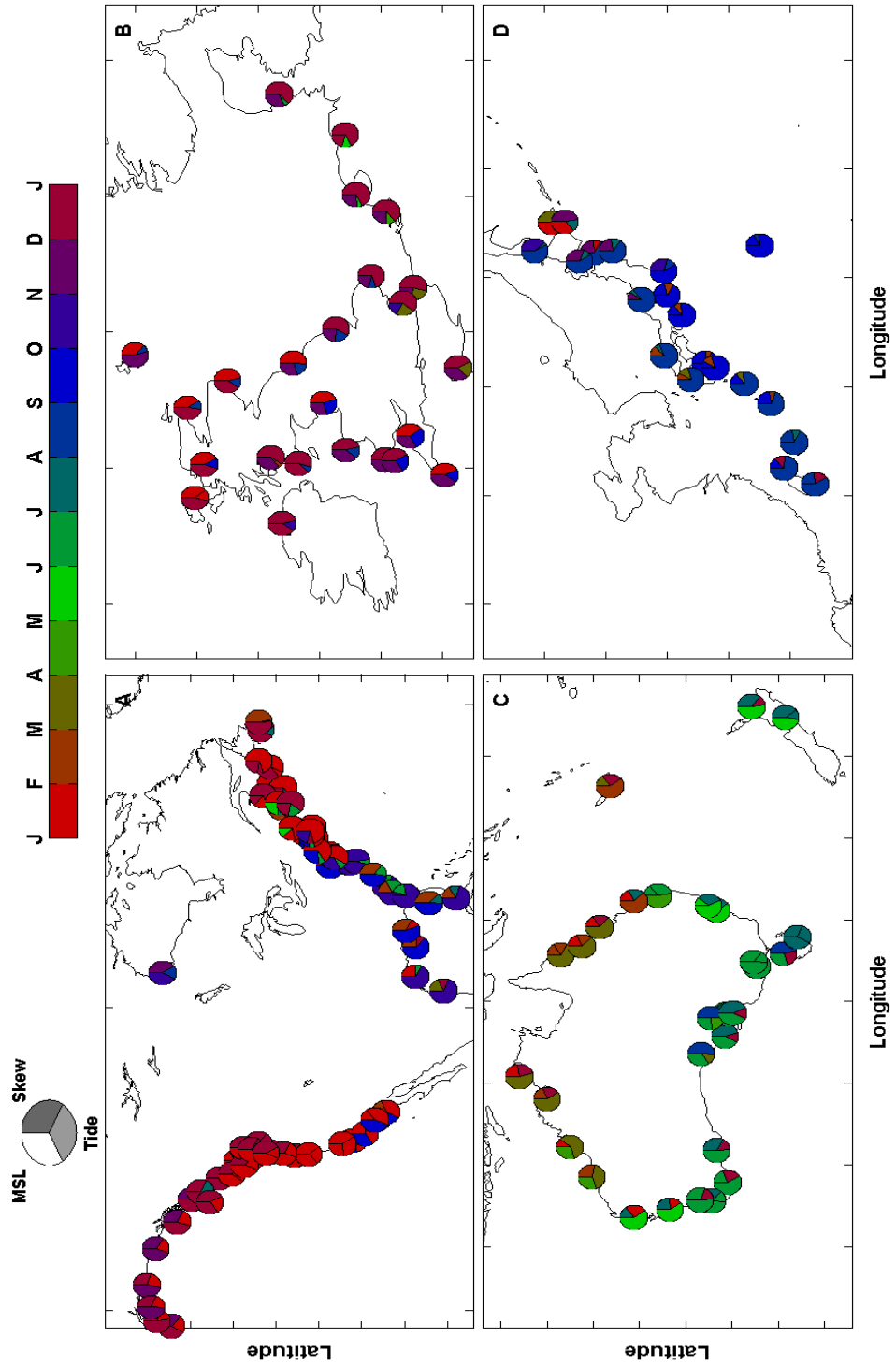

Figure 6.8**:** Regional maps showing the relative magnitude and timing of peaks in the seasonal cycles of MSL, tide and skew surge for four data dense regions (a) North America, (b) Europe, (c) Japan and (d) Australia. Each circle is divided into three segments for the seasonal cycles of MSL, tide, SS, with the segments plotted in this order anti-clockwise from 00:00 hrs. The size of the each segment shows the percentage of seasonal variability given by that component, and the colour corresponds to the month in which the peak in each seasonal cycle occurred.

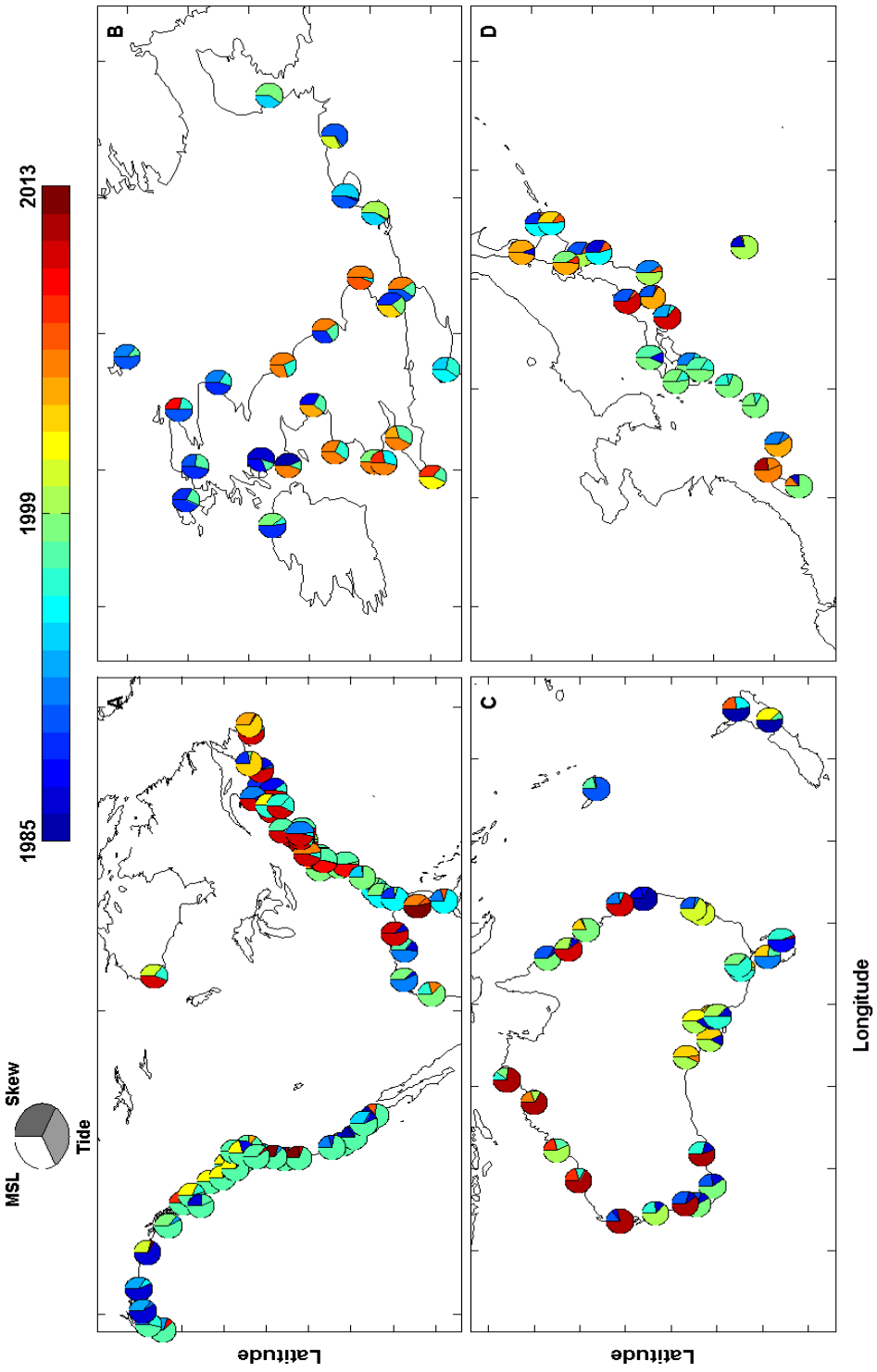

Figure 6.9**:** Regional maps showing the relative magnitude and timing of peaks in the inter-annual signals of MSL, tide and skew surge for four data dense regions (a) North America, (b) Europe, (c) Australia and (d) Japan. Each circle is divided into three segments for the inter-annual cycles of MSL, tide, SS, with the segments plotted in this order anti-clockwise from 00:00 hrs. The size of the each segment shows the percentage of inter-annual variability given by each component, and the colour corresponds to the year in which the peak in each inter-annual cycle occurred.

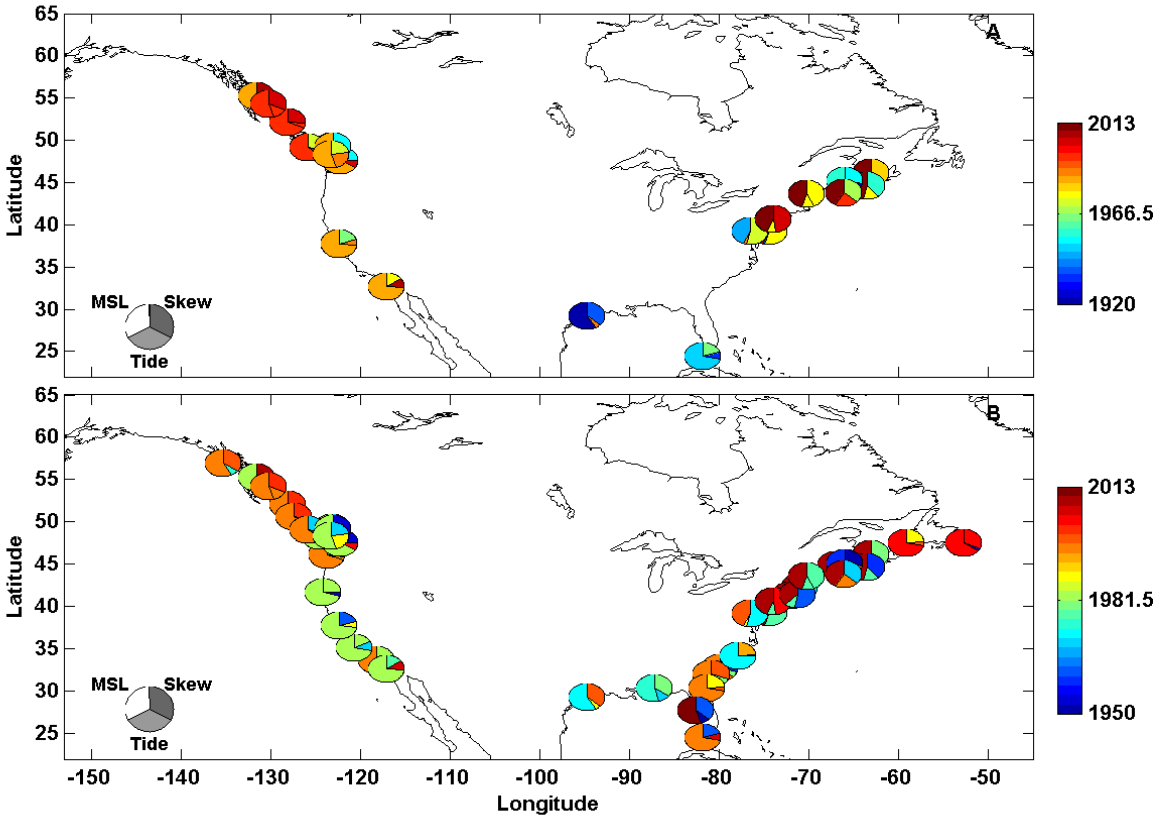

Figure 6.10**:** Regional map of North America showing the relative magnitude and timing of peaks in the inter-annual signals of MSL, tide and skew surge for (a) 1920-2013, (b) 1950-2013. Each circle is divided into three segments for the inter-annual cycles of MSL, tide, SS, with the segments plotted in this order anti-clockwise from 00:00 hrs . The size of the each segment shows the percentage of inter-annual variability given by each component, and the colour corresponds to the year in which the peak in each inter-annual cycle occurred

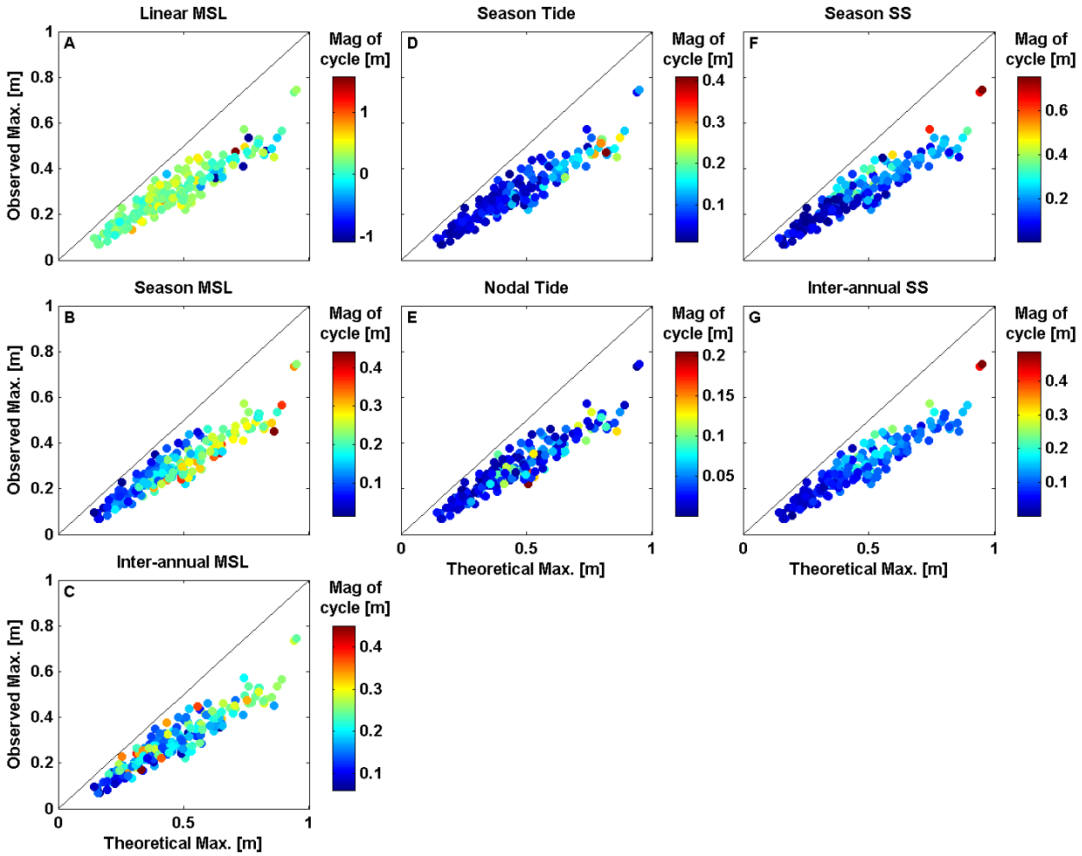

Figure 6.11**:** Comparison of maximum observed ESL to a maximum theoretical ESL. Each site is represented by a dot coloured by the magnitude of the signals in: a) secular MSL; b) seasonal MSL; c) inter-annual MSL; d) seasonal tide; e) nodal tide; f) seasonal skew surge; g) inter-annual skew surge. The lines on each panel represents 1:1 ratio of observed to theoretical maximum ESL.

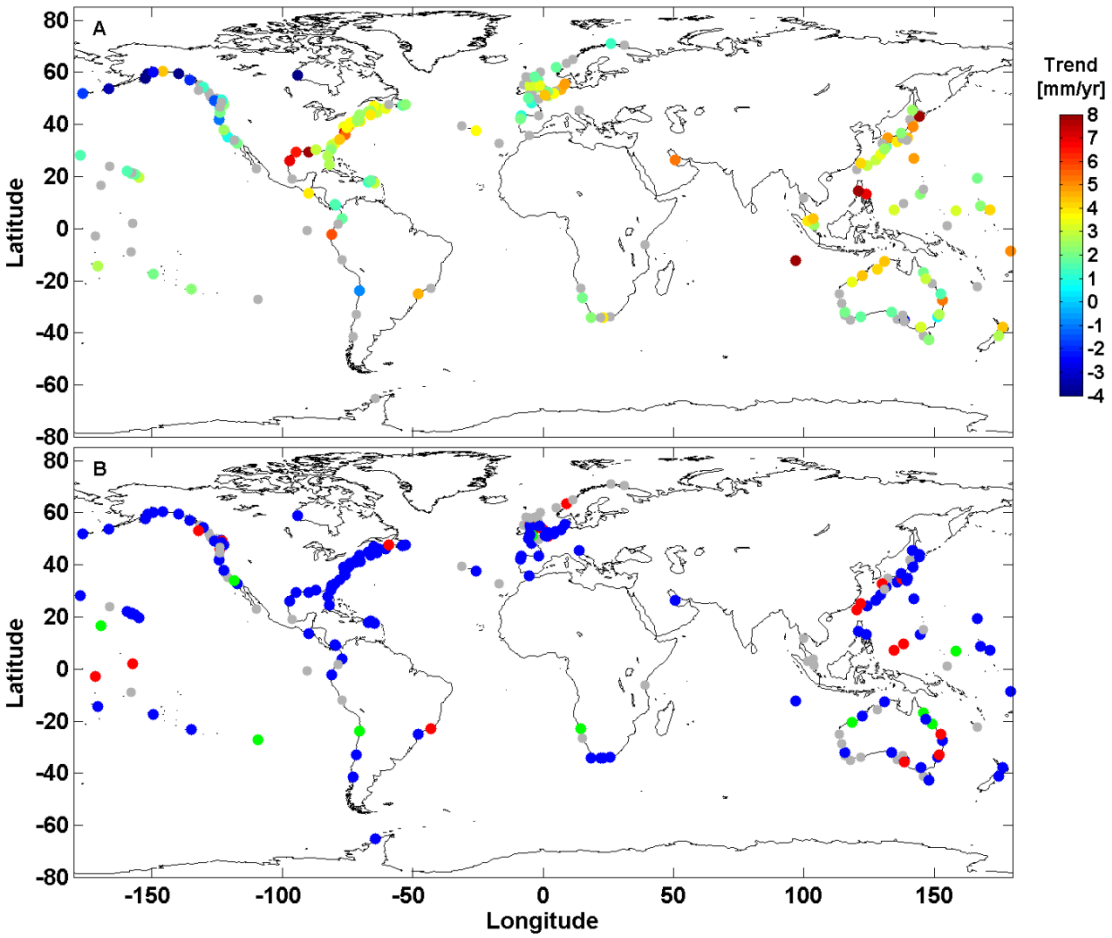

Figure 6.12**:** (A) Map of the magnitude of the trend in the 99th percentile of total sea level; (B) Map showing the component with the largest significant linear trend at each site: MSL (blue), MHHW (red), 99th percentile of skew surge (green), no significant trends in any component (grey).

Chapter 7: Conclusions and Implications

The overall aim of this thesis was to quantify the variability and secular trends in each of the three main components of sea level in order to better understand variability and secular trends in ESL on a global scale, over time scales from seasons to centuries. To achieve this I extended the GESLA tide gauge dataset, and analysed sea level records over 28 years in length from 220 sites around the world. Previous research has shown that changes in ESL are predominantly controlled by the secular increase in MSL, but that variability in other components and on other timescales is important at some sites. My study shows that changes in ESL have been caused by variability, on timescales from seasons to centuries, in all three components of sea level, and while the secular trend in MSL dominates over the centennial scale all components and timescales are important at some sites.

This chapter will first summarise the key findings of the three objectives, before drawing the conclusions together to provide a holistic view of the causes, magnitude and sign of ESL change in the historical record, and an indication of how it may change over the 21st century.

7.1 Secular Changes in Tidal Levels

The first objective of the thesis was to investigate secular changes in a range of different tidal levels, the findings of which are presented in Chapter 4. Tidal levels are often assumed stationary on a centennial timescale, since the astronomical forcing that generates the tides is constant over centennial timescales. However, a growing body of evidence has suggested that tidal constituents and tidal levels have changed at a number of locations over the last century, and that this may continue over the 21st century in response to global MSL rise amongst other mechanisms. To investigate changes in the tide this study estimated trends in 15 different tidal levels, at 220 sites around the world, to present the first global assessment of changes in tidal levels. Previous global studies of changes in the tide have focussed on individual tidal constituents, but it is difficult to quantify in terms useful to practitioners exactly how changes in individual constituents combine to alter the observed tidal curve at a specific location.

This chapter finds that significant changes in tidal levels have occurred over the last century, with the magnitude of MTR exceeding 1 mm/yr at 37 of the 220 sites analysed. At these 37 sites the magnitude of trends in tidal levels are currently comparable to those in MSL, and therefore should be considered for calculations of ESL. Significant trends occurred at between 36% and 60% of the

sites, depending on the tidal level used, and were distributed at different locations around the world. The differences in the percentage of significant trends shows for the first time that changes in different tidal levels were not consistent at all sites, with 56 sites exhibiting significant differences between the magnitudes of different tidal levels within the same set (i.e. tidal range, HW or LW). Regionally coherent increases in tidal range and high water levels were observed in the north-east Pacific and German Bight.

On a global scale, there were significantly more positive trends in the high water tidal levels, than negative trends, which suggest a global mechanism may be forcing the changes observed in tidal constituents and levels. The most likely mechanism is the global increase in MSL, but the correlation between trends of any tidal level and MSL is not significant (95% confidence level). However, using the output of a global tidal model (from a study by Pickering, 2014) forced with 0.5 m of SLR, it was found that for large changes in MHW (> 10 mm), SLR generates more positive changes than negative globally. The link between changes in the tide and MSL is well established, and the continued rise in global MSL through the 21st century will likely cause further changes in tidal levels. Direct comparisons of model and tide gauge results are complicated by the inaccuracy of the model in coastal regions, but the comparisons do show that, although changes in MSL have altered tidal levels there are many other mechanisms in action. For example, the coherent increases in HW levels in the north-east Pacific are not observed in the model, which suggests that hypothesised changes in internal tides or large scale wind patterns could be the cause of the observed changes.

In summary, secular changes in tidal levels should be considered in ESL projections, at locations where the changes are comparable with observed MSL rates. The widespread use of tidal levels for many different purposes mean that these changes will have an impact on many practical applications, including: impacts on navigable channels (at high and low water), changes to the potential tidal energy available for extraction, changes in sediment transport and tidal mixing fronts, alterations of national and international boundaries, and changes to the protection of intertidal ecosystems. However, the application of the changes is complicated by my novel finding that trends are not consistent between different tidal levels. Further work is therefore required to understand how to implement, for example, changes that may be larger for spring tides than neap tides.

7.2 Temporal and spatial variability of skew surge

The second objective of the thesis was to assess the secular and inter-annual variability in the meteorological component of sea level. Secular changes in storm surge have been postulated as a response to the predicted increase in storm frequency and/or intensity and duration driven by global warming. However, previous research has been inconclusive about the changes that have occurred historically over the last few centuries, since the substantial inter-annual variability present in the NTR component leads to large uncertainties. Most previous studies have used the NTR component of sea level to assess change in storm surges, but in recent years, skew surge has been suggested as a more appropriate parameter for assessing the meteorologically induced component of sea level. Therefore, I conducted the first global assessment of the distribution and magnitude of tide-surge interaction, and examined whether skew surge is a better parameter to represent the meteorological effect on sea level than the NTR. Further to this, I assessed the variability of skew surge magnitude, both spatially and temporally, by assessing the correlation between study sites and with regional climate indices.

Tide-surge interaction significantly altered the NTR at 81% of the study sites, based on the tidal-phase method and 59%, based on the tidal-level method. At most coastal locations therefore, skew surge is a better parameter for the assessment of the meteorological component. However, for the first time on a global scale many different shapes were observed in distribution of tide-surge interaction were observed. Sites with the strongest interaction typically had peaks in NTR occurring away from predicted HW, but at other sites with weaker but still significant interaction, the peaks in NTR occurred more frequently at times of predicted HW. More site specific research is required to understand how the tide-surge interaction manifests itself at each site.

The number of sites with significant trends in skew surge is low, which supports previous research, but a novel finding was that there were fewer negative trends in time-series of skew surge than NTR. The reduced number of negative trends may be due to the improved data quality that results from using skew surge, since phase offsets are not present in skew surge time-series by definition. At present, the low numbers of positive trends across the study sites suggest that there is not a significant global trend apparent in storm surges. However, if changes in storm surges do occur in the future (as predictions suggest), then using skew surge time series will allow us to detect these changes earlier than using the NTR component of sea level. Large uncertainties around trends in skew surge are caused by the substantial inter-annual variability at higher percentiles. This variability has been correlated to regional climate variations in previous studies, but despite strong correlations between some regional skew surge indices and climate indices,

However, none were statistically significant (at 95% confidence level) when serial autocorrelation was accounted for.

In summary, in undertaking the first global assessment of tide-surge interaction, I found that at most study locations the tide and NTR components are dependent, and as such, skew surge is a more appropriate parameter for assessing the 'true' meteorologically driven component of sea level. Using skew surge removes the non-linear tide-surge interaction (as a recent study has shown; Horsburgh and Williams, 2016) and the effect of phase offsets, caused by invalid measurements. Therefore, trends in skew surge are more representative of changes in meteorological component of sea level and its forcing mechanisms. Further assessment of inter-annual variability will aid the detection of future secular changes. Although this study does not find significant correlations between regions or with climate indices, many previous studies have established a link between them. The lack of statistically significant correlations is related to auto-correlation, which is an important consideration in the use of filters.

7.3 Changes in ESL assessed on a component by component approach

Building on the results from objectives 1 and 2, summarised above, the third objective of the thesis was to evaluate how the variability in the tidal and meteorological components of sea level, together with changes in MSL, influence the seasonal, inter-annual and secular changes in ESLs. Specifically my key goal here was to assess which component, and what time-scales, has the greatest influence on the variability in ESL at different sites, over the record lengths available. Seasonal, inter-annual and secular linear trends signals were extracted from each component, and from these the following are assessed: a) the magnitude of each cycle; b) the phase coherence between different components; and c) a theoretical maximum ESL. My study assessed the medium to long-term variability (>6 months) to create an understanding of the processes that generate the baseline upon which the high-frequency variability, associated with individual storms, then adds.

In agreement with previous studies the magnitudes of ESLs was found to have increased at most locations around the world, with the change being driven primarily by increases in MSL. While the secular trend in MSL is the primary cause of the long-term increased observed in ESLs, the considerable variability in each of the other sea level components strongly influenced variability in ESLs over a range of time-scales, resulting in periods of elevated or depressed ESLs.

The magnitude of variability was greatest in MSL signals on seasonal, inter-annual and secular timescales, but the magnitudes of seasonal and inter-annual skew surge signals were of the same order of magnitude. At some sites, the seasonal, nodal and secular signals in the tide also had important contributions to ESL variability. Secular trends skew surge and variations due to the perigean cycle are generally negligible relative to total ESL variability. The importance of secular trends will increase with time as their cumulative contribution to ESL continues. The magnitude of variability ESLs changes considerably around the world, with the largest variability occurring in the North Sea, where the baseline ESL could vary up to 2.4 m if all signals act constructively.

Seasonal cycles of MSL, tide and skew surge occur in phase in the NE Pacific and Japan, but at most locations concurrent peaks in different seasonal or inter-annual signals do not occur. A novel method of estimating a theoretical maximum was used to assess the increase in ESL that would occur if all independent signals were in phase. At sites where these cycles had occurred in phase during the historical record the observed maximum and the theoretical maximum would be similar. However, at all sites in this study the observed maximum is smaller than the theoretical maximum, which means that the magnitude of ESL could increase due to increased constructiveness of individual signals as well as changes in the magnitude of them. Where the theoretical maximum is over twice the observed maximum, the reasons include: peaks in the nodal cycle and the inter-annual cycles of MSL or skew surge being out of phase; and peaks in the inter-annual cycles occurring away from the maximum contribution from the secular trends.

The focus of this final objective was to better understand and quantify the relative importance of variability in the three main sea level components, on three different timescales, to the combined variability present in ESLs. At most sites the secular trend in MSL was the largest contributor to variability, but the variability on seasonal and inter-annual signals in both MSL and skew surge was similar in magnitude. Variability in ESL is dependent on the relative phase of different signals as well as their magnitude. I show that at all study sites, the maximum ESL could increase if independent signals became more constructive by coming more into phase. Although this does not account for the magnitude of individual storm surges, this assessment of baseline ESL shows that the magnitude of ESL may change in the future with or without an increase in magnitude of any low-frequency signals.

7.4 Summary

The overall aim of this thesis was to quantify the variability and secular trends in each of the three main components of sea level, first individually, and then in combination, in order to better

understand the variability and longer-term trends in ESL on a global scale, over time scales from seasons to centuries. A key motivation was to determine the degree to which the assertion that MSL is the dominant cause of changes in ESL held true. Before addressing the scientific question, several methodological issues needed to be resolved in order to accurately assess each component individually. Using the improvements in methodology, assessments were made of the global distribution of secular changes in tidal levels, and then the secular and inter-annual variability in the meteorological component. Considering these findings along with previous research this study then assessed the combined effect of changes in ESLs.

The first methodological question was whether trends estimated from different tidal levels were consistent in sign and magnitude. Tidal levels represent the average height of the observed tide, and because of this, they are used for many practical purposes. However, there are many different tidal levels used around the world, each is calculated from different subsets of HWs and LWs, and therefore represent different aspects of the tide. For example, MHWS is calculated from the average height of HW during spring periods (which in itself can be defined differently), while MHHW is calculated from the average of the highest HW of each day. Previous research into changes in tidal levels had concentrated almost exclusively on the MTR, with one study also using the DTR. This study provides the first assessment of changes in a wide range of different tidal levels (15 in total - 5 HW, 5 LW and 5 tidal range), and how the trends in the different levels compare. The significant differences that I found at 56 of the 220 sites mean that the trend for a particular level should not be inferred from another level.

The second methodological question was whether skew surge was a more appropriate parameter for assessing the meteorological component of sea level, than the more traditional NTR. The NTR is the remainder of the sea level after MSL and the astronomical tidal component have been removed. The skew surge has recently been used around north-west Europe and the USA, since it removes the influence of tide-surge interaction and phase offsets. Where tide-surge interaction or phase-offset errors have a large impact at a particular site, skew surge would be a more suitable parameter to represent the ‘real’ meteorologically induced change in sea level.

Significant tide-surge interaction was identified at most of the 220 study sites, but the pattern of the interaction varied. Previous research, primarily in the North Sea, had identified a pattern where most peaks in the NTR occurred away from predicted HW. Although this pattern was observed at many sites, particularly those in shallow coastal seas with large tidal ranges, other patterns were also observed at sites with smaller tidal ranges, and where the tide-surge interaction was typically weaker, but still statistically significant (at 95% level). Some of these included sites with a greater frequency of peaks in NTR at the same time as predicted HW. This

had been observed in one previous study of the Irish Sea, but this is the first study to show the different distributions at sites around the world, and therefore the mechanisms behind the different patterns have not been investigated in depth.

As well as tide-surge interaction, some sites have errors in the time-series, introduced by phase offsets. It can be difficult to separate natural signals from those caused by these errors, and therefore some phase offsets remain in the data, even in 'research quality' datasets. The use of skew surge reduces the impact of these, because, by definition, it is based only on the relative heights of the observed and predicted HW, ignoring the time between them. These suggest that the removal of phase offsets by skew surge is responsible for the reduction in the occurrence of negative trends in the skew surge time-series compared to the (relatively) large number of negative trends found when using the NTR. Phase offsets were more likely to occur early in the dataset, when measurement and recording techniques were less accurate. The removal of the negative bias that exists in the calculated trend of NTR may lead to an earlier identification of the predicted positive changes in magnitude and frequency of storm surges in the future, in response to climate change.

Given the large number of sites with significant tide-surge interaction around the world, and considering the benefits using skew surge has with regard to phase offsets, skew surge should be the preferred parameter for the representation of the meteorological component of sea level.One caveat of its use though, is that individual storm characteristics can differ from the average. Therefore, simultaneous occurrence of peaks in tide and NTR may occur in areas where tide-surge interaction typically causes peaks in NTR to occur away from the predicted HW.

The investigation of the methodological questions above means that the effect of each component of sea level on variability in ESL can be assessed independently. The first objective was to conduct the first global assessment of secular changes in different tidal levels. At some sites the magnitude of the trend in tidal level is comparable to the increase in global MSL, and therefore the effective increase in the observed HW (inclusive of MSL and tide), may be double the increase if only MSL is considered. This has important implications for projections of ESL, which do not account for changes in the tide at present, in most studies. Further work is required to understand the interaction of mechanisms that contribute to these changes, but changes are observed at locations across the world and on many different spatial scales. Local signals are observed in response to hydrological or bathymetric changes. Regional changes may be related to changes in MSL, internal tide generation or large-scale wind patterns, and global changes may be related to changes in global MSL. Comparisons between the tide gauge data and the output of a global tidal

model, show that while MSL can change tidal levels, other mechanisms may be dominant in some regions, such as in the north-east Pacific.

The second objective was to assess changes in the meteorological component of sea level. Skew surge time-series were used, instead of the NTR (because of the level of tide-surge interaction identified at most study sites) to assess the secular and inter-annual variability in the meteorological component. At most sites however, the trends in skew surge and NTR are similar and therefore allow comparisons with previous studies that have used the NTR. Secular trends (in both parameters) were observed at very few sites, typically because the inter-annual variability is large and this creates large uncertainties around the trend. Significant correlations have been observed, between the meteorological component and regional climate in previous studies, but no significant correlations are observed in this study. Strong correlations ($r > 0.5$) were observed, but these were not statistically significant (at 95% level) because the high level of autocorrelation introduced by the filter increased the size of the corresponding confidence intervals. Filters extract the low-frequency signal that reflects the inter-annual variability, but the length of the regional skew surge indices means that significant correlations are not observed. The significance of correlations are strongly affected by the inclusion of autocorrelation, and therefore studies should make it clear whether serial auto-correlation is included or not when estimating trends – in most previous studies it is not included.

The first two objectives improved understanding of the variability in the tide and meteorological components of sea level. On secular timescales, these changes are large at a few sites and may grow in importance in response to climate change over the remainder of the 21st century. However, total variability in ESL is dominated by secular changes in MSL, and seasonal and inter-annual variability in MSL and skew surge. The third objective, considering these findings, was to determine how ESL had changed in response to changes in the magnitude and phase of each of these individual signals. Many studies have investigated changes in ESL as a whole, or changes in individual components, but this novel study assessed the changes in ESL in response to variations in all components on all long-term timescales greater than 6 months. Variability in the magnitude of each signal can combine to generate variations in the baseline ESL of almost 2 m, if the peaks in all signals occurred simultaneously. Not all peaks can occur at the same time in reality due to inter-dependencies between the different components.

Another novel aspect of this thesis is the global assessment of the relative phases of the seasonal and inter-annual signals. At only a few sites do the seasonal cycles of all three components occur in phase, while the extra degrees of freedom on inter-annual timescales mean that peaks in the these signals rarely coincide. However, the relative phase of signals may change because of the

probability of independent signals acting constructively, or by changes in forcing mechanisms. If all independent signals acted constructively, the theoretical maximum would exceed the observed maximum at all sites. The main reasons for this are because the peak in inter-annual MSL and skew surge occurred during a trough in the nodal tidal cycle, or the peak in inter-annual signal occurred away from the maximum contribution from a large secular change (normally MSL). This highlights the importance of all aspects of this study. Secular trends are small relative to the seasonal and inter-annual variability in signals of all components, but their cumulative effect leads to significant changes in ESL. Capturing the variability on seasonal and inter-annual cycles is important for understanding, when ESLs might occur, since changes in the phase and/or the magnitude of these signals can change the magnitude of ESL.

This novel investigation into changes of individual components of sea level on different timescales and their combined effect on ESL, represents the most comprehensive study of factors affecting ESL (to my knowledge). This thesis shows that the assumption that secular changes in ESL are only driven by secular changes in MSL, does not hold true at all sites. Although at most sites the secular trend in MSL is the dominant mechanism causing changes in ESLs, there are significant secular changes in tidal levels at some sites, as well as large seasonal and inter-annual variability in all components. Therefore, all components and timescales should be considered in projections of future ESLs. Changes in the constructiveness of phasing between signals could also change ESL, without any change in the magnitude of variability. The magnitude of many signals that effect ESL will change in the future, and therefore accurate estimates of these changes and the impact they have on ESL are an important requirement for ensuring the safety and continued use of the coastal zone.

7.5 Outlook for further work

There are many areas of further work that have been suggested by this study. They are broadly summarised below.

Exploration of the mechanisms causing changes in the tide

Site specific analysis, such as that done for Astoria (USA; Jay et al., 2011) or Churchill (Canada; Ray, 2016), allows a thorough understanding of the nature of the changes observed in the and therefore better insight into the forcing mechanisms. Specific logs of changes in river discharge, natural or man-made changes in coastal morphodynamics, changes in seawater properties (e.g. temperature and salinity) or sea-ice concentrations, may be available at some sites. This would be

particularly interesting in the North Sea, where the response to MSL rise and changes in coastal morphology have been suggested as possible mechanisms amongst others.

Regional or global scale mechanisms could be investigated using numerical models. The outputs of the 1/8th degree tidal model used in this thesis does not resolve all important features (e.g. physical parameters of seawater or morphological), especially at the coast. Results from a 1/60th degree regional model have been shown to replicate observed changes in the tide gauge records more closely (Carless et al., 2015). Global tidal models examining the response to MSL rise should also capture the fingerprint of the MSL rise accurately. However, a number of different models are likely to be required to resolve regional mechanisms that include changes in MSL, sea-ice concentration, water column stratification and large-scale wind patterns.

Improvements to the tide gauge dataset.

Extension of datasets is recommended by most studies, and despite this thesis adding data to the GESLA dataset, more data is available. By the end of 2017 another 37 sites already within the GESLA dataset will meet the criteria, used in this thesis, of having at least 28 years of data. Many of these sites are in under-represented areas (11 in Malaysia, 5 in South America, 2 each in Bangladesh, the Indian Ocean islands and Africa). The UHSLC database also has another 13 sites with over 28 years of data. Among these are 4 in New Zealand, 3 in South Africa, and Hong Kong in China. Attempts to access data in locations where it is present but not publicly available should be continued, since analysis of this data by different researchers benefits both the global community and the holder of that data. A GESLA2 dataset is currently being compiled by a team of researchers (see www.gesla.org), with additional sites from the above sources. However, the variability of the sea level components is complex and there will never be enough tide gauges to capture it all completely and therefore other sources of sea level data should be considered to create a global database of sea level time-series.

The quality of the data also needs to be assured. The QC conducted as part of this study shows that although the data on platforms (such as UHSLC, NOAA, BODC etc.) are classed as research quality some erroneous data remains. This is partly due to prudence since many natural signals (e.g. meteotsunamis) are very similar, especially in hourly data, to those introduced by errors in measurement or analysis. However, a more thorough documentation would improve confidence in the analyses that use these datasets.

Assess the suitability of linear trends

The application of linear trends to secular changes implies that they are occurring at a constant rate through time. However, the long-term changes in all components have an inter-annual signal,

and in the case of MSL a possible acceleration. This project found that the linear trend accounted for a large proportion (based on R^2 values) of the variance, but at some sites these values were low. Discontinuities in the linear trends observed in the southern North Sea are one example, which as discussed above, might be a response to the construction of Deltaworks. Changes in the tide in this region are occurring, but before they are applied to ESL projection then we need to be sure that they are caused by relevant recent changes. Work by Visser et al. (2014) showed the importance of choosing a suitable regression to fit sea level data, and this could be built upon.

Determine how to apply changes in tidal levels

The finding of differences between trends of different tidal levels mean that applying changes in tidal levels to ESL projections is more complicated. Changes in the magnitude of spring-tropic tidal levels will lead to greater changes in magnitude of ESL than changes in neap-equatorial tidal levels.

Understand mechanisms of tide-surge interaction at each site.

The North Sea pattern of tide-surge interaction is well established, but this study and that of Olbert et al. (2013) have shown that timing of peaks in NTR do not always occur away from predicted HW. Regional studies (e.g. the whole of the UK) to assess the tide-surge interaction at each site should be conducted to determine whether local as well as external factors are important to this interaction at some sites.

Determine whether the magnitude of tide-surge interaction has changed over time

No changes in the level of tide-surge interaction have been observed in previous research, but this study is the largest assessment of the magnitude of tide-surge interaction, and it provides an ideal opportunity to assess this assumption at many more sites. Some of these sites have different patterns from those of the North Sea and English Channel, which were the regions in which the assumption of temporal stability in tide-surge interaction was determined.

On shorter time-scales, it would be good to assess whether differences occur during spring or neap tides. A combination of the two χ^2 methods (tidal level and tidal phase) could show the relative timing of peaks in NTR, but also dependent on the magnitude of the tide.

Determine if skew surge is always the best parameter

Investigate whether skew surge allows accurate extreme value analysis at all sites. At some sites (i.e. Brest, France) individual storms do not follow the typical pattern. For example, the peak NTR generated by Typhoon Ioke struck the island of Yap, in the Pacific, 6 hours before predicted HW.

This meant that the skew surge was 0.5 m smaller than the NTR, even though no significant tide-surge interaction is observed at the site. Therefore, the timing of peak NTR, including that of a storm like Typhoon Ioke, could occur at the same time as predicted HW. It is only in instances like this that the skew surge may underestimate the magnitude of the storm surge, but it is important to understand where this could occur.

Account for the variability in the seasonal cycles for the theoretical maximum

In this study, the seasonal cycle of each component is represented by sinusoidal curves with a fixed magnitude and phase. However, research has shown that these cycles can vary, especially in MSL and skew surge. Much of the variability in the magnitude was included in the inter-annual signal, but a small change in the phase in one seasonal cycle could change the magnitude of the combined seasonal signal.

The seasonal cycle could be calculated for many more sites, since an accurate seasonal cycle can be calculated from only 5 years of data (Marcos and Tsimplis, 2007).

Regional climatology

Improvements to the assessment of regional climatology would be made by using re-analysis data. Climate indices provide a simple method of representing temporal variations in regional climate, but the response of skew surge indices to temperatures in different parts of the Pacific Ocean shows that the spatial differences are important.

Appendices

Appendix A: Quality control notes for all sites

Appendix B: List of Identified Tsunamis.

Appendix C: Site Metadata

Appendix D: Supplementary material to Section 4

Appendix E: Supplementary material to Section 5.

Appendix F: Supplementary material to Section 6

Appendix A Quality Control Notes for All Sites

Data Sources

UK - https://www.bodc.ac.uk/data/online_delivery/ntslf/processed_customise_time_selection/
USA - http://tidesandcurrents.noaa.gov/station_retrieve.shtml?type=Historic+Tide+Data

- All data downloaded in metres, in UTC, relative to STND and hourly data.

Canada - http://www.meds-sdmm.dfo-mpo.gc.ca/isdm-gdsi/twl-mne/maps-cartes/inventory-inventaire-eng.asp

- All data downloaded in metres, in UTC, relative to STND and hourly data.

Australia - http://www.bom.gov.au/oceanography/projects/abslmp/data/index.shtml
South Pacific - http://www.bom.gov.au/oceanography/projects/spslcmp/data/index.shtml
NZ - http://www.linz.govt.nz/hydro/tidal-info/gauges/sea-level-data-downloads
Mexico - http://www.mareografico.unam.mx/Mareografico/

Quality Control

All quality control was conducted using a suite of MATLAB scripts saved here (C:\Users\rjm305\Documents\PhD\1_Project\1_Research\5_MATLAB_Scripts\2_DataQC).

Figures were generated to compare whether one dataset is better than another and whether the data quality of either is sufficient for further analysis. Where no noticeable different in the data was observed the longest site was typically chosen

During analysis of the data particular aspects are looked for:

1. Datum shift, manifests itself as a jump in the mean sea level. Can be corrected.
2. Outliers, peaks. Erroneous value is replaced by an interpolated value.
3. Long-term shift. Due to problem with instrument. Values are removed.
4. Silting of the stilling tubes or wells. The curve is distorted as the water no longer circulates normally. Data are invalid.
5. Time shift. Data can be corrected if time shift is uniform, but sometimes a clock drift occurs which makes this correction difficult and sometimes impossible.

Flags

Following quality control at each site the data were flagged so that interesting events could be noted. Two types of flags were used.

The QC flag identifies what type of error it is:

0 = Meteorological (e.g. Seiche, Meteotsunami),
1 = Spike,
2 = Phase Offset,
3 = Tsunami,
4 = Other

The GESLA flag, determines how it is treated during analysis and follows the same practice as in the inherited dataset (Note, values identified as spikes in this QC are flagged as 3, since they are not used in the analysis.

0 = no quality control
1 = correct value
2 = interpolated value
3 = doubtful value (Not used in analysis)
4 = isolated spike or wrong value
5 = missing value
6 = tsunami (Not used in analysis)

Abashiri, Japan (44.019°N, 144.286°E)

Inherited:

Filename	V1 no.	Start	End	Yrs
Abashiri,japan-001-glossdm-bodc.txt	2	01/01/2001	31/12/2003	3
Abashiri-347a-japan-uhslc.txt	3	01/01/1968	31/12/2005	37

Extended:

V1 filename	Abashiri-347a-japan-uhslc.txt (**3**)
v2 Filename	002_Abashiri-JPN_GESLA_v2.mat
Source of Extra Data	UHSLC
Extra Data filename	347a
Date of Download	12/08/2013
Time of Extra Data	01/01/2006 to 31/12/2010
Load in for Extra Data	UHSLC
Comparison Comments	Comparison between inherited (**3**) and extra are perfect.

Quality Control:

Type	Date Affected	Comments	QC Flag	GESLA Flag
Phase	02/03/1968 to 14/03/1968		2	3
Phase	03/07/1969 to 25/07/1969		2	3
Phase	14/08/1969 to 22/08/1969		2	3
Phase	18/04/1970 to 26/04/1970		2	3
Phase	13/12/1970 to 03/05/1971		2	3
Phase	12/12/1971 to 01/01/1972		2	3

(QC Flag: 0 = Meteorological (e.g. Seiche, Meteo-tsunami), 1 = Spike, 2 = Phase Offset, 3 = Tsunami, 4 = Other)

Analysis Comments

- Mixed tide means switch between diurnal and semi-diurnal gaps.

Aberdeen, UK (57.144°N, 2.077°W)

Inherited:

Filename	V1 no.	Start	End	Yrs
aberdeen-p038-uk-bodc.mat	4	29/05/1930	31/12/2006	46

Extended:

V1 filename	aberdeen-p038-uk-bodc.mat (4)
v2 Filename	003_Aberdeen-GBR_GESLA_v2.mat
Source of Extra Data	BODC
Extra Data filename	RN-7246_1372253428497/Aberdeen_19851231_20130331.txt
Date of Download	
Time of Extra Data	31/12/2006 to 28/02/2013
Load in for Extra Data	BODC2
Comparison Comments	Comparison between inherited (4) and extra are perfect.

Quality Control:

Type	Date Affected	Comments	QC Flag	GESLA Flag
Threshold		Remove data -0.5 < x > 8	1	3

(QC Flag: 0 = Meteorological (e.g. Seiche, Meteo-tsunami), 1 = Spike, 2 = Phase Offset, 3 = Tsunami, 4 = Other)

Analysis Comments:

- Skew surge statistics match those presented in H&W (2007) and therefore gives confidence that the script is performing correctly.
- Tidal range sensitivity tests show no changes in trend (w/o nodal or autocorrelation considered).
- No data for two big events in the North Sea of 1953 and 1978.

Aburatsu, Japan (31.567°N, 131.417°E)

Inherited:

Filename	V1 no.	Start	End	Yrs
Abaratsu,japan-001-glossdm-bodc.txt	5	01/01/1961	31/12/2003	44
Abaratsu354a-japan-uhslc.txt	6	01/01/1961	31/12/2005	46

Extended:

V1 Filename	Abaratsu354a-japan-uhslc.txt (6)
V2 Filename	004_Aburatsu-JPN_GESLA_v2.mat
Source of Extra Data	UHSLC
Extra Data filename	h354a
Date of Download	12/08/2013
Length of Extra Data	Ends 28/02/2013
Load in for Extra Data	BODC2
Comparison Comments	Comparison between inherited (6) and extra are perfect.

Quality Control:

Type	Date Affected	Comments	QC Flag	GESLA Flag
Phase	01/07/1968 to 31/10/1968		2	3

(QC Flag: 0 = Meteorological (e.g. Seiche, Meteo-tsunami), 1 = Spike, 2 = Phase Offset, 3 = Tsunami, 4 = Other)

Analysis Comments:

- Higher surge percentiles appear very noisy, data have been rechecked and the noisiness is due to the infrequent nature of storms that generate them.

Acajutla, El Salvador (13.567°N, 89.833°W)

Inherited:

Filename	V1 no.	Start	End	Yrs
'acajutla-082a-el_salvador-uhslc.mat'	7	01/01/1971	28/02/2001	26

Extended:

V1 Filename	acajutla-082a-el_salvador-uhslc.txt (**7**)
V2 Filename	005_Acajutla-SLV_GESLA_v2.mat
Source of Extra Data	N/A
Extra Data filename	N/A
Date of Download	N/A
Length of Extra Data	N/A
Load in for Extra Data	N/A
Comparison Comments	N/A

Quality Control:

Type	Date Affected	Comments	QC Flag	GESLA Flag
Phase	01/09/1973 09:00 to 03/09/1973		2	3
Phase	05/02/1977 to 09/02/1977		2	3
Phase	30/04/1977 to 03/05/1977		2	3
Phase	15/12/1979 to 06/01/1980		2	3
Phase	14/12/1996 to 17/12/1996		2	3
Phase	25/04/1998 to 28/04/1998		2	3
Phase	23/05/1998 to 26/05/1998		2	3

(QC Flag: 0 = Meteorological (e.g. Seiche, Meteo-tsunami), 1 = Spike, 2 = Phase Offset, 3 = Tsunami, 4 = Other)

Analysis Comments:

- Data set is noisy throughout. Although it looks like instrument noise there is no change in this with time and therefore be natural.

Adak, USA (Alaska) (51.863°N, 176.632°W)

Inherited:

Filename	V1 no.	Start	End	Yrs
'adak,alaska-040a-usa-uhslc.mat'	9	17/03/1950	31/12/2005	49
'adak-001-glossdm-bodc.mat'	10	17/03/1950	31/12/2000	43

Extended:

V1 filename	adak,alaska-040a-usa-uhslc.txt (**9**)
v2 Filename	007_Adak-USA_GESLA_v2.mat
Source of Extra Data	UHSLC/NOAA
Extra Data filename	040a/NOAA_Adak.txt
Date of Download	26/06/2013
End of Extra Data	31/12/2012
Load in for Extra Data	UHSLC/NOAA
Comparison Comments	Comparisons between datasets are perfect

Quality Control:

Type	Date Affected	Comments	QC Flag	GESLA Flag
Tsunami	04/11/1952 18:00 to 08/11/1952	Kuril Island Earthquake	3	6
Tsunami	23/05/1960 12:00 to 27/05/1960	Valdivia Earthquake	3	6
Tsunami	28/02/2010 to 03/03/2010	Chile Earthquake	3	6
Tsunami	11/03/2011 to 16/03/2011	Tohuku Earthquake	3	6

(QC Flag: 0 = Meteorological (e.g. Seiche, Meteo-tsunami), 1 = Spike, 2 = Phase Offset, 3 = Tsunami, 4 = Other)

Albany, Australia (35.034°S, 117.893°E)

Inherited:

Filename	V1 no.	Start	End	Yrs
'albany-001-australia-johnhunter.txt '	**11**	31/05/1960	31/12/2004	38

Extended:

v1 filename	'albany-001-australia-johnhunter.txt (**11**)
v2 Filename	008_Albany-AUS_GESLA_v2.mat
Source of Extra Data	N/A
Extra Data filename	N/A
Date of Download	N/A
End of Extra Data	N/A
Load in for Extra Data	N/A
Comparison Comments	N/A

Quality Control:

Type	Date Affected	Comments	QC Flag	GESLA Flag
Spike	14/04/1983 05:00		1	3
Spike	19/02/1984 18:00		1	3

(QC Flag: 0 = Meteorological (e.g. Seiche, Meteo-tsunami), 1 = Spike, 2 = Phase Offset, 3 = Tsunami, 4 = Other)

Analysis Comments

- First year of valid data is 1966.

Antofagasta, Chile (23.650°S, 70.400°W)

Inherited:

Filename	V1 no.	Start	End	Yrs
antofagasta-080a-chile-uhslc.mat	**20**	06/12/1945	31/12/2002	57

Extended:

v1 filename	antofagasta-080a-chile-uhslc.txt (**20**)
v2 Filename	017_Antofagasta-CHL_GESLA_v2.mat
Source of Extra Data	UHSLC
Extra Data filename	H80a
Date of Download	16/01/2014
End of Extra Data	31/12/2012
Load in for Extra Data	UHSLC
Comparison Comments	New data matching perfectly the inherited.

Quality Control:

Type	Date Affected	Comments	QC Flag	GESLA Flag
Tsunami	24/06/2001 to 26/06/2001	Southern Peru Earthquake	3	6
Tsunami	27/02/2010 to 03/03/2010	Chile Earthquake	3	6
Tsunami	11/03/2011 to 16/03/2011	Tohuku Earthquake	3	6

(QC Flag: 0 = Meteorological (e.g. Seiche, Meteo-tsunami), 1 = Spike, 2 = Phase Offset, 3 = Tsunami, 4 = Other)

Argentia, Canada (Newfoundland) (47.300°N, 53.983°W)

Inherited:

Filename	V1 no.	Start	End	Yrs
argentia,nf-00835-canada-meds.mat	**25**	11/02/1971	31/10/2008	36

Extended:

v1 filename	argentia,nf-00835-canada-meds.mat (**25**)
v2 Filename	021_Argentia-CAN_GESLA_v2.mat
Source of Extra Data	MEDS
Extra Data filename	835_01-JAN-2008_slev
Date of Download	30/07/2013
End of Extra Data	31/12/2012
Load in for Extra Data	MEDS
Comparison Comments	New data matching perfectly the inherited.

Quality Control:

Type	Date Affected	Comments	QC Flag	GESLA Flag
Phase	01/01/2008 to 05/01/2008		2	3

(QC Flag: 0 = Meteorological (e.g. Seiche, Meteo-tsunami), 1 = Spike, 2 = Phase Offset, 3 = Tsunami, 4 = Other)

Analysis Comments

- Peak NTR occurs on 10/01/1982 caused by storm documented in this paper 'Numerical Simulation of the Storm Surge of January 1982 on the South Coast of Newfoundland' by Murty & Greenberg.
- Surge on 5 Jan 1989 at same time as intense Atlantic storm.
- Residual on 10/09/1995, caused by Hurricane Luis
- Residual on 11/09/2012, caused by Hurricane Leslie

Astoria, USA (Oregon) (46.208°N, 123.767°W)

Inherited:

Filename	V1 no.	Start	End	Yrs
'astoria,or-572a-usa-uhslc.mat'	**29**	25/01/1925	31/12/2005	80

Extended:

v1 filename	astoria,or-572a-usa-uhslc.mat' (**29**)
v2 Filename	024_Astoria_USA_GESLA_v2.mat
Source of Extra Data	UHSLC
Extra Data filename	H572a
Date of Download	17/01/2014
End of Extra Data	31/12/2012
Load in for Extra Data	UHSLC
Comparison Comments	Comparison between inherited and new data show no differences.

Quality Control:

Type	Date Affected	Comments	QC Flag	GESLA Flag
Phase shift	23/12/1926	Offset of 1hr causes small residual	2	3
Phase shift	21/01/1929	Offset of 1hr causes small residual	2	3
Phase shift	05/11/1929	Offset of 1hr causes small residual	2	3
Phase shift	01/02/1933	Offset of 1hr causes small residual	2	3
Phase shift	02/12/1933	Offset of 1hr causes small residual	2	3
Phase shift	31/05/1934	Offset of 1hr causes small residual	2	3
Phase shift	01/09/1983 to 01/04/1984	Phase offset leading to erroneous tide and residual values	2	3
Phase	01/01/1989 to 02/04/1989		2	3
Phase	30/10/1989 to 31/12/1989		2	3

(QC Flag: 0 = Meteorological (e.g. Seiche, Meteo-tsunami), 1 = Spike, 2 = Phase Offset, 3 = Tsunami, 4 = Other)

Analysis Comments

- Clear seasonal cycle in residual associated with winter storms.
- Peak residual occurs on 17/12/1961 associated with known strong winds at Astoria on this day.
- Another big event occurs on 15/12/2006 and is associated with Hanukkah Eve storm that swept across NW USA.

Atlantic City, USA (39.355°N, 74.418°W)

Inherited:

Filename	V1 no.	Start	End	Yrs
'atlantic_city-264a-usa-uhslc.mat'	**30**	19/08/1911	31/12/2005	88
'atlanticcity-003-usa-johnhunter.mat'	**31**	19/08/1911	28/02/2006	59

Extended:

v1 filename	atlantic_city-264a-usa-uhslc.mat' (**30**)
v2 Filename	025_AtlanticCity-USA_GESLA_v2.mat
Source of Extra Data	UHSLC/NOAA
Extra Data filename	264a/ COOPS_AtlanticCity
Date of Download	22/05/2014
End of Extra Data	31/12/2013
Load in for Extra Data	UHSLC/NOAA
Comparison Comments	Comparison between selected inherited (30) and new data show no differences.

Quality Control:

Type	Date Affected	Comments	QC Flag	GESLA Flag
		No erroneous values to remove		

(QC Flag: 0 = Meteorological (e.g. Seiche, Meteo-tsunami), 1 = Spike, 2 = Phase Offset, 3 = Tsunami, 4 = Other)

Analysis Comments

- Skew surge statistics show bimodal distribution with peak HW-3, and HW+5. Not clearest of signals possibly because of narrow continental shelf.
- Surges of similar magnitude to tidal range. Predominantly during winter ET events, but also related to some hurricanes.
- Max. residual on 27/09/1985 caused by Hurricane Gloria.
- Max. sea level on 13/12/1992 caused by huge northeaster.
- Large residuals also on 30/01/1966 (North American Blizzard), 10/02/1978 (Storm with blizzard) & 29/10/2012 (Hurricane Sandy)

Balboa, Panama (8.962°N, 79.573°W)

Inherited:

Filename	V1 no.	Start	End	Yrs
balboa-302a-panama-uhslc.mat	**34**	19/06/1907	31/12/1997	88

Extended:

v1 filename	balboa-302a-panama-uhslc.mat (**34**)
v2 Filename	028_Balboa-PAN_GESLA_v2.mat
Source of Extra Data	UHSLC
Extra Data filename	H302a
Date of Download	Unknown
End of Extra Data	31/07/2010
Load in for Extra Data	UHSLA
Comparison Comments	Comparisons between inherited and extra data is perfect.

Quality Control:

Type	Date Affected	Comments	QC Flag	GESLA Flag
Spike	15/01/1908 09:00 to 14:00		1	3
Spike	15/07/1908 09:00 to 14:00		1	3
Phase	15/08/1908 to 01/09/1908		2	3
Phase	21/04/1943 to 26/04/1943		2	3
Phase	26/02/1948 to 28/02/1948		2	3
Phase	03/10/1948 18:00 to 04/10/1948 18:00		2	3
Phase	14/05/1949 to 17/05/1949		2	3
Phase	01/04/1952 12:00 to 04/04/1952 18:00		2	3
Phase	10/06/1972 to 19/06/1972		2	3
Phase	08/05/1973 12:00 to 10/05/1973		2	3
Phase	01/02/1975 to 07/02/1975		2	3
Phase	20/08/1975 to 28/08/1975		2	3
Phase	14/08/1977 to 05/09/1977		2	3
Phase	18/12/1977 to 01/01/1978		2	3
Phase	13/01/1978 to 21/01/1978		2	3
Phase	12/10/1980 to 15/10/1980		2	3
Phase	28/05/1981 to 02/06/1981		2	3
Phase	01/08/1981 to 05/08/1981		2	3
Phase	13/05/1983 to 20/05/1983		2	3
Phase	01/01/1984 to 04/01/1984		2	3
Phase	18/01/1991 12:00 to 22/01/1991 12:00		2	3
Phase	24/09/1992 12:00 to 30/09/1992		2	3
Phase	10/10/1992 to 15/10/1992 12:00		2	3
Phase	03/06/1996 12:00 to 17/06/1992		2	3
Phase	01/01/1997 to 01/02/1997		2	3
Phase	01/12/1997 to 01/01/1998		2	3
Phase	01/11/1998 to 01/12/1998		2	3
Phase	01/01/1999 to 07/03/1999		2	3
Phase	23/01/2007 12:00 to 24/01/2007 12:00		2	3

(QC Flag: 0 = Meteorological (e.g. Seiche, Meteo-tsunami), 1 = Spike, 2 = Phase Offset, 3 = Tsunami, 4 = Other)

Analysis Comments

- Strong skew surge affect with bi-modal distribution showing peaks 3-4 before or after HW. Likely due to the extent of shallow water around it in the Gulf of Panama, which allows the wind to act on the shallow water.

Baltimore, USA (39.267°N, 76.583°W)

Inherited:

Filename	V1 no.	Start	End	Yrs
'baltimore-004-usa-johnhunter.mat'	**35**	01/07/1902	28/02/2006	103

Extended:

v1 filename	'baltimore-004-usa-johnhunter.mat' (**35**)
v2 Filename	029_Baltimore_USA_GESLA_v2.mat
Source of Extra Data	NOAA-COOPS
Extra Data filename	CO-OPS_Baltimore.csv
Date of Download	17/01/2014
End of Extra Data	31/12/2013
Load in for Extra Data	NewNOAA
Comparison Comments	Comparison between inherited and new data show no differences.

Quality Control:

Type	Date Affected	Comments	QC Flag	GESLA Flag
		No erroneous values to remove		

(QC Flag: 0 = Meteorological (e.g. Seiche, Meteo-tsunami), 1 = Spike, 2 = Phase Offset, 3 = Tsunami, 4 = Other)

Analysis Comments

- Peak residual (+2.2 m) occurs on 24/08/1933 associated with Chesapeake-Potomac Hurricane.
- Another large event (> 2 m) on 19/09/2003 caused by Hurricane Isabel.
- Lowest residual (-1.6 m) occurs on 19/09/1936 associated with East Coast Hurricane
- The background residual size is often large, probably because of the position of the recorder up Chesapeake Bay which makes it susceptible to storm surges and the influence of river flow.
- Invalid data is harder to identify at this site since residual values are higher.

Bamfield, Canada (48.836°N, 125.136°W)

Inherited:

Filename	V1 no.	Start	End	Yrs
'bamfield,bc-08545-canada-meds.mat'	**40**	27/09/1969	27/09/2008	39

Extended:

v1 filename	'bamfield,bc-08545-canada-meds.mat (**41**)
v2 Filename	031_Bamfield-CAN_GESLA_v2.mat
Source of Extra Data	MEDS
Extra Data filename	8545-01-JAN-2007_slev.csv
Date of Download	17/01/2014
End of Extra Data	31/12/2012
Load in for Extra Data	MEDS
Comparison Comments	Comparison with new data downloaded in UTC from MEDS website on 17/01/2014 shows that inherited data is -16 hr different. I correct the data with the assumption that the newly downloaded data is correct, such that the inherited dataset has been shifted forward 16 hrs. Comparison between are otherwise good.

Quality Control:

Type	Date Affected	Comments	QC Flag	GESLA Flag
		No erroneous values to remove		

(QC Flag: 0 = Meteorological (e.g. Seiche, Meteo-tsunami), 1 = Spike, 2 = Phase Offset, 3 = Tsunami, 4 = Other)

Bella Bella, Canada (52.163°N, 128.143°W)

Inherited:

Filename	V1 no.	Start	End	Yrs
'bellabella,bc-08976-canada-meds.mat'	**44**	27/09/1969	27/09/2008	39

Extended:

v1 filename	'bellabella,bc-08976-canada-meds.mat (**41**)
v2 Filename	035_BellaBella-CAN_GESLA_v2.mat
Source of Extra Data	MEDS
Extra Data filename	8976-01-JAN-2008_slev.csv
Date of Download	17/01/2014
End of Extra Data	31/12/2012
Load in for Extra Data	MEDS
Comparison Comments	Comparison with new data downloaded in UTC from MEDS website on 17/01/2014 shows that inherited data is -16 hr different. I correct the data with the assumption that the newly downloaded data is correct, such that the inherited dataset has been shifted forward 16 hrs. Comparison between are otherwise good.

Quality Control:

Type	Date Affected	Comments	QC Flag	GESLA Flag
Other	1906 (Whole Year)	See below	4	3
Spike	22/12/1965 03:00		1	3
Spike	26/12/1965 07:00		1	3
Spike	16/04/1968 13:00		1	3
Spike	18/04/1968 14:00		1	3
Phase Shift	20/10/ 1968 to 26/10/1968		2	3
Phase Shift	14/09/1978 12:00 to 20/09/1978 23:00		2	3
Phase Shift	31/10/1978 03:00 to 01/11/1978 19:00		2	3
Phase Shift	14/03/1980 18:00 to 18/03/1980 06:00		2	3

(QC Flag: 0 = Meteorological (e.g. Seiche, Meteo-tsunami), 1 = Spike, 2 = Phase Offset, 3 = Tsunami, 4 = Other)

Analysis Comments

- 1906 is only year of valid data until 1960. The signal is similar but the phase for the M2 and S2 constituents is different to 1960 to 2012.
- Clear seasonal cycle with storm season over winter.
- Noisy signal the response of location which is sheltered from sea by fjords.

Boston, USA (42.355°N, 71.052°W)

Inherited:

Filename	V1 no.	Start	End	Yrs
'boston,ma-741a-usa-uhslc.mat'	**54**	03/05/1921	31/12/2005	83
'boston-002-usa-johnhunter.mat'	**55**	03/05/1921	28/02/2006	83

Extended:

v1 filename	'boston,ma-741a-usa-uhslc.mat'
v2 Filename	042_Boston-USA_GESLA_v2.mat
Source of Extra Data	UHSLC/NOAA
Extra Data filename	H741a/COOP_Boston
Date of Download	28/01/2014
End of Extra Data	31/12/2013
Load in for Extra Data	UHSLC/newNOAA
Comparison Comments	Comparison with inherited data is almost perfect.

Quality Control:

Type	Date Affected	Comments	QC Flag	GESLA Flag
Phase	19/09/1923 06:00 to 18:00.		2	3
Phase	21/09/1923 18:00 to 22/09/1923 01:00		2	3
Phase	03/08/1938 03:00 to 04/08/1938 06:00		2	3
Phase	06/08/1938 00:00 to 08/08/1938 12:00		2	3
Phase	07/05/1963 03:00 to 08/08/1963 04:00		2	3
Phase	14/03/1970 06:00 to 17/03/1970 00:00		2	3
Phase	13/08/1971 00:00 to 15/08/1971 12:00		2	3
Phase	01/01/1986 21:00 to 06/01/1986 18:00		2	3
Phase	14/08/1987 15:00 to 17/08/1987 16:00		2	3
Phase	09/09/1988 15:00 to 12/09/1988 12:00		2	3

(QC Flag: 0 = Meteorological (e.g. Seiche, Meteo-tsunami), 1 = Spike, 2 = Phase Offset, 3 = Tsunami, 4 = Other)

Analysis Comments

- Minimum residual value associated with Groundhog Day storm on 2 February 1976.
- Large residual caused by storm on 5 Feb 1978
- Peak residual caused by winter storm (http://en.wikipedia.org/wiki/February_25%E2%80%9327,_2010_North_American_blizzard) but the residual values does look a little suspicious. Will be left in unless further evidence emerges.

Brest, France (48.383°N, 4.500°W)

Inherited:

Filename	V1 no.	Start	End	Yrs
brest-bre-france-shom.txt	**56**	04/01/1846	31/12/2006	146
brest-822a-france-uhslc.txt	**57**	04/01/1846	10/01/2008	147

Extended:

v1 filename	brest-822a-france-uhslc.txt (**57**)
v2 Filename	043_Brest-France_GESLA_v2.mat
Source of Extra Data	N/A
Extra Data filename	N/A
Date of Download	N/A
End of Extra Data	N/A
Load in for Extra Data	N/A
Comparison Comments	N/A

Quality Control:

Type	Date Affected	Comments	QC Flag	GESLA Flag
Phase	31-Dec-1846		2	3
Phase	31/01/1850		2	3
Phase	28/12/1851 to 11/01/1852		2	3
Phase	20/03/1868 00:00 to 12:00		2	3
Phase	14/02/1869 to 17/02/1869		2	3
Phase	27/02/1869 12:00 to 28/02/1869 12:00		2	3
Phase	01/02/1870		2	3
Phase	07/08/1871		2	3
Phase	19/05/1872 to 20/05/1872		2	3
Phase	05/05/1876		2	3
Phase	29/12/1876		2	3
Datum	29/10.1887	0.5 m for 6 hr	4	3
Spike	25/02/1888 16:00 to 21:00		1	3
Phase	02/03/1897		2	3
Datum	30/10/1897	0.5 m for 6 hr	4	3
Phase	09/06/1898 to 20/06/1898 12:00		2	3
Phase	31/01/1907 21:00 to 01/02/1907 12:00		2	3
Phase	01/05/1907 12:00 to 03/05/1907		2	3
Phase	24/09/1907 10:00 to 26/09/1907		2	3
Spike	01/11/1908 03:00		1	3
Phase	31/08/1909 21:00 to 01/09/1909 12:00		2	3
Phase	02/04/1910 to 04/04/1910		2	3
Phase	17/12/1910 21:00 to 18/12/1910 06:00		2	3
Spike	28/03/1911 to 29/03/1911		1	3
Datum	01/09/1912 to 15/09/1912	Residual = 0.4	4	3
Phase	01-Mar-1913		2	3
Phase	14/07/1915 00:00 to 06:00		2	3
Phase	18/05/1916		2	3
Phase	27/02/1917		2	3
Spike	18/09/1920 to 19/09/1920		1	3
Spike	15/12/1922 to 16/12/1922		1	3
Phase	29/07/1923 to 01/08/1923		2	3
Phase	04/02/1939 00:00 to 08:00		2	3
Phase	06/07/1939 12:00 to 21:00		2	3
Phase	01/11/1939 10:00 to 20:00		2	3
Phase	01/07/1940 to 04/07/1940		2	3
Phase	12/02/1953 to 16/02/1953		2	3
Phase	19/03/1953		2	3
Phase	29/04/1954		2	3
Phase	01/11/1955 06:00 to 02/11/1955		2	3
Phase	21/05/1956 to 24/05/1956		2	3
Datum	18/08/1956	0.5 m	4	3
Phase	03/10/1956 to 05/10/1956 12:00		2	3
Phase	02/08/1958		2	3
Phase	19/02/1961		2	3
Datum	09/09/1963		4	3
Phase	16/09/1963		2	3
Phase	14/06/1965		2	3
Phase	16/02/1969 16:00 to 22:00		2	3
Phase	27/11/1969 to 28/11/1969		2	3
Phase	28/10/1970 03:00 to 09:00		2	3
Phase	19/10/1972 06:00 to 15:00		2	3
Phase	11-Aug-1975		2	3
Phase	19-Aug-1979		2	3
Other	05-Oct-1979		4	3
Phase	31-Dec-1979		2	3
Phase	30/12/1982 to 31/12/1982		2	3
Phase	16-Oct-1987		2	3
Phase	26-Nov-1999		2	3

(QC Flag: 0 = Meteorological (e.g. Seiche, Meteo-tsunami), 1 = Spike, 2 = Phase Offset, 3 = Tsunami, 4 = Other)

Brisbane, AUS (27.468°S, 153.028°E)

Inherited:

Filename	V1 no.	Start	End	Yrs
'brisbane-002-australia-johnhunter.mat'	**58**	14/11/1957	31/12/2004	32
'brisbane-331a-australia-uhslc.mat'	**59**	01/01/1984	31/12/2006	23

Extended:

v1 filename	'brisbane-002-australia-johnhunter.mat (**58**)
v2 Filename	044_Brisbane-AUS_GESLA_v2.mat
Source of Extra Data	UHSLC
Extra Data filename	H331a
Date of Download	28/01/2014
End of Extra Data	31/12/2014
Load in for Extra Data	UHSLC
Comparison Comments	Comparison with inherited data is almost perfect.

Quality Control:

Type	Date Affected	Comments	QC Flag	GESLA Flag
Phase	09/10/1966 13:00 to 11/10/1966 15:00		2	3
Phase	08/02/1980 to 17/02/1980		2	3
Phase	20/04/1980 to 01/05/1980		2	3
Phase	18/05/1980 to 29/05/1980		2	3
Phase	14/03/1981 to 22/03/1981		2	3
Phase	30/03/1981 to 12/04/1981		2	3
Phase	17/05/1981 to 27/05/1981		2	3
Phase	29/05/1981 to 03/06/1981		2	3
Phase	16/08/1981 to 03/09/1981		2	3
Phase	07/09/1981 to 17/09/1981		2	3
Phase	07/11/1981 to 11/11/1981		2	3
Phase	16/07/1982 to 29/07/1982		2	3
Phase	01/08/1982 to 04/08/1982		2	3
Phase	07/08/1982 to 30/09/1982 12:00		2	3
Phase	16/10/1982 to 21/10/1982		2	3
Phase	27/10/1982 to 02/11/1982		2	3
Phase	03/02/1983 15:00 to 04/02/1983 03:00		2	3
Phase	03/05/1983 08:00 to 04/05/1983 00:00		2	3
Phase	02/01/1984 to 17/01/1984		2	3
Phase	20/12/1984 to 24/12/1984		2	3
Phase	05/05/1986 06:00 to 18:00		2	3
Phase	21/10/1986 to 24/10/1986		2	3
Phase	06/06/1988 to 10/06/1988		2	3

(QC Flag: 0 = Meteorological (e.g. Seiche, Meteo-tsunami), 1 = Spike, 2 = Phase Offset, 3 = Tsunami, 4 = Other)

Analysis Comments

- Jumps in tidal amplitude of M2 seen around 1990 and 2000 need further investigation.
- Negative ESL on 10 February 1972 caused by Cyclone Wendy.
- Max. residual on 5/3/2004 caused by Cyclone Ingrid

Broome, AUS (17.955°S, 122.242°E)

Inherited:

Filename	V1 no.	Start	End	Yrs
'broome-004-australia-johnhunter.mat'	**60**	02/07/1966	31/12/2005	28
'broome-166a-australia-uhslc.mat'	**61**	12/07/1986	31/12/2006	16

Extended:

v1 filename	'broome-004-australia-johnhunter.mat (**60**)
v2 Filename	045_Broome-AUS_GESLA_v2.mat
Source of Extra Data	UHSLC/BOM
Extra Data filename	H166a/Broome_BOM_2012-13
Date of Download	28/01/2014
End of Extra Data	31/12/2013
Load in for Extra Data	UHSLC/BOM
Comparison Comments	Datum shift of -2 m applied to BOM to matches UHSLC. Then applied -1.139 m shift to match extra to inherited.

Quality Control:

Type	Date Affected	Comments	QC Flag	GESLA Flag
Phase	12/12/1967 00:00 to 03/01/1968 00:00		2	3
Phase	19/02/1969 00:00 to 21/02/1969 00:00		2	3
Phase	01/08/1969 10:00 to 02/08/1969 17:00		2	3
Phase	12/03/1972 to 01/10/1972		2	3
Phase	25/12/1973 to 03/01/1974		2	3
Datum	27/12/1974 19:00 to 28/12/1974 07:00		4	3
Gaps	17/09/1975 to 09/11/1975		4	3
Phase	19/02/1978 to 26/02/1978		2	3
Phase	09/03/1978 to 15/03/1978		2	3
Datum	08/02/1979 04:00 to 21/03/1979 06:00		4	3
Datum	09/07/1979 to 11/07/1979		4	3
Phase	13/02/1980 to 20/02/1980		2	3
Spike	15/03/1980 00:00 to 22/03/1980 04:00		1	3
Phase	01/04/1980 to 05/04/1980		2	3

(QC Flag: 0 = Meteorological (e.g. Seiche, Meteo-tsunami), 1 = Spike, 2 = Phase Offset, 3 = Tsunami, 4 = Other)

Analysis Comments

- Cyclone Rosito causes larges residual on 20/04/2000.
- Data before 1989 is noisy (both residual and tide) with jumps in MSL.
- The residuals (observed data minus predicted tides are very noisy, probably due to shallow water and complex coastal geometry effects that are not resolved by the harmonic analysis (UHSLC documentation)

Buenaventura, Colombia (3.900°N, 77.100°W)

Inherited:

Filename	V1 no.	Start	End	Yrs
'buenaventura-085a-colombia-uhslc.mat	**62**	12/05/1953	31/12/2000	43

Extended:

v1 filename	'buenaventura-085a-colombia-uhslc.mat (**62**)
v2 Filename	046_Buenaventura-COL_GESLA_v2.mat
Source of Extra Data	UHSLC
Extra Data filename	H085a
Date of Download	28/01/2014
End of Extra Data	31/03/2011
Load in for Extra Data	UHSLC
Comparison Comments	Data extension agrees perfectly with inherited dataset.

Quality Control:

Type	Date Affected	Comments	QC Flag	GESLA Flag
Phase	31/05/1962 00:00 to 31/05/1962 23:00		2	3
Phase	04/08/1967 02:00 to 06/08/1967 06:00		2	3
Phase	02/02/1971 02:00 to 05/02/1971 05:00		2	3
Phase	22/01/1975 to 29/01/1975		2	3
Phase	05/10/1975 to 12/10./1975		2	3
Phase	22/10/1975 to 12/12/1975		2	3
Phase	24/05/1976 to 30/05/1976		2	3
Phase	14/08/1977 to 28/08/1977		2	3
Phase	01/10/1978 21:00 to 05/10/197800:00		2	3
Phase	02/10/1979 21:00 to 04/10/1979 18:00		2	3
Phase	27/10/1985 to 31/10/1985 12:00		2	3
Phase	22/10/1988 to 31/10/1988 06:00		2	3
Phase	09/11/1988 12:00 to 11/11/1988 12:00		2	3
Phase	13/04/1991 15:00 to 15/04/1991 12:00		2	3
Phase	25/07/1991 to 26/07/1991 03:00		2	3
Phase	06/08/1995 to 15/08/1995		2	3
Phase	26/09/1996 to 02/10/1996		2	3
Phase	23/03/1997 to 27/03/1997		2	3
Phase	02/10/2003 to 19/10/2003 08:00		2	3
Phase	25/10/2003 to 01/11/2003		2	3
Phase	01/12/2003 00:00 21:00		2	3
Phase	15/07/2005 12:00 to 16/07/2005 12:00		2	3
Phase	20/08/2005 to 20/09/2005 12:00		2	3
Phase	05/10/2005 to 08/10/2005		2	3
Phase	10/03/2006 06:00 to 12/03/2009 14:00		2	3
Phase	26/08/2006 to 28/10/2006		2	3
Phase	2007 (all)		2	3
Phase	22/08/2008 to 27/08/2008		2	3
Phase	10/03/2009 06:00 to 11/03/2009 12:00		2	3
Phase	01/04/2009 to 01/05/2009		2	3

Phase	07/05/2009 10:00 to 12/05/2009 14:00		2	3
Phase	22/09/2009 to 23/09/2009 14:00		2	3

(QC Flag: 0 = Meteorological (e.g. Seiche, Meteo-tsunami), 1 = Spike, 2 = Phase Offset, 3 = Tsunami, 4 = Other)

Analysis Comments

- Whole of 2007 has large residual values, with the whole year seemingly out of phase with the predicted tide. Can this be time shifted? Removed from analysis at present, until time available for thorough analysis.
- A number of big spikes in the data especially towards the end need attention before the data are used.

Bunbury, Australia (33.327°S, 115.637°E)

Inherited:

Filename	V1 no.	Start	End	Yrs
bunbury-006-australia-johnhunter.mat	**64**	01/11/1963	31/12/2004	38

Extended:

v1 filename	bunbury-006-australia-johnhunter.mat (**64**)
v2 Filename	048_Bunbury-AUS_GESLA_v2.mat
Source of Extra Data	N/A
Extra Data filename	N/A
Date of Download	N/A
End of Extra Data	N/A
Load in for Extra Data	N/A
Comparison Comments	N/A

Quality Control:

Type	Date Affected	Comments	QC Flag	GESLA Flag
Datum	Data from start to end-1969.	Large magnitude jump in constituents and tidal levels.	4	3

(QC Flag: 0 = Meteorological (e.g. Seiche, Meteo-tsunami), 1 = Spike, 2 = Phase Offset, 3 = Tsunami, 4 = Other)

Bundaberg, Australia (24.866°S, 152.349°E)

Inherited:

Filename	V1 no.	Start	End	Yrs
bundaberg,australia-001-glossdm-bodc.mat'	**65**	01/01/1997	31/12/1998	2
'bundaberg-003-australia-johnhunter.mat'	**66**	16/02/1966	31/12/2004	36
'bundaberg-332a-australia-uhslc.mat'	**67**	01/01/1984	31/12/2006	23

Extended:

v1 filename	'bundaberg-003-australia-johnhunter.mat (**67**)
v2 Filename	049_Bundaberg-AUS_GESLA_v2.mat
Source of Extra Data	UHSLC
Extra Data filename	H332a
Date of Download	29/01/2014
End of Extra Data	31/12/2012
Load in for Extra Data	UHSLC
Comparison Comments	Data extension agrees perfectly with inherited dataset.

Quality Control:

Type	Date Affected	Comments	QC Flag	GESLA Flag
Phase	02/11/1966 21:00 to 09/11/1966 00:00		2	3
Phase	28/08/1974 to 03/09/1974		2	3
Spike	25/10/1975 06:00 to 07:00		1	3
Phase	02/02/1981 to 03/02/1981		2	3
Spike	02/08/1981 00:00 to 02/08/1981 21:00		1	3
Phase	10/04/1987 to 23/04/1987		2	3
Phase	25/04/1987 21:00 to 30/04/1987		2	3
Phase	03/05/1987 to 10/05/1987 12:00		2	3
Phase	14/05/1987 12:00 to 18/05/1987 00:00		2	3
Phase	22/05/1987 04:00 to 23/05/1987 07:00		2	3
Phase	25/05/1987 15:00 to 26/05/1987 19:00		2	3

(QC Flag: 0 = Meteorological (e.g. Seiche, Meteo-tsunami), 1 = Spike, 2 = Phase Offset, 3 = Tsunami, 4 = Other)

Analysis Comments

- Peak residual occurs on 10/02/1971, is due to Tropical Cyclone Dora. Unfortunately there is a period of missing data immediately prior to storm.
- Large residual occurs on 10/01/1968 but does not agree with any documented cyclone or tsunamis . Data to be left in.

Burnie, Australia (41.053°S, 145.906°E)

Inherited:

Filename	V1 no.	Start	End	Yrs
burnie-005-australia-johnhunter.mat	**68**	15/07/1952	31/12/2004	29

Extended:

v1 filename	burnie-005-australia-johnhunter.mat (**68**)
v2 Filename	050_Burnie-AUS_GESLA_v2.mat
Source of Extra Data	BOM
Extra Data filename	Burnie_BOM_2004-13.csv
Date of Download	30/01/2014
End of Extra Data	31/12/2013
Load in for Extra Data	BOM
Comparison Comments	Perfect agreement between inherited data and extension

Quality Control:

Type	Date Affected	Comments	QC Flag	GESLA Flag
Datum	Up to 1985		4	3
Spike	04/07/1986 06:00 to 08:00		1	3
Spike	26/08/1986 02:00 to 06:00		1	3
Spike	06/09/1986 01:00 to 04:00		1	3
Phase	23/10/1986 00:00 to 25/10/1986 00:00		2	3
Phase	07/11/1986		2	3
Phase	16/07/1988 to 28/07/1988		2	3

(QC Flag: 0 = Meteorological (e.g. Seiche, Meteo-tsunami), 1 = Spike, 2 = Phase Offset, 3 = Tsunami, 4 = Other)

Analysis Comments

- Data prior to 1980 appear very different to present data, suggest removing all data before 1980, but data after this period seems consistent. **Data removed prior to 1985**.
- Remaining data at high percentiles are noisy, but there are only small events so small variations look larger.

Cabo San Lucas, Mexico (22.880°N, 109.908°W)

Inherited:

Filename	V1 no.	Start	End	Yrs
cabo_san_lucas-034a-mexico-uhslc.mat	**69**	12/06/1973	31/12/2003	21
cabosanlucas,mexico-001-glossdm-bodc.mat	**70**	12/06/1973	31/12/1998	18

Extended:

v1 filename	'cabo_san_lucas-034a-mexico-uhslc.mat (69)
v2 Filename	051_CaboSanLucas-Mexico_GESLA_v2.mat
Source of Extra Data	N/A
Extra Data filename	N/A
Date of Download	N/A
End of Extra Data	N/A
Load in for Extra Data	N/A
Comparison Comments	No extra data available

Quality Control:

Type	Date Affected	Comments	QC Flag	GESLA Flag
Phase	01/03/1983 00:00 to 24/03/1983 00:00		2	3
Phase	09/05/1983 to 16/05/1983		2	3
Phase	23/05/1983 to 30/05/1983		2	3
Phase	20/08/1983 to 13/09/1983		2	3
Phase	15/12/1983 to 21/12/1983		2	3
Phase	19/01/1984 00:00 to 19/01/1984 21:00		2	3
Phase	27/01/1984 to 05/02/1984		2	3
Phase	16/02/1984 06:00 to 17/02/1984 01:00		2	3
Phase	18/02/1984 18:00 to 22/02/1984		2	3
Phase	05/03/1984 to 08/03/1984 12:00		2	3
Phase	28/03/1984 to 30/03/1984		2	3
Phase	09/05/1984 12:00 to 13/05/1984		2	3
Phase	08/06/1984 12:00 to 17/06/1984		2	3
Phase	25/06/1984 to 28/06/1984 18:00		2	3
Phase	18/07/1984 to 05/08/1984		2	3
Phase	20/12/1984 to 23/12/1984		2	3
Phase	14/09/1984 12:00 to 15/09/1984 06:00		2	3
Phase	21/09/1984 to 28/09/1984		2	3
Phase	25/11/1984 08:00 to 26/11/1984 08:00		2	3

(QC Flag: 0 = Meteorological (e.g. Seiche, Meteo-tsunami), 1 = Spike, 2 = Phase Offset, 3 = Tsunami, 4 = Other)

Analysis Comments

- Data after 1989 are much less noisy, therefore more extensive QC has been carried out before this date.
- Min. residual 02/10/1976 caused by Hurricane Liza.
- Max. residual 28/09/2001 caused by Hurricane Juliette

Cairns, Australia (16.925°S, 145.775°E)

Inherited:

Filename	V1 no.	Start	End	Yrs
cairns-007-australia-johnhunter.mat	**71**	31/05/1960	31/12/2004	31

Extended:

v1 filename	cairns-007-australia-johnhunter.mat (**71**)
v2 Filename	052_Cairns-AUS_GESLA_v2.mat
Source of Extra Data	N/A
Extra Data filename	N/A
Date of Download	N/A
End of Extra Data	N/A
Load in for Extra Data	N/A
Comparison Comments	N/A

Quality Control:

Type	Date Affected	Comments	QC Flag	GESLA Flag
Phase	02/03/1973 23:00 to 04/03/1973 05:00		2	3
Spike	26/04/1987 13:00 to 14:00		1	3
Spike	02/12/1987 05:00 to 06:00		1	3
Phase	05/12/1987 01:00		2	3
Phase	07/12/1987 02:00		2	3
Noise	28/07/1992 to 27/08/1992		N/A	1

(QC Flag: 0 = Meteorological (e.g. Seiche, Meteo-tsunami), 1 = Spike, 2 = Phase Offset, 3 = Tsunami, 4 = Other)

Analysis Comments

- Max. residual occurs on 28/02/2000 caused by Cyclone Steve.

Calais, France (50.967°N, 1.867°E)

Inherited:

Filename	V1 no.	Start	End	Yrs
calais-cal-france-shom.mat	**72**	03/05/1941	10/01/2008	28

Extended:

v1 filename	calais-cal-france-shom.mat (**72**)
v2 Filename	053_Calais-FRA_GESLA_v2.mat
Source of Extra Data	N/A
Extra Data filename	N/A
Date of Download	N/A
End of Extra Data	N/A
Load in for Extra Data	N/A
Comparison Comments	N/A

Quality Control:

(QC Flag: 0 = Meteorological (e.g. Seiche, Meteo-tsunami), 1 = Spike, 2 = Phase Offset, 3 = Tsunami, 4 = Other)

Analysis Comments

- Invalid values towards the end of the data to be removed (removed by max. threshold of 10 m).
- Max. residual occurs on 28 November 1974, but cannot find reference to the storm that may cause it. Data during this period does is not recorded at Dover. Data at Heysham does show an increase during this period before the sea level record stops, but the harmonic analysis has not be conducted for 1974 due to low data coverage for the year as a whole.
- Larger event in 1993 is real.

Callao, Peru (12.050°S, 77.150°W)

Inherited:

Filename	V1 no.	Start	End	Yrs
'callao-a,peru-001-glossdm-bodc.mat'	**75**	01/01/1950	31/12/1965	16
'callao-b,peru-001-glossdm-bodc.mat'	**76**	01/01/1970	30/04/1994	24
'callao_a-093a-peru-uhslc.mat'	**77**	01/01/1950	31/12/1965	16
'callao_b-093b-peru-uhslc.mat'	**78**	01/01/1970	31/12/2003	34

Extended:

v1 filename	callao_b-093b-peru-uhslc.mat (**78**)
v2 Filename	055_Callao-PER_GESLA_v2.mat
Source of Extra Data	UHSLC
Extra Data filename	H093b
Date of Download	30/01/2014
End of Extra Data	31/12/2012
Load in for Extra Data	UHSLC
Comparison Comments	Perfect comparison between inherited data and extension

Quality Control:

Type	Date Affected	Comments	QC Flag	GESLA Flag
Phase	23/05/1982 to 01/06/1982 00:00		2	3
Phase	29/08/1982 to 04/09/1982		2	3
Phase	11/08/1982 to 12/08/1982 09:00		2	3
Phase	25/07/1983 to 26/07/1983 00:00		2	3
Phase	24/09/1983 10:00 to 26/09/1983 14:00		2	3
Phase	02/10/1983 to 06/10/1983 18:00		2	3
Phase	30/11/1986 06:00 to 01/12/1986 06:00		2	3
Phase	31/12/1986 12:00 to 01/01/1987 00:00		2	3
Phase	15/01/1987 to 17/01/1987 12:00		2	3
Phase	13/02/1987 12:00 to 14/02/1987 12:00		2	3
Phase	16/02/1987 12:00 to 17/02/1987 12:00		2	3
Phase	31/03/1987 03:00 to 01/04/1987 06:00		2	3
Phase	14/04/1987 12:00 to 16/04/1987 12:00		2	3
Phase	28/04/1987 14:00 to 30/04/1987 00:00		2	3
Phase	16/02/1989 06:00 to 18/02/1989 12:00		2	3
Phase	06/11/1994 10:00 to 07/11/1994 14:00		2	3
Datum	28/04/1997 00:00 to 01/05/1997 12:00		4	3
Phase	03/05/1997 23:00 to 04/05/1997 13:00		2	3
Datum	16/05/1997 12:00 to 20/05/1997 00:00		4	3
Phase	29/06/1997 to 01/07/1997 08:00		2	3
Phase	05/09/1997 to 06/09/1997 18:00		2	3
Phase	31/12/1997 18:00 to 03/01/1998 00:00		2	3
Phase	15/02/1998 to 01/03/1998		2	3
Phase	01/06/1998 to 02/06/1998		2	3
Phase	31/07/1998 to 03/08/1998		2	3
Phase	12/08/1998 to 18/08/1998		2	3
Phase	13/06/1999 12:00 to 14/06/1999		2	3
Phase	03/09/1999 to 15/09/1999		2	3
Phase	01/08/2000 to 03/08/2000		2	3
Phase	09/08/2000 to 10/08/2000		2	3
Phase	07/04/2001 to 08/04/2001		2	3
Datum	25/08/2001 to 02/09/2001		4	3
Phase	21/04/2002 to 14/05/2002		2	3
Phase	26/04/2002 06:00 to 27/04/2002 18:00		2	3
Phase	16/07/2002 06:00 to 16/07/2002 21:00		2	3
Phase	17/03/2003 22:00 to 21/03/2003 00:00		2	3
Phase	02/06/2003 to 03/06/2003 00:00		2	3
Phase	08/06/2003 12:00 to 10/06/2003		2	3
Phase	16/06/2003 12:00 to 19/06/2003		2	3
Phase	26/12/2003 10:00 to 02/01/2004 03:00		2	3
Phase	21/01/2004 08/02/2004		2	3
Phase	23/04/2004 25/05/2004 00:00		2	3
Phase	12/09/2004 to 24/09/2004		2	3
Phase	23/11/2004 15:00 to 25/11/2004 15:00		2	3
Phase	07/01/2005 to 15/01/2005		2	3
Phase	07/02/2005 12:00 to 10/02/2005 00:00		2	3
Spike	05/04/2005 21:00		1	3
Phase	07/04/2005 10:00 to 08/04/2005 10:00		2	3
Phase	10/05/2005 00:00 to 13/05/2005 00:00		2	3
Phase	06/12/2005 00:00 to 08/12/2005 06:00		2	3

(QC Flag: 0 = Meteorological (e.g. Seiche, Meteo-tsunami), 1 = Spike, 2 = Phase Offset, 3 = Tsunami, 4 = Other)

Analysis Comments

- 093b station info. Gives many examples of data being input from various sources, datum shifts caused by earthquakes and other anomalies. These need to be taken into account during analysis.
- While 093a data is good quality there is no way information to tie the two datasets into each other and therefore comparison is not possible.
- Data from 2010 onwards have much lower residual values. This may invalidate residual values before this.
- Surge values are increasing rapidly (post-2010 excluded) but skew surge values are not, suggesting that there is a significant change in the tide-surge interaction or reduction in the impact of phase offsets

Campbell River, Canada (50.042°N, 125.247°W)

Inherited:

Filename	V1 no.	Start	End	Yrs
campbellriver,bc-08074-canada-meds.mat	**79**	07/08/1958	30/09/2008	37

Extended:

v1 filename	campbellriver,bc-08074-canada-meds.mat (**79**)
v2 Filename	056_CampbellRiver-CAN_GESLA_v2.mat
Source of Extra Data	MEDS
Extra Data filename	8074-01-JAN-2007_slev.csv
Date of Download	04/02/2014
End of Extra Data	31/12/2013
Load in for Extra Data	MEDS
Comparison Comments	Comparison with new data downloaded in UTC from MEDS website on 17/01/2014 shows that inherited data is -16 hr different. I correct the data with the assumption that the newly downloaded data is correct, such that the inherited dataset has been shifted forward 16 hrs. Comparison between are otherwise good.

Quality Control:

Type	Date Affected	Comments	QC Flag	GESLA Flag
Datum	Data before 01/01/1979	Removed all	4	3

(QC Flag: 0 = Meteorological (e.g. Seiche, Meteo-tsunami), 1 = Spike, 2 = Phase Offset, 3 = Tsunami, 4 = Other)

Analysis Comments

- Magnitude and phase of main tidal constituents show a discontinuity between 1976 and 1977. Data removed before 1977.

Cananeia, Brazil (25.017°S, 47.925°W)

Inherited:

Filename	V1 no.	Start	End	Yrs
'cananeia-281a-brazil-uhslc.mat'	**80**	26/02/1954	31/12/2006	52

Extended:

v1 filename	cananeia-281a-brazil-uhslc.mat (**80**)
v2 Filename	057_Cananeia-BRA_GESLA_v2.mat
Source of Extra Data	N/A
Extra Data filename	N/A
Date of Download	N/A
End of Extra Data	N/A
Load in for Extra Data	N/A
Comparison Comments	N/A

Quality Control:

Type	Date Affected	Comments	QC Flag	GESLA Flag
Phase	05/10/1969 to 24/10/1969		2	3
Phase	31/10/1969 10:00 to 03/11/1969 14:00		2	3
Phase	10/11/1969 02:00 to 11/11/1969 04:00		2	3
Phase	06/12/1969 16:00 to 07/12/1969 12:00		2	3
Phase	22/12/1969 10:00 to 08/01/1970 05:00		2	3
Phase	22/01/1970 to 02/02/1970		2	3
Phase	08/02/1970 19:00 to 10/02/1970 00:00		2	3
Phase	22/02/1970 06:00 to 23/02/1970 05:00		2	3
Phase	01/07/1973 06:00 to 02/07/1973 05:00		2	3
Phase	28/07/1973 12:00 to 02/08/1973		2	3
Spikes	29/03/1999 06:00 to 30/03/1999 12:00		1	3
Phase	03/10/1999 03:00 to 15:00		2	3
Spikes	29/10/1999 06:00 to 30/10/1999 18:00		1	3
Phase	09/06/2002 16:00 to 10/06/2002 00:00		2	3
Datum	06/02/2003 10:00 to 07/02/2003 14:00		4	3
Phase	23/12/2003 12:00 to 24/12/2003 16:00		2	3

(QC Flag: 0 = Meteorological (e.g. Seiche, Meteo-tsunami), 1 = Spike, 2 = Phase Offset, 3 = Tsunami, 4 = Other)

Analysis Comments

- Peak residual occurs on 29/10/1999. Signal may be real but event is > 2m greater than any other and there is no reference to the event. Nothing is recorded at Rio de Janeiro (700 km along the coast). **Data to be removed**.
- Residual data generally noisy due to small tidal component.

Cape May, USA (38.968°N, 74.960°W)

Inherited:

Filename	V1 no.	Start	End	Yrs
cape_may,nj-746a-usa-uhslc.mat	**81**	21/11/1965	31/12/2005	34

Extended:

v1 filename	cape_may,nj-746a-usa-uhslc.mat (**81**)
v2 Filename	058_CapeMay-USA_GESLA_v2.mat
Source of Extra Data	UHSLC/NOAA
Extra Data filename	H746a / CO-OPS_CapeMay.csv
Date of Download	04/02/2014
End of Extra Data	31/12/2013
Load in for Extra Data	UHSLC/NOAA
Comparison Comments	Comparison of new UHSLC and new NOAA data showing perfect continuity as does the inherited and extended datasets.

Quality Control:

Type	Date Affected	Comments	QC Flag	GESLA Flag
Phase	28/07/1967 14:00 to 15/08/1967 15:00		2	3
Phase	01/01/1968 21:00 to 03/01/1968 18:00		2	3

(QC Flag: 0 = Meteorological (e.g. Seiche, Meteo-tsunami), 1 = Spike, 2 = Phase Offset, 3 = Tsunami, 4 = Other)

Analysis Comments

- Lowest sea level caused by large –ve residual caused by Great Blizzard of 1966 (01-Feb).
- Min. residual caused by ET storm on 13/03/1993
- Max residuals caused by ET storm on 03/01/1996 and Hurricane Sandy 29/10/2012, both similar magnitude.

Carnarvon, Australia (24.884°S, 113.657°E)

Inherited:

Filename	V1 no.	Start	End	Yrs
'carnarvon-008-australia-johnhunter.mat'	**83**	01/11/1965	31/12/2004	27
'carnarvon-167a-australia-uhslc.mat'	**84**	07/04/1984	31/12/2005	16

Extended:

v1 filename	'carnarvon-167a-australia-uhslc.mat' (**83**)
v2 Filename	060_Carnarvon-AUS_GESLA_v2.mat
Source of Extra Data	UHSLC
Extra Data filename	H167a
Date of Download	04/02/2014
End of Extra Data	31/12/2012
Load in for Extra Data	UHSLC
Comparison Comments	A small offset exists between the two datasets so a shift of -0.14 m was applied to the data extension.

Quality Control:

Type	Date Affected	Comments	QC Flag	GESLA Flag
Phase	27/02/1973 12:00 to 02/03/1973 00:00			3
Phase	1973-74			1
Phase	10/12/1978 to 12/12/1978			3
Phase	15/12/1978 to 17/12/1978			3

(QC Flag: 0 = Meteorological (e.g. Seiche, Meteo-tsunami), 1 = Spike, 2 = Phase Offset, 3 = Tsunami, 4 = Other)

Analysis Comments

- Two peaks close to each other in Feb 1970, probably caused by Cyclone Glynnis (04/02/1970) and Cyclone Ingrid (17/02/1970), although details back that far are not certain.
- Cyclone Hazel (14/03/1979).
- Tidal phase shows discontinuity for data in 1973/74. Despite, this not being seen in magnitude.

Ceuta, Spain (35.900°N, 5.317°E)

Inherited:

Filename	V1 no.	Start	End	Yrs
'ceuta-207a-spain-uhslc.mat'	**92**	01/03/1944	31/12/2006	60
'ceuta-a,spain-001-glossdm-bodc.mat'	**93**	01/01/1971	24/08/1974	3
'ceuta-c,spain-001-glossdm-bodc.mat'	**94**	01/01/1978	13/04/1980	2
'ceuta-ceut-spain-ieo.mat'	**95**	01/03/1944	31/12/2006	60
'ceuta-d,spain-001-glossdm-bodc.mat'	**96**	29/04/1980	31/12/1991	9

Extended:

v1 filename	ceuta-207a-spain-uhslc.mat (**92**)
v2 Filename	066_Ceuta-ESP_GESLA_v2.mat
Source of Extra Data	UHSLC
Extra Data filename	H207a
Date of Download	05/02/2014
End of Extra Data	31/12/2008
Load in for Extra Data	UHSLC
Comparison Comments	Inherited data taken from 92 because of the extra data it has. Perfect comparison between inherited and extra data, but it is from the same source!

Quality Control:

Type	Date Affected	Comments	QC Flag	GESLA Flag
	No erroneous data to remove			

(QC Flag: 0 = Meteorological (e.g. Seiche, Meteo-tsunami), 1 = Spike, 2 = Phase Offset, 3 = Tsunami, 4 = Other)

Charleston, OR – USA (43.345°N, 124.322°W)

Inherited:

Filename	V1 no.	Start	End	Yrs
charleston,or-575a-usa-uhslc.mat	**98**	01/07/1978	31/12/2004	26

Extended:

v1 filename	charleston,or-575a-usa-uhslc.mat (**98**)
v2 Filename	068_Charleston,OR-USA_GESLA_v2.mat
Source of Extra Data	UHSLC/NOAA
Extra Data filename	H575a/COOPS_Charleston,OR
Date of Download	05/02/2014
End of Extra Data	31/12/2013
Load in for Extra Data	UHSLC/NOAA
Comparison Comments	Perfect comparison between two new datesets during overlap period of 2012. Also perfect comparison between inherited and extra data.

Quality Control:

Type	Date Affected	Comments	QC Flag	GESLA Flag
Phase	10/03/1981 to 18/03/1981		2	3
Phase	06/09/1983 14:00 to 23/09/1983 10:00		2	3
Phase	04/07/1999 to 17/07/1999 06:00		2	3

(QC Flag: 0 = Meteorological (e.g. Seiche, Meteo-tsunami), 1 = Spike, 2 = Phase Offset, 3 = Tsunami, 4 = Other)

Charleston,SC – USA (32.782°N, 79.925°W)

Inherited:

Filename	V1 no.	Start	End	Yrs
'charleston,sc-261a-usa-uhslc.mat'	**99**	01/10/1921	31/12/2005	84
'charleston,usa-001-glossdm-bodc.mat'	**100**	01/01/1985	31/12/1996	12
'charleston-005-usa-johnhunter.mat'	**101**	01/10/1921	28/02/2006	84

Extended:

v1 filename	charleston,sc-261a-usa-uhslc.mat (**99**)
v2 Filename	069_Charleston,SC-USA_GESLA_v2.mat
Source of Extra Data	UHSLC/NOAA
Extra Data filename	H261a/COOPS_Charleston,SC
Date of Download	05/02/2014
End of Extra Data	31/12/2013
Load in for Extra Data	UHSLC/NOAA
Comparison Comments	Inherited data taken from 99 because of the extra data it has and the consistency with the extra data. Comparison between 2 new datasets is perfect as are the inherited against the extra.

Quality Control:

Type	Date Affected	Comments	QC Flag	GESLA Flag
Phase	28/05/1965 to 30/05/1965 06:00		2	3
Phase	30/05/1973 to 13/06/1973		2	3
Phase	24/10/1987 to 28/10/1987		2	3

(QC Flag: 0 = Meteorological (e.g. Seiche, Meteo-tsunami), 1 = Spike, 2 = Phase Offset, 3 = Tsunami, 4 = Other)

Analysis Comments

- 29/09/1959 – Hurricane Gracie, but peak residual occurs at low tide and therefore total sea level is barely above normal HW level.
- 22/09/1989 – Hurricane Hugo
- Min. residual caused on 14/03/1993 by major nor'easter that also affected the sea level at Cape May, which is approx. 1000 km away.
- Trend in MHW is large from 1920 to 1960 but after this the trend is flat.

Charlotte Amalie, Virgin Islands (18.335°N, 64.920°W)

Inherited:

Filename	V1 no.	Start	End	Yrs
charlotte_amalie-255a-usa-uhslc.mat	**102**	01/10/1978	01/12/2005	23

Extended:

v1 filename	charlotte_amalie-255a-usa-uhslc.mat (**102**)
v2 Filename	070_CharlotteAmalie-VIR_GESLA_v2.mat
Source of Extra Data	UHSLC
Extra Data filename	H255a
Date of Download	05/02/2014
End of Extra Data	01/12/2012
Load in for Extra Data	UHSLC
Comparison Comments	Perfect comparison between extra and inherited

Quality Control:

Type	Date Affected	Comments	QC Flag	GESLA Flag
	No erroneous data to remove			

(QC Flag: 0 = Meteorological (e.g. Seiche, Meteo-tsunami), 1 = Spike, 2 = Phase Offset, 3 = Tsunami, 4 = Other)

Analysis Comments

- Max. residual caused by Hurricane Marilyn on 16/09/1995. Regular storm surge seen during hurricane season, with particular peaks in 1989, 1998 and 1999.
- Seasonal cycle observed in MSL, with peak in October

Charlotte Town, Canada (46.233°N, 63.117°W)

Inherited:

Filename	V1 no.	Start	End	Yrs
charlottetown,pei-01700-canada-meds.mat	**103**	31/03/1911	31/10/2008	71

Extended:

v1 filename	charlottetown,pei-01700-canada-meds.mat
v2 Filename	071_CharlotteTown-CAN_GESLA_v2.mat
Source of Extra Data	MEDS
Extra Data filename	1700-01-JAN-2008_slev.csv
Date of Download	05/02/2014
End of Extra Data	31/12/2013
Load in for Extra Data	MEDS
Comparison Comments	Comparison between new MEDS data and inherited data shows an 8hr time offset. Therefore -8 hrs is applied to the data on import, but the whole extended dataset is shifted forward by 8hrs to UTC (assuming the extra data is correct).

Quality Control:

Type	Date Affected	Comments	QC Flag	GESLA Flag
Spike	14/03/1962 03:00		1	3
Spike	17/03/1962 14:00		1	3
Spike	17/03/1962 18:00		1	3
Spike	19/03/1962 05:00		1	3
Spike	20/03/1962 09:00		1	3
Spike	24/03/1962 19:00		1	3
Spike	25/03/1962 12:00		1	3
Spike	26/03/1962 22:00		1	3
Spike	27/03/1962 00:00		1	3
Spike	28/03/1962 12:00		1	3
Spike	31/03/1962 15:00		1	3

(QC Flag: 0 = Meteorological (e.g. Seiche, Meteo-tsunami), 1 = Spike, 2 = Phase Offset, 3 = Tsunami, 4 = Other)

Analysis Comments

- Max. residual caused by winter storm on 28/12/2004 referenced in this bulletin (http://www.atl.ec.gc.ca/weather/bulletins/pe/20041228021900.txt.en).
- Residual data is noisy with strong positive and negative surges occurring throughout the data but especially during the winter. This is probably caused by the large body of shallow water around Prince Edward Island.

Cherbourg, France (49.650°N, 1.617°W)

Inherited:

Filename	V1 no.	Start	End	Yrs
cherbourg-che-france-shom.mat	**104**	30/03/1943	09/01/2008	34

Extended:

v1 filename	cherbourg-che-france-shom.mat
v2 Filename	072_Cherbourg-FRA_GESLA_v2.mat
Source of Extra Data	N/A
Extra Data filename	N/A
Date of Download	N/A
End of Extra Data	N/A
Load in for Extra Data	N/A
Comparison Comments	No extra data available for extension

Quality Control:

Type	Date Affected	Comments	QC Flag	GESLA Flag
Spike	06/06/1975 00:00 to 12:00		1	3
Phase	10/07/1980 20:00 to 15/07/1980		2	3
Spike	23/09/1983 20:00 to 22:00		2	3

(QC Flag: 0 = Meteorological (e.g. Seiche, Meteo-tsunami), 1 = Spike, 2 = Phase Offset, 3 = Tsunami, 4 = Other)

Chesapeake Bay, USA (36.967°N, 76.113°W)

Inherited:

Filename	V1 no.	Start	End	Yrs
chesapeake_bbt-749a-usa-uhslc.mat	**105**	29/01/1975	31/12/2004	30

Extended:

v1 filename	chesapeake_bbt-749a-usa-uhslc.mat
v2 Filename	073_ChesapeakeBay-USA_GESLA_v2.mat
Source of Extra Data	UHSLC/NOOA
Extra Data filename	h749a / COOPS_ChesapeakeBBT
Date of Download	05/02/2014
End of Extra Data	31/12/2013
Load in for Extra Data	UHSLC/NOAA
Comparison Comments	NOAA data is 4 m higher than the UHSLC despite being downloaded relative to station datum. This has been corrected for and the comparison is perfect after this.

Quality Control:

Type	Date Affected	Comments	QC Flag	GESLA Flag
		No erroneous data to remove		

(QC Flag: 0 = Meteorological (e.g. Seiche, Meteo-tsunami), 1 = Spike, 2 = Phase Offset, 3 = Tsunami, 4 = Other)

Chichijima, Japan (27.100°N, 142.183°E)

Inherited:

Filename	V1 no.	Start	End	Yrs
'chichijima,japan-001-glossdm-bodc.mat'	**106**	31/03/1975	31/12/2003	28
'chichijima-047a-japan-uhslc.mat'	**107**	31/03/1975	31/12/2005	31

Extended:

v1 filename	chichijima-047a-japan-uhslc.mat
v2 Filename	074_Chichijima-JPN_GESLA_v2.mat
Source of Extra Data	UHSLC
Extra Data filename	H047a
Date of Download	05/02/2014
End of Extra Data	31/12/2012
Load in for Extra Data	UHSLC
Comparison Comments	Perfect comparison between inherited and extra data

Quality Control:

Type	Date Affected	Comments	QC Flag	GESLA Flag
		No erroneous data to remove		

(QC Flag: 0 = Meteorological (e.g. Seiche, Meteo-tsunami), 1 = Spike, 2 = Phase Offset, 3 = Tsunami, 4 = Other)

Analysis Comments

- Typhoon Ben caused max. residual on 28/09/1986
- Many typhoons are evident in the data, the ESL associated with them are exacerbated by the seasonal cycle in MSL which peaks around October
- Noisy high percentiles, caused by typhoons but also the low magnitude of events at the site.

Christmas, Kiribati (1.982°N, 157.472°W)

Inherited:

Filename	V1	Start	End	Yrs
'christmas-a,lineis.kiribati-001-glossdm-bodc.mat'	**108**	01/12/1955	01/04/1972	14
'christmas-b,lineis.kiribati-001-glossdm-bodc.mat'	**109**	06/02/1974	31/12/1998	23
'christmas_a-011a-rep._of_kiribati-uhslc.mat'	**110**	01/12/1955	01/04/1972	14
christmas_b-011b-rep._of_kiribati-uhslc.mat'	**111**	06/02/1974	31/12/2003	27

Extended:

v1 filename	christmas_b-011b-rep._of_kiribati-uhslc.mat (**111**)
v2 Filename	075_ChristmasIsland-KIR_GESLA_v2.mat
Source of Extra Data	
Extra Data filename	
Date of Download	
End of Extra Data	03/04/2012
Load in for Extra Data	
Comparison Comments	

Quality Control:

Type	Date Affected	Comments	QC Flag	GESLA Flag
Noisy	01/01/1974 to 01/06/1975		4	3

(QC Flag: 0 = Meteorological (e.g. Seiche, Meteo-tsunami), 1 = Spike, 2 = Phase Offset, 3 = Tsunami, 4 = Other)

Churchill, Canada (58.783°N, 94.200°W)

Inherited:

Filename	V1 no.	Start	End	Yrs
'churchill,canada-001-glossdm-bodc.mat'	**113**	01/11/1961	01/01/2002	33
'churchill-274a-canada-uhslc.mat'	**114**	01/11/1961	31/12/2000	32

Extended:

v1 filename	'churchill-274a-canada-uhslc.mat (114)
v2 Filename	077_Churchill-CAN_GESLA_v2.mat
Source of Extra Data	UHSLC/MEDS
Extra Data filename	H274a / 5010_01_JAN_2010_slev.csv
Date of Download	06/02/2014
End of Extra Data	31/12/2014
Load in for Extra Data	UHSLC/MEDS
Comparison Comments	Comparison between inherited data and both extended datasets are perfect. No timing offset with the data suggests that MEDS data in the inherited data had the wrong time.

Quality Control:

Type	Date Affected	Comments	QC Flag	GESLA Flag
Phase	19/08/1966 04:00 to 22/08/1966 10:00		2	3
Phase	06/08/1967 21:00 to 10/09/1967 12:00		2	3
Phase	13/04/1972 to 02/05/1972		2	3
Phase	14/07/1975 12:00 to 18/07/1975 12:00		2	3
Phase	01/04/1987 to 10/04/1987		2	3

(QC Flag: 0 = Meteorological (e.g. Seiche, Meteo-tsunami), 1 = Spike, 2 = Phase Offset, 3 = Tsunami, 4 = Other)

Analysis Comments

- Peak residual on 05/10/1990 caused by large long period surge. Check local phenomena to see if this is likely.
- The decrease in HW and tidal range has also been observed Ray (personal communication) who suggests that the change might be due to reduced sea-ice cover across the Hudson Bay or changes in hydrology in the Churchill River. Although a localized cause is more likely since altimeter data show no change for the central Hudson Bay.

Cocos Islands, Australia (12.117°S, 96.883°E)

Inherited:

Filename	V1 no.	Start	End	Yrs
'cocos-171a-australia-uhslc.mat'	**119**	11/12/1985	31/12/2006	20
'cocosis.,australia-001-glossdm-bodc.mat'	**120**	11/12/1985	31/12/2001	15

Extended:

v1 filename	'cocos-171a-australia-uhslc.mat (119)
v2 Filename	081_CocosIsland-AUS_GESLA_v2.mat
Source of Extra Data	UHSLC/BOM
Extra Data filename	H171a/Cocos_BOM_2011-13.csv
Date of Download	06/02/2014
End of Extra Data	31/12/2013
Load in for Extra Data	UHSLC/BOM
Comparison Comments	Comparisons are perfect

Quality Control:

Type	Date Affected	Comments	QC Flag	GESLA Flag
Phase	14/02/1986 to 21/02/1986 10:00		2	3

(QC Flag: 0 = Meteorological (e.g. Seiche, Meteo-tsunami), 1 = Spike, 2 = Phase Offset, 3 = Tsunami, 4 = Other)

Cordova, USA (60.558°N, 145.753°W)

Inherited:

Filename	V1 no.	Start	End	Yrs
cordova_b,alaska-583b-usa-uhslc.mat	**122**	01/05/1964	31/12/2005	35

Extended:

v1 filename	cordova_b,alaska-583b-usa-uhslc.mat (122)
v2 Filename	083_Cordova-USA_GESLA_v2.mat
Source of Extra Data	UHSLC/NOAA
Extra Data filename	H583a / CO-OPS_Cordova.csv
Date of Download	06/02/2014
End of Extra Data	31/12/2013
Load in for Extra Data	UHSLC/NOAA
Comparison Comments	Comparisons are perfect

Quality Control:

Type	Date Affected	Comments	QC Flag	GESLA Flag
Phase	24/02/1970 18:00 to 07/03/1970		2	3
Phase	16/09/1970 to 24/09/1970		2	3
Phase	21/03/1971 to 01/11/1971		2	3
Phase	26/06/1973 12:00 to 01/07/1973		2	3
Noise	01/09/1974 18:00 to 04/09/1974		4	3

(QC Flag: 0 = Meteorological (e.g. Seiche, Meteo-tsunami), 1 = Spike, 2 = Phase Offset, 3 = Tsunami, 4 = Other)

Analysis Comments

- Noisy data, seen in early years of the data.

Coruna, Spain (43.367°N, 8.400°W)

Inherited:

Filename	V1 no.	Start	End	Yrs
'coruna-coru-spain-ieo.mat'	**123**	01/03/1943	31/12/2006	63
'la_coruna-830a-spain-uhslc.mat'	**305**	01/03/1943	31/12/2006	63

Extended:

v1 filename	'la_coruna-830a-spain-uhslc.mat (305)
v2 Filename	084_Coruna-ESP_GESLA_v2.mat
Source of Extra Data	UHSLC
Extra Data filename	H830a
Date of Download	06/02/2014
End of Extra Data	31/12/2008
Load in for Extra Data	UHSLC
Comparison Comments	Comparisons are perfect

Quality Control:

Type	Date Affected	Comments	QC Flag	GESLA Flag
Phase	1943-1944	Large sections of data had phase offsets.	2	3
Phase	21/04/1952 10:00 to 02/05/1952		2	3
Phase	11/09/1958 10:00 to 18/09/1958 12:00		2	3
Phase	20/02/1963 to 20/04/1963		2	3
Phase	15/12/1972 to 17/12/1972		2	3
Phase	28/04/1973 to 21/05/1973		2	3
Phase	07/10/1973 to 22/12/1973		2	3
Phase	04/01/1974 to 31/01/1974		2	3
Phase	07/05/1975 to 18/06/1975		2	3
Phase	05/03/1989 to 12/03/1989		2	3
Phase	01/01/1995 to 05/02/1995		2	3
Phase	12/02/1995 to 19/02/1995		2	3
Phase	09/04/1995 to 21/04/1995		2	3
Phase	08/05/1995 to 21/05/1995		2	3
Phase	01/01/2003 to 25/01/2003		2	3

(QC Flag: 0 = Meteorological (e.g. Seiche, Meteo-tsunami), 1 = Spike, 2 = Phase Offset, 3 = Tsunami, 4 = Other)

Crescent City, USA (41.745°N, 124.183°W)

Inherited:

Filename	V1 no.	Start	End	Yrs
'crescent_city,ca-556a-usa-uhslc.mat'	**125**	11/04/1933	31/12/2005	63
'crescentcity,california-001-glossdm-bodc.mat'	**126**	01/01/1951	01/09/2000	34

Extended:

v1 filename	'crescent_city,ca-556a-usa-uhslc.mat (125)
v2 Filename	086_CrescentCity-USA_GESLA_v2.mat

Source of Extra Data	UHSLC/NOAA
Extra Data filename	H556a/CO-OPS_CrescentCity.csv
Date of Download	06/02/2014
End of Extra Data	31/12/2013
Load in for Extra Data	UHSLC/NOAA
Comparison Comments	Comparisons are perfect

Quality Control:

Type	Date Affected	Comments	QC Flag	GESLA Flag
Phase	01/04/1946 15:00 to 05/04/1946			
Tsunami	04/11/1952 to 10/11/1952:	Alaskan Tsunami		
Phase	17/10/1955 18:00 to 18/10/1955 12:00			
Phase	28/11/1955 06:00 to 29/11/1955 08:00			
Tsunami	23/05/1960 to 27/05/1960:	Chile Earthquake		
Phase	16/02/1972 00:00 to 23:00			
Phase	16/06/1973 to 19/06/1973			
Phase	05/10/1994 to 06/10/1994			
Phase	07/01/2010 to 20/02/2010			
Tsunami	28/02/2010 to 03/03/2010:	Chile		
Tsunami	11/03/2011 12:00 to 15/03/2011:	Tohoku, Japan Earthquake		

(QC Flag: 0 = Meteorological (e.g. Seiche, Meteo-tsunami), 1 = Spike, 2 = Phase Offset, 3 = Tsunami, 4 = Other)

Analysis Comments

- Max. residual occurs on 14/11/1981.

Cristobal, Panama (9.355°N, 79.915°W)

Inherited:

Filename	V1 no.	Start	End	Yrs
'cristobal-266a-panama-uhslc.mat'	**127**	03/04/1907	31/12/1997	87

Extended:

v1 filename	'cristobal-266a-panama-uhslc.mat (127)
v2 Filename	087_Cristobal-PAN_GESLA_v2.mat
Source of Extra Data	UHSLC
Extra Data filename	H266a
Date of Download	06/02/2014
End of Extra Data	31/12/2012
Load in for Extra Data	UHSLC
Comparison Comments	Comparisons are perfect

Quality Control:

Type	Date Affected	Comments	QC Flag	GESLA Flag
Phase	05/09/1973 to 18/09/1973		2	3
Phase	23/05/1974 to 30/05/1974		2	3
Phase	31/12/1974 to 11/01/1975		2	3
Phase	08/09/1978 15:00 to 15/09/1978		2	3

(QC Flag: 0 = Meteorological (e.g. Seiche, Meteo-tsunami), 1 = Spike, 2 = Phase Offset, 3 = Tsunami, 4 = Other)

Analysis Comments

- Extra data does seem to have a datum shift from the inherited data, but it is presented as one continuous dataset on the UHSLC website.

Darwin, Australia (12.416°S, 130.842°E)

Inherited:

Filename	V1 no.	Start	End	Yrs
'darwin,australia-001-glossdm-bodc.mat'	**137**	01/01/1984	31/12/2001	17
'darwin-009-australia-johnhunter.mat'	**138**	01/01/1959	31/12/2004	39
'darwin-168a-australia-uhslc.mat'	**139**	01/01/1984	31/12/2006	22

Extended:

v1 filename	'darwin-009-australia-johnhunter.mat (138)
v2 Filename	093_Darwin-AUS_GESLA_v2.mat
Source of Extra Data	UHSLC/ BOM
Extra Data filename	H168e / Darwin_BOM_2012-13.csv
Date of Download	07/02/2014
End of Extra Data	31/12/2013
Load in for Extra Data	UHSLC/BOM
Comparison Comments	Perfect comparison between UHSLC and BOM data used for Extra data. However, inherited data (**138**) is offset from Extra data by 0.12 m. The inherited data was shifted up by 0.12m after assuming that the Extra data is correct. Comparison with shifted data is perfect which suggests that combining datasets is okay to do.

Quality Control:

Type	Date Affected	Comments	QC Flag	GESLA Flag
Phase	22/09/1961 to 25/09/1961		2	3
Phase	22/10/1961 to 29/10/1969		2	3
Phase	02/11/1961 to 08/11/1961		2	3
Phase	04/04/1966 to 10/04/1966		2	3
Phase	05/05/1966 to 12/05/1966		2	3
Phase	09/10/1966 to 19/10/1966		2	3
Phase	27/10/1966 to 01/11/1966		2	3
Phase	13/11/1966 18:00 to 14/11/1966 12:00		2	3
Phase	07/12/1966 to 18/12/1966		2	3
Phase	25/12/1966 to 05/02/1967		2	3
Phase	07/02/1967 to 10/02/1967		2	3
Phase	25/02/1967 to 03/03/1967		2	3
Phase	20/05/1967 to 30/05/1967		2	3
Phase	13/10/1967 to 18/10/1967 08:00		2	3
Phase	04/11/1967 to 08/11/1967		2	3
Phase	27/11/1967 to 07/12/1967		2	3
Phase	26/12/1967 to 03/02/1968		2	3
Phase	13/02/1968 to 24/03/1968		2	3
Phase	01/04/1968 to 07/04/1968		2	3
Phase	11/04/1968 to 03/05/1968		2	3
Phase	22/10/1968 to 07/02/1969		2	3
Phase	13/02/1969 to 11/03/1969		2	3
Phase	23/07/1969 to 02/09/1969		2	3
Phase	07/12/1969 to 11/12/1969		2	3
Phase	20/08/1971 to 30/08/1971		2	3
Phase	04/09/1971 to 08/09/1971 03:00		2	3
Datum	14/08/1972 to 17/08/1972		4	3
Phase	02/09/1972 to 17/09/1972		2	3
Phase	01/05/1073 to 01/06/1973		2	3
Phase	07/09/1973 to 14/09/1973		2	3
Phase	22/09/1973 to 25/09/1973		2	3
Phase	07/12/1973 to 14/12/1973		2	3
Phase	04/06/1974 to 04/08/1974		2	3
Phase	24/12/1974 to 04/02/1975		2	3
Phase	26/05/1976 to 14/06/1976		2	3
Phase	24/08/1976 to 12/12/1976		2	3
Phase	21/12/1976 to 24/12/1976		2	3
Phase	01/02/1977 to 13/02/1977		2	3
Phase	20/02/1977 to 26/02/1977		2	3
Phase	02/03/1977 to 13/03/1977		2	3
Phase	01/04/1977 to 10/04/1977		2	3
Phase	17/08/1977 to 21/08/1977		2	3
Phase	01/09/1977 to 02/09/1977 03:00		2	3
Phase	07/02/1979 to 22/02/1979		2	3
Phase	01/03/1979 to 04/03/1979		2	3
Phase	07/06/1979 to 18/06/1979		2	3
Phase	06/07/1979 to 16/07/1979		2	3
Phase	02/10/1979 to 13/10/1979		2	3
Phase	12/08/1980 to 20/08/1980		2	3
Phase	01/12/1980 t o16/12/1980		2	3
Phase	04/07/1981 10:00 to 06/07/1981		2	3
Phase	12/07/1981 to 16/07/1981		2	3
Phase	01/09/1982 to 12/09/1982		2	3
Datum	12/04/1985 to 24/04/1985		4	3
Phase	20/05/1985 to 27/05/1985		2	3
Phase	30/06/1985 to 19/07/1985		2	3
Phase	12/09/1985 to 04/11/1985		2	3

Phase	08/12/1985 to 15/12/1985		2	3
Phase	09/03/1986 to 16/03/1986		2	3
Phase	02/06/1986 to 12/06/1986		2	3
Phase	16/07/1986 to 27/07/1986		2	3
Phase	13/11/1986 to 23/11/1986		2	3
Phase	10/12/1986 to 14/12/1986		2	3
Phase	12/03/1987 to 22/03/1987		2	3
Phase	06/09/1987 to 13/09/1987		2	3
Phase	22/12/1987 10:00 to 29/12/1987		2	3
Phase	17/01/1988 to 31/01/1988		2	3
Phase	26/07/1988 to 06/08/1988		2	3
Phase	25/08/1988 to 15/09/1988		2	3
Phase	25/09/1988 to 16/10/1988		2	3
Phase	04/01/1989 to 12/01/1989		2	3
Phase	10/03/1989 to 14/03/1989		2	3
Phase	04/04/1989 to 11/04/1989		2	3
Phase	19/03/1990 to 03/04/1990		2	3

(QC Flag: 0 = Meteorological (e.g. Seiche, Meteo-tsunami), 1 = Spike, 2 = Phase Offset, 3 = Tsunami, 4 = Other)

Analysis Comments

- Data from 01/04/1990 is far less noisy than data previously. This suggests that noisiness in the data before this data is an artefact of the data measurements and not real. Need to go through and remove noisy periods as well as out of phase measurements..

Delfzijl, Netherlands (53.326°N, 6.933°E)

Inherited:

Filename	V1 no.	Start	End	Yrs
delfzijl-del-nl-rws.mat'	**145**	01/01/1971	31/12/2007	37

Extended:

v1 filename	delfzijl-del-nl-rws.mat (145)
v2 Filename	097_Delfzijl-NDL_GESLA_v2.mat.
Source of Extra Data	N/A
Extra Data filename	N/A
Date of Download	N/A
End of Extra Data	N/A
Load in for Extra Data	N/A
Comparison Comments	No extra data available for extension.

Quality Control:

Type	Date Affected	Comments	QC Flag	GESLA Flag
		No erroneous data to remove		

(QC Flag: 0 = Meteorological (e.g. Seiche, Meteo-tsunami), 1 = Spike, 2 = Phase Offset, 3 = Tsunami, 4 = Other)

Analysis Comments

- Clear seasonal cycle with stormy season in NH winter.
- Very high residuals in Nov-1973, but looks like storm surge signal.
- Peak residual on 02/01/1976 caused by gale that affected whole of north sea (http://en.wikipedia.org/wiki/Gale_of_January_1976)
- Apparent change in trend around 1978. Data compared to 098_DenHelder where similar pattern is observed suggesting that change could be due to some local adjustment possibly due to coastal engineering on the Dutch or German coasts.

Den Helder, Netherlands (52.965°N, 4.746°E)

Inherited:

Filename	V1 no.	Start	End	Yrs
'denhelder-hel-nl-rws.mat	**146**	01/01/1971	31/12/2007	37

Extended:

v1 filename	'denhelder-hel-nl-rws.mat (146)
v2 Filename	098_DenHelder-NLD_GESLA_v2.mat.
Source of Extra Data	N/A
Extra Data filename	N/A
Date of Download	N/A
End of Extra Data	N/A
Load in for Extra Data	N/A
Comparison Comments	No extra data available for extension.

Quality Control:

Type	Date Affected	Comments	QC Flag	GESLA Flag
		No erroneous data to remove		

(QC Flag: 0 = Meteorological (e.g. Seiche, Meteo-tsunami), 1 = Spike, 2 = Phase Offset, 3 = Tsunami, 4 = Other)

Dover, UK (51.114°N, 1.323°E)

Inherited:

Filename	V1 no.	Start	End	Yrs
'dover-p012-uk-bodc.mat'	**153**	06/01/1924	31/12/2006	47

Extended:

v1 filename	'dover-p012-uk-bodc.mat (153)
v2 Filename	102_Dover-GBR_GESLA_v2.mat
Source of Extra Data	BODC
Extra Data filename	RN-7246_1372253428497.zip
Date of Download	26/06/2013
End of Extra Data	31/12/2012
Load in for Extra Data	BODC2
Comparison Comments	Comparison if perfect

Quality Control:

Type	Date Affected	Comments	QC Flag	GESLA Flag
Threshold		> 10, < -1	1	3
Phase	24-Feb-2012 00:00 to 27-Feb-2012 16:00		2	3

(QC Flag: 0 = Meteorological (e.g. Seiche, Meteo-tsunami), 1 = Spike, 2 = Phase Offset, 3 = Tsunami, 4 = Other)

Analysis Comments

- Low data return before 1959 leads to high residuals, remove data before 1959 to increase confidence in generated trend.
- MSL seems higher in early records.
- Large –ve residual caused by storm surge on 01/03/1967.

Duck Pier, USA (36.183°N, 75.740°W)

Inherited:

Filename	V1 no.	Start	End	Yrs
'duck,n.c.-001-glossdm-bodc.mat'	**156**	01/11/1979	31/12/2000	21
'duck_pier,nc-260a-usa-uhslc.mat'	**157**	01/06/1978	31/12/2005	27

Extended:

v1 filename	'duck_pier,nc-260a-usa-uhslc.mat (157)
v2 Filename	105_DuckPier-USA_GESLA_v2.mat.
Source of Extra Data	UHSLC/NOAA
Extra Data filename	H260a/COOP_DuckPier.csv
Date of Download	11/02/2014
End of Extra Data	31/12/2013
Load in for Extra Data	UHSLC/NOAA
Comparison Comments	Data comparisons between UHSLC extension data (h260a) and the NOAA extension data to end 2013 (COOPS_DuckPier) are perfect as is the comparison with the inherited data.

Quality Control:

Type	Date Affected	Comments	QC Flag	GESLA Flag
Phase	02/06/1992 15:00 to 04/06/1992 18:00		2	3

(QC Flag: 0 = Meteorological (e.g. Seiche, Meteo-tsunami), 1 = Spike, 2 = Phase Offset, 3 = Tsunami, 4 = Other)

Analysis Comments

- Peak residual on 20/09/2003, caused by hurricane Isabel (Cat. 5).
- Superstorm Sandy hits (end October 2012) and the records stop. Therefore event not captured in residual component since MSL calculation requires 15 days before and after time stamp.

Dutch Harbour, USA (53.880°N, 166.537°W)

Inherited:

Filename	V1 no.	Start	End	Yrs
'dutch_harbor_b,ak-041b-usa-uhslc.mat'	**160**	01/01/1982	31/12/2005	22

Extended:

v1 filename	'dutch_harbor_b,ak-041b-usa-uhslc.mat (160)
v2 Filename	107_DutchHarbour-USA_GESLA_v2.mat.
Source of Extra Data	UHSLC/NOAA
Extra Data filename	H041b/CO-OPS_Unalaska.csv
Date of Download	11/02/2014
End of Extra Data	31/12/2013
Load in for Extra Data	UHSLC/NOAA
Comparison Comments	Comparisons are perfect

Quality Control:

Type	Date Affected	Comments	QC Flag	GESLA Flag
Tsunami	28/02/2010 to 02/02/2010	Chilean Tsunami	3	6
Tsunami	11/03/2011 10:00 to 15/03/2011	Tohuku Earthquake	3	6

(QC Flag: 0 = Meteorological (e.g. Seiche, Meteo-tsunami), 1 = Spike, 2 = Phase Offset, 3 = Tsunami, 4 = Other)

Analysis Comments

- Negative trend in sea level due to its location in Alaska and the isostatic rebound.

Easter Island, Chile (27.150°S, 109.448°W)

Inherited:

Filename	V1 no.	Start	End	Yrs
'easter_c-022c-chile-uhslc.mat'	**162**	02/04/1970	06/12/2002	25
'isladapascua-a,chile-001-glossdm-bodc.mat'	**251**	16/01/1957	31/12/1958	2
'isladapascua-b,chile-001-glossdm-bodc.mat'	**252**	27/01/1962	17/04/1963	1
'isladapascua-d,chile-001-glossdm-bodc.mat'	**253**	22/03/1977	07/08/1984	7
'isladapascua-e,chile-001-glossdm-bodc.mat'	**254**	01/01/1985	31/12/1998	13

Extended:

v1 filename	'easter_c-022c-chile-uhslc.mat (162)
v2 Filename	109_EasterIsland-CHL_GESLA_v2.mat.
Source of Extra Data	UHSLC
Extra Data filename	H022c
Date of Download	11/02/2014
End of Extra Data	06/12/2012
Load in for Extra Data	UHSLC
Comparison Comments	Comparisons are perfect

Quality Control:

Type	Date Affected	Comments	QC Flag	GESLA Flag
Phase	27/02/1974 to 02/03/1974		2	3
Tsunami	16/11/2006 03:00 to 18/11/2006:	Kuril Earthquake	3	6
Tsunami	27/02/2010 10:00 to 02/03/2010	Chile Earthquake	3	6
Tsunami	11/03/2011 22:00 to 15/03/2011	Tohuku Earthquake	3	6

(QC Flag: 0 = Meteorological (e.g. Seiche, Meteo-tsunami), 1 = Spike, 2 = Phase Offset, 3 = Tsunami, 4 = Other)

Analysis Comments

- First patch of noisy data is on 15/08/1999. Nothing beforehand that looks similar.
- Data on 15/06/2006 appear to be the response to a tsunami, but there are no reports of one anywhere at that time. Data left in as it may be a seiching signal, but more research is required.
- Other noisy periods : 05/04/2007 to 08/04/2007 and 08/06/2009 to 11/06/2009:

Eastport, USA (44.903°N, 66.985°W)

Inherited:

Filename	V1 no.	Start	End	Yrs
'eastport,me-740a-usa-uhslc.mat'	**163**	12/09/1929	31/12/2005	68

Extended:

v1 filename	'eastport,me-740a-usa-uhslc.mat (163)
v2 Filename	110_Eastport-USA_GESLA_v2.mat.
Source of Extra Data	UHSLC/NOAA
Extra Data filename	H740a/COOP_Eastport.csv
Date of Download	11/02/2014
End of Extra Data	31/12/2013
Load in for Extra Data	UHSLC/NOAA
Comparison Comments	Comparisons are perfect

Quality Control:

Type	Date Affected	Comments	QC Flag	GESLA Flag
Phase	08/02/1931 18:00 to 09/02/1931 08:00		2	3
Phase	13/05/1931 01:00 to 06:00		2	3
Phase	13/05/1931 18:00 to 23:00		2	3
Phase	25/02/1934 to 05/03/1934		2	3
Phase	10/08/1934 to 17/08/1934		2	3
Phase	16/12/1934 to 05/01/1935		2	3
Phase	03/03/1935 to 08/03/1935		2	3
Phase	02/09/1940 12:00 to 03/09/1940 12:00		2	3
Phase	12/09/1941 04:00 to 13/09/1941 08:00		2	3
Phase	14/12/1941 12:00 to 15/12/1941 10:00		2	3
Phase	21/12/1941 to 23/12/1941		2	3
Phase	08/10/1944 t0 20/10/1944		2	3
Phase	03/02/1946 to 05/02/1946		2	3
Phase	21/11/1949 03:00 to 23/11/1949 08:00		2	3
Phase	05/03/1952 12:00 to 20:00		2	3
Phase	16/03/1952 04:00 to 17/03/1952 08:00		2	3
Phase	05/09/1952 18:00 to 08/09/1952		2	3
Phase	28/09/1952 to 11/10/1952		2	3
Phase	18/10/1953 04:00 to 19/10/1953 08:00		2	3
Phase	03/01/1959 20:00 to 04/01/1959 05:00		2	3
Phase	17/01/1959 to 20/01/1959		2	3
Phase	08/01/1962 00:00 to 21:00		2	3
Phase	18/08/1962 to 22/08/1962		2	3
Phase	05/10/1962 to 16/10/1962		2	3
Phase	01/11/1962 to 04/11/1962		2	3
Phase	08/11/1962 to 20/12/1962		2	3
Phase	28/06/1965 to 09/07/1965		2	3
Phase	28/06/1965 to 09/07/1965		2	3
Phase	27/06/1966 15:00 to 04/07/1966		2	3
Phase	03/08/1966 to 13/08/1966		2	3
Phase	16/05/1967 to 24/05/1967		2	3
Phase	08/06/1967 to 15/06/1967		2	3
Phase	21/06/1967 to 29/06/1967		2	3
Phase	02/07/1967 to 21/07/1967		2	3
Phase	03/08/1967 to 20/08/1967		2	3
Phase	25/08/1967 to 13/09/1967		2	3
Phase	02/06/1968 to 25/06/1968		2	3
Phase	01/07/1968 to 04/08/1968		2	3
Spike	28/04/1970 20:00 to 29/04/1970 10:00		1	3
Phase	01/06/1970 18:00 to 03/06/1970		2	3
Phase	01/01/1971 to 12/03/1971		2	3
Phase	28/03/1971 to 08/04/1971		2	3
Phase	15/06/1971 to 18/08/1971		2	3
Phase	16/05/1967 to 24/05/1967		2	3
Phase	08/06/1967 to 15/06/1967		2	3
Phase	21/06/1967 to 29/06/1967		2	3
Phase	02/07/1967 to 21/07/1967		2	3
Phase	03/08/1967 to 20/08/1967		2	3
Phase	25/08/1967 to 13/09/1967		2	3
Phase	02/06/1968 to 25/06/1968		2	3
Phase	01/07/1968 to 04/08/1968		2	3
Spike	28/04/1970 20:00 to 29/04/1970 10:00		1	3
Phase	01/06/1970 18:00 to 03/06/1970		2	3
Phase	01/01/1971 to 12/03/1971		2	3
Phase	28/03/1971 to 08/04/1971		2	3
Phase	15/06/1971 to 18/08/1971		2	3
Phase	19/09/1971 to 11/11/1971		2	3
Phase	25/11/1971 to 08/02/1972		2	3
Phase	12/03/1972 to 25/05/1972		2	3
Phase	25/06/1972 to 29/09/1972		2	3
Phase	19/12/1972 to 25/01/1973		2	3
Noise	01/06/1973 to 05/06/1973		4	3
Phase	17/06/1973 to 30/09/1973		2	3
Phase	14/11/1980 to 06/12/1980		2	3
Phase	27/01/1983 to 22/02/1983		2	3
Phase	19/03/1983 to 15/05/1983		2	3
Phase	18/12/1983 to 31/01/1984		2	3
Phase	08/03/1984 to 22/03/1984		2	3
Phase	24/06/1984 to 15/07/1984		2	3

Phase	03/04/1987 12:00 to 10/04/1987		2	3
Phase	10/03/1988 to 14/03/1988		2	3
Phase	26/03/1988 12:00 to 28/03/1988 12:00		2	3
Phase	02/03/1989 21:00 to 08/03/1989 18:00		2	3
Phase	04/04/1989 to 15/04/1989		2	3
Phase	02/01/1990 to 08/01/1990		2	3
Phase	09/09/1991 to 16/09/1991		2	3
Phase	03/11/2007 18:00 to 05/11/2007 08:00		2	3
Phase	30/12/2012 to 02/01/2013		2	3
Phase	09/02/2013 to 11/02/2013		2	3

(QC Flag: 0 = Meteorological (e.g. Seiche, Meteo-tsunami), 1 = Spike, 2 = Phase Offset, 3 = Tsunami, 4 = Other)

Analysis Comments

- Residuals in 1971 appear to have a phase offset, but this may be due to incorrect assignment of harmonic constituents.
- Period of data in 1976 appears to have a datum shift.

Esbjerg, Denmark (55.467°N, 8.433°E)

Inherited:

Filename	V1 no.	Start	End	Yrs
'esbjerg-130121-denmark-dmi.mat'	**166**	01/01/1950	31/12/2001	50

Extended:

v1 filename	'esbjerg-130121-denmark-dmi.mat (166)
v2 Filename	113_Esbjerg-DNK_GESLA_v2.mat
Source of Extra Data	N/A
Extra Data filename	N/A
Date of Download	N/A
End of Extra Data	N/A
Load in for Extra Data	N/A
Comparison Comments	No extra data available

Quality Control:

Type	Date Affected	Comments	QC Flag	GESLA Flag
Phase	25/09/1983 to 01/10/1983		2	3
Phase	09/11/1983 00:00 to 23:00		2	3
Phase	11/01/1987 to 18/01/1987		2	3
Phase	16/03/1987 to 01/04/1987		2	3
Phase	05/04/1987 to 12/04/1987		2	3
Phase	06/11/1988 21:00 to 09/11/1988		2	3
Phase	30/04/1989 to 08/05/1989 12:00		2	3
Phase	19/12/2001 to 21/12/2001		2	3

(QC Flag: 0 = Meteorological (e.g. Seiche, Meteo-tsunami), 1 = Spike, 2 = Phase Offset, 3 = Tsunami, 4 = Other)

Analysis Comments

- Peak residual occurs on 2 November 1965, looks like a surge signal but no report of storm on internet except for shipwreck off Friesland on that date.
- Peak water level occurs on 24/11/1981, caused by North Friesian Flood, but data finishes at the peak and not captured in residual because MSL is not calculable.
- Offset in tide between 1982 and 1983.
- Possible jumps in MSL in 2001 but difficult to fully detect. Leave the data.

Esperance, Australia (33.861°S, 121.891°E)

Inherited:

Filename	V1 no.	Start	End	Yrs
'esperance-010-australia-johnhunter.mat'	**167**	10/12/1965	31/12/2005	39
'esperance-176a-australia-uhslc.mat'	**168**	01/01/1985	31/12/2006	21
'esperence,australia-001-glossdm-bodc.mat'	**170**	01/01/1990	31/12/2001	1

Extended:

v1 filename	esperance-010-australia-johnhunter.mat (167)
v2 Filename	114_Esperance-AUS_GESLA_v2.mat
Source of Extra Data	UHSLC/BOM
Extra Data filename	H167a/Esperance_BOM_2012-13.csv
Date of Download	04/02/2014
End of Extra Data	31/12/2013
Load in for Extra Data	UHSLC/BOM
Comparison Comments	Comparisons are perfect

Quality Control:

Type	Date Affected	Comments	QC Flag	GESLA Flag
Phase	03/02/1983 to 07/02/1983		2	3
Phase	15/04/1983 to 02/06/1983		2	3
Phase	06/07/1983 to 08/07/1983		2	3
Phase	09/04/1986 to 27/04/1986		2	3

(QC Flag: 0 = Meteorological (e.g. Seiche, Meteo-tsunami), 1 = Spike, 2 = Phase Offset, 3 = Tsunami, 4 = Other)

Faraday, Antarctica (65.250°S, 64.267°W)

Inherited:

Filename	V1 no.	Start	End	Yrs
'faraday-700a-united_kingdom-uhslc.mat'	**173**	01/03/1984	31/12/2004	21
'faradaybase,phase0-001-glossdm-bodc.mat'	**174**	15/10/1959	28/02/1971	11
'vernadsky-a003-uk+ukraine-pol.mat'	**640**	01/03/1984	31/12/2006	23

Extended:

v1 filename	N/A
v2 Filename	118_Faraday-ATA_GESLA_v2.mat
Source of Extra Data	UHSLC
Extra Data filename	H700a
Date of Download	12/02/2014
End of Extra Data	31/12/2009
Load in for Extra Data	UHSLC
Comparison Comments	The new UHSLC datasets extends from 1959 to 2009 and is therefore used in its entirety.

Quality Control:

Type	Date Affected	Comments	QC Flag	GESLA Flag
Phase	19/05/1966 00:00 to 14:00		2	3
Phase	21/05/1966 00:00 to 14:00		2	3
Phase	01/06/1986 to 07/06/1986		2	3
Phase	01/01/2000 to 03/03/2000		2	3
Phase	23/04/2000 15:00 to 24/04/2000 15:00		2	3
Phase	08/05/2000 00:00 to 15:00		2	3
Spike	31/05/2000 01:00		1	3
Spike	06/06/2000 08:00		1	3
Spike	01/07/2000 08:00		1	3
Spike	13/07/2000 07:00		1	3
Spike	01/08/2000 02:00		1	3
Spike	02/09/2000 17:00		1	3
Spike	19/12/2000 20:00		1	3
Spike	28/12/2000 13:00		1	3
Spike	31/05/2002 23:00		1	3
Spike	04/06/2002 23:00		2	3
Phase	25/03/2004 to 29/03/2004		2	3
Phase	27/12/2006 to 01/01/2007		2	3
Phase	12/03/2007 to 03/05/2007		2	3
Phase	21/08/2007 to 01/09/2007		2	3
Phase	24/09/2007 to 03/10/2007		2	3
Phase	30/10/2007 to 03/11/2007		2	3
Phase	03/06/2008 18:00 to 05/06/2008		2	3
Phase	21/08/2008 12:00 to 22/08/2008 15:00		2	3
Phase	28/07/2009 06:00 to 30/07/2009		2	3
Phase	19/09/2009 to 06/10/2009		2	3

(QC Flag: 0 = Meteorological (e.g. Seiche, Meteo-tsunami), 1 = Spike, 2 = Phase Offset, 3 = Tsunami, 4 = Other)

Fernandina Beach, USA (30.672°N, 81.467°W)

Inherited:

Filename	V1 no.	Start	End	Yrs
'fernandina_beach-240a-usa-uhslc.mat'	**175**	01/01/1985	31/12/2005	19

Extended:

v1 filename	N/A
v2 Filename	119_FernandinaBeach-USA_GESLA_v2.mat
Source of Extra Data	UHSLC/ NOAA
Extra Data filename	H240a/ COOPS_FernandinaBeach.csv
Date of Download	12/02/2014
End of Extra Data	31/12/2013
Load in for Extra Data	UHSLC/NOAA
Comparison Comments	The new UHSLC datasets extends from 1897 to 2012 and is therefore used in its entirety.

Quality Control:

Type	Date Affected	Comments	QC Flag	GESLA Flag
Phase	18/09/1906 to 23/09/1906		2	3
Phase	22/07/1907 06:00 to 23/07/1907 10:00		2	3
Phase	27/08/1910 12:00 to 28/08/1910 15:00		2	3
Phase	13/10/1910 to 23/10/1910		2	3
Phase	30/10/1910 to 02/11/1910		2	3
Phase	04/11/1910 to 18/11/1910		2	3
Phase	19/06/1912 00:00 to 23:00		2	3
Phase	22/06/1912 12:00 to 22:00		2	3
Phase	04/12/1912 to 10/12/1912		2	3
Phase	14/10/1913 12:00 to 16/10/1913 12:00		2	3
Phase	16/12/1914 to 19/12/1914		2	3
Phase	17/02/1915 to 21/02/1915		2	3
Phase	01/03/1915 00:00 to 22:00		2	3
Phase	27/03/1919 to 10/04/1919		2	3
Phase	22/04/1919 to 11/05/1919		2	3
Phase	26/01/1920 to 05/02/1920		2	3
Phase	26/06/1923 to 02/07/1923		2	3
Phase	17/04/1994 to 01/05/1994		2	3
Phase	30/05/2012 00:00 to 23:00		2	3
Phase	05/06/2012 to 07/06/2012		2	3
Phase	02/02/2013 15:00 to 05/02/2013 15:00		2	3

(QC Flag: 0 = Meteorological (e.g. Seiche, Meteo-tsunami), 1 = Spike, 2 = Phase Offset, 3 = Tsunami, 4 = Other)

Analysis Comments

- Min. residual is caused by –ve surge in response to the storm of the century on 14/03/1993 (http://en.wikipedia.org/wiki/1993_Storm_of_the_Century)

Fishguard, UK (52.014°N, 4.983°W)

Inherited:

Filename	V1 no.	Start	End	Yrs
fishgaurd-p055-uk-bodc.mat	**176**	05/01/1963	31/12/2006	40

Extended:

v1 filename	fishgaurd-p055-uk-bodc.mat (176)
v2 Filename	120_Fishguard-GBR_GESLA_v2.mat
Source of Extra Data	BODC
Extra Data filename	RN-7246_1372253428497.zip
Date of Download	26/06/2013
End of Extra Data	31/12/2013
Load in for Extra Data	BODC2
Comparison Comments	Comparisons are perfect

Quality Control:

Type	Date Affected	Comments	QC Flag	GESLA Flag
Threshold		> 8 or < -2	4	3
Phase	18/08/2012 05:00 to 20/08/2012 12:00		2	3
Phase	14/03/2012 09:00 to 15/03/2012 20:00		2	3
Phase	13/01/2011 09:00 to 14/01/2011 15:00		2	3
Phase	18/07/2012 04:00 to 18/07/2012 15:00		2	3

(QC Flag: 0 = Meteorological (e.g. Seiche, Meteo-tsunami), 1 = Spike, 2 = Phase Offset, 3 = Tsunami, 4 = Other)

Analysis Comments

- Peak surge caused by October 1989 storm.

Flores, Portugal (Azores) (39.453°N, 31.120°W)

Inherited:

Filename	V1 no.	Start	End	Yrs
'flores,azores-210a-portugal-uhslc.mat'	**177**	09/07/1976	31/12/1996	14

Extended:

v1 filename	'flores,azores-210a-portugal-uhslc.mat (177)
v2 Filename	121_Flores-PRT_GESLA_v2.mat
Source of Extra Data	UHSLC
Extra Data filename	H210a
Date of Download	12/02/2014
End of Extra Data	31/12/2009
Load in for Extra Data	UHSLC
Comparison Comments	Comparisons are perfect

Quality Control:

Type	Date Affected	Comments	QC Flag	GESLA Flag
Phase	22/11/1977 to 25/11/1977		2	3
Phase	06/08/1979 to 16/09/1979		2	3
Phase	16/07/1986 to 26/07/1986		2	3
Pre-Gap	31/08/1986 to 02/09/1986		4	3

(QC Flag: 0 = Meteorological (e.g. Seiche, Meteo-tsunami), 1 = Spike, 2 = Phase Offset, 3 = Tsunami, 4 = Other)

Analysis Comments

- Peak water level occurs on 25/12/1996 from what appears to be a storm surge.
- Event in 1984 looks valid as well.
- Peak residual on 24/01/2007 potentially caused by ice storm that dissipates (moves away from North America) around this date. No other storm system referenced, but definite surge signal.

Fort Denison, Australia (33.855°S, 151.226°E)

Inherited:

Filename	V1 no.	Start	End	Yrs
'fort_denison-333a-australia-uhslc.mat'	**179**	01/01/1965	31/12/2006	40
'fortdenison,australia-001-glossdm-bodc.mat'	**183**	01/01/1985	31/12/1998	6
'fortdenison-011-australia-johnhunter.mat'	**184**	31/05/1914	31/12/2004	89

Extended:

v1 filename	'fortdenison-011-australia-johnhunter.mat (184)
v2 Filename	123_FortDenison-AUS_GESLA_v2.mat
Source of Extra Data	UHSLC
Extra Data filename	H333a
Date of Download	21/06/2013
End of Extra Data	31/12/2012
Load in for Extra Data	UHSLC
Comparison Comments	Data built upon **184** since length of data is greater. Comparison between the three datasets show strong agreement, with only a few minor differences. Comparisons with new data are perfect.

Quality Control:

Type	Date Affected	Comments	QC Flag	GESLA Flag
Phase	04/02/1924 to 05/02/1924		2	3
Phase	25/01/1929 21:00 to 26/01/1929 12:00		2	3
Phase	15/01/1943 18:00 to 23:00		2	3
Phase	17/01/1943 00:00 to 12:00		2	3
Phase	13/02/1943 to 15/02/1943		2	3
Phase	14/08/1943 00:00 23:00		2	3
Phase	27/08/1943 to 30/08/1943		2	3
Phase	29/12/1949 00:00 23:00		2	3
Phase	28/01/1953 21:00 to 31/01/1953		2	3
Phase	18/01/1958 to 20/01/1958		2	3
Phase	28/12/1966 08:00 to 12:00		2	3
Phase	08/10/1971 to 09/10/1971		2	3
Phase	15/01/1972 08:00 to 23:00		2	3
Phase	03/10/1975 to 08/10/1975		2	3
Phase	04/11/1975 to 05/11/1975		2	3
Spike	19/08/1976 00:00		1	3
Phase	10/02/1982 22:00 to 11/02/1982 08:00		2	3
Phase	14/01/1983 00:00 to 12:00		2	3
Phase	28/09/1983 00:00 to 29/09/1983 04:00		2	3

Phase	15/10/1984 00:00 to 13:00		2	3
Phase	21/01/1985 15:00 to 22/01/1985		2	3
Phase	08/04/1988 to 10/04/1988		2	3

(QC Flag: 0 = Meteorological (e.g. Seiche, Meteo-tsunami), 1 = Spike, 2 = Phase Offset, 3 = Tsunami, 4 = Other)

Fort Pulaski, USA (32.033°N, 80.902°W)

Inherited:

Filename	V1 no.	Start	End	Yrs
'fort_pulaski,ga-752a-usa-uhslc.mat'	**180**	01/07/1935	31/12/2005	65

Extended:

v1 filename	fort_pulaski,ga-752a-usa-uhslc.mat (180)
v2 Filename	124_FortPulaski-USA_GESLA_v2.mat
Source of Extra Data	UHSLC/NOAA
Extra Data filename	H752a / COOP_FortPulaski
Date of Download	13/02/2014
End of Extra Data	31/12/2013
Load in for Extra Data	UHSLC/NOAA
Comparison Comments	Comparisons are perfect

Quality Control:

Type	Date Affected	Comments	QC Flag	GESLA Flag
Phase	11/12/1944 15:00 to 12/12/1944 12:00		2	3
Phase	06/07/1964 to 11/07/1964		2	3
Gaps	1976		4	3

(QC Flag: 0 = Meteorological (e.g. Seiche, Meteo-tsunami), 1 = Spike, 2 = Phase Offset, 3 = Tsunami, 4 = Other)

Analysis Comments

- Peak residual occurs on 19/10/1944 caused by the Cuba-Florida Hurricane.
- Large residual on 04/09/1979 at the time Hurricanes David and Frederic were around
- Min residual caused by Storm of the Century 14/03/1993. Much smaller than any other event.
- Nearly all tidal levels have an outlier in 1976. This is a year that is surrounding by years that do not have sufficient data coverage in that year for analysis. The difference is large in many TD and has therefore been removed.

Fremantle, Australia (32.053°S, 115.746°E)

Inherited:

Filename	V1 no.	Start	End	Yrs
'fremantle-012-australia-johnhunter.mat'	**185**	10/01/1897	31/12/2004	97
'fremantle-175a-australia-uhslc.mat'	**186**	01/01/1984	31/12/2006	23

Extended:

v1 filename	fremantle-012-australia-johnhunter.mat (185)
v2 Filename	126_Fremantle-US_GESLA_v2.mat
Source of Extra Data	UHSLC
Extra Data filename	H175a
Date of Download	17/02/2014
End of Extra Data	31/12/2012
Load in for Extra Data	UHSLC
Comparison Comments	Comparisons are perfect

Quality Control:

Type	Date Affected	Comments	QC Flag	GESLA Flag
Phase	01/01/1904 to 04/01/1904		2	3
Phase	28/02/1904 to 08/04/1904		2	3
Phase	26/11/1917 to 31/11/1917		2	3
Phase	10/02/1920 to 13/02/1920		2	3
Flat line	18/04/1956 12:00 to 20/04/1956		4	3
Flat line	24/04/1956 06:00 to 25/04/1956 06:00		4	3
Flat line	25/05/1956 08:00 to 27/05/1956		4	3
Flat line	29/05/1956 12:00 to 30/05/1956		4	3
Flat line	19/06/1956 06:00 to 20/06/1956		4	3
Flat line	03/08/1956 to 05/08/1956		4	3
Flat line	18/08/1956 16:00 to 20/08/1956		4	3
Flat line	06/09/1956 to 10/09/1956 12:00		4	3
Phase	14/12/1956 08:00 to 15/12/1956 08:00		2	3
Spike	14/01/1964 19:00		1	3
Flat line	01/12/1966 to 02/12/1966 12:00		4	3
Flat line	13/12/1966 08:00 to 15/12/1966		4	3
Phase	05/01/1969 to 16/01/1969		2	3

(QC Flag: 0 = Meteorological (e.g. Seiche, Meteo-tsunami), 1 = Spike, 2 = Phase Offset, 3 = Tsunami, 4 = Other)

Analysis Comments

- Period from 1971 to 1978 where water level is recorded only to 1 d.p. Before and after it is 2 d.p., with 3 d.p. starting in 1996.

French Frigate Shoals, HI, USA (23.867°N, 166.290°W)

Inherited:

Filename	V1 no.	Start	End	Yrs
'french_frigate_s.-014a-usa-uhslc.mat'	**187**	03/07/1974	31/12/2001	26
frenchfrigateshoal,usa-001-glossdm-bodc.mat	**188**	03/07/1974	31/12/1998	23

Extended:

v1 filename	'french_frigate_s.-014a-usa-uhslc.mat (187)
v2 Filename	127_FrenchFrigateShoals-USA _GESLA_v2.mat
Source of Extra Data	UHSLC
Extra Data filename	H014a
Date of Download	17/02/2014
End of Extra Data	31/12/2007
Load in for Extra Data	UHSLC
Comparison Comments	Comparisons are perfect. Data for 014a end in 2007, and 014b takes over. No datum control had been conducted and therefore this data has not been used.

Quality Control:

Type	Date Affected	Comments	QC Flag	GESLA Flag
		No erroneous data to remove.		

(QC Flag: 0 = Meteorological (e.g. Seiche, Meteo-tsunami), 1 = Spike, 2 = Phase Offset, 3 = Tsunami, 4 = Other)

Analysis Comments

- Peak residual occurs on 05/11/1988, although it is difficult to attribute to Hurricane Joan which was occurring at the same time near Mexico.
- A number of noisy periods of data (previously seen on Easter Island) start to appear in the data in December 1998. Leave data in for time being but check during analysis what impact these noisy periods have. No obvious impact on surge percentiles.

Funafuti, Tuvalu (8.525°S, 179.195°E)

Inherited:

Filename	V1 no.	Start	End	Yrs
'funafuti,tuvalu-001-glossdm-bodc.mat'	**190**	17/10/1977	31/12/2001	24
'funafuti_a-025a-tuvalu-uhslc.mat'	**191**	17/10/1977	31/12/1999	22
'funafuti_b-025b-tuvalu-uhslc.mat'	**192**	24/03/1993	31/12/2006	13

Extended:

v1 filename	'funafuti_a-025a-tuvalu-uhslc.mat (191)
v2 Filename	129_Funafuti-TUV_GESLA_v2.mat
Source of Extra Data	UHSLC
Extra Data filename	H025b
Date of Download	17/02/2014
End of Extra Data	31/12/2012
Load in for Extra Data	UHSLC
Comparison Comments	UHSLC states that combining of data files is possible given the 6 years of overlapping. The data from 191 have been shifted up 0.77 m to match the datums. Data during this period show only miniscule differences approx. 1-2 mm and therefore the combined data file will continue to analysis.

Quality Control:

Type	Date Affected	Comments	QC Flag	GESLA Flag
Phase	09/03/1978 to 30/04/1978		2	3
Phase	30/07/1978 to 05/11/1978		2	3
Phase	25/08/1982 to 17/09/1982		2	3
Phase	26/09/1982 to 03/10/1982		2	3
Phase	07/11/1982 to 14/01/1983		2	3
Phase	09/06/1987 to 17/06/1987		2	3

(QC Flag: 0 = Meteorological (e.g. Seiche, Meteo-tsunami), 1 = Spike, 2 = Phase Offset, 3 = Tsunami, 4 = Other)

Funchal, Portugal (32.640°N, 16.907°W)

Inherited:

Filename	V1 no.	Start	End	Yrs
'funchal_b-218b-portugal-uhslc.mat'	**193**	06/10/1976	30/06/2006	19

Extended:

v1 filename	'funchal_b-218b-portugal-uhslc.mat (193)
v2 Filename	130_Funchal-PRT _GESLA_v2.mat
Source of Extra Data	UHSLC
Extra Data filename	H218a
Date of Download	17/02/2014
End of Extra Data	31/12/2009
Load in for Extra Data	UHSLC
Comparison Comments	Small differences observed between the inherited and downloaded data. Therefore only the new data is used.

Quality Control:

Type	Date Affected	Comments	QC Flag	GESLA Flag
Phase	24/10/1995 to 23/11/1995		2	3
Phase	12/12/1995 to 04/02/1996		2	3
Phase	01/03/1996 to 08/03/1996		2	3
Phase	21/03/1996 to 27/03/1996		2	3
Phase	25/04/1996 to 19/05/1996		2	3
Phase	09/12/1996 to 29/12/1996		2	3
Phase	12/01/1997 to 15/01/1997		2	3
Phase	14/04/1997 12:00 to 16/04/1997 12:00		2	3
Phase	18/10/1997 to 09/11/1997		2	3
Phase	14/12/1997 to 21/12/1997		2	3
Phase	09/01/1998 to 14/01/1998		2	3
Phase	26/01/1998 to 05/02/1998		2	3
Phase	13/04/1998 03:00 to 12:00		2	3
Phase	24/04/1998 16:00 to 23:00		2	3
Phase	27/04/1998 10:00 to 18:00		2	3
Spike	06/05/1998 14:00		1	3
Phase	19/05/1998 12:00 to 22:00		2	3
Phase	20/05/1998 12:00 to 22:00		2	3
Spike	18/06/1998 18:00		1	3
Phase	31/03/2000 to 17/04/2000		2	3

(QC Flag: 0 = Meteorological (e.g. Seiche, Meteo-tsunami), 1 = Spike, 2 = Phase Offset, 3 = Tsunami, 4 = Other)

Galveston Pier, USA (29.310°N, 94.793°W)

Inherited:

Filename	V1 no.	Start	End	Yrs
galveston,p.pier-767a-usa-uhslc.mat	**195**	21/08/1957	31/12/2005	46
galveston,pier_21-775a-usa-uhslc.mat	**196**	01/01/1904	31/12/2001	93
Galveston-008-usa-johnhunter.mat	**197**	01/01/1904	28/02/2006	98

Extended:

v1 filename	galveston,p.pier-767a-usa-uhslc.mat (195)
v2 Filename	132_GalvestonPier-USA _GESLA_v2.mat
Source of Extra Data	UHSLC/NOAA
Extra Data filename	H767a / 196_NOAA_GalvestonPier.txt
Date of Download	09/04/2013
End of Extra Data	31/12/2012
Load in for Extra Data	UHSLC/NOAA
Comparison Comments	Comparisons are perfect

Quality Control:

Type	Date Affected	Comments	QC Flag	GESLA Flag
		No erroneous data to remove		

(QC Flag: 0 = Meteorological (e.g. Seiche, Meteo-tsunami), 1 = Spike, 2 = Phase Offset, 3 = Tsunami, 4 = Other)

Analysis Comments

- Large residual on 14/08/1932 caused by Hurricane Two.
- Large residual on 12/09/1961 caused by Hurricane Carla.

- Hurricane Ike (09/2008) shows clearly in data, but WLR fails during event. Nearby gauge shows increase of residual during missing period. Water level 0.5 m higher at nearby station during missing period than times that for which there are data
- No other WLR with valid observations during the period.

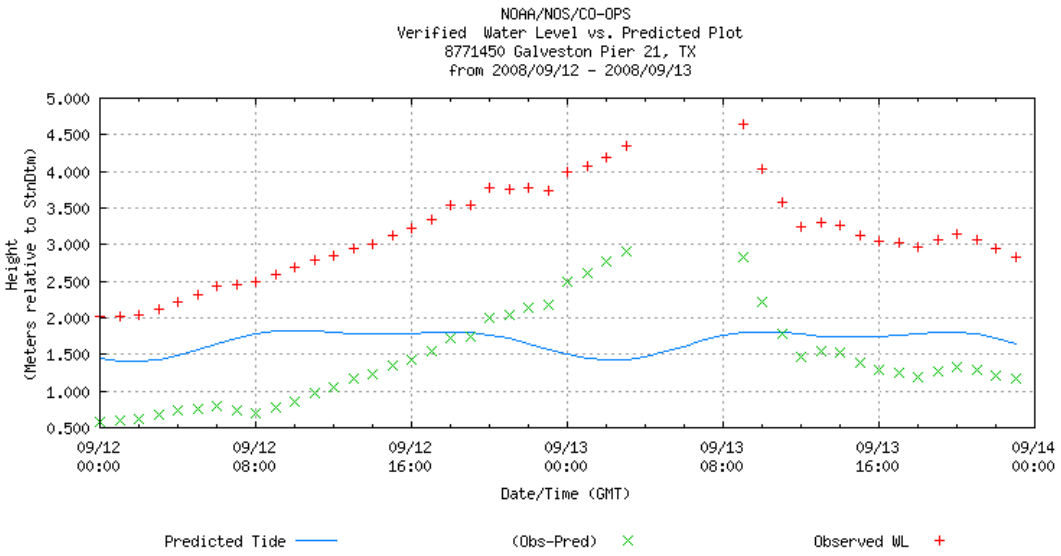

http://tidesandcurrents.noaa.gov/cgi-bin-mp/data_plot.cgi?mins=&datum=0&unit=0&stn=8771450&bdate=20080912&edate=20080913&data_type=wl&relative=&type=Historic%20Tide%20Data&shift=g&plot_size=large&relative=&wl_sensor_hist=W2&plot_backup=

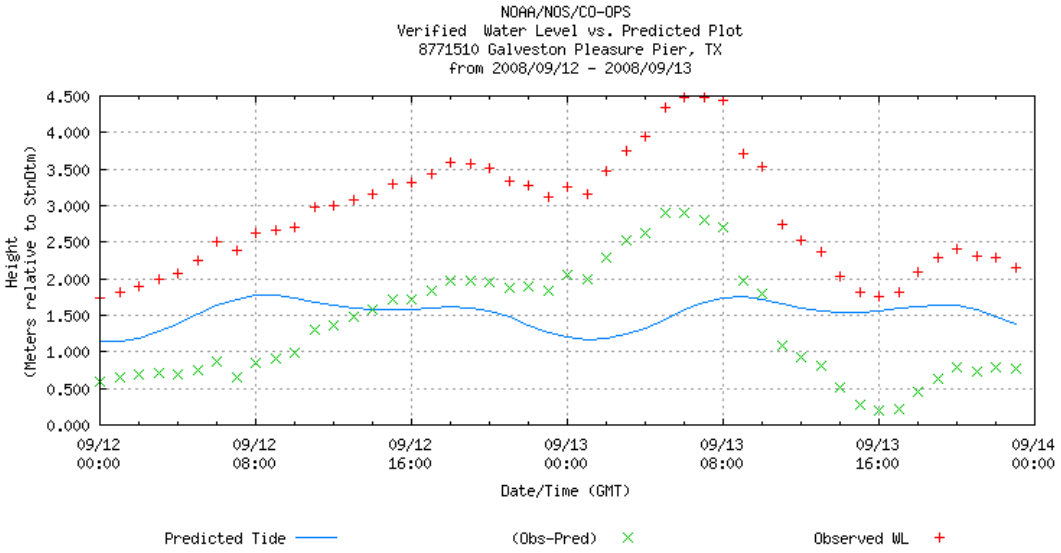

http://tidesandcurrents.noaa.gov/cgi-bin-mp/data_plot.cgi?mins=&datum=0&unit=0&stn=8771510&bdate=20080912&edate=20080913&data_type=wl&relative=&type=Historic%20Tide%20Data&shift=g&plot_size=large&relative=&wl_sensor_hist=W2&plot_backup=

Geelong, Australia (38.147°S, 144.361°E)

Inherited:

Filename	V1 no.	Start	End	Yrs
'geelong-013-australia-johnhunter.mat'	**200**	01/09/1965	31/12/2004	29

Extended:

v1 filename	geelong-013-australia-johnhunter.mat (200)
v2 Filename	134_Geelong-AUS_GESLA_v2.mat
Source of Extra Data	N/A
Extra Data filename	N/A
Date of Download	N/A
End of Extra Data	N/A
Load in for Extra Data	N/A
Comparison Comments	No extra data available

Quality Control:

Type	Date Affected	Comments	QC Flag	GESLA Flag
Noise	21/03/1970 08:00 to 23/03/1970		4	3
Noise	21/12/1992 00:00 to 23:00		4	3

(QC Flag: 0 = Meteorological (e.g. Seiche, Meteo-tsunami), 1 = Spike, 2 = Phase Offset, 3 = Tsunami, 4 = Other)

Analysis Comments

- Peak residual on 25/03/1984 possibly caused by storm event a week before that is documented as causing widespread flooding in Melbourne. Geelong is in the same bay and there may be a delayed response.

Geraldton, Australia (28.773°S, 114.611°E)

Inherited:

Filename	V1 no.	Start	End	Yrs
'geraldton-014-australia-johnhunter.mat'	**202**	31/10/1963	31/12/2004	39

Extended:

v1 filename	'geraldton-014-australia-johnhunter.mat (202)
v2 Filename	136_Geraldton-AUS_GESLA_v2.mat
Source of Extra Data	N/A
Extra Data filename	N/A
Date of Download	N/A
End of Extra Data	N/A
Load in for Extra Data	N/A
Comparison Comments	No extra data available

Quality Control:

Type	Date Affected	Comments	QC Flag	GESLA Flag
Phase	02/06/1967 to 06/06/1967		2	3
Tsunami	26/12/2004 to 01/01/2005	Indian Ocean Tsunami	3	6

(QC Flag: 0 = Meteorological (e.g. Seiche, Meteo-tsunami), 1 = Spike, 2 = Phase Offset, 3 = Tsunami, 4 = Other)

Grand Isle, USA (Louisiana), (29.263°N, 89.957°W)

Inherited:

Filename	V1 no.	Start	End	Yrs
'grand_isle,la-765a-usa-uhslc.mat'	**207**	01/01/1980	31/12/2005	26

Extended:

v1 filename	grand_isle,la-765a-usa-uhslc.mat (207)
v2 Filename	140_GrandIsle-USA_GESLA_v2.mat
Source of Extra Data	UHSLC/NOAA
Extra Data filename	H765a/COOP_GrandIsle.csv
Date of Download	17/02/2014
End of Extra Data	31/12/2013
Load in for Extra Data	UHSLC/NOAA
Comparison Comments	Comparisons are perfect

Quality Control:

Type	Date Affected	Comments	QC Flag	GESLA Flag
		No erroneous data to remove		

(QC Flag: 0 = Meteorological (e.g. Seiche, Meteo-tsunami), 1 = Spike, 2 = Phase Offset, 3 = Tsunami, 4 = Other)

Analysis Comments

- Storm cluster in September 2002 as Hurricane Isidore and Lili impact nearby one week apart.
- Peak residual is caused by Hurricane Katrina on 30 August 2005. Hurricane Rita also has large effect on 23 September 2005.
- Another two storms occur in 2008: 02/09/2008 Hurricane Gustav and 12/09/2008 Hurricane Ike.
- Peak water level occurs on 29/08/2012 caused by Hurricane Isaac.
- Take care when using data since TR is small and small jumps occur in the predicted tide between years.

Guam, Apra Harbour (13.433°N, 144.650°E)

Inherited:

Filename	V1 no.	Start	End	Yrs
'guam,usa-001-glossdm-bodc.mat'	**208**	10/03/1948	31/12/2000	48
'guam-053a-usa_trust-uhslc.mat'	**209**	10/03/1948	31/12/2005	51

Extended:

v1 filename	guam-053a-usa_trust-uhslc.mat (209)
v2 Filename	141_ApraHarbour-GUM_GESLA_v2.mat
Source of Extra Data	UHSLC/NOAA
Extra Data filename	H053a/COOP_ApraHarbour.csv
Date of Download	17/02/2014
End of Extra Data	31/12/2013
Load in for Extra Data	UHSLC/NOAA
Comparison Comments	Comparisons are perfect

Quality Control:

Type	Date Affected	Comments	QC Flag	GESLA Flag
Phase	10/05/1951 to 14/05/1951		2	3
Tsunami	22/05/1960 to 29/05/1960	Chilean Tsunami	3	6
Gaps	21/06/1964 to 28/06/1964		2	3
Phase	23/08/1964 to 04/09/1964		2	3
Phase	08/03/1966 12:00 to 10/03/1966 15:00		2	3
Phase	01/04/1970 to 02/04/1970 12:00		2	3
Phase	18/07/1973 12:00 to 19/07/1973 21:00		2	3
Phase	24/03/1987 00:00 to 23:00		2	3
Phase	07/03/1988 to 12/03/1988		2	3

(QC Flag: 0 = Meteorological (e.g. Seiche, Meteo-tsunami), 1 = Spike, 2 = Phase Offset, 3 = Tsunami, 4 = Other)

Hachinohe, Japan (40.533°N, 141.533°E)

Inherited:

Filename	V1 no.	Start	End	Yrs
'hachinohe-375a-japan-uhslc.mat'	**212**	01/01/1980	31/12/2005	26

Extended:

v1 filename	'hachinohe-375a-japan-uhslc.mat (212)
v2 Filename	144_Hachinohe-JPN_GESLA_v2.mat
Source of Extra Data	UHSLC
Extra Data filename	H375a
Date of Download	17/02/2014
End of Extra Data	31/12/2010
Load in for Extra Data	UHSLC
Comparison Comments	Comparisons are perfect

Quality Control:

Type	Date Affected	Comments	QC Flag	GESLA Flag
		No erroneous data to remove		

(QC Flag: 0 = Meteorological (e.g. Seiche, Meteo-tsunami), 1 = Spike, 2 = Phase Offset, 3 = Tsunami, 4 = Other)

Analysis Comments

- 05/12/2004: Peak residual possibly associated with Typhoon Nanmadol, although it would have been dissipating at this point. No other potential storms

Hakodate, Japan (41.783°N, 140.733°E)

Inherited:

Filename	V1 no.	Start	End	Yrs
'hakodate,japan-001-glossdm-bodc.mat'	**214**	09/03/1967	31/12/2003	35
'hakodate-364a-japan-uhslc.mat'	**215**	30/06/1964	31/12/2005	38

Extended:

v1 filename	'hakodate-364a-japan-uhslc.mat (215)
v2 Filename	146_Hakodate-JPN_GESLA_v2.mat
Source of Extra Data	UHSLC
Extra Data filename	h364a
Date of Download	17/02/2014
End of Extra Data	31/12/2012
Load in for Extra Data	UHSLC
Comparison Comments	Comparisons are perfect

Quality Control:

Type	Date Affected	Comments	QC Flag	GESLA Flag
Phase	06/10/1967 to 18/10/1967		2	3
Phase	12/05/1969 to 22/05/1969		2	3

(QC Flag: 0 = Meteorological (e.g. Seiche, Meteo-tsunami), 1 = Spike, 2 = Phase Offset, 3 = Tsunami, 4 = Other)

Analysis Comments

- Peak values in 1970 and 1979 both have typical storm signatures.

Halifax, Canada (44.667°N, 63.583°W)

Inherited:

Filename	V1 no.	Start	End	Yrs
'halifax,canada-001-glossdm-bodc.mat'	**216**	01/01/1920	31/12/2001	31
'halifax,ns-00490-canada-meds.mat'	**217**	06/10/1919	31/10/2008	89
'halifax-275a-canada-uhslc.mat'	**218**	01/01/1920	31/12/2001	81

Extended:

v1 filename	'halifax,ns-00490-canada-meds.mat (217)
v2 Filename	147_Halifax-CAN_GESLA_v2.mat
Source of Extra Data	MEDS
Extra Data filename	490-01-JAN-2007_slev.csv
Date of Download	17/02/2014
End of Extra Data	31/10/2013
Load in for Extra Data	MEDS
Comparison Comments	Time shift of -8 hrs was applied to the extra data to tie up with inherited data. This is corrected in QC and shifted to GMT by adding 8 hrs onto the entire data. There were a few duplicate points in the extra data downloaded from MEDS. These points on the 12/04/2012 were removed from the csv file in Notepad so that the data format was not changed. Comparisons between the extra dataset and the inherited dataset are perfect.

Quality Control:

Type	Date Affected	Comments	QC Flag	GESLA Flag
Phase	29/07/1926 15:00 to 01/08/1926		2	3
Datum	11/01/1927 18:00 to 12/01/1927 10:00		4	3
Phase	03/06/1931 08:00 to 21:00		2	3
Phase	02/10/1933 20:00 to 03/10/1933 20:00		2	3
Phase	13/12/1933 15:00 to 15/12/1933 15:00		2	3
Phase	03/03/1934 18:00 to 04/03/1934 21:00		2	3
Phase	10/08/1938 to 18/08/1938		2	3
Phase	26/08/1946 10:00 to 29/08/1946		2	3
Spike	30/08/1946 08:00		1	3
Phase	01/01/1961 to 05/02/1961		2	3
Phase	19/09/1961 to 01/01/1962		2	3
Phase	01/01/1970 to 22/01/1970 12:00		2	3
Datum	31/08/1970 to 23/09/1970		4	3
Phase	20/10/1974 00:00 to 23:00		2	3
Phase	24/04/1992 to 29/04/1992		2	3
Gaps	10/12/2000 to 20/03/2001		4	3
Phase	11/06/2012 to 20/06/2012 08:00		2	3
Spike	30/07/2012 08:00 to 10:00		1	3
Phase	09/12/2012 to 19/12/2012		2	3

(QC Flag: 0 = Meteorological (e.g. Seiche, Meteo-tsunami), 1 = Spike, 2 = Phase Offset, 3 = Tsunami, 4 = Other)

Hamada, Japan (34.900°N, 132.067°E)

Inherited:

Filename	V1 no.	Start	End	Yrs
'hamada,japan-001-glossdm-bodc.mat'	**219**	01/01/2001	31/12/2003	2
'hamada-348a-japan-uhslc.mat'	**220**	29/02/1984	31/12/2005	22

Extended:

v1 filename	'hamada-348a-japan-uhslc.mat (220)
v2 Filename	148_Hamada-JPN_GESLA_v2.mat
Source of Extra Data	UHSLC
Extra Data filename	H348a
Date of Download	17/02/2014
End of Extra Data	31/12/2012
Load in for Extra Data	UHSLC
Comparison Comments	Comparisons are perfect

Quality Control:

Type	Date Affected	Comments	QC Flag	GESLA Flag
		No erroneous data to remove		

(QC Flag: 0 = Meteorological (e.g. Seiche, Meteo-tsunami), 1 = Spike, 2 = Phase Offset, 3 = Tsunami, 4 = Other)

Analysis Comments

- Peak residual on 27/09/1991 caused by Typhoon Mirielle.
- Min. residual on16/09/1997 caused by Typhoon Oliwa
- Peak water level occurs on 19/08/2005, due to coincidence of peak in seasonal MSL signal and Typhoon Mawar (potential, although timings are completely convincing).

Harwich, UK (51.947°N, 1.285°E)

Inherited:

Filename	V1 no.	Start	End	Yrs
harwich-p022-uk-bodc.txt	**223**	05/01/1954	31/12/2006	17

Extended:

v1 filename	harwich-p022-uk-bodc.txt (223)
v2 Filename	223_Harwich-GBR_GESLA_v2.mat
Source of Extra Data	BODC
Extra Data filename	RN-7246_1372253428497.zip
Date of Download	26/06/2013
End of Extra Data	31/12/2012
Load in for Extra Data	BODC2
Comparison Comments	Comparisons are perfect

Quality Control:

Type	Date Affected	Comments	QC Flag	GESLA Flag
Threshold		<-2, >10	4	3
	10/02/2007 06:00 to 07/03/2007 11:00		4	3
	30/03/2007 00:00 to 09/04/2007 06:00		4	3
	12/04/2007 22:00 to 15/04/2007 07:00		4	3
	24/10/2007 13:00 to 14/11/2007 04:00		4	3
	29/02/2008 07:00 to 14/04/2008 17:00		4	3
	28/11/2008 08:00 to 18/03/2009 01:00		4	3
	03/04/2009 01:00 to 04/04/2009 22:00		4	3
	09/05/2009 07:00 to 06/07/2009 20:00		4	3
	20/07/2009 13:00 to 20/07/2009 19:00		4	3
	23/04/2012 09:00 to 25/04/2012 15:00		4	3
	13/09/2012 12:00 to 23/09/2012 01:00		4	3

(QC Flag: 0 = Meteorological (e.g. Seiche, Meteo-tsunami), 1 = Spike, 2 = Phase Offset, 3 = Tsunami, 4 = Other)

Analysis Comments

- Information regarding water level recorder can be found here on link to BODC website: file:///C:/Users/rjm305/Documents/PhD/1_Project/1_Research/0_Data/0_SeaLevel/5_BODC/0_Downloaded/RN-7246_1372253428497/Harwich.html

Heimsjoe, Norway (63.433°N, 9.117°E)

Inherited:

Filename	V1 no.	Start	End	Yrs
'heimsjoe-001-norway-mapping.mat'	**224**	01/01/1970	31/12/2008	39

Extended:

v1 filename	'heimsjoe-001-norway-mapping.mat (224)
v2 Filename	151_Heimsjoe-NOR_GESLA_v2.mat
Source of Extra Data	N/A
Extra Data filename	N/A
Date of Download	N/A
End of Extra Data	N/A
Load in for Extra Data	N/A
Comparison Comments	Extra data is available through the NMA website but can only be downloaded 30 days at a time. I have decided not to perform this labour intensive task at the moment.

Quality Control:

Type	Date Affected	Comments	QC Flag	GESLA Flag
Phase	05/01/1970 to 31/12/1972		2	3

(QC Flag: 0 = Meteorological (e.g. Seiche, Meteo-tsunami), 1 = Spike, 2 = Phase Offset, 3 = Tsunami, 4 = Other)

Analysis Comments

- Lot of noise in the data in the early years. Location in a fjord could lead to a complex tidal regime, but noise signals appear to be incorrect phase and this is backed up by data from 1973 onwards which does not have the noise in the data.
- Most of the data from the period before 1973 is invalid and as therefore it is difficult to trust the data remaining since it will constitute a low percentage of the original data. Therefore all data before 1973 is flagged as erroneous.

Heysham, UK (54.033°N, 2.912°W)

Inherited:

Filename	V1 no.	Start	End	Yrs
heysham-p050-uk-bodc.mat	**225**	05/01/1964	31/12/2006	31

Extended:

v1 filename	heysham-p050-uk-bodc.mat (225)
v2 Filename	152_Heysham-GBR_GESLA_v2.mat
Source of Extra Data	BODC
Extra Data filename	RN-7246_1372253428497.zip
Date of Download	26/06/2013
End of Extra Data	31/12/2012
Load in for Extra Data	BODC2
Comparison Comments	Comparisons are perfect

Quality Control:

Type	Date Affected	Comments	QC Flag	GESLA Flag
Threshold		Data >12 & < -2	4	3
	19/02/2007 09:00 to 22/02/2007 18:00		4	3
	06/08/2007 13:00 to 08/08/2007 21:00		4	3
	24/03/2009 08:00 to 24/03/2009 23:00		4	3
Spike	10/09/2010 11:00		1	3
	21/032011 15:00 to 23/03/2011 17:00		4	3
	11/05.2011 02:00 to 12/05/2011 16:00		4	3
	29/11/2011 12:00 to 02/12/2011 18:00		4	3
	11/07/2012 01:00 to 11/07.2012 09:00		4	3

(QC Flag: 0 = Meteorological (e.g. Seiche, Meteo-tsunami), 1 = Spike, 2 = Phase Offset, 3 = Tsunami, 4 = Other)

Analysis Comments

- Number of storm surge, with most in the winter season.

Hilo-Hawaii, USA (19.733°N, 155.067°W)

Inherited:

Filename	V1 no.	Start	End	Yrs
'hilo,_hawaii-060a-usa-uhslc.mat'	**226**	22/01/1927	31/12/2005	64
'hilo,hawaii,usa-001-glossdm-bodc.mat'	**227**	22/01/1927	31/12/2000	6

Extended:

v1 filename	hilo,_hawaii-060a-usa-uhslc.mat (226)
v2 Filename	**153**_Hilo-Hawaii-USA_GESLA_v2.mat
Source of Extra Data	UHSLC/NOAA
Extra Data filename	H060a / 226_NOAA_Hilo-Hawaii.txt
Date of Download	09/04/2013
End of Extra Data	31/12/2012
Load in for Extra Data	UHSLC/NOAA
Comparison Comments	Comparisons are perfect

Quality Control:

Type	Date Affected	Comments	QC Flag	GESLA Flag
Offset	Before 1946.		4	3
Tsunami	05/11/1952 to 09/11/1952	Aleutian Islands	3	6
Tsunami	09/03/1957 12:00 to 13/03/1957	Andreanov Island	3	6
Tsunami	23/05/1960 to 28/05/1960	Valdivia	3	6
Phase	22/12/1961 to 25/12/1961		2	
Phase	07/02/1962 12:00 to 09/02/1962		2	
Tsunami	28/03/1964 to 02/04/1964	Alaskan	3	6
Tsunami	04/02/1965 to 06/02/1962	Rat Islands	3	6
Phase	07/03/1974 12:00 to 08/03/1974 12:00		2	
Phase	14/10/1984 to 24/10/1984		2	
Tsunami	30/07/1995 12:00 to 02/08/1995	Antofagasta	3	6
Spike	22/06/2001 09:00		1	
Tsunami	24/06/2001 06:00 to 27/06/2001	Southern Peru	3	6
Tsunami	15/11/2006 to 19/11/2006	Kuril Islands	3	6
Tsunami	11/03/2011 06:00 to 15/03/2011	Tohuku	3	6
Tsunami	28/10/2012 06:00 to 29/10/2012	Queen Charlotte	3	6

(QC Flag: 0 = Meteorological (e.g. Seiche, Meteo-tsunami), 1 = Spike, 2 = Phase Offset, 3 = Tsunami, 4 = Other)

Analysis Comments

- After initial QC it is clear that data in the 1920s is different to the rest of the data. In particular the phase of many constituents is up to 10 degrees different and without the data from in intervening years it is not possible to verify this as a legitimate change.
- Data before 1946 are therefore deemed invalid.

Hoek van Holland, Netherlands (51.978°N, 4.120°E)

Inherited:

Filename	V1 no.	Start	End	Yrs
'hoekvanholla-hvh-nl-rws.mat'	**232**	01/01/1971	31/12/2007	37

Extended:

v1 filename	'hoekvanholla-hvh-nl-rws.mat (232)
v2 Filename	156_HoekVonHolland-NDL_GESLA_v2.mat
Source of Extra Data	N/A
Extra Data filename	N/A
Date of Download	N/A
End of Extra Data	N/A
Load in for Extra Data	N/A
Comparison Comments	No extra data available

Quality Control:

Type	Date Affected	Comments	QC Flag	GESLA Flag
		No erroneous data to remove		

(QC Flag: 0 = Meteorological (e.g. Seiche, Meteo-tsunami), 1 = Spike, 2 = Phase Offset, 3 = Tsunami, 4 = Other)

Analysis Comments

- Peak residual on 21/02/1993, associated with internal surge that caused flooding in Norfolk.
- Complex double low tide leads to misleading assignment of LHW during LW. **Take care when using anything but MHHW or MLLW.**

Holyhead, UK (53.308°N, 4.631°W)

Inherited:

Filename	V1 no.	Start	End	Yrs
'holyhead-p054-uk-bodc.mat'	**233**	05/01/1964	31/12/2006	31

Extended:

v1 filename	'holyhead-p054-uk-bodc.mat (233)
v2 Filename	157_Holyhead-GBR_GESLA_v2.mat
Source of Extra Data	BODC
Extra Data filename	RN-7246_1372253428497.zip
Date of Download	26/06/2013
End of Extra Data	31/03/2013
Load in for Extra Data	BODC2
Comparison Comments	Comparisons are perfect

Quality Control:

Type	Date Affected	Comments	QC Flag	GESLA Flag
Phase	14/08/2008 to 22/08/2008		2	3
Phase	12/09/2008 to 19/09/2008		2	3
Phase	15/01/2010 00:00 to 23:00		2	3
Phase	13/02/2010 18:00 to 14/02/2010 15:00		2	3
Spike	27/08/2010 11:00		1	3
Phase	31/08/2010 00:00 to23:00		2	3
Spike	10/01/2011 13:00		1	3
Spike	13/07/2011 08:00		1	3
Spike	24/08/2011 08:00		1	3
Spike	31/08/2011 08:00		1	3
Spike	31/10/2011 00:00 to 16:00		1	3

(QC Flag: 0 = Meteorological (e.g. Seiche, Meteo-tsunami), 1 = Spike, 2 = Phase Offset, 3 = Tsunami, 4 = Other)

Analysis Comments

- Number of invalid points to be removed using threshold of + 7.5 m and -0.5 m.

Honningsvaag, Norway (70.983°N, 25.983°E)

Inherited:

Filename	V1 no.	Start	End	Yrs
'honningsvaag-002-norway-mapping.mat'	**239**	04/06/1970	31/12/2008	35

Extended:

v1 filename	'honningsvaag-002-norway-mapping.mat (239)
v2 Filename	160_Honningsvaag-NOR_GESLA_v2.mat
Source of Extra Data	N/A
Extra Data filename	N/A
Date of Download	N/A
End of Extra Data	N/A
Load in for Extra Data	N/A
Comparison Comments	No extra data available, but email sent to NMA. Only inherited data carried forward.

Quality Control:

Type	Date Affected	Comments	QC Flag	GESLA Flag
Phase	31/10/1978 to 13/11/1978		2	3
Phase	27/11/1978 to 10/12/1978		2	3
Phase	26/12/1978 to 30/12/1978		2	3
Phase	09/12/1979 to 17/12/1979		2	3
Phase	30/01/1980 12:00 to 04/02/1980 15:00		2	3
Phase	06/03/1980 21:00 to 08/03/1980 12:00		2	3
Phase	28/05/1981 10:00 to 23:00		2	3
Phase	31/05/1981 20:00 to 02/06/1981 10:00		2	3
Phase	28/09/1981 to 04/10/1981		2	3
Datum	27/11/1981 12:00 to 22:00		4	3

(QC Flag: 0 = Meteorological (e.g. Seiche, Meteo-tsunami), 1 = Spike, 2 = Phase Offset, 3 = Tsunami, 4 = Other)

Analysis Comments

- Data is noisy throughout due to its location, possibly a sea ice influence in winter?
- Characteristic of the noise changes. Older data has more phase issues that are not present after 1982, which justifies removing the erroneous data before this date.
- Data pre-1990 show a phase shift to those afterwards although this is not seen in the amplitude data and therefore nothing is flagged.

Honolulu, USA (Hawaii) (21.307°N, 157.867°W)

Inherited:

Filename	V1 no.	Start	End	Yrs
'honolulu_a,hawaii-057a-usa-uhslc.mat'	**240**	21/06/1877	13/07/1892	3
'honolulu_b,hawaii-057b-usa-uhslc.mat'	**241**	01/01/1905	31/12/2005	100
'honululu,hawaii,usa-001-glossdm-bodc.mat'	**242**	02/01/1905	31/12/2000	41

Extended:

v1 filename	'honolulu_b,hawaii-057b-usa-uhslc.mat (241)
v2 Filename	161_Honolulu-USA_GESLA_v2.mat
Source of Extra Data	UHSLC/NOAA
Extra Data filename	H057b / COOP_Honolulu.csv
Date of Download	19/02/2014
End of Extra Data	31/12/2013
Load in for Extra Data	UHSLC/NOAA
Comparison Comments	Comparisons are perfect

Quality Control:

Type	Date Affected	Comments	QC Flag	GESLA Flag
Phase	02/12/1907 to 03/12/1907		2	3
Phase	18/07/1911 15:00 to 19/07/1911 21:00		2	3
Phase	26/08/1911 18:00 to 27/08/1911 18:00		2	3
Phase	15/07/1916 to 21/07/1916		2	3
Phase	05/06/1917 20:00 to 06/06/1917 20:00		2	3
Phase	14/06/1917 00:00 to 12:00		2	3
Phase	18/04/1920 to 20/04/1920		2	3
Phase	29/10/1920 to 12/11/1920		2	3
Phase	27/05/1923 to 20/06/1923		2	3
Phase	27/06/1923 to 01/07/1923		2	3
Phase	10/11/1929 12:00 to 12/11/1929 21:00		2	3
Phase	01/06/1936 08:00 to 04/06/1936 12:00		2	3
Tsunami	01/04/1946 12:00 to 02/04/1946 12:00	Aleutian Islands	3	6
Tsunami	04/11/1952 21:00 to 08/11/1952	Kuril Islands	3	6
Tsunami	09/03/1957 12:00 to 12/03/1957	Andreanov Islands	3	6
Tsunami	23/05/1960 08:00 to 29/05/1960	Chile	3	6
Phase	16/08/1962 12:00 to 17/08/1962 12:00		2	3
Tsunami	28/03/1964 06:00 to 30/03/1964	Alaska		
Phase	01/06/1966 00:00 to 12:00		2	3
Datum	01/08/1976 to 11/08/1976		4	
Phase	06/01/1982 18:00 to 07/01/1982 15:00		2	3
Phase	07/11/1982 to 16/11/1982		2	3
Phase	19/10/1982 00:00 to 23:00		2	3
Phase	26/07/1984 00:00 to 21:00		2	3
Tsunami	27/02/2010 28:00 to 02/03/2010	Chile	3	6
Tsunami	11/03/2011 12:00 to 14/03/2011	Tohuku	3	6

(QC Flag: 0 = Meteorological (e.g. Seiche, Meteo-tsunami), 1 = Spike, 2 = Phase Offset, 3 = Tsunami, 4 = Other)

Analysis Comments

- Peak water level on 12/09/1992. Although check about associated storm.
- Large residual on 13/01/1970 does not coincide with known tsunami and is therefore classed as a storm surge.
- Large residual on 24/11/1982 caused by Hurricane Iwa.

Ilfracombe, UK (51.211°N, 4.111°W)

Inherited:

Filename	V1 no.	Start	End	Yrs
'ilfracombe-p061-uk-bodc.mat'	**245**	30/01/1968	31/12/2006	19

Extended:

v1 filename	'ilfracombe-p061-uk-bodc.mat (245)
v2 Filename	164_Ilfracombe-GBR_GESLA_v2.mat
Source of Extra Data	BODC
Extra Data filename	RN-7246_1372253428497.zip
Date of Download	26/06/2013
End of Extra Data	31/03/2013
Load in for Extra Data	BODC2
Comparison Comments	Comparisons are perfect

Quality Control:

Type	Date Affected	Comments	QC Flag	GESLA Flag
Threshold		< -1 & > 11	4	3
Phase	09/03/2008 to 13/03/2008		2	3
Phase	31/03/2010 to 02/04/2010		2	3
Other	10/10/2011 to 11/10/2011 10:00	Flat line	4	3
Other	25/03/2012 15:00 to 26/03/2012 12:00	Flat line	4	3

(QC Flag: 0 = Meteorological (e.g. Seiche, Meteo-tsunami), 1 = Spike, 2 = Phase Offset, 3 = Tsunami, 4 = Other)

Immingham, UK (53.633°N, 0.187°W)

Inherited:

Filename	V1 no.	Start	End	Yrs
'immingham-p026-uk-bodc.mat'	**248**	28/01/1953	31/12/2006	46

Extended:

v1 filename	'immingham-p026-uk-bodc.mat (248)
v2 Filename	167_Immingham-GBR_GESLA_v2.mat
Source of Extra Data	BODC
Extra Data filename	RN-7246_1372253428497.zip
Date of Download	26/06/2013
End of Extra Data	31/03/2013
Load in for Extra Data	BODC2
Comparison Comments	Comparisons are perfect

Quality Control:

Type	Date Affected	Comments	QC Flag	GESLA Flag
Threshold		< -0.5 & > 10	4	3
Phase	07/05/2008 06:00 to 13/05/2008 12:00		2	3
Other	12/05/2011 08:00 to 15/05/2011	Flat line	4	3
Spike	27/09/2012 13:00		1	3

(QC Flag: 0 = Meteorological (e.g. Seiche, Meteo-tsunami), 1 = Spike, 2 = Phase Offset, 3 = Tsunami, 4 = Other)

Analysis Comments

- Peak residual occurs on 14/02/1989. Big windstorm affected Scotland mostly.
- Clear seasonal storm season during NH winter.

Ishigaki, Japan (24.333°N, 124.150°E)

Inherited:

Filename	V1 no.	Start	End	Yrs
'ishigaki,japan-001-glossdm-bodc.mat'	**249**	01/01/1975	31/12/2003	27
'ishigaki-365a-japan-uhslc.mat'	**250**	01/01/1969	31/12/2005	37

Extended:

v1 filename	'ishigaki-365a-japan-uhslc.mat (250)
v2 Filename	168_Ishigaki-JPN_GESLA_v2.mat
Source of Extra Data	UHSLC
Extra Data filename	H365a
Date of Download	19/02/2014
End of Extra Data	31/12/2012
Load in for Extra Data	UHSLC
Comparison Comments	Comparisons are perfect

Quality Control:

Type	Date Affected	Comments	QC Flag	GESLA Flag
		No erroneous data to remove		

(QC Flag: 0 = Meteorological (e.g. Seiche, Meteo-tsunami), 1 = Spike, 2 = Phase Offset, 3 = Tsunami, 4 = Other)

Analysis Comments

- Large residual on 09/08/1976.
- Peak residual on 06/10/2007.

Johnston Island, USA (Hawaii) (16.738°N, 169.530°W)

Inherited:

Filename	V1 no.	Start	End	Yrs
'johnston-052a-usa_trust-uhslc.mat'	**256**	01/05/1947	19/02/2003	49
'johnstonisland,usa-001-glossdm-bodc.mat'	**257**	01/05/1947	31/12/2000	47

Extended:

v1 filename	'johnston-052a-usa_trust-uhslc.mat (256)
v2 Filename	170_JohnstonIsland-USA_GESLA_v2.mat
Source of Extra Data	UHSLC
Extra Data filename	H052a
Date of Download	19/02/2014
End of Extra Data	31/12/2012
Load in for Extra Data	UHSLC
Comparison Comments	Comparisons are perfect

Quality Control:

Type	Date Affected	Comments	QC Flag	GESLA Flag
Tsunami	23/05/1960 10:00 to 25/05/1960	Chile	3	6
Phase	16/05/1973 10:00 to 17/05/1973 12:00		2	3
Phase	18/05/1973 10:00 to 19/05/1973 12:00		2	3

(QC Flag: 0 = Meteorological (e.g. Seiche, Meteo-tsunami), 1 = Spike, 2 = Phase Offset, 3 = Tsunami, 4 = Other)

Analysis Comments

- Peak residual on 13/01/1958, looks like .a valid event.
- Large water level in Jan 1962, but tide and surge not possible because of poor data coverage in 1962.

Johor Baharu, Malaysia (1.412°N, 103.792°E)

Inherited:

Filename	V1 no.	Start	End	Yrs
'johor_baharu-321a-malaysia-uhslc.mat'	**258**	18/12/1983	31/12/2005	22

Extended:

v1 filename	'johor_baharu-321a-malaysia-uhslc.mat (258)
v2 Filename	171_JohorBaharu-MYS_GESLA_v2.mat
Source of Extra Data	UHSLC
Extra Data filename	H321a
Date of Download	19/02/2014
End of Extra Data	31/12/2011
Load in for Extra Data	UHSLC
Comparison Comments	Comparisons are perfect

Quality Control:

Type	Date Affected	Comments	QC Flag	GESLA Flag
		No erroneous data to remove		

(QC Flag: 0 = Meteorological (e.g. Seiche, Meteo-tsunami), 1 = Spike, 2 = Phase Offset, 3 = Tsunami, 4 = Other)

Kahului, USA (Hawaii) (20.900°N, 156.467°W)

Inherited:

Filename	V1 no.	Start	End	Yrs
'kahului,maui,hawaii,usa-001-glossdm-bodc.mat'	**264**	19/10/1950	31/12/2000	46
'kahului-059a-usa-uhslc.mat'	**265**	19/10/1950	31/12/2005	51

Extended:

v1 filename	'kahului-059a-usa-uhslc.mat (265)
v2 Filename	174_Kahului-USA_GESLA_v2.mat
Source of Extra Data	UHSLC/NOAA
Extra Data filename	H059a / COOPS_Kahului
Date of Download	19/02/2014
End of Extra Data	31/12/2013
Load in for Extra Data	UHSLC/NOAA
Comparison Comments	Comparisons are perfect

Quality Control:

Type	Date Affected	Comments	QC Flag	GESLA Flag
Tsunami	28/03/1964 08:00 to 02/04/1964	Aleutian Islands	3	6
Phase	18/04/1968 18:00 to 19/04/1968 12:00		2	3
Tsunami	16/05/1968 06:00 to 18/05/1968	Tokachi	3	6
Phase	15/01/1969 06:00 to 16/01/1969 12:00		2	3
Phase	01/08/1970 to 05/08/1970		2	3
Phase	01/11/1974 06:00 to 21:00		2	3
Phase	04/07/1982 to 24/07/1982		2	3
Phase	02/07/1983 21:00 to 03/07/1983 08:00		2	3
Phase	19/10/1983 to 03/11/1983		2	3

Tsunami	04/10/1994 18:00 to 07/10/1994	Kuril Islands	3	6
Tsunami	30/07/1995 15:00 to 02/08/1995	Antofagasta	3	6
Tsunami	24/06/2001 12:00 to 27/06/2001	Southern Peru	3	6
Tsunami	17/11/2003 10:00 to 23/11/2003	Rat Island	3	6
Tsunami	15/11/2006 15:00 to 18/11/2006	Kuril Islands	3	6
Tsunami	16/08/2007 to 20/08/2007	Peru	3	6
Tsunami	30/09/2009 to 04/10/2009	Samoan	3	6
Tsunami	27/02/2010 21:00 to 07/03/2010	Chile	3	6
Tsunami	11/03/2011 12:00 to 18/03/2011	Tohuku	3	6
Tsunami	28/10/2012 08:00 to 30/10/2012	Queen Charlotte	3	6

(QC Flag: 0 = Meteorological (e.g. Seiche, Meteo-tsunami), 1 = Spike, 2 = Phase Offset, 3 = Tsunami, 4 = Other)

Analysis Comments

- Max. residual caused by Chilean 2010 Earthquake while min. residual caused by 2011 Tohuku Earthquake. Both flagged as erroneous.
- Check for documented tsunamis but not found anything so data left in on the following dates: 22/01/1982, 04/12/1999, 04/12/2007.

Kanton, Kiribati (2.810°S, 171.718°W)

Inherited:

Filename	V1 no.	Start	End	Yrs
'kanton-a,kiribati-001-glossdm-bodc.mat'	**267**	28/05/1949	15/09/1967	17
'kanton-b,kiribati-001-glossdm-bodc.mat'	**268**	02/05/1972	31/12/1998	23
'kanton_a-013a-rep._of_kiribati-uhslc.mat'	**269**	28/05/1949	15/09/1967	17
'kanton_b-013b-rep._of_kiribati-uhslc.mat'	**270**	02/05/1972	03/08/2001	25

Extended:

v1 filename	'kanton_b-013b-rep._of_kiribati-uhslc.mat (270)
v2 Filename	176_Kanton-KIR_GESLA_v2.mat
Source of Extra Data	UHSLC
Extra Data filename	H013b
Date of Download	19/02/2014
End of Extra Data	03/08/2012
Load in for Extra Data	UHSLC
Comparison Comments	Comparisons are perfect

Quality Control:

Type	Date Affected	Comments	QC Flag	GESLA Flag
Phase	21/10/1973 to 24/10/1973		2	3
Phase	22/11/1973 to 27/11/1973		2	3
Phase	30/09/1974 to 07/10/1974		2	3
Phase	01/03/1976 00:00 to 23:00		2	3
Phase	01/03/1979 to 07/03/1979		2	3

(QC Flag: 0 = Meteorological (e.g. Seiche, Meteo-tsunami), 1 = Spike, 2 = Phase Offset, 3 = Tsunami, 4 = Other)

Analysis Comments

- Generally low residual up to 0.2 m with no obvious signal of storm surges.

Kaohsiung, Taiwan (22.615°N, 120.280°E)

Inherited:

Filename	V1 no.	Start	End	Yrs
'kaohsiung-340a-republic_of_china-uhslc.mat'	**271**	01/01/1980	31/12/2006	27

Extended:

v1 filename	kaohsiung-340a-republic_of_china-uhslc.mat (271)
v2 Filename	177_Kaohsiung-TWN_GESLA_v2.mat
Source of Extra Data	UHSLC
Extra Data filename	H340a
Date of Download	19/02/2014
End of Extra Data	31/12/2012
Load in for Extra Data	UHSLC
Comparison Comments	Comparisons between inherited and extra show a datum shift which is documented on the UHSLC station info. Historic data (1980-2007) were adjusted to the TG by adding -47 cm. Only the newly downloaded data is used for this site.

Quality Control:

Type	Date Affected	Comments	QC Flag	GESLA Flag
Phase	26/11/1981 to 03/12/1981		2	3
Phase	18/06/2001 00:00 to 12:00		2	3
Phase	23/06/2001 00:00 to 15:00:		2	3
Phase	22/06/2002 15:00 to 24/06/2002		2	3
Phase	09/11/2005 12:00 to 15/11/2005		2	3
Tsunami	11/03/2011 09:00 to 13/03/2011	Tohuku	3	6

(QC Flag: 0 = Meteorological (e.g. Seiche, Meteo-tsunami), 1 = Spike, 2 = Phase Offset, 3 = Tsunami, 4 = Other)

Analysis Comments

- Some data in 1980 appears to have some tidal signal carried through to the surge component (i.e. no noise in residual just some tidal signal?). Is this tide-surge interaction during the following periods: 01/01/1980 to 01/04/1980; 01/01/1981 to 01/02/1981; 25/02/1981 to 15/08/1982

Kapingamarangi, Micronesia (1.098°N, 154.777°E)

Inherited:

Filename	V1 no.	Start	End	Yrs
'kapingamarangi,fed.micronesia-001-glossdm-bodc.mat'	**272**	08/09/1978	31/12/1998	18
'kapingamarangi-029a-fd._st._micronesia-uhslc.mat'	**273**	08/09/1978	31/12/2003	22

Extended:

v1 filename	'kapingamarangi-029a-fd._st._micronesia-uhslc.mat (273)
v2 Filename	178_Kapingamarangi-FSM_GESLA_v2.mat
Source of Extra Data	UHSLC
Extra Data filename	H029a
Date of Download	19/02/2014
End of Extra Data	31/12/2009
Load in for Extra Data	UHSLC
Comparison Comments	Comparisons are perfect

Quality Control:

Type	Date Affected	Comments	QC Flag	GESLA Flag
Phase	20/09/1987 to 01/01/1988		2	3

(QC Flag: 0 = Meteorological (e.g. Seiche, Meteo-tsunami), 1 = Spike, 2 = Phase Offset, 3 = Tsunami, 4 = Other)

Analysis Comments

- Peak residual 27/06/2002.
- A lot of noise in the surge residuals but it all appears valid. Caused by infrequent storms and changes in MSL.

Keelung, Taiwan (25.147°N, 121.745°E)

Inherited:

Filename	V1 no.	Start	End	Yrs
'keelung-341a-republic_of_china-uhslc.mat'	**277**	01/01/1980	31/12/2006	21

Extended:

v1 filename	'keelung-341a-republic_of_china-uhslc.mat (277)
v2 Filename	182_Keelung-TWN_GESLA_v2.mat
Source of Extra Data	UHSLC
Extra Data filename	H341a
Date of Download	19/02/2014
End of Extra Data	31/12/2012
Load in for Extra Data	UHSLC
Comparison Comments	Comparisons between inherited and extra show a datum shift which is documented on the UHSLC station info. Historic data (1980-2007) were adjusted to the KP by adding -92 cm. Only the newly downloaded data is used for this site.

Quality Control:

Type	Date Affected	Comments	QC Flag	GESLA Flag
Phase	13/10/1981 to 18/10/1981		2	3

(QC Flag: 0 = Meteorological (e.g. Seiche, Meteo-tsunami), 1 = Spike, 2 = Phase Offset, 3 = Tsunami, 4 = Other)

Analysis Comments

- Peak residual 18/08/1997

Kelang, Malaysia (3.050°N, 101.358°E)

Inherited:

Filename	V1 no.	Start	End	Yrs
'kelang-140a-malaysia-uhslc.mat'	**278**	15/12/1983	31/12/2005	22

Extended:

v1 filename	'kelang-140a-malaysia-uhslc.mat (278)
v2 Filename	183_Kelang-MYS_GESLA_v2.mat
Source of Extra Data	UHSLC
Extra Data filename	H140a
Date of Download	19/02/2014
End of Extra Data	31/12/2011
Load in for Extra Data	UHSLC
Comparison Comments	Comparisons are perfect

Quality Control:

Type	Date Affected	Comments	QC Flag	GESLA Flag
Phase	21/10/1991 to 27/10/1991		2	3
Phase	29/09/2008 18:00 to 30/09/2008 06:00		2	3
Other	15/10/2008 to 19/11/2008		4	3
Phase	27/01/2010 to 03/02/2010		2	3
Phase	14/01/2011 to 17/01/2011		2	3
Other	17/07/2011 to 20/07/2011		4	3
Other	25/08/2011 to 10/09/2011		4	3
Phase	18/12/2011 to 23/12/2011		2	3

(QC Flag: 0 = Meteorological (e.g. Seiche, Meteo-tsunami), 1 = Spike, 2 = Phase Offset, 3 = Tsunami, 4 = Other)

Ketchikan, USA (Alaska) (55.333°N, 131.625°W)

Inherited:

Filename	V1 no.	Start	End	Yrs
'ketchikan,ak-571a-usa-uhslc.mat'	**282**	12/10/1918	31/12/2005	64
'ketchikan,usa-001-glossdm-bodc.mat'	**283**	01/01/1949	31/12/2000	49

Extended:

v1 filename	'ketchikan,ak-571a-usa-uhslc.mat (282)
v2 Filename	187_Ketchikan-USA_GESLA_v2.mat
Source of Extra Data	UHSLC/NOAA
Extra Data filename	H571a / COOPS_Ketchikan
Date of Download	19/02/2014
End of Extra Data	31/12/2003
Load in for Extra Data	UHSLC/NOAA
Comparison Comments	Comparisons are perfect

Quality Control:

Type	Date Affected	Comments	QC Flag	GESLA Flag
Phase	28/02/1919 to 02/03/1919		2	3
Datum	31/12/1920 12:00 to 02/01/1921		4	3
Phase	30/12/1923 to 01/01/1924		2	3
Phase	05/07/1960 08:00 to 06/07/1960 10:00		2	3
Phase	07/08/1960 to 11/08/1960		2	3
Phase	03/12/1960 00:00 to 12:00		2	3
Noise	27/05/1961 to 01/06/1961		4	3
Phase	28/09/1961 00:00 to 21:00		2	3
Phase	09/11/1962 to 14/11/1962		2	3
Phase	03/03/1974 to 11/03/1974		2	3
Phase	21/08/1974 to 25/08/1974		2	3
Phase	28/01/1975 to 14/02/1975		2	3
Phase	25/03/1975 to 02/04/1975		2	3
Phase	29/04/1975 18:00 to 30/04/1975 10:00		2	3
Phase	07/09/1975 00:00 23:00		2	3
Phase	12/12/1975 to 28/12/1975		2	3
Phase	25/01/1978 18:00 to 26/01/1978 21:00		2	3
Noise	03/11/1978 to 17/11/1978		4	3
Phase	30/04/1979 00:00 to 01/05/1979 08:00		2	3
Phase	16/10/1980 to 18/10/1980		2	3
Phase	27/12/1980 03:00 to 28/12/1980 12:00		2	3
Phase	12/06/2007 13:00 to 14:00		2	3
Phase	14/06/2007 13:00 to 16:00		2	3
Phase	15/06/2007 14:00 to 18:00		2	3

Phase	16/06/2007 15:00 to 19:00		2	3
Phase	17/06/2007 15:00 to 20:00		2	3
Phase	18/06/2007 15:00 to 20:00		2	3
Phase	29/06/2007 12:00 to 22:00		2	3
Phase	30/06/2007 12:00 to 22:00		2	3
Phase	01/07/2007 12:00 to 22:00		2	3
Phase	02/07/2007 12:00 to 22:00		2	3
Phase	03/07/2007 12:00 to 22:00		2	3
Phase	04/07/2007 12:00 to 22:00		2	3
Phase	05/07/2007 12:00 to 22:00		2	3
Phase	11/07/2007 12:00 to 22:00		2	3
Phase	12/07/2007 12:00 to 22:00		2	3
Phase	13/07/2007 12:00 to 22:00		2	3
Phase	14/07/2007 12:00 to 22:00		2	3
Phase	15/07/2007 12:00 to 22:00		2	3
Phase	16/07/2007 12:00 to 22:00		2	3
Phase	17/07/2007 12:00 to 22:00		2	3
Phase	18/07/2007 12:00 to 22:00		2	3
Phase	19/07/2007 12:00 to 22:00		2	3
Phase	20/07/2007 12:00 to 22:00		2	3

(QC Flag: 0 = Meteorological (e.g. Seiche, Meteo-tsunami), 1 = Spike, 2 = Phase Offset, 3 = Tsunami, 4 = Other)

Key West, USA (Florida) (24.553°N, 81.808°W)

Inherited:

Filename	V1 no.	Start	End	Yrs
'key_west,fl-242a-usa-uhslc.mat'	**284**	19/01/1913	31/12/2005	91
'keywest,fl-001-glossdm-bodc.mat'	**285**	01/01/1926	31/12/2000	28
'keywest-006-usa-johnhunter.mat'	**286**	19/01/1913	28/02/2006	91

Extended:

v1 filename	'key_west,fl-242a-usa-uhslc.mat (284)
v2 Filename	188_KeyWest-USA_GESLA_v2.mat
Source of Extra Data	UHSLC/NOAA
Extra Data filename	H242a / COOPS_KeyWest
Date of Download	19/02/2014
End of Extra Data	31/12/2013
Load in for Extra Data	UHSLC/NOAA
Comparison Comments	Comparisons are perfect

Quality Control:

Type	Date Affected	Comments	QC Flag	GESLA Flag
Phase	29/04/1923 to 06/05/1923		2	3
Phase	24/01/1932 to 28/01/1932		2	3
Phase	26/11/1939 20:00 to 27/11/1939 04:00		2	3
Spike	27/04/1980 15:00 to 23:00		1	3
Phase	05/02/1984 to 09/02/1984		2	3
Phase	11/03/2006 12:00 to 16/03/2006 18:00		2	3
Phase	12/02/2012 06:00 to 13/02/2012 18:00		2	3

(QC Flag: 0 = Meteorological (e.g. Seiche, Meteo-tsunami), 1 = Spike, 2 = Phase Offset, 3 = Tsunami, 4 = Other)

Analysis Comments

- Peak residual on 18/10/1944 caused by Cuba-Florida Hurricane.
- Peak water level (= max. residual) on 24/10/2005. Caused by Hurricane Wilma.
- Other events in 1965, 1965 and 1998 are also prominent.

Knysna, South Africa (34.080°S, 23.050°E)

Inherited:

No inherited file.

Extended:

v1 filename	N/A
v2 Filename	464_Kynsna-ZAF_GESLA_v2.mat
Source of Extra Data	UHSLC
Extra Data filename	H186a
Date of Download	19/02/2014
End of Extra Data	31/12/2012
Load in for Extra Data	UHSLC
Comparison Comments	N/A

Quality Control:

Type	Date Affected	Comments	QC Flag	GESLA Flag
Phase	30/09/1978 to 03/10/1978		2	3
Phase	23/07/1980 to 28/07/1980		2	3
Phase	24/08/1980 to 30/08/1980		2	3
Phase	08/09/1980 12:00 to 12/09/1980 12:00		2	3
Phase	30/10/1981 to 08/11/1981 15:00		2	3
Phase	03/01/1985 12:00 to 06/01/1985 12:00		2	3

(QC Flag: 0 = Meteorological (e.g. Seiche, Meteo-tsunami), 1 = Spike, 2 = Phase Offset, 3 = Tsunami, 4 = Other)

Ko Lak, Thailand (11.795°N, 99.817°E)

Inherited:

Filename	V1 no.	Start	End	Yrs
'ko_lak-328a-thailand-uhslc.mat'	**290**	01/01/1985	28/12/2006	22

Extended:

v1 filename	'ko_lak-328a-thailand-uhslc.mat (290)
v2 Filename	192_KoLak-THA-USA_GESLA_v2.mat
Source of Extra Data	UHSLC
Extra Data filename	H328a
Date of Download	19/02/2014
End of Extra Data	28/12/2012
Load in for Extra Data	UHSLC
Comparison Comments	Comparisons are perfect

Quality Control:

Type	Date Affected	Comments	QC Flag	GESLA Flag
Phase	05/05/1996 00:00 to 18:00		2	3
Phase	07/05/1996 00:00 to 18:00		2	3
Phase	19/04/2001 to 03/06/2001		2	3
Phase	25/10/2002 to 16/01/2003		2	3
Phase	22/06/2003 to 01/07/2003		2	3
Phase	27/06/2004 to 07/07/2004 12:00		2	3
Phase	02/07/2008 12:00 to 03/07/2008 06:00		2	3
Phase	20/11/2011 12:00 to 22/11/2011 18:00		2	3

(QC Flag: 0 = Meteorological (e.g. Seiche, Meteo-tsunami), 1 = Spike, 2 = Phase Offset, 3 = Tsunami, 4 = Other)

Analysis Comments

- Min. residual occurred on 03/11/1997 caused by Cyclone Linda (Openg)

Kodiak Island, USA (Alaska) (57.732°N, 152.512°W)

Inherited:

Filename	V1 no.	Start	End	Yrs
'kodiak_isl.,alaska-039a-usa-uhslc.mat'	**292**	01/01/1975	31/12/2005	26
'kodiakisland,usa-001-glossdm-bodc.mat'	**293**	01/01/1975	31/12/2000	21

Extended:

v1 filename	'kodiak_isl.,alaska-039a-usa-uhslc.mat (292)
v2 Filename	194_KodiakIsland-USA_GESLA_v2.mat
Source of Extra Data	UHSLC/NOAA
Extra Data filename	H039a/COOPS_KodiakIsland
Date of Download	19/02/2014
End of Extra Data	31/12/2013
Load in for Extra Data	UHSLC/NOAA
Comparison Comments	Comparisons are perfect

Quality Control:

Type	Date Affected	Comments	QC Flag	GESLA Flag
Phase	16/02/1976 08:00 to 17/02/1976 12:00		2	3
Phase	01/12/1982 to 05/12/1982		2	3
Phase	23/01/2007 to 27/01/2007		2	3
Tsunami	28/02/2010 to 02/03/2010	Chile	3	6
Tsunami	11/03/2011 18:00 to 16/03/2011	Tohuku	3	6
Spikes	14/06/2013 08:00 to 15/06/2013 06:00		1	3
Phase	16/06/2013 21:00 to 17/06/2013 04:00		2	3
Phase	17/06/2013 21:00 to 18/06/2013 06:00		2	3

(QC Flag: 0 = Meteorological (e.g. Seiche, Meteo-tsunami), 1 = Spike, 2 = Phase Offset, 3 = Tsunami, 4 = Other)

Kuantan, Malaysia (3.975°N, 103.430°E)

Inherited:

Filename	V1 no.	Start	End	Yrs
'kuantan-322a-malaysia-uhslc.mat'	**295**	21/12/1983	31/12/2005	22

Extended:

v1 filename	'kuantan-322a-malaysia-uhslc.mat (295)
v2 Filename	196_Kuantan-MYS_GESLA_v2.mat
Source of Extra Data	UHSLC
Extra Data filename	H322a
Date of Download	20/02/2014
End of Extra Data	31/12/2012
Load in for Extra Data	UHSLC
Comparison Comments	Comparisons are perfect

Quality Control:

Type	Date Affected	Comments	QC Flag	GESLA Flag
Spike	02/11/2005 03:00		1	2

(QC Flag: 0 = Meteorological (e.g. Seiche, Meteo-tsunami), 1 = Spike, 2 = Phase Offset, 3 = Tsunami, 4 = Other)

Analysis Comments

- Peak residual occurs on 06/03/2005. No documented cyclone but definite storm surge.

Kushimoto, Japan (33.467°N, 135.783°E)

Inherited:

Filename	V1 no.	Start	End	Yrs
'kushimoto,japan-001-glossdm-bodc.mat'	**298**	01/01/1961	31/12/2003	42
'kushimoto-353a-japan-uhslc.mat'	**299**	01/01/1961	31/12/2005	44

Extended:

v1 filename	'kushimoto-353a-japan-uhslc.mat (299)
v2 Filename	199_Kushimoto-JPN_GESLA_v2.mat
Source of Extra Data	UHSLC
Extra Data filename	H353a
Date of Download	20/02/2014
End of Extra Data	31/12/2012
Load in for Extra Data	UHSLC
Comparison Comments	Comparisons are perfect

Quality Control:

Type	Date Affected	Comments	QC Flag	GESLA Flag
Phase	02/01/1964 12:00 to 04/01/1964 15:00		2	3
Phase	18/09/1970 to 20/09/1970		2	3

(QC Flag: 0 = Meteorological (e.g. Seiche, Meteo-tsunami), 1 = Spike, 2 = Phase Offset, 3 = Tsunami, 4 = Other)

Analysis Comments

- Peak residual on 16/09/1961 caused by Cyclone Nancy (Cat 5)
- Peak water level on 02/09/2011, storm surge caused by TS Talas small but coincides with peak of seasonal MSL signal and spring tides.

Kushiro, Japan (42.967°N, 144.383°E)

Inherited:

Filename	V1 no.	Start	End	Yrs
kushiro,japan-001-glossdm-bodc.mat	**300**	01/01/1963	31/12/2003	38
kushiro-350a-japan-uhslc.mat	**301**	01/01/1963	31/12/2005	41

Extended:

v1 filename	kushiro-350a-japan-uhslc.mat (301)
v2 Filename	200_Kushiro-JPN_GESLA_v2.mat
Source of Extra Data	UHSLC
Extra Data filename	H350a
Date of Download	20/02/2014
End of Extra Data	31/12/2012
Load in for Extra Data	UHSLC
Comparison Comments	Comparisons are perfect

Quality Control:

Type	Date Affected	Comments	QC Flag	GESLA Flag
		No erroneous data to remove		

(QC Flag: 0 = Meteorological (e.g. Seiche, Meteo-tsunami), 1 = Spike, 2 = Phase Offset, 3 = Tsunami, 4 = Other)

Analysis Comments

- Huge trends in MSL of 8 mm/yr
- Double high tide, causes some issues when selecting HW and LW.
- Peak residual on 19/10/1979, caused (probably) by Super Typhoon Tip.
- Peak water level on 08/10/2006, but no obvious generating storm.

Kwajalein, Marshall Islands (8.733°N, 167.733°E)

Inherited:

Filename	V1 no.	Start	End	Yrs
'kwajalein,marshallis.-001-glossdm-bodc.mat'	302	07/06/1946	31/12/2000	53
'kwajalein-055a-rep._of_marshall_i-uhslc.mat'	303	07/06/1946	31/12/2005	58

Extended:

v1 filename	'kwajalein-055a-rep._of_marshall_i-uhslc.mat (303)
v2 Filename	201_Kwajalein-MHL_GESLA_v2.mat
Source of Extra Data	UHSLC/NOAA
Extra Data filename	H055a/COOP_Kwajalein
Date of Download	20/02/2014
End of Extra Data	31/12/2013
Load in for Extra Data	UHSLC/NOAA
Comparison Comments	Comparisons are perfect

Quality Control:

Type	Date Affected	Comments	QC Flag	GESLA Flag
Phase	10/09/1947 to 31/12/11947 23:00		2	3
Phase	01/01/1949 to 20/01/1949		2	3
Phase	28/01/1949 to 01/02/1949		2	3
Phase	12/03/1949 to 20/03/1949		2	3
Phase	15/06/1949 to 16/07/1949		2	3
Phase	17/12/1949 to 31/12/1949 23:00		2	3
Phase	30/01/1950 to 06/02/1950		2	3
Phase	04/03/1950 to 11/03/1950		2	3
Phase	29/04/1950 to 05/05/1950		2	3
Phase	10/05/1950 to 22/08/1950		2	3
Tsunami	05/11/1952 to 07/11/1952	Severo-Kulisk	3	6
Phase	23/09/1956 to 27/09/1956		2	3
Phase	01/04/1958 18:00 to 05/04/1958		2	3
Phase	12/04/1958 to 17/04/1958		2	3
Phase	17/08/1958 to 30/08/1958		2	3
Phase	06/01/1959 to 12/01/1959		2	3
Phase	07/06/1959 to 15/06/1959		2	3
Tsunami	23/05/1960 to 27/05/1960	Valdivia	3	6
Phase	14/05/1963 to 17/05/1963		2	3
Phase	18/10/1964 to 24/10/1964		2	3
Phase	21/11/1968 to 24/11/1968		2	3
Phase	05/09/1970 21:00 to 08/09/1970		2	3
Phase	30/12/1970 to 04/01/1971		2	3
Phase	02/09/1975 to 12/09/1975		2	3
Phase	02/10/1975 to 10/10/1975		2	3
Phase	24/10/1975 to 27/10/1975		2	3
Phase	23/01/1976 to 03/02/1976		2	3
Phase	15/02/1980 to 17/02/1980		2	3
Phase	22/03/1985 21:00 to 24/03/1985		2	3
Phase	13/04/1991 to 02/05/1991		2	3
Phase	13/04/2006 to 28/04/2006		2	3
Tsunami	18/01/2009 to 25/01/2009	Kermadoc Islands	3	6
Phase	09/01/2010 to 11/01/2010		2	3
Tsunami	11/03/2011 06:00 to 15/03/2011	Tohuku	3	6

(QC Flag: 0 = Meteorological (e.g. Seiche, Meteo-tsunami), 1 = Spike, 2 = Phase Offset, 3 = Tsunami, 4 = Other)

La Libertad, Ecuador (-2.200°S, 80.927°W)

Inherited:

Filename	V1 no.	Start	End	Yrs
'la_libertad-091a-ecuador-uhslc.mat'	**307**	01/09/1949	31/12/2003	52

Extended:

v1 filename	'la_libertad-091a-ecuador-uhslc.mat (307)
v2 Filename	204_LaLibertad-ECU_GESLA_v2.mat
Source of Extra Data	UHSLC
Extra Data filename	H091a
Date of Download	20/02/2014
End of Extra Data	31/12/2012
Load in for Extra Data	UHSOLC
Comparison Comments	Offset between inherited and downloaded data suggest that a shift has been applied to all data on the UHSLC website since previous download. Only used extra data

Quality Control:

Type	Date Affected	Comments	QC Flag	GESLA Flag
Tsunami	05/11/1952 08:00 to 10/11/1952	Severo-Kulisk	3	6
Phase	06/01/1954 to 12/01/1954		2	3
Phase	15/02/1954 to 18/02/1954		2	3
Tsunami	23/05/1960 to 01/06/1960: Valdivia		2	3
Tsunami	28/03/1964 15:00 to 03/04/1964	Alaskan	3	6
Phase	01/09/1981 to 10/09/1981		2	3
Phase	10/07/1988 12:00 to 11/07/1988 12:00		2	3
Phase	20/01/1990 18:00 to 21/01/1990 12:00		2	3
Phase	05/12/1990 12:00 to 11/12/1990		2	3
Phase	09/02/1992 to 27/02/1992		2	3
Phase	02/11/1997 to 04/11/1997		2	3
Noise	1998-1999		4	3
Phase	27/07/2000 to 24/08/2000		2	3
Phase	07/06/2001 to 11/06/2001		2	3
Noise	23/11/2001 to 23/02/2003		4	3
Phase	14/12/2004 00:00 to 23:00		2	3
Phase	24/05/2006 00:00 to 23:00		2	3
Tsunami	27/02/2010 to 04/03/2010	Chile	3	6
Tsunami	12/03/2011 to 16/003/2011	Tohuku	3	6
Phase	27/09/2011 00:00 to 10:00		2	3

(QC Flag: 0 = Meteorological (e.g. Seiche, Meteo-tsunami), 1 = Spike, 2 = Phase Offset, 3 = Tsunami, 4 = Other)

Analysis Comments

- During 1998-1999 there is a lot of high frequency noise in the residual. UHSLC stats that "The originators did not detect any problems the gauge during this period and assume the noise was caused by agitated local seas".
- The signal is not the same for the rest of the data and therefore skews the results, but they noisy patches 1983, 1998 and 2002 roughly correlate with El Nino events that may have some indirect effect on noise in the data..

Legaspi, Philippines (13.150°N, 123.750°E)

Inherited:

Filename	V1 no.	Start	End	Yrs
'legaspi-371a-philippines-uhslc.mat'	**318**	01/01/1984	31/12/2004	19

Extended:

v1 filename	'legaspi-371a-philippines-uhslc.mat (318)
v2 Filename	213_Legaspi-PHL_GESLA_v2.mat
Source of Extra Data	UHSLC
Extra Data filename	H371a
Date of Download	24/02/2014
End of Extra Data	30/09/2012
Load in for Extra Data	UHSLC
Comparison Comments	Comparisons are perfect

Quality Control:

Type	Date Affected	Comments	QC Flag	GESLA Flag
Phase	31/01/1985 08:00 to 11/02/1985 18:00		2	3

(QC Flag: 0 = Meteorological (e.g. Seiche, Meteo-tsunami), 1 = Spike, 2 = Phase Offset, 3 = Tsunami, 4 = Other)

Analysis Comments

- Peak residual in Dec-1992 not associated with a particular storm. However, the city is located at the end of a long bay, so large events could be forced by met conditions a long way from the site.

Lerwick, UK (60.154°N, 1.140°W)

Inherited:

Filename	V1 no.	Start	End	Yrs
lerwick-001-glossdm-bodc.txt	320	03/03/1980	31/12/1991	7
lerwick-293a-united_kingdom-uhslc.txt	321	01/01/1959	31/12/2001	42
lerwick-p041-uk-bodc.txt	322	05/01/1959	31/12/2006	43

Extended:

v1 filename	lerwick-293a-united_kingdom-uhslc.txt (321)
v2 Filename	214_Lerwick-GBR_GESLA_v2.mat
Source of Extra Data	BODC
Extra Data filename	RN-7246_1372253428497.zip
Date of Download	26/06/2013
End of Extra Data	31/12/2012
Load in for Extra Data	BODC2
Comparison Comments	Comparisons are perfect

Quality Control:

Type	Date Affected	Comments	QC Flag	GESLA Flag
Threshold		< -1 & > 20	4	3
Other	30/10/2006 21:00 to 13/07/2007		4	3
Other	27/08/2007 15:00 to 28/08/2007 18:00		4	3
Other	26/04/2012 07:00 to 01/05/2012 03:00		4	3

(QC Flag: 0 = Meteorological (e.g. Seiche, Meteo-tsunami), 1 = Spike, 2 = Phase Offset, 3 = Tsunami, 4 = Other)

Lewes, USA (Delaware) (38.782°N, 71.120°W)

Inherited:

Filename	V1 no.	Start	End	Yrs
'lewes,de-747a-usa-uhslc.mat'	**323**	01/01/1957	31/12/2005	47

Extended:

v1 filename	'lewes,de-747a-usa-uhslc.mat (323)
v2 Filename	215_Lewes-USA_GESLA_v2.mat
Source of Extra Data	UHSLC/NOAA
Extra Data filename	H747a / COOPS_Lewes
Date of Download	24/02/2014
End of Extra Data	31/12/2013
Load in for Extra Data	UHSLC/NOAA
Comparison Comments	Comparisons are perfect

Quality Control:

Type	Date Affected	Comments	QC Flag	GESLA Flag
		No erroneous data to remove.		

(QC Flag: 0 = Meteorological (e.g. Seiche, Meteo-tsunami), 1 = Spike, 2 = Phase Offset, 3 = Tsunami, 4 = Other)

Analysis Comments

- Peak residual and water level occur on 08/03/1962 caused by Ash Wednesday storm that impacted the Atlantic Coast of the mid-USA.

Lime Tree Bay, US Virgin Islands (17.697°N, 64.753°W)

Inherited:

Filename	V1 no.	Start	End	Yrs
'limetree_bay-254a-usa-uhslc.mat'	325	02/02/1982	31/12/2005	21
'st.croix,(akalimetreebay)-001-glossdm-bodc.mat'	588	01/01/1991	31/12/2000	8

Extended:

v1 filename	'limetree_bay-254a-usa-uhslc.mat (325)
v2 Filename	217_LimeTreeBay-VIR_GESLA_v2.mat
Source of Extra Data	UHSLC/NOAA
Extra Data filename	H254a / COOPS_LimeTreeBay
Date of Download	24/02/2014
End of Extra Data	31/12/2013
Load in for Extra Data	UHSLC/NOAA
Comparison Comments	Comparison between inherited and extra datasets is perfect. Comparison between downloaded UHSLC and NOAA shows a datum shift of 9.144 m, which was taken from NOAA data allows perfect comparison between datasets.

Quality Control:

Type	Date Affected	Comments	QC Flag	GESLA Flag

(QC Flag: 0 = Meteorological (e.g. Seiche, Meteo-tsunami), 1 = Spike, 2 = Phase Offset, 3 = Tsunami, 4 = Other)

Analysis Comments

- Peak residual and water level occur on 17/11/1999 caused by Hurricane Lenny, which made landfall not far from the gauge.
- Generally small residuals except for occasional TS.
- Very small tidal signal, with some cases of double highs causing incorrect assignment of LW.

Los Angeles, USA (33.720°N, 118.271°W)

Inherited:

Filename	V1 no.	Start	End	Yrs
'los_angeles,ca-567a-usa-uhslc.mat'	335	29/11/1923	31/12/2001	74

Extended:

v1 filename	'los_angeles,ca-567a-usa-uhslc.mat
v2 Filename	224_LosAngeles-USA_GESLA_v2.mat
Source of Extra Data	UHSLC/NOAA
Extra Data filename	H576a / COOPS_LosAngeles
Date of Download	24/02/2014
End of Extra Data	31/12/2013
Load in for Extra Data	UHSLC/NOAA
Comparison Comments	Comparisons are perfect

Quality Control:

Type	Date Affected	Comments	QC Flag	GESLA Flag
Phase	27/03/1928 06:00 to 28/03/1928 10:00	Severo-Kulisk	2	3
Phase	27/02/1947 06:00 to 18:00		2	3
Tsunami	05/11/1952 to 09/11/1952	Kuril Islands	3	6
Tsunami	09/03/1957 20:00 to 12/03/1957	Andreanov	3	6
Tsunami	23/05/1960 08:00 to 29/05/1960	Valdivia	3	6
Tsunami	28/03/1964 06:00 to 02/04/1964	Alaskan	3	6
Phase	16/11/1965 12:00 to 17/11/1965 12:00		2	3
Phase	20/03/1966 to 23/03/1966		2	3
Phase	01/11/1966 06:00 to 21:00		2	3
Phase	13/11/1966 12:00 to 14/11/1966 18:00		2	3
Phase	29/10/1967 to 31/10/1967		2	3
Phase	19/07/1969 00:00 to 23:00		2	3
Phase	10/07/1991 to 17/07/1991		2	3
Tsunami	27/02/2010 21:00 to 03/03/2010	Chile	3	6
Tsunami	11/03/2011 12:00 to 15/03/2011	Tohuku	3	6

(QC Flag: 0 = Meteorological (e.g. Seiche, Meteo-tsunami), 1 = Spike, 2 = Phase Offset, 3 = Tsunami, 4 = Other)

Analysis Comments

- Nodal tide fit for MHLW, MLHW and therefore LDTR does not appear very good with the amplitude of the nodal component seemingly too small. Nothing changed, but interesting to note.

Lower Escuminac, Canada (47.0833°N, 64.883°W)

Inherited:

Filename	V1 no.	Start	End	Yrs
'lowerescuminac,nb-02000-canada-meds.mat'	**336**	06/08/1963	31/10/2008	32

Extended:

v1 filename	'lowerescuminac,nb-02000-canada-meds.mat (336)
v2 Filename	225_LowerEscuminac-CAN_GESLA_v2.mat
Source of Extra Data	MEDS
Extra Data filename	2001_01-JAN-2007.csv
Date of Download	24/02/2014
End of Extra Data	31/10/2013
Load in for Extra Data	MEDS
Comparison Comments	Time offset observed (as standard with Canadian sites). -8 hrs applied to the extra data, but then converted back to GMT once the data were combined. Comparison between inherited and extra datasets is perfect.

Quality Control:

Type	Date Affected	Comments	QC Flag	GESLA Flag

(QC Flag: 0 = Meteorological (e.g. Seiche, Meteo-tsunami), 1 = Spike, 2 = Phase Offset, 3 = Tsunami, 4 = Other)

Analysis Comments

- First section of data in 1962 too short to be included in analysis, therefore data will start in 1973.

Lowestoft, UK (52.482°N, 1.752°E)

Inherited:

Filename	V1 no.	Start	End	Yrs
'lowestoft-p024-uk-bodc.mat'	337	05/01/1964	31/12/2006	43

Extended:

v1 filename	'lowestoft-p024-uk-bodc.mat (337)
v2 Filename	226_Lowestoft-GBR_GESLA_v2.mat
Source of Extra Data	BODC
Extra Data filename	RN-7246_1372253428497.zip
Date of Download	26/06/2013
End of Extra Data	31/03/2013
Load in for Extra Data	BODC2
Comparison Comments	Comparison are perfect

Quality Control:

Type	Date Affected	Comments	QC Flag	GESLA Flag
Spike	04/10/2007 12:00		1	3
Phase	07/02/200912:00 to 10/02/2009		2	3
Phase	17/02/2009 08:00 to 21:00		2	3
Phase	26/02/2009 to 27/02/2009 08:00		2	3
Phase	22/09/2010 12:00 to 23/09/2010 12:00		2	3
Phase	24/05/2011 to 04/06/2011		2	3
Phase	19/01/2012 06:00 to 18:00		2	3
Phase	04/07/2012 06:00 to 18:00		2	3

(QC Flag: 0 = Meteorological (e.g. Seiche, Meteo-tsunami), 1 = Spike, 2 = Phase Offset, 3 = Tsunami, 4 = Other)

Analysis Comments

- Threshold QC applied to remove erroneous values <-1 and >5.
- Peak water level occurs on 29/09/1968

Luderitz, Namibia (26.630°S, 15.150°E)

Inherited:

No inherited file.

Extended:

v1 filename	N/A
v2 Filename	465_Luderitz-NAM_GESLA_v2.mat
Source of Extra Data	UHSLC
Extra Data filename	H702a
Date of Download	24/02/2014
End of Extra Data	05/07/2012
Load in for Extra Data	UHSLC
Comparison Comments	N/A

Quality Control:

Type	Date Affected	Comments	QC Flag	GESLA Flag
Phase	22/04/1961 to 28/04/1961		2	3
Phase	06/03/1962 to 10/03/1962 06:00		2	3
Phase	14/04/1962 TO 18/04/1962 06:00		2	3
Phase	14/08/1963 to 18/08/1963 12:00		2	3
Phase	27/01/1964 to 29/01/1964 12:00		2	3
Phase	19/11/1964 12:00 to 21/11/1964 12:00		2	3
Phase	21/07/1965 12:00 to 24/07/1965 12:00		2	3
Phase	06/09/1976 to 15/09/1976 12:00		2	3
Phase	01/11/1976 12:00 to 06/11/1976 12:00		2	3
Phase	29/11/1977 to 30/11/1977 06:00		2	3
Phase	22/01/1978 to 01/02/1978		2	3
Phase	22/02/1978 to 01/07/1978		2	3
Phase	02/09/1978 to 09/09/1978		2	3
Phase	25/09/1978 to 19/10/1978		2	3
Phase	29/10/1978 to 05/12/1978		2	3
Phase	24/12/1978 to 01/01/1979		2	3
Phase	12/02/1979 to 16/02/1979		2	3
Phase	09/04/1979 03:00 to 21:00		2	3
Phase	31/12/1979 to 03/01/1980		2	3
Phase	20/03/1982 18:00 to 23/03/1982 06:00		2	3
Phase	26/03/1982 18:00 to 27/03/1982 12:00		2	3
Phase	28/03/1982 18:00 to 29/03/1982 12:00		2	3
Phase	07/04/1982 21:00 to 08/04/1982 18:00		2	3
Phase	10/04/1982 00:00 to 23:00		2	3
Phase	19/04/1982 18:00 to 20/04/1982 12:00		2	3
Phase	21/04/1982 18:00 to 22/04/1982 12:00		2	3
Phase	03/05/1982 to 06/05/1982 18:00		2	3
Phase	03/09/1982 to 10/09/1982		2	3
Phase	18/01/1985 to 21/01/1985 12:00		2	3
Phase	28/12/1985 to 31/12/1985 12:00		2	3

(QC Flag: 0 = Meteorological (e.g. Seiche, Meteo-tsunami), 1 = Spike, 2 = Phase Offset, 3 = Tsunami, 4 = Other)

Analysis Comments

- Seems to be a jump in MSL between 1992 and 1994, but nothing is mentioned in the UHSLC metadata.

Maaloey, Norway (61.933°N, 5.117°E)

Inherited:

Filename	V1 no.	Start	End	Yrs
'maaloey-003-norway-mapping.mat'	**341**	01/01/1970	31/12/2008	37

Extended:

v1 filename	'maaloey-003-norway-mapping.mat (341)
v2 Filename	229_Maaloey-NOR_GESLA_v2.mat
Source of Extra Data	N/A
Extra Data filename	N/A
Date of Download	N/A
End of Extra Data	N/A
Load in for Extra Data	N/A
Comparison Comments	No extra data available

Quality Control:

Type	Date Affected	Comments	QC Flag	GESLA Flag
Phase	17/11/1981 00:00 to 23:00		2	3

(QC Flag: 0 = Meteorological (e.g. Seiche, Meteo-tsunami), 1 = Spike, 2 = Phase Offset, 3 = Tsunami, 4 = Other)

Analysis Comments

- Max. & min. residual occurs on 14/02/1989 caused by same event.

Mackay, Australia (21.143°S, 149.187°E)

Inherited:

Filename	V1 no.	Start	End	Yrs
'mackay-018-australia-johnhunter.mat'	**342**	01/06/1960	31/12/2004	31

Extended:

v1 filename	'mackay-018-australia-johnhunter.mat (342)
v2 Filename	230_Mackay-AUS_GESLA_v2.mat
Source of Extra Data	N/A
Extra Data filename	N/A
Date of Download	N/A
End of Extra Data	N/A
Load in for Extra Data	N/A
Comparison Comments	No extra data available

Quality Control:

Type	Date Affected	Comments	QC Flag	GESLA Flag
Phase	24/01/1968 to 30/01/1968		2	3
Phase	29/02/1968 to 12/04/1968		2	3
Phase	05/12/1968 to 09/12/1968		2	3
Phase	05/01/1969 to 26/01/1969		2	3
Phase	28/05/1970 to 08/06/1970		2	3
Phase	18/06/1970 to 22/06/1970		2	3
Spike	19/08/1971 15:00		1	3
Spike	20/08/1971 05:00		1	3
Spike	21/08/1971 00:00		1	3
Spike	21/08/1971 20:00 to 21:00		1	3
Spike	24/08/1971 02:00		1	3
Spike	21/09/1972 04:00		1	3
Noise	24/09/1972 to 26/09/1972		4	3
Phase	28/11/1972 to 18/12/1972		2	3
Spike	31/12/1972 01:00		1	3
Phase	06/07/1976 to 08/07/1976 08:00		2	3
Phase	18/08/1976 to 27/08/1976		2	3
Phase	15/02/1977 to 24/02/1977		2	3
Phase	10/08/1985 to 15/08/1985		2	3
Noise	1985		4	3
Phase	20/07/1989 to 01/08/1989		2	3
Phase	20/08/1989 to 29/08/1989		2	3
Phase	26/09/1989 to 15/10/1989		2	3
Phase	25/10/1989 t0 07/11/1989		2	3
Noise	1991		4	3

(QC Flag: 0 = Meteorological (e.g. Seiche, Meteo-tsunami), 1 = Spike, 2 = Phase Offset, 3 = Tsunami, 4 = Other)

Analysis Comments

- Missing data in 1985 leads to noisier data. Does the missing data in a year mean that certain constituents cannot be determined from the length of data. This is seen at many sites.
- 1991 also has high noise content.

Magueyes Island, USA (17.972°N, 67.047°W)

Inherited:

Filename	V1 no.	Start	End	Yrs
'magueyes_island,pr-246a-usa-uhslc.mat'	**347**	01/01/1965	31/12/2004	37

Extended:

v1 filename	'magueyes_island,pr-246a-usa-uhslc.mat (347)
v2 Filename	234_MagueyesIsland-PRI_GESLA_v2.mat
Source of Extra Data	UHSLC/NOAA
Extra Data filename	H246a / COOPS_MagueyesIsland.csv
Date of Download	24/02/2014
End of Extra Data	31/12/2003
Load in for Extra Data	UHSLC/NOAA
Comparison Comments	Comparisons are perfect

Quality Control:

Type	Date Affected	Comments	QC Flag	GESLA Flag
Phase	18/11/1975 06:00 to 18:00		2	3
Phase	30/09/1976 to 05/10/1976		2	3
Phase	03/02/1977 00:00 to 15:00		2	3

(QC Flag: 0 = Meteorological (e.g. Seiche, Meteo-tsunami), 1 = Spike, 2 = Phase Offset, 3 = Tsunami, 4 = Other)

Analysis Comments

- Peak water level seems to be caused by storm surge but this is not captured in residual because tide has not been calculated because data coverage for 1979 is lower than 75%.
- Peak residual therefore occurs on 22/09/1998, caused by hurricane …

- Noisy patch from 26/11/1999 to 03/12/1999, looks like a tsunami signal but there are no tsunamis in this basin at this time. Same again 08/11/2006 to 14/11/2006. Same on 03/04/2010 to 07/04/2010. Meteo-tsunamis?

Maisaka, Japan (34.683°N, 137.617°E)

Inherited:

Filename	V1 no.	Start	End	Yrs
'maisaka-356a-japan-uhslc.mat'	**348**	01/01/1968	31/12/2005	37

Extended:

v1 filename	'maisaka-356a-japan-uhslc.mat (348)
v2 Filename	235_Maisaka-JPN_GESLA_v2.mat
Source of Extra Data	UHSLC
Extra Data filename	H356a
Date of Download	25/02/2014
End of Extra Data	31/12/2012
Load in for Extra Data	UHSLC
Comparison Comments	Comparisons are perfect

Quality Control:

Type	Date Affected	Comments	QC Flag	GESLA Flag
		No erroneous data to remove		

(QC Flag: 0 = Meteorological (e.g. Seiche, Meteo-tsunami), 1 = Spike, 2 = Phase Offset, 3 = Tsunami, 4 = Other)

Analysis Comments

- Peak water level and residual occur on 19/10/1979 caused by Typhoon Tip.
- Another large surge on 21/09/2011 caused by Typhoon Roke

Majuro, Marshall Islands (7.107°N, 171.373°E)

Inherited:

Filename	V1 no.	Start	End	Yrs
'majuro,marshallislands-001-glossdm-bodc.mat'	**349**	06/10/1968	31/12/2001	30
'majuro_a-005a-rep._of_marshall_i-uhslc.mat'	**350**	06/10/1968	31/12/1999	28
'majuro_b-005b-rep._of_marshall_i-uhslc.mat'	**351**	14/05/1993	31/12/2006	13

Extended:

v1 filename	'majuro_a-005a-rep._of_marshall_i-uhslc.mat (350)
v2 Filename	236_Majuro-MHL_GESLA_v2.mat
Source of Extra Data	UHSLC
Extra Data filename	H005a
Date of Download	
End of Extra Data	
Load in for Extra Data	
Comparison Comments	UHSLC website says that 005a & b can be combined if checks are conducted. Comparisons between 005a and 005b show a small offset which is corrected by subtracting 0.179 m from the inherited data. However small differences of approx. 2-3 mm occasionally occur between the two datasets. No discontinuity in amplitude or phase of tidal constituents between 1999 & 2000 when dataset changes and therefore assume that combined dataset is good to use.

Quality Control:

Type	Date Affected	Comments	QC Flag	GESLA Flag
Phase	30/01/1977 to 26/02/1977		2	3
Phase	15/05/1977 to 05/06/1977		2	3
Phase	26/07/1977 to 02/08/1977		2	3
Phase	01/09/1977 to 24/09/1977		2	3
Phase	09/10/1977 to 16/11/1977		2	3
Phase	29/08/1978 to 07/09/1978		2	3
Phase	01/10/1978 to 09/10/1978		2	3
Phase	01/03/1979 to 06/03/1979		2	3
Phase	17/08/1979 00:00 to 23:00		2	3
Spike	01/09/2006 18:00 to 02/09/2006 06:00		1	3

(QC Flag: 0 = Meteorological (e.g. Seiche, Meteo-tsunami), 1 = Spike, 2 = Phase Offset, 3 = Tsunami, 4 = Other)

Malakal, Belau (7.330°N, 134.463°E)

Inherited:

Filename	V1 no.	Start	End	Yrs
'malakal,rep.ofbelau-001-glossdm-bodc.mat'	**352**	18/05/1969	31/12/1998	28
'malakal_a-007a-republic_of_belau-uhslc.mat'	**353**	01/01/1926	10/12/1939	12
'malakal_b-007b-republic_of_belau-uhslc.mat'	**354**	18/05/1969	30/04/2003	32

Extended:

v1 filename	'malakal_b-007b-republic_of_belau-uhslc.mat (354)
v2 Filename	237_Malakal-PLW_GESLA_v2.mat
Source of Extra Data	UHSLC
Extra Data filename	H007b
Date of Download	25/02/2014
End of Extra Data	30/04/2012
Load in for Extra Data	UHSLC
Comparison Comments	Comparisons are perfect

Quality Control:

Type	Date Affected	Comments	QC Flag	GESLA Flag
Phase	04/04/1973 00:00 to 23:00		2	3
Phase	30/04/1973 to 05/05/1973		2	3

(QC Flag: 0 = Meteorological (e.g. Seiche, Meteo-tsunami), 1 = Spike, 2 = Phase Offset, 3 = Tsunami, 4 = Other)

Analysis Comments

- Peak residual on 10/11/1990 caused by Typhoon Mike, but nowhere near max. water level since it coincided with neap tides. Also occurred for storm in 1976 and 2001.

Malin Head, Ireland (55.372°N, 7.330°W)

Inherited:

Filename	V1 no.	Start	End	Yrs
'malinhead-001-glossdm-bodc.mat'	**358**	16/01/1958	31/12/2001	41

Extended:

v1 filename	'malinhead-001-glossdm-bodc.mat (358)
v2 Filename	240_MalinHead-IRL_GESLA_v2.mat
Source of Extra Data	N/A
Extra Data filename	N/A
Date of Download	N/A
End of Extra Data	N/A
Load in for Extra Data	N/A
Comparison Comments	No extra data available

Quality Control:

Type	Date Affected	Comments	QC Flag	GESLA Flag
		No erroneous data to remove		

(QC Flag: 0 = Meteorological (e.g. Seiche, Meteo-tsunami), 1 = Spike, 2 = Phase Offset, 3 = Tsunami, 4 = Other)

Manila, Philippines (14.583°N, 120.967°E)

Inherited:

Filename	V1 no.	Start	End	Yrs
'manila-370a-philippines-uhslc.mat'	**360**	01/01/1984	22/10/2002	19

Extended:

v1 filename	'manila-370a-philippines-uhslc.mat (360)
v2 Filename	241_Manila-PHL_GESLA_v2.mat
Source of Extra Data	UHSLC
Extra Data filename	H370a
Date of Download	25/02/2014
End of Extra Data	31/12/2012
Load in for Extra Data	UHSLC
Comparison Comments	Comparisons are perfect

Quality Control:

Type	Date Affected	Comments	QC Flag	GESLA Flag
Phase	1985		2	3
Phase	26/11/1987 to 28/11/1987	See below	2	3
Phase	21/10/1994 00:00 to 21:00		2	3

Phase	03/11/1995 to 04/11/1995		2	3
Phase	28/12/2006 to 30/12/2006		2	3
Phase	13/07/2010 12:00 to 15/07/2010		2	3
Phase	29/07/2012 08:00 to 31/07/2012		2	3

(QC Flag: 0 = Meteorological (e.g. Seiche, Meteo-tsunami), 1 = Spike, 2 = Phase Offset, 3 = Tsunami, 4 = Other)

Analysis Comments

- Phase offsets marked above as see below have the same periodic 4x a day signal anomaly. Periodic signal occurs for 1-2 days occasionally, with 4 oscillations during a day. Too regular for a tsunami or storm surge, and no associated causal events.

Mayport, USA (Florida) (30.395°N, 81.432°W)

Inherited:

Filename	V1 no.	Start	End	Yrs
'mayport,fl-753a-usa-uhslc.mat'	**374**	26/04/1928	31/12/2000	72

Extended:

v1 filename	'mayport,fl-753a-usa-uhslc.mat (374)
v2 Filename	250_Mayport-USA_GESLA_v2.mat
Source of Extra Data	N/A
Extra Data filename	N/A
Date of Download	N/A
End of Extra Data	N/A
Load in for Extra Data	N/A
Comparison Comments	No extra data on UHSLC website. Data is available from 2001-2013 on the NOAA website but there is a gap of 1 month between datasets that means that the datum shift that is evident between the two datasets cannot be resolved.

Quality Control:

Type	Date Affected	Comments	QC Flag	GESLA Flag
Phase	11/03/1960 to 24/03/1960		2	3
Phase	29/07/1975 to 01/08/1975		2	3
Phase	06/01/2000 12:00 to 11/01/2000		2	3

(QC Flag: 0 = Meteorological (e.g. Seiche, Meteo-tsunami), 1 = Spike, 2 = Phase Offset, 3 = Tsunami, 4 = Other)

Analysis Comments

- Peak residual on 19/10/1944 caused by Cuba-Florida Hurricane
- Min. residual on 14/03/1993 caused by Storm of the Century

Mera, Japan (34.917°N, 139.833°E)

Inherited:

Filename	V1 no.	Start	End	Yrs
'mera,japan-001-glossdm-bodc.mat'	**376**	01/01/1965	31/12/2003	35
'mera-352a-japan-uhslc.mat'	**377**	01/01/1965	31/12/2005	38

Extended:

v1 filename	'mera-352a-japan-uhslc.mat (377)
v2 Filename	252_Mera-JPN_GESLA_v2.mat
Source of Extra Data	UHSLC
Extra Data filename	H352a
Date of Download	26/02/2014
End of Extra Data	31/12/2012
Load in for Extra Data	UHSLC
Comparison Comments	Comparisons are perfect

Quality Control:

Type	Date Affected	Comments	QC Flag	GESLA Flag
		No erroneous values to remove		

(QC Flag: 0 = Meteorological (e.g. Seiche, Meteo-tsunami), 1 = Spike, 2 = Phase Offset, 3 = Tsunami, 4 = Other)

Analysis Comments

- Peak residual on 01/10/2002 caused by Typhoon Higos
- Peak water level on 19/10/1979 caused by Typhoon Tip.

Midway, USA (Hawaii) (28.217°N, 177.367°W)

Inherited:

Filename	V1 no.	Start	End	Yrs
'midway,usa-001-glossdm-bodc.mat'	**379**	08/02/1947	31/12/2000	51
'midway-050a-usa_trust-uhslc.mat'	**380**	08/02/1947	31/12/2004	55

Extended:

v1 filename	'midway-050a-usa_trust-uhslc.mat (380)
v2 Filename	254_Midway-USA_GESLA_v2.mat
Source of Extra Data	UHSLC
Extra Data filename	H050a
Date of Download	26/02/2014
End of Extra Data	31/12/2012
Load in for Extra Data	UHSLC
Comparison Comments	Comparisons are perfect

Quality Control:

Type	Date Affected	Comments	QC Flag	GESLA Flag
Tsunami	22/05/1960 12:00 to 26/05/1960	Valdivia	2	3
Spike	01/08/1963 00:00		2	3
Phase	02/08/1968 to 10/08/1968		2	3
Tsunami	11/03/2011 08:00 to 15/03/2011	Valdivia	2	3

(QC Flag: 0 = Meteorological (e.g. Seiche, Meteo-tsunami), 1 = Spike, 2 = Phase Offset, 3 = Tsunami, 4 = Other)

Milford Haven, UK (51.702°N, 5.014°W)

Inherited:

Filename	V1 no.	Start	End	Yrs
'milfordhaven-p056-uk-bodc.mat'	**381**	01/08/1953	31/12/2006	51

Extended:

v1 filename	'milfordhaven-p056-uk-bodc.mat (381)
v2 Filename	255_Milford-GBR_GESLA_v2.mat
Source of Extra Data	BODC
Extra Data filename	RN-7246_1372253428497
Date of Download	26/06/2013
End of Extra Data	31/03/2013
Load in for Extra Data	BODC2
Comparison Comments	Comparisons are perfect

Quality Control:

Type	Date Affected	Comments	QC Flag	GESLA Flag
Threshold		< -0.6 & > 10	4	3
Phase	29/09/2009 to 01/10/2009		2	3
Phase	28/11/2010 21:00 to 29/11/2010 06:00		2	3
Spike	16/06/2011 16:00		1	3
Phase	07/11/2011 to 08/11/2011 12:00		2	3
Phase	15/11/2011 to 18/11/2011		2	3
Phase	26/11/2011 15:00 to 23:00		2	3
Phase	27/11/2001 to 30/11/2011		2	3
Phase	07/12/2011 to 09/12/2011		2	3
Phase	11/12/2011 to 13/12/2011		2	3
Phase	18/12/2011 08:00 to 19/12/2011 16:00		2	3
Phase	23/12/2011 12:00 to 24/12/2011 18:00		2	3
Phase	31/12/2011 to 03/01/2012 12:00		2	3
Phase	07/01/2012 to 09/01/2012		2	3
Phase	26/01/2012 03:00 to 12:00		2	3
Phase	27/01/2012 15:00 to 30/01/2012 12:00		2	3
Spike	31/01/2012 12:00 to 18:00		1	3
Phase	02/02/2012 12:00 to 03/02/2012 15:00		2	3
Phase	04/02/2012 12:00 to 07/02/2012		2	3

(QC Flag: 0 = Meteorological (e.g. Seiche, Meteo-tsunami), 1 = Spike, 2 = Phase Offset, 3 = Tsunami, 4 = Other)

Analysis Comments

- First year of with >75% data coverage is 1968. 2nd year is 1980
- Peak residual on 27/03/1987

Millport, UK (55.750°N, 4.906°W)

Inherited:

Filename	V1 no.	Start	End	Yrs
'millport-p049-uk-bodc.mat'	**382**	05/01/1978	31/12/2006	25

Extended:

v1 filename	'millport-p049-uk-bodc.mat (382)
v2 Filename	256_Millport-GBR_GESLA_v2.mat
Source of Extra Data	BODC
Extra Data filename	RN-7246_1372253428497
Date of Download	26/06/2013
End of Extra Data	31/03/2013
Load in for Extra Data	BODC2
Comparison Comments	Comparisons are perfect

Quality Control:

Type	Date Affected	Comments	QC Flag	GESLA Flag
Threshold		< -0.8 & > 5.2	4	3
Phase	08/02/2005 to 10/02/2005		2	3
Phase	28/11/2011 to 29/11/2011		2	3
Phase	07/12/2011 to 09/12/2011 12:00		2	3

(QC Flag: 0 = Meteorological (e.g. Seiche, Meteo-tsunami), 1 = Spike, 2 = Phase Offset, 3 = Tsunami, 4 = Other)

Analysis Comments

- First year of with >75% data coverage is 1968. 2nd year is 1980
- Peak residual on 27/03/1987

Mina Sulman, Bahrain (26.233°N, 50.600°E)

Inherited:

Filename	V1 no.	Start	End	Yrs
'mina_sulman-182a-bahrain-uhslc.mat'	**383**	01/01/1979	31/12/2005	18

Extended:

v1 filename	'mina_sulman-182a-bahrain-uhslc.mat (383)
v2 Filename	257_MinaSulman-BHR_GESLA_v2.mat
Source of Extra Data	UHSLC
Extra Data filename	H182a
Date of Download	26/02/2014
End of Extra Data	05/11/2007
Load in for Extra Data	UHSLC
Comparison Comments	Comparisons are perfect

Quality Control:

Type	Date Affected	Comments	QC Flag	GESLA Flag
		No erroneous values to remove		

(QC Flag: 0 = Meteorological (e.g. Seiche, Meteo-tsunami), 1 = Spike, 2 = Phase Offset, 3 = Tsunami, 4 = Other)

Analysis Comments

- Max. residual on 11/12/1995 could be a winter shamal, but no event documented.

Miyakejima, Japan (34.060°N, 139.483°E)

Inherited:

Filename	V1 no.	Start	End	Yrs
'miyakejima-357a-japan-uhslc.mat'	**385**	31/01/1964	31/12/2003	40

Extended:

v1 filename	'miyakejima-357a-japan-uhslc.mat'(385)
v2 Filename	259_Miyakejima-JPN_GESLA_v2.mat
Source of Extra Data	UHSLC
Extra Data filename	H357a
Date of Download	26/02/2014
End of Extra Data	31/12/2012
Load in for Extra Data	UHSLC
Comparison Comments	Comparisons are perfect

Quality Control:

Type	Date Affected	Comments	QC Flag	GESLA Flag
Phase	14/02/1972 to 21/02/1972		2	3
Phase	25/03/1972 12:00 to 27/03/1972		2	3

(QC Flag: 0 = Meteorological (e.g. Seiche, Meteo-tsunami), 1 = Spike, 2 = Phase Offset, 3 = Tsunami, 4 = Other)

Analysis Comments

- Large increase in MSL, between 1999 and 2003. Initial inspection suggests natural cause. UHSLC says that it is due to subsidence after a volcanic eruption on the island. Leave in as this is a natural signal, but flag where appropriate.
- Peak residual on 19/10/1979 caused by Typhoon Tip.
- Peak water level on 21/10/2004 caused by Typhoon Tip.

Mokuolue, USA (Hawaii) (21.433°N, 157.800°W)

Inherited:

Filename	V1 no.	Start	End	Yrs
'mokuoloe-061a-usa-uhslc.mat'	**386**	01/05/1957	31/12/2005	37

Extended:

v1 filename	'mokuoloe-061a-usa-uhslc.mat (386)
v2 Filename	260_Mokuolue-USA_GESLA_v2.mat
Source of Extra Data	UHSLC/NOAA
Extra Data filename	H061a / COOPS_Mokolue
Date of Download	26/02/2014
End of Extra Data	31/12/2013
Load in for Extra Data	UHSLC/NOAA
Comparison Comments	Comparisons are perfect

Quality Control:

Type	Date Affected	Comments	QC Flag	GESLA Flag
Tsunami	23/05/1960 08:00 to 27/05/1960	Valdivia	3	6
Tsunami	28/03/1964 06:00 to 01/04/1964	Alaskan	3	6
Phase	26/02/1967 18:00 to 27/02/1967 18:00		2	3
Phase	10/10/1969 12:00 to 14/10/1969		2	3
Phase	15/01/1992 18:00 to 18/01/1992		2	3
Phase	05/06/2005 21:00 to 09/06/2005		2	3
Phase	04/11/2008 to 23/11/2008		2	3
Tsunami	11/03/2011 12:00 to 14/03/2011	Tohuku	3	6

(QC Flag: 0 = Meteorological (e.g. Seiche, Meteo-tsunami), 1 = Spike, 2 = Phase Offset, 3 = Tsunami, 4 = Other)

Analysis Comments

- Peak residual occurs on 10/04/1968 caused by unknown event.
- Large residual on 24/11/1982 caused by Hurricane Iwa.

Montauk, USA (New York) (41.083°N, 71.960°W)

Inherited:

Filename	V1 no.	Start	End	Yrs
'montauk,ny-279a-usa-uhslc.mat'	**389**	01/01/1959	31/10/2005	40

Extended:

v1 filename	'montauk,ny-279a-usa-uhslc.mat (389)
v2 Filename	262_Montauk-USA_GESLA_v2.mat
Source of Extra Data	UHSLC/NOAA
Extra Data filename	H279a / COOPS_Montauk
Date of Download	26/02/2014
End of Extra Data	31/12/20013
Load in for Extra Data	UHSLC/NOAA
Comparison Comments	Comparisons are perfect

Quality Control:

Type	Date Affected	Comments	QC Flag	GESLA Flag
		No erroneous values to remove		

(QC Flag: 0 = Meteorological (e.g. Seiche, Meteo-tsunami), 1 = Spike, 2 = Phase Offset, 3 = Tsunami, 4 = Other)

Analysis Comments.

- Peak water level caused by Hurricane Sandy.

Monterey, USA (California) (36.605°N, 121.883°E)

Inherited:

Filename	V1 no.	Start	End	Yrs
'monterey,ca-555a-usa-uhslc.mat'	**390**	08/11/1973	31/12/2005	32

Extended:

v1 filename	'monterey,ca-555a-usa-uhslc.mat (390)
v2 Filename	263_Monterey-USA_GESLA_v2.mat
Source of Extra Data	UHSLC/NOAA
Extra Data filename	H555a / COOPS_Monterey
Date of Download	26/02/2014
End of Extra Data	31/12/2013
Load in for Extra Data	UHSLC/NOAA
Comparison Comments	Comparisons are perfect

Quality Control:

Type	Date Affected	Comments	QC Flag	GESLA Flag
Phase	09/07/1980 to 12/07/1980		2	3
Tsunami	08/11/1980 12:00 to 11/11/1980	N. California	3	6
Phase	12/09/1981 to 27/09/1981		2	3
Tsunami	27/02/2010 18:00 to 02/03/2011	Chile	3	6
Tsunami	11/03/2011 12:00 to 18/03/2011	Tokuku	3	6

(QC Flag: 0 = Meteorological (e.g. Seiche, Meteo-tsunami), 1 = Spike, 2 = Phase Offset, 3 = Tsunami, 4 = Other)

Analysis Comments

- Tsunami like signal on 03/11/1984 but no documentation of associated earthquake.

Mossel Bay, South Africa (34.183°S, 22.150°E)

Inherited:

No inherited dataset

Extended:

v1 filename	N/A
v2 Filename	466_MosselBay-ZAF_GESLA_v2.mat
Source of Extra Data	UHSLC
Extra Data filename	H185a
Date of Download	26/02/2014
End of Extra Data	31/12/2012
Load in for Extra Data	UHSLC
Comparison Comments	Comparisons are perfect

Quality Control:

Type	Date Affected	Comments	QC Flag	GESLA Flag
Phase	30/06/1980 to 08/07/1980		2	3
Phase	19/03/1982 06:00 to 21/03/1982		2	3
Phase	27/03/1982 20:00 to 28/03/1982 12:00		2	3
Phase	29/03/1982 20:00 to 30/03/1982 12:00		2	3
Phase	03/04/1982 20:00 to 05/04/1982 12:00		2	3
Phase	12/07/1982 to 16/07/1982		2	3
Phase	04/08/1982 to 13/08/1982		2	3
Phase	25/10/1982 12:00 to 23:00		2	3
Phase	27/10/1982 12:00 to 23:00		2	3
Phase	22/11/1982 to 26/11/1982		2	3
Phase	01/01/1984 to 01/05/1984		2	3
Phase	26/12/1987 12:00 to 28/12/1987 12:00		2	3
Phase	07/01/1990 15:00 to 09/01/1990		2	3
Phase	11/02/1991 06:00 to 13/02/1991		2	3
Phase	15/02/1991 18:00 to 19/02/1991		2	3
Phase	05/03/1991 to 06/03/1991 12:00		2	3
Phase	12/03/1991 to 14/03/1991		2	3
Phase	23/03/1991 06:00 to 23:00		2	3
Phase	26/03/1991 03:00 to 23:00		2	3
Phase	10/04/1991 to 13/04/1991		2	3
Phase	17/05/1991 to 22/05/1991		2	3
Phase	01/11/1991 to 04/01/1991		2	3
Phase	27/01/1994 18:00 to 29/01/1994		2	3
Phase	07/03/1994 to 29/05/1994		2	3
Phase	20/08/1995 to 24/08/1995		2	3

Phase	29/09/1995 to 01/10/1995		2	3
Phase	24/10/1995 to 27/10/1995		2	3
Phase	12/11/1995 to 18/11/1995		2	3
Phase	17/12/1995 12:00 to 19/12/1995 12:00		2	3

(QC Flag: 0 = Meteorological (e.g. Seiche, Meteo-tsunami), 1 = Spike, 2 = Phase Offset, 3 = Tsunami, 4 = Other)

Nagasaki, Japan (32.733°N, 129.867°E)

Inherited:

Filename	V1 no.	Start	End	Yrs
'nagasaki,japan-001-glossdm-bodc.mat'	**391**	01/01/1964	31/12/2003	36
'nagasaki-362a-japan-uhslc.mat'	**392**	01/01/1985	31/12/2005	21

Extended:

v1 filename	'nagasaki,japan-001-glossdm-bodc.mat (391)
v2 Filename	264_Nagasaki-JPN_GESLA_v2.mat
Source of Extra Data	UHSLC
Extra Data filename	H362a
Date of Download	27/02/2014
End of Extra Data	30/12/2012
Load in for Extra Data	UHSLC
Comparison Comments	Comparisons are perfect

Quality Control:

Type	Date Affected	Comments	QC Flag	GESLA Flag
		No erroneous values to remove		

(QC Flag: 0 = Meteorological (e.g. Seiche, Meteo-tsunami), 1 = Spike, 2 = Phase Offset, 3 = Tsunami, 4 = Other)

Analysis Comments

- Max. residual on 27/09/1991 caused by Typhoon Mirielle.

Naha, Japan (26.217°N, 127.667°E)

Inherited:

Filename	V1 no.	Start	End	Yrs
'naha,japan-001-glossdm-bodc.mat'	**393**	31/07/1966	31/12/2003	36
'naha-355a-japan-uhslc.mat'	**394**	31/07/1966	31/12/2005	39

Extended:

v1 filename	'naha-355a-japan-uhslc.mat (394)
v2 Filename	265_Naha-JPN_GESLA_v2.mat
Source of Extra Data	UHSLC
Extra Data filename	H355a
Date of Download	27/02/2014
End of Extra Data	31/12/2012
Load in for Extra Data	UHSLC
Comparison Comments	Comparisons are perfect

Quality Control:

Type	Date Affected	Comments	QC Flag	GESLA Flag
Phase	22/02/1967 to 02/03/1967		2	3
Phase	03/10/1971 to 08/10/1971		2	3
Phase	21/01/1974 to 29/01/1974		2	3
Phase	21/04/1986 to 03/09/1986		2	3

(QC Flag: 0 = Meteorological (e.g. Seiche, Meteo-tsunami), 1 = Spike, 2 = Phase Offset, 3 = Tsunami, 4 = Other)

Analysis Comments

- Peak water level occurs on 15/10/2012 caused by Typhoon Sanba, but the peak residual occurs on 29/09/2012 caused by Typhoon Jelawat Another storm a few weeks before shows strong clustering of storms during this period.

Nantucket Island, USA (MA) (41.285°N, 70.097°W)

41.2850 -70.0967

Inherited:

Filename	V1 no.	Start	End	Yrs
'nantucket,ma-743a-usa-uhslc.mat'	**396**	01/02/1965	31/12/2005	39

Extended:

v1 filename	'nantucket,ma-743a-usa-uhslc.mat (396)
v2 Filename	267_NantucketIsland-USA_GESLA_v2.mat
Source of Extra Data	UHSLC/NOAA
Extra Data filename	H743a / COOPS_Nantucket
Date of Download	27/02/2014
End of Extra Data	31/12/2013
Load in for Extra Data	UHSLC/NOAA
Comparison Comments	Comparisons are perfect

Quality Control:

Type	Date Affected	Comments	QC Flag	GESLA Flag
Threshold		> 5 m	4	3
Phase	29/01/1977 to 10/02/1977		2	3
Phase	10/01/1981 to 21/01/1981		2	3
Spike	01/10/2000 00:00 to 05:00		1	3

(QC Flag: 0 = Meteorological (e.g. Seiche, Meteo-tsunami), 1 = Spike, 2 = Phase Offset, 3 = Tsunami, 4 = Other)

Analysis Comments

- Drop in residual after gap on 04/02/1976, may be negative surge but find a storm.
- Peak residual on 31/10/1991, ET storm signal.
- Another large ET storm on 09/02/2013.

Nawiliwili, USA (Hawaii) (21.967°N, 159.35°W)

Inherited:

Filename	V1 no.	Start	End	Yrs
'nawiliwili,kauai,hawaii,usa-001-glossdm-bodc.mat'	**402**	01/12/1954	31/12/2000	46
'nawiliwili-058a-usa-uhslc.mat'	**403**	01/12/1954	31/12/2005	51

Extended:

v1 filename	'nawiliwili-058a-usa-uhslc.mat (403)
v2 Filename	271_Nawiliwili-USA_GESLA_v2.mat
Source of Extra Data	UHSLC/NOAA
Extra Data filename	H058a / COOPS_Nawiliwili
Date of Download	27/02/2014
End of Extra Data	31/12/2013
Load in for Extra Data	UHSLC/NOAA
Comparison Comments	Comparisons are perfect

Quality Control:

Type	Date Affected	Comments	QC Flag	GESLA Flag
Tsunami	09/03/1957 18:00 to 12/03/1957	Andreanov	3	6
Spike	01/09/1959 00:00		2	3
Tsunami	23/05/1960 12:00 to 27/05/1960	Valdivia	3	6
Phase	29/09/1962 12:00 to 01/10/1962 12:00		2	3
Phase	17/02/1966 to 18/02/1966 12:00		2	3
Tsunami	27/02/2010 18:00 to 02/03/2010	Chile	3	6
Tsunami	11/03/2011 10:00 to 15/03/2011	Tohuku	3	6
Spike	28/10/2012/ 09:00		2	3

(QC Flag: 0 = Meteorological (e.g. Seiche, Meteo-tsunami), 1 = Spike, 2 = Phase Offset, 3 = Tsunami, 4 = Other)

Analysis Comments

- Peak wl and residual are on 12/09/1992 caused by Hurricane Iniki.

Naze, Japan (28.382°N, 129.495°E)

Inherited:

Filename	V1 no.	Start	End	Yrs
'naze,japan-001-glossdm-bodc.mat'	**404**	01/01/1965	31/12/1998	33
'naze-359a-japan-uhslc.mat'	**405**	08/04/1957	31/12/2003	44

Extended:

v1 filename	'naze-359a-japan-uhslc.mat (405)
v2 Filename	272_Naze-JPN_GESLA_v2.mat
Source of Extra Data	UHSLC
Extra Data filename	H359a
Date of Download	Unknown
End of Extra Data	31/12/2010
Load in for Extra Data	UHSLC
Comparison Comments	Comparisons are perfect

Quality Control:

Type	Date Affected	Comments	QC Flag	GESLA Flag
Phase	03/04/1959 to 28/06/1959		2	3
Phase	10/07/1959 to 20/08/1959		2	3
Phase	30/09/1959 to 30/10/1959		2	3
Spike	31/01/1961 10:00 to 21:00		1	3
Phase	14/10/1961 to 16/10/1961		2	3
Phase	15/03/1963 15:00 to 23:00		2	3
Phase	Pre-1965		2	3
Phase	01/03/1969 to 04/03/1969		2	3
Phase	24/07/1969 to 04/08/1969		2	3
Phase	30/08/1969 to 01/09/1969 12:00		2	3
Phase	20/10/1969 to 14/11/1969		2	3
Phase	22/11/1969 00:00 to 23:00		2	3
Phase	05/12/1969 to 08/12/1969		2	3
Phase	29/12/1969 to 05/01/1970		2	3
Phase	09/01/1970 12:00 to 12/01/1970 12:00		2	3
Phase	05/03/1970 to 13/03/1970		2	3
Phase	21/03/1970 to 28/03/1970		2	3
Phase	01/07/1970 to 02/07/1970 06:00		2	3
Phase	28/03/1971 to 01/04/1971		2	3
Phase	12/11/1971 to 16/11/1971		2	3
Phase	14/01/1972 15:00 to 17/01/1972		2	3
Phase	29/01/1972 to 04/02/1972		2	3
Phase	31/03/1972 to 08/04/1972		2	3
Phase	03/05/1972 12:00 to 04/05/1972 15:00		2	3
Phase	13/09/1973 12:00 to 15/09/1973		2	3
Phase	09/10/1973 to 19/10/1973		2	3
Phase	26/10/1973 10:00 to 28/10/1973 12:00		2	3
Phase	10/11/1973 to 12/11/1973		2	3
Phase	09/02/1974 to 12/02/1974		2	3
Phase	25/03/1974 18:00 to 27/03/1974		2	3
Phase	17/06/1974 to 24/06/1974		2	3
Phase	06/07/1974 to 09/07/1974		2	3
Phase	15/07/1974 12:00 to 19/07/1974		2	3
Phase	13/09/1974 to 23/09/1974		2	3
Phase	26/11/1977 to 28/11/1977		2	3

(QC Flag: 0 = Meteorological (e.g. Seiche, Meteo-tsunami), 1 = Spike, 2 = Phase Offset, 3 = Tsunami, 4 = Other)

Analysis Comments

- Noise in early years of data is not matched by recent data, which suggests that noise is created by measurement error and not real.
- UHSLC states that timing of records from 1962-64 are 15-30 minutes offset, but there does not appear to be any resultant change in the magnitude or phase.

Neah Bay, USA (Washington) (48.368°N, 124.617°W)

Inherited:

Filename	V1 no.	Start	End	Yrs
'neah_bay,wa-558a-usa-uhslc.mat'	**406**	01/08/1934	31/12/2005	69
'neahbay,usa-001-glossdm-bodc.mat'	**407**	01/08/1934	31/12/1944	10

Extended:

v1 filename	'neah_bay,wa-558a-usa-uhslc.mat (406)
v2 Filename	273_NeahBay-USA_GESLA_v2.mat
Source of Extra Data	UHSLC/NOAA
Extra Data filename	H558a / COOPS_NeahBay
Date of Download	27/02/2014
End of Extra Data	31/12/2013
Load in for Extra Data	UHSLC/NOAA
Comparison Comments	Comparisons are perfect

Quality Control:

Type	Date Affected	Comments	QC Flag	GESLA Flag
Phase	18/02/1960 08:00 to 19/02/1960 08:00		2	3
Tsunami	23/05/1960 10:00 to 27/05/1960	Valdivia	3	6
Phase	20/12/1960 03:00 to 09:00		2	3
Phase	09/01/1961 06:00 to 10/01/1961 12:00		2	3
Phase	01/06/1962 08:00 to 18:00		2	3
Phase	01/06/1962 12:00 to 21:00		2	3
Phase	07/08/1962 06:00 to 21:00		2	3

Phase	01/09/1962 12:00 to 02/09/1962 21:00		2	3
Tsunami	28/03/1964 06:00 to 31/03/1964	Alaskan	3	6
Phase	16/08/1965 06:00 to 18/08/1965 18:00		2	3
Spike	04/12/1965 15:00 to 23:00		1	3
Spike	08/12/1965 18:00 to 09/12/1965 03:00		1	3
Spike	18/12/1965 18:00 to 19/12/1965 06:00		1	3
Spike	19/12/1965 18:00 to 20/12/1965 06:00		1	3
Spike	20/12/1965 12:00 to 21/12/1965 06:00		1	3
Spike	21/12/1965 18:00 to 22/12/1965 06:00		1	3
Spike	28/12/1965 00:00 to 12:00		1	3
Phase	24/11/1965 10:00 to 26/11/1965		2	3
Phase	27/06/1968 to 29/06/1968		2	3
Phase	25/01/1973 12:00 to 26/01/1973 08:00		2	3
Phase	16/02/1973 12:00 to 17/02/1973 15:00		2	3
Phase	26/03/1975 to 28/03/1975		2	3
Phase	08/04/1975 06:00 to 09/04/1975 10:00		2	3
Spikes	01/07/1975 to 10/08/1975		1	3
Phase	27/07/1977 15:00 to 29/07/1977 21:00		2	3
Phase	09/03/1980 21:00 to 12/03/1980		2	3
Phase	01/09/1984 to 07/09/1984		2	3
Phase	02/08/2007 to 08/08/2007		2	3
Tsunami	11/03/2011 12:00 to 15/03/2011	Tohuku	3	6
Phase	09/07/2011 to 11/07/2011		2	3

(QC Flag: 0 = Meteorological (e.g. Seiche, Meteo-tsunami), 1 = Spike, 2 = Phase Offset, 3 = Tsunami, 4 = Other)

Analysis Comments

- First few years to 1942 seem to be offset from the rest, but there is no documentation regarding this on the UHSLC website. These differences are observed in individual constituents as well as in tidal datums (especially MTR).
- MHW before 1943 appears to be 2.5 cm higher, while MLW seems 2.5 cm lower during this period.
- 14/11/1952 – large ET storm.

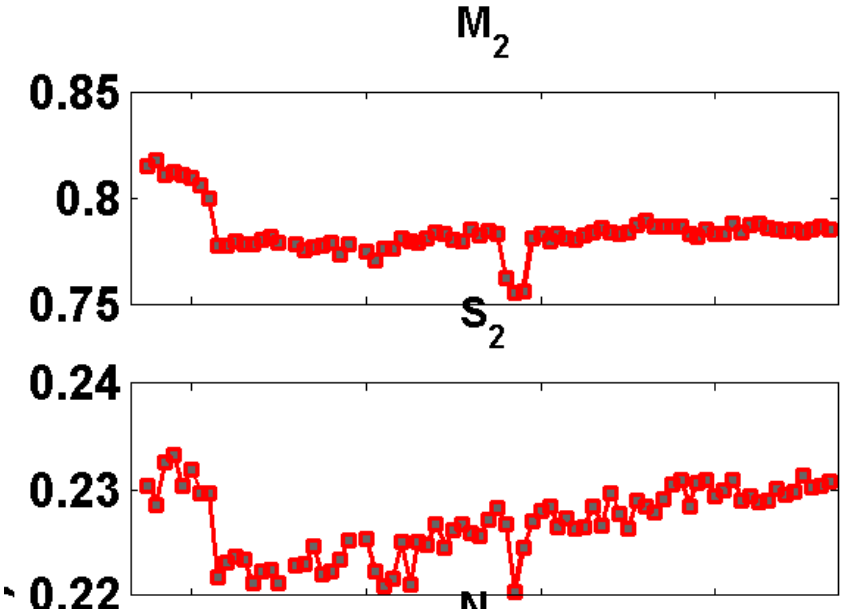

New London, USA (Connecticut) (41.355°N, 72.087°W)

Inherited:

Filename	V1 no.	Start	End	Yrs
'new_london,ct-744a-usa-uhslc.mat'	**408**	12/06/1938	31/12/2005	63

Extended:

v1 filename	'new_london,ct-744a-usa-uhslc.mat (408)
v2 Filename	274_NewLondon-USA_GESLA_v2.mat
Source of Extra Data	UHSLC/NOAA
Extra Data filename	H744a / COOPS_NewLondon
Date of Download	27/02/2014
End of Extra Data	31/12/2013
Load in for Extra Data	UHSLC/NOAA
Comparison Comments	Comparisons are perfect

Quality Control:

Type	Date Affected	Comments	QC Flag	GESLA Flag
		No erroneous values to remove		

(QC Flag: 0 = Meteorological (e.g. Seiche, Meteo-tsunami), 1 = Spike, 2 = Phase Offset, 3 = Tsunami, 4 = Other)

Analysis Comments

- Peak residual and wl caused by Hurricane Carol on 02/09/1954

New York, USA (New York) (40.700°N, 74.150°W)

Inherited:

Filename	V1 no.	Start	End	Yrs
'new_york,ny-745a-usa-uhslc.mat'	**409**	01/05/1958	31/12/2005	33

Extended:

v1 filename	'new_york,ny-745a-usa-uhslc.mat (409)
v2 Filename	275_NewYork-USA_GESLA_v2.mat
Source of Extra Data	UHSLC/NOAA
Extra Data filename	H745a/COOPS_NewYork
Date of Download	27/02/2014
End of Extra Data	31/12/2013
Load in for Extra Data	UHSLC/NOAA
Comparison Comments	Comparisons are perfect

Quality Control:

Type	Date Affected	Comments	QC Flag	GESLA Flag
		No erroneous values to remove		

(QC Flag: 0 = Meteorological (e.g. Seiche, Meteo-tsunami), 1 = Spike, 2 = Phase Offset, 3 = Tsunami, 4 = Other)

Analysis Comments

- Hurricane Sandy gives peak water level by over 1 m.
- A number of other hurricanes impact the site, with an oscillatory signal observed after the initial surge (some kind of seiche affect?).

Newcastle, Australia (32.926°S, 151.781°E)

Inherited:

Filename	V1 no.	Start	End	Yrs
'newcastle-019-australia-johnhunter.mat'	**410**	14/11/1957	31/12/2004	39

Extended:

v1 filename	'newcastle-019-australia-johnhunter.mat (410)
v2 Filename	276_Newcastle-AUS_GESLA_v2.mat
Source of Extra Data	N/A
Extra Data filename	N/A
Date of Download	N/A
End of Extra Data	N/A
Load in for Extra Data	N/A
Comparison Comments	No extra data available

Quality Control:

Type	Date Affected	Comments	QC Flag	GESLA Flag
Phase	03/10/1966 to 05/10/1966		2	3
Phase	20/01/1968 21:00 to 23/01/1968 06:00		2	3
Other	09/02/1968 18:00 to 12/02/1968 12:00		4	3
Phase	10/08/1969 12:00 to 12/08/1969		2	3
Phase	15/08/1969 to 17/08/1969 12:00		2	3
Phase	26/10/1970 03:00 to 18:00		2	3
Phase	01/11/1970 18:00 to 03/11/1970		2	3
Phase	23/02/1971 00:00 to 23:00		2	3
Spike	27/02/1971 18:00		1	3
Phase	23/08/1971 18:00 to 25/08/1971		2	3
Phase	24/11/1974 00:00 to 23:00		2	3
Phase	05/03/1977 to 12/03/1977		2	3
Phase	15/12/1977 12:00 to 17/12/1977		2	3
Phase	17/08/1978 to 20/08/1978		2	3
Phase	29/11/1978 17:00 to 20:00		2	3
Phase	15/01/1979 to 16/01/1979 12:00		2	3
Phase	04/07/1979 12:00 to 23:00		2	3
Phase	30/11/1982 00:00 to 12:00		2	3

Phase	27/06/1984 to 30/06/1984		2	3
Phase	16/09/1984 to 17/09/1984 03:00		2	3
Phase	13/08/1985 18:00 to 14/08/1985		2	3
Phase	01/01/1986 18:00 to 03/01/1986		2	3

(QC Flag: 0 = Meteorological (e.g. Seiche, Meteo-tsunami), 1 = Spike, 2 = Phase Offset, 3 = Tsunami, 4 = Other)

Newlyn, UK (50.103°N, 5.543°W)

Inherited:

Filename	V1 no.	Start	End	Yrs
Newlyn,_cornwall-294a-united_kingdom-uhslc.txt	**411**	22/04/1915	31/12/2001	85
Newlyn-001-glossdm-bodc.txt	**412**	01/01/1916	31/12/1944	29
Newlyn-p001-uk-bodc txt	**413**	22/04/1915	31/12/2006	74

Extended:

v1 filename	Newlyn,_cornwall-294a-united_kingdom-uhslc.txt
v2 Filename	287_Newlyn-GBR_GESLA_v2.mat
Source of Extra Data	BODC
Extra Data filename	RN-7246_1372253428497.zip
Date of Download	26/06/2013
End of Extra Data	31/12/2010
Load in for Extra Data	BODC2
Comparison Comments	Comparisons are perfect

Quality Control:

Type	Date Affected	Comments	QC Flag	GESLA Flag
Phase	16/07/1916 to 29/07/1916		2	3
Phase	24/06/1919 to 30/06/1919 12:00		2	3
Phase	09/08/1939 to 14/08/1939 12:00		2	3
Phase	13/04/1944 to 14/04/1944 12:00		2	3
Phase	08/07/1944 to 01/08/1944		2	3
Phase	05/08/1953 to 10/08/1953 12:00		2	3
Phase	04/11/1953 to 08/11/1953 12:00		2	3
Phase	03/12/2009 18:00		2	3
Datum	12/01/2010 to 15/08/2010 12:00		4	3

(QC Flag: 0 = Meteorological (e.g. Seiche, Meteo-tsunami), 1 = Spike, 2 = Phase Offset, 3 = Tsunami, 4 = Other)

Analysis Comments

- Large residual on 12/01/2010 probably caused by storm event that cleared previously cold weather, not obvious though. Data for this event and through to 15/08/2010 have been removed on the UHSLC website and therefore will be removed from this analysis.

Newport, USA (Rhode Island) (41.505°N, 71.327°W)

Inherited:

Filename	V1 no.	Start	End	Yrs
'newport,ri-253a-usa-uhslc.mat'	**414**	10/09/1930	31/12/2005	70

Extended:

v1 filename	'newport,ri-253a-usa-uhslc.mat (414)
v2 Filename	278_Newport-USA_GESLA_v2.mat
Source of Extra Data	UHSLC/NOAA
Extra Data filename	H253a / COOPS_Newport
Date of Download	01/04/2014
End of Extra Data	31/12/2013
Load in for Extra Data	UHSLC/NOAA
Comparison Comments	Comparisons are perfect

Quality Control:

Type	Date Affected	Comments	QC Flag	GESLA Flag
Phase	04/09/1977 to 08/09/1977		2	3
Phase	20/08/1978 to 31/12/1978 23:00		2	3

(QC Flag: 0 = Meteorological (e.g. Seiche, Meteo-tsunami), 1 = Spike, 2 = Phase Offset, 3 = Tsunami, 4 = Other)

Analysis Comments

- Apparent spikes on 27/10/1923 may be caused by hurricane that tracked along the US East Coast.
- Peak residual on 20/08/1991, Hurricane Bob

Nishinoomote, Japan (30.735°N, 130.992°E)

Inherited:

Filename	V1 no.	Start	End	Yrs
'nishinoomote,japan-001-glossdm-bodc.mat'	**416**	21/04/1965	30/04/1998	32
'nishinoomote-363a-japan-uhslc.mat'	**417**	21/04/1965	31/12/2003	38

Extended:

v1 filename	'nishinoomote-363a-japan-uhslc.mat (417)
v2 Filename	280_Nishinoomote-JPN_GESLA_v2.mat
Source of Extra Data	UHSLC
Extra Data filename	H363a
Date of Download	01/04/2014
End of Extra Data	31/12/2010
Load in for Extra Data	UHSLC
Comparison Comments	Comparisons are perfect

Quality Control:

Type	Date Affected	Comments	QC Flag	GESLA Flag
Phase	12/10/1966 to 14/10/1966		2	3
Phase	23/03/1967 to 04/04/1967		2	3
Phase	23/06/1967 to 26/06/1967		2	3
Phase	07/07/1967 to 11/07/1967		2	3
Phase	16/11/1967 to 23/11/1967		2	3
Phase	20/06/1968 to 05/07/1968		2	3
Phase	08/08/1968 to 14/08/1968		2	3
Phase	29/12/1968 to 07/01/1969		2	3
Phase	09/02/1969 to 23/02/1969		2	3
Phase	06/09/1969 to 17/09/1969		2	3
Phase	21/05/1970 to 03/06/1970		2	3
Phase	22/05/1971 to 24/05/1971		2	3
Phase	08/08/1971 to 12/08/1971		2	3
Phase	17/01/1973 to 22/01/1973		2	3
Phase	03/05/1973 to 21/05/1973		2	3
Phase	27/10/1973 to 30/10/1973		2	3
Phase	21/02/1974 to 27/02/1974		2	3
Phase	25/03/1980 to 31/03/1980		2	3
Phase	29/12/1981 to 02/12/1981		2	3
Phase	24/02/1982 to 27/02/1982		2	3
Phase	19/06/1986 to 01/07/1986		2	3
Phase	18/07/1986 to 01/08/1986		2	3
Phase	16/08/1986 to 01/09/1986		2	3
Phase	27/11/2006 00:00 to 23:00		2	3

(QC Flag: 0 = Meteorological (e.g. Seiche, Meteo-tsunami), 1 = Spike, 2 = Phase Offset, 3 = Tsunami, 4 = Other)

Analysis Comments

- Discontinuity seen in constituent amplitude and tidal datum time series. Remove all data before 1973.

North Shields, UK (55.007°N, 1.440°W)

Inherited:

Filename	V1 no.	Start	End	Yrs
northshields-p032-uk-bodc.mat	**419**	24/01/1946	31/12/2006	33

Extended:

v1 filename	northshields-p032-uk-bodc.mat (419)
v2 Filename	292_NorthShields-GBR_GESLA_v2.mat
Source of Extra Data	BODC
Extra Data filename	RN-7246_1372253428497.zip
Date of Download	26/06/2013
End of Extra Data	29/12/2012
Load in for Extra Data	BODC2
Comparison Comments	Comparisons are perfect

Quality Control:

Type	Date Affected	Comments	QC Flag	GESLA Flag
		No erroneous values to remove		

(QC Flag: 0 = Meteorological (e.g. Seiche, Meteo-tsunami), 1 = Spike, 2 = Phase Offset, 3 = Tsunami, 4 = Other)

Analysis Comments

- Outliers were removed (> 6, < -1).

North Sydney, Canada (46.217°N, 60.250°W)

Inherited:

Filename	V1 no.	Start	End	Yrs
'northsydney,ns-00612-canada-meds.mat'	**420**	07/01/1970	31/10/2008	39

Extended:

v1 filename	'northsydney,ns-00612-canada-meds.mat (420)
v2 Filename	283_NorthSydney-CAN_GESLA_v2.mat
Source of Extra Data	MEDS
Extra Data filename	612_01-JAN-2008.csv
Date of Download	01/04/2014
End of Extra Data	31/10/2013
Load in for Extra Data	MEDS
Comparison Comments	Comparisons between inherited and the extra data are perfect with a -16 hr offset applied to extra data to match inherited. Some duplicate records on 26/04/2011 were removed from the csv file before concatenation.

Quality Control:

Type	Date Affected	Comments	QC Flag	GESLA Flag
Spike	22/10/2011 02:00		1	3

(QC Flag: 0 = Meteorological (e.g. Seiche, Meteo-tsunami), 1 = Spike, 2 = Phase Offset, 3 = Tsunami, 4 = Other)

Analysis Comments

- Slightly noisy signal potentially caused by small tidal signal

Noumea, New Caledonia (22.292°SN, 166.437°E)

Inherited:

Filename	V1 no.	Start	End	Yrs
'noumea,newcaledonia-001-glossdm-bodc.mat'	**422**	24/02/1967	31/12/1998	32
'noumea-019a-france-uhslc.mat'	**423**	24/02/1967	31/08/2003	36

Extended:

v1 filename	'noumea-019a-france-uhslc.mat (423)
v2 Filename	285_Noumea-NCL_GESLA_v2.mat
Source of Extra Data	N/A
Extra Data filename	N/A
Date of Download	N/A
End of Extra Data	N/A
Load in for Extra Data	N/A
Comparison Comments	No extra data available for 019a. 019b has data from 2005-2012, but no overlapping period to tie the datums to each other.

Quality Control:

Type	Date Affected	Comments	QC Flag	GESLA Flag
Phase	06/06/1985 10:00 to 23:00		2	3
Spike	01/08/1994 00:00		1	3

(QC Flag: 0 = Meteorological (e.g. Seiche, Meteo-tsunami), 1 = Spike, 2 = Phase Offset, 3 = Tsunami, 4 = Other)

Ofunato, Japan (39.067°N, 141.717°E)

Inherited:

Filename	V1 no.	Start	End	Yrs
'ofunato,japan-001-glossdm-bodc.mat'	**429**	01/01/1965	31/12/2003	38
'ofunato-351a-japan-uhslc.mat'	**430**	01/01/1965	31/12/2005	41

Extended:

v1 filename	'ofunato-351a-japan-uhslc.mat (430)
v2 Filename	289_Ofunato-JPN_GESLA_v2.mat
Source of Extra Data	UHSLC
Extra Data filename	H351a
Date of Download	01/05/2014
End of Extra Data	31/12/2012
Load in for Extra Data	UHSLC
Comparison Comments	New data has been shifted after the 2011 Tohoku Earthquake as documented on the UHSLC website. "The Geospatial Information Authority of Japan estimated a vertical crustal movement of -801 mm after the 11 Mar 2011 Tohoku Earthquake. The historic series (1965-11 Mar 2011) was adjusted to the new level by adding 801 mm.

Quality Control:

Type	Date Affected	Comments	QC Flag	GESLA Flag
Phase	12/05/1965 18:00 to 14/05/1965 06:00		2	3
Phase	28/05/1965 18:00 to 30/05/1965 06:00		2	3
Phase	15/01/1968 to 19/01/1968 06:00		2	3

(QC Flag: 0 = Meteorological (e.g. Seiche, Meteo-tsunami), 1 = Spike, 2 = Phase Offset, 3 = Tsunami, 4 = Other)

Analysis Comments

- Peak residual on 23/08/1981, associated with Typhoon Thad.
- Peak sea level on 08/10/2006, not associated with a particular storm, and has a signal more akin to that of ET storms!

Pago Pago, American Samoa (14.283°S, 170.683°W)

Inherited:

Filename	V1 no.	Start	End	Yrs
pago_pago-056a-usa_trust-uhslc.mat'	**434**	08/09/1948	31/12/2005	54
pagopago,americansamoa,usa-001-glossdm-bodc.mat'	**435**	08/09/1948	01/09/2000	48

Extended:

v1 filename	pago_pago-056a-usa_trust-uhslc.mat (434)
v2 Filename	293_PagoPago-ASM_GESLA_v2.mat
Source of Extra Data	UHSLC/NOAA
Extra Data filename	H056a / 434_NOAA_PagoPago
Date of Download	31/07/2013
End of Extra Data	31/12/2012
Load in for Extra Data	UHSLC/NOAA
Comparison Comments	Overlap between inherited and extra is good, despite a seeming offset between last two years of data (NOAA) and extra data from UHSLC. Comparisons show overlap of NOAA and UHSLC data though. May be result of La Nina event as 1997 El Nino event shows very clearly at site.

Quality Control:

Type	Date Affected	Comments	QC Flag	GESLA Flag
Tsunami	05/11/1952 to 08/11/1952	Severo-Kulisk	3	6
Tsunami	10/03/1957 to 13/03/1957	Andreanov	3	6
Tsunami	23/05/1960 to 27/05/1960	Valdivia	3	6
Phase	30/10/1962 to 31/10/1962 12:00		2	3
Tsunami	28/03/1964 12:00 to 01/04/1964	Alaska	3	6
Phase	12/11/1968 12:00 to 16/11/1968		2	3
Phase	13/10/1974 to 15/10/1974		2	3
Phase	28/01/1975 to 04/02/1975		2	3
Phase	28/08/1976 to 01/09/1976		2	3
Tsunami	24/06/2001 06:00 to 28/06/2001	S. Peru	3	6
Tsunami	03/05/2006 12:00 to 07/05/2006	Tonga	3	6
Tsunami	15/11/2006 18:00 to 20/11/2006	Kuril Islands	3	6
Tsunami	29/09/2009 12:00 to 03/10/2009	Samoan	3	6
Tsunami	27/02/2010 18:00 to 04/03/2010	Chile	3	6
Tsunami	11/03/2011 12:00 to 16/03/2011	Tohuku	3	6

(QC Flag: 0 = Meteorological (e.g. Seiche, Meteo-tsunami), 1 = Spike, 2 = Phase Offset, 3 = Tsunami, 4 = Other)

Analysis Comments

- Severe Tropical Cyclone Val struck on 10/12/1991 and caused the maximum skew surge, followed immediately by lowest skew surge.

Papeete, French Polynesia (17.532°S, 149.567°W)

Inherited:

Filename	V1 no.	Start	End	Yrs
'papeete-a,frenchpolynesia-001-glossdm-bodc.mat'	**439**	01/05/1969	31/05/1975	5
'papeete-b,frenchpolynesia-001-glossdm-bodc.mat'	**440**	08/06/1975	31/12/1998	23
'papeete_b-015b-french_polynesia-uhslc.mat'	**441**	08/06/1975	05/09/2002	26

Extended:

v1 filename	'papeete_b-015b-french_polynesia-uhslc.mat (441)
v2 Filename	297_Papeete-PYF_GESLA_v2.mat
Source of Extra Data	UHSLC
Extra Data filename	H015b
Date of Download	01/05/2014
End of Extra Data	26/02/2012
Load in for Extra Data	UHSLC
Comparison Comments	Comparisons are perfect

Quality Control:

Type	Date Affected	Comments	QC Flag	GESLA Flag
		No erroneous values to remove		

(QC Flag: 0 = Meteorological (e.g. Seiche, Meteo-tsunami), 1 = Spike, 2 = Phase Offset, 3 = Tsunami, 4 = Other)

Analysis Comments

- Extra data downloaded from UHSLC website (015b) on 01/05/2014 and added to 441, for consistency. Papeete-A is referenced to a different TGZ and therefore cannot be added to B..
- Peak residual on 05/10/2010 associated with Cyclone Oli.
- Also large events on 10/03/1981 and 11/12/1991.

Patricia Bay, Canada (48.654°N, 123.452°W)

Inherited:

Filename	V1 no.	Start	End	Yrs
'patriciabay,bc-07277-canada-meds.mat'	**442**	30/06/1966	30/09/2008	31

Extended:

v1 filename	'patriciabay,bc-07277-canada-meds.mat (442)
v2 Filename	298_PatriciaBay-CAN_GESLA_v2.mat
Source of Extra Data	MEDS
Extra Data filename	7277_01-JAN-2008_slev
Date of Download	01/05/2014
End of Extra Data	31/12/2013
Load in for Extra Data	
Comparison Comments	Comparisons between inherited and extra data are perfect if a -16hr offset is applied to the new data. This is then corrected back to UTC by adding 16 hrs to the whole dataset.

Quality Control:

Type	Date Affected	Comments	QC Flag	GESLA Flag
		No erroneous values to remove		

(QC Flag: 0 = Meteorological (e.g. Seiche, Meteo-tsunami), 1 = Spike, 2 = Phase Offset, 3 = Tsunami, 4 = Other)

Penhryn, Cook Islands (8.977°S, 158.053°W)

Inherited:

Filename	V1 no.	Start	End	Yrs
'penrhyn,cookislands-001-glossdm-bodc.mat'	**444**	16/04/1977	31/12/1998	21
'penrhyn-024a-cook_islands-uhslc.mat'	**445**	16/04/1977	31/12/2003	26

Extended:

v1 filename	'penrhyn-024a-cook_islands-uhslc.mat (445)
v2 Filename	300_Penhryn-COK_GESLA_v2.mat
Source of Extra Data	UHSLC
Extra Data filename	H024a
Date of Download	02/05/2014
End of Extra Data	03/03/2012
Load in for Extra Data	UHSLC
Comparison Comments	Comparisons are perfect

Quality Control:

Type	Date Affected	Comments	QC Flag	GESLA Flag
		No erroneous values to remove		

(QC Flag: 0 = Meteorological (e.g. Seiche, Meteo-tsunami), 1 = Spike, 2 = Phase Offset, 3 = Tsunami, 4 = Other)

Analysis Comments

- Peak sea level on 22/01/2010 associated with TS 17 (possibly).
- Peak residual on 21/07/1996 looks real but cannot find associated storm.

Pensacola, USA (30.403°N, 87.213WE)

Inherited:

Filename	V1 no.	Start	End	Yrs
pensacola,fl-762a-usa-uhslc.mat'	**446**	01/05/1923	31/12/2005	79
pensacola-007-usa-johnhunter.mat'	**447**	01/05/1923	28/02/2006	78

Extended:

v1 filename	pensacola,fl-762a-usa-uhslc.mat'
v2 Filename	301_Pensacola-USA_GESLA_v2.mat
Source of Extra Data	UHSLC/NOAA
Extra Data filename	H762a / 446_NOAA_Pensacola
Date of Download	25/07/2013
End of Extra Data	31/12/2012
Load in for Extra Data	UHSLC/NOAA
Comparison Comments	Comparisons are perfect

Quality Control:

Type	Date Affected	Comments	QC Flag	GESLA Flag
Threshold		< 1m		
Phase	12/08/1950 22:00 to 31/08/1950		2	3

(QC Flag: 0 = Meteorological (e.g. Seiche, Meteo-tsunami), 1 = Spike, 2 = Phase Offset, 3 = Tsunami, 4 = Other)

Analysis Comments

- Data in 1950 drifts before there is a gap in the data, need to determine where this drift begins and remove data from there. Flag from 01/07/1950.
- Huge event in 1926 associated with the Great Miami Hurricane.
- Large event in 2004 associated with Hurricane Ivan (Cat-5), WLR failure around time of landfall, keep event in despite event not being fully described.
- 2005 – Dennis (July) Katrina (August).
- Other large events are: Sep-1947, Aug-1969, Sep-1979 (Frederic), Oct-1995 (Opal), Sep-1998 (Georges)

Pohnpei, States of Micronesia (6.987°N, 158.243°E)

Inherited:

Filename	V1 no.	Start	End	Yrs
'pohnpei-a,carolines-001-glossdm-bodc.mat'	**449**	08/05/1969	28/02/1971	1
'pohnpei-b,carolines-001-glossdm-bodc.mat'	**450**	21/04/1974	31/12/2001	24
'pohnpei_b-001b-fd._st._micronesia-uhslc.mat'	**451**	21/04/1974	31/12/2004	30

Extended:

v1 filename	N/A
v2 Filename	303_Pohnpei-FSM_GESLA_v2.mat
Source of Extra Data	UHSLC
Extra Data filename	H001b
Date of Download	02/05/2014
End of Extra Data	31/12/2004
Load in for Extra Data	UHSLC
Comparison Comments	Extra data replaced inherited, because of corrections to the data. No data after 2004, because new tide gauge was deployed to give 001c, which has a slightly different tidal regime and therefore cannot be combined.

Quality Control:

Type	Date Affected	Comments	QC Flag	GESLA Flag
		No erroneous values to remove		

(QC Flag: 0 = Meteorological (e.g. Seiche, Meteo-tsunami), 1 = Spike, 2 = Phase Offset, 3 = Tsunami, 4 = Other)

Analysis Comments

- UHSLC website states that the harmonic analysis does not resolve all constituents.

Point Atkinson, Canada (BC) (49.337°N, 123.253°W)

Inherited:

Filename	V1 no.	Start	End	Yrs
'pointatkinson,bc-07795-canada-meds.mat'	**453**	30/04/1914	30/09/2008	64

Extended:

v1 filename	'pointatkinson,bc-07795-canada-meds.mat (453)
v2 Filename	305_PointAtkinson-CAN_GESLA_v2.mat
Source of Extra Data	M EDS
Extra Data filename	7795_01-JAN-2008_slev
Date of Download	02/05/2014
End of Extra Data	31/12/2013
Load in for Extra Data	MEDS
Comparison Comments	Comparisons between inherited and extra data are perfect if a -16hr offset is applied to the new data. This is then corrected back to UTC by adding 16 hrs to the whole dataset.

Quality Control:

Type	Date Affected	Comments	QC Flag	GESLA Flag
Phase	30/11/1939 18:00 to 03/12/1939		2	3
Phase	21/05/1978 to 27/06/1978		2	3

(QC Flag: 0 = Meteorological (e.g. Seiche, Meteo-tsunami), 1 = Spike, 2 = Phase Offset, 3 = Tsunami, 4 = Other)

Ponta Delgada, Portugal (37.735°N, 25.672°W)

Inherited:

Filename	V1 no.	Start	End	Yrs
'ponta_delgada-211a-portugal-uhslc.mat'	**455**	19/05/1978	31/12/2005	15
'pontadelgada,azores-001-glossdm-bodc.mat'	**456**	19/05/1978	31/12/1998	8

Extended:

v1 filename	'ponta_delgada-211a-portugal-uhslc.mat (455)
v2 Filename	307_PontaDelgada-PRT_GESLA_v2.mat
Source of Extra Data	UHSLC
Extra Data filename	H211a
Date of Download	02/05/2014
End of Extra Data	03/04/2012
Load in for Extra Data	UHSLC
Comparison Comments	Comparisons are perfect

Quality Control:

Type	Date Affected	Comments	QC Flag	GESLA Flag
		No erroneous values to remove		

(QC Flag: 0 = Meteorological (e.g. Seiche, Meteo-tsunami), 1 = Spike, 2 = Phase Offset, 3 = Tsunami, 4 = Other)

Port-aux-Basques, Canada (NF) (47.567°N, 59.133°W)

Inherited:

Filename	V1 no.	Start	End	Yrs
'port-aux-basques,nf-00665-canada-meds.mat'	**457**	12/08/1935	31/10/2008	44

Extended:

v1 filename	'port-aux-basques,nf-00665-canada-meds.mat (457)
v2 Filename	308_PortAuxBasques-CAN_GESLA_v2.mat
Source of Extra Data	MEDS
Extra Data filename	665-01-JAN-2008_slev.csv
Date of Download	02/05/2014
End of Extra Data	31/12/2013
Load in for Extra Data	MEDS
Comparison Comments	Comparisons between inherited and extra data are perfect if a -7hr offset is applied to the new data. This is then corrected back to UTC by adding 7 hrs to the whole dataset. Duplicate data point detected on 09/04/2012 13:30 by MATLAB, but cannot see anything in the imported dataset. Duplicate point removed in Extra.D.data and script is able to run.

Quality Control:

Type	Date Affected	Comments	QC Flag	GESLA Flag
Phase	26/06/1959 to 01/07/1959		2	3
Phase	22/08/1959 to 25/08/1959		2	3
Phase	24/07/1973 to 01/08/1973 06:00		2	3

(QC Flag: 0 = Meteorological (e.g. Seiche, Meteo-tsunami), 1 = Spike, 2 = Phase Offset, 3 = Tsunami, 4 = Other)

Analysis Comments

- Large gap between first valid year and majority of the data. Appears not to affect trend and therefore they have been left in.

Port Elizabeth, South Africa (33.960°S, 25.630°E)

Inherited:

Filename	V1 no.	Start	End	Yrs
'port_elizabeth-184a-south_africa-uhslc.mat'	**459**	01/01/1985	31/12/2000	8
'portelizabeth,southafrica-001-glossdm-bodc.mat'	**471**	01/03/1973	31/12/2000	14

Extended:

v1 filename	N/A
v2 Filename	310_PortElizabeth-ZAF_GESLA_v2.mat
Source of Extra Data	UHSLC
Extra Data filename	H184a
Date of Download	07/05/2014
End of Extra Data	31/07/2011
Load in for Extra Data	UHSLC
Comparison Comments	Comparisons between inherited and extra data show discrepancy. UHSLC states that thorough calibration was conducted and the data were adjusted in 2008. Therefore only new downloaded data from the UHSLC (which now dates back to 1973) is used.

Quality Control:

Type	Date Affected	Comments	QC Flag	GESLA Flag
Phase	13/02/1980 12:00 to 15/02/1980 06:00		2	3
Phase	14/07/1980 12:00 to 19/07/1980		2	3
Phase	07/04/1993 to 13/04/1993		2	3
Phase	06/05/1993 to 08/05/1993		2	3
Phase	01/01/2009 to 11/04/2009		2	3
Phase	22/11/2009 to 31/12/2009 23:00		2	3

(QC Flag: 0 = Meteorological (e.g. Seiche, Meteo-tsunami), 1 = Spike, 2 = Phase Offset, 3 = Tsunami, 4 = Other)

Analysis Comments

- First Yr > 75% is 1979.
- Big jump in amplitude and phase of tide in 1993.

Port Hedland, Australia (20.314°S, 118.578°E)

Inherited:

Filename	V1 no.	Start	End	Yrs
'port_hedland-169a-australia-uhslc.mat'	**460**	01/01/1984	31/12/2005	21
'porthedland-022-australia-johnhunter.mat'	**474**	31/05/1960	31/12/2004	32

Extended:

v1 filename	'porthedland-022-australia-johnhunter.mat (474)
v2 Filename	311_PortHedland-AUS_GESLA_v2.mat
Source of Extra Data	UHSLC
Extra Data filename	H169a
Date of Download	07/05/2014
End of Extra Data	03/04/2012
Load in for Extra Data	UHSLC
Comparison Comments	Comparisons are perfect

Quality Control:

Type	Date Affected	Comments	QC Flag	GESLA Flag
		No erroneous values to remove		

(QC Flag: 0 = Meteorological (e.g. Seiche, Meteo-tsunami), 1 = Spike, 2 = Phase Offset, 3 = Tsunami, 4 = Other)

Analysis Comments

- First Yr > 75% is 1966.
- Peak residual on 22/01/1973, caused by Cyclone Kerry.
- Possible datum shift between 1978 and 1984. Only data from 1984 is documented on UHSLC, which suggests that it is not possible to use data previous to this date. The jump in amplitude in major constituents is good evidence that the measurements have changed unnaturally.

Port Isabel, USA (Texas) (26.060°N, 97.215°W)

Inherited:

Filename	V1 no.	Start	End	Yrs
'port_isabel,tx-772a-usa-uhslc.mat'	**461**	26/01/1977	31/12/2005	27

Extended:

v1 filename	'port_isabel,tx-772a-usa-uhslc.mat (461)
v2 Filename	312_PortIsabel-USA_GESLA_v2.mat
Source of Extra Data	UHSLC/NOAA
Extra Data filename	H772a / COOPS_PortIsabel
Date of Download	07/05/2014
End of Extra Data	31/12/2013
Load in for Extra Data	UHSLC/NOAA
Comparison Comments	Comparisons between inherited and extra data are perfect. Comparisons between UHSLC and NOAA show offset of 0.121 m, for the majority of overlap, but for 3 months the UHSLC is the same.

Quality Control:

Type	Date Affected	Comments	QC Flag	GESLA Flag
		No erroneous values to remove		

(QC Flag: 0 = Meteorological (e.g. Seiche, Meteo-tsunami), 1 = Spike, 2 = Phase Offset, 3 = Tsunami, 4 = Other)

Analysis Comments

- Large residual and sea level recorded on 09/08/1980 associated with Hurricane Allen, but TG breaks during event so event is not completely captured.
- Possible datum shift around 1984, seen in amplitude of M2 constituent but not in any other indicator plot. Check for documentation regarding this.
- Events in 1977, 2008 clearly hurricanes occurring along Gulf Coast.

Port San Luis, USA (California) (35.177°N, 120.760°W)

Inherited:

Filename	V1 no.	Start	End	Yrs
'port_san_luis,_ca-565a-usa-uhslc.mat'	**465**	01/01/1983	31/12/2005	20

Extended:

v1 filename	N/A
v2 Filename	316_PortSanLuis-USA_GESLA_v2.mat
Source of Extra Data	UHSLC/NOAA
Extra Data filename	H565a / COOPS_PortSan Luis
Date of Download	07/05/2014
End of Extra Data	31/12/2013
Load in for Extra Data	UHSLC/NOAA
Comparison Comments	Comparisons are perfect, but only the extra data is used because the dataset on UHSLC has been extended back to 1948.

Quality Control:

Type	Date Affected	Comments	QC Flag	GESLA Flag
Phase	27/08/1953 to 31/08/1953 03:00		2	3
Phase	01/08/1957 to 03/08/1957 18:00		2	3
Spike	28/07/1957 03:00		1	3
Phase	10/11/1958 08:00 to 11/11/1958 10:00		2	3
Phase	24/05/1963 to 26/05/1963		2	3
Tsunami	28/03/1964 06:00 to 31/03/1964	Alaskan	3	6
Phase	31/10/1966 20:00 to 01/11/1966 02:00		2	3
Phase	01/01/1969 to 31/12/1969		2	3
Phase	05/02/1973 to 08/02/1973		2	3
Phase	30/04/1974 12:00 to 01/05/1974 12:00		2	3
Phase	06/09/1974 08:00 to 07/09/1974 08:00		2	3
Phase	30/09/1976 00:00 to 23:00		2	3
Tsunami	15/11/2006 to 18/11/2006	Kuril Island	3	6
Phase	23/07/2009 to 01/08/2009		2	3
Tsunami	30/09/2009 to 02/10/2009	Samoan	3	6
Tsunami	11/03/2011 12:00 to 18/03/2011	Tohuku	3	6

(QC Flag: 0 = Meteorological (e.g. Seiche, Meteo-tsunami), 1 = Spike, 2 = Phase Offset, 3 = Tsunami, 4 = Other)

Analysis Comments

- Big jump in amplitude and phase of tide in 1969. All data for year flagged.
- Noisy period around 1986 to 1988 like noisy data superimposed on a longer period event.
- Peak residual in 1983.

Port Adelaide (Outer), Australia (34.926°S, 135.600°E)

Inherited:

Filename	V1 no.	Start	End	Yrs
'portadelaideinner-021-australia-johnhunter.mat'	**469**	01/01/1933	31/12/1999	42
'portadelaideouter-020-australia-johnhunter.mat'	**470**	09/11/1940	31/12/2004	62

Extended:

v1 filename	'portadelaideouter-020-australia-johnhunter.mat (470)
v2 Filename	319_PortAdelaide-AUS_GESLA_v2.mat
Source of Extra Data	N/A
Extra Data filename	N/A
Date of Download	N/A
End of Extra Data	N/A
Load in for Extra Data	N/A
Comparison Comments	No extra data available. Using the Outer site since data coverage is better and longer.

Quality Control:

Type	Date Affected	Comments	QC Flag	GESLA Flag
Phase	17/02/1941 to 05/03/1941		2	3
Phase	12/06/1941 12:00 to 24/06/1941		2	3
Phase	13/07/1941 to 19/07/1941		2	3
Phase	25/07/1961 21:00 to 01/08/1961		2	3
Phase	09/10/1961 06:00 to 23:00		2	3
Phase	12/01/1963 12:00 to 13/01/1963 18:00		2	3
Phase	14/02/1963 00:00 to 18:00		2	3
Phase	09/06/1963 00:00 to 18:00		2	3
Phase	05/03/1969 18:00 to 06/03/1969 03:00		2	3
Phase	14/06/1969 12:00 to 15/06/1969 15:00		2	3
Phase	05/06/1972 to 06/06/1972		2	3
Phase	23/02/1975 21:00 to 24/02/1975 03:00		2	3

(QC Flag: 0 = Meteorological (e.g. Seiche, Meteo-tsunami), 1 = Spike, 2 = Phase Offset, 3 = Tsunami, 4 = Other)

Analysis Comments

- Data quality improves after 1966. Up to this point there is a lot of noise in the data, but it is difficult to determine whether signal is real or not.
- Peak residual on 18/05/1953, storm??

Port Hardy, Canada (BC) (50.722°N, 127.489°W)

Inherited:

Filename	V1 no.	Start	End	Yrs
'porthardy,bc-08408-canada-meds.mat'	**473**	03/06/1964	30/09/2008	42

Extended:

v1 filename	'porthardy,bc-08408-canada-meds.mat (473)
v2 Filename	321_PortHardy-CAN_GESLA_v2.mat
Source of Extra Data	MEDS
Extra Data filename	8047_01-JAN-2008_slev.csv
Date of Download	08/05/2014
End of Extra Data	31/12/2013
Load in for Extra Data	MEDS
Comparison Comments	Comparison between inherited and extra data are perfect if -16hr time shift is applied to the extra data downloaded. However, because the data were downloaded in UTC all the dataset is then shifted forward 16 hrs to return data to UTC.

Quality Control:

Type	Date Affected	Comments	QC Flag	GESLA Flag
Spike	17/02/1965 04:00 to 10:00		1	3
Spike	23/03/1968 07:00		1	3
Spike	27/03/1968 01:00		1	3
Spike	31/03/1968 02:00		1	3
Spike	05/05/1968 18:00		1	3
Spike	10/05/1968 10:00		1	3
Spike	11/05/1968 19:00 to 22:00		1	3
Spike	13/05/1968 10:00		1	3
Spike	13/05/1968 17:00		1	3
Spike	16/05/1968 16:00		1	3
Spike	20/05/1968 20:00		1	3

Phase	23/12/1969 to 28/12/1969		2	3
Phase	19/10/1980 to 29/10/1980		2	3

(QC Flag: 0 = Meteorological (e.g. Seiche, Meteo-tsunami), 1 = Spike, 2 = Phase Offset, 3 = Tsunami, 4 = Other)

Analysis Comments

- Tsunami signal is not evident at the site. Is that because it is facing away from the Pacific on Vancouver Island?

Portland, USA (Maine) (43.657°N, 70.247°W)

Inherited:

Filename	V1 no.	Start	End	Yrs
'portland,me-252a-usa-uhslc.mat'	**475**	04/03/1910	31/12/2005	91
'portlandmaine-001-usa-johnhunter.mat'	**477**	04/03/1910	28/02/2006	91

Extended:

v1 filename	'portland,me-252a-usa-uhslc.mat (475)
v2 Filename	322_Portland-USA_GESLA_v2.mat
Source of Extra Data	UHSLC/NOAA
Extra Data filename	H252a / COOPS_Portland
Date of Download	08/05/2014
End of Extra Data	31/12/2013
Load in for Extra Data	UHSLC/NOAA
Comparison Comments	Comparisons are perfect

Quality Control:

Type	Date Affected	Comments	QC Flag	GESLA Flag
Spike	08/11/1910 13:00		1	3
Phase	10/11/1910 to 18/12/1910		2	3
Phase	08/09/1912 to 12/09/1912		2	3
Phase	15/05/1913 to 20/05/1913		2	3
Phase	03/04/1918 to 04/04/1918		2	3
Phase	17/01/1921 to 29/01/1921		2	3
Phase	1942	Whole Year!	2	3
Phase	26/02/1943 03:00 to 15:00		2	3
Phase	31/12/1943 23:00 to 01/01/1944 04:00		2	3
Phase	06/09/1951 03:00 to 07/09/1951 06:00		2	3
Phase	13/07/1962 to 25/07/1962		2	3
Phase	07/04/1974 to 26/07/1974		2	3

(QC Flag: 0 = Meteorological (e.g. Seiche, Meteo-tsunami), 1 = Spike, 2 = Phase Offset, 3 = Tsunami, 4 = Other)

Analysis Comments

- First year of valid data (1910) has smaller amplitudes of tide, possibly because the first 2 months of the year are missing. Flag data. Possibly consider changing threshold of valid data per year as it seems to allow erroneous years through. Remaining data were noisy and a small section was removed, which reduces the data % below 75 for 1910.

Port Lincoln, Australia (34.720°S, 135.858°E)

Inherited:

Filename	V1 no.	Start	End	Yrs
'portlincoln-023-australia-johnhunter.mat'	**478**	03/05/1965	31/12/2004	39

Extended:

v1 filename	'portlincoln-023-australia-johnhunter.mat (478)
v2 Filename	324_PortLincolm-AUS_GESLA_v2.mat
Source of Extra Data	N/A
Extra Data filename	N/A
Date of Download	N/A
End of Extra Data	N/A
Load in for Extra Data	N/A
Comparison Comments	No extra data available

Quality Control:

Type	Date Affected	Comments	QC Flag	GESLA Flag
Phase	11/04/1971 to 13/04/1971		2	3
Phase	16/04/1971 12:00 to 18/04/1971		2	3
Phase	14/11/1977 to 17/11/1977		2	3

(QC Flag: 0 = Meteorological (e.g. Seiche, Meteo-tsunami), 1 = Spike, 2 = Phase Offset, 3 = Tsunami, 4 = Other)

Port Lonsdale, Australia (35.909°S, 138.498°E)

Inherited:

Filename	V1 no.	Start	End	Yrs
'portlonsdale-017-australia-johnhunter.mat'	**479**	27/11/1962	31/12/2004	42

Extended:

v1 filename	'portlonsdale-017-australia-johnhunter.mat (479)
v2 Filename	325_PortLonsdale-AUS_GESLA_v2.mat
Source of Extra Data	N/A
Extra Data filename	N/A
Date of Download	N/A
End of Extra Data	N/A
Load in for Extra Data	N/A
Comparison Comments	No extra data available

Quality Control:

Type	Date Affected	Comments	QC Flag	GESLA Flag
Phase	17/09/1983 09:00 to 15:00		2	3
Phase	19/01/1984 00:00 to 15:00		2	3
Phase	06/03/1984 to 09/03/1984		2	3
Phase	07/06/1984 to 10/06/1984		2	3
Phase	24/12/1984 00:00 to 23:00		2	3
Phase	23/02/1985 09:00 to 12:00		2	3
Phase	02/03/1985 to 05/03/1985		2	3

(QC Flag: 0 = Meteorological (e.g. Seiche, Meteo-tsunami), 1 = Spike, 2 = Phase Offset, 3 = Tsunami, 4 = Other)

Port Patrick, UK (54.843°N, 5.120°W)

Inherited:

Filename	V1 no.	Start	End	Yrs
portpatrick-p063-uk-bodc.mat	484	05/01/1968	31/12/2006	35

Extended:

v1 filename	portpatrick-p063-uk-bodc.mat (484)
v2 Filename	327_PortPatrick-GBR_GESLA_v2.mat
Source of Extra Data	BODC
Extra Data filename	RN-7246_1372253428497.zip
Date of Download	26/06/2013
End of Extra Data	29/12/2012
Load in for Extra Data	BODC2
Comparison Comments	Comparisons are perfect

Quality Control:

Type	Date Affected	Comments	QC Flag	GESLA Flag
Threshold		< -5 & > 7	4	3
Spikes	03/2010 to 08/2010	See below	1	3
Phase	28/10/2011 15:00 to 21/11/2011 13:00		2	3
Spike	02/09/2010 15:00 to 02/09/2010 17:00		1	3

(QC Flag: 0 = Meteorological (e.g. Seiche, Meteo-tsunami), 1 = Spike, 2 = Phase Offset, 3 = Tsunami, 4 = Other)

Analysis Comments

- A number of small spikes appear from Mar-2010 to Aug-2010, this may the result of small timing errors. They are mostly small downwards spikes in the residual, but can be up to 0.7 m.

Port Pirie, Australia (33.177°S, 138.010°E)

Inherited:

Filename	V1 no.	Start	End	Yrs
'portpirie-024-australia-johnhunter.mat'	**485**	04/01/1941	31/12/2004	64

Extended:

v1 filename	'portpirie-024-australia-johnhunter.mat (485)
v2 Filename	328_PortPirie-AUS_GESLA_v2.mat
Source of Extra Data	N/A
Extra Data filename	N/A
Date of Download	N/A
End of Extra Data	N/A
Load in for Extra Data	N/A
Comparison Comments	No extra data available

Quality Control:

Type	Date Affected	Comments	QC Flag	GESLA Flag
Phase	19/07/1944 00:00 to 15:00		2	3
Phase	04/01/1951 09:00 to 05/01/1951 15:00		2	3
Phase	26/06/1952 00:00 to 23:00		2	3
Phase	11/06/1959 to 14/06/1959		2	3
Phase	25/07/1959 to 28/07/1959		2	3
Phase	30/01/1960 18:00 to 23:00		2	3
Phase	1961: Phase may be 1 hr off.		2	3
Phase	31/12/1963 03:00 to 21:00		2	3
Phase	16/12/1964 to 17/12/1964 06:00		2	3
Phase	30/07/1968 to 01/08/1968		2	3
Phase	01/05/1972 to 01/07/1972		2	3
Phase	01/01/1980 to 31/01/1980		2	3
Phase	24/06/1987 00:00 to 23:00		2	3

(QC Flag: 0 = Meteorological (e.g. Seiche, Meteo-tsunami), 1 = Spike, 2 = Phase Offset, 3 = Tsunami, 4 = Other)

Prince Rupert, Canada (54.317°N, 130.324°W)

Inherited:

Filename	V1 no.	Start	End	Yrs
prince_rupert_b-540b-canada-uhslc.mat'	**490**	01/01/1963	31/12/1999	37
princerupert,bc-09354-canada-meds.mat'	**491**	01/01/1909	30/09/2008	77
princerupert,canada-001-glossdm-bodc.mat'	**492**	01/01/1909	31/12/1999	13

Extended:

v1 filename	princerupert,bc-09354-canada-meds.mat (491)
v2 Filename	330_PortRupert-CAN_GESLA_v2.mat
Source of Extra Data	MEDS
Extra Data filename	9354-01-JAN-2008_slev.csv
Date of Download	25/07/2013
End of Extra Data	31/12/2012
Load in for Extra Data	MEDS
Comparison Comments	Inherited data are in PST(UTC-8) as standard MEDS format, and therefore they are shifted to be in UTC to match the extra data.

Quality Control:

Type	Date Affected	Comments	QC Flag	GESLA Flag
Phase	30/08/1917 to 03/09/1917		2	3
Phase	14/12/1944 to 21/12/1944 06:00		2	3
Phase	13/12/1945 15:00 to 25/12/1945 20:00		2	3
Phase	10/01/1963 04:00 to 10/01/1963 07:00		2	3
Phase	12/01/1963 06:00 to 12/01/1963 08:00		2	3
Phase	25/03/1972 13:00 to 01/04/1972 09:00		2	3

(QC Flag: 0 = Meteorological (e.g. Seiche, Meteo-tsunami), 1 = Spike, 2 = Phase Offset, 3 = Tsunami, 4 = Other)

Analysis Comments

- Fitted linear models with nodal component do not fit the data for GDTR, MHHW or MLLW. All other tidal datums are well accounted for.

Puerto Montt, Chile (41.483°S, 72.967°W)

Inherited:

Filename	V1 no.	Start	End	Yrs
'puerto_montt-684a-chile-uhslc.mat'	**504**	02/04/1980	31/12/2002	20

Extended:

v1 filename	'puerto_montt-684a-chile-uhslc.mat (504)
v2 Filename	338_PuertoMontt-CHL_GESLA_v2.mat
Source of Extra Data	UHSLC
Extra Data filename	H684a
Date of Download	09/05/2014
End of Extra Data	31/12/2012
Load in for Extra Data	UHSLC
Comparison Comments	Comparisons are perfect

Quality Control:

Type	Date Affected	Comments	QC Flag	GESLA Flag
Phase	23/03/1981 to 27/03/1981		2	3
Phase	03/03/1984 to06/03/1984		2	3
Phase	02/05/1984 to 21/05/1984		2	3
Phase	18/04/1987 12:00 to 22/04/1987		2	3
Phase	09/07/1987 to 17/07/1987		2	3
Phase	03/08/1987 to 03/10/1987		2	3
Phase	05/02/1989 to 10/04/1989		2	3
Phase	03/09/1989 to 05/11/1989		2	3
Phase	14/09/1990 to 06/11/1990		2	3
Phase	01/01/1991 to 24/03/1991		2	3
Phase	02/06/1991 to 07/06/1991		2	3
Phase	14/07/1991 to 20/07/1991		2	3
Phase	09/08/1991 to 31/08/1991		2	3
Phase	16/11/1991 to 29/11/1991		2	3
Phase	23/12/1991 to 31/12/1991 23:00		2	3
Phase	10/01/1992 to 13/01/1992		2	3
Phase	14/02/1992 to 02/04/1992		2	3
Phase	22/05/1992 to 26/05/1992		2	3
Phase	27/06/1992 to 01/07/1992		2	3
Phase	30/09/1992 06:00 to 04/10/1992		2	3
Phase	01/01/1994 to 18/04/1994		2	3
Phase	04/04/1995 to 08/05/1995		2	3
Phase	27/06/1995 to 02/07/1995		2	3
Phase	20/01/1996 to 23/01/1996		2	3
Phase	30/06/1996 to 30/03/1997		2	3
Phase	17/05/1997 to 27/05/1997		2	3
Phase	14/06/1997 to 02/08/1997		2	3
Phase	21/09/1997 to 01/11/1997		2	3

(QC Flag: 0 = Meteorological (e.g. Seiche, Meteo-tsunami), 1 = Spike, 2 = Phase Offset, 3 = Tsunami, 4 = Other)

Analysis Comments

- Data much noisier pre-2000 than after. Have removed as many phase offsets as possible but it is clear in the surge percentiles that there is still a strong influence there. The magnitude of constituents is more variable before 2000 as well.
- Continue to use in analysis, but be aware of data issues.

Queen Charlotte City, Canada (53.252°N, 132.072°W)

Inherited:

Filename	V1 no.	Start	End	Yrs
'queencharlottecity,bc-09850-canada-meds.mat'	**509**	01/06/1957	30/09/2008	42

Extended:

v1 filename	'queencharlottecity,bc-09850-canada-meds.mat (509)
v2 Filename	342_QueenCharlotteCity-CAN_GESLA_v2.mat
Source of Extra Data	MEDS
Extra Data filename	9850_01-JAN-2007_slev.csv
Date of Download	09/05/2014
End of Extra Data	31/12/2013
Load in for Extra Data	MEDS
Comparison Comments	Comparisons are perfect between inherited and extra data, if -16hr time offset is applied to extra data. However, because the extra data was downloaded in UTC a correction of +16hrs is applied to all the data after concatenation.

Quality Control:

Type	Date Affected	Comments	QC Flag	GESLA Flag
Spike	06/07/1966 16:00		1	3
Spike	08/07/1966 05:00		1	3
Spike	31/07/1966 08:00		1	3
Spike	01/08/1966 01:00		1	3
Spike	02/09/1966 15:00		1	3
Spike	21/06/1967 04:00 to 05:00		1	3
Phase	01/06/1968 to 03/06/1968		2	3
Phase	31/01/1972 to 02/02/1972		2	3

(QC Flag: 0 = Meteorological (e.g. Seiche, Meteo-tsunami), 1 = Spike, 2 = Phase Offset, 3 = Tsunami, 4 = Other)

Rikitea, French Polynesia (23.125°S, 134.953°W)

Inherited:

Filename	V1 no.	Start	End	Yrs
'rikitea,frenchpolynesia-001-glossdm-bodc.mat'	**521**	05/10/1969	31/12/1998	25
'rikitea-016a-french_polynesia-uhslc.mat'	**522**	05/10/1969	30/06/2003	28

Extended:

v1 filename	'rikitea-016a-french_polynesia-uhslc.mat (522)
v2 Filename	349_Rikitea-PYF_GESLA_v2.mat
Source of Extra Data	UHSLC
Extra Data filename	H016a
Date of Download	09/05/2014
End of Extra Data	03/04/2012
Load in for Extra Data	UHSLC
Comparison Comments	Comparisons are perfect

Quality Control:

Type	Date Affected	Comments	QC Flag	GESLA Flag
Phase	01/02/1970 to 02/05/1970		2	3
Phase	24/07/1970 to 26/07/1970		2	3
Phase	14/02/1971 to 16/02/1971		2	3
Phase	13/12/1971 to 01/01/1972		2	3
Phase	01/06/1972 to 24/09/1972		2	3
Phase	01/10/1972 to 10/10/1972		2	3
Phase	18/10/1972 to 10/11/1972		2	3
Phase	18/11/1972 to 26/11/1972		2	3
Phase	01/01/01974 to 27/02/1974		2	3
Phase	24/03/1974 to 04/04/1974		2	3
Phase	29/04/1974 to 07/05/1974		2	3
Phase	01/03/1976 00:00 to 12:00		2	3
Other	01/04/2004 to 01/10/2007	HW values missing	4	3

(QC Flag: 0 = Meteorological (e.g. Seiche, Meteo-tsunami), 1 = Spike, 2 = Phase Offset, 3 = Tsunami, 4 = Other)

Analysis Comments

- Data before 1976 appear noisier.
- Data from 2004-2008 appear to not records HW, with a threshold seemingly applied at 1.304 m.

Rio de Janeiro, Brazil (22.933°S, 43.133°W)

Inherited:

Filename	V1 no.	Start	End	Yrs
rio_de_janeiro,cg-709a-brazil-uhslc.txt	523	01/01/1955	31/12/1968	10

Extended:

v1 filename	N/A
v2 Filename	350_RiodeJaneiro-BRA_GESLA_v2.mat
Source of Extra Data	UHSLC
Extra Data filename	H709a
Date of Download	Unknown
End of Extra Data	31/12/2010
Load in for Extra Data	UHSLC
Comparison Comments	Comparison of current UHSLC data with GESLA dataset shows difference during overlapping period. This is not discussed on UHSLC website (ftp://ilikai.soest.hawaii.edu/rqds/atlantic/doc/qa280a.dmt). Just new downloaded data, although not mentioned on UHSLC why difference may have occurred.

Quality Control:

Type	Date Affected	Comments	QC Flag	GESLA Flag
Phase	11/10/1966 to 16/10/1966		2	3
Phase	19/08/1967 to 12/09/1967		2	3
Phase	07/04/1968 to 16/04/1968		2	3
Phase	30/11/1968 to 09/12/1968		2	3
Phase	10/01/1971 to 11/01/1971 04:00		2	3
Phase	12/12/1972 12:00 to 14/12/1972 12:00		2	3
Phase	24/09/1977 06:00 to 25/09/1977 15:00		2	3
Phase	05/01/1997 08:00 to 07/01/1997 12:00		2	3
Phase	01/07/1984 to 01/10/1984		2	3
Phase	01/01/1986 to 08/01/1986		2	3
Phase	06/12/1991 12:00 to 07/12/1991 12:00		2	3
Phase	05/05/1994 to 3/05/1994		2	3
Phase	27/12/1996 00:00 to 28/12/1996 12:00		2	3
Phase	16/12/2002 to 24/12/2002		2	3

(QC Flag: 0 = Meteorological (e.g. Seiche, Meteo-tsunami), 1 = Spike, 2 = Phase Offset, 3 = Tsunami, 4 = Other)

Analysis Comments

- Drop in tidal range in 1984. No obvious anomaly in the data.
- Very strange section of seemingly large tides in 1994.
- All but the LDTR datums are poorly resolved by the fits.

Roervik, Norway (64.867°N, 11.250°E)

Inherited:

Filename	V1 no.	Start	End	Yrs
'roervik-005-norway-mapping.mat'	**528**	01/01/1970	31/12/2008	38
'rorvik-001-glossdm-bodc.mat'	**529**	18/08/1969	31/12/2003	33

Extended:

v1 filename	'roervik-005-norway-mapping.mat (528)
v2 Filename	354_Roervik-NOR_GESLA_v2.mat
Source of Extra Data	NMA
Extra Data filename	Water level observations Roervik_2009-2013.txt
Date of Download	03/2014
End of Extra Data	23/02/2014
Load in for Extra Data	NMA
Comparison Comments	Comparisons between inherited (528) and extra data show magnitude offset of 1.253 m. This figure is confirmed by NMA after correspondence and is caused by use of different reference levels. Data file documents the data being in UTC+1 therefore the data had a time offset to give data in UTC.

Quality Control:

Type	Date Affected	Comments	QC Flag	GESLA Flag
		No erroneous values to remove		

(QC Flag: 0 = Meteorological (e.g. Seiche, Meteo-tsunami), 1 = Spike, 2 = Phase Offset, 3 = Tsunami, 4 = Other)

Analysis Comments

- Peak residual on 02/11/1971 looks real.

Saint John, Canada (NB) (45.251°N, 66.063°W)

Inherited:

Filename	V1 no.	Start	End	Yrs
'saintjohn,nb-00065-canada-meds.mat'	**534**	01/06/1905	05/10/2008	81

Extended:

v1 filename	'saintjohn,nb-00065-canada-meds.mat (534)
v2 Filename	358_SaintJohn,NB-CAN_GESLA_v2.mat
Source of Extra Data	MEDS
Extra Data filename	65_01-JAN-2008_slev.csv
Date of Download	12/05/2014
End of Extra Data	31/12/2013
Load in for Extra Data	MEDS
Comparison Comments	Comparisons between inherited (534) and extra data show offset are perfect, if a -8hr offset is applied. Since the extra data were downloaded in UTC, a correction of +8hr is applied to the data after concatenation. An error occurred when combining the two datasets, so after good comparisons were checked the overlapping section of the extra data was removed and the extra data was then appended on to the inherited data.

Quality Control:

Type	Date Affected	Comments	QC Flag	GESLA Flag
Phase	10/10/1909 to 19/10/1909		2	3
Phase	15/10/1910 to 18/10/1910		2	3
Phase	11/02/1929 16:00 to 12/02/1929 00:00		2	3
Phase	12/02/1929 16:00 to 13/02/1929 00:00		2	3
Phase	13/02/1929 16:00 to 14/02/1929 00:00		2	3
Phase	14/02/1929 16:00 to 15/02/1929 00:00		2	3
Phase	15/02/1929 16:00 to 16/02/1929 00:00		2	3
Phase	12/05/1948 to 27/05/1948		2	3
Phase	12/06/1948 to 22/06/1948		2	3
Phase	23/02/1950 to 01/03/1950		2	3
Phase	17/03/1950 to 24/03/1950		2	3
Phase	05/04/1950 22:00 to 06/04/1950 12:00		2	3
Spike	26/04/1950 21:00		1	3
Phase	03/06/1950 18:00 to 23:00		2	3
Phase	04/06/1950 23:00 to 05/06/1950 23:00		2	3
Phase	03/10/1950 to 10/10/1950 12:00		2	3
Spike	12/03/1951 02:00		1	3
Phase	30/06/1954 to 07/07/1954		2	3
Phase	04/10/1954 to 12/10/1954		2	3
Phase	30/01/1955 to 08/02/1955		2	3
Phase	22/05/1955 to 24/05/1955 12:00		2	3
Phase	31/05/1956 03:00 to 21:00		2	3
Phase	21/12/1956 to 28/12/1956		2	3
Phase	20/07/1957 to 29/07/1957		2	3
Phase	05/10/1959 06:00 to 07/10/1959 08:00		2	3
Phase	25/04/1960 to 03/05/1960		2	3
Phase	13/02/1961 to 15/02/1961 12:00		2	3
Spike	03/05/1963 20:00		1	3
Phase	28/06/1963 to 07/07/1963		2	3
Phase	26/11/1969 to 01/12/1969 12:00		2	3
Phase	16/10/1970 12:00 to 19/10/1970 12:00		2	3
Phase	21/04/1971 12:00 to 22/04/1971 15:00		2	3
Other	18/07/1997 to 28/02/2000:	Missing LW	4	3

(QC Flag: 0 = Meteorological (e.g. Seiche, Meteo-tsunami), 1 = Spike, 2 = Phase Offset, 3 = Tsunami, 4 = Other)

Analysis Comments

- Data between 06/1998 and 01/2000 does not have valid LW captured and therefore will probably have to remove data during this period.

Saipan, North Mariana Islands (15.227°N, 145.742°E)

Inherited:

Filename	V1 no.	Start	End	Yrs
'saipan,northmarianaisland-001-glossdm-bodc.mat'	**535**	19/09/1978	31/12/1998	18
'saipan_b-028b-n._mariana_islands-uhslc.mat'	**536**	19/09/1978	31/08/2003	22

Extended:

v1 filename	'saipan_b-028b-n._mariana_islands-uhslc.mat (536)
v2 Filename	359_Saipan-MNP_GESLA_v2.mat
Source of Extra Data	UHSLC
Extra Data filename	h028a
Date of Download	12/05/2014
End of Extra Data	03/04/2012
Load in for Extra Data	UHSLC
Comparison Comments	Comparisons are perfect

Quality Control:

Type	Date Affected	Comments	QC Flag	GESLA Flag
		No erroneous values to remove		

(QC Flag: 0 = Meteorological (e.g. Seiche, Meteo-tsunami), 1 = Spike, 2 = Phase Offset, 3 = Tsunami, 4 = Other)

Analysis Comments

- Peak residual on 25/10/1994, associated with Typhoon Wilda.
- Peak sea level on 03/12/1986, caused by Typhoon Kim. May have been largest residual but gap just before means MSL is not calculated during storm, but rough estimate is almost 1.2 m surge.
- Valid events in 1991 and 1997.

San Diego, USA (32.713°N, 117.173°W)

Inherited:

Filename	V1 no.	Start	End	Yrs
san_diego-569a-usa-uhslc.mat'	**542**	21/01/1906	31/12/2005	98
sandiego,california-001-glossdm-bodc.mat'	**543**	21/01/1906	31/12/2000	42
sandiego-009-usa-johnhunter.mat'	**544**	21/01/1906	28/02/2006	52

Extended:

v1 filename	san_diego-569a-usa-uhslc.mat (542)
v2 Filename	364_SanDiego-USA_GESLA_v2.mat
Source of Extra Data	UHSLC/NOAA
Extra Data filename	H569a / COOPS_SanDiego
Date of Download	11/11/2013 & 25/03/2014
End of Extra Data	31/12/2012
Load in for Extra Data	UHSLC/NOAA
Comparison Comments	Comparisons are perfect

Quality Control:

Type	Date Affected	Comments	QC Flag	GESLA Flag
Phase	08/07/1907 10:00 to 22:00		2	3
Phase	29/12/1908 03:00 to 30/12/1908 06:00		2	3
Phase	1919	Regularly all year	2	3
Datum	Pre-1926		4	3
Phase	01/09/1931 to 01/12/1931		2	3
Phase	10/01/1933 t0 01/06/1933		2	3
Tsunami	05/11/1952 to 10/11/1952	Kuril Islands	3	6
Tsunami	23/05/1960 to 30/05/1960	Valdivia	3	6
Tsunami	28/03/1964 to 02/04/1964	Alaska	3	6
Other	18/12/1968 to 24/12/1968	Large tides	2	6
Phase	14/02/1973 to 17/02/1973		2	3
Phase	11/07/1975 to 15/07/1975		2	3
Phase	21/09/1975 to 02/11/1975		2	3
Tsunami	28/02/2010 to 03/03/2010	Chile	3	6
Tsunami	11/03/2011 12:00 to 18/03/2011	Tohuku	3	6

(QC Flag: 0 = Meteorological (e.g. Seiche, Meteo-tsunami), 1 = Spike, 2 = Phase Offset, 3 = Tsunami, 4 = Other)

Analysis Comments

- There appears to be a jump in the data around 1926. This is documented on the UHSLC station info. as being a change of instrument, and something that has been corrected for. Changes in magnitude and phase of tide suggest that affects have not been removed and therefore the data pre-1926 will be removed from analysis
- .

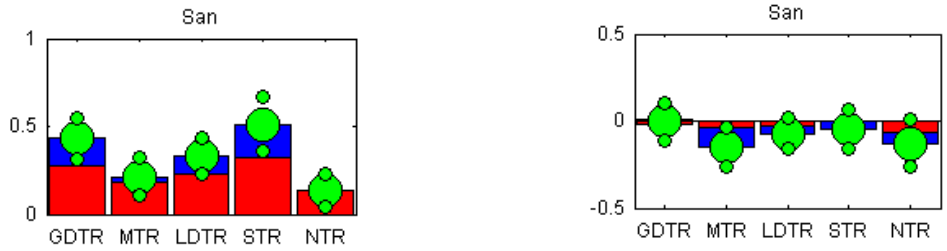

Above are the trends calculated with (left) and without (right) data before 1926, which were deemed invalid in final processing. Trends are reversed and become non-significant except for MTR, which becomes a significant negative trend.

- Peak residual on 21/01/2009 occurs at neap tides.

San Francisco, USA (CA) (37.807°N, 122.465°W)

Inherited:

Filename	V1 no.	Start	End	Yrs
'san_francisco-551a-usa-uhslc.mat'	**544**	01/01/1901	31/12/2004	104
'sanfrancisco,usa-001-glossdm-bodc.mat'	**553**	01/01/1901	31/12/1944	44
'sanfrancisco-010-usa-johnhunter.mat'	**554**	01/01/1901	28/02/2006	105

Extended:

v1 filename	N/A
v2 Filename	366_SanFrancisco-USA_GESLA_v2.mat
Source of Extra Data	UHSLC/NOAA
Extra Data filename	G551a/COOPS_SanFrancisco
Date of Download	12/05/2014
End of Extra Data	31/12/2012
Load in for Extra Data	UHSLC/NOAA
Comparison Comments	Comparisons are perfect. However, data on the UHSLC now goes back to 1897 and given the perfect comparison only the extra (newly downloaded data) is used for this dataset.

Quality Control:

Type	Date Affected	Comments	QC Flag	GESLA Flag
Phase	08/09/1904 to 26/09/1904		2	3
Phase	02/10/1904 to 20/10/1904		2	3
Phase	04/09/1905 to 09/09/1905		2	3
Phase	24/06/1922 04:00 to 18:00		2	3
Phase	25/06/1922 04:00 to 18:00		2	3
Phase	26/06/1922 04:00 to 18:00		2	3
Phase	27/06/1922 04:00 to 18:00		2	3
Phase	28/06/1922 04:00 to 18:00		2	3
Phase	17/10/1926 10:00 to 18/10/1926 12:00		2	3
Phase	08/12/1926 to 16/12/1926		2	3
Phase	22/04/1928 to 02/05/1928		2	3
Phase	24/06/1928 to 26/06/1928		2	3
Phase	23/01/1929 12:00 to 26/01/1929 12:00		2	3
Phase	29/06/1947 06:00 to 30/06/1947 09:00		2	3
Tsunami	23/05/1960 to 27/05/1960	Chile	3	6
Tsunami	28/03/1964 to 01/04/1964	Alaska	3	6
Phase	18/02/1967 to 18/03/1967		2	3
Phase	30/12/1971 to 01/01/1972		2	3
Phase	28/02/1972 00:00 to 23:00		2	3
Phase	28/03/1979 to 28/04/1979		2	3
Phase	03/09/1985 to 07/09/1985		2	3
Phase	19/05/1987 18:00 to 21/05/1987 06:00		2	3
Phase	30/05/1987 to 03/06/1987		2	3
Phase	27/07/1989 00:00 to 23:00		2	3
Phase	02/08/1989 06:00 to 18:00		2	3

(QC Flag: 0 = Meteorological (e.g. Seiche, Meteo-tsunami), 1 = Spike, 2 = Phase Offset, 3 = Tsunami, 4 = Other)

San Juan, USA (Puerto Rico) (18.460°N, 66.117°W)

Inherited:

Filename	V1 no.	Start	End	Yrs
'san_juan,pr-245a-usa-uhslc.mat'	**546**	01/01/1985	31/12/2005	20
'sanjuan,puertorico,usa-001-glossdm-bodc.mat'	**555**	01/01/1985	31/12/2000	15

Extended:

v1 filename	N/A
v2 Filename	368_SanJuan-USA_GESLA_v2.mat
Source of Extra Data	UHSLC/NOAA
Extra Data filename	H245a/COOPS_SanJuan
Date of Download	12/05/2014
End of Extra Data	31/12/2013
Load in for Extra Data	UHSLC/NOAA
Comparison Comments	Comparisons are perfect. Data on the UHSLC now goes back to 1979 and given the perfect comparison only the extra (newly downloaded data) is used for this dataset.

Quality Control:

Type	Date Affected	Comments	QC Flag	GESLA Flag
		No erroneous values to remove		

(QC Flag: 0 = Meteorological (e.g. Seiche, Meteo-tsunami), 1 = Spike, 2 = Phase Offset, 3 = Tsunami, 4 = Other)

Analysis Comments

- Peak residual on 22/09/1998, caused by Hurricane Georges.
- Peak sea level on 18/09/1989 caused by Hurricane Hugo, but not seen in residual because large data gaps earlier in the year mean tides cannot be extracted.

Santa Cruz, Ecuador (0.755°S, 90.313°W)

Inherited:

Filename	V1 no.	Start	End	Yrs
'santa_cruz-030a-ecuador-uhslc.mat'	**557**	19/10/1978	31/12/2004	24
'santacruz,galapagos,ecuador-001-glossdm-bodc.mat'	**559**	19/10/1978	31/12/1998	18

Extended:

v1 filename	'santa_cruz-030a-ecuador-uhslc.mat (557)
v2 Filename	374_SantaCruz-ECU_GESLA_v2.mat
Source of Extra Data	UHSLC
Extra Data filename	H030a
Date of Download	14/05/2014
End of Extra Data	03/04/2012
Load in for Extra Data	UHSLC
Comparison Comments	Comparisons are perfect

Quality Control:

Type	Date Affected	Comments	QC Flag	GESLA Flag
Phase	12/12/1979 12:00 to 27/12/1979		2	3
Tsunami	30/07/1995 to 01/08/1995		3	6
Phase	30/12/2000 23:00		2	3
Tsunami	24/06/2001 to 29/06/2001	Peru	3	6
Tsunami	27/12/2004 to 31/12/2004	Indonesia	3	6
Tsunami	04/05/2006 to 07/05/2006	Tonga	3	6
Tsunami	16/11/2006 to 19/11/2006	Kuril Islands	3	6

(QC Flag: 0 = Meteorological (e.g. Seiche, Meteo-tsunami), 1 = Spike, 2 = Phase Offset, 3 = Tsunami, 4 = Other)

Santa Monica, USA (CA) (34.008°N, 118.500°W)

Inherited:

Filename	V1 no.	Start	End	Yrs
'santa_monica,_ca-578a-usa-uhslc.mat'	**558**	01/01/1995	31/12/2005	10

Extended:

v1 filename	N/A
v2 Filename	375_SantaMonica-USA_GESLA_v2.mat
Source of Extra Data	UHSLC/NOAA
Extra Data filename	H578a/COOPS_SantaMonica
Date of Download	14/05/2014
End of Extra Data	31/12/2013
Load in for Extra Data	UHSLC/NOAA
Comparison Comments	Comparisons are perfect, but only the extra data is used because the data on UHSLC now goes back to 1973.

Quality Control:

Type	Date Affected	Comments	QC Flag	GESLA Flag
Datum	18/07/1980 to 26/08/1980		4	3
Tsunami	02/06/1985 to 09/06/1985	Antofagasta	3	6
Tsunami	27/02/2010 12:00 to 03/03/2010	Chile	3	6
Tsunami	11/03/2011 12:00 to 18/03/2011	Tohuku	3	6

(QC Flag: 0 = Meteorological (e.g. Seiche, Meteo-tsunami), 1 = Spike, 2 = Phase Offset, 3 = Tsunami, 4 = Other)

Analysis Comments

- Data is noisy until 1995, when instrument noise reduces.

Seattle, USA (47.600°N, 122.333°W)

Inherited:

Filename	V1 no.	Start	End	Yrs
seattle-011-usa-johnhunter.txt	**560**	01/01/1901	28/02/2006	105

Extended:

v1 filename	seattle-011-usa-johnhunter.txt (560)
v2 Filename	376_Seattle-USA_GESLA_v2.mat
Source of Extra Data	NOAA
Extra Data filename	560_NOAA_Seattle
Date of Download	06/04/2013
End of Extra Data	31/12/2012
Load in for Extra Data	NOAA
Comparison Comments	Comparisons are perfect

Quality Control:

Type	Date Affected	Comments	QC Flag	GESLA Flag
Spike	07/04/1902 15:00		1	3
Spike	14/05/1902 03:00		1	3
Phase	23/06/1902 12:00 to 24/06/1902 06:00		2	3
Spike	30/10/1902 04:00		1	3
Phase	26/10/1903 to 28/10/1903		2	3
Phase	22/08/1906 18:00 to 23/08/1906 12:00		2	3
Phase	30/12/1907 21:00 to 31/12/1907 21:00		2	3
Phase	07/07/1910 12:00 to 08/07/1910 06:00		2	3
Spike	12/08/1912 18:00		1	3
Spike	26/11/1912 09:00		1	3
Spike	27/11/1912 07:00		1	3
Spike	02/09/1916 17:00		1	3
Spike	24/10/1922 06:00		1	3
Phase	26/10/1922 09:00 to 21:00		2	3
Spike	02/02/1923 08:00		1	3
Phase	11/03/1923 to 12/03/1923 12:00		2	3
Phase	17/05/1923 12:00 to 23:00		2	3
Phase	10/01/1925 to 11/01/1925 15:00		2	3
Phase	07/06/1926 08:00 to 23:00		2	3
Phase	18/07/1926 to 19/07/1926 12:00		2	3
Phase	28/08/1927 to 30/08/1923		2	3
Spike	22/02/1928 11:00		1	3
Phase	23/03/1930 18:00 to 24/03/1930 18:00		2	3
Phase	18/04/1930 to 19/04/1930 06:00		2	3
Phase	13/06/1930 to 18/06/1930		2	3
Phase	12/10/1930 to 13/10/1930 06:00		2	3
Phase	25/10/1930 12:00 to 27/10/1930		2	3
Phase	03/02/1931 to 05/02/1931		2	3
Spike	15/12/1933 07:00		1	3
Phase	28/12/1933 to 03/01/1934		2	3
Spike	16/01/1934 03:00		1	3
Spike	05/05/1934 03:00		1	3
Phase	11/06/1934 06:00 to 21:00		2	3
Spike	21/08/1935 16:00		1	3
Spike	25/10/1935 03:00		1	3
Phase	01/07/1937 15:00 to 02/07/1937 12:00		2	3
Phase	28/12/1956 00:00 to 12:00		2	3
Spike	09/05/1957 05:00		1	3
Spike	20/05/1957 02:00		1	3
Spike	30/05/1957 15:00		1	3
Spike	28/07/1957 23:00		1	3
Phase	20/05/1959 18:00 to 23:00		1	3
Phase	20/05/1959 00:00 to 07:00		2	3
Phase	30/01/1960 06:00 to 31/01/1960 12:00		2	3
Spike	29/05/1961 21:00		1	3
Phase	06/03/1962 00:00 to 15:00		2	3
Phase	24/01/1964 04:00 to 08:00		2	3
Spike	19/01/1966 01:00		1	3
Spike	22/02/1966 19:00		1	3
Spike	28/03/1966 01:00		1	3
Datum	01/05/1966 to 07/05/1966		4	3
Phase	28/10/1970 18:00 to 03/11/1970		2	3
Phase	25/03/1976 15:00 to 30/03/1976		2	3
Phase	03/04/1980 17:00 to 20:00		2	3
Phase	23/04/1980 09:00 to 23:00		2	3
Phase	09/09/1983 15:00 to 15/03/1983		2	3
Phase	23/09/1983 18:00 to 26/09/1983		2	3
Phase	01/09/1987 00:00 to 23:00		2	3
Phase	31/12/1995 12:00 to 23:00		2	3

(QC Flag: 0 = Meteorological (e.g. Seiche, Meteo-tsunami), 1 = Spike, 2 = Phase Offset, 3 = Tsunami, 4 = Other)

Seldovia, USA (Alaska) (59.440°N, 151.720°W)

Inherited:

Filename	V1 no.	Start	End	Yrs
'seldovia-561a-usa-uhslc.mat'	**562**	01/10/1979	31/12/2005	26

Extended:

v1 filename	N/A
v2 Filename	378_Seldovia-USA_GESLA_v2.mat
Source of Extra Data	UHSLC/NOAA
Extra Data filename	H561a/COOPS_Seldovia
Date of Download	14/05/2014
End of Extra Data	31/12/2013
Load in for Extra Data	UHSLC/NOAA
Comparison Comments	Comparisons are perfect, but only the extra data is used because the data on UHSLC now goes back to 1975.

Quality Control:

Type	Date Affected	Comments	QC Flag	GESLA Flag
Phase	18/01/1980 to 27/01/1980		2	3
Phase	22/12/1980 to 26/12/1980		2	3
Phase	07/09/1981 to 04/10/1981		2	3
Phase	09/10/1981 to 02/11/1981		2	3
Phase	02/08/1985 to 07/08/1985		2	3
Spike	31/12/1985 23:00		1	3
Spike	31/12/1986 23:00		1	3
Spike	31/12/1987 23:00		1	3
Spike	31/12/1988 23:00		1	3
Spike	31/12/1989 23:00		1	3
Phase	02/06/2005 12:00 to 04/06/2005 06:00		2	3
Phase	09/06/2005 00:00 to 23:00		2	3
Phase	21/03/2007 to 27/03/2007 06:00		2	3
Phase	14/07/2010 to 16/07/2010		2	3
Phase	21/05/2010 to 25/07/2010		2	3
Phase	31/05/2011 06:00 to 18:00		2	3

(QC Flag: 0 = Meteorological (e.g. Seiche, Meteo-tsunami), 1 = Spike, 2 = Phase Offset, 3 = Tsunami, 4 = Other)

Seward, USA (Alaska) (60.120°N, 149.427°W)

Inherited:

Filename	V1 no.	Start	End	Yrs
'seward_c,ak-560c-usa-uhslc.mat'	**566**	01/01/1967	31/12/2005	33

Extended:

v1 filename	'seward_c,ak-560c-usa-uhslc.mat (566)
v2 Filename	380_Seward-USA_GESLA_v2.mat
Source of Extra Data	UHSLC/NOAA
Extra Data filename	H566c/COOPS_Seward
Date of Download	14/05/2014
End of Extra Data	31/12/2013
Load in for Extra Data	UHSLC/NOAA
Comparison Comments	Comparisons are perfect

Quality Control:

Type	Date Affected	Comments	QC Flag	GESLA Flag
Phase	27/06/1968 15:00 to 28/06/1968 18:00		2	3
Spike	01/05/1970 00:00		1	3
Phase	14/12/1989 to 18/12/1989		2	3
Phase	15/09/2002 to 25/09/2002		2	3

(QC Flag: 0 = Meteorological (e.g. Seiche, Meteo-tsunami), 1 = Spike, 2 = Phase Offset, 3 = Tsunami, 4 = Other)

Sheerness, UK (51.443°N, 0.750°E)

Inherited:

Filename	V1 no.	Start	End	Yrs
'sheerness-p015-uk-bodc.mat'	**568**	05/01/1952	31/12/2006	36

Extended:

v1 filename	'sheerness-p015-uk-bodc.mat (568)
v2 Filename	382_Sheerness-GBR_GESLA_v2.mat
Source of Extra Data	BODC
Extra Data filename	RN-7246_1372253428497.zip
Date of Download	26/02/2014
End of Extra Data	30/04/2013
Load in for Extra Data	BODC2
Comparison Comments	Comparisons are perfect

Quality Control:

Type	Date Affected	Comments	QC Flag	GESLA Flag
Threshold		< -0.5 & > 10	4	3
Datum	05/07/2007 to 22/07/2007		4	3
Datum	20/12/2007 to 28/12/2007		4	3
Spike	14/09/2009 02:00		1	3
Spike	19/10/2009 15:00		1	3
Spike	20/10/2009 03:00		1	3
Spike	20/10/2009 15:00		1	3
Datum	26/10/2009 18:00 to 21:00		4	3
Datum	12/11/2009 00:00 to 12:00		4	3
Datum	13/11/2009 12:00 to 23:00		4	3
Datum	28/05/2010 00:00 to 23:00		4	3
Datum	25/06/2010 to 28/06/2010		4	3
Datum	31/07/2010 06:00 to 12:00		4	3
Datum	24/08/2010 00:00 to 23:00		4	3
Datum	20/04/2011 to 23/04/2011		4	3
Datum	21/08/2011 to 29/01/2012		4	3
Spike	15/02/2012 14:00		1	3
Datum	01/01/2013 to 01/05/2013		4	3

(QC Flag: 0 = Meteorological (e.g. Seiche, Meteo-tsunami), 1 = Spike, 2 = Phase Offset, 3 = Tsunami, 4 = Other)

Simon's Town, South Africa (34.183°S, 18.433°E)

Inherited:

Filename	V1 no.	Start	End	Yrs
'simon''s_bay-221a-south_africa-uhslc.mat'	**572**	31/01/1958	30/12/1996	36
'simonstown,southafrica-001-glossdm-bodc.mat'	**573**	31/01/1958	30/12/1996	34

Extended:

v1 filename	N/A
v2 Filename	386_SimonsTown-ZAF_GESLA_v2.mat
Source of Extra Data	UHSLC
Extra Data filename	H221a
Date of Download	13/04/2013
End of Extra Data	30/12/2009
Load in for Extra Data	UHSLC
Comparison Comments	Note in on UHSLC website states that in September 2008 all data from this site was amended after a thorough calibration and correction. Therefore all data in v2 dataset has been re-downloaded from the UHSLC website and is all new. (ftp://ilikai.soest.hawaii.edu/rqds/atlantic/doc/qa221a.dmt)

Quality Control:

Type	Date Affected	Comments	QC Flag	GESLA Flag
Phase	22/11/1974 to 06/12/1974		2	3
Phase	15/11/1975 to 23/11/1975		2	3
Phase	20/06/1978 to 28/06/1978		2	3
Phase	27/07/1984 to 01/08/1984		2	3
Phase	14/02/1991 to 21/02/1991		2	3
Phase	07/04/1991 to 17/04/1991		2	3
Phase	02/05/1991 to 16/05/1991		2	3
Phase	26/05/1991 to 09/06/1991		2	3
Phase	30/06/1991 to 11/07/1991		2	3
Phase	07/12/1993 to 14/12/1993		2	3
Phase	01/02/2003 to 06/02/2003		2	3
Phase	19/07/2004 to 31/07/2004		2	3

(QC Flag: 0 = Meteorological (e.g. Seiche, Meteo-tsunami), 1 = Spike, 2 = Phase Offset, 3 = Tsunami, 4 = Other)

Analysis Comments

- Data at end 0f 1997 appears to be offset. This corresponds to a new acoustic SRD tide gauge being installed. Need to check against nearby Cape Town to determine validity of this period.

Sitka, USA (Alaska) (57.052°N, 135.342°W)

Inherited:

Filename	V1 no.	Start	End	Yrs
'sitka,ak-559a-usa-uhslc.mat'	**575**	05/01/1952	31/12/2006	36

Extended:

v1 filename	N/A
v2 Filename	388_Sitka-USA_GESLA_v2.mat
Source of Extra Data	UHSLC/NOAA
Extra Data filename	H569a/COOPS_Sitka
Date of Download	14/05/2014
End of Extra Data	31/12/2013
Load in for Extra Data	UHSLC/NOAA
Comparison Comments	Comparisons are perfect, but since the dataset on UHSLC has been extended back to 1938 only the extra (newly downloaded data is used in this analysis.

Quality Control:

Type	Date Affected	Comments	QC Flag	GESLA Flag
Tsunami	23/05/1960 to 28/05/1960	Valdivia	3	6
Tsunami	28/03/1964 to 31/03/1964	Alaskan	3	6
Spike	01/01/1987 00:00		1	3
Spike	01/01/1991 00:00		1	3
Spike	01/01/1992 00:00		1	3
Tsunami	11/03/2011 12:00 to 15/03/2011	Tohuku	3	6

(QC Flag: 0 = Meteorological (e.g. Seiche, Meteo-tsunami), 1 = Spike, 2 = Phase Offset, 3 = Tsunami, 4 = Other)

Socoa, France (43.400°N, 1.683°W)

Inherited:

Filename	V1 no.	Start	End	Yrs
'socoa-soc-france-shom.mat'	**577**	20/11/1942	10/01/2008	36

Extended:

v1 filename	'socoa-soc-france-shom.mat (577)
v2 Filename	390_Socoa-FRA_GESLA_v2.mat
Source of Extra Data	N/A
Extra Data filename	N/A
Date of Download	N/A
End of Extra Data	N/A
Load in for Extra Data	N/A
Comparison Comments	No extra data available

Quality Control:

Type	Date Affected	Comments	QC Flag	GESLA Flag
Phase	02/11/1967 to 08/11/1967		2	3
Phase	28/11/1967 to 05/12/1967		2	3
Phase	14/10/1970 to 21/10/1970		2	3
Phase	29/10/1970 09:00 to 18:00		2	3
Spike	05/01/1971 10:00		1	3
Phase	06/04/1974 00:00 to 18:00		2	3
Phase	06/06/1974 00:00 to 15:00		2	3
Phase	03/12/1974 09:00 to 23:00		2	3
Phase	23/06/1979 00:00 to 23:00		2	3
Phase	08/02/2005 to 12/02/2005		2	3

(QC Flag: 0 = Meteorological (e.g. Seiche, Meteo-tsunami), 1 = Spike, 2 = Phase Offset, 3 = Tsunami, 4 = Other)

Analysis Comments

- Many invalid values removed by applying a threshold of >6 m.

South Beach, USA (Oregon) (44.625°N, 124.043°W)

Inherited:

Filename	V1 no.	Start	End	Yrs
'south_beach,or-592a-usa-uhslc.mat'	**578**	01/02/1967	31/12/2005	39

Extended:

v1 filename	'south_beach,or-592a-usa-uhslc.mat (578)
v2 Filename	391_SouthBeach-USA_GESLA_v2.mat
Source of Extra Data	UHSLC/NOAA
Extra Data filename	H592a/COOPS_SouthBeach
Date of Download	14/05/2014
End of Extra Data	31/12/2013
Load in for Extra Data	UHSLC/NOAA
Comparison Comments	Comparisons are perfect

Quality Control:

Type	Date Affected	Comments	QC Flag	GESLA Flag
Phase	23/07/1967 15:00 to 24/07/1967 15:00		2	3
Phase	11/12/1970 00:00 to 08:00		2	3
Phase	20/07/1974 to 28/07/1974		2	3
Phase	10/10/1976 01:00		2	3
Phase	06/09/1980 06:00 to 18:00		2	3
Phase	07/09/1980 06:00 to 18:00		2	3
Phase	23/09/1980 09:00 to 24/09/1980 18:00		2	3
Phase	27/09/1980 09:00 to 21:00		2	3
Phase	01/10/1980 12:00 to 23:00		2	3
Phase	03/10/1980 12:00 to 23:00		2	3
Phase	04/10/1980 12:00 to 05/10/1980 03:00		2	3
Phase	07/10/1980 18:00 to 23:00		2	3
Phase	08/10/1980 06:00 to 15:00		2	3
Tsunami	11/03/2011 to 15/03/2011	Tohuku	3	6

(QC Flag: 0 = Meteorological (e.g. Seiche, Meteo-tsunami), 1 = Spike, 2 = Phase Offset, 3 = Tsunami, 4 = Other)

Analysis Comments

- Peak residual on 03/10/1967, caused by … ?
- Noisy period from 1967 to 1971 appears valid.

Spring Bay, Australia (42.550°S, 147.933°E)

Inherited:

Filename	V1 no.	Start	End	Yrs
'spring_bay-335a-australia-uhslc.mat'	**582**	12/04/1985	31/12/2006	20
'springbay,australia-001-glossdm-bodc.mat'	**583**	01/01/1991	31/12/2001	11

Extended:

v1 filename	'spring_bay-335a-australia-uhslc.mat (582)
v2 Filename	394_SpringBay-AUS_GESLA_v2.mat
Source of Extra Data	UHSLC/BOM
Extra Data filename	H335a/ SpringBay_BOM_2012-13
Date of Download	14/05/2014
End of Extra Data	31/12/2013
Load in for Extra Data	UHSLC/BOM
Comparison Comments	Comparisons are perfect

Quality Control:

Type	Date Affected	Comments	QC Flag	GESLA Flag
		No erroneous values to remove		

(QC Flag: 0 = Meteorological (e.g. Seiche, Meteo-tsunami), 1 = Spike, 2 = Phase Offset, 3 = Tsunami, 4 = Other)

St. Johns, Canada (NF) (47.467°N, 52.717°W)

Inherited:

Filename	V1 no.	Start	End	Yrs
'st._john''s_a-276a-canada-uhslc.mat'	**586**	01/11/1961	31/05/1993	30
'st.johns,canada-001-glossdm-bodc.mat'	**589**	01/11/1961	31/12/2001	39
'st.johns,nf-00905-canada-meds.mat'	**590**	02/08/1935	31/10/2008	50

Extended:

v1 filename	'st.johns,nf-00905-canada-meds.mat (590)
v2 Filename	397_StJohns,NF-CAN_GESLA_v2.mat
Source of Extra Data	MEDS
Extra Data filename	905_01-JAN-2008_slev.csv
Date of Download	19/05/2014
End of Extra Data	31/12/2013
Load in for Extra Data	MEDS
Comparison Comments	Comparisons between inherited and extra data are perfect if a time offset of -7hrs is applied to the data. Since the data were downloaded in UTC, +7hrs is applied to all data after concatenation to return data to UTC.

Quality Control:

Type	Date Affected	Comments	QC Flag	GESLA Flag
Phase	18/06/1961 to 25/06/1961		2	3
Phase	01/09/1974 to 10/09/1974		2	3
Phase	28/10/1974 to 04/11/1974		2	3
Phase	15/11/1974 00:00 to 23:00		2	3

(QC Flag: 0 = Meteorological (e.g. Seiche, Meteo-tsunami), 1 = Spike, 2 = Phase Offset, 3 = Tsunami, 4 = Other)

St. Petersburg, USA (Florida) (27.760°N, 82.627°W)

Inherited:

Filename	V1 no.	Start	End	Yrs
'st._petersburg,_fl-759a-usa-uhslc.mat'	**587**	18/12/1946	31/12/2005	56

Extended:

v1 filename	'st._petersburg,_fl-759a-usa-uhslc.mat (587)
v2 Filename	398_StPetersburg-USA_GESLA_v2.mat
Source of Extra Data	UHSLC/NOAA
Extra Data filename	H759a/COOPS_StPetersburg
Date of Download	19/05/2014
End of Extra Data	31/12/2013
Load in for Extra Data	UHSLC/NOAA
Comparison Comments	Comparisons are perfect

Quality Control:

Type	Date Affected	Comments	QC Flag	GESLA Flag
		No erroneous values to remove		

(QC Flag: 0 = Meteorological (e.g. Seiche, Meteo-tsunami), 1 = Spike, 2 = Phase Offset, 3 = Tsunami, 4 = Other)

Analysis Comments

- Large residual on 19/06/1972 preceding a gap in the data caused by Hurricane Agnes.
- Peak residual on 13/03/1993, caused by Storm of Century.
- Peak sea level on 31/08/1985 caused by Hurricane Elena.

Stornoway, UK (58.208°N, 6.388°W)

Inherited:

Filename	V1 no.	Start	End	Yrs
stornoway-001-glossdm-bodc.mat'	**595**	01/01/1976	31/12/1991	11
stornoway-295a-united_kingdom-uhslc.mat'	**596**	01/01/1976	31/12/2001	21
stornoway-p042-uk-bodc.mat'	**597**	05/01/1976	31/12/2006	26

Extended:

v1 filename	stornoway-p042-uk-bodc.mat (597)
v2 Filename	413_Stornoway-GBR_GESLA_v2.mat
Source of Extra Data	BODC
Extra Data filename	RN-7246_1372253428497.zip
Date of Download	26/02/2014
End of Extra Data	31/12/2012
Load in for Extra Data	BODC2
Comparison Comments	Comparisons are perfect

Quality Control:

Type	Date Affected	Comments	QC Flag	GESLA Flag
Phase	10/09/2007 12:00 to 10/09/2007 17:00		2	3
Phase	29/01/2008 02:00 to 21/05/2008 17:00		2	3

Phase	15/02/2011 21:00 to 22/02/2011 12:00		2	3
Spike	24/08/2011 13:00		1	3
Phase	01/09/2011 18:00 to 11/03/2012 13:00		2	3

(QC Flag: 0 = Meteorological (e.g. Seiche, Meteo-tsunami), 1 = Spike, 2 = Phase Offset, 3 = Tsunami, 4 = Other)

Analysis Comments

- LW between 24-Dec-2011 to 11-Mar-2012 not captured as SL below zero not recorded.
- Outliers were removed (> 8, < -1). Before sections of data were removed.

Tauranga, New Zealand (37.650°S, 176.183°E)

Inherited:

Filename	V1 no.	Start	End	Yrs
'tauranga-073a-new_zealand-uhslc.mat'	**611**	01/08/1984	31/12/2005	17

Extended:

v1 filename	'tauranga-073a-new_zealand-uhslc.mat (611)
v2 Filename	410_Tauranga-NZL_GESLA_v2.mat
Source of Extra Data	UHSLC
Extra Data filename	H073a
Date of Download	19/05/2014
End of Extra Data	31/12/2012
Load in for Extra Data	UHSLC
Comparison Comments	Comparisons are perfect

Quality Control:

Type	Date Affected	Comments	QC Flag	GESLA Flag
Tsunami	27/02/2010 to 02/03/2010	Chile	3	6
Tsunami	11/03/2011 to 16/03/2011	Tohuku	3	6

(QC Flag: 0 = Meteorological (e.g. Seiche, Meteo-tsunami), 1 = Spike, 2 = Phase Offset, 3 = Tsunami, 4 = Other)

Analysis Comments

- Peak residual on 30/12/1996, caused by Cyclone Fergus (became ET when it reached NZ).
- Peak sea level on 23/01/2011, caused by Cyclone Wilma.

Thevenard, Australia (32.146°S, 133.653°E)

Inherited:

Filename	V1 no.	Start	End	Yrs
'thevenard-026-australia-johnhunter.mat'	**614**	01/01/1966	31/12/2004	39

Extended:

v1 filename	'thevenard-026-australia-johnhunter.mat (614)
v2 Filename	413_Thevenard-AUS_GESLA_v2.mat
Source of Extra Data	UHSLC/BOM
Extra Data filename	H128a/ Thevenard_BOM_2012-13
Date of Download	19/05/2014
End of Extra Data	31/12/2013
Load in for Extra Data	UHSLC/BOM
Comparison Comments	Comparisons are perfect

Quality Control:

Type	Date Affected	Comments	QC Flag	GESLA Flag
Phase	29/12/1986 00:00 to 23:00		2	3

(QC Flag: 0 = Meteorological (e.g. Seiche, Meteo-tsunami), 1 = Spike, 2 = Phase Offset, 3 = Tsunami, 4 = Other)

Analysis Comments

- Peak sea level on 14/08/1990, probably caused by an ET storm.

Tofino, Canada (BC) (49.154°N, 125.913°W)

Inherited:

Filename	V1 no.	Start	End	Yrs
'tofino,bc-08615-canada-meds.mat'	**616**	01/10/1909	30/09/2008	67
'tofino,canada-001-glossdm-bodc.mat'	**617**	01/01/1963	31/12/1999	32
'tofino-542a-canada-uhslc.mat'	**618**	01/01/1963	31/12/1999	32

Extended:

v1 filename	'tofino,bc-08615-canada-meds.mat (616)
v2 Filename	415_Tofino-CAN_GESLA_v2.mat
Source of Extra Data	MEDS
Extra Data filename	8615_01-JAN-2008_slev.csv
Date of Download	20/05/2014
End of Extra Data	31/12/2013
Load in for Extra Data	MEDS
Comparison Comments	Comparisons between inherited and extra data show time offset of -16 hrs The extra data is shifted to combine with the inherited data initially, but because the extra data was downloaded in UTC time stamp then we apply a correction of +16 hrs to the whole dataset to return all data to UTC.

Quality Control:

Type	Date Affected	Comments	QC Flag	GESLA Flag
Phase	28/11/1947 18:00 to 04/12/1987		2	3
Tsunami	11/03/2011 to 15/03/2011	Tohuku	3	6

(QC Flag: 0 = Meteorological (e.g. Seiche, Meteo-tsunami), 1 = Spike, 2 = Phase Offset, 3 = Tsunami, 4 = Other)

Analysis Comments

- residual on 29/12/1952, probably ET storm, but not documented online.

Townsville, Australia (19.258°S, 146.818°E)

Inherited:

Filename	V1 no.	Start	End	Yrs
'townsville,australia-001-glossdm-bodc.mat'	**620**	01/01/1985	31/12/1998	14
'townsville-025-australia-johnhunter.mat'	**621**	04/01/1959	31/12/2004	46
'townsville-334a-australia-uhslc.mat'	**622**	01/01/1984	31/12/2006	23

Extended:

v1 filename	'townsville-025-australia-johnhunter.mat (621)
v2 Filename	417_Townsville-AUS_GESLA_v2.mat
Source of Extra Data	UHSLC
Extra Data filename	H334a
Date of Download	20/05/2014
End of Extra Data	31/12/2012
Load in for Extra Data	UHSLC
Comparison Comments	Comparisons are perfect

Quality Control:

Type	Date Affected	Comments	QC Flag	GESLA Flag
Phase	27/04/1959 to 29/04/1959		2	3
Phase	31/08/1959 to 04/09/1959		2	3
Spike	04/01/1960 02:00		1	3
Spike	05/01/1960 02:00		1	3
Spike	09/01/1960 03:00		1	3
Spike	24/01/1960 17:00		1	3
Spike	21/02/1960 03:00		1	3
Spike	18/03/1960 12:00		1	3
Spike	19/05/1960 21:00		1	3
Spike	11/06/1960 11:00		1	3
Spike	10/08/1960 05:00		1	3
Spike	14/08/1960 12:00		1	3
Spike	14/08/1960 22:00		2	3
Phase	17/08/1960 00:00 to 03:00		2	3
Phase	29/08/1960 21:00 to 23:00		2	3
Phase	30/08/1960 21:00 to 23:00		2	3
Phase	26/09/1960 09:00 to 15:00		2	3
Phase	27/09/1960 09:00 to 15:00		2	3
Phase	30/09/1960 09:00 to 15:00		2	3
Phase	01/10/1960 09:00 to 15:00		2	3
Phase	02/10/1960 09:00 to 15:00		2	3
Phase	18/10/1960 09:00 to 15:00		2	3
Phase	19/10/1960 09:00 to 15:00		2	3
Phase	20/10/1960 09:00 to 15:00		2	3
Phase	23/10/1960 15:00 to 18:00		2	3
Phase	25/10/1960 06:00 to 15:00		2	3
Phase	01/11/1960 09:00 to 23:00		2	3
Phase	02/11/1960 09:00 to 23:00		2	3
Phase	03/11/1960 09:00 to 23:00		2	3
Spike	01/01/1961 00:00		1	3

Spike	11/01/1961 06:00		1	3
Spike	01/02/1961 03:00		1	3
Spike	04/02/1961 23:00		1	3
Spike	21/02/1961 11:00		1	3
Spike	13/04/1961 07:00		1	3
Spike	28/04/1961 19:00		1	3
Spike	29/04/1961 11:00		1	3
Phase	07/11/1961 00:00 to 18:00		2	3
Phase	06/02/1962 20:00 to 23:00		2	3
Phase	07/02/1962 20:00 to 23:00		2	3
Spike	12/02/1962 14:00		1	3
Spike	12/02/1962 21:00		1	3
Phase	14/02/1962 10:00 to 18:00		2	3
Spike	20/02/1962 02:00		1	3
Phase	11/03/1962 18:00 to 23:00		2	3
Phase	16/03/1962 21:00 to 23:00		2	3
Phase	18/03/1962 15:00 to 23:00		2	3
Spike	30/09/1962 13:00		1	3
Spike	02/10/1962 12:00		1	3
Phase	10/12/1962 to 18/12/1962		2	3
Noise	01/04/1963 to 08/04/1963		4	3
Phase	06/04/1963 18:00 to 22:00		2	3
Phase	08/05/1963 00:00 to 12:00		2	3
Phase	09/05/1963 00:00 to 12:00		2	3
Phase	10/05/1963 00:00 to 12:00		2	3
Phase	11/05/1963 00:00 to 12:00		2	3
Phase	12/05/1963 00:00 to 12:00		2	3
Phase	13/05/1963 00:00 to 12:00		2	3
Phase	14/05/1963 00:00 to 12:00		2	3
Spike	24/06/1963 13:00		1	3
Spike	05/07/1963 02:00		1	3
Spike	13/07/1963 22:00		1	3
Phase	01/10/1963 12:00 to 02/10/1963 06:00		2	3
Phase	25/11/1963 12:00 to 13:00		2	3
Phase	25/12/1963 to 29/12/1963		2	3
Phase	13/01/1964 09:00 to 23:00		2	3
Phase	14/01/1964 09:00 to 23:00		2	3
Phase	15/01/1964 09:00 to 23:00		2	3
Phase	16/01/1964 09:00 to 23:00		2	3
Noise	04/04/1964 to 10/04/1964		4	3
Phase	02/09/1964 to 06/09/1964		2	3
Phase	02/10/1964 to 12/10/1964		2	3
Phase	14/01/1965 to 29/01/1965		2	3
Spike	08/10/1967 22:00		1	3
Phase	16/10/1967 to 23/10/1967		2	3
Phase	09/11/1967 12:00 to 10/11/1967 06:00		2	3
Phase	07/12/1967 21:00 to 08/12/1967 15:00		2	3
Phase	18/12/1967 12:00 to 19/12/1967 12:00		2	3
Phase	21/12/1967 to 27/12/1967		2	3
Spike	10/07/1971 00:00		2	3
Phase	25/05/1972 12:00 to 26/05/1972		2	3
Phase	02/11/1976 12:00 to 03/11/1976 12:00		2	3
Spike	21/12/1976 18:00		1	3
Phase	02/09/1980 to 08/09/1980		2	3
Phase	21/09/1980 to 29/09/1980		2	3
Phase	06/08/1985 06:00 to 12:00		2	3

(QC Flag: 0 = Meteorological (e.g. Seiche, Meteo-tsunami), 1 = Spike, 2 = Phase Offset, 3 = Tsunami, 4 = Other)

Analysis Comments

- Peak sea level and residual occur on 24/12/1971, caused by Cyclone Althea.
- Another peak sea level occurred on 03/02/2011, caused by Cyclone Yasi

Toyama, Japan (36.767°N, 137.217°E)

Inherited:

Filename	V1 no.	Start	End	Yrs
'toyama,japan-001-glossdm-bodc.mat'	**623**	01/01/2001	31/12/2003	3
'toyama-349a-japan-uhslc.mat'	**624**	30/04/1967	31/12/2005	38

Extended:

v1 filename	'toyama-349a-japan-uhslc.mat (624)
v2 Filename	418_Toyama-JPN_GESLA_v2.mat
Source of Extra Data	UHSLC
Extra Data filename	H349a
Date of Download	20/05/2014
End of Extra Data	31/12/2012
Load in for Extra Data	UHSLC
Comparison Comments	Comparisons are perfect

Quality Control:

Type	Date Affected	Comments	QC Flag	GESLA Flag
Phase	12/08/1970 to 05/10/1970		2	3
Phase	20/08/2004 to 24/09/2004		2	3
Phase	04/09/2005 to 18/09/2005		2	3

(QC Flag: 0 = Meteorological (e.g. Seiche, Meteo-tsunami), 1 = Spike, 2 = Phase Offset, 3 = Tsunami, 4 = Other)

Analysis Comments

- Small tides may be an issue.
- Large seasonal cycle (approx.. 0.4 m, with peak in Summer)

Trieste, Italy (45.650°N, 13.750°E)

Inherited:

Filename	V1 no.	Start	End	Yrs
'trieste-270061-italy-itt.mat'	**627**	01/01/1971	31/12/2006	36

Extended:

v1 filename	'trieste-270061-italy-itt.mat (627)
v2 Filename	420_Trieste-ITA_GESLA_v2.mat
Source of Extra Data	N/A
Extra Data filename	N/A
Date of Download	N/A
End of Extra Data	N/A
Load in for Extra Data	N/A
Comparison Comments	No extra data available

Quality Control:

Type	Date Affected	Comments	QC Flag	GESLA Flag
		No erroneous values to remove		

(QC Flag: 0 = Meteorological (e.g. Seiche, Meteo-tsunami), 1 = Spike, 2 = Phase Offset, 3 = Tsunami, 4 = Other)

Analysis Comments

- Events identified as possible phase offsets appear to coincide with documented 'aqua alta' in Venice caused when high tides are added to by a seiching affect caused by wind conditions in the Adriatic.
- Peak sea level on 22/12/1979 coincides with 2nd highest modern 'aqua alta' in Venice.
- Small tides may be an issue.

Tumaco, Colombia (1.833°N, 78.733°W)

Inherited:

Filename	V1 no.	Start	End	Yrs
tumaco-303a-colombia-uhslc.txt	**629**	01/11/1951	31/12/2000	39

Extended:

v1 filename	N/A
v2 Filename	421_Tumaco-COL_GESLA_v2.mat
Source of Extra Data	UHSLC
Extra Data filename	H303a
Date of Download	09/08/2013
End of Extra Data	31/12/2012
Load in for Extra Data	UHSLC
Comparison Comments	Data comparison of inherited and extra shows datum offset. This is explained in station info on UHSLC website (ftp://ilikai.soest.hawaii.edu/rqds/pacific/doc/qa303a.dmt). All data were calibrated and corrected with the whole dataset replaced in May 2013.

Quality Control:

Type	Date Affected	Comments	QC Flag	GESLA Flag
Phase	13/07/1955 to 27/07/1955		2	3
Phase	06/08/1955 to 12/08/1955		2	3
Phase	26/08/1955 to 06/09/1955		2	3
Phase	16/09/1955 to 22/09/1955		2	3
Phase	27/11/1955 to 03/03/1956		2	3
Phase	15/03/1956 06:00 to 15:00		2	3
Phase	16/03/1956 06:00 to 15:00		2	3
Phase	16/03/1956 15:00 to 21:00		2	3
Phase	26/04/1956 00:00 to 12:00		2	3
Phase	22/06/1956 06:00 to 15:00		2	3
Phase	14/07/1956 00:00 to 09:00		2	3
Phase	06/06/1960 to 18/06/1960		2	3
Phase	11/08/1960 12:00 to 13/08/1960		2	3
Noise	26/08/1961 to 30/09/1961		4	3
Spike	16/07/1965 17:00		1	3
Spike	21/07/1965 21:00		1	3
Spike	31/07/1965 16:00		1	3
Phase	12/08/1965 00:00 to 06:00		2	3
Other	06/09/1965 06:00 to 07/09/1965 09:00		2	3
Phase	14/11/1965 to 31/12/1965 23:00		2	3
Phase	11/08/1966 12:00 to 12/08/1966 06:00		2	3
Phase	06/11/1966 03:00 to 07/11/1966 06:00		2	3
Phase	24/10/1967 03:00 to 25/10/1967 06:00		2	3
Phase	25/11/1967 to 03/12/1967		2	3
Phase	23/12/1967 to 08/02/1968		2	3
Phase	17/02/1968 09:00 to 15:00		2	3
Phase	11/03/1968 to 24/03/1968		2	3
Phase	24/07/1968 03:00 to 26/07/1968 06:00		2	3
Phase	22/08/1969 03:00 to 15:00		2	3
Phase	31/08/1969 15:00 to 01/09/1969 09:00		2	3
Phase	25/09/1969 to 04/10/1969		2	3
Phase	23/10/1969 08:00 to 24/10/1969 08:00		2	3
Phase	09/12/1969 to 31/12/1969 23:00		2	3
Phase	15/09/1970 to 18/10/1970		2	3
Phase	01/11/1970 to 05/11/1970		2	3
Phase	05/04/1973 03:00 to 08/04/1973 06:00		2	3
Phase	10/05/1973 09:00 to 11/05/1973 06:00		2	3
Phase	20/05/1973 to 21/05/1973 12:00		2	3
Phase	25/06/1973 to 28/06/1973		2	3
Phase	18/07/1973 to 02/08/1973		2	3
Phase	21/08/1973 00:00 to 09:00		2	3
Phase	24/09/1973 to 26/09/1973		2	3
Phase	04/12/1973 03:00 to 05/12/1973 06:00		2	3
Phase	08/12/1973 to 16/12/1973		2	3
Phase	23/03/1974 to 11/04/1974		2	3
Phase	18/06/1974 to 24/06/1974		2	3
Phase	05/08/1974 to 07/08/1974 06:00		2	3
Phase	21/09/1974 to 24/09/1974		2	3
Phase	14/11/1974 to 17/11/1974		2	3
Phase	16/09/1975 03:00 to 17/09/1975 06:00		2	3
Phase	27/07/1976 to 03/08/1976		2	3
Phase	26/08/1976 to 02/09/1976		2	3
Phase	13/11/1976 15:00 to 15/11/1976		2	3
Phase	17/07/1979 06:00 to 18:00		2	3
Phase	22/07/1979 12:00 to 23/07/1979 06:00		2	3
Phase	01/09/1979 00:00 to 23:00		2	3
Phase	08/01/1981 to 22/01/1981		2	3
Phase	05/03/1981 to 14/03/1981		2	3
Phase	19/07/1981 to 02/08/1981		2	3
Phase	28/08/1981 to 03/09/1981		2	3
Phase	24/09/1981 to 07/10/1981		2	3
Phase	25/10/1981 to 02/11/1981		2	3
Phase	21/05/1982 to 02/06/1982		2	3
Phase	08/07/1982 18:00 to 20/07/1982		2	3
Phase	07/08/1982 09:00 to 15:00		2	3
Phase	01/01/1983 to 05/01/1983		2	3
Phase	19/12/1984 to 24/12/1984		2	3
Phase	02/12/1985 to 13/12/1985		2	3
Datum	22/07/1986 to 01/08/1986		4	3
Datum	01/10/1986 to 01/11/1986		4	3
Phase	28/12/1986 to 10/01/1987		2	3

Phase	09/06/1987 12:00 to 11/06/1987 18:00		2	3
Phase	15/06/1987 00:00 to 23:00		2	3
Phase	02/08/1987 to 23/08/1987		2	3
Phase	21/07/1988 to 28/07/1988		2	3
Phase	23/04/1993 to 29/04/1993		2	3
Phase	01/01/1994 to 18/01/1994		2	3
Phase	01/09/1994 to 01/01/1995		2	3
Phase	20/01/1996 to 11/02/1996		2	3
Phase	23/04/1996 to 10/05/1996		2	3
Phase	01/06/1996 to 30/06/1996		2	3
Phase	01/08/1996 to 02/08/1996		2	3
Phase	23/09/1996 to 31/10/1996		2	3
Phase	12/12/1996 to 20/12/1996		2	3
Phase	08/02/1997 to 27/04/1997		2	3
Phase	20/06/1997 18:00 to 22/06/1997		2	3
Phase	02/08/1997 to 24/08/1997		2	3
Phase	13/09/1997 to 24/09/1997		2	3
Phase	11/10/1997 to 18/10/1997		2	3
Phase	04/11/1997 to 20/11/1997		2	3
Phase	14/12/1997 to 31/12/1998 23:00		2	3
Phase	01/03/1999 to 24/03/1999		2	3
Phase	14/05/1999 to 19/05/1999		2	3
Phase	07/11/1999 to 27/12/1999		2	3
Phase	05/02/2000 12:00 to 07/02/2000 12:00		2	3
Phase	14/02/2000 18:00 to 15/02/2000 06:00		2	3
Phase	19/02/2000 12:00 to 20/02/2000 15:00		2	3
Phase	07/03/2000 to 14/03/2000		2	3
Phase	17/03/2000 to 23/03/2000		2	3
Phase	06/04/2000 18:00 to 09/04/2000		2	3
Phase	20/04/2000 08:00 to 15:00		2	3
Phase	04/05/2000 to 06/05/2000		2	3
Phase	01/06/2000 to 12/06/2000		2	3
Phase	06/07/2000 to 10/07/2000		2	3
Phase	18/07/2000 to 24/07/2000		2	3
Phase	19/08/2000 to 09/09/2000		2	3
Spike	14/10/2000 04:00		1	3
Phase	26/10/2000 00:00 to 15:00		2	3
Phase	15/11/2000 12:00 to 16/11/2000 15:00		2	3
Phase	26/03/2001 to 13/04/2001		2	3
Phase	04/05/2001 to 13/05/2001		2	3
Phase	05/07/2002 to 09/07/2002 06:00		2	3
Phase	11/08/2002 03:00 to 12/08/2002 06:00		2	3
Phase	22/11/2002 03:00 to 23/11/2002 06:00		2	3
Phase	29/01/2006 to 20/04/2006		2	3
Phase	17/07/2006 to 21/07/2006		2	3
Phase	01/01/2007 to 25/01/2007		2	3
Phase	02/02/2007 09:00 to 15:00		2	3
Phase	18/02/2007 09:00 to 15:00		2	3
Phase	10/03/2007 to 25/03/2007		2	3
Phase	11/04/2007 to 13/04/2007 06:00		2	3
Phase	03/05/2007 09:00 to 15:00		2	3
Phase	17/05/2007 15:00 to 23:00		2	3
Phase	08/06/2007 12:00 to 21:00		2	3
Phase	13/06/2007 to 19/06/2007 09:00		2	3
Phase	08/07/2007 21:00 to 09/07/2007 06:00		2	3
Phase	26/07/2007 09:00 to 15:00		2	3
Phase	31/07/2007 09:00 to 15:00		2	3
Phase	21/08/2007 12:00 to 22/08/2007 09:00		2	3
Phase	24/08/2007 09:00 to 15:00		2	3
Phase	01/09/2007 06:00 to 18:00		2	3
Phase	04/09/2007 12:00 to 05/09/2007 03:00		2	3
Phase	06/09/2007 09:00 to 07/09/2007 06:00		2	3
Phase	10/09/2007 18:00 to 11/09/2007 12:00		2	3
Phase	01/10/2007 to 02/10/2007 06:00		2	3
Phase	09/12/2007 00:00 to 06:00		2	3

(QC Flag: 0 = Meteorological (e.g. Seiche, Meteo-tsunami), 1 = Spike, 2 = Phase Offset, 3 = Tsunami, 4 = Other)

Analysis Comments

- Overall, quality of the data appears poor throughout and data needs to be used carefully in future analysis.
- After first pass it is clear that data is noisy for most of the data coverage. From 2009-onwards the quality of data improves and this has been taken as the appropriate level of residual noise for the data set. Further data removal is therefore required for preceding years.

Ullapool, UK (57.895°N, 5.158°W)

Inherited:

Filename	V1 no.	Start	End	Yrs
ullapool-p043-uk-bodc.mat	630	05/01/1966	31/12/2006	28

Extended:

v1 filename	ullapool-p043-uk-bodc.mat (630)
v2 Filename	422_Ullapool-GBR_GESLA_v2.mat
Source of Extra Data	BODC
Extra Data filename	RN-7246_1372253428497.zip
Date of Download	26/02/2014
End of Extra Data	31/12/2012
Load in for Extra Data	BODC2
Comparison Comments	Comparisons are perfect

Quality Control:

Type	Date Affected	Comments	QC Flag	GESLA Flag
Threshold		< -2 & > 12	4	3
Phase	22/08/2011 04:00 to 24/08/2011 13:00		2	3
Phase	11/12/2011 23:00 to 16/12/201 16:00		2	3

(QC Flag: 0 = Meteorological (e.g. Seiche, Meteo-tsunami), 1 = Spike, 2 = Phase Offset, 3 = Tsunami, 4 = Other)

Valparaiso, Chile (-33 033°S, 71.633°W)

Inherited:

Filename	V1 no.	Start	End	Yrs
'valparaiso-081a-chile-uhslc.mat'	**633**	02/01/1944	31/12/2002	49
'valparaiso-a,chile-001-glossdm-bodc.mat'	**634**	02/01/1944	03/11/1944	1
'valparaiso-b,chile-001-glossdm-bodc.mat'	**635**	01/08/1982	31/12/1998	16

Extended:

v1 filename	'valparaiso-081a-chile-uhslc.mat (633)
v2 Filename	425_Valparaiso-CHL_GESLA_v2.mat
Source of Extra Data	UHSLC
Extra Data filename	H081a
Date of Download	26/03/2014
End of Extra Data	31/12/2012
Load in for Extra Data	UHSLC
Comparison Comments	Comparisons are perfect

Quality Control:

Type	Date Affected	Comments	QC Flag	GESLA Flag
Phase	25/09/1984 to 04/10/1984		2	3
Phase	01/04/1989 to 09/04/1989		2	3
Tsunami	24/06/2001 to 27/06/2001	S. Peru	3	6
Tsunami	27/02/2010 to 03/03/2010	Chile	3	6
Tsunami	12/03/2011 to 18/03/2011	Tohuku	3	6
Spike	31/08/2011 16:00		1	3

(QC Flag: 0 = Meteorological (e.g. Seiche, Meteo-tsunami), 1 = Spike, 2 = Phase Offset, 3 = Tsunami, 4 = Other)

Analysis Comments

- Fitted linear models with nodal component do not fit the data for GDTR, MHHW or MLLW. All other tidal datums are well accounted for.

Vancouver, Canada (BC) (49.287°N, 123.110°W)

Inherited:

Filename	V1 no.	Start	End	Yrs
'vancouver,bc-07735-canada-meds.mat'	**636**	01/11/1909	30/09/2008	80

Extended:

v1 filename	'vancouver,bc-07735-canada-meds.mat (636)
v2 Filename	426_Vancouver-CAN_GESLA_v2.mat
Source of Extra Data	MEDS
Extra Data filename	7735_01-JAN-2008_slev.csv
Date of Download	21/05/2014
End of Extra Data	31/12/2013
Load in for Extra Data	MEDS
Comparison Comments	Comparisons between inherited (636) and extra data are perfect if -16hr time offset is applied to the extra data. The extra data were downloaded in UTC and

	therefore a +16hr time shift is applied to all the data once it is combined to return to UTC time zone.

Quality Control:

Type	Date Affected	Comments	QC Flag	GESLA Flag
Datum	Before 01/01/1917		4	3
Phase	15/01/1943 21:00 to 16/01/1943 06:00		2	3
Spike	09/01/1963 16:00		1	3
Phase	02/01/1967 06:00 to 18:00		2	3

(QC Flag: 0 = Meteorological (e.g. Seiche, Meteo-tsunami), 1 = Spike, 2 = Phase Offset, 3 = Tsunami, 4 = Other)

Analysis Comments

- Data before 1917 appears to be have a shift in datum compared to data after this date. Remove data as it gives unrealistic high trends.

Vardoe, Norway (70.333°N, 31.100°E)

Inherited:

Filename	V1 no.	Start	End	Yrs
'vardo,norway-001-glossdm-bodc.mat'	**638**	11/09/1947	31/12/2003	30

Extended:

v1 filename	'vardo,norway-001-glossdm-bodc.mat (638)
v2 Filename	428_Vardoe-NOR_GESLA_v2.mat
Source of Extra Data	NMA
Extra Data filename	Water level observations Vardoe_2009-2013
Date of Download	02/04/2014
End of Extra Data	31/21/2013
Load in for Extra Data	NMA
Comparison Comments	Comparisons between inherited and extra data are not possible, since there is a gap between them, but the offset supplied by NMA in email of 2.857 m does appear to provide a continuous datum. Initial comparison shows a phase offset in all constituents of 30 degrees or 1 hr. A time offset is therefore applied to the data from NMA of -1hr to return the data to UTC. Phase offset is removed by this action.

Quality Control:

Type	Date Affected	Comments	QC Flag	GESLA Flag
		No erroneous values to remove		

(QC Flag: 0 = Meteorological (e.g. Seiche, Meteo-tsunami), 1 = Spike, 2 = Phase Offset, 3 = Tsunami, 4 = Other)

Veracruz, Mexico (19.200°N, 96.133°W)

Inherited:

Filename	V1 no.	Start	End	Yrs
'veracruz_a,ver.-250a-mexico-uhslc.mat'	**639**	01/02/1985	31/12/1995	11

Extended:

v1 filename	'veracruz_a,ver.-250a-mexico-uhslc.mat (639)
v2 Filename	429_Veracruz-MEX_GESLA_v2.mat
Source of Extra Data	UHSLC
Extra Data filename	H250a
Date of Download	21/05/2014
End of Extra Data	31/12/2012
Load in for Extra Data	UHSLC
Comparison Comments	Comparisons are perfect

Quality Control:

Type	Date Affected	Comments	QC Flag	GESLA Flag
		No erroneous values to remove		

(QC Flag: 0 = Meteorological (e.g. Seiche, Meteo-tsunami), 1 = Spike, 2 = Phase Offset, 3 = Tsunami, 4 = Other)

Victor Harbour, Australia (35.553°S, 138.622°E)

Inherited:

Filename	V1 no.	Start	End	Yrs
'victorharbor-027-australia-johnhunter.mat'	**641**	15/05/1965	31/12/2004	38

Extended:

v1 filename	'victorharbor-027-australia-johnhunter.mat (641)
v2 Filename	430_VictorHarbour-AUS_GESLA_v2.mat
Source of Extra Data	N/A
Extra Data filename	N/A
Date of Download	N/A
End of Extra Data	N/A
Load in for Extra Data	N/A
Comparison Comments	No extra data available

Quality Control:

Type	Date Affected	Comments	QC Flag	GESLA Flag
		No erroneous values to remove		

(QC Flag: 0 = Meteorological (e.g. Seiche, Meteo-tsunami), 1 = Spike, 2 = Phase Offset, 3 = Tsunami, 4 = Other)

Analysis Comments

- Peak residual on 28/06/1972.

Victoria Harbour, Canada (BC) (48.417°N, 123.367°W)

Inherited:

Filename	V1 no.	Start	End	Yrs
'victoria,bc-543a-canada-uhslc.mat'	**642**	18/02/1909	31/12/1964	54
'victoriaharbour,bc-07120-canada-meds.mat'	**644**	17/02/1909	30/09/2008	47

Extended:

v1 filename	N/A
v2 Filename	431_VictoriaHarbour-CAN_GESLA_v2.mat
Source of Extra Data	UHSLC
Extra Data filename	H543a
Date of Download	21/05/2014
End of Extra Data	31/12/2012
Load in for Extra Data	UHSLC
Comparison Comments	Comparisons between inherited (642) and extra data show an offset of 3.050 m which is documented on the UHSLC as being caused by a reanalysis of the data. Only extra data downloaded from UHSLC 543a is used in GESLA_v2.

Quality Control:

Type	Date Affected	Comments	QC Flag	GESLA Flag
Phase	06/12/1915 03:00 to 18:00		2	3
Phase	04/02/1928 21:00 to 05/02/1928 09:00		2	3
Phase	26/10/1928 18:00 to 27/10/1928 18:00		2	3
Phase	12/02/1931 18:00 to 14/02/1931		2	3
Phase	22/02/1931 18:00 to 23/02/1931 18:00		2	3
Phase	07/06/1932 06:00 to 21:00		2	3
Phase	24/12/1935 to 04/01/1936		2	3
Phase	24/12/1937 to 17/12/1937		2	3
Phase	18/08/1938 06:00 to 19/08/1938 12:00		2	3
Phase	31/10/1938 06:00 to 18:00		2	3
Phase	25/06/1939 to 04/07/1939		2	3

(QC Flag: 0 = Meteorological (e.g. Seiche, Meteo-tsunami), 1 = Spike, 2 = Phase Offset, 3 = Tsunami, 4 = Other)

Vigo, Spain (42.233°N, 8.733°W)

Inherited:

Filename	V1 no.	Start	End	Yrs
vigo-208a-spain-uhslc.txt	645	08/03/1943	31/12/1990	48

Extended:

v1 filename	vigo-208a-spain-uhslc.txt (645)
v2 Filename	442_Vigo-ESP_GESLA_v2.mat
Source of Extra Data	IEO
Extra Data filename	Vigo_1991_2004_Format1/Vigo_2005_2010_Format2
Date of Download	20/06/2013
End of Extra Data	31/21/2010
Load in for Extra Data	IEO
Comparison Comments	Comparisons are perfect, between inherited and both formats of the extended data

Quality Control:

Type	Date Affected	Comments	QC Flag	GESLA Flag
Phase	01/07/1951 to 24/07/1951		2	3
Phase	12/10/1954 to 16/10/1954		2	3
Phase	16/08/1955 to 24/08/1955		2	3
Phase	22/01/1959 12:00 to 24/01/1959		2	3
Phase	01/09/1962 to 06/09/1962		2	3
Phase	01/08/1964 to 14/09/1964		2	3
Phase	27/01/1968 to 09/02/1968		2	3
Phase	11/04/1968 to 18/04/1968		2	3
Phase	24/12/1968 to 26/12/1968		2	3
Phase	23/11/1977 to 01/04/1984	Consistent	2	3
Phase	01/09/1985 12:00 to 03/09/1985 12:00		2	3

(QC Flag: 0 = Meteorological (e.g. Seiche, Meteo-tsunami), 1 = Spike, 2 = Phase Offset, 3 = Tsunami, 4 = Other)

Analysis Comments

- 1980-83: Strange patterns in surge and the tide. There are some unusual variations in tidal constituents at this time. Identified by UHSLC QC.
- 1990 ish: large jumps in the phase of the major constituents, at the time of old data set. Caused by time offset +1hr on inherited data. **CORRECTED** by applying a time offset of -1 hr applied to data to fit to UTC.

Wake Island, USA (Pacific) (19.283°N, 166.617°E)

Inherited:

Filename	V1 no.	Start	End	Yrs
'wake-051a-usa_trust-uhslc.mat'	**648**	30/05/1950	31/12/2004	49
'wakeisland,usa-001-glossdm-bodc.mat'	**649**	30/05/1950	31/12/2000	45

Extended:

v1 filename	'wake-051a-usa_trust-uhslc.mat (648)
v2 Filename	434_WakeIsland-USA_GESLA_v2.mat
Source of Extra Data	UHSLC/NOAA
Extra Data filename	H051a/COOPS_WakeIsland
Date of Download	21/05/2014
End of Extra Data	31/12/2013
Load in for Extra Data	UHSLC/NOAA
Comparison Comments	Comparisons are perfect

Quality Control:

Type	Date Affected	Comments	QC Flag	GESLA Flag
Tsunami	23/05/1960 12:00 to 25/05/1960	Valdivia	3	6
Phase	07/02/1973 to 09/02/1973		2	3
Phase	17/11/1975 00:00 to 23:00		2	3
Phase	03/03/1976 00:00 to 23:00		2	3
Phase	13/03/1976 to 16/03/1976		2	3
Phase	17/09/1977 to 20/09/1977		2	3
Phase	16/03/1984 to 19/03/1984		2	3
Phase	14/11/1986 12:00 to 23:00		2	3
Phase	15/08/1989 to 25/08/1989		2	3

(QC Flag: 0 = Meteorological (e.g. Seiche, Meteo-tsunami), 1 = Spike, 2 = Phase Offset, 3 = Tsunami, 4 = Other)

Analysis Comments

- Noisy period from 15/08/1986 to 25/08/1986 is probably caused by TS Georgette crossing the Pacific and changing into Cyclone Tip.
- Another noisy period between 11/09/1987 and 16/09/1987 also simultaneous to the passing of nearby Super Typhoon Holly. Appears that site responds in this manner to the passing of storms a little distance away.
- Another period from 13/08/1974 to 18/08/1974 has the same signal and is assumed to be valid despite not identifying a simultaneous storm event.
- Typhoon Dan passed almost directly over Wake Island and causes a large short storm surge (standard shape) on 28/10/1992.
- Peak sea level and residual on 01/09/2006 caused by Typhoon Ioke (Cat 4 at the time)

Wakkanai, Japan (45.417°N, 141.683°E)

Inherited:

Filename	V1 no.	Start	End	Yrs
'wakkanai-001-glossdm-bodc.mat'	**650**	01/01/2001	31/12/2003	3
'wakkanai-360a-japan-uhslc.mat'	**651**	01/01/1967	31/12/2005	39

Extended:

v1 filename	'wakkanai-360a-japan-uhslc.mat (651)
v2 Filename	435_Wakkanai-JPN_GESLA_v2.mat
Source of Extra Data	UHSLC
Extra Data filename	H360a
Date of Download	21/05/2014
End of Extra Data	31/12/2012
Load in for Extra Data	UHSLC
Comparison Comments	Comparisons are perfect

Quality Control:

Type	Date Affected	Comments	QC Flag	GESLA Flag
		No erroneous values to remove		

(QC Flag: 0 = Meteorological (e.g. Seiche, Meteo-tsunami), 1 = Spike, 2 = Phase Offset, 3 = Tsunami, 4 = Other)

Analysis Comments

- Tide appears to have been resolved well despite the low magnitude.

Walvis Bay, Namibia (22.950°S, 14.500°E)

Inherited:

Filename	V1 no.	Start	End	Yrs
'walvis_bay-220a-namibia-uhslc.mat'	**652**	01/01/1959	23/11/1998	21
'walvisbay,namibia-001-glossdm-bodc.mat'	**653**	19/08/1991	23/11/1998	3

Extended:

v1 filename	N/A
v2 Filename	436_WalvisBay-NAM_GESLA_v2.mat
Source of Extra Data	UHSLC
Extra Data filename	H220a
Date of Download	21/05/2014
End of Extra Data	31/12/2012
Load in for Extra Data	UHSLC
Comparison Comments	Comparisons between inherited (653) and extra data show offset. This is caused because a thorough check and recalibration of the data was conducted in 2008 and therefore the new data is all that should be used (UHSLC website).

Quality Control:

Type	Date Affected	Comments	QC Flag	GESLA Flag
Phase	21/03/1959 to 30/03/1959		2	3
Noise	01/06/1979 to 05/06/1979		4	3
Phase	21/08/1979 18:00 to 23/08/1979		2	3
Phase	21/01/1980 06:00 to 22/01/1980 12:00		2	3
Phase	25/07/1980 00:00 to 23:00		2	3
Phase	27/09/1980 09:00 to 28/09/1980 21:00		2	3
Phase	07/02/1982 00:00 to 23;00		2	3
Phase	13/03/1982 00:00 to 23:00		2	3
Phase	20/03/1982 06:00 to 15:00		2	3
Phase	05/10/1982 to 07/10/1982		2	3
Phase	11/12/1982 to 14/12/1982		2	3
Phase	25/02/1983 to 01/03/1983		2	3
Phase	23/12/1985 00:00 to 12:00		2	3
Phase	06/06/1992 to 15/05/1992		2	3
Phase	30/06/1992 18:00 to 06/07/1992		2	3

(QC Flag: 0 = Meteorological (e.g. Seiche, Meteo-tsunami), 1 = Spike, 2 = Phase Offset, 3 = Tsunami, 4 = Other)

Analysis Comments

- Only 18 years of valid data spread over 54 years may lead to invalid trends, but use site until proved invalid because this region is not well represented.
- Noisy data through years to 2009.

Wellington, New Zealand (41.283°S, 174.783°E)

Inherited:

Filename	V1 no.	Start	End	Yrs
wellington-071a-new_zealand-uhslc..txt	654	18/11/1944	31/12/2005	59

Extended:

v1 filename	wellington-071a-new_zealand-uhslc..txt (654)
v2 Filename	437_Wellington-NZL_GESLA_v2.mat
Source of Extra Data	UHSLC
Extra Data filename	H071a
Date of Download	25/06/2013
End of Extra Data	31/12/2012
Load in for Extra Data	UHSLC
Comparison Comments	Comparisons are perfect. More data available from LINZ ftp website, but an offset was identified between this and the UHSLC dataset, that was not constant with time. Therefore, we do not use the LINZ data.

Quality Control:

Type	Date Affected	Comments	QC Flag	GESLA Flag
Phase	01/07/1945 to 06/08/1945			

(QC Flag: 0 = Meteorological (e.g. Seiche, Meteo-tsunami), 1 = Spike, 2 = Phase Offset, 3 = Tsunami, 4 = Other)

Wick, UK (58.441°N, 3.086°W)

Inherited:

Filename	V1 no.	Start	End	Yrs
'wick-p035-uk-bodc.mat'	**656**	05/01/1965	31/12/2006	38

Extended:

v1 filename	'wick-p035-uk-bodc.mat (656)
v2 Filename	439_Wick-GBR_GESLA_v2.mat
Source of Extra Data	UHSLC
Extra Data filename	RN-7246_1372253428497.zip
Date of Download	26/02/2014
End of Extra Data	31/03/2013
Load in for Extra Data	BODC2
Comparison Comments	Comparisons are perfect

Quality Control:

Type	Date Affected	Comments	QC Flag	GESLA Flag
Phase	01/01/2011 to 23/03/2011		2	3
Phase	12/11/2011 to 15/11/2011		2	3
Phase	08/03/2012 12:00 to 23:00		2	3
Phase	21/03/2013 12:00 to 21:00		2	3

(QC Flag: 0 = Meteorological (e.g. Seiche, Meteo-tsunami), 1 = Spike, 2 = Phase Offset, 3 = Tsunami, 4 = Other)

Analysis Comments

- Number of big spikes were also removed.

Willapa Bay, USA (Washington) (46.708°N, 123.965°W)

Inherited:

Filename	V1 no.	Start	End	Yrs
'willapa_bay,_wa-564a-usa-uhslc.mat'	**657**	01/01/1996	31/12/2005	10

Extended:

v1 filename	N/A
v2 Filename	440_WillapaBay-USA_GESLA_v2.mat
Source of Extra Data	UHSLC/NOAA
Extra Data filename	H564a/COOPS_WillapaBay
Date of Download	21/05/2014
End of Extra Data	31/12/2013
Load in for Extra Data	UHSLC/NOAA
Comparison Comments	Comparisons are perfect, however, the data has been extended back to 1972 and therefore only extra data is used in GESLA_v2. UHSLC data called Toke Point

Quality Control:

Type	Date Affected	Comments	QC Flag	GESLA Flag
Phase	25/12/1975 to 09/01/1976		2	3
Phase	05/06/1976 to 10/06/1976		2	3
Phase	13/08/1976 to 17/08/1976		2	3
Phase	15/08/1981 to 22/08/1981		2	3
Phase	19/07/2002 09:00 to 21:00		2	3
Phase	26/07/2002 06:00 to 12:00		2	3
Phase	27/07/2002 06:00 to 28/07/2002 03:00		2	3

Phase	28/07/2002 15:00 to 29/07/2002 03:00		2	3
Phase	26/08/2002 18:00 to 28/08/2002		2	3
Phase	06/09/2002 00:00 to 12:00		2	3
Phase	16/02/2003 to 20/02/2003		2	3
Phase	26/02/2003 to 28/02/2003		2	3
Phase	05/03/2003 03:00 to 15:00		2	3
Phase	06/03/2003 03:00 to 15:00		2	3
Phase	17/03/2003 to 20/03/2003		2	3
Phase	13/07/2003 00:00 to 15:00		2	3
Phase	12/06/2008 to 27/06/2008		2	3

(QC Flag: 0 = Meteorological (e.g. Seiche, Meteo-tsunami), 1 = Spike, 2 = Phase Offset, 3 = Tsunami, 4 = Other)

Williamstown, Australia (37.857°S, 144.898°E)

Inherited:

Filename	V1 no.	Start	End	Yrs
'williamstown-028-australia-johnhunter.mat'	**658**	28/01/1966	31/12/2004	39

Extended:

v1 filename	'williamstown-028-australia-johnhunter.mat (658)
v2 Filename	441_Williamstown-AUS_GESLA_v2.mat
Source of Extra Data	N/A
Extra Data filename	N/A
Date of Download	N/A
End of Extra Data	N/A
Load in for Extra Data	N/A
Comparison Comments	No extra data available

Quality Control:

Type	Date Affected	Comments	QC Flag	GESLA Flag
		No erroneous values to remove		

(QC Flag: 0 = Meteorological (e.g. Seiche, Meteo-tsunami), 1 = Spike, 2 = Phase Offset, 3 = Tsunami, 4 = Other)

Wilmington, USA (North Carolina) (34.227°N, 77.953°W)

Inherited:

Filename	V1 no.	Start	End	Yrs
'wilmington,nc-750a-usa-uhslc.mat'	**659**	28/12/1935	31/12/2005	69

Extended:

v1 filename	'wilmington,nc-750a-usa-uhslc.mat (659)
v2 Filename	442_Wilmington-USA_GESLA_v2.mat
Source of Extra Data	UHSLC/NOAA
Extra Data filename	H750a/COOPS_Wilmington
Date of Download	21/05/2014
End of Extra Data	31/12/2013
Load in for Extra Data	UHSLC/NOAA
Comparison Comments	Comparisons are perfect

Quality Control:

Type	Date Affected	Comments	QC Flag	GESLA Flag
Phase	09/07/1961 to 11/07/1961 12:00		2	3

(QC Flag: 0 = Meteorological (e.g. Seiche, Meteo-tsunami), 1 = Spike, 2 = Phase Offset, 3 = Tsunami, 4 = Other)

Analysis Comments

- Period end 09/1945 where a large increase in MSL is observed, probably caused by Hurricane that tracked along the coast around this time a dumped substantial rainfall. Raised sea level is probably caused by river water, which will have an impact given the location of the gauge up the Northeast Cape Fear River.
- Peak sea level on 15/10/1954 caused by Hurricane Hazel.
- Peak residual on 06/09/1996 caused by Hurricane Fran matched on 14/08/2004 by surge caused by Hurricane Charley.
- Min. residual on 12/09/1984 caused by Hurricane Diana, with a large peak coming 1 day later.
- Change in trends of TD occurs around 1983, but there is no mention of datum shifts on UHSLC or NOAA websites. No mention of construction of dams since the 1930s.
- Other notable storms surges: 13/03/1993 (Storm of Century, nor'easter), 26/08/1998 (Bonnie), 16/09/1999 (Floyd), 06/09/2008 (Hanna)

Wood's Hole, USA (MA) (41.523°N, 70.672°W)

Inherited:

Filename	V1 no.	Start	End	Yrs
'woods_hole,ma-742a-usa-uhslc.mat'	**662**	01/01/1957	31/12/2005	43

Extended:

v1 filename	'woods_hole,ma-742a-usa-uhslc.mat (662)
v2 Filename	445_WoodsHole-USA _GESLA_v2.mat
Source of Extra Data	UHSLC/NOAA
Extra Data filename	H742a / COOPS_WoodsHole
Date of Download	21/05/2014
End of Extra Data	31/12/2013
Load in for Extra Data	UHSLC/NOAA
Comparison Comments	Comparisons are perfect

Quality Control:

Type	Date Affected	Comments	QC Flag	GESLA Flag
		No erroneous values to remove		

(QC Flag: 0 = Meteorological (e.g. Seiche, Meteo-tsunami), 1 = Spike, 2 = Phase Offset, 3 = Tsunami, 4 = Other)

Analysis Comments

- Major storm surges include: 13/09/1960 (Donna), 03/02/1976 (Groundhog Gale, negative surge), 19/08/1991 (Bob; cause max wl and ntr)

Wyndham, Australia (15.000°S, 128.100°E)

Inherited:

Filename	V1 no.	Start	End	Yrs
'wyndham-029-australia-johnhunter.mat'	**663**	17/04/1966	31/12/2004	31
'wyndham-165a-australia-uhslc.mat'	**664**	08/08/1984	31/12/2005	21

Extended:

v1 filename	'wyndham-029-australia-johnhunter.mat (663)
v2 Filename	446_Wyndham-AUS _GESLA_v2.mat
Source of Extra Data	UHSLC
Extra Data filename	H165a
Date of Download	21/05/2104
End of Extra Data	31/12/2012
Load in for Extra Data	UHSLC
Comparison Comments	Comparisons between inherited (663) and extra data show slight offset of 0.26 m. This offset was constant during overlapping period data and therefore inherited data had 0.26 m added to it. The position stated by the John Hunter dataset (36.9S, 149.6E) is wrong, therefore the position from the UHSLC (15S, 128.1E) is used in analysis.

Quality Control:

Type	Date Affected	Comments	QC Flag	GESLA Flag
		No erroneous values to remove		

(QC Flag: 0 = Meteorological (e.g. Seiche, Meteo-tsunami), 1 = Spike, 2 = Phase Offset, 3 = Tsunami, 4 = Other)

Analysis Comments

- Data has a high background noise signal.
- Large residuals often have a typical storm surge appearance, but cannot match them to a storm event.

Yakutat, USA (Alaska) (59.548°N, 139.735°W)

Inherited:

Filename	V1 no.	Start	End	Yrs
'yakutat,ak-570a-usa-uhslc.mat'	**666**	17/04/1966	31/12/2004	31
'yakutat,usa-001-glossdm-bodc.mat'	**667**	08/08/1984	31/12/2005	21

Extended:

v1 filename	'yakutat,ak-570a-usa-uhslc.mat (666)
v2 Filename	448_Yakutat-USA _GESLA_v2.mat
Source of Extra Data	UHSLC/NOAA
Extra Data filename	H570a/COOPS_Yakutat
Date of Download	21/05/2014
End of Extra Data	31/12/2013
Load in for Extra Data	UHSLC/NOAA
Comparison Comments	Comparisons are perfect

Quality Control:

Type	Date Affected	Comments	QC Flag	GESLA Flag
Phase	21/12/1967 18:00 to 27/12/1967		2	3
Phase	09/01/1970 to 14/01/1970		2	3
Phase	07/09/1970 to 22/09/1970		2	3

(QC Flag: 0 = Meteorological (e.g. Seiche, Meteo-tsunami), 1 = Spike, 2 = Phase Offset, 3 = Tsunami, 4 = Other)

Analysis Comments

- Peak residual on 05/05/1970 appears to coincide with low pressure system documented on (http://www.wunderground.com/history/airport/PAYA/1970/5/5/WeeklyHistory.html, accessed on 29/05/2014). Information on ET storms are difficult to find. Event is suspicious because no other events are even 50% of it.
- Similar looking event on 21/07/1974 does not have recorded storm.
- Residual much noisier before 1980.

Yap, Micronesia (9.508°N, 138.128°E)

Inherited:

Filename	V1 no.	Start	End	Yrs
'yap-a,fed.micronesia-001-glossdm-bodc.mat'	**668**	28/02/1951	31/12/1952	2
'yap-b,fed.micronesia-001-glossdm-bodc.mat'	**669**	10/05/1969	31/12/1998	27
'yap_b-008b-fd._st._micronesia-uhslc.mat'	**670**	10/05/1969	31/12/2004	33

Extended:

v1 filename	'yap_b-008b-fd._st._micronesia-uhslc.mat (670)
v2 Filename	449_Yap-FSM _GESLA_v2.mat
Source of Extra Data	UHSLC
Extra Data filename	H008b
Date of Download	21/05/2014
End of Extra Data	03/04/2012
Load in for Extra Data	UHSLC
Comparison Comments	Comparisons are perfect

Quality Control:

Type	Date Affected	Comments	QC Flag	GESLA Flag
		No erroneous values to remove		

(QC Flag: 0 = Meteorological (e.g. Seiche, Meteo-tsunami), 1 = Spike, 2 = Phase Offset, 3 = Tsunami, 4 = Other)

Analysis Comments

- Datum shift between 1996-97? 1997 appears to be lower than other years.
- Max. sea level and residual on 09/04/2004 caused by Typhoon Sudal
- Large residual on 03/03/2002, caused by Typhoon Mitag.

Yarmouth, Canada (Nova Scotia) (43.833°N, 66.117°W)

Inherited:

Filename	V1 no.	Start	End	Yrs
'yarmouth,ns-00365-canada-meds.mat'	**671**	01/01/1900	31/10/2008	38

Extended:

v1 filename	'yarmouth,ns-00365-canada-meds.mat (671)
v2 Filename	450_Yarmouth-CAN _GESLA_v2.mat
Source of Extra Data	MEDS
Extra Data filename	365_01-JAN-2008_slev.csv
Date of Download	21/05/2014
End of Extra Data	31/10/2013
Load in for Extra Data	MEDS
Comparison Comments	Comparisons between inherited (670) and extra data are perfect if a time offset of -8 hrs is applied to the newly downloaded data. After the data are combined a time shift is applied to all data to return it to UTC. This shift is +8hrs.

Quality Control:

Type	Date Affected	Comments	QC Flag	GESLA Flag
Phase	20/01/1967 to 03/02/1967		2	3
Phase	16/04/1967 to 06/08/1967		2	3
Phase	19/10/1967 to 22/10/1967		2	3
Phase	02/11/1967 00:00 to 23:00		2	3
Spike	05/11/1967 19:00		1	3
Phase	28/12/1967 to 11/01/1968		2	3
Phase	07/07/1970 to 21/07/1970		2	3
Phase	04/09/1970 to 26/09/1970		2	3
Phase	30/12/1970 to 03/01/1971		2	3
Phase	18/02/1971 to 02/03/1971		2	3
Phase	20/03/1971 to 05/05/1971		2	3
Phase	19/08/1988 to 26/08/1988		2	3
Phase	18/11/1988 to 25/11/1988		2	3
Phase	07/08/1989 03:00 to 08/08/1989 09:00		2	3

(QC Flag: 0 = Meteorological (e.g. Seiche, Meteo-tsunami), 1 = Spike, 2 = Phase Offset, 3 = Tsunami, 4 = Other)

Analysis Comments

- Data in 1900, will need to be removed since there is then no data until 1950s. Long term trends derived with this data in could be misleading.

Zanzibar, Tanzania (6.155°S, 39.190°E)

Inherited:

Filename	V1 no.	Start	End	Yrs
'zanzibar,tanzania-001-glossdm-bodc.mat'	**673**	01/03/1984	31/12/1998	15
'zanzibar-151a-tanzania-uhslc.mat'	**674**	01/03/1984	30/09/2004	20

Extended:

v1 filename	'zanzibar-151a-tanzania-uhslc.mat (674)
v2 Filename	452_Zanzibar-TZA _GESLA_v2.mat
Source of Extra Data	UHSLC
Extra Data filename	H151a
Date of Download	21/05/2014
End of Extra Data	03/04/2012
Load in for Extra Data	UHSLC
Comparison Comments	Comparisons are perfect

Quality Control:

Type	Date Affected	Comments	QC Flag	GESLA Flag
Phase	06/03/1985 to 09/03/1985		2	3
Phase	02/06/1991 00:00 to 12:00		2	3
Phase	09/09/2006 to 14/09/2006		2	3

(QC Flag: 0 = Meteorological (e.g. Seiche, Meteo-tsunami), 1 = Spike, 2 = Phase Offset, 3 = Tsunami, 4 = Other)

Analysis Comments

- An 6th diurnal signal appears in the residual. This may not be captured by the harmonic analysis.

Appendix B List of Identified Tsunamis

The below table shows a list of all tsunamis identified during QC procedures, along with the associated earthquake.

Year	Basin	Name	Lat.	Long.	Mag. (Mw)	Sites observed at (Site ID, see Table A1)
01/04/1946	Pacific	Aleutian Islands	52.800	163.500		161
04/11/1952	Pacific	Severo-Kulisk Earthquake	52.300	161.000	9.0	007, 086, 153, 161, 201, 204, 224, 293, 364
09/03/1957	Pacific	Andreanof Islands	51.500	-175.700		153, 161, 224, 271, 293
22/05/1960	Pacific	Valdivia	-38.235	-73.047	9.5	007, 086, 141, 153, 161, 170, 201, 204, 224, 254, 260, 271, 273, 293, 364, 366, 388, 435
27/03/1964	Pacific	Alaska	61.050	-147.480	9.2	153, 161, 174, 204, 224, 260, 273, 293, 316, 364, 366, 388
04/02/1965	Pacific	Rat Islands	51.210	178.498	8.7	153
16/05/1968	Pacific	Tokachi	40.900	143.350	8.3	174
08/11/1980	Pacific	Northern California	41.110	-124.300	7.3	263
04/10/1994	Pacific	Kuril Islands	43.706	147.328	8.2	174
30/07/1995	Pacific	Antofagasta	-23.650	-70.900	8.0	153, 174, 374, 375
23/06/2001	Pacific	Southern Peru	-16.260	-73.640	8.4	017, 153, 174, 293, 374, 435
17/11/2003	Pacific	Rat Island, Alaska	50.749	178.443	7.8	174
26/12/2004	Indian	Sumatra	3.316	95.854	9.2	136, 193, 374
03/05/2006	Pacific	Tonga	-20.130	-174.164	8.0	293, 374
15/11/2006	Pacific	Kuril Islands	46.607	153.230	8.3	109, 153, 174, 293, 316, 374
15/08/2007	Pacific	Peru	-13.380	-76.610	8.0	174
29/09/2009	Pacific	Samoan	-15.509	-172.034		174, 293, 316
27/02/2010	Pacific	Chilean	-36.290	-73.239	8.8	007, 017, 086, 109, 161, 174, 194, 203, 224, 263, 271, 293, 364, 375, 410, 435
11/03/2011	Pacific	Tohoku	38.322	142.369	9.0	007, 017, 086, 109, 153, 161, 174, 177, 194, 201, 204, 224, 254, 260, 263, 271, 273, 293, 316, 364, 375, 388, 391, 410, 415, 425
28/10/2012	Pacific	Queen Charlotte Islands	52.769	-131.927	7.8	153, 174

Appendix C Site Metadata

Table C1: Metadata for all 220 sites selected in the analysis

Site ID	Location	Lat.	Long.	Start	End	Valid Yrs.
2	Abashiri, Japan	144.28	44.02	1968	2010	42
3	Aberdeen	-2.07	57.14	1946	2012	46
4	Aburatsu	131.42	31.57	1961	2010	50
5	Acajutla, El Salvador	-89.83	13.58	1971	2000	26
7	Adak, USA	-176.63	51.86	1950	2012	55
8	Albany, Australia	117.88	-35.02	1967	2004	38
17	Antofagasta, Chile	-70.40	-23.65	1946	2012	61
21	Argentia, Canada	-53.98	47.30	1971	2012	40
24	Astoria, USA	-123.77	46.21	1925	2012	86
25	Atlantic City, USA	-74.42	39.35	1912	2013	96
28	Balboa, Panama	-79.57	8.96	1908	2009	99
29	Baltimore, USA	-76.58	39.27	1903	2013	111
31	Bamfield, Canada	-125.14	48.84	1971	2012	42
35	Bella Bella, Canada	-128.14	52.16	1906	2012	51
42	Boston, USA	-71.05	42.36	1922	2013	91
43	Brest, France	-4.50	48.38	1846	2007	147
44	Brisbane, Australia	153.03	-27.47	1966	2012	40
45	Broome, Australia	122.24	-17.96	1967	2013	36
46	Buenaventura, Colombia	-77.10	3.90	1954	2009	52
48	Bunbury, Australia	115.64	-33.33	1970	2004	34
49	Bundaberg, Australia	152.35	-24.87	1966	2012	44
50	Burnie, Australia	145.91	-41.05	1953	2013	38
51	Cabo San Lucas, Mexico	-109.91	22.88	1974	2001	21
52	Cairns, Australia	145.78	-16.93	1966	2004	31
53	Calais, France	1.87	50.97	1965	2007	28
55	Callao, Peru	-77.15	-12.05	1970	2012	43
56	Campbell River, Canada	-125.25	50.04	1967	2013	43
57	Cananeia, Brazil	-47.93	-25.02	1954	2005	52
58	Cape May, USA	-74.96	38.97	1966	2013	42
60	Carnarvon, Australia	113.66	-24.88	1967	2012	35
66	Ceuta, Spain	-5.32	35.90	1944	2008	62
68	Charleston - OR, USA	-124.32	43.35	1979	2013	35
69	Charleston - SC, USA	-79.93	32.78	1922	2013	92
70	Charlotte Amalie, Virgin Islands	-64.92	18.34	1982	2012	29
71	Charlotte Town, Canada	-63.12	46.23	1912	2012	75
72	Cherbourg, France	-1.62	49.65	1943	2007	34
73	Chesapeake Bay, USA	-76.11	36.97	1975	2013	39
74	Chichijima,Japan	142.18	27.10	1975	2012	38
75	Christmas Island, Kiribati	-157.47	1.98	1974	2011	34
77	Churchill, Canada	-94.20	58.78	1962	2013	45
81	Cocos Island, Australia	96.88	-12.12	1986	2013	27
83	Cordova, USA	-145.75	60.56	1965	2013	43
84	Coruna, Spain	-8.40	43.37	1943	2008	65
86	Crescent City, USA	-124.18	41.75	1934	2013	71

87	Cristobal, Panama	-79.92	9.36	1908	2012	96
93	Darwin, Australia	130.84	-12.46	1961	2013	48
97	Delfzijl, Netherlands	6.93	53.33	1971	2007	37
98	Den Helder, Netherlands	4.75	52.97	1971	2007	37
102	Dover, UK	1.32	51.11	1924	2012	53
105	Duck Pier, USA	-75.74	36.18	1979	2013	35
107	Dutch Harbour, USA	-166.54	53.88	1982	2013	30
109	Easter Island, Chile	-109.45	-27.15	1971	2012	33
110	Eastport, USA	-66.99	44.90	1930	2013	76
113	Esbjerg, Denmark	8.43	55.47	1950	2001	50
114	Esperance, Australia	121.89	-33.86	1966	2013	47
118	Faraday Base, Antarctica	-64.27	-65.25	1960	2009	37
119	Fernandina Beach, USA	-81.47	30.67	1898	2013	52
120	Fishguard, UK	-4.98	52.01	1963	2012	46
121	Flores - Azores, Portugal	-31.12	39.45	1977	2007	15
123	Fort Denison, Australia	151.23	-33.86	1915	2009	94
124	Fort Pulaski, USA	-80.90	32.03	1936	2013	73
126	Fremantle, Australia	115.75	-32.05	1897	2012	105
127	French Frigate Shoal, USA	-166.29	23.87	1975	2005	29
129	Funafuti, Tuvalu	179.20	-8.53	1978	2012	35
130	Funchal, Portugal	-16.91	32.64	1977	2009	23
132	Galveston, USA	-94.79	29.31	1904	2012	103
134	Geelong, Australia	144.36	-38.15	1966	2004	29
136	Geraldton, Australia	114.61	-28.77	1966	2004	39
140	Grand Isle, USA	-89.96	29.26	1980	2013	34
141	Apra Harbour, Guam	144.65	13.43	1949	2013	58
144	Hachinohe, Japan	141.53	40.53	1980	2010	31
146	Hakodate, Japan	140.73	41.78	1967	2012	45
147	Halifax, Canada	-63.58	44.67	1920	2013	94
148	Hamada, Japan	132.07	34.90	1984	2012	29
150	Harwich, UK	1.28	51.95	1954	2012	23
151	Heimsjoe, Norway	9.12	63.43	1970	2008	39
152	Heysham, UK	-2.91	54.03	1964	2012	37
153	Hilo - Hawaii, USA	-155.07	19.73	1927	2012	71
156	Hoek van Holland, Netherlands	4.12	51.98	1971	2007	37
157	Holyhead, UK	-4.63	53.31	1964	2012	37
160	Honningsvaag, Norway	25.98	70.98	1971	2008	35
161	Honolulu	-157.87	21.31	1905	2013	108
164	Ilfracombe, UK	-4.11	51.21	1969	2012	25
167	Immingham, UK	-0.19	53.63	1956	2012	52
168	Ishigaki, Japan	124.15	24.33	1969	2012	44
170	Johnston Island, USA	-169.53	16.74	1950	2012	54
171	Johor Baharu, Malaysia	103.79	1.46	1984	2011	28
174	Kahului, USA	-156.47	20.90	1951	2013	59
176	Kanton, Kiribati	-171.72	-2.81	1973	2011	33
177	Kaohsiung, Taiwan	120.28	22.62	1980	2012	33
178	Kapingamarangi, Micronesia	154.78	1.10	1979	2008	27
182	Keelung, Taiwan	121.75	25.15	1980	2012	27
183	Kelang, Malaysia	101.36	3.05	1984	2011	27
187	Ketchikan, USA	-131.63	55.33	1919	2013	72
188	Key West, USA	-81.81	24.55	1913	2013	99

192	Ko Lak, Thailand	99.82	11.80	1985	2012	28
194	Kodiak Island, USA	-152.51	57.73	1975	2013	34
196	Kuantan, Malaysia	103.43	3.98	1984	2011	28
199	Kushimoto, Japan	135.78	33.47	1961	2012	51
200	Kushiro, Japan	144.38	42.97	1963	2012	48
201	Kwajalein, Marshall Islands	167.73	8.73	1947	2013	65
204	La Libertad, Ecuador	-80.92	-2.20	1950	2012	61
213	Legaspi, Philippines	123.75	13.15	1984	2011	24
214	Lerwick, UK	-1.14	60.16	1959	2012	53
215	Lewes, USA	-75.12	38.78	1957	2013	55
217	Lime Tree Bay, USA	-64.75	17.70	1984	2013	29
224	Los Angeles, USA	-118.27	33.72	1924	2013	89
225	Lower Escuminac, Canada	-64.88	47.08	1973	2013	37
226	Lowestoft, UK	1.75	52.48	1964	2012	49
229	Maaloey, Norway	5.12	61.93	1970	2008	37
230	Mackay, Australia	149.19	-21.14	1966	2004	31
234	Magueyes Island, USA	-67.05	17.97	1965	2013	46
235	Maisaka, Japan	137.62	34.68	1968	2012	44
236	Majuro, Marshall Islands	171.37	7.11	1969	2012	41
237	Malakal, Belau (Palau)	134.46	7.33	1970	2011	40
239	Malin Head, UK	-7.33	55.37	1958	2001	41
241	Manila, Philippines	120.97	14.58	1984	2012	27
250	Mayport, USA	-81.43	30.40	1929	2000	72
252	Mera, Japan	139.83	34.92	1965	2012	45
254	Midway, USA	-177.37	28.22	1947	2012	63
255	Milford Haven, UK	-5.01	51.70	1968	2012	32
256	Millport, UK	-4.91	55.75	1978	2012	31
257	Mina Sulman, Bahrain	50.60	26.23	1979	2006	19
259	Miyakejima, Japan	139.48	34.06	1964	2011	48
260	Mokuoloe, USA	-157.80	21.43	1958	2013	45
262	Montauk, USA	-71.96	41.05	1960	2013	47
263	Monterey, USA	-121.89	36.61	1974	2013	40
264	Nagasaki, Japan	129.87	32.73	1964	2012	46
265	Naha, Japan	127.67	26.22	1967	2012	46
267	Nantucket, USA	-70.10	41.29	1965	2013	47
271	Nawiliwili, USA	-159.35	21.97	1955	2013	59
272	Naze, Japan	129.50	28.38	1958	2010	51
273	Neah Bay, USA	-124.62	48.37	1935	2013	77
274	New London, USA	-72.09	41.36	1939	2013	71
275	New York (Battery), USA	-74.02	40.70	1921	2013	73
276	Newcastle, Australia	151.78	-32.93	1966	2004	39
277	Newlyn, UK	-5.54	50.10	1916	2012	94
278	Newport, USA	-71.33	41.51	1931	2013	77
280	Nishinoomote, Japan	130.99	30.74	1966	2010	45
282	North Shields, UK	-1.44	55.01	1962	2012	39
283	North Sydney, Canada	-60.25	46.22	1970	2013	44
285	Noumea, New Caledonia	166.44	-22.29	1967	2002	36
289	Ofunato, Japan	141.72	39.07	1965	2010	46
293	Pago Pago, American Samoa	-170.68	-14.28	1949	2012	61
297	Papeete, French Polynesia	-149.57	-17.53	1976	2011	34
298	Patricia Bay, Canada	-123.45	48.65	1977	2013	37

300	Penhryn, Cook Islands	-158.05	-8.98	1978	2011	33
301	Pensacola, USA	-87.21	30.40	1924	2012	86
303	Pohnpei, Micronesia	158.24	6.99	1975	2004	30
305	Point Atkinson, Canada	-123.25	49.34	1915	2013	69
307	Ponta Delgada, Azores	-25.67	37.74	1979	2011	20
308	Port aux Basques, Canada	-59.13	47.57	1936	2008	44
310	Port Elizabeth, South Africa	25.63	-33.96	1979	2010	25
311	Port Hedland, Australia	118.58	-20.31	1966	2011	39
312	Port Isabel, USA	-97.22	26.06	1977	2013	35
316	Port San Luis, USA	-120.76	35.18	1948	2013	58
319	Port Adelaide, Australia	138.60	-34.93	1941	2004	62
321	Port Hardy, Canada	-127.49	50.72	1965	2013	48
322	Portland, USA	-70.25	43.66	1912	2013	96
324	Port Lincoln, Australia	135.86	-34.72	1966	2004	39
325	Port Lonsdale, Australia	138.50	-35.10	1963	2004	42
327	Port Patrick, UK	-5.12	54.84	1968	2012	41
328	Port Pirie, Australia	138.01	-33.18	1941	2004	62
330	Prince Rupert, Canada	-130.32	54.32	1909	2012	82
338	Puerto Montt, Chile	-72.97	-41.48	1981	2012	25
342	Queen Charlotte City, Canada	-132.07	53.25	1958	2013	48
349	Rikitea, French Polynesia	-134.95	-23.13	1971	2011	30
350	Rio de Janeiro, Brazil	-43.13	-22.93	1963	2010	45
354	Rørvik, Norway	11.25	64.87	1970	2013	43
358	Saint John, Canada	-66.06	45.25	1906	2013	82
359	Saipan, North Mariana Islands	145.74	15.23	1979	2010	26
364	San Diego, USA	-117.17	32.71	1906	2013	106
366	San Francisco, USA	-122.47	37.81	1898	2013	116
368	San Juan, USA	-66.12	18.46	1978	2013	34
374	Santa Cruz, Ecuador	-90.31	-0.76	1979	2011	31
375	Santa Monica, USA	-118.50	34.01	1975	2013	36
376	Seattle, USA	-122.33	47.60	1901	2012	112
378	Seldovia, USA	-151.72	59.44	1980	2013	34
380	Seward, USA	-149.43	60.12	1968	2013	41
382	Sheerness, UK	0.75	51.44	1952	2012	40
386	Simon's Town, S. Africa	18.43	-34.18	1960	2009	36
388	Sitka, USA	-135.34	57.05	1939	2013	74
390	Socoa, France	-1.68	43.40	1964	2007	36
391	South Beach, USA	-124.04	44.63	1967	2013	47
394	Spring Bay, Australia	147.93	-42.55	1986	2013	27
397	St. John's, Canada	-52.72	47.57	1936	2013	55
398	St. Petersburg, USA	-82.63	27.76	1948	2013	64
403	Stornoway, UK	-6.39	58.21	1976	2012	30
410	Tauranga, New Zealand	176.18	-37.65	1985	2012	24
413	Thevenard, Australia	133.65	-32.15	1966	2013	48
415	Tofino, Canada	-125.91	49.15	1910	2013	73
417	Townsville, Australia	146.82	-19.26	1959	2012	54
418	Toyama, Japan	137.22	36.77	1968	2012	45
420	Trieste, Italy	13.75	45.65	1971	2006	36
421	Tumaco, Colombia	-78.73	1.83	1954	2012	41
422	Ullapool, UK	-5.16	57.90	1966	2012	34
425	Valparaiso, Chile	-71.63	-33.03	1944	2012	58

426	Vancouver, Canada	-123.11	49.29	1910	2013	86
428	Vardo, Norway	31.10	70.33	1948	2013	35
429	Veracruz, Mexico	-96.13	19.20	1985	2012	16
430	Victor Harbour, Australia	138.62	-35.55	1966	2004	38
431	Victoria, Canada	-123.37	48.42	1909	2012	102
432	Vigo, Spain	-8.73	42.23	1943	2010	62
434	Wake Island, USA	166.62	19.28	1951	2013	57
435	Wakkanai, Japan	141.68	45.42	1967	2012	46
436	Walvis Bay, Namibia	14.50	-22.95	1959	2012	18
437	Wellington, New Zealand	174.78	-41.28	1945	2010	64
439	Wick, UK	-3.09	58.44	1965	2012	44
440	Willapa Bay, USA	-123.97	46.71	1973	2013	40
441	Williamstown, Australia	144.90	-37.86	1966	2004	39
442	Wilmington, USA	-77.95	34.23	1936	2013	77
445	Woods Hole, USA	-70.67	41.52	1957	2013	50
446	Wyndham, Australia	149.65	-36.93	1967	2012	39
448	Yakutat, USA	-139.74	59.55	1961	2013	48
449	Yap, Micronesia	138.13	9.51	1970	2011	37
450	Yarmouth, Canada	-66.12	43.83	1968	2013	42
452	Zanzibar, Tanzania	39.19	-6.16	1984	2011	26
464	Knysna, South Africa	23.05	-34.08	1966	2012	27
465	Luderitz, Namibia	15.15	-26.63	1961	2010	28
466	Mossel Bay, South Africa	22.15	-34.18	1966	2012	31

Appendix D Supplementary Material to Chapter 4

Figures D1.1 to D1.5: Significance of trends at each site for all tidal levels

Figures D2.1 to D2.5: Magnitude of trends at each site for all tidal levels

Figures D3.1 to D3.5: Percentage magnitude of trends at each site for all tidal levels

Figures D4.1 to D4.11: Tidal range trends and contribution from associated high waters and low water trends for each site Figure D

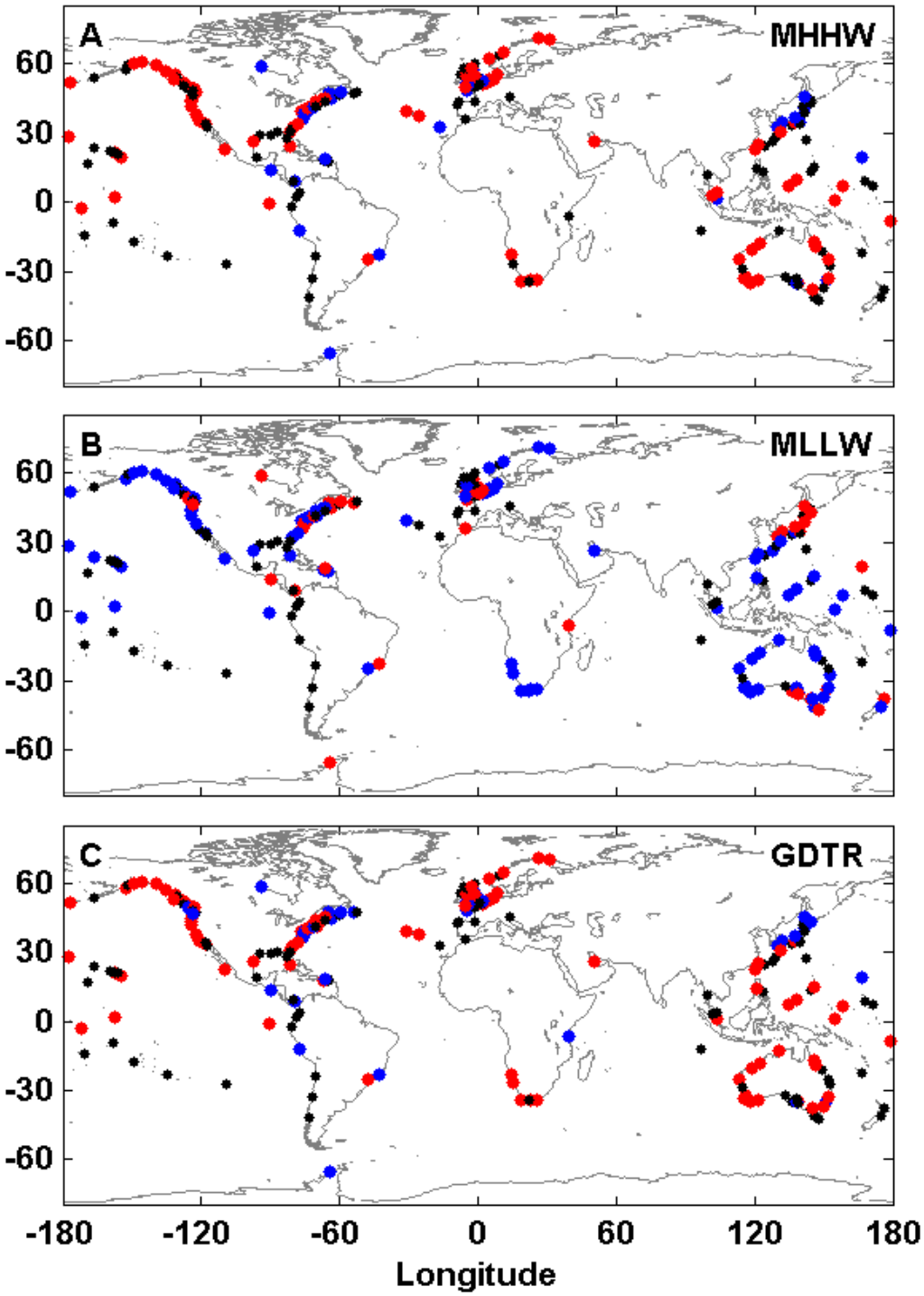

Figure D1.1: Global map showing where trends in MHHW (a), MLLW (b) and GDTR (c) are: significant positive (red), significant negative (blue) or non-significant (black). Significance means trend is significantly different to zero.

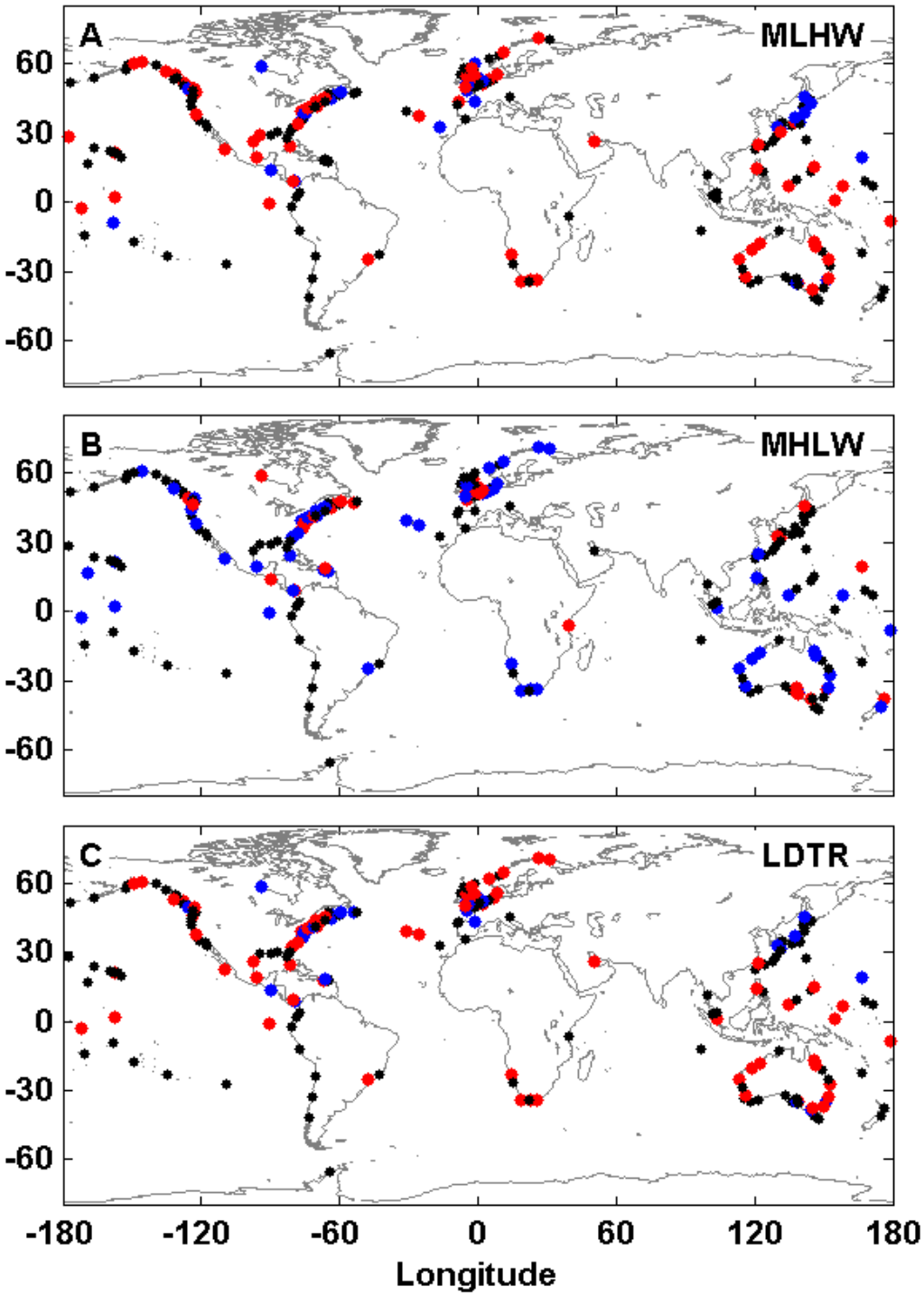

Figure B1.2: Global map showing where trends in MHW (a), MLW (b) and MTR (c) are: significant positive (red), significant negative (blue) or non-significant (black). Significance means trend is significantly different to zero.

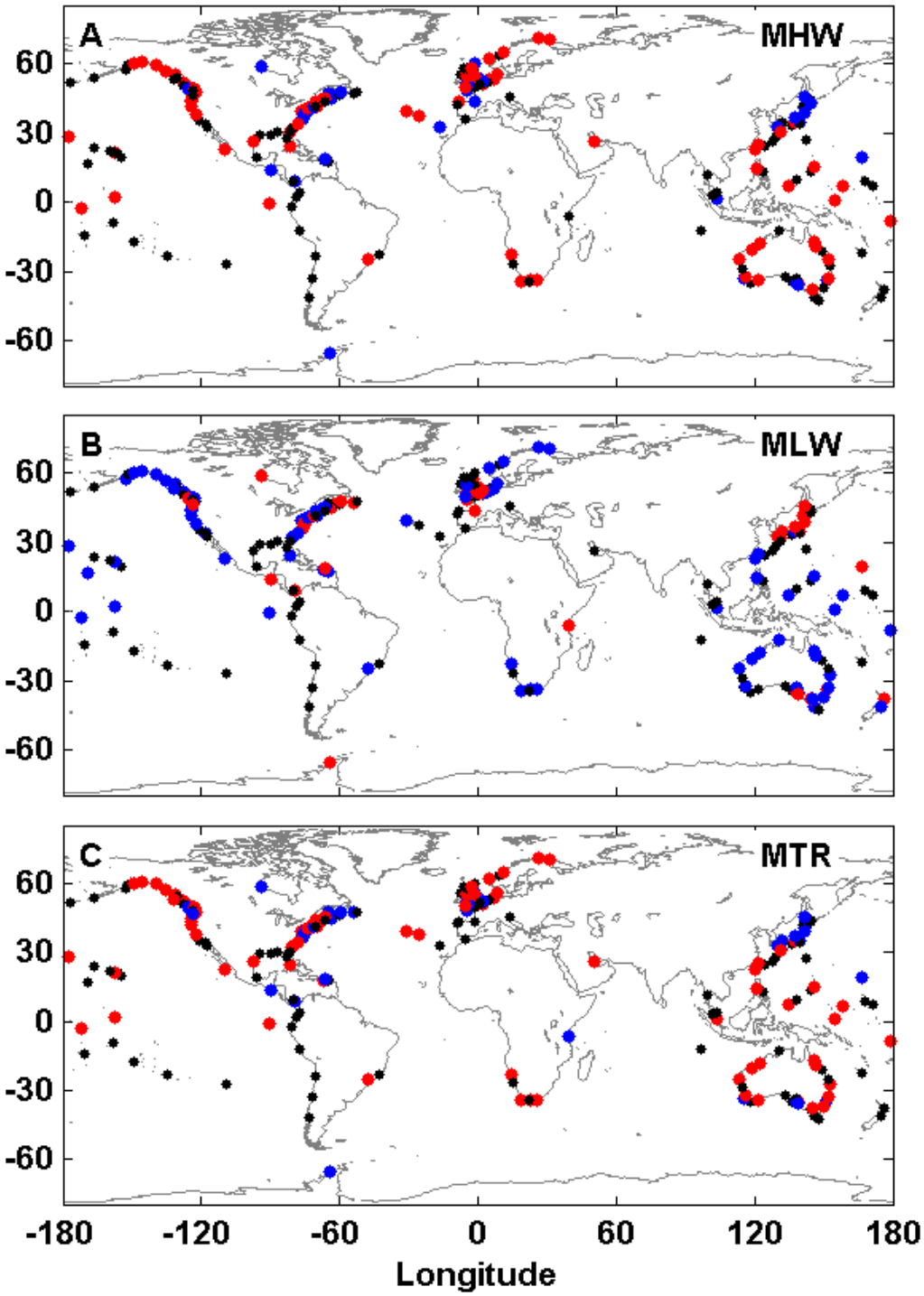

Figure D1.3: Global map showing where trends in MLHW (a), MHLW (b) and LDTR (c) are: significant positive (red), significant negative (blue) or non-significant (black). Significance means trend is significantly different to zero.

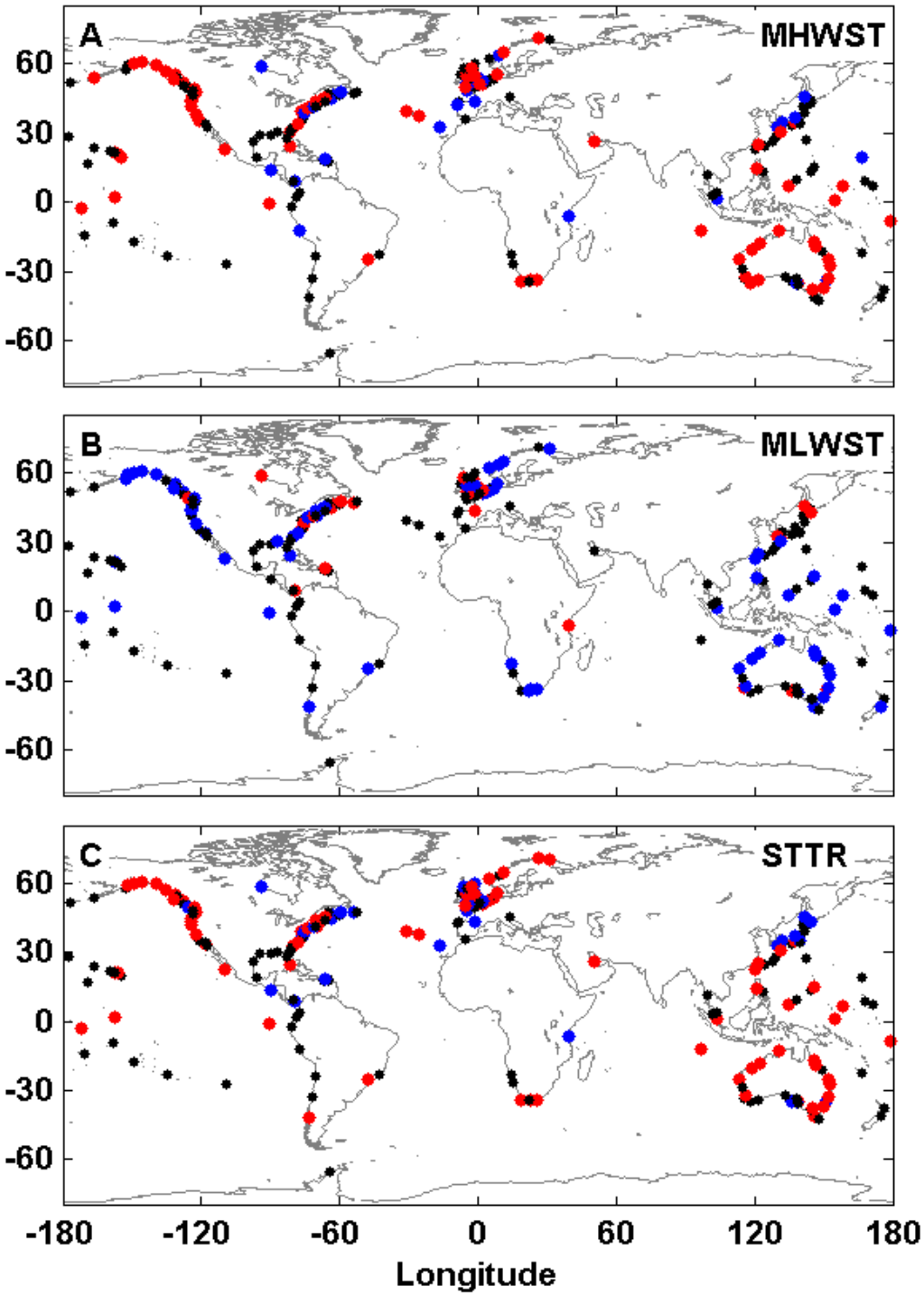

Figure D1.4: Global map showing where trends in MHWST (a), MLWST (b) and STTR (c) are: significant positive (red), significant negative (blue) or non-significant (black). Significance means trend is significantly different to zero.

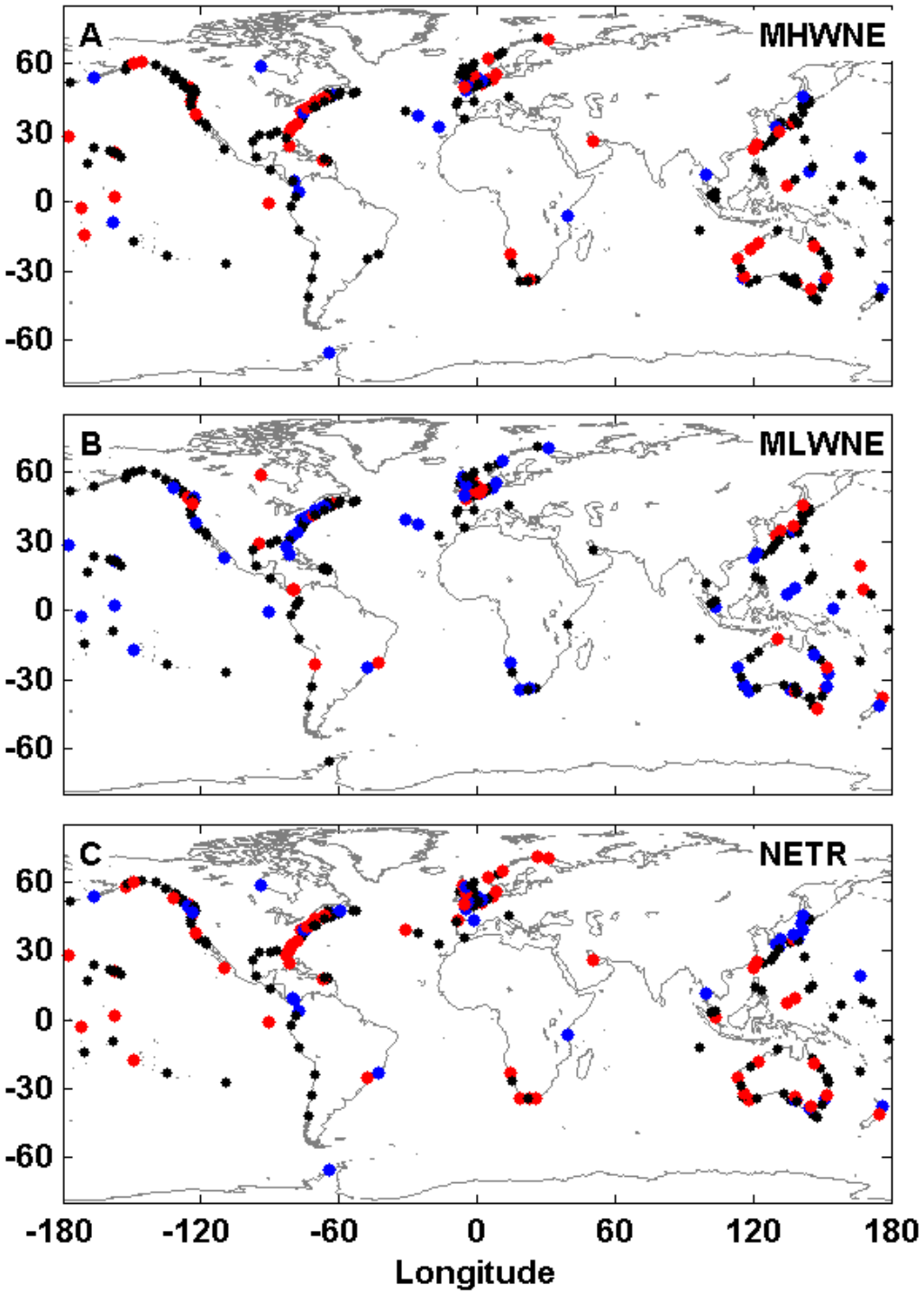

Figure D1.5: Global map showing where trends in MHWNE (a), MLWNE (b) and NETR (c) are: significant positive (red), significant negative (blue) or non-significant (black). Significance means trend is significantly different to zero.

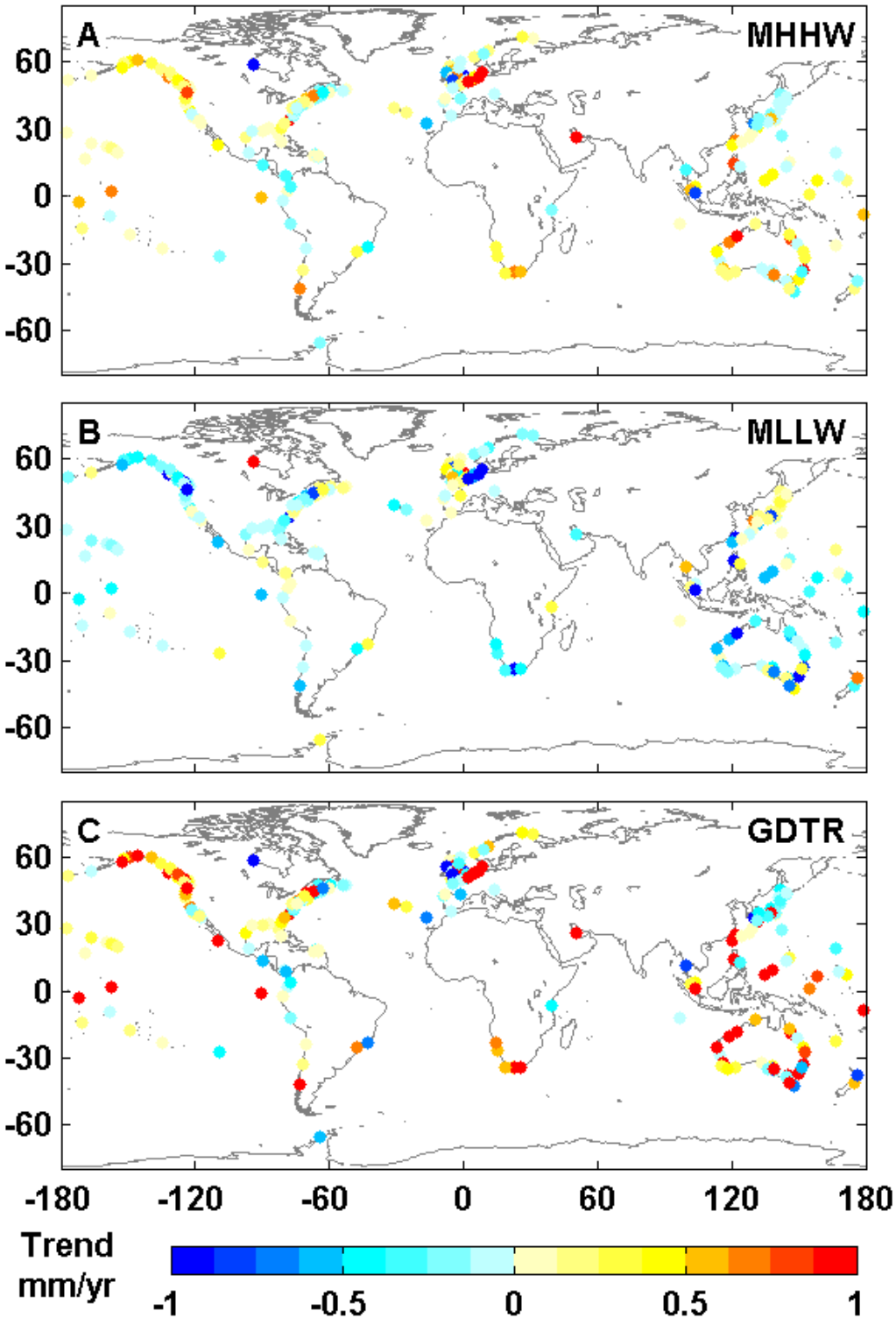

Figure D2.1: Global map showing magnitude of trends in mm/yr for MHHW (a), MLLW (b) and GDTR (c) for all locations.

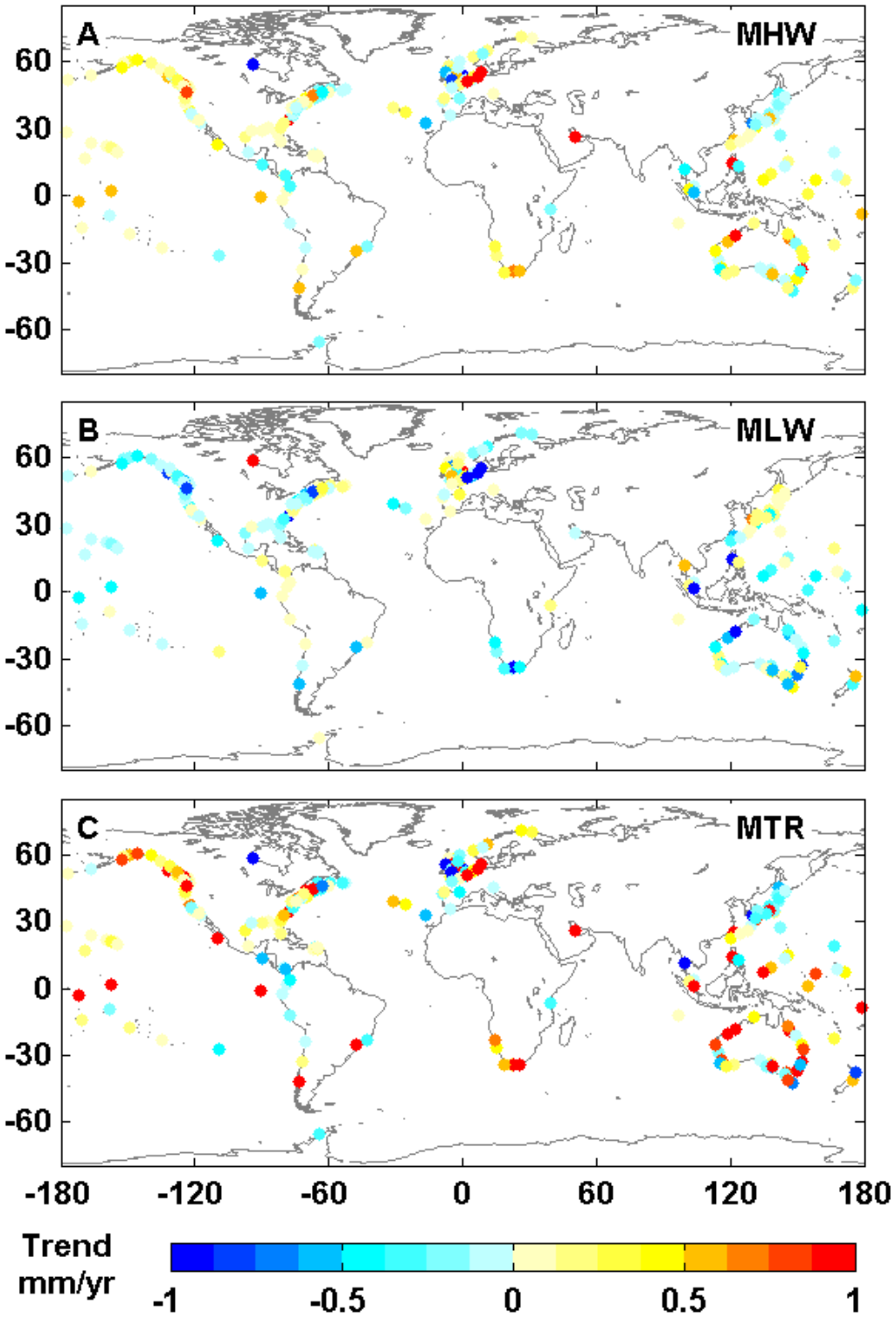

Figure D2.2: Global map showing magnitude of trends in mm/yr for MHW (a), MLW (b) and MTR (c) for all locations.

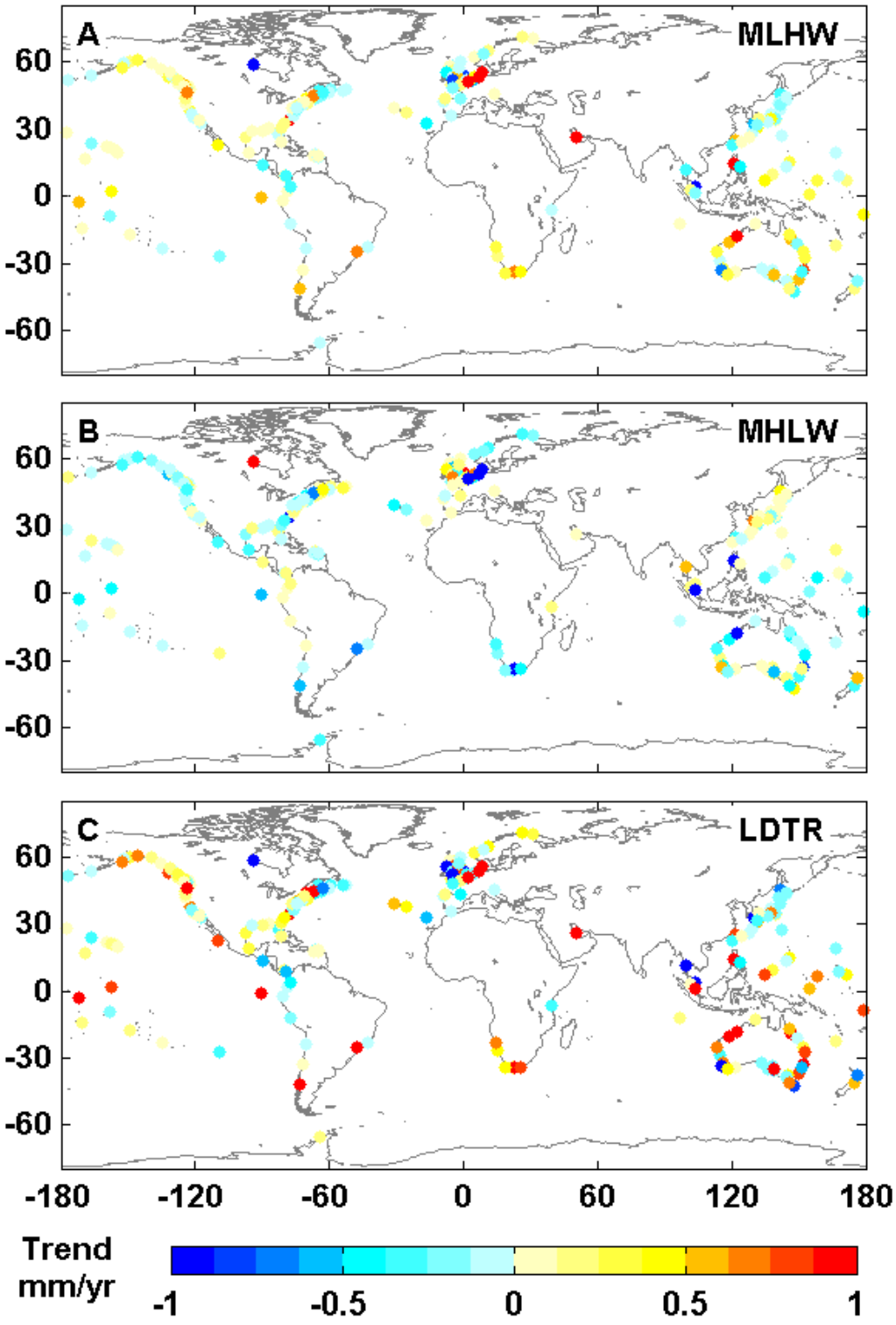

Figure D2.3: Global map showing magnitude of trends in mm/yr for MLHW (a), MHLW (b) and LDTR (c) for all locations.

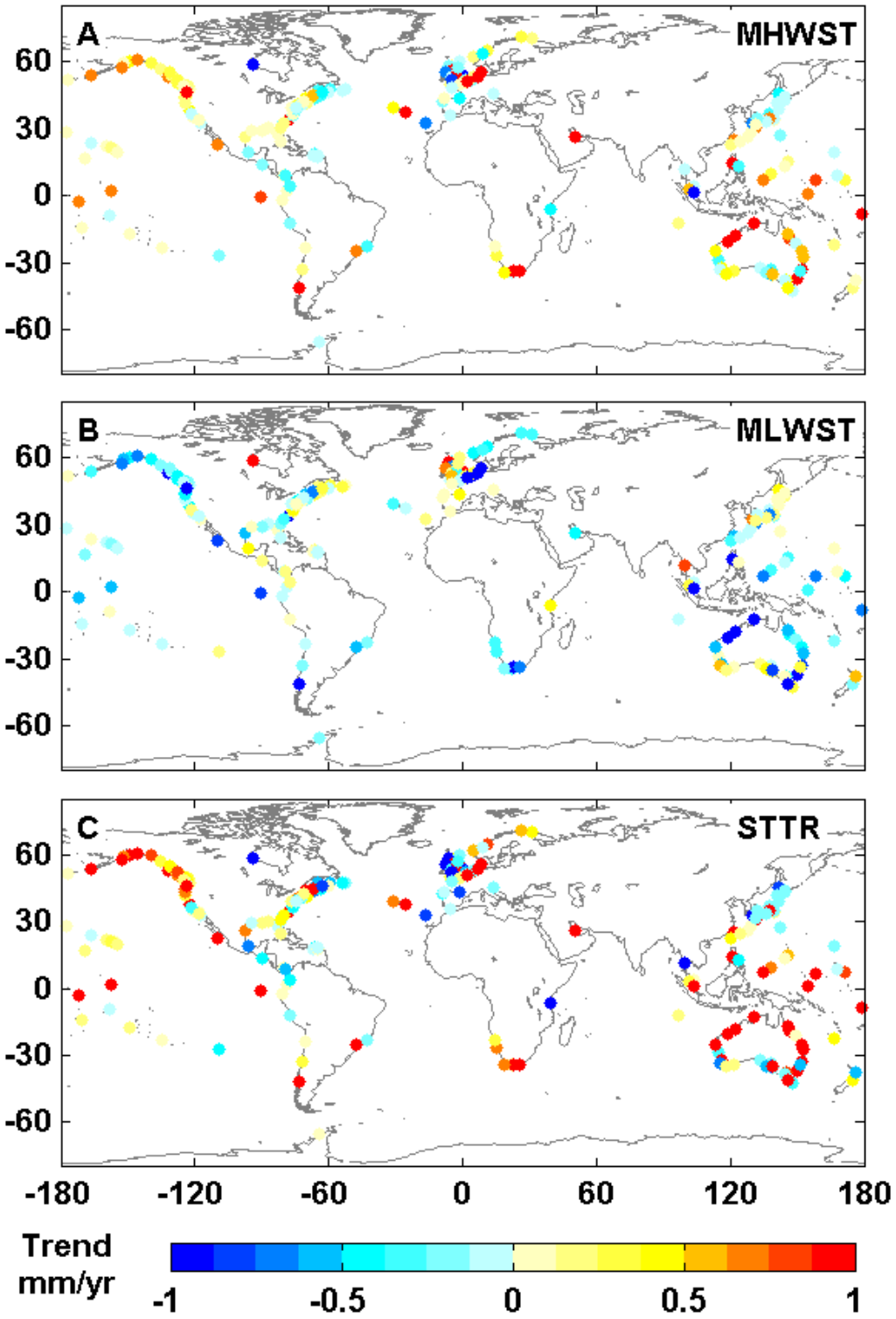

Figure D2.4: Global map showing magnitude of trends in mm/yr for MHWST (a), MLWST (b) and STTR (c) for all locations.

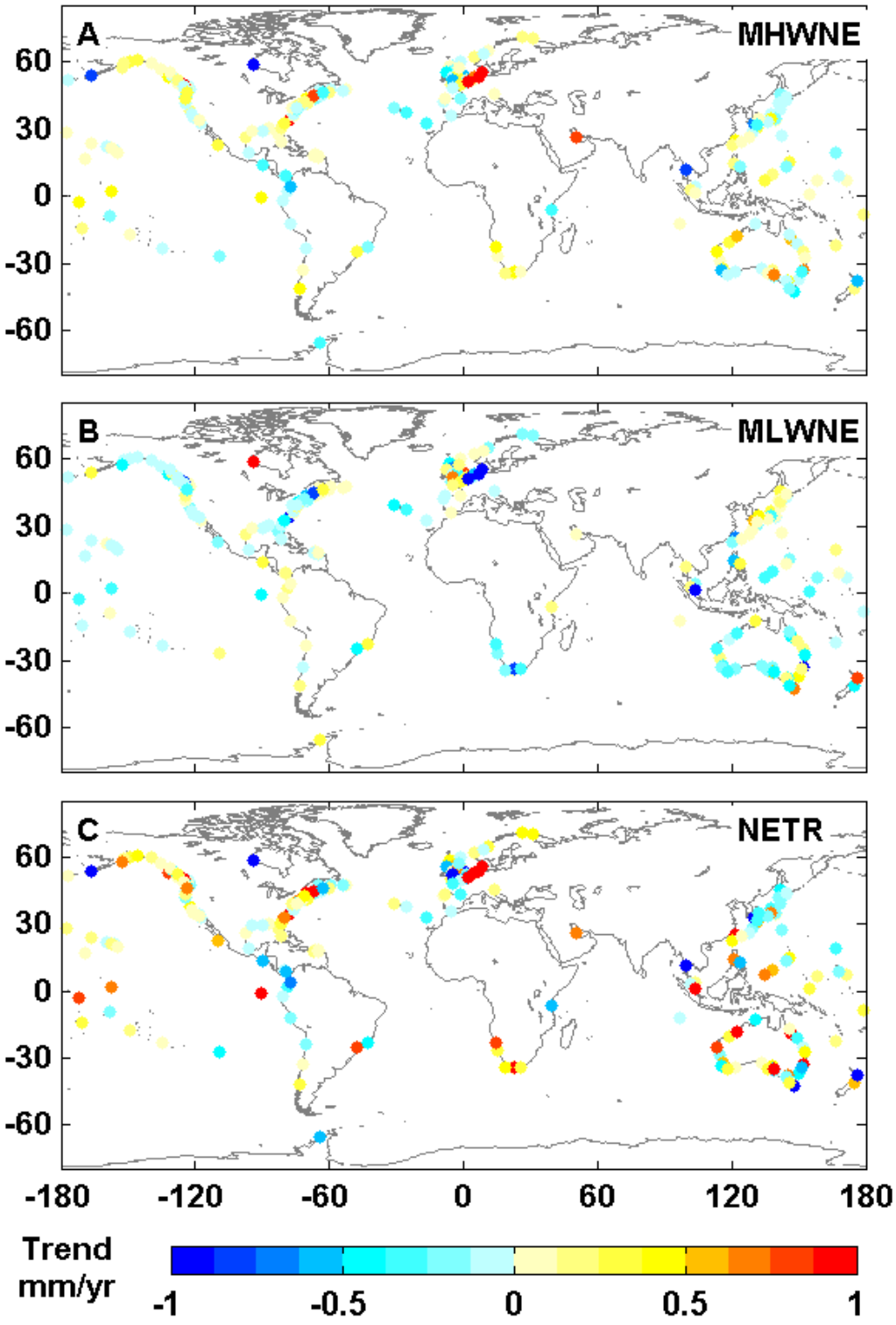

Figure D2.5: Global map showing magnitude of trends in mm/yr for MHWNE (a), MLWNE (b) and NETR (c) for all locations.

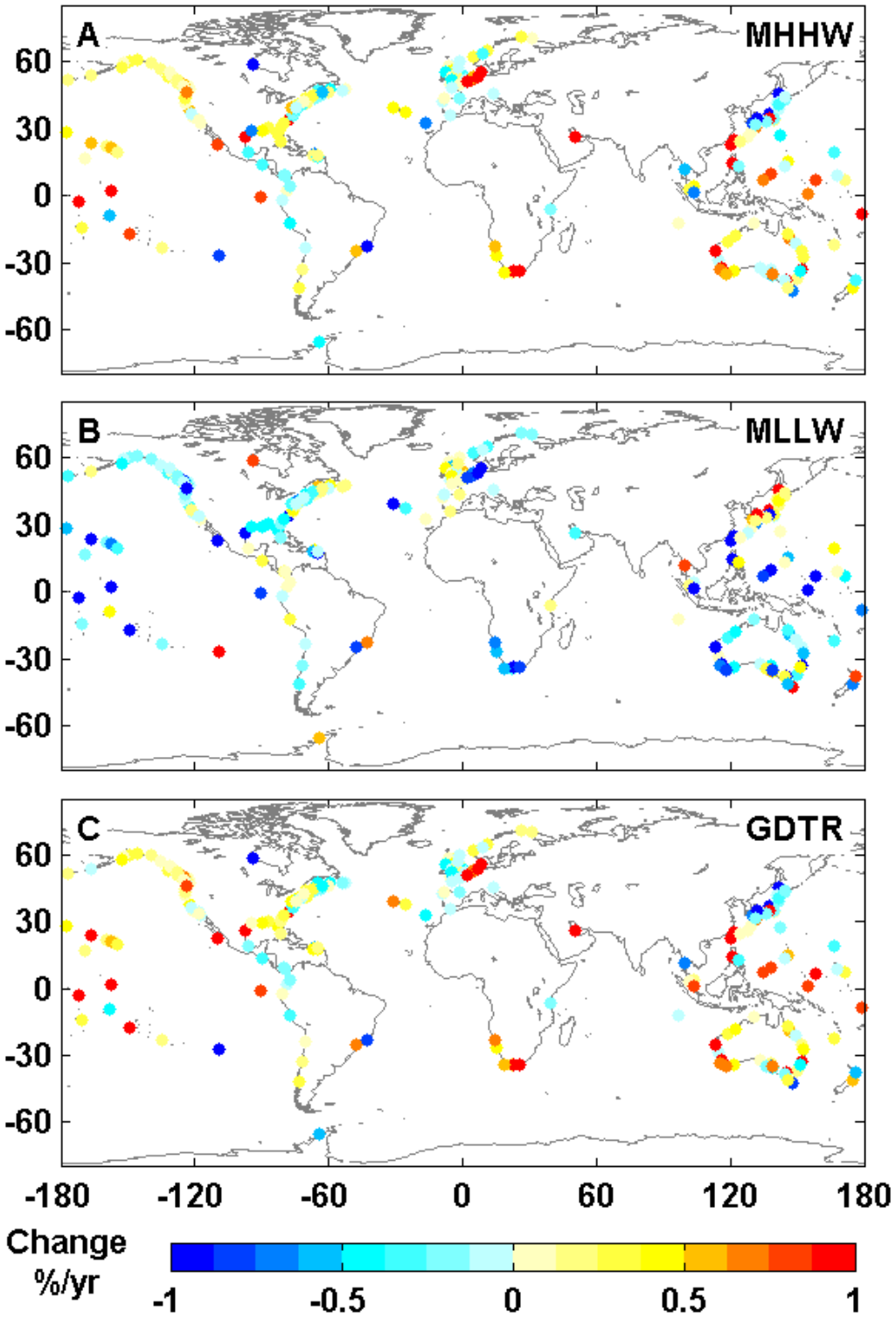

Figure D3.1: Global map showing percentage changes in %/yr for MHHW (a), MLLW (b) and GDTR (c) for all locations.

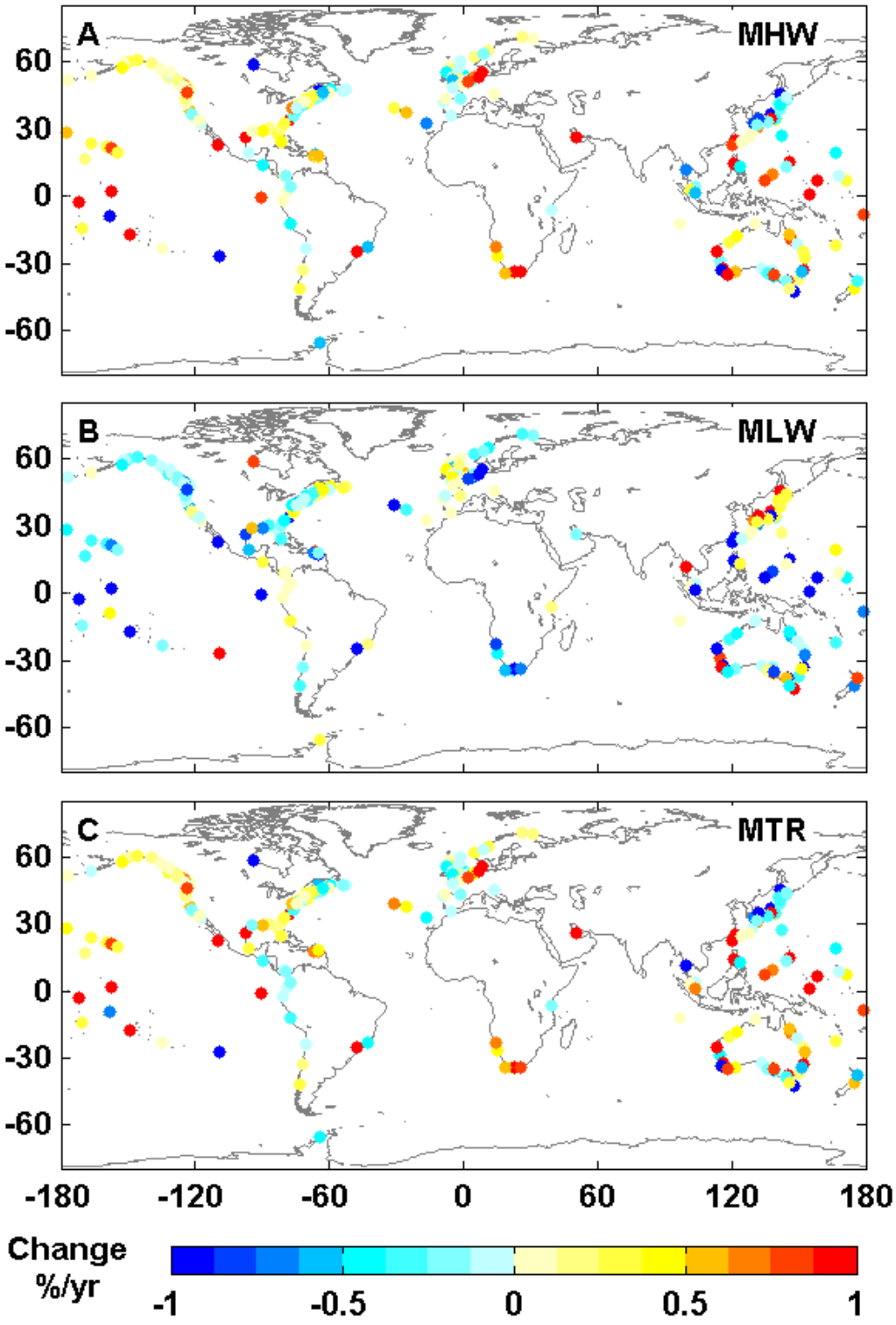

Figure D3.2: Global map showing percentage changes in %/yr for MHW (a), MLW (b) and MTR (c) for all locations.

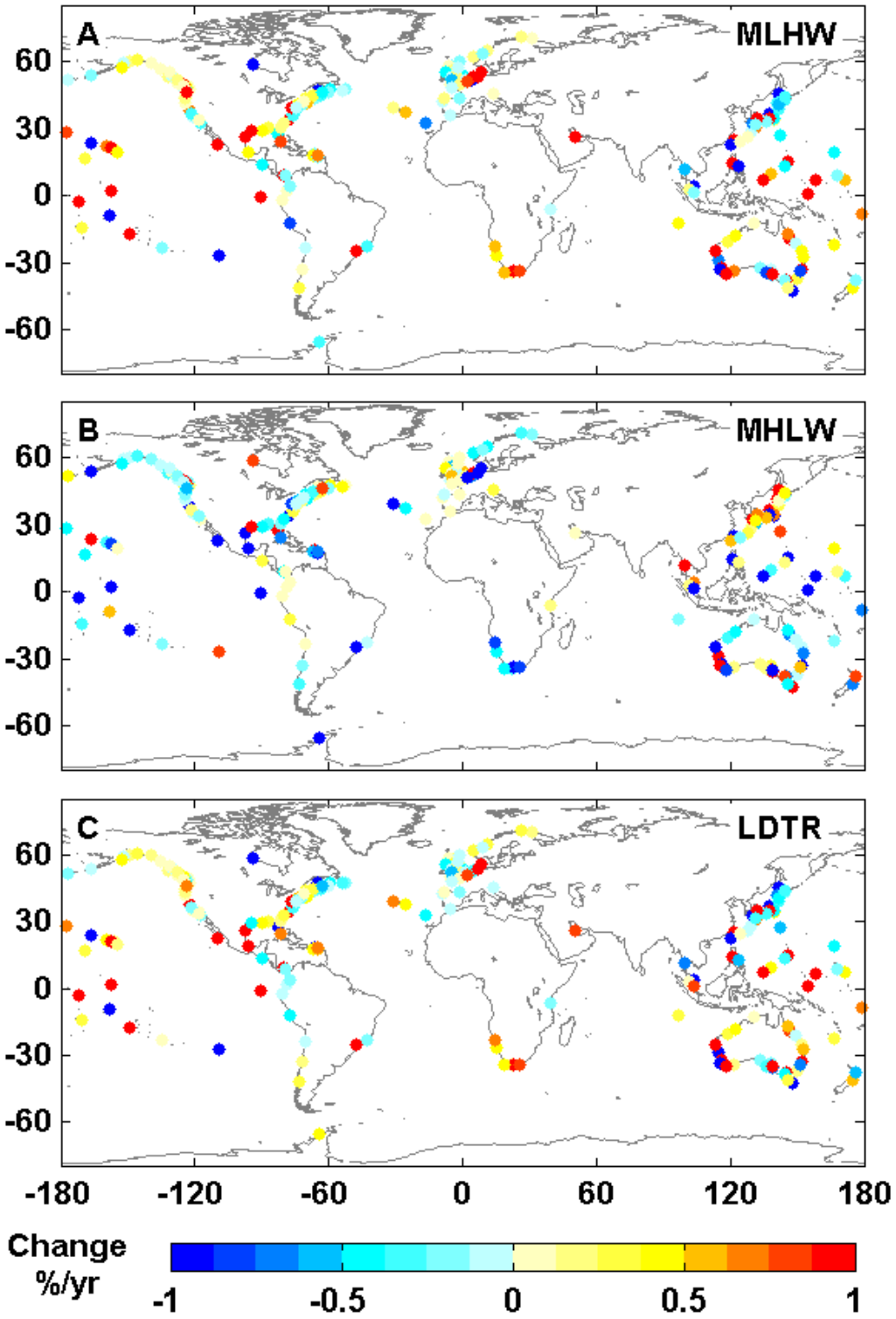

Figure D3.3: Global map showing percentage changes in %/yr for MLHW (a), MHLW (b) and LDTR (c) for all locations.

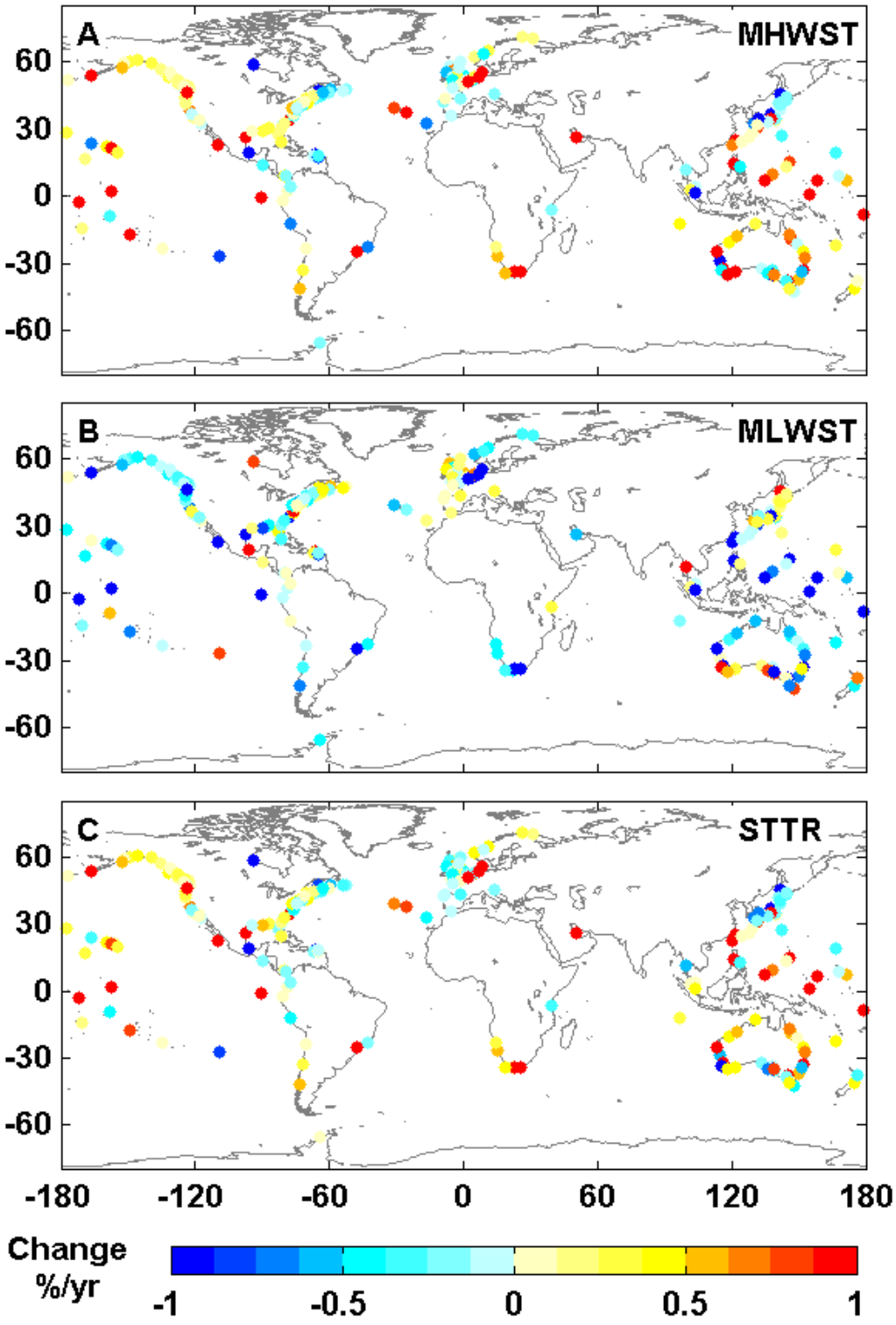

Figure D3.4: Global map showing percentage changes in %/yr for MHWST (a), MLWST (b) and STTR (c) for all locations.

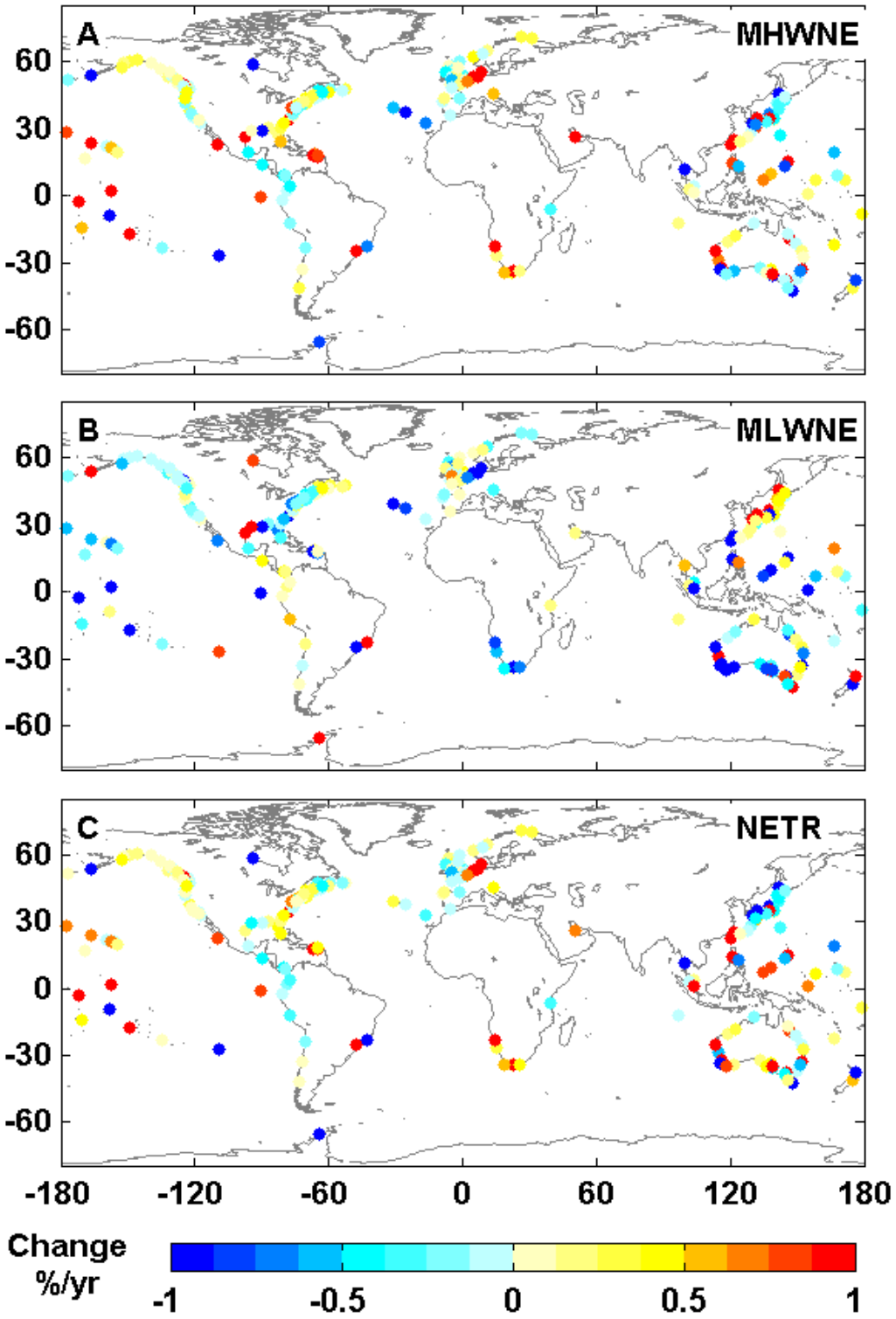

Figure D3.5: Global map showing percentage changes in %/yr for MHWNE (a), MLWNE (b) and NETR (c) for all locations.

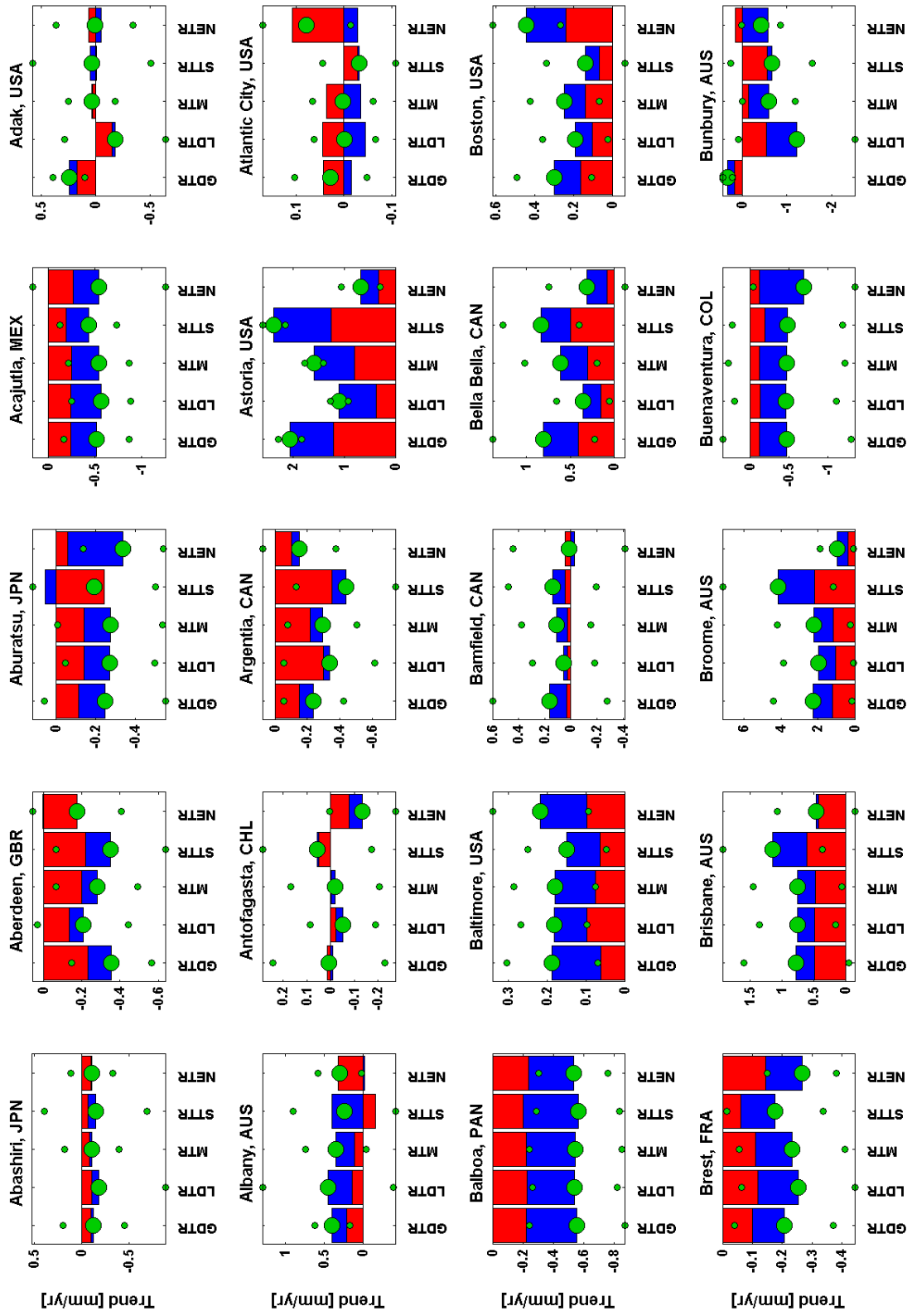

Figure D4.1: Plots showing the magnitude of linear trends in tidal levels at all sites. The trend in tidal range (large green dots) is plotted with 95% confidence limits (small green dots) for five tidal range (see Table 1). Stacked bar charts show the contribution towards the tidal range trend of changes in the respective HW subsets (red) and LW subsets (blue).

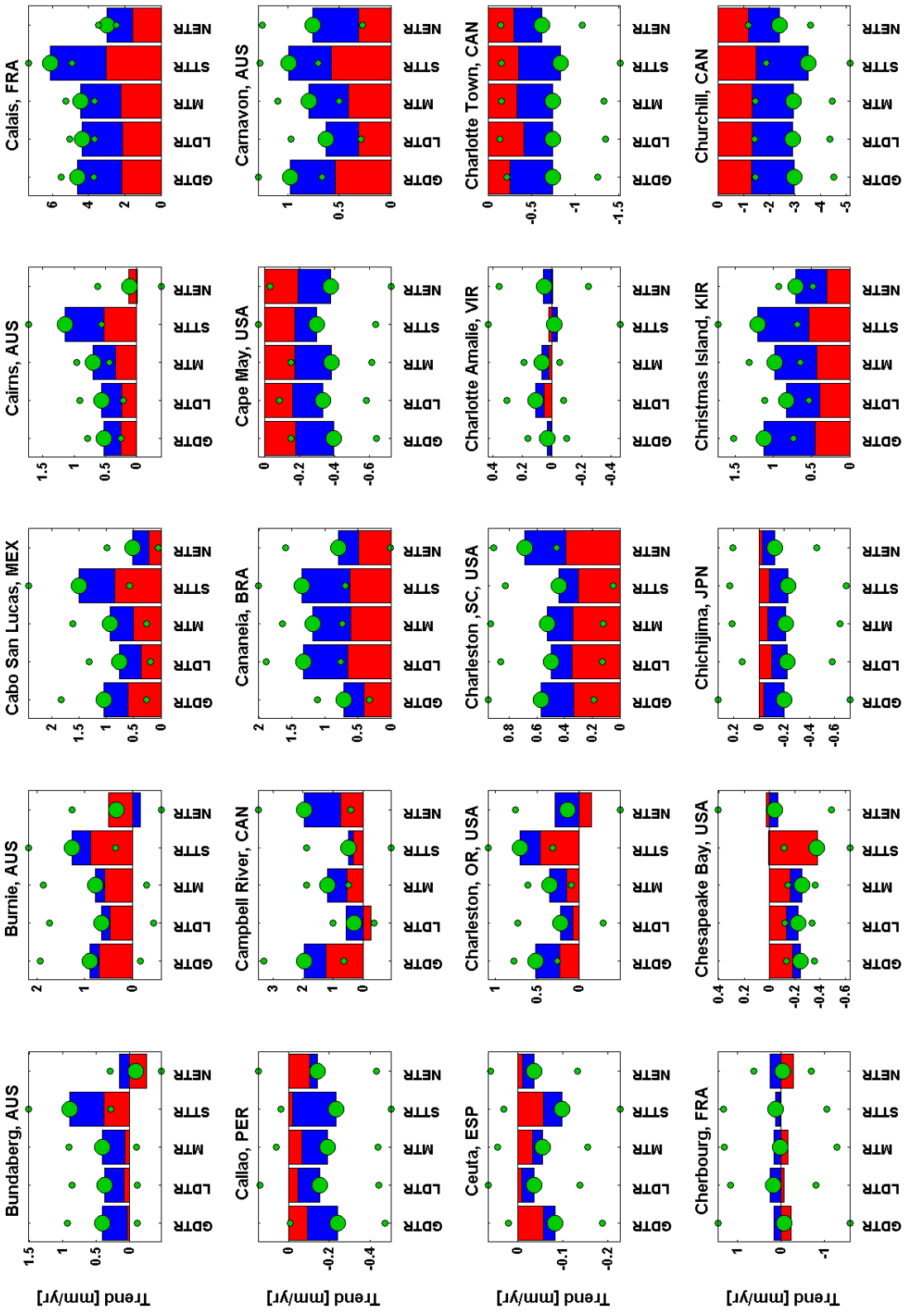

Figure D4.2: Plots showing the magnitude of linear trends in tidal levels at all sites. The trend in tidal range (large green dots) is plotted with 95% confidence limits (small green dots) for five tidal range (see Table 1). Stacked bar charts show the contribution towards the tidal range trend of changes in the respective HW subsets (red) and LW subsets (blue).

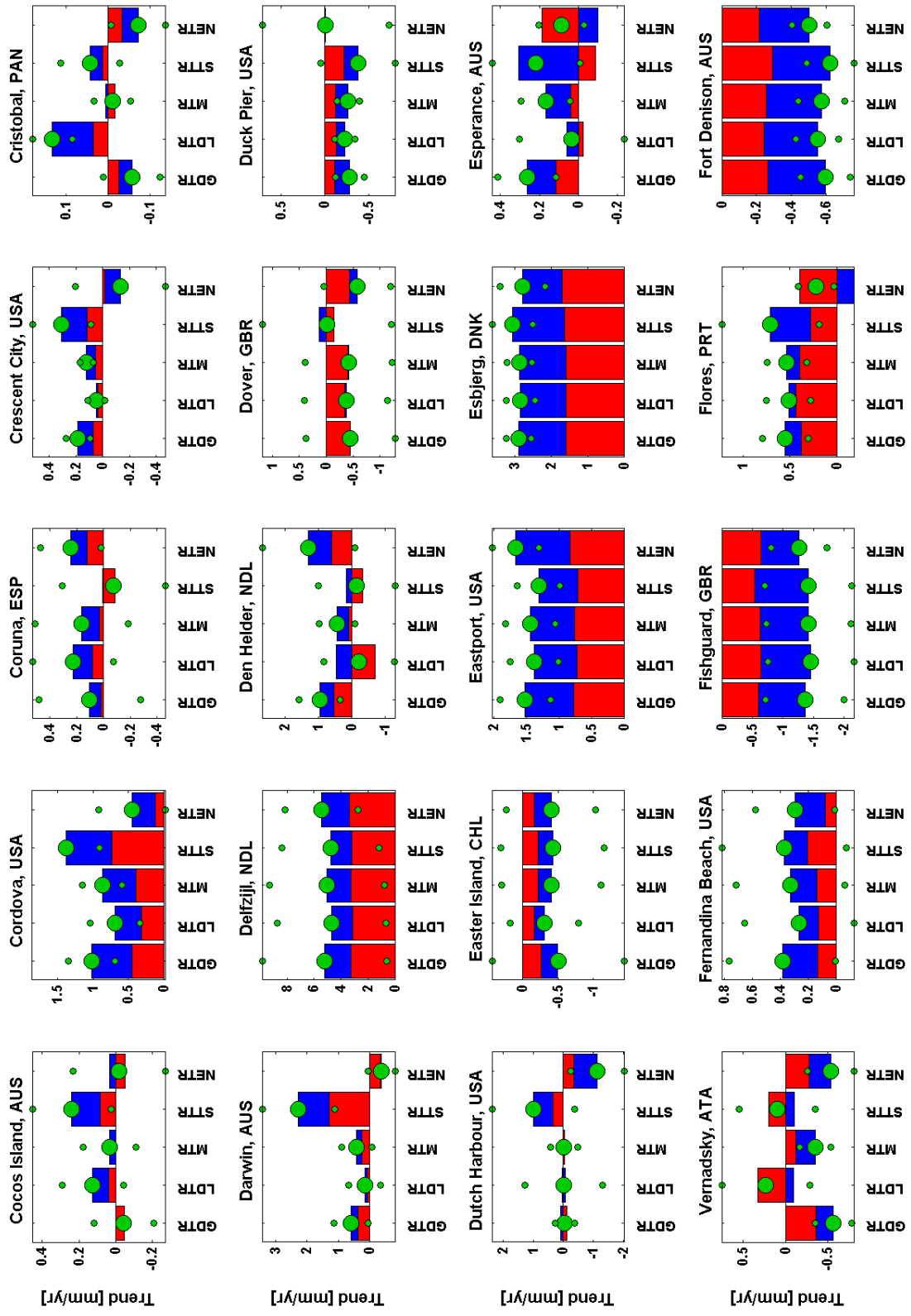

Figure D4.3: Plots showing the magnitude of linear trends in tidal levels at all sites. The trend in tidal range (large green dots) is plotted with 95% confidence limits (small green dots) for five tidal range (see Table 1). Stacked bar charts show the contribution towards the tidal range trend of changes in the respective HW subsets (red) and LW subsets (blue).

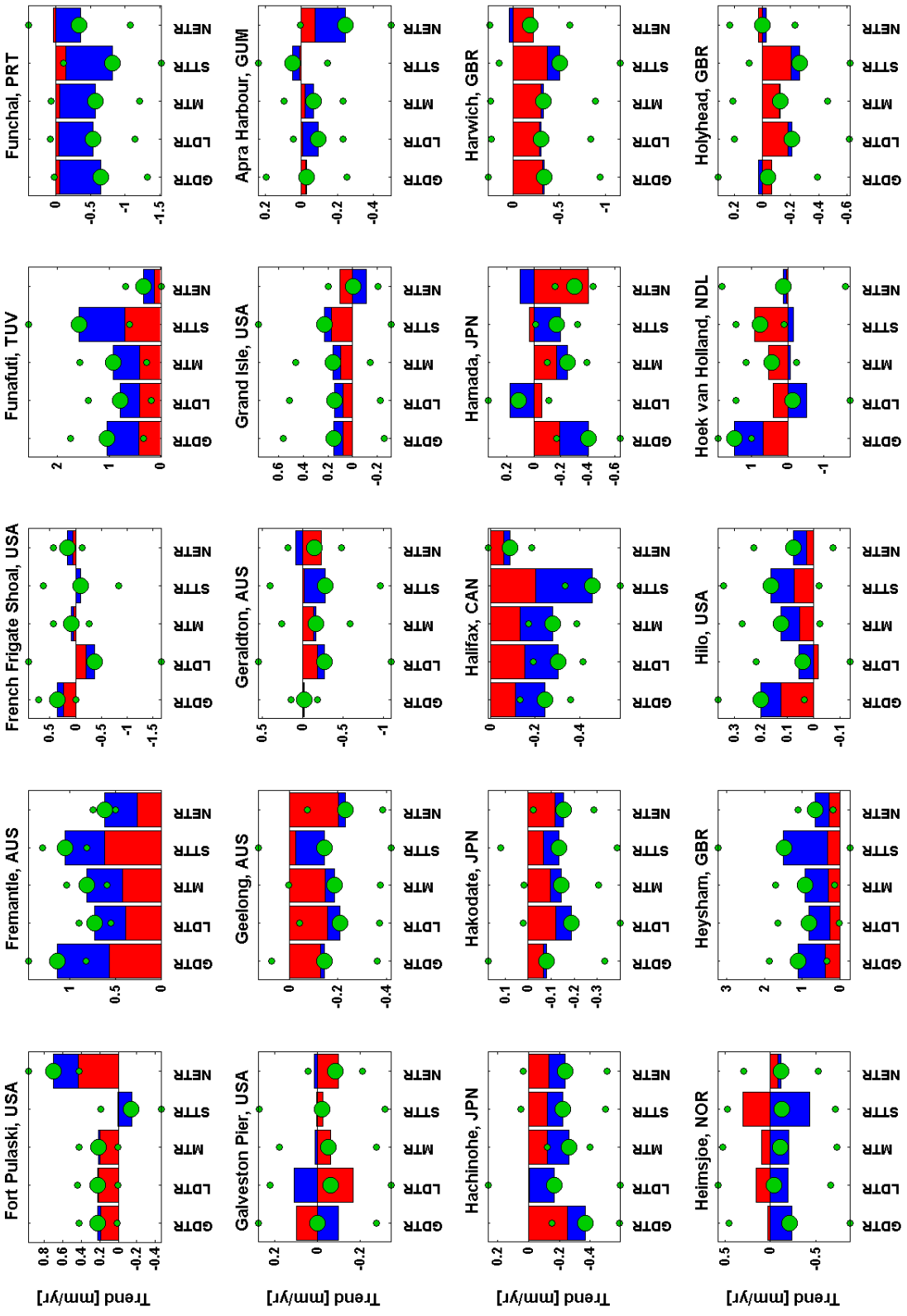

Figure D4.4: Plots showing the magnitude of linear trends in tidal levels at all sites. The trend in tidal range (large green dots) is plotted with 95% confidence limits (small green dots) for five tidal range (see Table 1). Stacked bar charts show the contribution towards the tidal range trend of changes in the respective HW subsets (red) and LW subsets (blue).

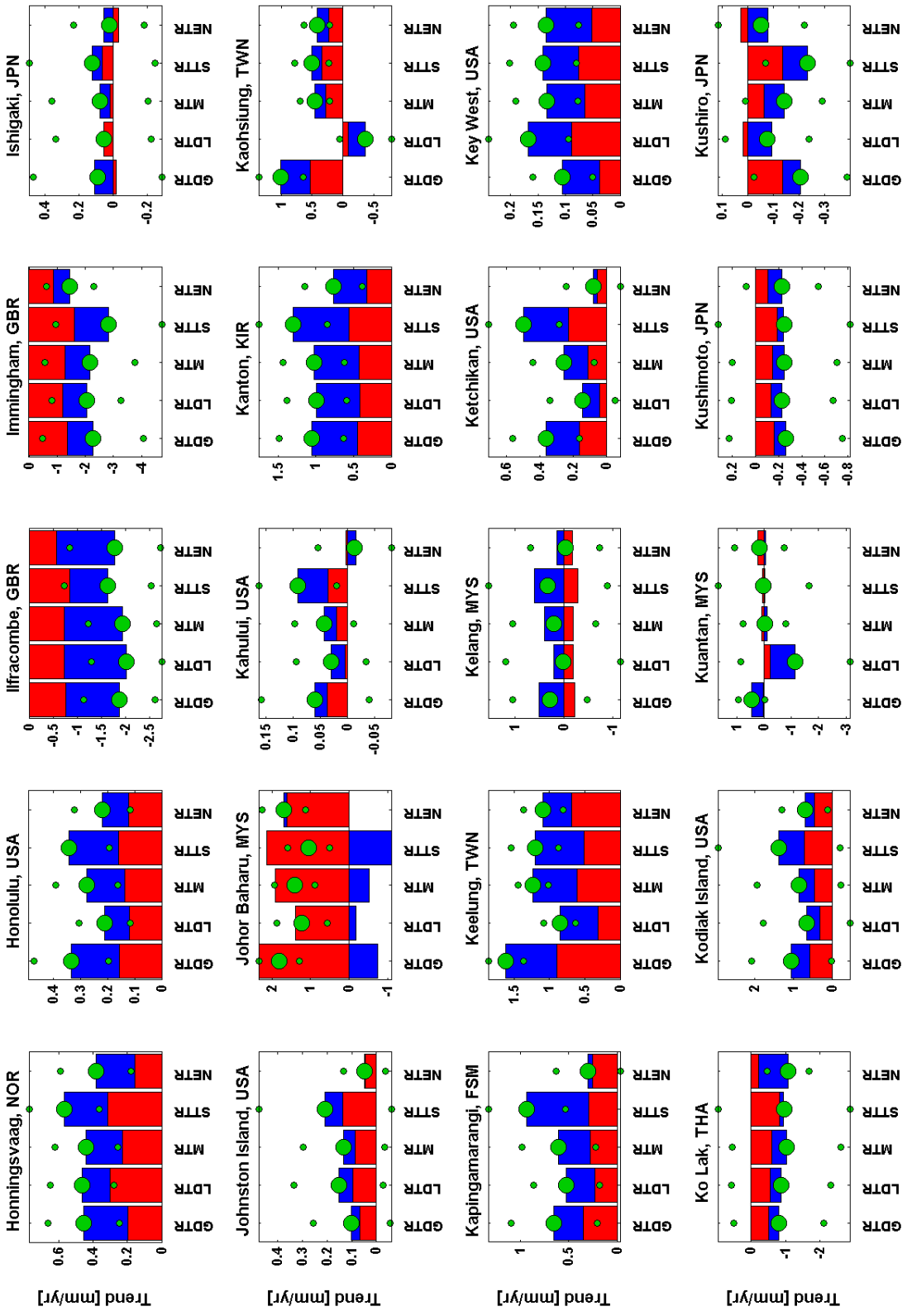

Figure D4.5: Plots showing the magnitude of linear trends in tidal levels at all sites. The trend in tidal range (large green dots) is plotted with 95% confidence limits (small green dots) for five tidal range (see Table 1). Stacked bar charts show the contribution towards the tidal range trend of changes in the respective HW subsets (red) and LW subsets (blue).

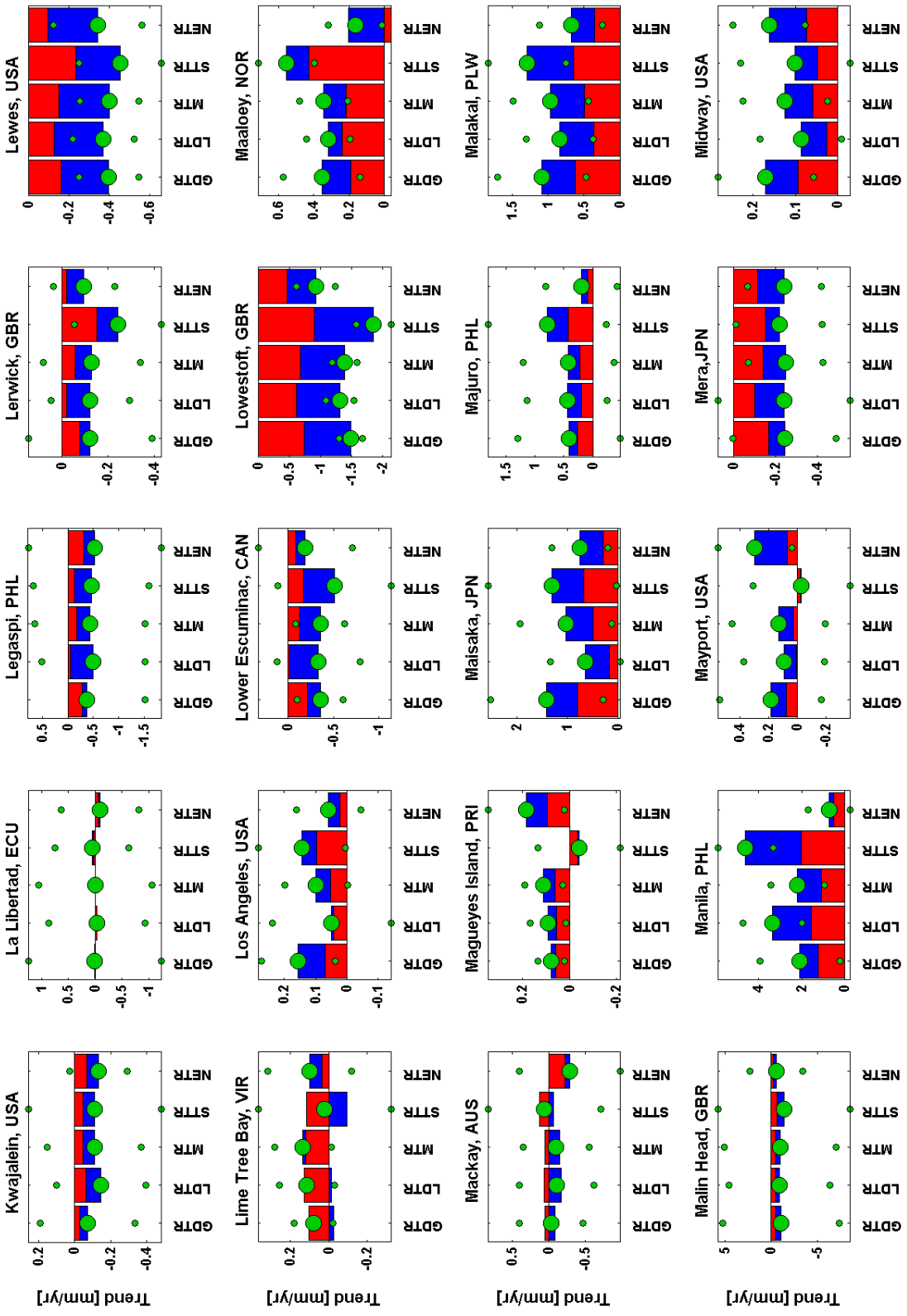

Figure D4.6: Plots showing the magnitude of linear trends in tidal levels at all sites. The trend in tidal range (large green dots) is plotted with 95% confidence limits (small green dots) for five tidal range (see Table 1). Stacked bar charts show the contribution towards the tidal range trend of changes in the respective HW subsets (red) and LW subsets (blue).

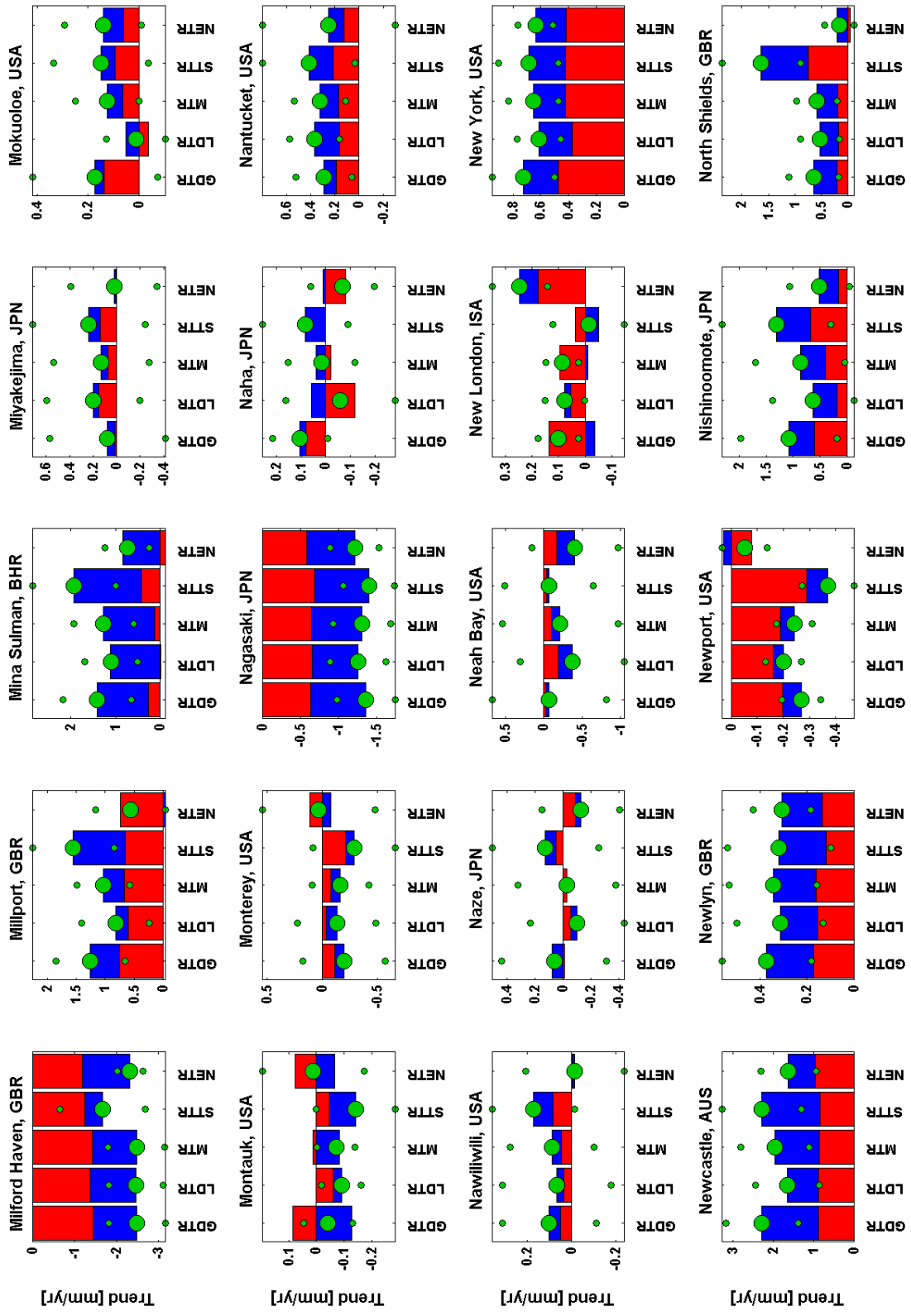

Figure D4.7: Plots showing the magnitude of linear trends in tidal levels at all sites. The trend in tidal range (large green dots) is plotted with 95% confidence limits (small green dots) for five tidal range (see Table 1). Stacked bar charts show the contribution towards the tidal range trend of changes in the respective HW subsets (red) and LW subsets (blue).

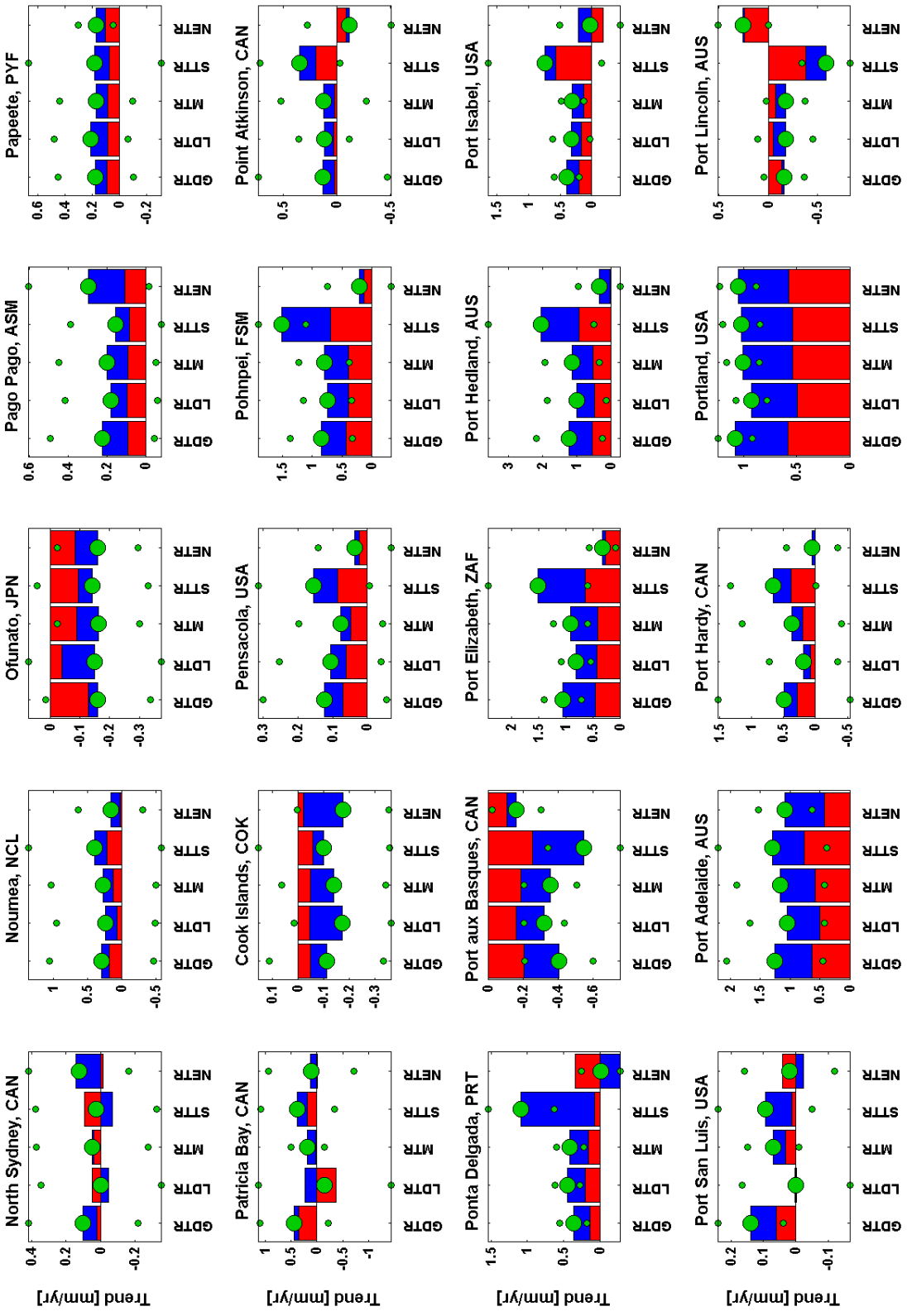

Figure D4.8: Plots showing the magnitude of linear trends in tidal levels at all sites. The trend in tidal range (large green dots) is plotted with 95% confidence limits (small green dots) for five tidal range (see Table 1). Stacked bar charts show the contribution towards the tidal range trend of changes in the respective HW subsets (red) and LW subsets (blue).

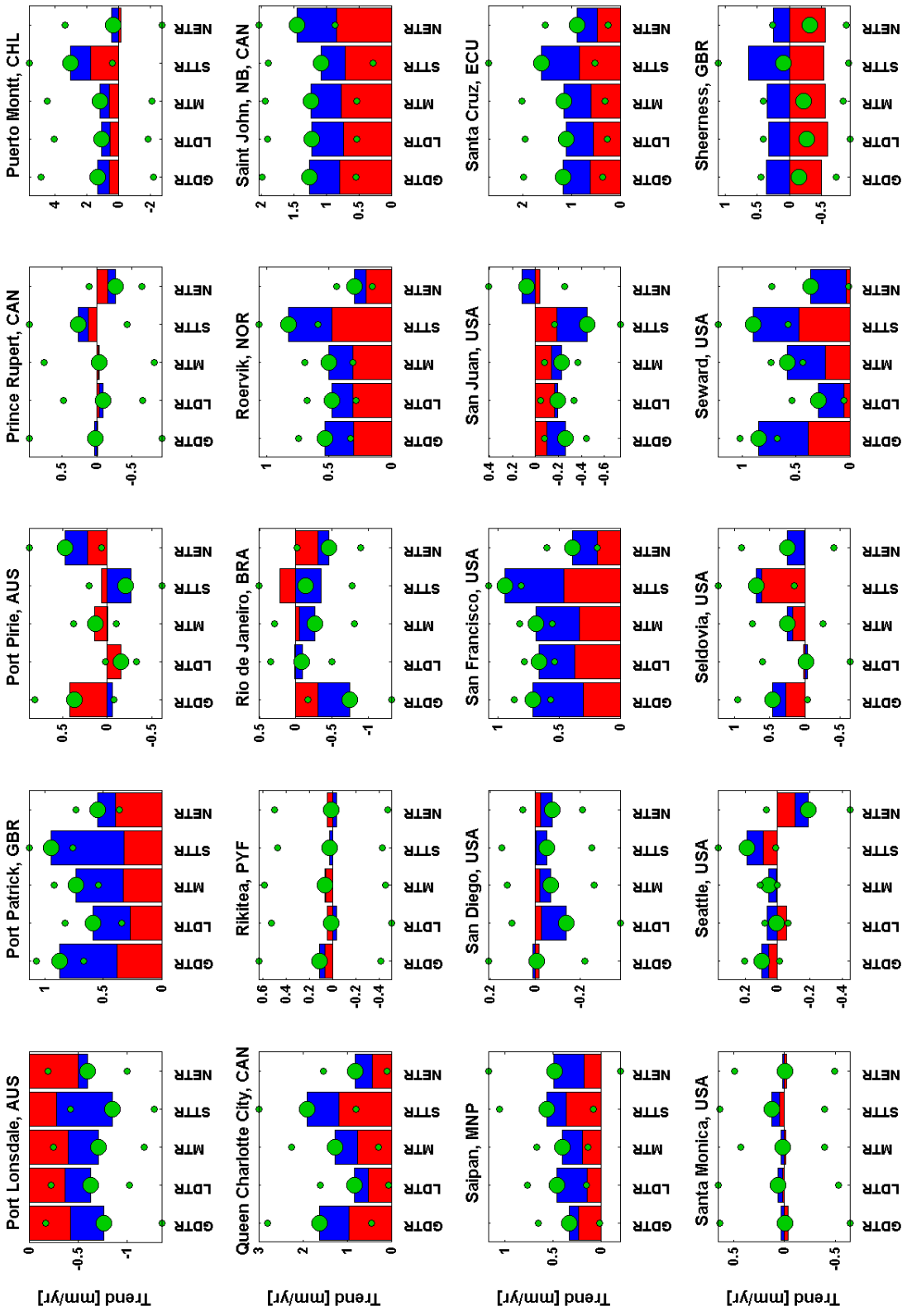

Figure D4.9: Plots showing the magnitude of linear trends in tidal levels at all sites. The trend in tidal range (large green dots) is plotted with 95% confidence limits (small green dots) for five tidal range (see Table 1). Stacked bar charts show the contribution towards the tidal range trend of changes in the respective HW subsets (red) and LW subsets (blue).

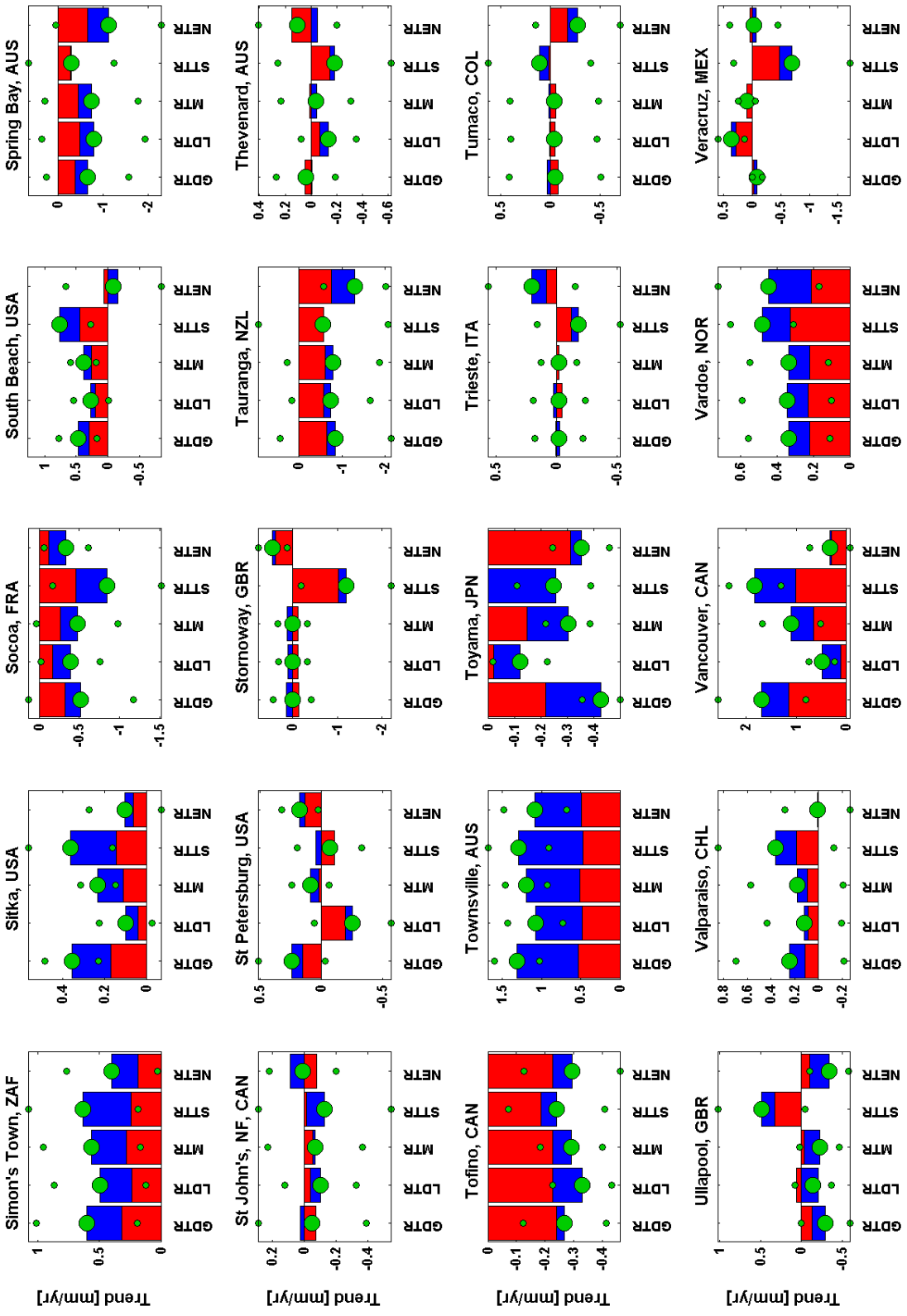

Figure D4.10: Plots showing the magnitude of linear trends in tidal levels at all sites. The trend in tidal range (large green dots) is plotted with 95% confidence limits (small green dots) for five tidal range (see Table 1). Stacked bar charts show the contribution towards the tidal range trend of changes in the respective HW subsets (red) and LW subsets (blue).

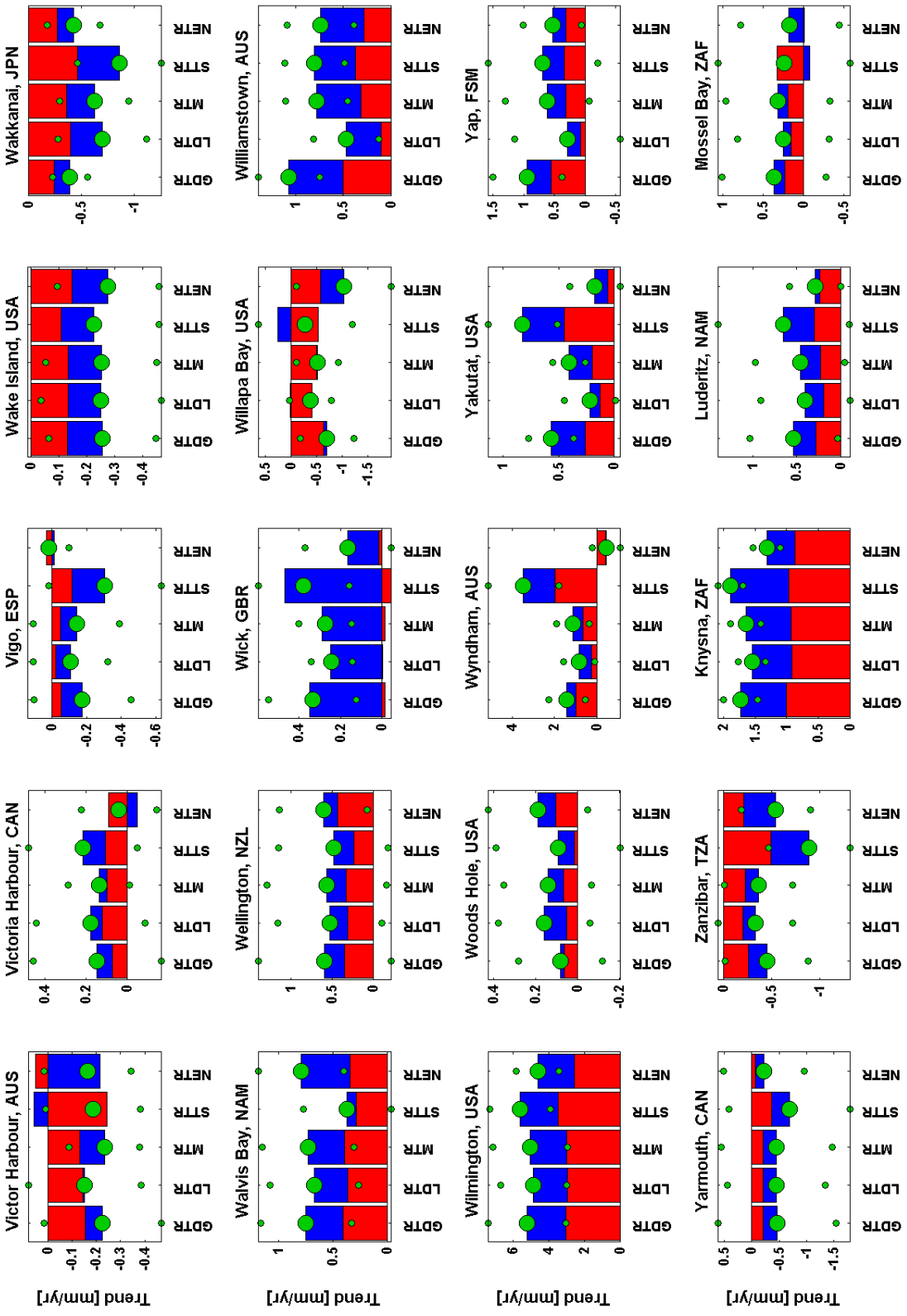

Figure D4.11: Plots showing the magnitude of linear trends in tidal levels at all sites. The trend in tidal range (large green dots) is plotted with 95% confidence limits (small green dots) for five tidal range (see Table 1). Stacked bar charts show the contribution towards the tidal range trend of changes in the respective HW subsets (red) and LW subsets (blue).

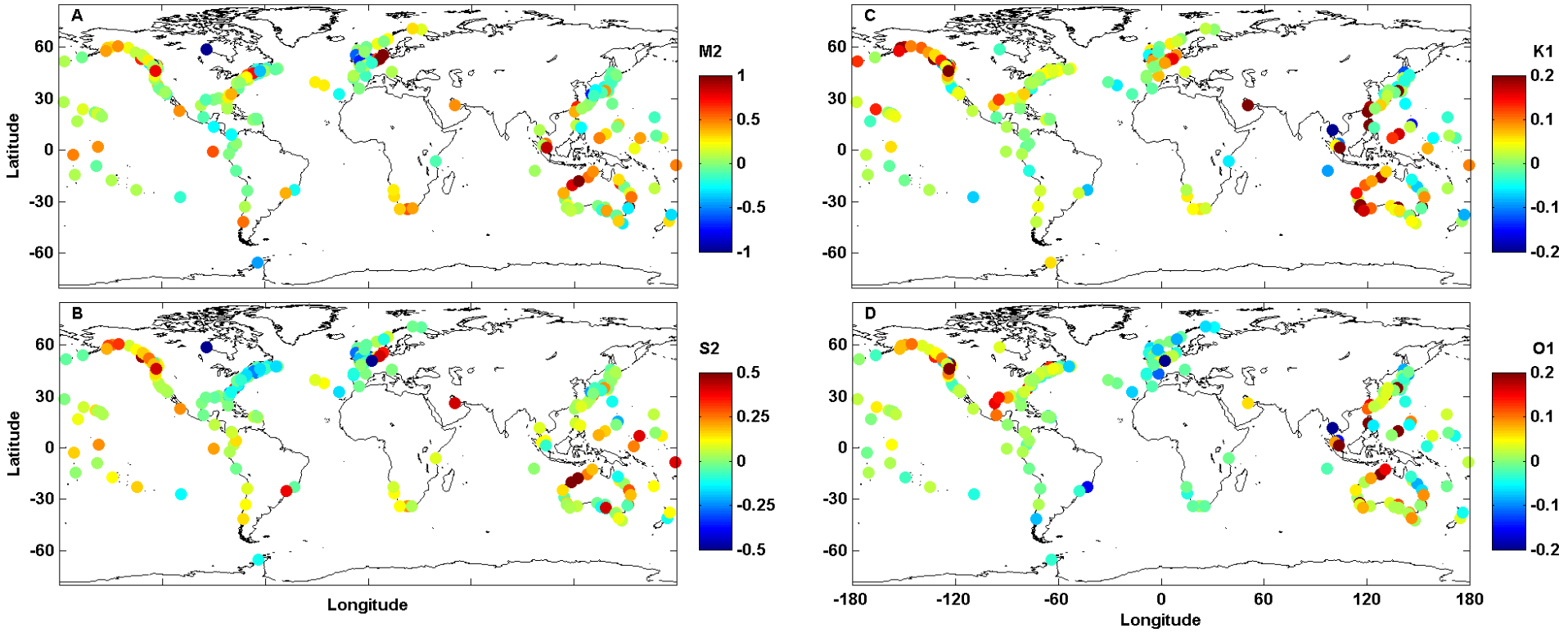

Figure D5.1: Maps show the trend in the magnitude of 4 tidal constituents (M2, S2, K1 & O1) in mm/yr. range (see Table 1). Stacked bar charts show the contribution towards the tidal range trend of changes in the respective HW subsets (red) and LW subsets (blue)

Appendix E Supplementary Material to Chapter 5

Figure E1 shows the histogram of the timing relative to predicted high water of the 100 largest independent NTR events.

Figure E2 shows scatter plots of the 100 largest independent NTR events and their associated skew surge value.

Figures E3.1 to E3.4 show the trends in the 99th percentile of skew surge for the last 20-80 years (at sites with enough data) and compared to the trend for the entire length of the data at each site.

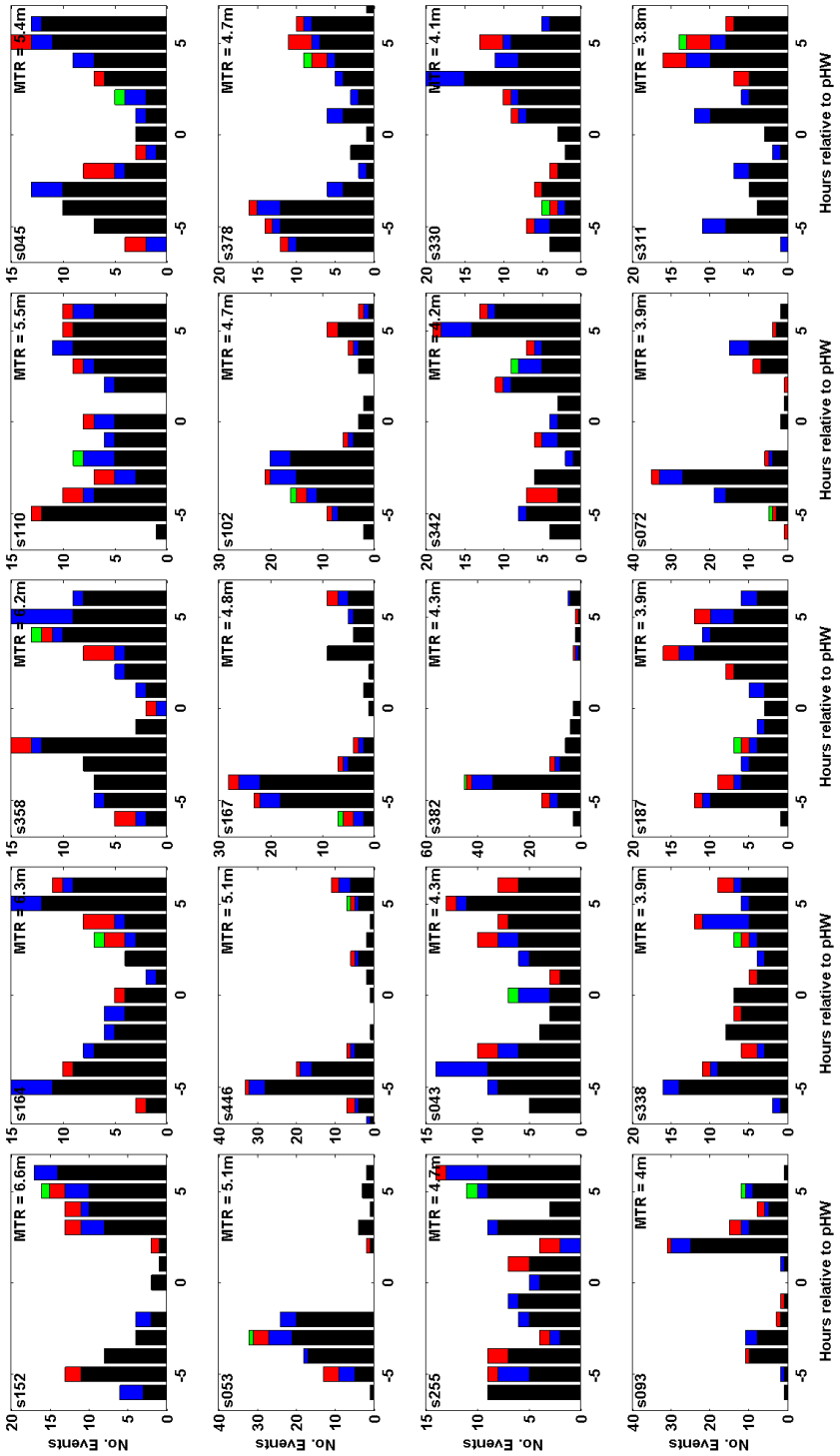

Figure E1.1: Histogram of the timing relative to predicted high water of the 100 largest independent NTR events. Colours indicate rank according to magnitude of NTR: green = maximum, red = top 10, blue = top 50. Plots are ordered by magnitude of MTR, which is written in the top right corner, while the site ID is written in the top left corner.

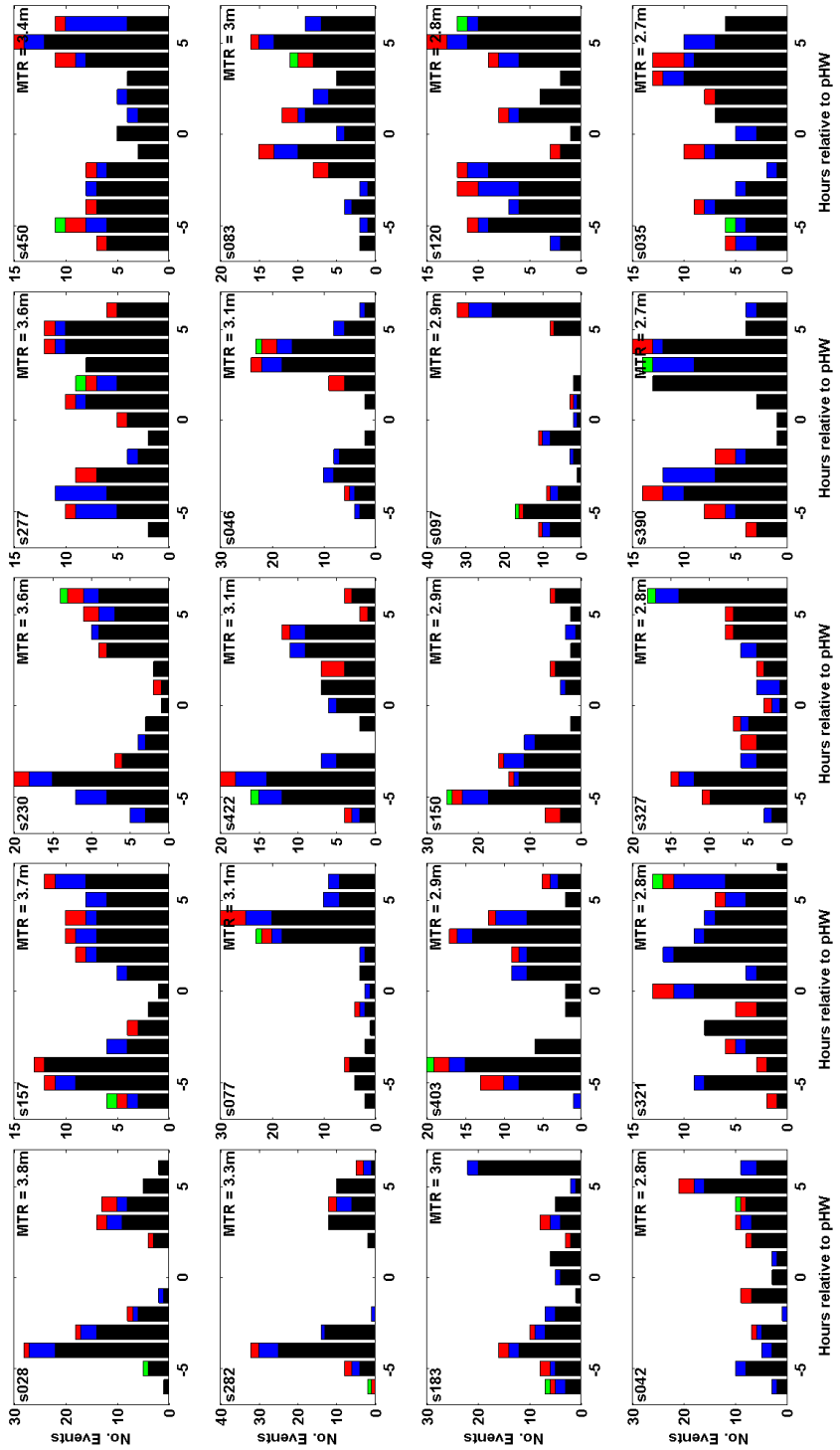

Figure E1.2: Histogram of the timing relative to predicted high water of the 100 largest independent NTR events. Colours indicate rank according to magnitude of NTR: green = maximum, red = top 10, blue = top 50. Plots are ordered by magnitude of MTR, which is written in the top right corner, while the site ID is written in the top left corner.

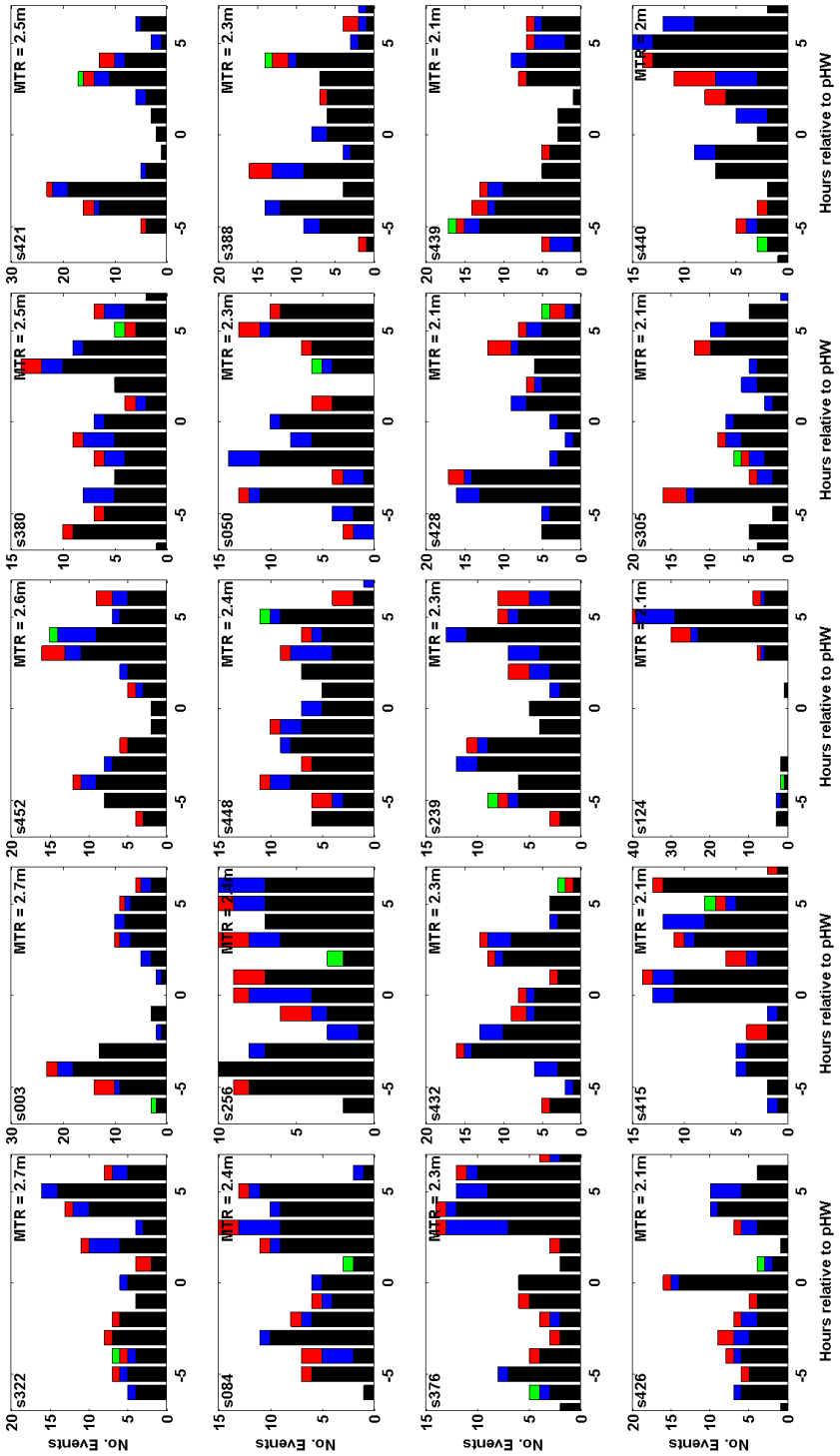

Figure E1.3: Histogram of the timing relative to predicted high water of the 100 largest independent NTR events. Colours indicate rank according to magnitude of NTR: green = maximum, red = top 10, blue = top 50. Plots are ordered by magnitude of MTR, which is written in the top right corner, while the site ID is written in the top left corner.

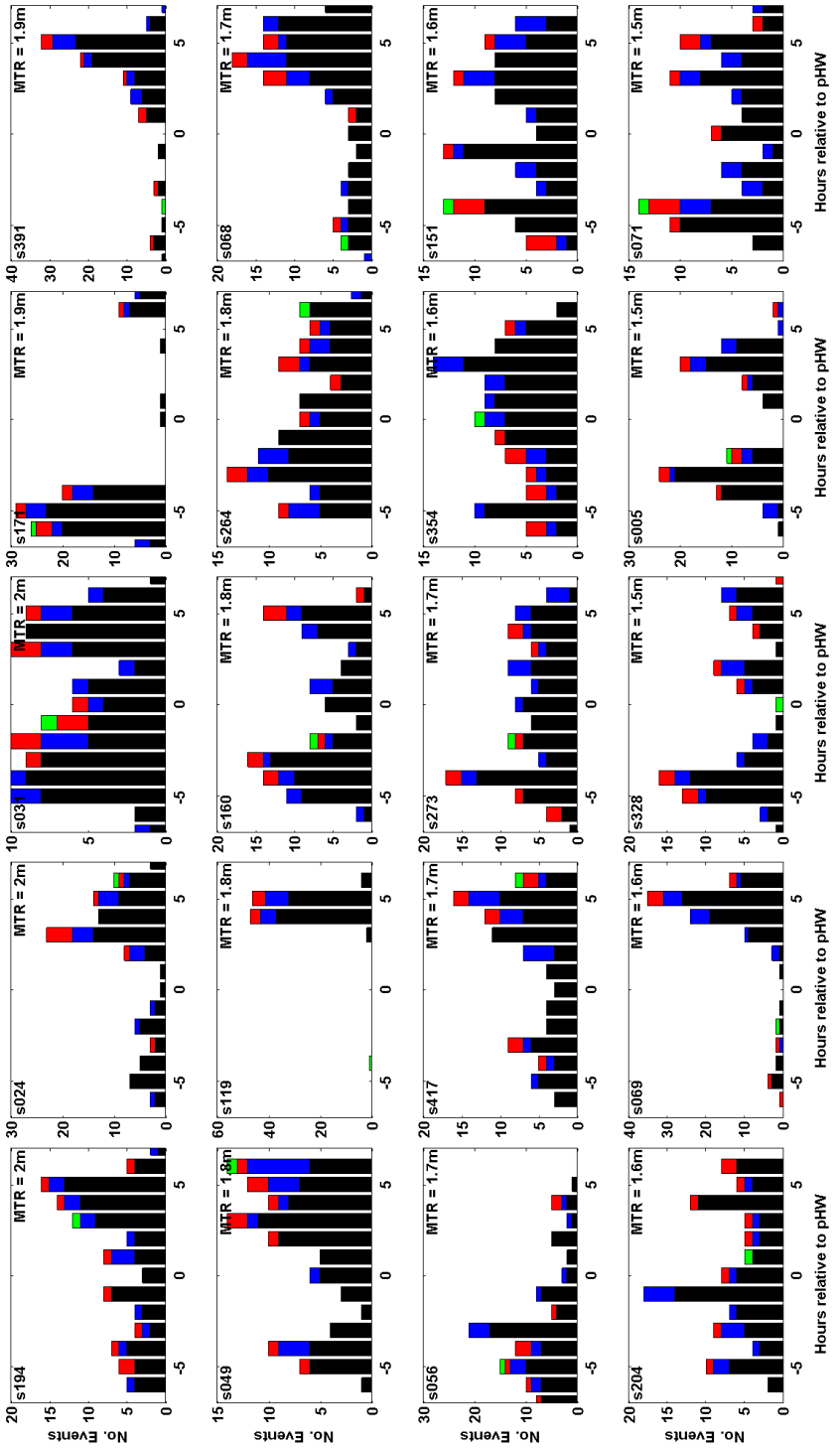

Figure E1.4: Histogram of the timing relative to predicted high water of the 100 largest independent NTR events. Colours indicate rank according to magnitude of NTR: green = maximum, red = top 10, blue = top 50. Plots are ordered by magnitude of MTR, which is written in the top right corner, while the site ID is written in the top left corner.

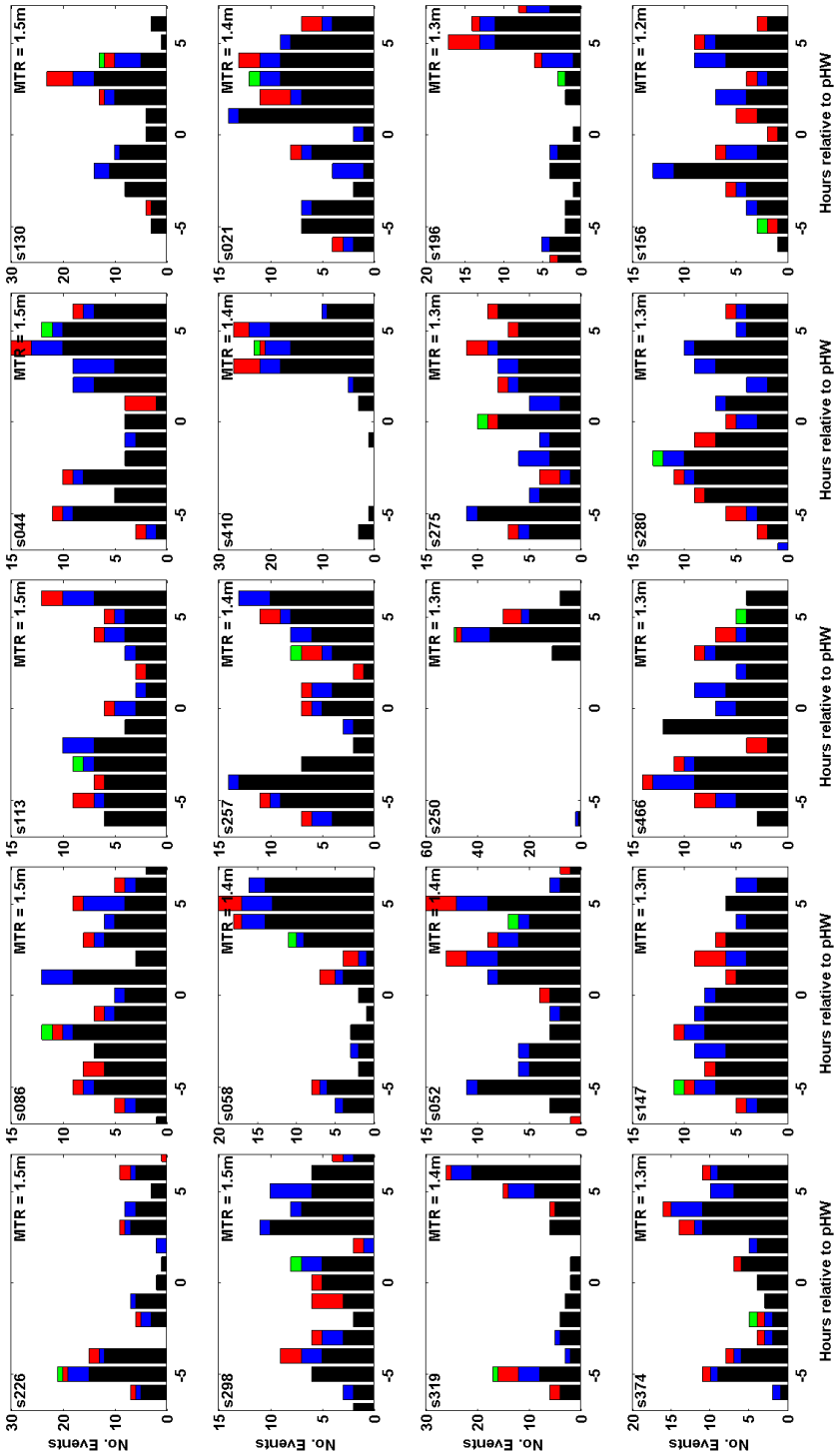

Figure E1.5: Histogram of the timing relative to predicted high water of the 100 largest independent NTR events. Colours indicate rank according to magnitude of NTR: green = maximum, red = top 10, blue = top 50. Plots are ordered by magnitude of MTR, which is written in the top right corner, while the site ID is written in the top left corner.

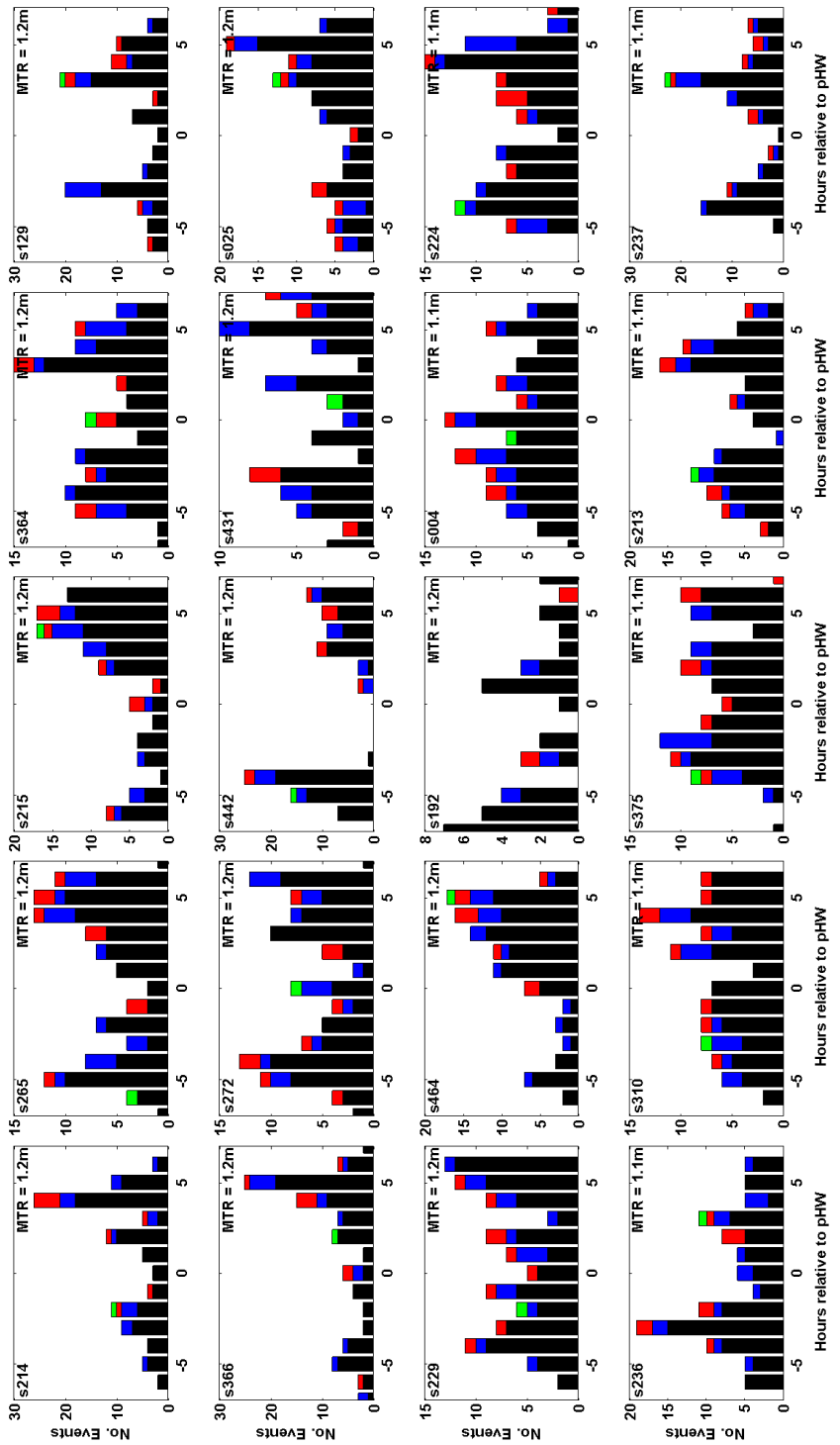

Figure E1.6: Histogram of the timing relative to predicted high water of the 100 largest independent NTR events. Colours indicate rank according to magnitude of NTR: green = maximum, red = top 10, blue = top 50. Plots are ordered by magnitude of MTR, which is written in the top right corner, while the site ID is written in the top left corner.

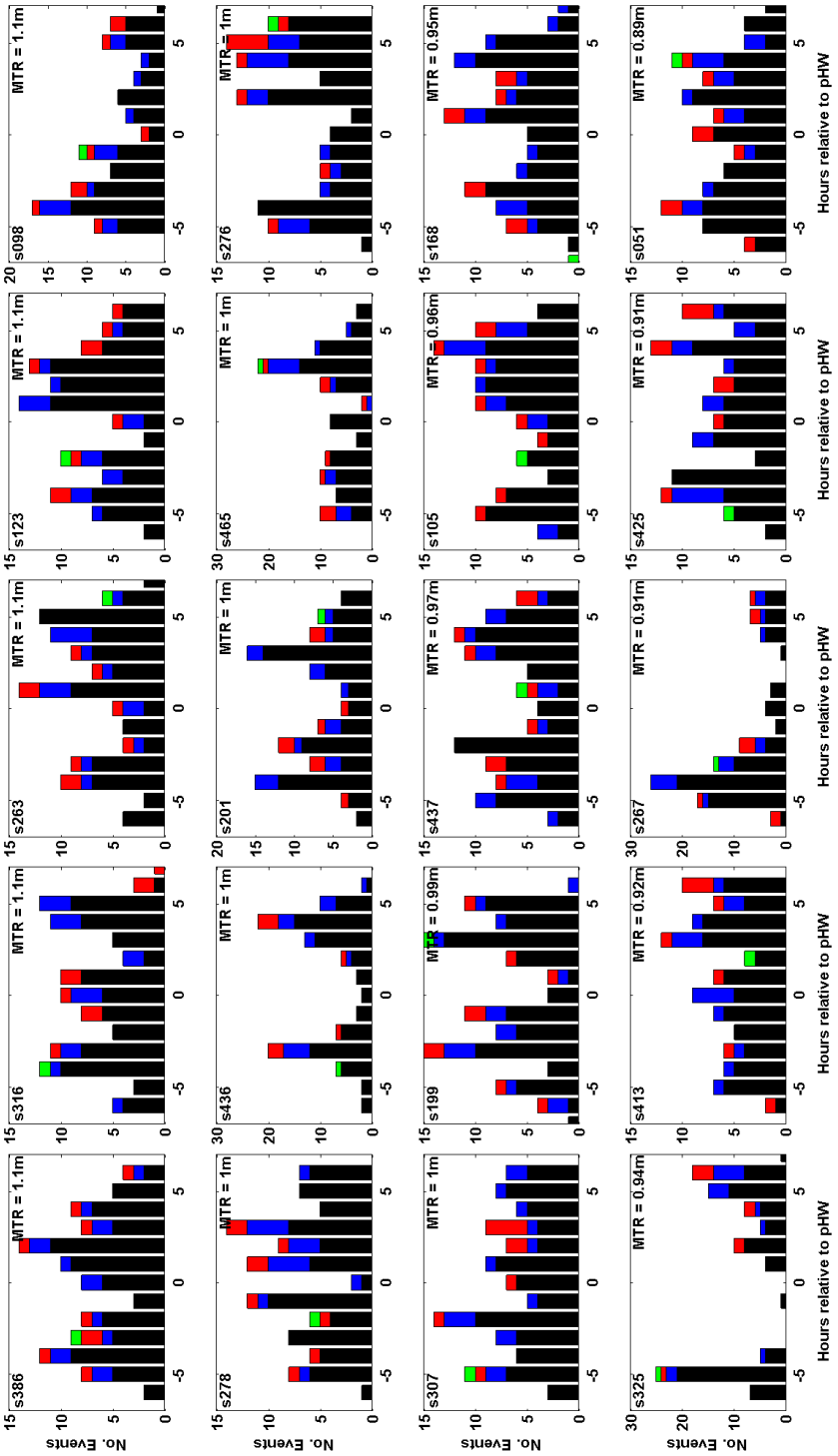

Figure E1.7: Histogram of the timing relative to predicted high water of the 100 largest independent NTR events. Colours indicate rank according to magnitude of NTR: green = maximum, red = top 10, blue = top 50. Plots are ordered by magnitude of MTR, which is written in the top right corner, while the site ID is written in the top left corner.

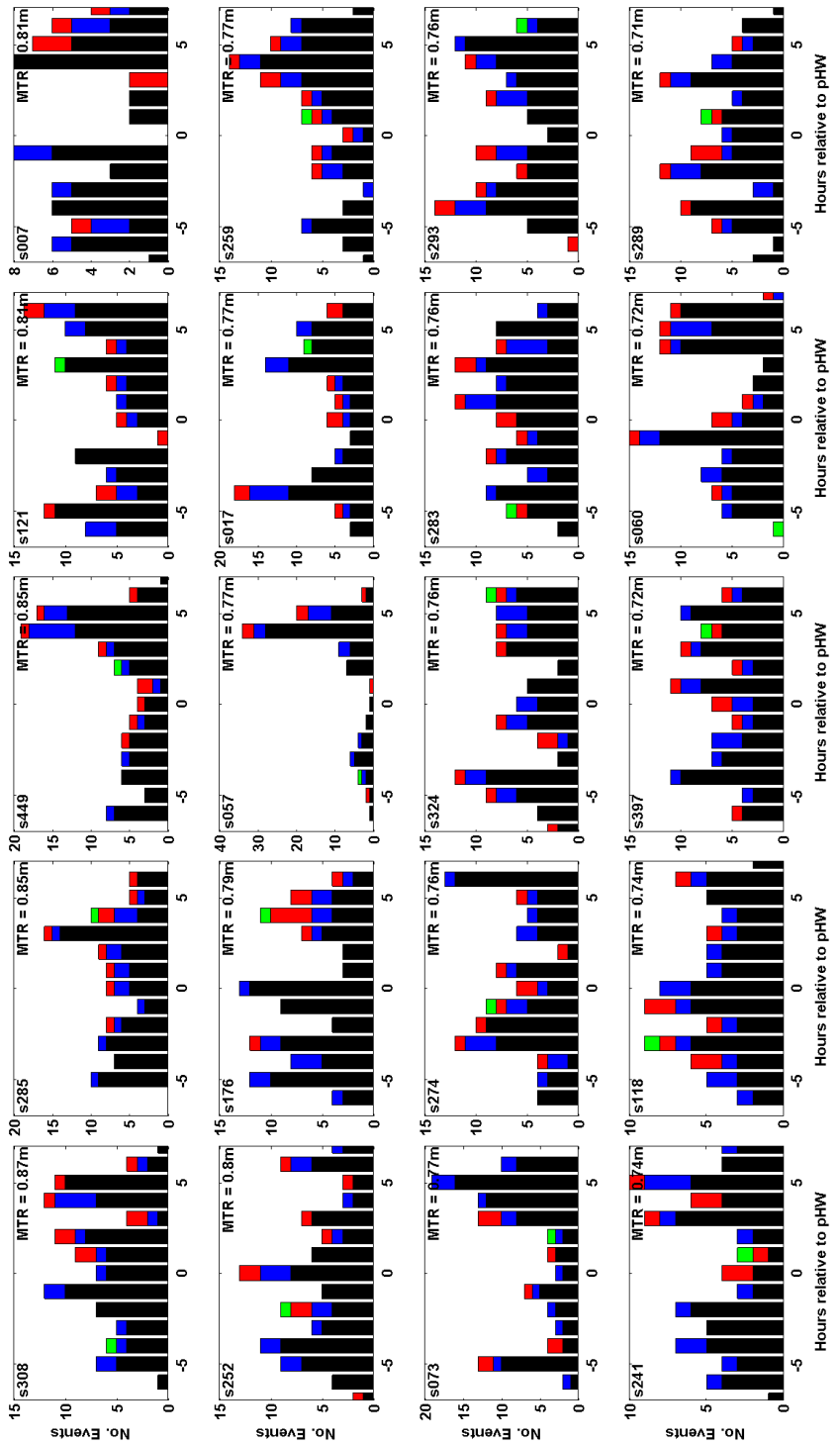

Figure E1.8: Histogram of the timing relative to predicted high water of the 100 largest independent NTR events. Colours indicate rank according to magnitude of NTR: green = maximum, red = top 10, blue = top 50. Plots are ordered by magnitude of MTR, which is written in the top right corner, while the site ID is written in the top left corner.

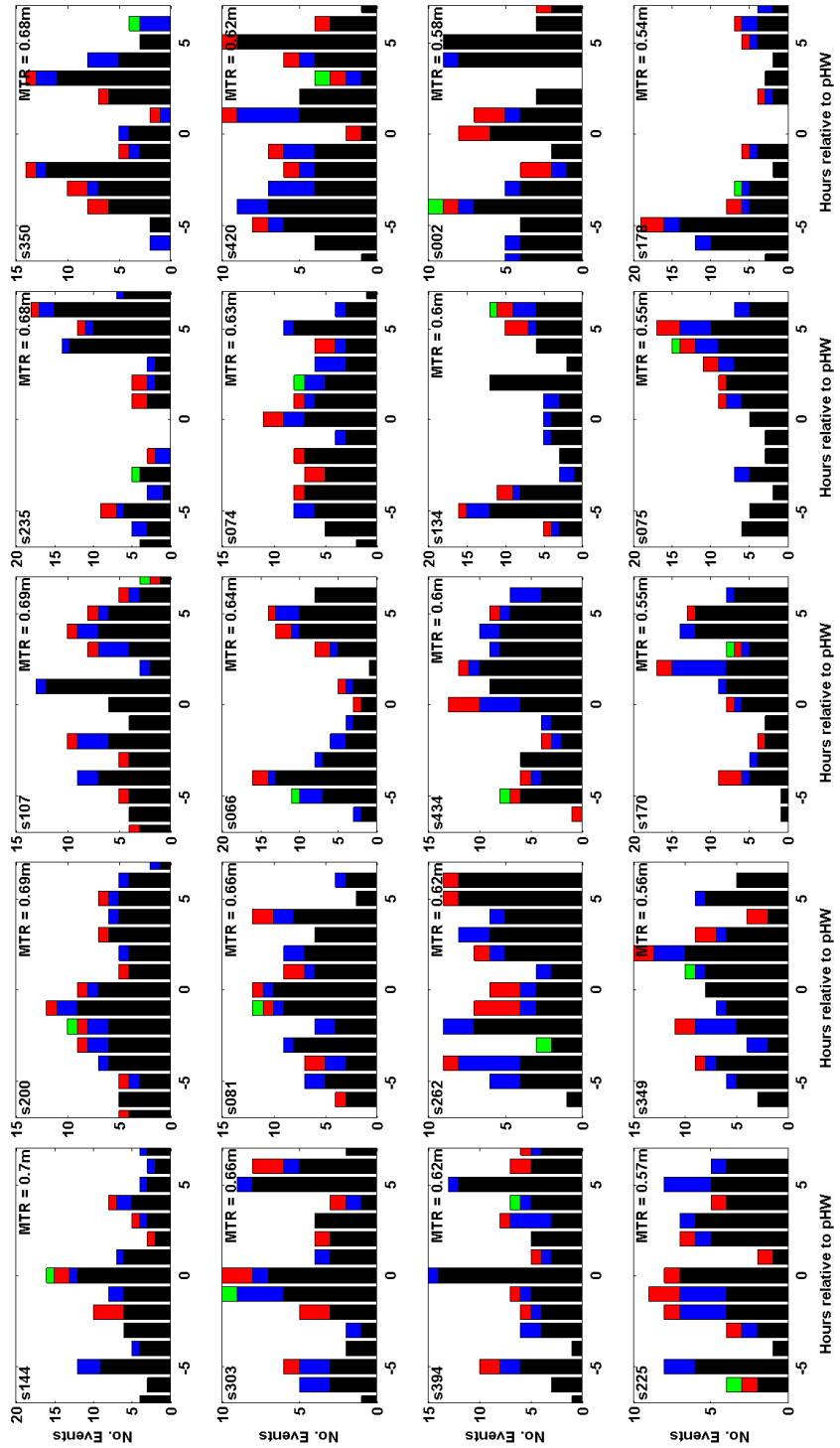

Figure E1.9: Histogram of the timing relative to predicted high water of the 100 largest independent NTR events. Colours indicate rank according to magnitude of NTR: green = maximum, red = top 10, blue = top 50. Plots are ordered by magnitude of MTR, which is written in the top right corner, while the site ID is written in the top left corner.

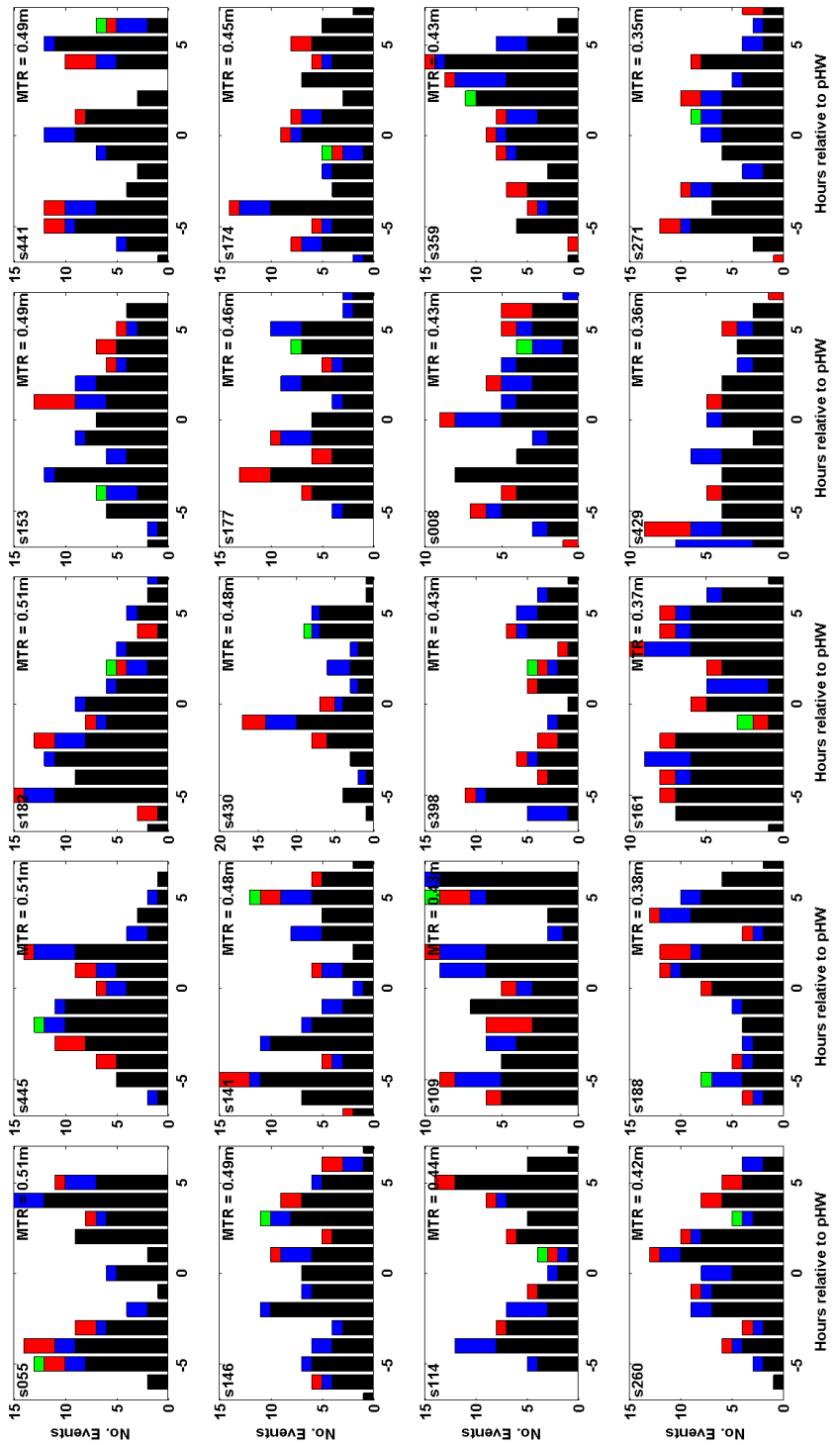

Figure E1.10: Histogram of the timing relative to predicted high water of the 100 largest independent NTR events. Colours indicate rank according to magnitude of NTR: green = maximum, red = top 10, blue = top 50. Plots are ordered by magnitude of MTR, which is written in the top right corner, while the site ID is written in the top left corner.

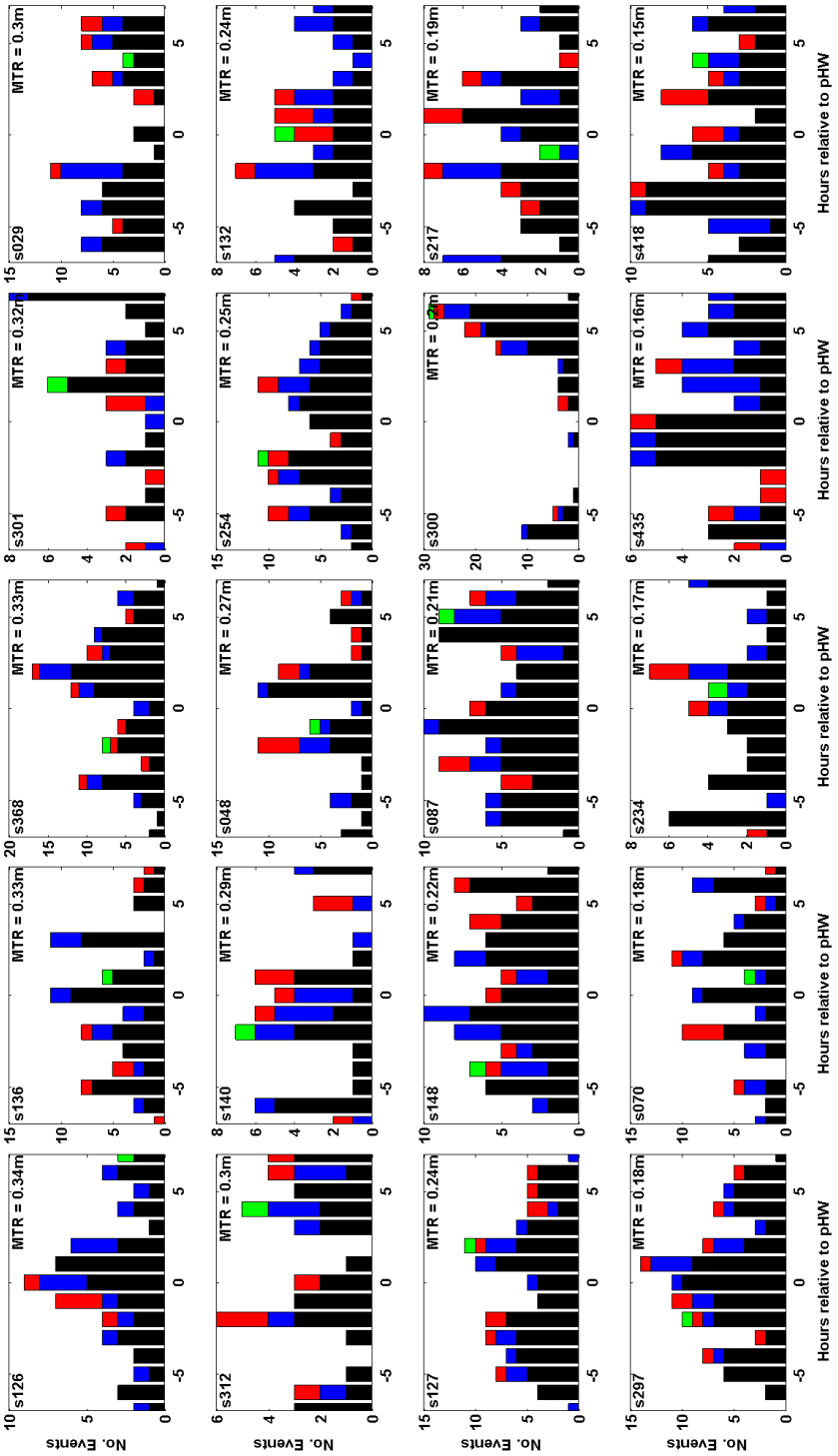

Figure E1.11: Histogram of the timing relative to predicted high water of the 100 largest independent NTR events. Colours indicate rank according to magnitude of NTR: green = maximum, red = top 10, blue = top 50. Plots are ordered by magnitude of MTR, which is written in the top right corner, while the site ID is written in the top left corner.

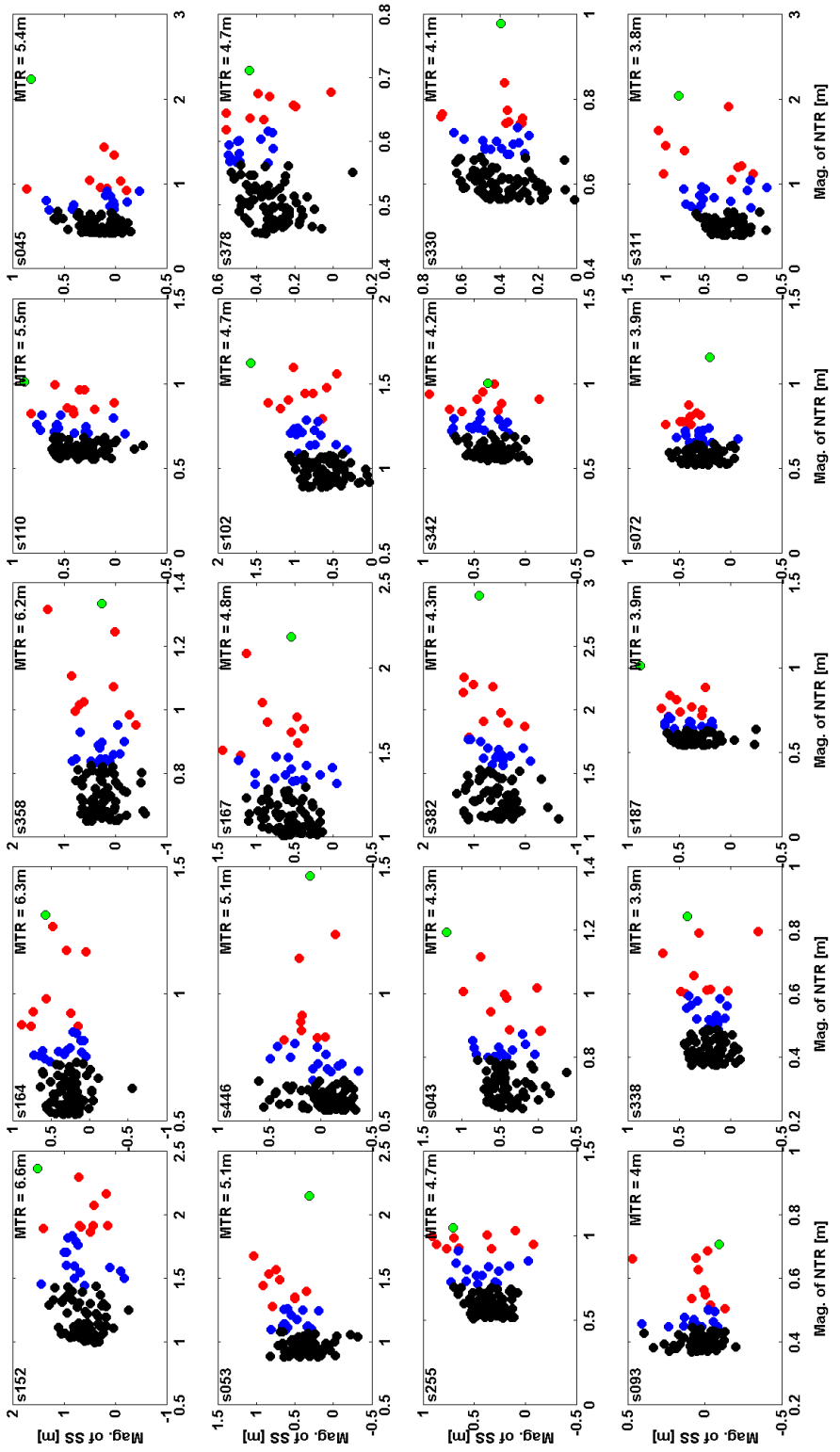

Figure E2.1: Scatter plots of the 100 largest independent NTR events and their associated skew surge value. Colours indicate rank according to magnitude of NTR: green = maximum, red = top 10, blue = top 50 (plots are ordered by magnitude of MTR).

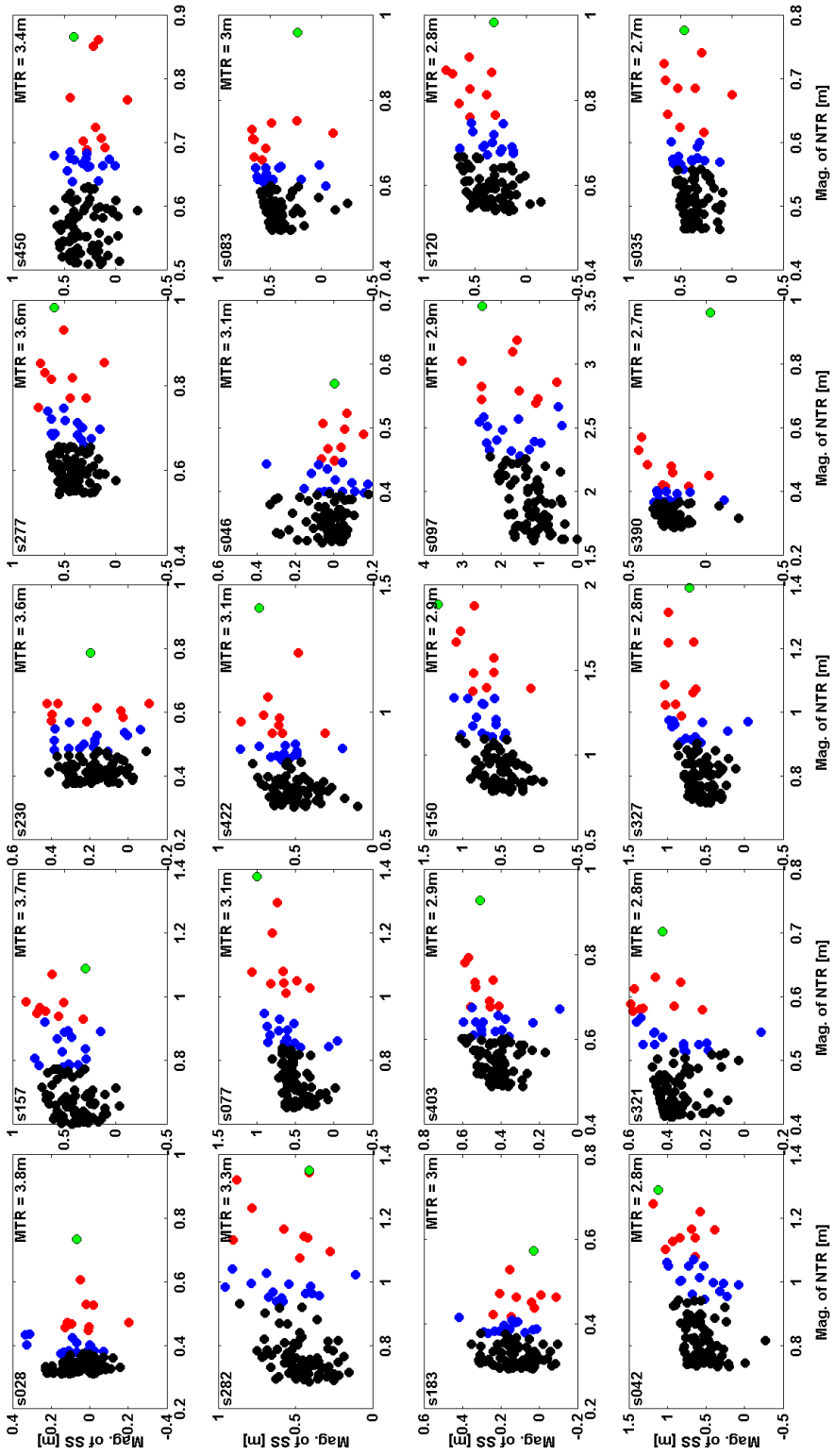

Figure E2.2: Scatter plots of the 100 largest independent NTR events and their associated skew surge value. Colours indicate rank according to magnitude of NTR: green = maximum, red = top 10, blue = top 50 (plots are ordered by magnitude of MTR).

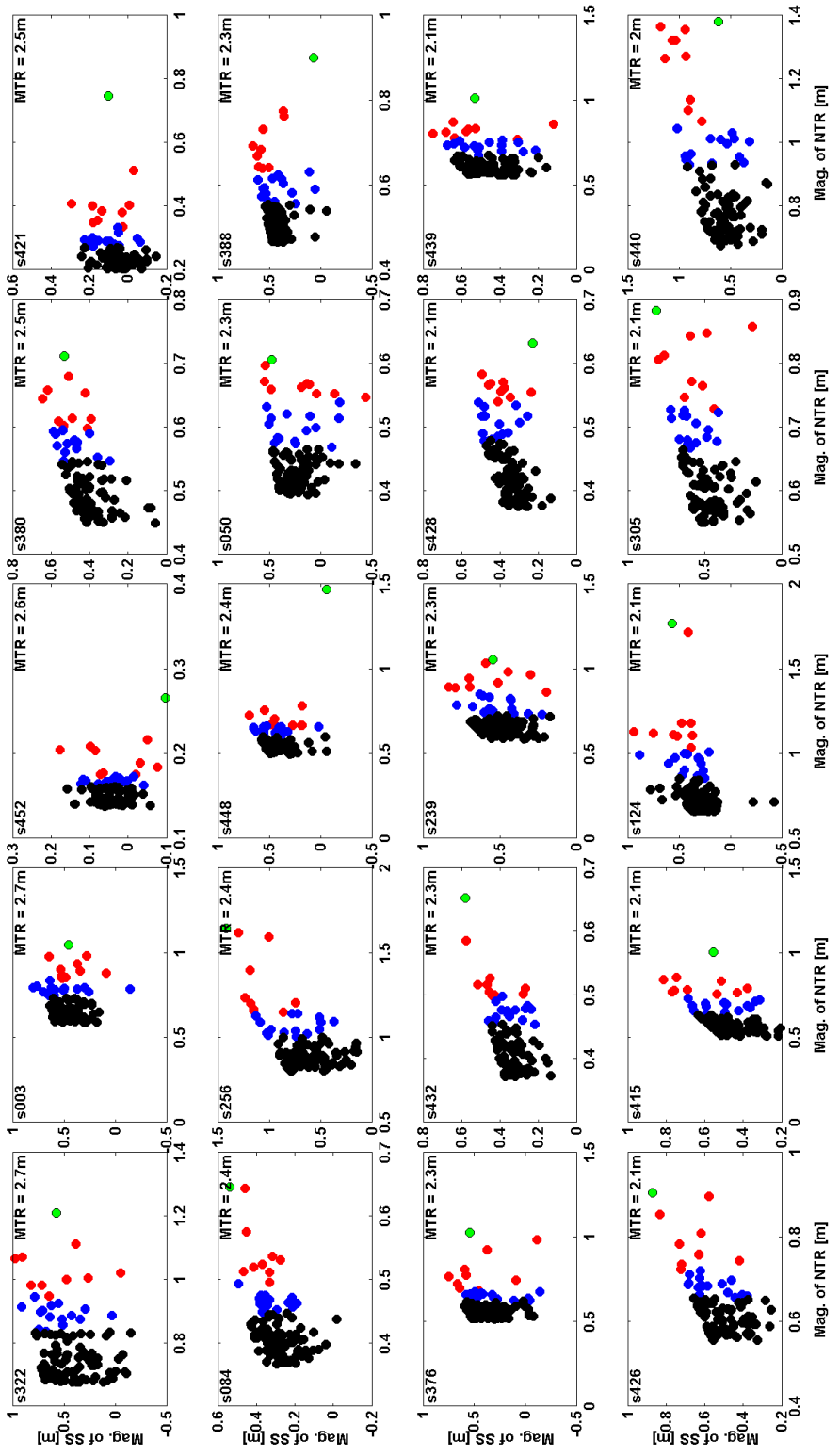

Figure E2.3: Scatter plots of the 100 largest independent NTR events and their associated skew surge value. Colours indicate rank according to magnitude of NTR: green = maximum, red = top 10, blue = top 50 (plots are ordered by magnitude of MTR).

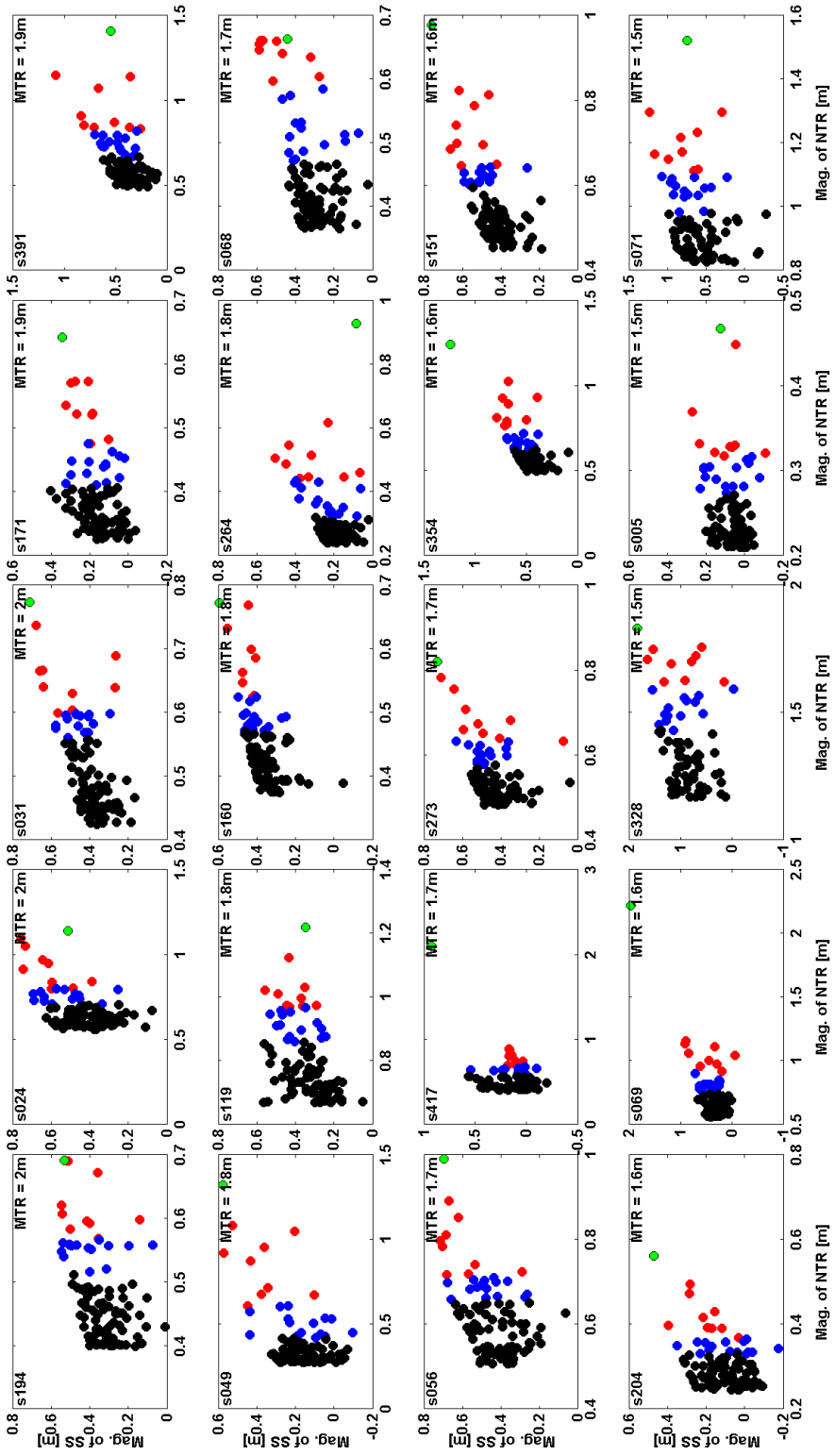

Figure E2.4: Scatter plots of the 100 largest independent NTR events and their associated skew surge value. Colours indicate rank according to magnitude of NTR: green = maximum, red = top 10, blue = top 50 (plots are ordered by magnitude of MTR).

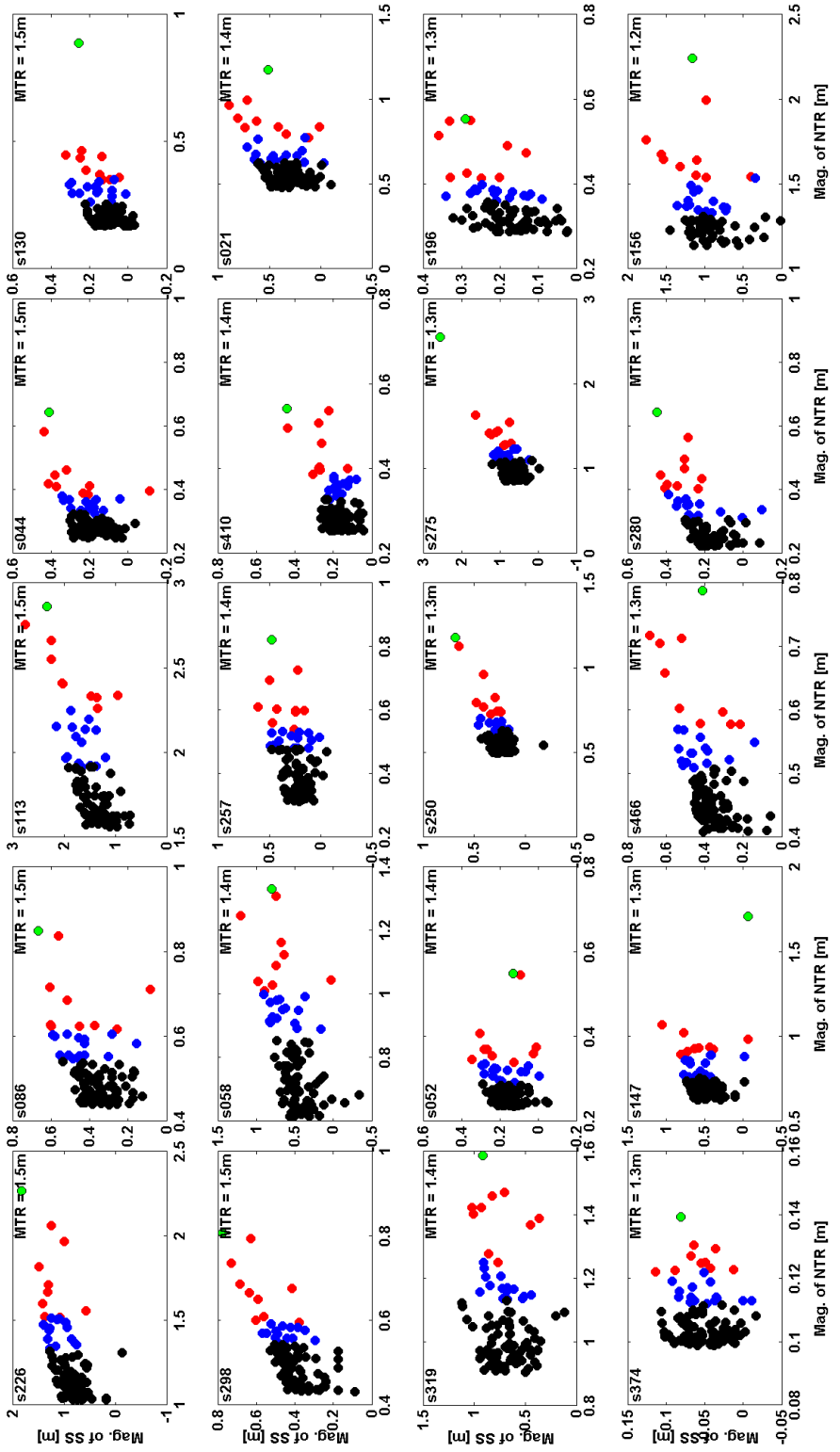

Figure E2.5: Scatter plots of the 100 largest independent NTR events and their associated skew surge value. Colours indicate rank according to magnitude of NTR: green = maximum, red = top 10, blue = top 50 (plots are ordered by magnitude of MTR).

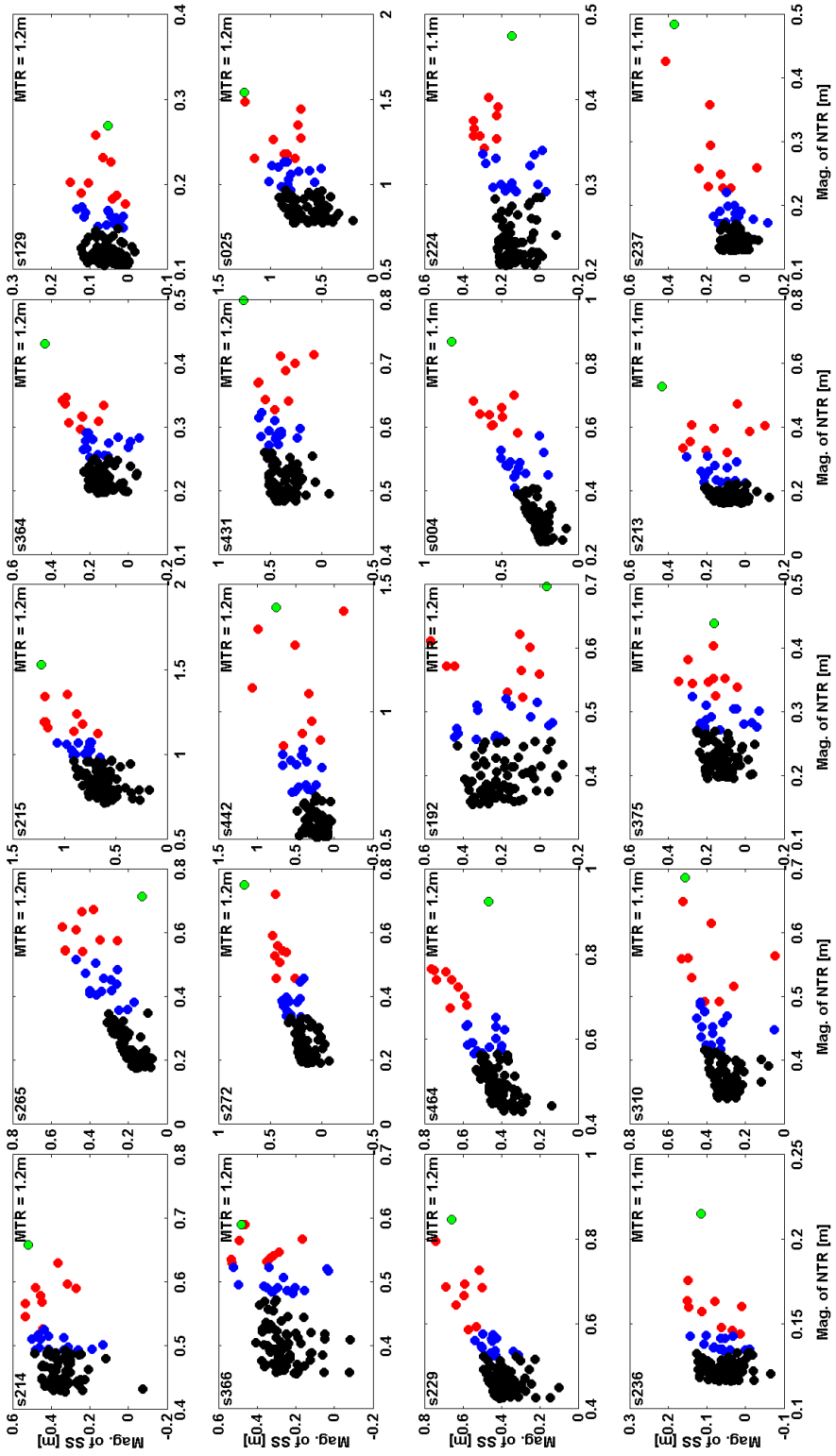

Figure E2.6: Scatter plots of the 100 largest independent NTR events and their associated skew surge value. Colours indicate rank according to magnitude of NTR: green = maximum, red = top 10, blue = top 50 (plots are ordered by magnitude of MTR).

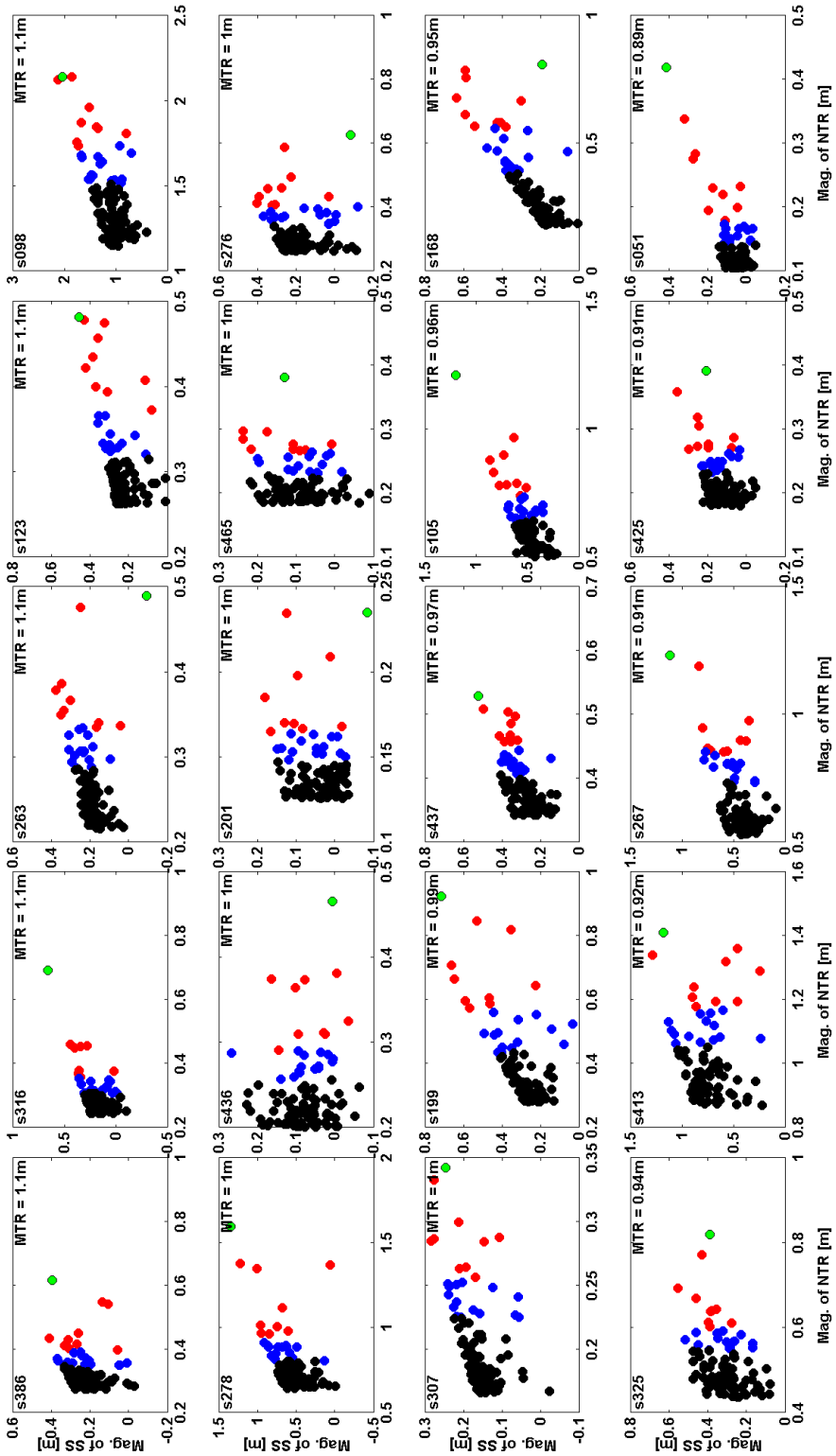

Figure E2.7: Scatter plots of the 100 largest independent NTR events and their associated skew surge value. Colours indicate rank according to magnitude of NTR: green = maximum, red = top 10, blue = top 50 (plots are ordered by magnitude of MTR).

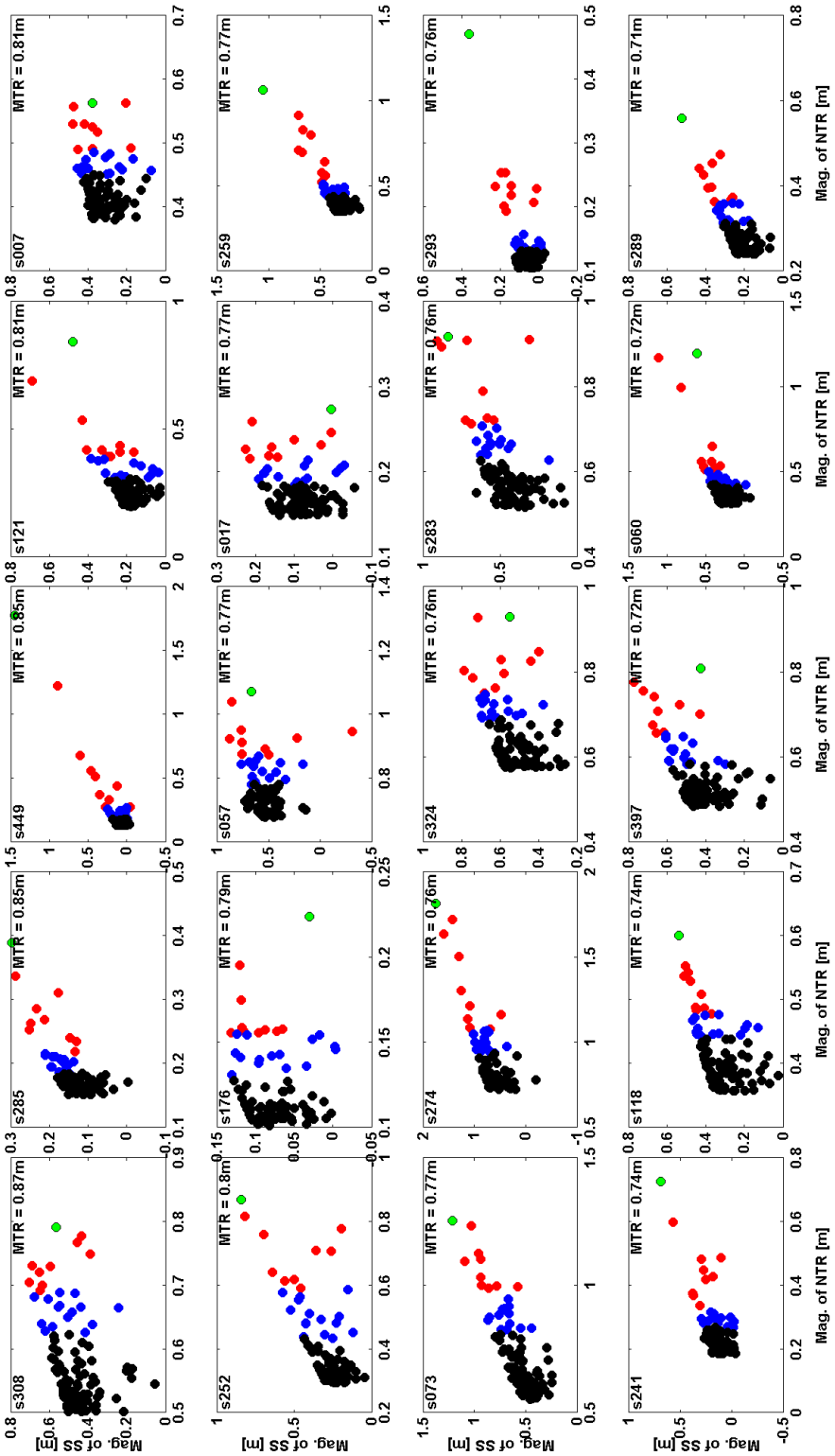

Figure E2.8: Scatter plots of the 100 largest independent NTR events and their associated skew surge value. Colours indicate rank according to magnitude of NTR: green = maximum, red = top 10, blue = top 50 (plots are ordered by magnitude of MTR).

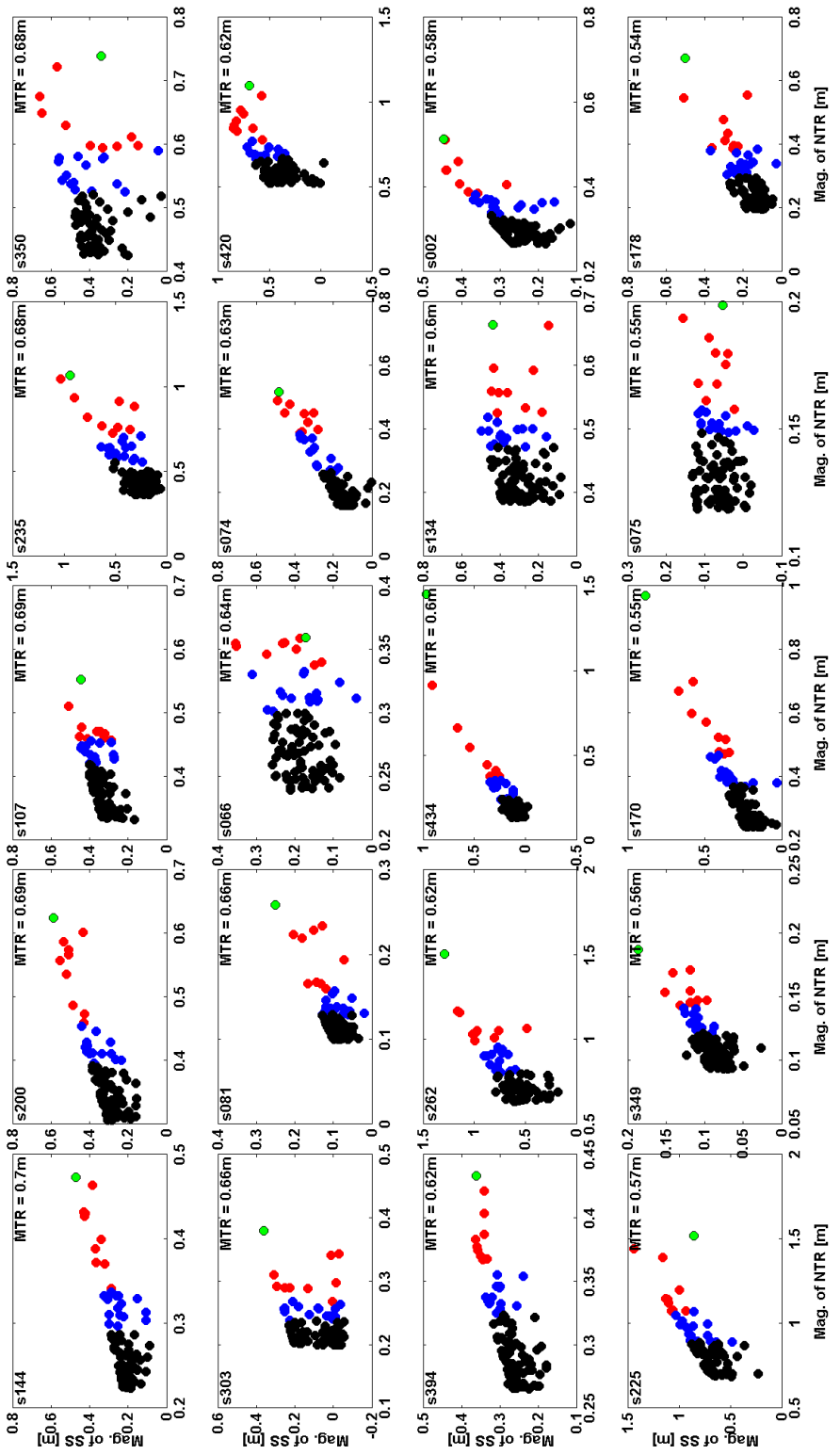

Figure E2.9: Scatter plots of the 100 largest independent NTR events and their associated skew surge value. Colours indicate rank according to magnitude of NTR: green = maximum, red = top 10, blue = top 50 (plots are ordered by magnitude of MTR).

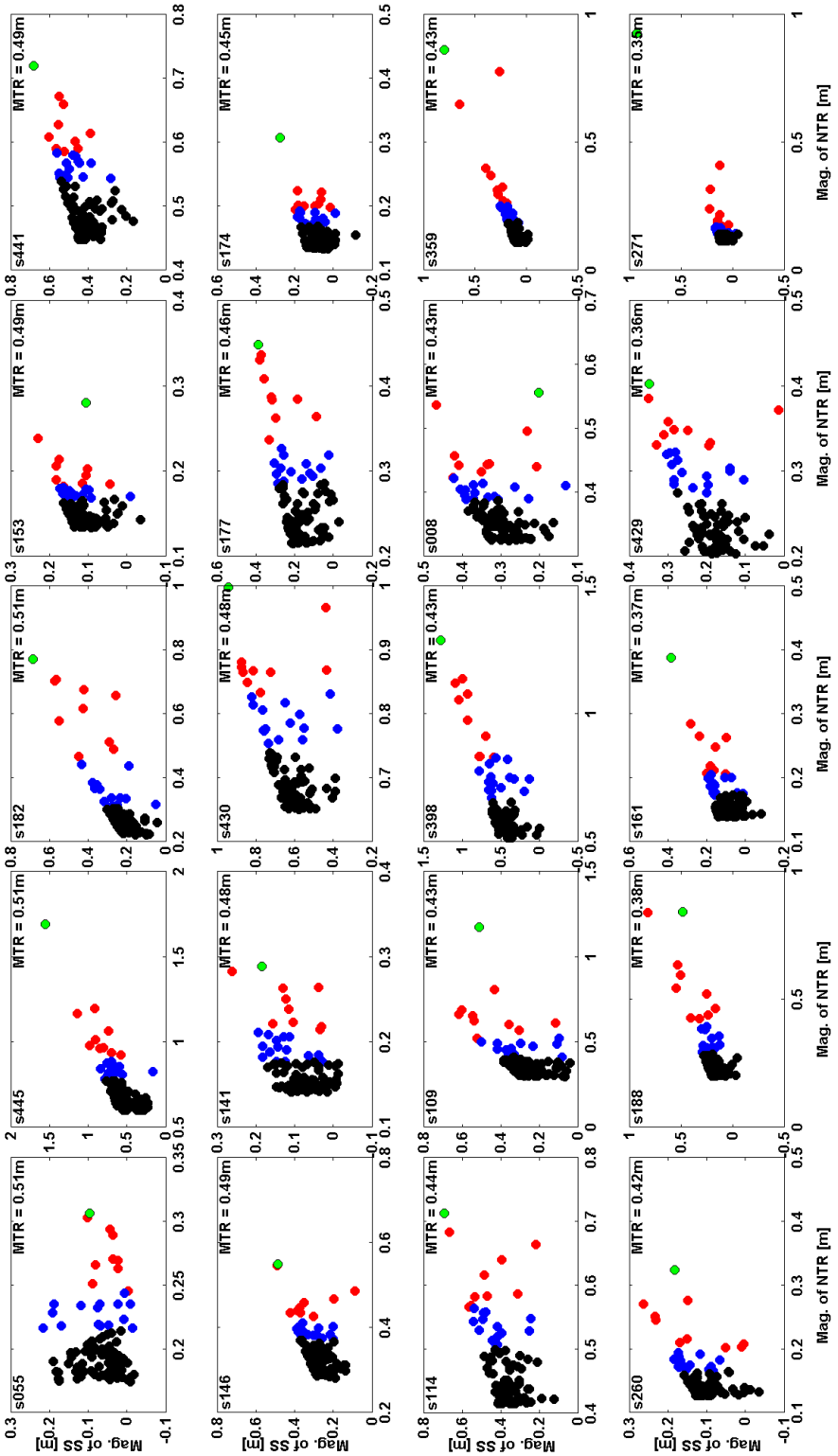

Figure E2.10: Scatter plots of the 100 largest independent NTR events and their associated skew surge value. Colours indicate rank according to magnitude of NTR: green = maximum, red = top 10, blue = top 50 (plots are ordered by magnitude of MTR).

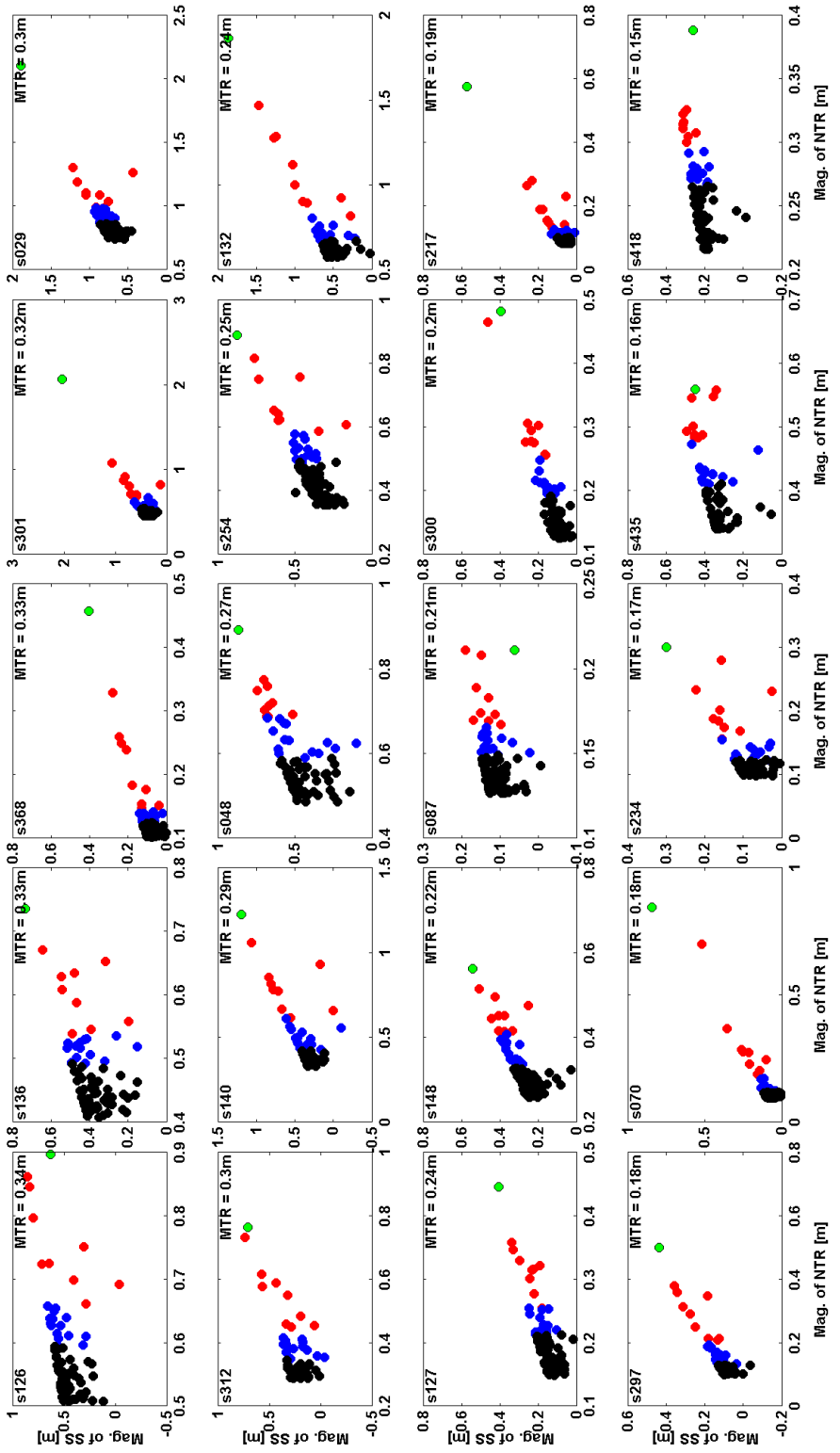

Figure E2.11: Scatter plots of the 100 largest independent NTR events and their associated skew surge value. Colours indicate rank according to magnitude of NTR: green = maximum, red = top 10, blue = top 50 (plots are ordered by magnitude of MTR).

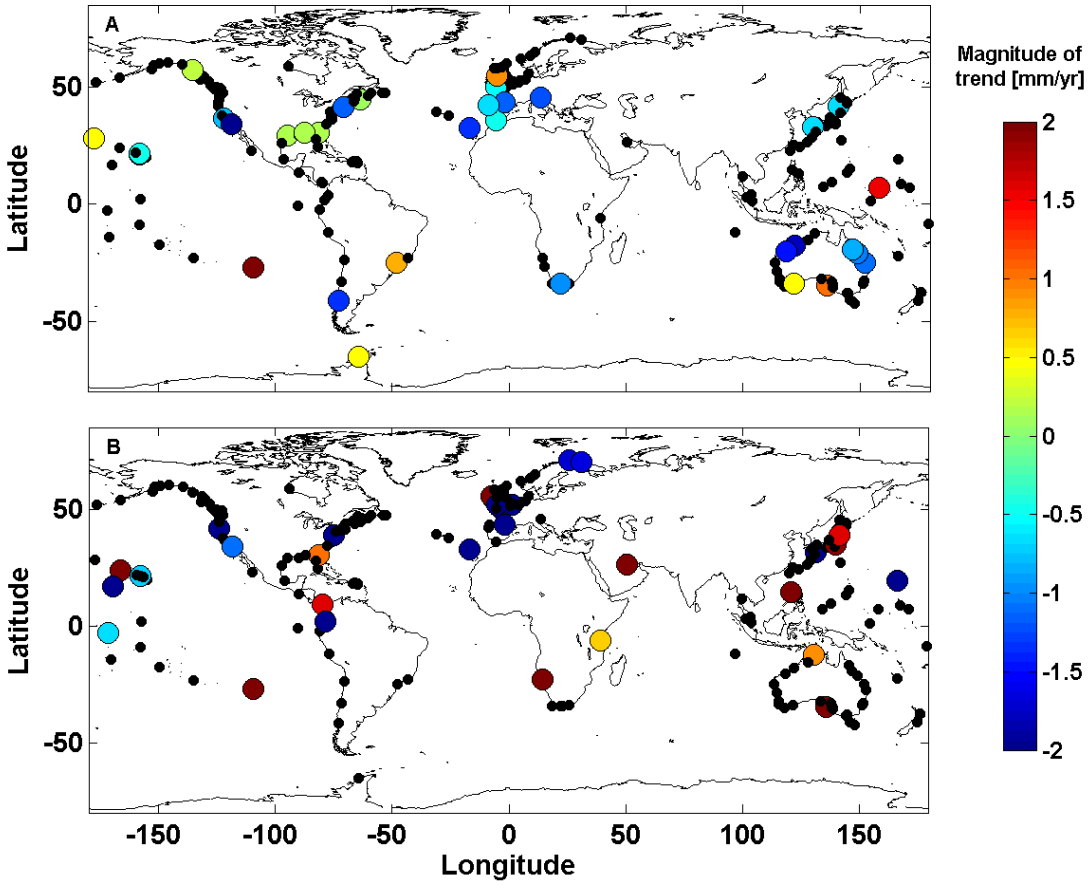

Figure E3.1**:** Shows the magnitude of the trend in in the 99th percentile of skew surge for (a) the entire length of the data at each site, and (b) the last 20 years, where the site has enough data. Large dots show that the trend is significant at the 95% level.

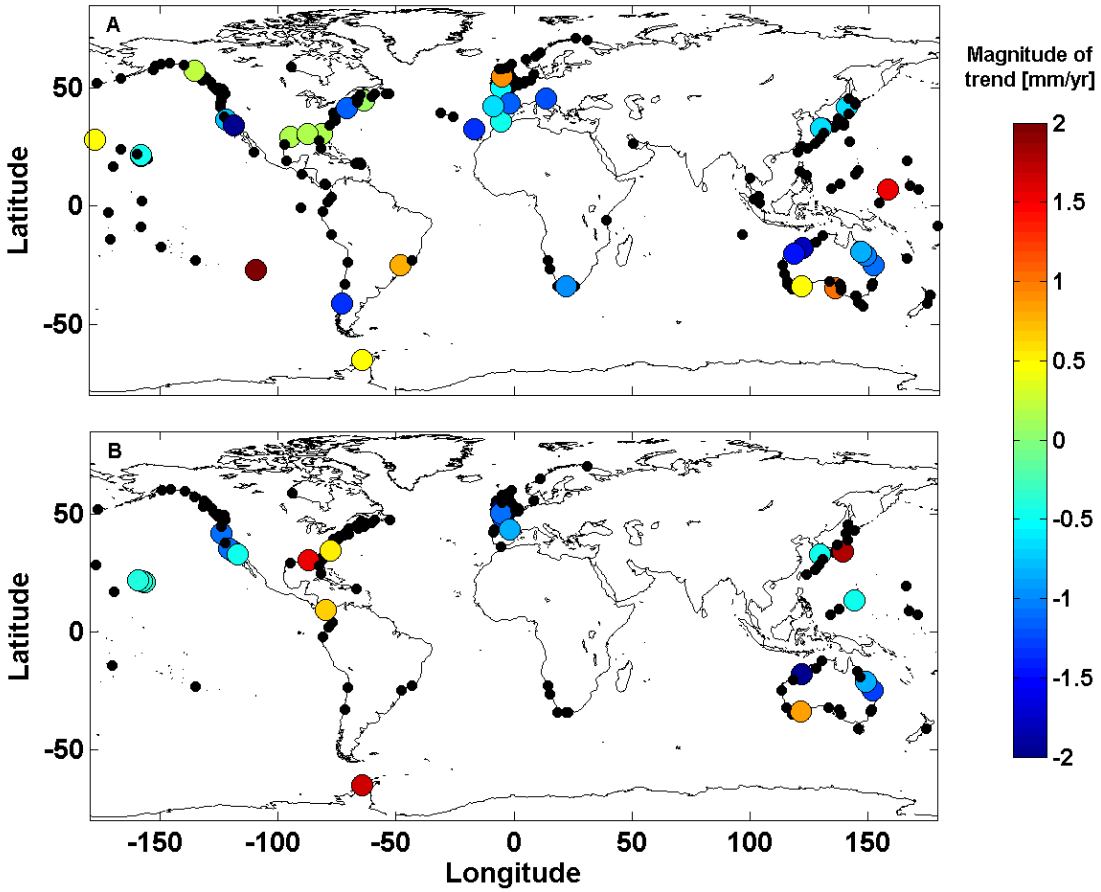

Figure E3.2**:** Shows the magnitude of the trend in in the 99th percentile of skew surge for (a) the entire length of the data at each site, and (b) the last 40 years, where the site has enough data. Large dots show that the trend is significant at the 95% level.

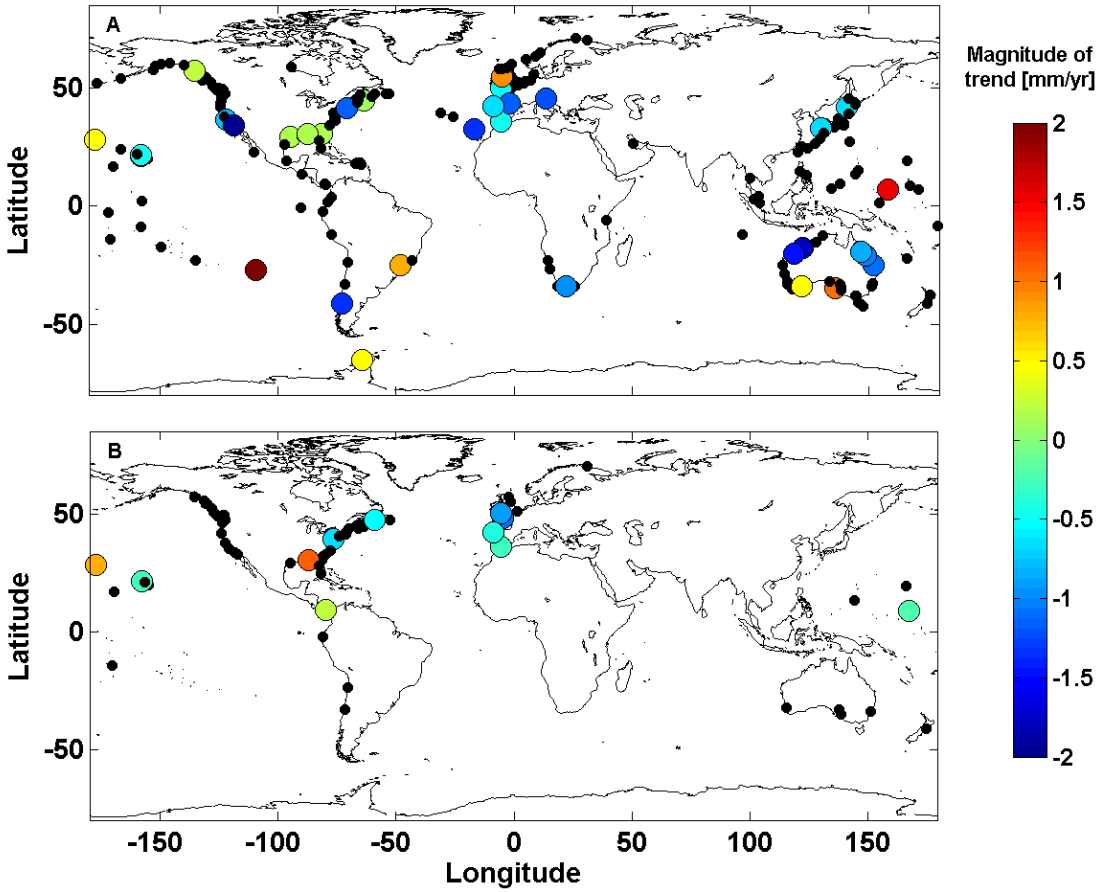

Figure E3.3**:** Shows the magnitude of the trend in in the 99th percentile of skew surge for (a) the entire length of the data at each site, and (b) the last 60 years, where the site has enough data. Large dots show that the trend is significant at the 95% level.

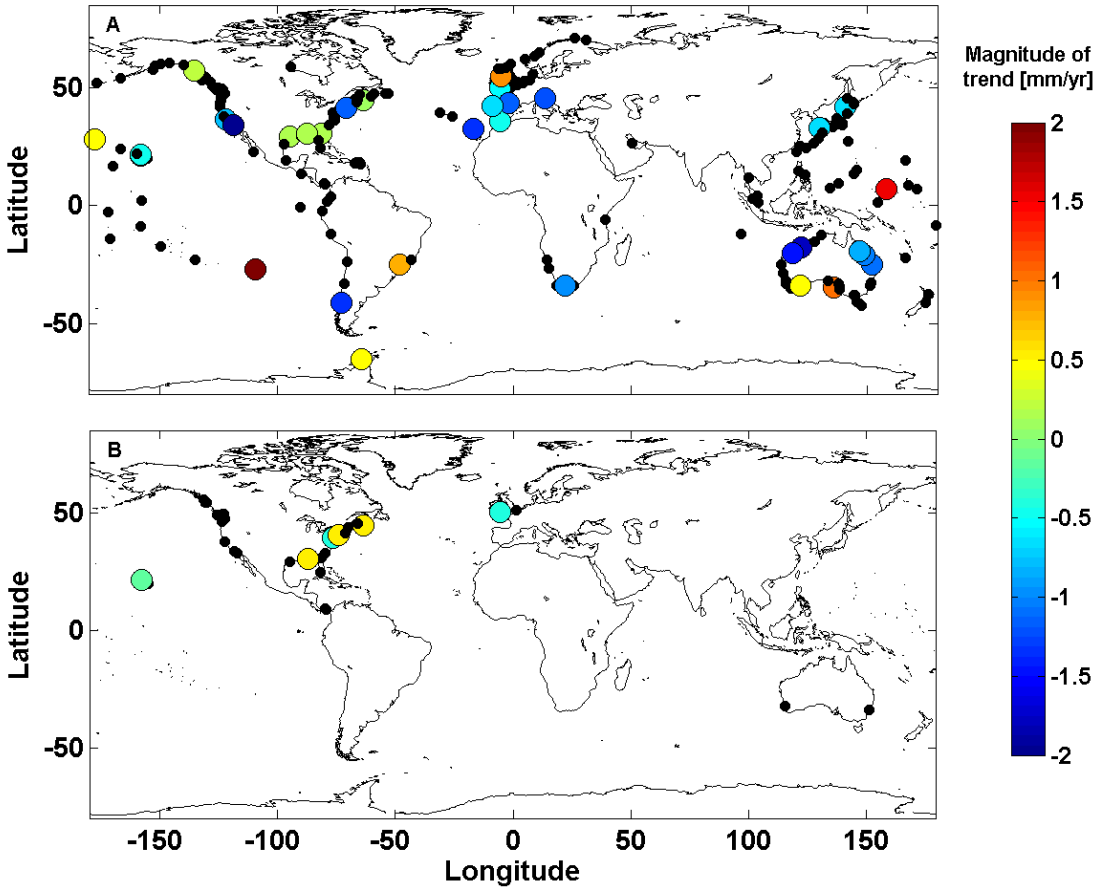

Figure E3.4**:** Shows the magnitude of the trend in in the 99th percentile of skew surge for (a) the entire length of the data at each site, and (b) the last 80 years, where the site has enough data. Large dots show that the trend is significant at the 95% level.

Appendix F Supplementary Material to Chapter 6

Figures F1.1 to F1.5 show examples of the extracted signals for Charlotte Amalie, Virgin Islands; Grand Isle, USA; Malakal, Palau; Patricia Bay, Canada; and Trieste, Italy respectively. The individual panels show: (A) the time-series of the monthly maximum sea level (red) compared to the combined time-series from the 10 extracted signals (black); (B) all 10 extracted signals, with their magnitude calculated from the maximum to minimum range over the entire time-series; (C) the three seasonal cycles, along with a combined seasonal signal (black line); (D) the four inter-annual signals, along with a combined inter-annual signal (black line). Maximum values of each seasonal and inter-annual time-series are shown as a coloured dot.

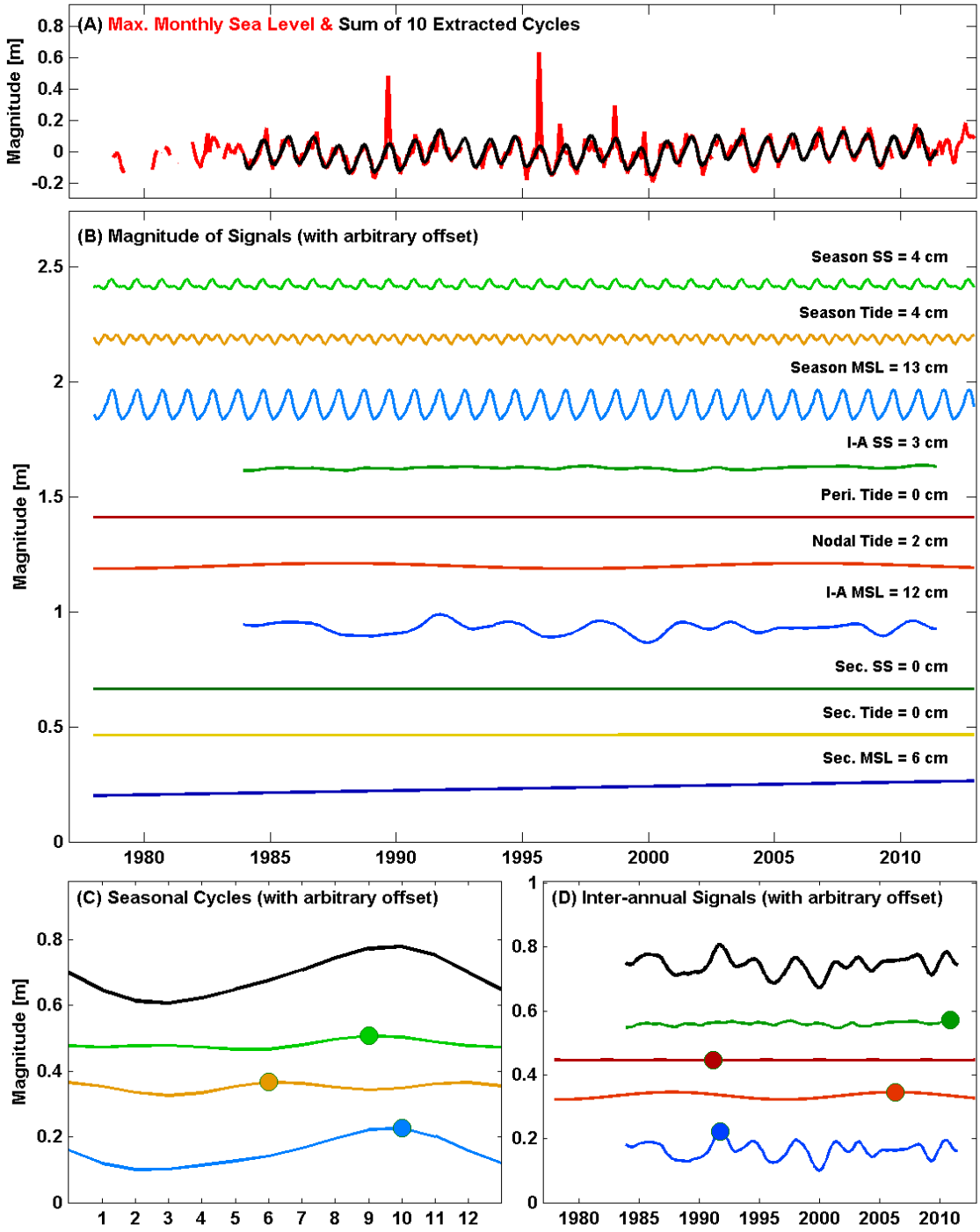

Figures F1.1: Example of the extracted signals for Charlotte Amalie, Virgin Islands.

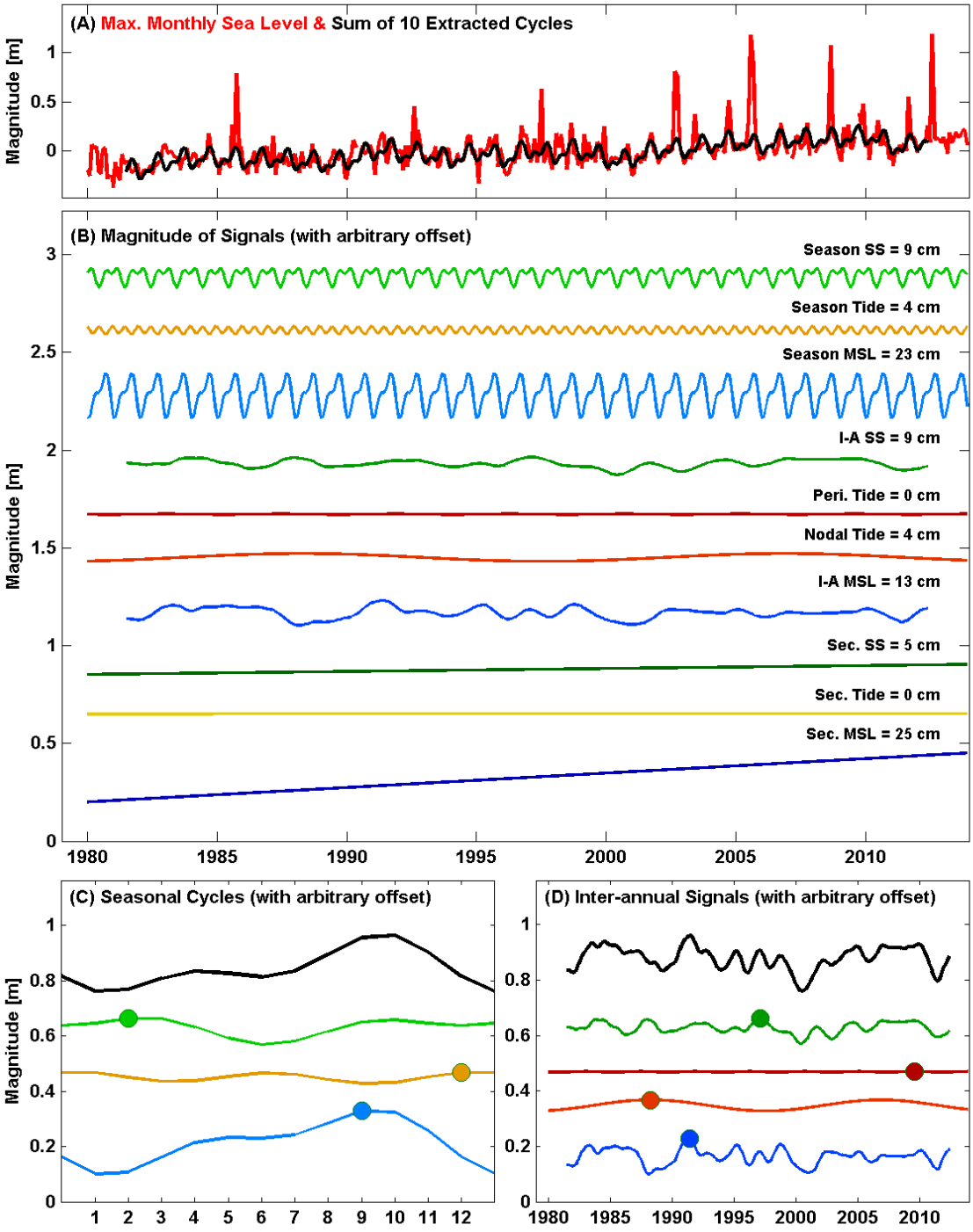

Figures F1.2: Example of the extracted signals for Grand Isle, USA.

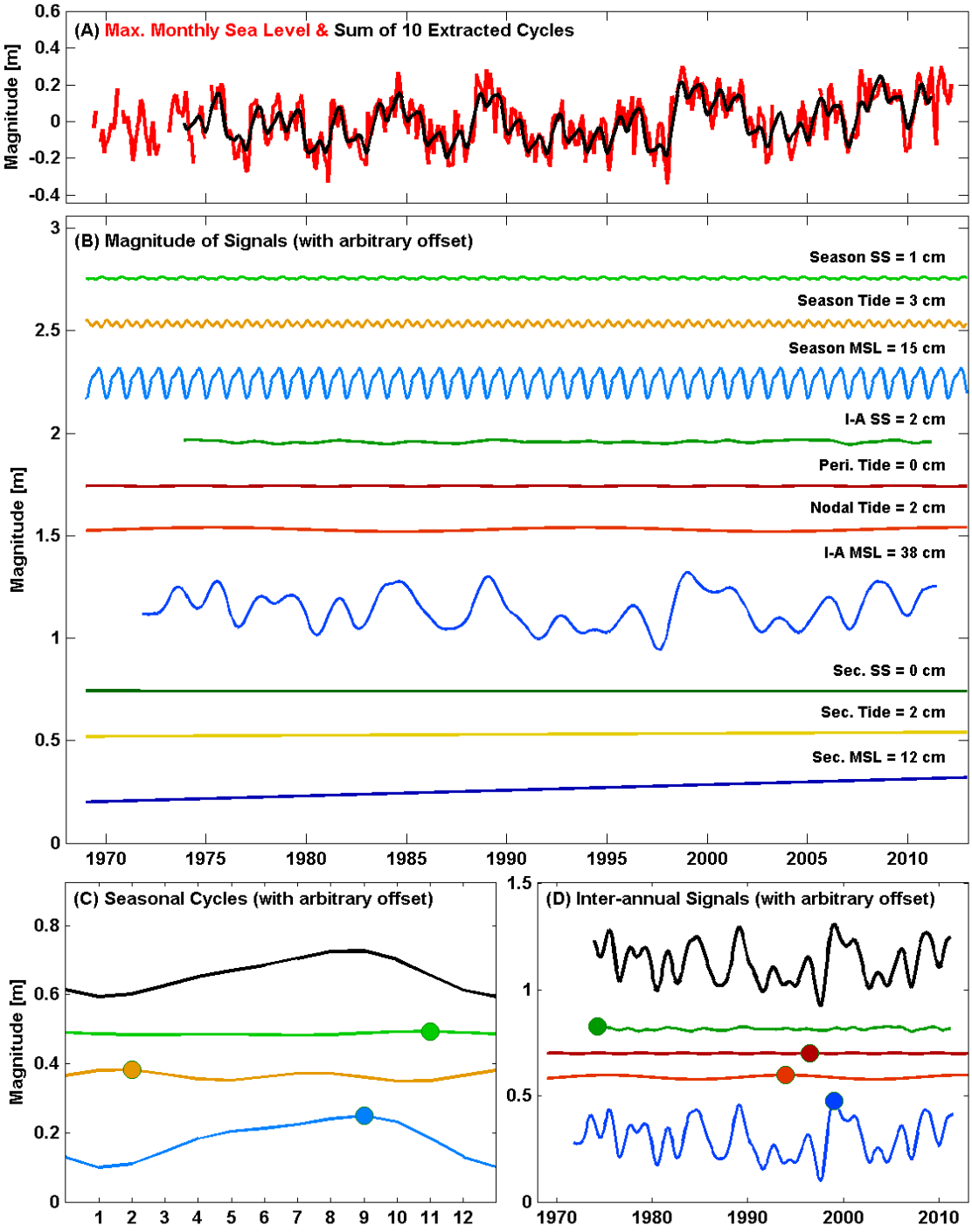

Figures F1.3: Example of the extracted signals for Malakal, Palau.

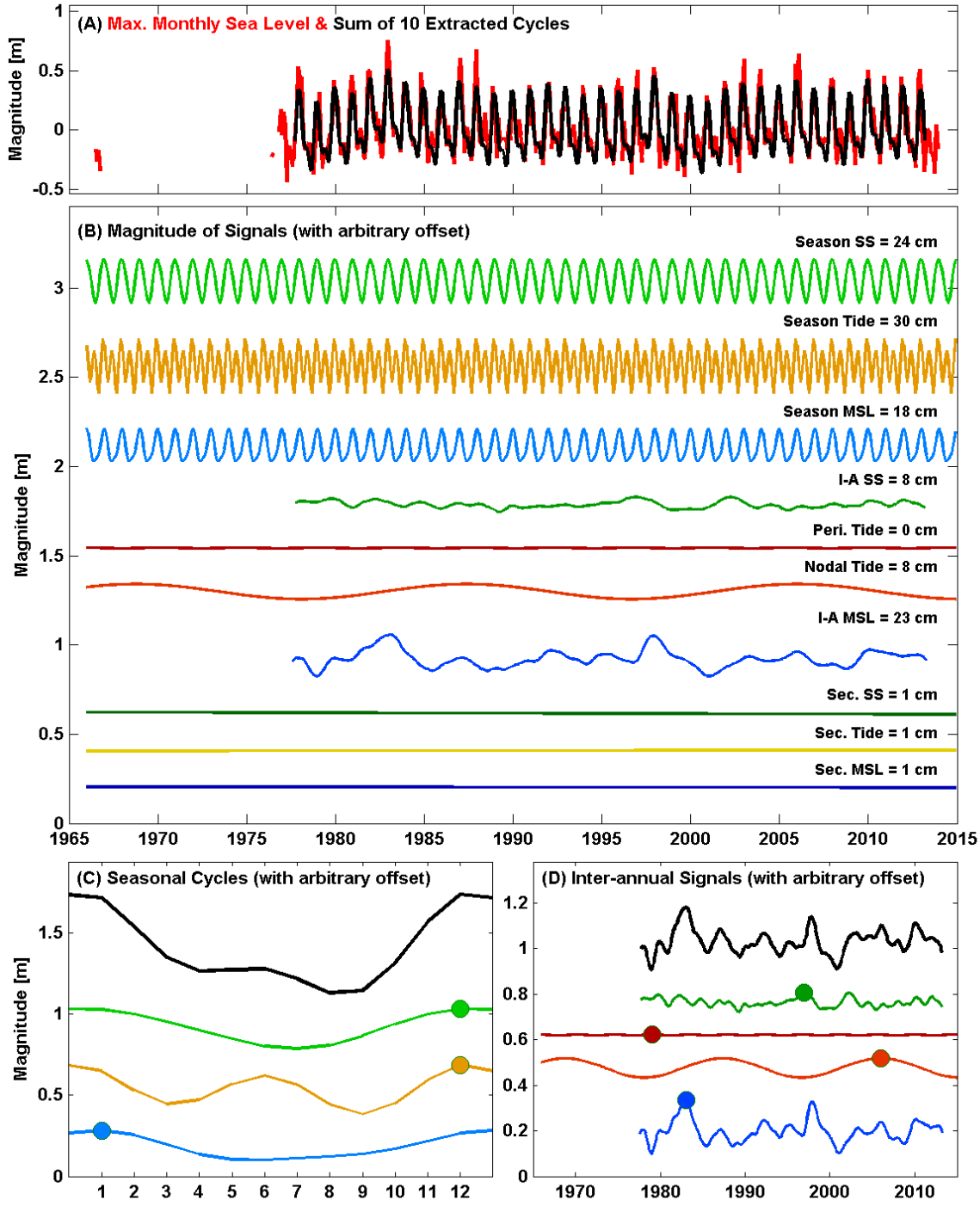

Figures F1.4: Example of the extracted signals for Patricia Bay, Canada.

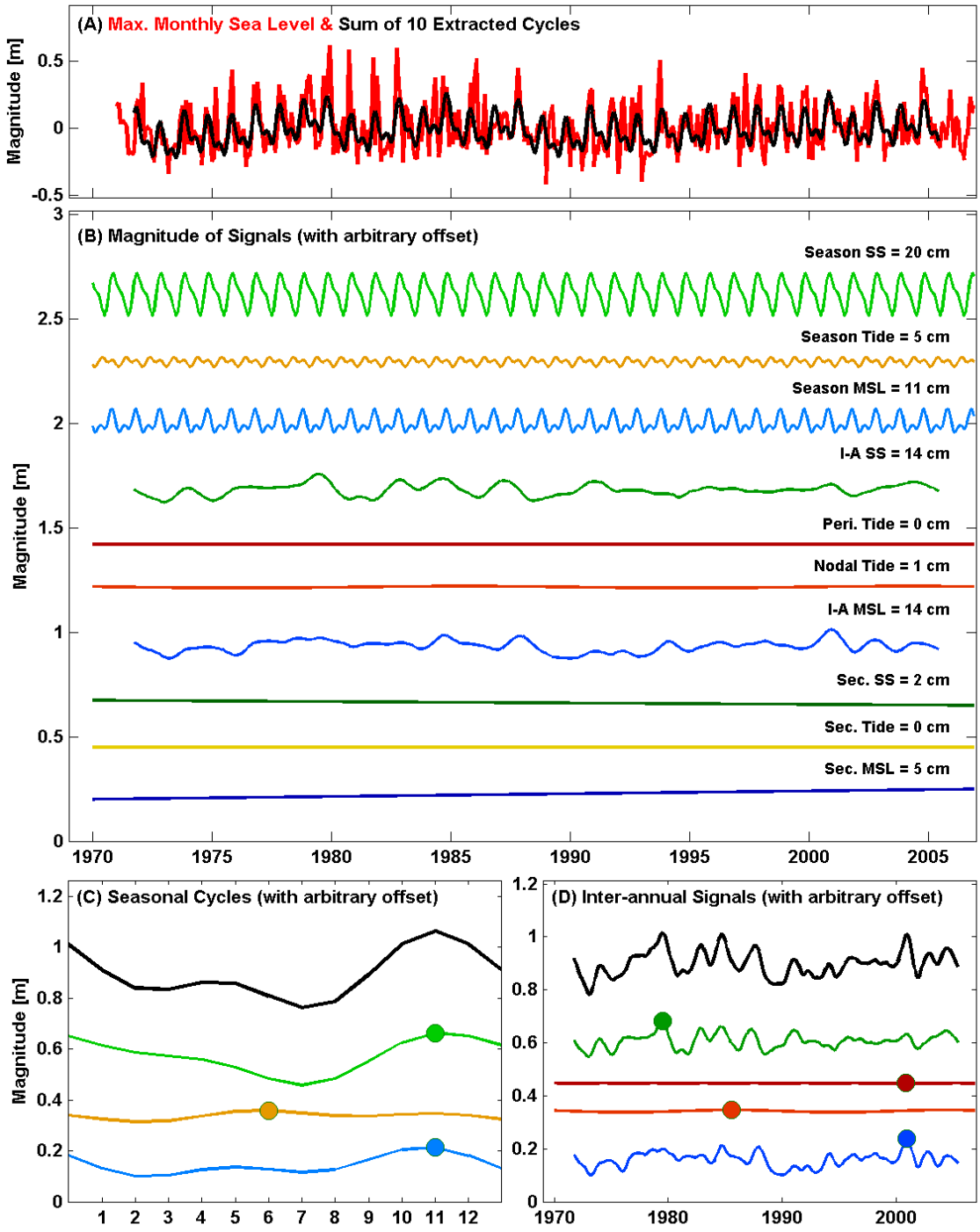

Figures F1.5: Example of the extracted signals for Trieste Italy.

List of References

Abeysirigunawardena, D. S., and I. J. Walker (2008), Sea Level Responses to Climatic Variability and Change in Northern British Columbia, Atmos Ocean, 46(3), 277-296.

Allen, G. P., J. Salomon, P. Bassoullet, Y. Du Penhoat, and C. De Grandpre (1980), Effects of tides on mixing and suspended sediment transport in macrotidal estuaries, Sedimentary Geology, 26(1), 69-90.

Alves, J.-H. G. M. (2006), Numerical modeling of ocean swell contributions to the global wind-wave climate, Ocean Modelling, 11(1–2), 98-122.

Amin, M. (1979), A note on extreme tidal levels, The International Hydrographic Review, 56(2), 133-141.

Amin, M. (1993), Changing mean sea level and tidal constants on the west coast of Australia, Marine and Freshwater Research, 44(6), 911-925.

Amiruddin, A. M., I. D. Haigh, M. N. Tsimplis, F. M. Calafat, and S. Dangendorf (2015), The seasonal cycle and variability of sea level in the South China Sea, Journal of Geophysical Research: Oceans, 120(8), 5490-5513.

Antony, C., and A. S. Unnikrishnan (2013), Observed characteristics of tide-surge interaction along the east coast of India and the head of Bay of Bengal, Estuarine, Coastal and Shelf Science, 131, 6-11.

Araujo, I. (2006), Sea level variability: examples from the Atlantic coast of Europe. PhD Thesis, 216 pp, University of Southampton, United Kingdom.

Araújo, I. B., and D. T. Pugh (2008), Sea Levels at Newlyn 1915–2005: Analysis of Trends for Future Flooding Risks, J Coastal Res, 24(4C), 203-212.

Araújo, I. B., J. M. Dias, and D. T. Pugh (2008), Model simulations of tidal changes in a coastal lagoon, the Ria de Aveiro (Portugal), Cont Shelf Res, 28(8), 1010-1025.

Arbic, B. K., P. St-Laurent, G. Sutherland, and C. Garrett (2007), On the resonance and influence of the tides in Ungava Bay and Hudson Strait, Geophys Res Lett, 34(17), L17606.

Bank, W. (2010), Improving the assessment of disaster risks to strengthen financial resilience.Rep.

Batstone, C., M. Lawless, J. Tawn, K. Horsburgh, D. Blackman, A. McMillan, D. Worth, S. Laeger, and T. Hunt (2013), A UK best-practice approach for extreme sea-level analysis along complex topographic coastlines, Ocean Eng, 71, 28-39.

Bell, G. D., and M. Chelliah (2006), Leading Tropical Modes Associated with Interannual and Multidecadal Fluctuations in North Atlantic Hurricane Activity, J Climate, 19(4), 590-612.

Bernier, N., and K. Thompson (2007), Tide-surge interaction off the east coast of Canada and northeastern United States, Journal of geophysical research, 112(C6), C06008.

Bijker, W. E. (2002), The Oosterschelde storm surge barrier: a test case for Dutch water technology, management, and politics, Technology and Culture, 43(3), 569-584.

Bister, M., and K. A. Emanuel (1998), Dissipative heating and hurricane intensity, Meteorol Atmos Phys, 65(3-4), 233-240.

Bowen, A. J. (1972), The Tidal Regime of the River Thames; Long-Term Trends and their Possible Causes, Philosophical Transactions of the Royal Society of London A: Mathematical, Physical and Engineering Sciences, 272(1221), 187-199.

Box, G. E. P., G. M. Jenkins, and G. C. Reinsel (1994), Time Series Analysis: Forecasting and Control. 3rd ed, Prentice-Hall, Upper Saddle River, NJ.

Bromirski, P. D., R. E. Flick, and D. R. Cayan (2003), Storminess Variability along the California Coast: 1858–2000, J Climate, 16(6), 982-993.

Brown, S., R. J. Nicholls, C. D. Woodroffe, S. Hanson, J. Hinkel, A. S. Kebede, B. Neumann, and A. T. Vafeidis (2013), Sea-Level Rise Impacts and Responses: A Global Perspective, in Coastal Hazards, edited by W. C. Finkl, pp. 117-149, Springer Netherlands, Dordrecht.

Calafat, F. M., D. P. Chambers, and M. N. Tsimplis (2013), Inter-annual to decadal sea-level variability in the coastal zones of the Norwegian and Siberian Seas: The role of atmospheric forcing, Journal of Geophysical Research: Oceans, 118(3), 1287-1301.

Carless, S., M. Green, and S. Wilmes (2015), The impact of global sea-level rise on tides: a revisit, paper presented at EGU General Assembly Conference Abstracts.

Cartwright, D. E. (1971), Tides and waves in the vicinity of Saint Helena, Philosophical Transactions for the Royal Society of London. Series A, Mathematical and Physical Sciences, 603-646.

Cartwright, D. E. (1972), Secular Changes in the Oceanic Tides at Brest, 1711–1936, Geophys J Int, 30(4), 433-449.

Cartwright, D. E. (1974), Years of peak astronomical tides, Nature, 248(5450), 656-657.

Cartwright, D. (1985), Tidal prediction and modern time scales, Int Hydrogr Rev, 62(1), 127-138.

Cartwright, D. E., and R. J. Tayler (1971), New Computations of the Tide-generating Potential, Geophys J Int, 23(1), 45-73.

Cartwright, D. E., and A. C. Edden (1973), Corrected Tables of Tidal Harmonics, Geophys J Int, 33(3), 253-264.

Cayan, D. R., P. D. Bromirski, K. Hayhoe, M. Tyree, M. D. Dettinger, and R. E. Flick (2008), Climate change projections of sea level extremes along the California coast, Climatic Change, 87, S57-S73.

Chelton, D. B., M. G. Schlax, R. M. Samelson, and R. A. de Szoeke (2007), Global observations of large oceanic eddies, Geophys Res Lett, 34(15), L15606.

Church, J. A., and N. J. White (2011), Sea-Level Rise from the Late 19th to the Early 21st Century, Surv Geophys, 32(4-5), 585-602.

Church, J. A., et al. (2013), Sea Level Change. In: Climate Change 2013: The Physical Science Basis. Contribution of Working Group I to the Fifth Assessment Report of the Intergovernmental Panel on Climate Change Stocker, T.F., D. Qin, G.-K. Plattner, M. Tignor, S.K. Allen, J. Boschung, A. Nauels, Y. Xia, V. Bex and P.M. Midgley (eds.)]. Cambridge University Press, Cambridge, United Kingdom and New York, NY, USARep.

Cleveland, W. S., and S. J. Devlin (1988), Locally Weighted Regression: An Approach to Regression Analysis by Local Fitting, Journal of the American Statistical Association, 83(403), 596-610.

Coles, S., and J. Tawn (2005), Bayesian modelling of extreme surges on the UK east coast, Philosophical Transactions of the Royal Society of London A: Mathematical, Physical and Engineering Sciences, 363(1831), 1387-1406.

Colosi, J. A., and W. Munk (2006), Tales of the Venerable Honolulu Tide Gauge*, J Phys Oceanogr, 36(6), 967-996.

Cummins, P. F., D. Masson, and M. G. G. Foreman (2000), Stratification and Mean Flow Effects on Diurnal Tidal Currents off Vancouver Island, J Phys Oceanogr, 30(1), 15-30.

Dangendorf, S., C. Mudersbach, T. Wahl, and J. Jensen (2013), Characteristics of intra-, inter-annual and decadal sea-level variability and the role of meteorological forcing: the long record of Cuxhaven, Ocean Dynam, 63(2), 209-224.

Dangendorf, S., F. M. Calafat, A. Arns, T. Wahl, I. D. Haigh, and J. Jensen (2014), Mean sea level variability in the North Sea: Processes and implications, Journal of Geophysical Research: Oceans, 119(10).

de Ronde, J. G. (1983), Changes of Relative Mean Sea-Level and of Mean Tidal Amplitude Along the Dutch Coast, in Seismicity and Seismic Risk in the Offshore North Sea Area, edited by A. R. Ritsema and A. Gürpinar, pp. 131-141, Springer Netherlands.

Dixon, M. J., and J. A. Tawn (1994), Extreme sea-levels at the UK A-class sites: site-by-site analyses, edited by I. D. Proudman Oceanographic Laboratory, p. 229pp.

Egbert, G. D., R. D. Ray, and B. G. Bills (2004), Numerical modeling of the global semidiurnal tide in the present day and in the last glacial maximum, Journal of Geophysical Research: Oceans, 109(C3), C03003.

Eliot, M. (2012), Sea level variability influencing coastal flooding in the Swan River region, Western Australia, Cont Shelf Res, 33, 14-28.

Emanuel, K. (2000), A Statistical Analysis of Tropical Cyclone Intensity, Mon Weather Rev, 128(4), 1139-1152.

Emanuel, K. (2005), Divine Wind-The History and Science of Hurricanes, Divine Wind-The History and Science of Hurricanes, by Kerry Emanuel, pp. 296. Foreword by Kerry Emanuel. Oxford University Press, Sep 2005. ISBN-10: 0195149416. ISBN-13: 9780195149418, 1.

Emanuel, K. A., R. Sundararajan, and J. Williams (2008), Hurricanes and global warming: Results from downscaling IPCC AR4 simulations. , B Am Meteorol Soc, 89(3), 346-367.

Ezer, T., and L. P. Atkinson (2014), Accelerated flooding along the U.S. East Coast: On the impact of sea-level rise, tides, storms, the Gulf Stream, and the North Atlantic Oscillations, Earth's Future, 2(8), 362-382.

Feng, X., and M. N. Tsimplis (2014), Sea level extremes at the coasts of China, Journal of Geophysical Research: Oceans, 119(3), 1593-1608.

Feng, X., M. N. Tsimplis, M. Marcos, F. M. Calafat, J. Zheng, G. Jordà, and P. Cipollini (2015), Spatial and temporal variations of the seasonal sea level cycle in the northwest Pacific, Journal of Geophysical Research: Oceans, 120(10), 7091-7112.

Feser, F., M. Barcikowska, O. Krueger, F. Schenk, R. Weisse, and L. Xia (2015), Storminess over the North Atlantic and northwestern Europe—A review, Q J Roy Meteor Soc, 141(687), 350-382.

Flather, R. A., T. F. Baker, P. L. Woodworth, I. M. Vassie, and D. L. Blackman (2001), Integrated effects of climate change on coastal extreme sea levels.Rep., 20pp pp, Proudman Oceanographic Laboratory Internal Document.

Flick, R., J. Murray, and L. Ewing (2003), Trends in United States Tidal Datum Statistics and Tide Range, Journal of Waterway, Port, Coastal, and Ocean Engineering, 129(4), 155-164.

Foreman, M. G. G. (1977), Manual of tidal heights analysis and prediction. Pacific Marine sciences Report 77-10. Institute of Ocean Sciences. Victoria.

Foreman, M. G. G., R. A. Walters, R. F. Henry, C. P. Keller, and A. G. Dolling (1995), A tidal model for eastern Juan de Fuca Strait and the southern Strait of Georgia, Journal of Geophysical Research: Oceans, 100(C1), 721-740.

Franco, P., L. Jeftic, P. Rizzoli, A. Michelato, and M. Orlic (1982), Descriptive model of the Northern Adriatic, Oceanologica Acta, 5(3), 379-389.

Frank, N. L., and S. Husain (1971), The deadliest tropical cyclone in history, B Am Meteorol Soc, 52(6), 438-445.

Gill, S. K., and J. R. Schultz (2001), Tidal datums and their applications, National Oceanic and Atmospheric Administration.

Godin, G. (1985), Frictional damping of the tide in the Gulf of California, Geofísica Internacional, 24(2).

Gönnert, G., S. Dube, T. Murty, and W. Siefert (2001), Global storm surges, Die Küste—Archive for research and technology on the North Sea and Baltic Sea coast, Kuratorium Forsch. Küsteningenieurwesen, 63, 623.

Green, J. A. M. (2010), Ocean tides and resonance, Ocean Dynam, 60(5), 1243-1253.

Greenberg, D. A., W. Blanchard, B. Smith, and E. Barrow (2012), Climate Change, Mean Sea Level and High Tides in the Bay of Fundy, Atmos Ocean, 50(3), 261-276.

Grinsted, A., J. C. Moore, and S. Jevrejeva (2012), Homogeneous record of Atlantic hurricane surge threat since 1923, P Natl Acad Sci USA, 109(48), 19601-19605.

Ha, T., J.-Y. Choi, J. Yoo, I. Chun, and J. Shim (2014), Transformation of small-scale meteorological tsunami due to terrain complexity on the western coast of Korea, J Coastal Res, 70(sp1), 284-289.

Haigh, I., R. Nicholls, and N. Wells (2009), Mean sea level trends around the English Channel over the 20th century and their wider context, Cont Shelf Res, 29(17), 2083-2098.

Haigh, I., R. Nicholls, and N. Wells (2010), Assessing changes in extreme sea levels: Application to the English Channel, 1900–2006, Cont Shelf Res, 30(9), 1042-1055.

Haigh, I. D., M. Eliot, and C. Pattiaratchi (2011), Global influences of the 18.61 year nodal cycle and 8.85 year cycle of lunar perigee on high tidal levels, Journal of Geophysical Research: Oceans, 116(C6), C06025.

Haigh, I. D., E. M. S. Wijeratne, L. R. MacPherson, C. B. Pattiaratchi, M. S. Mason, R. P. Crompton, and S. George (2014), Estimating present day extreme water level exceedance probabilities around the coastline of Australia: tides, extra-tropical storm surges and mean sea level, Clim Dynam, 42(1-2), 121-138.

Haigh, I. D., T. Wahl, E. J. Rohling, R. M. Price, C. B. Pattiaratchi, F. M. Calafat, and S. Dangendorf (2014), Timescales for detecting a significant acceleration in sea level rise, Nat Commun, 5.

Haigh, I. D., M. P. Wadey, S. L. Gallop, H. Loehr, R. J. Nicholls, K. Horsburgh, J. M. Brown, and E. Bradshaw (2015), A user-friendly database of coastal flooding in the United Kingdom from 1915–2014, Scientific Data, 2, 150021.

Hanson, S., R. Nicholls, N. Ranger, S. Hallegatte, J. Corfee-Morlot, C. Herweijer, and J. Chateau (2011), A global ranking of port cities with high exposure to climate extremes, Climatic Change, 104(1), 89-111.

Hartmann, D., A. Klein Tank, M. Rusicucci, L. Alexander, B. Broenniman, Y. Charabi, F. Dentener, E. Dlugokencky, D. Easterling, and A. Kaplan (2013), Observations: atmosphere and surface. In: Climate Chanage 2013: The Physical Scientific Basis. Working Group I Contribution to the Intergovernmental Panel on Climate Change 5th Assessment Report [Stocker, T.F., D. Qin, G.-K. Plattner, M. Tignor, S.K. Allen, J. Boschung, A. Nauels, Y. Xia, V. Bex and P.M. Midgley (eds.)]. Cambridge University Press, Cambridge, United Kingdom and New York, NY, USA.

Hibbert, A., H. Leach, P. Woodworth, C. W. Hughes, and V. Roussenov (2010), Quasi-Biennial Modulation of the Southern Ocean Coherent Mode, Q J Roy Meteor Soc, 136(648), 755-768.

Hibiya, T., and K. Kajiura Origin of theAbiki phenomenon (a kind of seiche) in Nagasaki Bay, Journal of the Oceanographical Society of Japan, 38(3), 172-182.

Hollebrandse, F. A. (2005), Temporal development of the tidal range in the southern North Sea, MS thesis, Delft Univ. of Technol., Delft, Netherlands.

Horrevoets, A. C., H. H. G. Savenije, J. N. Schuurman, and S. Graas (2004), The influence of river discharge on tidal damping in alluvial estuaries, J Hydrol, 294(4), 213-228.

Horsburgh, K. J., and C. Wilson (2007), Tide-surge interaction and its role in the distribution of surge residuals in the North Sea, J Geophys Res-Oceans, 112(C8).

Horsburgh, K., and S. Williams (2016), Changes to estimates of extreme sea levels for Wales when data from the 2013/2014 winter are included. Report for Natural Resources Wales.

Hünicke, B., and E. Zorita (2008), Trends in the amplitude of Baltic Sea level annual cycle, Tellus A, 60(1), 154-164.

Hunter, J. (2012), A simple technique for estimating an allowance for uncertain sea-level rise, Climatic Change, 113(2), 239-252.

Hunter, J. R., J. A. Church, N. J. White, and X. Zhang (2013), Towards a global regionally varying allowance for sea-level rise, Ocean Eng, 71(0), 17-27.

Idier, D., F. Dumas, and H. Muller (2012), Tide-surge interaction in the English Channel, Nat Hazard Earth Sys, 12(12), 3709-3718.

Jay, D. A. (2009), Evolution of tidal amplitudes in the eastern Pacific Ocean, Geophys Res Lett, 36(4), L04603.

Jay, D. A., K. Leffler, and S. Degens (2011), Long-Term Evolution of Columbia River Tides, Journal of Waterway, Port, Coastal, and Ocean Engineering, 137(4), 182-191.

Kang, S. K., K. T. Jung, J. J. Park, E. J. Kim, and J. K. So (2013), Tidal regime change due to the large scale of reclamation in the west coast of the Korean Peninsula in the Yellow and East China Seas, In: Conley, D.C., Masselink, G., Russell, P.E. and O'Hare, T.J. (eds.), Proceedings 12th International Coastal Symposium (Plymouth, England), Journal of Coastal Research, Special Issue No. 65, 254-259.

Kang, S. K., M. G. G. Foreman, H.-J. Lie, J.-H. Lee, J. Cherniawsky, and K.-D. Yum (2002), Two-layer tidal modeling of the Yellow and East China Seas with application to seasonal variability of the M2 tide, Journal of Geophysical Research: Oceans, 107(C3), 6-1-6-18.

Kolker, A. S., and S. Hameed (2007), Meteorologically driven trends in sea level rise, Geophys Res Lett, 34(23), L23616.

Kossin, J., K. Knapp, D. Vimont, R. Murnane, and B. Harper (2007), A globally consistent reanalysis of hurricane variability and trends, Geophys Res Lett, 34(4).

Lamb, H., and K. Frydendahl (1991), Historic Storms of the North Sea, British Isles and Northwest Europe, Cambridge University Press.

Lionello, P., R. Mufato, and A. Tomasin (2005), Sensitivity of free and forced oscillations of the Adriatic Sea to sea level rise, Climate Res, 29(1), 23-39.

Lionello, P., L. Cavaleri, K. M. Nissen, C. Pino, F. Raicich, and U. Ulbrich (2012), Severe marine storms in the Northern Adriatic: Characteristics and trends, Physics and Chemistry of the Earth, Parts A/B/C, 40–41, 93-105.

Livezey, R. E., and W. Y. Chen (1983), Statistical Field Significance and its Determination by Monte Carlo Techniques, Mon Weather Rev, 111(1), 46-59.

Mackay, D. J. C. (2008), Sustainable energy – without the hot air. UIT Cambridge, 2008. ISBN 978-0-0544529-3-3. <www.withouthotair.com>.

Marcos, M., and M. N. Tsimplis (2007), Variations of the seasonal sea level cycle in southern Europe, Journal of Geophysical Research: Oceans, 112(C12), n/a-n/a.

Marcos, M., M. N. Tsimplis, and A. G. P. Shaw (2009), Sea level extremes in southern Europe, Journal of Geophysical Research: Oceans, 114(C1).

Marcos, M., F. M. Calafat, Á. Berihuete, and S. Dangendorf (2015), Long-term variations in global sea level extremes, Journal of Geophysical Research: Oceans.

Mawdsley, R., and I. D. Haigh (2016), Spatial and temporal variability and long-term trends in skew surges globally, Frontiers in Marine Science, 3.

Mawdsley, R. J., I. D. Haigh, and N. C. Wells (2014), Global changes in mean tidal high water, low water and range., [Proceedings 13th International Coastal Symposium (Durban, South Africa)] Journal of Coastal Research, (SI 70), 343-348.

Mawdsley, R. J., I. D. Haigh, and N. C. Wells (2015), Global secular changes in different tidal high water, low water and range levels, Earth's Future.

McMillan, A., C. Batstone, D. Worth, J. Tawn, K. Horsburgh, and M. Lawless (2011), Coastal flood boundary conditions for UK mainland and islands. Project SC060064/TR2: Design sea levels.

Menéndez, M., and P. L. Woodworth (2010), Changes in extreme high water levels based on a quasi-global tide-gauge data set, Journal of Geophysical Research: Oceans, 115(C10), C10011.

Merrifield, M. A., A. S. Genz, C. P. Kontoes, and J. J. Marra (2013), Annual maximum water levels from tide gauges: Contributing factors and geographic patterns, Journal of Geophysical Research: Oceans, 118(5), 2535-2546.

Meyssignac, B., and A. Cazenave (2012), Sea level: A review of present-day and recent-past changes and variability, J Geodyn, 58, 96-109.

Mitchum, G. T., and S. M. Chiswell (2000), Coherence of internal tide modulations along the Hawaiian Ridge, Journal of Geophysical Research: Oceans, 105(C12), 28653-28661.

Mudersbach, C., T. Wahl, I. D. Haigh, and J. Jensen (2013), Trends in high sea levels of German North Sea gauges compared to regional mean sea level changes, Cont Shelf Res, 65(0), 111-120.

Müller, M. (2008), Synthesis of forced oscillations, Part I: Tidal dynamics and the influence of the loading and self-attraction effect, Ocean Modelling, 20(3), 207-222.

Müller, M. (2012), The influence of changing stratification conditions on barotropic tidal transport and its implications for seasonal and secular changes of tides, Cont Shelf Res, 47(0), 107-118.

Müller, M., B. K. Arbic, and J. X. Mitrovica (2011), Secular trends in ocean tides: Observations and model results, Journal of Geophysical Research: Oceans, 116(C5), C05013.

Müller, M., J. Y. Cherniawsky, M. G. G. Foreman, and J.-S. Storch (2014), Seasonal variation of the M 2 tide, Ocean Dynam, 64(2), 159-177.

Munk, W. H., and D. E. Cartwright (1966), Tidal Spectroscopy and Prediction, Philosophical Transactions of the Royal Society of London. Series A, Mathematical and Physical Sciences, 259(1105), 533-581.

Neumann, B., A. T. Vafeidis, J. Zimmermann, and R. J. Nicholls (2015), Future Coastal Population Growth and Exposure to Sea-Level Rise and Coastal Flooding-A Global Assessment, Plos One, 10(3), e0118571.

Nicholls, R. J. (2010), Impacts of and responses to sea-level rise, Understanding Sea-level rise and variability, 17-51.

Nicholls, R. J., P. P. Wong, V. Burkett, J. Codignotto, J. Hay, R. McLean, S. Ragoonaden, C. D. Woodroffe, P. Abuodha, and J. Arblaster (2007), Coastal systems and low-lying areas.

Olbert, A. I., S. Nash, C. Cunnane, and M. Hartnett (2013), Tide–surge interactions and their effects on total sea levels in Irish coastal waters, Ocean Dynam, 63(6), 599-614.

Ozsoy, O., I. D. Haigh, M. P. Wadey, R. J. Nicholls, and N. C. Wells (2016), High-frequency sea level variations and implications for coastal flooding: a case study of the Solent, UK., Cont Shelf Res, (in review).

Palmer, H. R. (1831), Description of a Graphical Registrer of Tides and Winds, Philosophical Transactions of the Royal Society of London, 121, 209-213.

Pawlowicz, R., B. Beardsley, and S. Lentz (2002), Classical tidal harmonic analysis including error estimates in MATLAB using T_TIDE, Computers & Geosciences, 28(8), 929-937.

Pelling, H., and J. Green (2013), Sea-level rise, tidal power, and tides in the Bay of Fundy, J. Geophys. Res, 118, 1-11.

Pelling, H. E., J. A. Mattias Green, and S. L. Ward (2013), Modelling tides and sea-level rise: To flood or not to flood, Ocean Modelling, 63(0), 21-29.

Peltier, W. R. (2001), Chapter 4 Global glacial isostatic adjustment and modern instrumental records of relative sea level history, in International Geophysics, edited by M. S. K. Bruce C. Douglas and P. L. Stephen, pp. 65-95, Academic Press.

Peng, D., H. Palanisamy, A. Cazenave, and B. Meyssignac (2013), Interannual Sea Level Variations in the South China Sea Over 1950–2009, Mar Geod, 36(2), 164-182.

Pickering, M. (2014), The impact of future sea-level rise on the tides, University of Southampton.

Pickering, M. D., N. C. Wells, K. J. Horsburgh, and J. A. M. Green (2012), The impact of future sea-level rise on the European Shelf tides, Cont Shelf Res, 35(0), 1-15.

Plag, H. P., and M. N. Tsimplis (1999), Temporal variability of the seasonal sea-level cycle in the North Sea and Baltic Sea in relation to climate variability, Global Planet Change, 20(2–3), 173-203.

Pugh, D. (1987), Tides, Surges and Mean Sea-Level: A Handbook for Engineers and Scientists, 472 pp, edited, John Wiley, Chichester, UK.

Pugh, D., and J. Vassie (1978), Extreme sea levels from tide and surge probability, Coastal Engineering Proceedings, 1(16).

Pugh, D., and P. Woodworth (2014), Sea-level Science: Understanding Tides, Surges, Tsunamis and Mean Sea-level Changes, Cambridge University Press.

Raicich, F. (2003), Recent evolution of sea-level extremes at Trieste (Northern Adriatic), Cont Shelf Res, 23(3-4), 225-235.

Rasheed, A. S., and V. P. Chua (2014), Secular Trends in Tidal Parameters along the Coast of Japan, Atmos Ocean, 52(2), 155-168.

Ray, R. D. (2006), Secular changes of the M tide in the Gulf of Maine, Cont Shelf Res, 26(3), 422-427.

Ray, R. D. (2009), Secular changes in the solar semidiurnal tide of the western North Atlantic Ocean, Geophys Res Lett, 36(19), L19601.

Ray, R. D. (2016), On Measurements of the Tide at Churchill, Hudson Bay, Atmos Ocean, 1-9.

Ray, R. D., and G. T. Mitchum (1997), Surface manifestation of internal tides in the deep ocean: observations from altimetry and island gauges, Prog Oceanogr, 40(1–4), 135-162.

Rhein, M. a., S. Rintoul, S. Aoki, E. Campos, D. Chambers, R. Feely, S. Gulev, G. Johnson, S. Josey, and A. Kostianoy (2013), Observations: ocean, Climate change, 255-315.

Rong, Z., Y. Liu, H. Zong, and Y. Cheng (2007), Interannual sea level variability in the South China Sea and its response to ENSO, Global Planet Change, 55(4), 257-272.

Seneviratne, S. I., et al. (2012), Changes in climate extremes and their impacts on the natural physical environment. In: Managing the Risks of Extreme Events and Disasters to Advance Climate Change Adaptation, [Field, C.B., V. Barros, T.F. Stocker, D. Qin, D.J. Dokken, K.L. Ebi, M.D. Mastrandrea, K.J. Mach, G.-K. Plattner, S.K. Allen, M. Tignor, and P.M. Midgley (eds.)]. A Special Report of Working Groups I and II of the Intergovernmental Panel on Climate Change (IPCC). Cambridge University Press, Cambridge, UK, and New York, NY, USA, pp. 109-230.

Šepić, J., I. Vilibić, A. B. Rabinovich, and S. Monserrat (2015), Widespread tsunami-like waves of 23-27 June in the Mediterranean and Black Seas generated by high-altitude atmospheric forcing, Scientific Reports, 5, 11682.

Shennan, I., and P. L. Woodworth (1992), A comparison of late Holocene and twentieth-century sea-level trends from the UK and North Sea region, Geophys J Int, 109(1), 96-105.

Sickmöller, M., R. Blender, and K. Fraedrich (2000), Observed winter cyclone tracks in the northern hemisphere in re-analysed ECMWF data, Q J Roy Meteor Soc, 126(563), 591-620.

Stevens, A., D. Clarke, R. Nicholls, and M. Wadey (2015), Estimating the long-term historic evolution of exposure to flooding of coastal populations, Natural Hazards and Earth System Sciences Discussions, 3(2), 1681-1715.

St-Laurent, P., F. J. Saucier, and J. F. Dumais (2008), On the modification of tides in a seasonally ice-covered sea, Journal of Geophysical Research: Oceans, 113(C11), C11014.

Stumpf, R. P., and J. W. Haines (1998), Variations in Tidal Level in the Gulf of Mexico and Implications for Tidal Wetlands, Estuarine, Coastal and Shelf Science, 46(2), 165-173.

Sündermann, J., and P. Brosche (1978), Numerical computation of tidal friction for present and ancient oceans, in Tidal Friction and the Earth's Rotation, edited, pp. 125-144, Springer.

SwissRe. (2013), Swiss Re's Sigma on Natural Catastrophes and Man-Made Disasters in 2012 Reports USD 77 Billion in Insured Losses and Economic Losses of USD 186 Billion., edited, Available: http://www.swissre.com/media/news_releases/nr_20130327_sigma_natcat_2012.html

Talke, S. A., P. Orton, and D. A. Jay (2014), Increasing storm tides in New York Harbor, 1844–2013, Geophys Res Lett, 41(9), 3149-3155.

Tappin, D. R., A. Sibley, K. Horsburgh, C. Daubord, D. Cox, and D. Long (2013), The English Channel 'tsunami' of 27 June 2011 – a probable meteorological source, Weather, 68(6), 144-152.

Tawn, J., and J. Vassie (1989), Extreme sea levels: the joint probabilities method revisited and revised.

Tawn, J., and J. Vassie (1991), Recent improvements in the joint probability method for estimating extreme sea levels. Tidal Hydrodynamics. BB Parker (ed.): 813-828, edited, Wiley. New York.

Thompson, P. R., and G. T. Mitchum (2014), Coherent sea level variability on the North Atlantic western boundary, Journal of Geophysical Research: Oceans, 119(9), 5676-5689.

Thompson, P. R., G. T. Mitchum, C. Vonesch, and J. Li (2013), Variability of Winter Storminess in the Eastern United States during the Twentieth Century from Tide Gauges, J Climate, 26(23), 9713-9726.

Thomson, R. E., A. B. Rabinovich, I. V. Fine, D. C. Sinnott, A. McCarthy, N. A. S. Sutherland, and L. K. Neil (2009), Meteorological tsunamis on the coasts of British Columbia and Washington, Physics and Chemistry of the Earth, Parts A/B/C, 34(17–18), 971-988.

Töppe, A., and A. Führböter (1994), Recent anomalies in mean and high tidal water levels at the German North Sea coastline, J Coastal Res, 206-209.

Torres, R. R., and M. N. Tsimplis (2011), Tides and long-term modulations in the Caribbean Sea, Journal of Geophysical Research: Oceans, 116(C10), C10022.

Torres, R. R., and M. N. Tsimplis (2013), Sea-level trends and interannual variability in the Caribbean Sea, Journal of Geophysical Research: Oceans, 118(6), 2934-2947.

Trenberth, K. E., et al. (2007), Observations: Surface and atmospheric climate change. In: Climate Change 2007: The Physical Science Basis. Contribution of Working Group I to the Fourth Assessment Report of the Intergovernmental Panel on Climate Change [Solomon, S., D. Qin, M. Manning, Z. Chen, M. Marquis, K.B. Averyt, M. Tignor and H.L. Miller (eds.)]. Cambridge University Press, Cambridge, UK, and New York, NY, pp. 235-336.

Tsimplis, M. N., and P. L. Woodworth (1994), The global distribution of the seasonal sea level cycle calculated from coastal tide gauge data, Journal of Geophysical Research: Oceans, 99(C8), 16031-16039.

Ullmann, A., P. A. Pirazzoli, and A. Tomasin (2007), Sea surges in Camargue: Trends over the 20th century, Cont Shelf Res, 27(7), 922-934.

UNESCO-IOC, M. Guides, 2006. Manual on Sea-level Measurements and Interpretation, Volume IVRep., JCOMM Technical report.

United Nations, D. o. E. a. S. A., Population Division (2014), World Urbanization Prospects: The 2014 Revision, edited.

Valle-Levinson, A., M. Olabarrieta, and A. Valle (2013), Semidiurnal perturbations to the surge of Hurricane Sandy, Geophys Res Lett, 40(10), 2211-2217.

van Rijn, L. (2011), Analytical and numerical analysis of tides and salinities in estuaries; part I: tidal wave propagation in convergent estuaries, Ocean Dynam, 61(11), 1719-1741.

Vecchi, G. A., and B. J. Soden (2007), Increased tropical Atlantic wind shear in model projections of global warming, Geophys Res Lett, 34(8).

Vinogradov, S. V., and R. M. Ponte (2010), Annual cycle in coastal sea level from tide gauges and altimetry, Journal of Geophysical Research: Oceans, 115(C4), n/a-n/a.

Vinogradov, S. V., R. M. Ponte, P. Heimbach, and C. Wunsch (2008), The mean seasonal cycle in sea level estimated from a data-constrained general circulation model, Journal of Geophysical Research: Oceans, 113(C3), n/a-n/a.

Visser, H., S. Dangendorf, and A. C. Petersen (2015), A review of trend models applied to sea level data with reference to the “acceleration-deceleration debate”, Journal of Geophysical Research: Oceans, 120(6), 3873-3895.

von Storch, H., and K. Woth (2008), Storm surges: perspectives and options, Sustain Sci, 3(1), 33-43.

Vučetić, T., I. Vilibić, S. Tinti, and A. Maramai (2009), The Great Adriatic flood of 21 June 1978 revisited: An overview of the reports, Physics and Chemistry of the Earth, Parts A/B/C, 34(17–18), 894-903.

Wadey, M. P., I. D. Haigh, R. J. Nicholls, J. M. Brown, K. Horsburgh, B. Carroll, S. Gallop, T. Mason, and E. Bradshaw (2015), A comparison of the 31 January – 1 February 1953 and 5 – 6 December 2013 coastal flood events around the UK, Frontiers in Marine Science, 2.

Wahl, T., and D. P. Chambers (2015), Evidence for multidecadal variability in US extreme sea level records, Journal of Geophysical Research: Oceans, 120(3), 1527-1544.

Wahl, T., and D. P. Chambers (2016), Climate controls multidecadal variability in U. S. extreme sea level records, Journal of Geophysical Research: Oceans.

Wahl, T., F. M. Calafat, and M. E. Luther (2014), Rapid changes in the seasonal sea level cycle along the US Gulf coast from the late 20th century, Geophys Res Lett, 41(2), 491-498.

Wahl, T., I. D. Haigh, P. L. Woodworth, F. Albrecht, D. Dillingh, J. Jensen, R. J. Nicholls, R. Weisse, and G. Wöppelmann (2013), Observed mean sea level changes around the North Sea coastline from 1800 to present, Earth-Science Reviews, 124, 51-67.

Ward, S., J. A. M. Green, and H. Pelling (2012), Tides, sea-level rise and tidal power extraction on the European shelf, Ocean Dynam, 62(8), 1153-1167.

Weisse, R., and H. Von Storch (2008), Marine climate and climate change : storms, wind waves and storm surges. 2010, Berlin Chichester: Springer-Verlag ;.

Weisse, R., H. von Storch, and F. Feser (2005), Northeast Atlantic and North Sea Storminess as Simulated by a Regional Climate Model during 1958–2001 and Comparison with Observations, J Climate, 18(3), 465-479.

Wolf, J. (1981), Surge-tide interaction in the North Sea and River Thames, Floods due to high winds and tides. Academic, London, 75-94.

Wolter, K., and M. S. Timlin (1998), Measuring the strength of ENSO events: How does 1997/98 rank?, Weather, 53(9), 315-324.

Wong, P. P., I. J. Losada, J. P. Gattuso, J. Hinkel, A. Khattabi, K. L. McInnes, Y. Saito, and A. Sallenger (2014), Coastal systems and low-lying areas, in Climate Change 2014: Impacts,

Adaptation, and Vulnerability. Part A: Global and Sectoral Aspects. Contribution of Working Group II to the Fifth Assessment Report of the Intergovernmental Panel of Climate Change, edited by C. B. Field, et al., pp. 361-409, Cambridge University Press, Cambridge, United Kingdom and New York, NY, USA.

Woodworth, P. L. (2010), A survey of recent changes in the main components of the ocean tide, Cont Shelf Res, 30(15), 1680-1691.

Woodworth, P. L. (2011), A Note on the Nodal Tide in Sea Level Records, J Coastal Res, 316-323.

Woodworth, P. L., and D. L. Blackman (2004), Evidence for Systematic Changes in Extreme High Waters since the Mid-1970s, J Climate, 17(6), 1190-1197.

Woodworth, P. L., and M. Menéndez (2015), Changes in the mesoscale variability and in extreme sea levels over two decades as observed by satellite altimetry, Journal of Geophysical Research: Oceans, 120(1), 64-77.

Woodworth, P. L., S. M. Shaw, and D. L. Blackman (1991), Secular trends in mean tidal range around the British Isles and along the adjacent European coastline, Geophys J Int, 104(3), 593-609.

Woodworth, P. L., A. Aman, and T. Aarup (2007), Sea level monitoring in Africa, Afr J Mar Sci, 29(3), 321-330.

Woodworth, P. L., M. Menendez, and W. R. Gehrels (2011), Evidence for Century-Timescale Acceleration in Mean Sea Levels and for Recent Changes in Extreme Sea Levels, Surv Geophys, 32(4-5), 603-618.

Woodworth, P. L., M. N. Tsimplis, R. A. Flather, and I. Shennan (1999), A review of the trends observed in British Isles mean sea level data measured by tide gauges, Geophys J Int, 136(3), 651-670.

Woodworth, P. L., F. N. Teferle, R. M. Bingley, I. Shennan, and S. D. P. Williams (2009), Trends in UK mean sea level revisited, Geophys J Int, 176(1), 19-30.

Yin, J. H. (2005), A consistent poleward shift of the storm tracks in simulations of 21st century climate, Geophys Res Lett, 32(18), n/a-n/a.

Zaron, E. D., and D. A. Jay (2014), An Analysis of Secular Change in Tides at Open-Ocean Sites in the Pacific, J Phys Oceanogr(2014).

Zetler, B. D., and R. E. Flick (1985), Predicted Extreme High Tides for Mixed-Tide Regimes, J Phys Oceanogr, 15(3), 357-359.

Zhang, X., and J. A. Church (2012), Sea level trends, interannual and decadal variability in the Pacific Ocean, Geophys Res Lett, 39(21), n/a-n/a.

Zhang, K. Q., B. C. Douglas, and S. P. Leatherman (2000), Twentieth-century storm activity along the US east coast, J Climate, 13(10), 1748-1761.